Straw Pressboard Composites

by

Chong Meng

A thesis

presented to the University of Waterloo

in fulfillment of the

thesis requirement for the degree of

Doctor of Philosophy

in

Chemical Engineering (Nanotechnology)

Waterloo, Ontario, Canada, 2020

Examining Committee Membership

The following served on the Examining Committee for this thesis. The decision of the Examining Committee is by majority vote.

External Examiner	Paul Charpentier Professor, Department of Chemical and Biochemical Engineering, Western University
Supervisor	Leonardo Simon Professor, Department of Chemical Engineering, University of Waterloo
Internal Members	Michael Pope Assistant Professor, Department of Chemical Engineering, University of Waterloo
	Tizazu Mekonnen Assistant Professor, Department of Chemical Engineering, University of Waterloo
Internal/External Member	Sheshakamal Jayaram Professor, Department of Electrical and Computer Engineering, University of Waterloo

AUTHOR'S DECLARATION

I hereby declare that I am the sole author of this thesis. This is a true copy of the thesis, including any required final revisions, as accepted by my examiners.

I understand that my thesis may be made electronically available to the public.

Abstract

To fully explore the potential of wheat straw and expand its use in composite applications, this thesis aimed to develop a feasible and effective manufacturing method for wheat straw based polymer pressboard composites.

The effects of hot-water and alkaline treatments of wheat straw raw material were evaluated in terms of wettability and binder absorption, surface morphology and thermal stability. Alkaline treatment was proved to significantly increase the wettability and binder absorption of hydrophilic binder system.

The curing kinetics of thermosetting polyester binders (Acrodur) were studied isothermally and non-isothermally using two complementary thermal analysis techniques (DSC and TGA). Onset and peak temperatures, reaction enthalpy, and activation energy were measured and evaluated to determine suitable conditions for curing Acrodur. This was an extensive and systematic study not previously available in the literature. The threshold temperatures for curing Acrodur were determined to be above 180°C for hermetic system for 10 minutes, and above 150°C for non-hermetic system. It was also concluded that the pressure influenced the onset of cure reaction. As a result of this study, a set of conditions of temperature, time and ventilation can be selected for compression molding.

The adhesion strength of Acrodur on wheat straw stem were measured and evaluated according to ASTM D3163 (for plastic) and ASTM D5868 (for fiber reinforced plastic). It was concluded that Acrodur at low concentrations was capable to provide sufficient adhesion in wheat straw based composites and straw was the weak point.

The wheat straw based composite pressboards were compression molded with different binder systems and processing conditions. The binder systems evaluated were polyamide 6, thermosetting Acrodur, CNF reinforced thermosetting Acrodur, thermoplastic Acrodur. The processing conditions evaluated were: straw loading level, compression molding temperature, pressure and time. The flexural strength and modulus of resultant pressboards were measured and evaluated according to ASTM D790; the dielectric breakdown voltage was also measured according to ASTM D149-09, method A.

The effect of wheat straw size, treatment, binder type, compression molding temperature and pressures on the mechanical properties was investigated. Wheat straw particle generally showed higher reinforcing effect than longer wheat straw fiber. The sodium hydroxide treated straw improved mechanical properties, which was attributed to increased compatibility and binder absorption.

Binder loading level of 40% exhibited better mechanical properties than 20% and 60%. Using polyamide 6 could result in thermal degradation on wheat straw. Thermosetting Acrodur significantly improved the mechanical properties. Incorporation of CNF led to improvement of mechanical properties of pressboards on untreated wheat straw. The thermoplastic Acrodur achieved the remarkable improvement on mechanical properties with both hot-water and alkaline treatments and both sizes of straw at low binder loading of 20%.

The flexural strength and modulus of pressboard prepared here were at high end in comparison with the results in the literature. The pressboards manufactured in this research met and exceeded the requirements for MDF (medium density fiberboard) and HDF (high density fiberboard) and car interior parts in automotive industry.

Acknowledgements

I would like to express my sincere gratitude to Dr. Leonardo C. Simon for his continuous guidance and support throughout the development of this thesis. His advices and support had been invaluable to me.

I would also like to thank my examining committee members, Dr. Paul Charpentier, Dr. Sheshakamal Jayaram, Dr. Michael Pope and Dr. Tizazu Mekonnen for their dedication and for taking the time for reading my thesis. Your valuable comments and suggestions are greatly appreciated.

This project would not have been possible without the financial support provided by Alok Goel, President of Omtec Inc. as well as NSERC. I am very grateful. Thanks also to our other industrial partners BASF, Suzano Pulp and Paper and Kal-Polymers Inc for their collaboration and in-kind donations.

Special thanks to all my friends and colleagues for making this journey more enjoyable. I am grateful to Dr. Charles Dal Castel for the constructive discussions and valuable information during the experiment and analysis processes, and to Dr. Mariana Beauvalet, Dr. Ryan Sungho Park, Dr. Andrew Finkle, Dr. Muhammad Arif, Douglas A Casetta, Jiaxin Xu, Yuhan Huang, Fahad Al-Faleh, Abdulelah Hakami, Syed Ali Shahid, for all their valuable help and kind understanding. Special thanks to two young people, Dinesha Ganesarajan and Ian Tivendale, for the valuable support in preparation for a conference and other things.

Thanks to Dr. Sheshakamal Jayaram, Dr. Marios Ioannidis and Ralph Dickhout for providing me their lab equipment for my experiments.

Dedication

To my parents, Xianren Meng and Caixia Wang;

To my wife, Jie Yan;

To my niece, Mengzhu Yuan;

To my daughter, Hannah Meng and son, Harrison Meng.

Table of Contents

List of Figures

List of Tables

Chapter 1
Introduction

1.1 Motivation and Objectives

Natural fibers are playing more important roles in today's composite pressboard production. As an agro-byproduct, straw is advantageous over other natural fibers because it is cheaper and greener due to its low cost, low energy input, environmental friendliness and biodegradability. The utilization of agricultural residues as supplements or as direct substitutes for wood products and other natural fibers in composites continues to be very attractive. It is the subject of intensive research all over the world. The alternative use of wheat straw in composites manufacturing has the potential to: 1) reduce the use of the petroleum resources; 2) promote the cost-effectiveness and environmental sustainability; 3) save energy since processing straw is less energy intensive than processing wood, and 4) diversify the agricultural economy in Ontario and Canada (Mohanty et al. 2005).

The goal of this research project is to explore the potential of using wheat straw in the composites products and to develop an effective and feasible manufacturing method of wheat straw based polymer composite pressboards. The potential applications of resultant wheat straw based pressboards can be 1) the insulation with supportive function in the oil immersed transformers, 2) the car parts in automotive, 3) the boards used in furniture, buildings and houses, and 4) the boards in packaging. The resultant pressboard must meet or exceed the requirements of these specific applications to justify its appropriation of utilization. Among these applications, the MDF (medium density fiberboard) and HDF (medium density fiberboard) require the flexural strength of 12.4 and 23.5 MPa, followed by car parts of 52 MPa and the insulation pressboards of $\geq$ 100 MPa in machine direction and $\geq$ 75 MPa for across machine direction.

The proposed manufacturing mothed should be transferrable to the existing methods of composites manufacturing to benefit from manufacturing equipment that is already available. In addition to wheat straw, the composites will make use of a binder that can be either thermoplastic or thermoset. The success of this project will dramatically add value to wheat straw, and enable its use the composites manufacturing industry as a novel and sustainable feedstock. Wheat straw is very abundant and readily available in industrialized areas. Approximately 2 parts of the wheat plant are straw and 1 part is grain.

1.2 Research Strategy

It has been challenging to expand the utilization of straw in composites, mainly due to the poor mechaqnical properties of composites products. To fulfil the task, specifically, to improve mechanical properties, the primary factors in this regard include the investigation of wheat straw, polymer binders, and the manufacturing method (technology and condition) that play an important role in determining the mechanical and other properties. These three factors need to work synergistically to give well-improved performance to meet the requirements of the target applications. The research strategy is schematically presented in Figure 1.1.

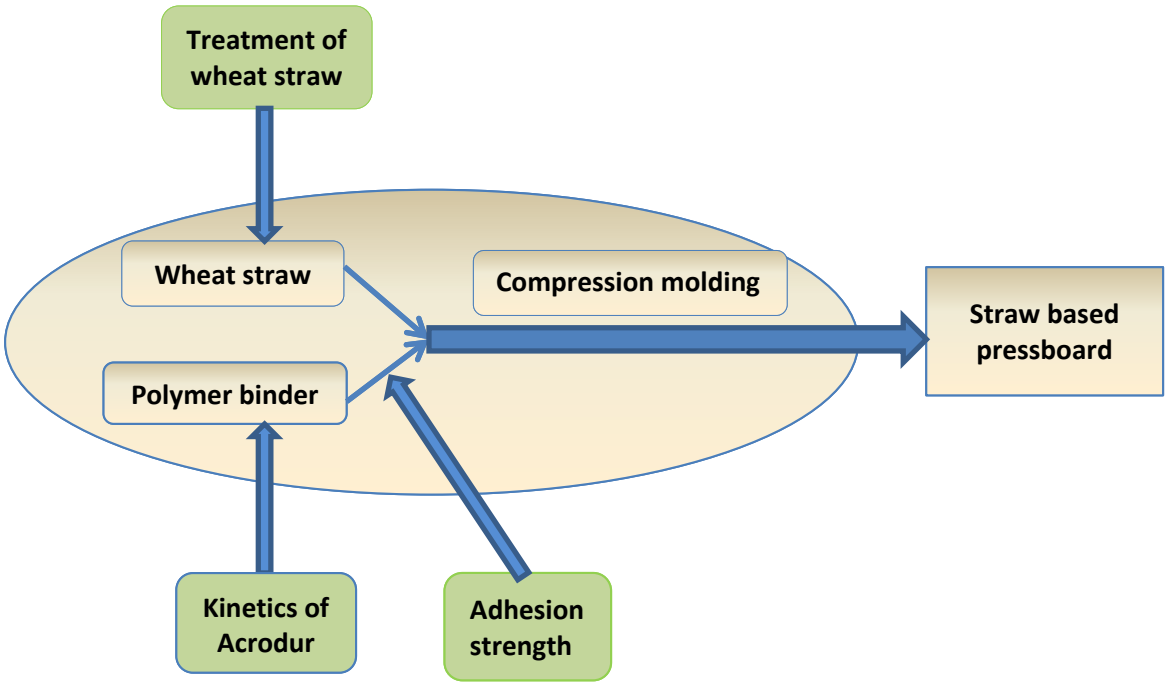

Figure 1.1 Schematic represention of research strategy

The utilization of wheat straw in the composites for load-bearing applications is challenging mainly because of its intrinsic inferior strength and incompatibility with polymeric binders if compared to glass fiber for example. To explore the full potential of wheat straw and expand its use in practical applications, this thesis is seeking to develop a feasible and effective manufacturing method for wheat straw based polymer composite pressboards, with improved mechanical, dielectric, and other properties.

There were a few questions that needed to be addressed before successful production of the pressboards. What treatments can improve the compatibility between straw and polymer binder at low cost? What are the compression molding conditions for curing the binder when thermoset Acrodur is used? Is thermoset Acrodur capable to provide sufficient adhesion in the composites, and how much of it is required? The specific research problems addressed in this thesis were identified by literature review and also throughout the research. To answer these questions, three sub-projects were conducted to support the final step: manufacturing of pressboards, corresponding to four specific goals:

1) To study the effect of straw surface on the compatibility and binder absorption. Two surface treatments were carried out on wheat straw raw material, and the effect of treatments were studied in terms of the wettability, binder absorption, surface morphology and thermal stability.

2) To measure the kinetics of thermosetting binder (namely Acrodur) during the cure reaction. The reaction was investigated isothermally and non-isothermally using thermal analysis methods. The temperature–time dependence of the conversion was established. The activation energy was estimated using iso-conversional method for three types of Acrodur binders and the prepregs. The conditions for curing temperature, time and pressure were selected.

3) To investigate the effect of binder content and straw surfaces on adhesion. The single lap adhesion strength of Acrodur on wheat straw were measured and evaluated.

4) To prepare the pressboards using the compression molding and to evaluate the properties. Two types of binders were investigated (thermoplastic polyamide 6, and thermosetting and thermoplastic Acrodur) while also investigating other parameters, like straw sizes, formulations, treatments and compression molding conditions. The effects of these parameters on the mechanical and dielectric properties were evaluated.

1.3 Chapter Outline

The subsequent chapters of this thesis address the above mentioned tasks and describe the experimental procedures through which the outlined research objectives were achieved. This thesis will make use of the scientific method and engineering tools to enable engineering research leading to development of pressboard using what straw.

Chapter 1 identifies the main research goals. Specific research objectives are identified in subsequent chapters.

Chapter 2 presents the literature review on the production of wheat straw based composite pressboards. Specifically, the chemical and structural properties of wheat straw, the characteristics of thermoplastic polyamide 6 and thermosetting polyester (Acrodur) and their typical applications in production of composite were reviewed. This chapter also identifies the research challenges.

Chapter 3 covers the application of treatment with hot-water and NaOH on wheat straw. The effects of these two treatments were evaluated in terms of contact angle, binder absorption, surface morphology, and thermal stability. This is relevant to understand the surface characteristic of the straw can be controlled with respect to its behavior controlling its interaction and location of the binder.

Chapter 4 presents the kinetics study of cure reaction of three thermosetting binders (three types of Acrodur) and wheat straw-Acrodur prepregs using thermal analysis methods. Thermogravimetric analysis (TGA) and differential scanning calorimetry (DSC) were used as complementary tools. The onset and peak temperature and the activation energy were measured, compared and correlated. The preferred compression molding conditions, consisting of temperature, time and pressure were assessed and selected. This is relevant because the properties of the composites are strongly defendant on the structure of the binder, which is a function of its curing kinetics. This information was not found in the previous literature.

Chapter 5 presents the single lap adhesion strength measurement of Acrodur and wheat straw under different conditions. Although this chapter is narrow in its scope, the information reported here is useful to understand certain limitations in terms of strength of straw and binder. This chapter is relevant because it provides solid information about the nature of the adhesion under controlled conditions, something that is often assumed to be known but it is seldom measured.

Chapter 6 describes the production of pressboards fabricated with polyamide 6 as binder, the mechanical properties were measured and the effects of binder loading, and compression molding temperature and pressure were evaluated using factorial design of experiment. This study is interesting because it evaluates the combination of two feedstocks that are currently undervalued – straw and recycled plastics – thus unveiling the potential for new sustainable products.

Chapter 7 describes the production of pressboard made with two types of Acrodur: thermosetting and thermoplastic. The mechanical properties were measured and the effects of wheat straw size, treatment, binder loading, Acrodur type, and compression molding temperature, time and pressure were evaluated. The major outcome of this chapter are the correlations between these factors (formulation

and processing) and the performance of the resultant composite pressboards. The quantitative correlations established here were not reported in the literature elsewhere and form a solid foundation to enable manufacturing of straw pressboard using industrial compression molding conditions.

At last, Chapters 8 summarizes the significant contributions for this research and its importance to the utilization of wheat straw in production of composite pressboards. The general conclusions from the research were discussed along with a discussion of the research limitations and recommendations for future work.

The list of references cited in the thesis and the appendices with additional information related to raw data of contact angle and binder absorption, kinectic analysis of Acrodur curing and statistical analysis of fitting wetting model and peak deconvolution, thermal degradation of wheat straw, DOE analysis, SEM images of wheat straw and pressboard are presented.

Chapter 2
Literature Review

2.1 Outline

The factors influencing the mechanical performance of natural fiber reinforced composites have been extensively studied in literature. The main factors in this regard include: 1) the reinforcing fiber processing and treatment; 2) the polymer binder; 3) the interfacial adhesion, and 4) the composite manufacturing technology and condition.

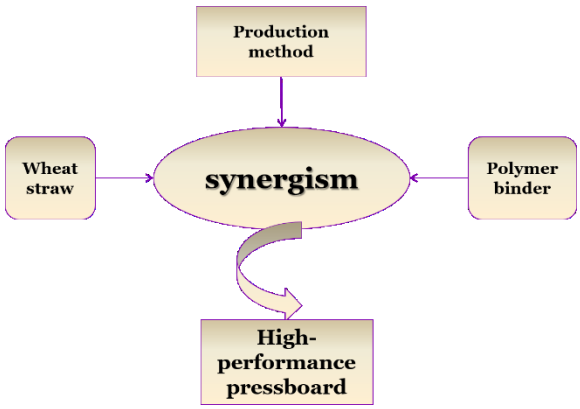

Figure 2.1 Controlling factors in production of natural fiber-polymer composite

This chapter (literature review) covers these three factors shown in Figure 2.1 with the purpose of providing a profound insight on wheat straw, polymer binder, and manufacturing method as well as the property evaluation methods. This chapter is structured as follows:

1) The general characteristics of the plant based natural fibers were reviewed. Wood and bast fibers, as two most relevant natural fibers, and their composites were reviewed and discussed.
2) Wheat straw was comprehensively examined in the context of fiber-reinforced composite materials, in terms of the anatomical component, the structure, the chemical composites, with the purpose of establishing a structure–property correlation with the properties of interest, such as the mechanical properties and the surface morphology. The commonly used treatment methods were reviewed and discussed. The typical and potential utilizations of wheat straw in the composites are reviewed and evaluated.

3) Both the thermoplastic and thermosetting polymeric binders were reviewed in this section. Their advantage and disadvantages, and the typical utilization in composite were reviewed and evaluated.
4) The manufacture technology, compression molding for the natural fiber reinforced composites pressboards was reviewed and discussed. The affecting factors, such as moisture content, fiber type and content, coupling agents and their influence on composites properties, were reviewed and discussed.
5) Characterization and evaluation technologies for mechanical, dielectric and other properties.

The review will conclude with a summary of wheat straw in composites as well as key issues that need to be addressed and resolved.

2.2 Natural Fiber

The natural fibers addressed here are cellulose based fibers that feature a short growth period, renewability and abundancy. The low density and relatively low cost of natural fibers are the main aspects referred to as the attractions for utilization of natural fiber composites in the applications. Also, natural fiber composites are claimed to offer multiple environmental benefits such as: reduced dependence on non-renewable energy and material sources, low pollutant emissions, low greenhouse gas emissions enhanced energy recovery and end of life biodegradability of components (Yahya et al. 2017).

However, the associated drawbacks greatly reduce the potential of natural fibers to be used as reinforcement in polymers, including large variation in properties and quality, high moisture absorption, low durability, low strength and low processing temperature, incompatibility with the hydrophobic polymer resin (Saheb and Jog 1999). These inherent downsides pose the topics for the researchers and producers to address and solve.

Wood Fibers

The use of wood fibers has a long history in paper making industry and the wood currently provides the basis for the vast majority of global pulp production. Paper and pressboard are made from a three dimensional structured network of wood fibers extracted through pulping process (Kraft process). The Kraft process is a conversion process, during which the cellulose fibers are liberated from its “matrix” of hemicelluloses and lignin.

The electrical grade paper and pressboard are made of Kraft pulp from pine wood softwood. The dried paper and pressboard after impregnated with the insulating oil are used as the electrical insulation in the high-voltage transformers. The electrical insulation system of the combination of oil-paper electrical insulation largely determines the life span of a transformer. The insulation pressboards in the electrical transformers perform two main functions: 1) structural support (mechanical properties) and 2) insulating media (electrical properties).

Bast Fibers

The bast fibers are obtained from the phloem or outer bark of jute, kenaf, flax and hemp plants. The bast fibers are annually renewable crops growing in 90 to 100 days. The bast fibers are multicellular and their individual fiber are small and short, but in bundles these fibers provide the reinforcement to stems and leaves. Their high content of cellulose along with high aspect ratio makes them appropriate for stress-bearing applications. As the most widely used non-wood lignocellulosic fibers due to their specific strength, modulus characteristics and availability, the bast fibers are reported in general to exhibit the comparable mechanical properties with those of synthetic fibers when used in reinforced composites (Summerscales et al. 2010a) (Summerscales et al. 2010b). Studies indicate that the natural fiber composites can contribute to a cost reduction of 20% and weight reduction of 30% of an automotive part (Shuda et al. 2008). Figure 2.2 shows the process from hemp fiber to door panel for a car.

Figure 2.2 Production of door panel in automotive from hemp fiber (Pollitt 2018)

2.3 Wheat Straw

Wheat (Triticum spelta) is an annual crop grown throughout the most populated areas in the world, such as India, China and North America. Wheat ranks second in total production as a cereal crop. Wheat straw is the above-ground parts of the wheat plants that remain after the nutrient grains or seeds have been removed. It comprises approximately two-thirds of the total dry weight of the crop. It is available in large quantities (about 600 million tons per year worldwide on average (2012–2014), estimated by Food and Agriculture Organization) at low cost (US$ 40 per ton).

As reinforcement in composites, the mechanical strength and stiffness of wheat straw plays a crucial role in determining the wheat straw reinforced polymer composites performance. In order to explore the full potential of wheat straw as reinforcement in composites, it is of most importance to characterize the physical and chemical characteristics of wheat straw and also necessary to understand how the factors affect the mechanical reinforcement performance of wheat straw and other relevant performances (Rowell et al. 2000).

2.3.1 Structure and Surface Properties of Straw

Wheat is a species of monocots and grows only vertically and does not thicken in diameter because of the lack of cambium. In wheat straw the fiber part (fibrous tissue) is around 67% (Jin and Chen 2007), which is much lower than 73–98% of the fiber part in wood (Halvarsson 2010). Wheat straw is the dry stems of wheat plant and is commonly approximately 50–100 cm long depending on overall growing environment and cultivation method. Wheat straw is usually gathered and stored in bales. Wheat straw in bales consists mostly of the stems unavoidably mixed with a small amount of the leaves, grains and chaffs. The mass balance of wheat straw bale was estimated as shown in Figure 2.3 (B), where the node, internode, leaf, and other parts were considered. The wheat stalk has two principal functions for plant wellness: structural supporting and conduction of nutrients and water. The stalk is made up of a variable number of internodes, separated by nodes at which the leaves are attached show in Figure 2.3 (A).

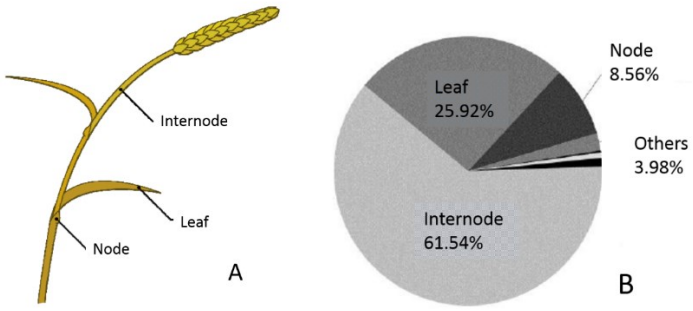

Figure 2.3 Parts of the wheat plant (A) (Halvarsson 2010) and mass balance of wheat straw bale by physical content (B) (Atik and Ates 2012)

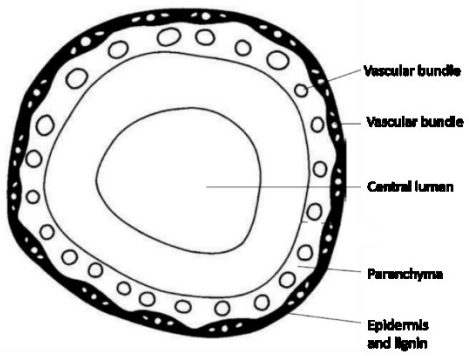

Figure 2.4 Transverse section of the internodes of wheat straw showing epidermis, vascular bundle, parenchyma tissue and pith from outside to inside (Theander and Aman 1984)

The internode is the predominant and most valuable part in wheat straw as it contains the fibers of sufficient amount and quality corresponding to its structural supporting function. The internode also known as stem develops as a hollow cylinder surrounded by a leaf sheath. The internodes is mainly comprised of epidermis, cellular inner region and central void called lumen from outside to inside as shown in Figure 2.4.

The epidermis functions to protect the internal parts of the plant and to retain water from evaporation. The cells in the epidermis are closely packed in parallel rows. The cell walls are rich in cellulose fibrils which are bound within an amorphous matrix of lignin and hemicellulose. And the cell walls in the

epidermis are thickened and covered with a thin water proof layer called the cuticle, in which waxes are deposited.

The inner cellular is a loose structure compared to epidermis, with 25–27% numerous vascular bundles embedded in a parenchyma ground tissue (Hornsby et al. 1997a). The vascular bundle is rich in cellulose and serves as the mechanical support and the nutrients conduction.

The pith occupies the central part of the stem and is composed of thin-walled parenchyma cells often with larger intercellular spaces than you would find in the epidermis. It has a loose and porous structure without any wax covered. Therefore cellulose and hemicellulose are accessible from inside and exhibit the hydrophilic property.

The nodes and leaves (including sheath) contain less amounts of fiber cell elements and more mineral ashes. They are hard and rigid to compression and rather useless when used as fiber reinforcement.

2.3.2 Chemical Composition and Distribution

The cell wall of wheat straw is a heterogeneous natural nanocomposite of cellulose, lignin, and hemicelluloses, with content, composition, and distribution varying over a wide range. The chemical components are distributed throughout the cell wall. Cellulose, hemicelluloses, and lignin account for more than 80% of the dry matter of the common cereal straws including wheat (Gordon and Phillips 1989).

Compared to other natural fibers, wheat straw fibers have lower cellulose content than cotton and linen but in the same range of cellulose content reported for kenaf (Ramaswamy et al. 1994) (Thygesen et al. 2005). The previous studies on the structure of cellulose in wheat straw have reported crystallinity in the range of 43–47% for cellulose obtained from various parts of wheat straw (Liu et al. 2005). Wheat straw fibers have lower cellulose content and crystallinity than cotton, linen, and kenaf. Therefore, wheat straw fibers may have lower strength but better moisture and chemical absorptions compared to cotton, linen, and kenaf. The cellulose crystals in wheat straw fibers are poorly oriented along the fiber axis compared to cotton and linen (Reddy and Yang 2007).

Generally, the bast fibers such as kenaf are lignified to a higher extent than lignocelluloses from agricultural byproducts such as wheat straw, rice straw and cornhusks, and therefore, the fibers from the straw have lower lignin contents than some of the common bast fibers (Reddy and Yang 2005a)

(Reddy and Yang 2005b). The ash content in wheat fibers is similar to cotton but lower than that of kenaf fibers (Reddy and Yang 2007).

Cellulose is the most abundant organic polymer on earth, with an estimated annual natural production of 1.5×10^{12} tons. Cellulose is a linear homopolymer of β-D glucose units (glucopyranose units) joined together by β-1, 4-glucosidic linkages, with a degree of polymerization ranging from 15 to as high as 10,000–14,000 (Evans 1979), or up to 15,000 (Marx-Figini 1971). Its chemical structure is shown in Figure 2.5.

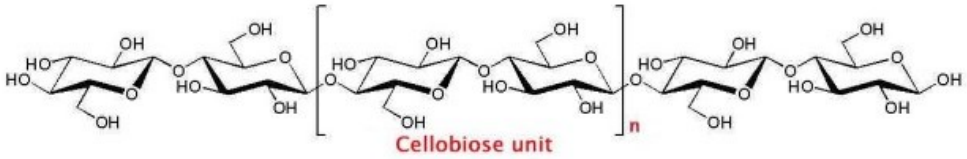

Figure 2.5 Chemical structure of cellulose (Klemm et al. 2005)

Because of the strong tendency for intra- or inter-molecular hydrogen bonding, bundles of cellulose molecules aggregate to microfibrils, which form either highly ordered (crystalline) or less ordered (amorphous) regions. Microfibrils are further aggregated to fibrils and finally to cellulose fibers. The fibrous structure along with strong hydrogen bonds makes cellulose resistant to the heat and most solvents while rendering it high mechanical properties (Wangaard 1979) (Godavarti 2005).

Hemicelluloses are noncrystalline heteropolysacharides and classically defined as the alkali soluble material after removal of the pectic substances. Chemically, hemicelluloses are heteropolymers of various 5- and 6-carbon sugars and have a degree of polymerization 10–1000 times lower than that of cellulose (Yao et al. 2008). Hemicellulose's highly branched and amorphous structure makes it the easiest component to solubilize during thermo-chemical pretreatments. Solubilization of hemicellulose begins at 150ºC under neutral conditions (Volynets and Dahman 2011). Hemicelluloses function as mechanical coupling agents in a two-phase composite between cellulose and lignin. They form hydrogen bonds with cellulose and covalent bonds (mainly α-benzyl ether linkages) with lignin (Sun 2010a).

Lignin is one of main components of wheat straw and ranks third after cellulose and hemicellulose. However, lignin is significantly different in properties, such as activity and solubility with carbohydrates. Lignin is essentially viewed as an amorphous composite of physically and chemically heterogeneous materials, comprising a family of amorphous branched non-carbohydrate polymers

made of mainly aromatics arising from an enzyme-mediated polymerization process. About 60–80% of the total lignin is located within the secondary wall (Saka and Goring 1988). As a summery, the characteristics of cellulose, hemicellulose, and lignin in wheat straw are tablated in Table 2.1.

Table 2.1 Structure and chemical composition and interdependency of fiber properties of cellulose, hemicellulose, and lignin in cell walls of wheat straw (Yang et al. 2008) (Dakar 2015)

	Cellulose	Hemicellulose	Lignin
Polysaccharides	Homo-polysaccharides	Hetero-polysaccharides	
Monomers	Same monomer (glucose)	Different sugar monomers (xylose, glucose, mannose, galactose, uronic acid)	Guaiacyl-propane (G), Syringyl-propane (S), p-Hydroxyphenyl-propane (H)
Branch	Unbranched	Branched	Branched
DP	500–20,000	150–200	4000
Structure	Crystalline (40%)	Amorphous	Amorphous
Characteristics	Rigid, linear polymer of glucose subunits	Branching polymers of C5, C6	Complex, crosslinked polymer of aromatic rings
Composition	Three-dimensional linear molecular composed of the crystalline region and the amorphous region	Three-dimensional, inhomogeneous molecular with a small crystalline region	Amorphous, inhomogeneous, Nonlinear three-dimensional polymer
Water affinity	Hydrophilic	Hydrophilic	Hydrophobic
Thermal Degradation	>200ºC	160ºC	110ºC (slow)
Functions	Strength	Bind microfibrils	Stiffness
Plant constituents influence	Biodegradation	Thermal degradation and moistrure absorption	UV degradation

On the surface of stem and leave is a dense coating called cuticle, which serves to protect the plant as diffusion barrier from the effects of water loss, from the effects of high and low temperatures, and from the effects of insect predation.

On the aerial parts of the plant, the cuticle is made up of cutin (lipophilic polymers) embedded in epicuticular wax layer, both of them are water-proofing. Cutin is an amorphous polymer largely held

together by ester linkages, comprising of aliphatic and aromatic subunits). Cutin can be depolymerized by the presence of alkali (Brown and Kolattukudy 1978). Wheat straw contains around 1% wax by weight (only 0.5–1.0% of the dry weight) (Hamilton 1995). The wax is usually a complex mixture of several classes of aliphatic components, such as hydrocarbons, esters, free alcohols, and acids. (Mo et al. 2005)

Ash represents the mineral content in wheat straw, with its content and level dependent on the soil and environmental conditions. All the agricultural fibers are rich in mineral matters while the softwood and hardwoods contain almost negligible amount of minerals. In general, the ash content of fibrous raw material is between 1% and 20% (Eroğlu and Deniz 1993). It is concentrated on the surface of stem and leaves (for wheat straw about half (50.90%) of the silica comes from leaves (Atik and Ates 2012)) (Halvarsson 2010). About 65–70% of the total mineral content is SiO_2. The role of silicon in plant cell wall is even more ambiguous. Silica has been reported to serve as protection of plant from insects and fungi (Sangster and Hodson 1986), also be beneficial for mechanical strengthening.

The chemical content of straw also varies appreciably according to the stage of maturity. The different fractions of straw vary in chemical composition. Table 2.2 shows that cellulose is higher in the internodes, and ash in which the main constituent is silica, insoluble ash, is high in leaf and leaf base. Lignin is high in the node cores. The stems account for 50–60 wt. % and are richer in cellulose while containing less ash. The leaves that account for around one third of biomass fraction contain more ash and nodes are higher in lignin. Chemically, the stems contain higher levels of cellulose and hemicellulose and a lower amount of lignin than other parts of wheat plant, making wheat straw a more efficient lignocellulose source for reinforcement use (Volynets and Dahman 2011).

Table 2.2 Chemical compositions of different parts of wheat straw

	Percentage of dry weight				
	Overall *	Internode**	Blade **	Sheath **	Node **
Cellulose	38.6	44.8	37.7	32.7	37.5
Hemicelluloses	32.6	33.8	32.4	34.2	32.7
Lignin	14.1	14.2	15.3	14.1	16.7
Hot-water-soluble	4.7	7.2	14.6	18.9	13.2
Ash	5.9	4.7	11.5	12.4	6.3
Wax	1.7	-	-	-	-

*(Sun and Tomkinson 2004), ** (Harper and Lynch 1981)

2.3.3 Processing and Treatment

Wheat straw can be processed and treated in various ways to yield the reinforcing elements with varied mechanical and other properties according to the requirements of the final product forms, end applications, and manufacturing methods.

The purpose of processing and treatment on wheat straw raw material is 1) to prepare appropriate forms of feedstock for pressboard production process, and 2) to improve the functional properties of final products by physically or chemically modifying wheat straw's structure and chemistry. For example, wheat straw requires the modification of the surface physio-chemistry to improve wettability or dimensional stability, thus to increase the adhesion with hydrophobic matrix (Ramesh et al. 2017) (Le Moigne et al. 2018). The appropriate processing and treatment can not only facilitate the production process but also improve the mechanical properties.

Due to the complexity of wheat straw structure and chemistry, a multiply-step strategy is normally involved in raw material processing depending on the application requirements as well as economic consideration. A comprehensive diagram is presented in Figure 2.6 after an extensive literature review. This diagram represents most possible methodologies available in the literature. It is useful to provide understanding of different paths to be taken in processing wheat straw and other natural fibers.

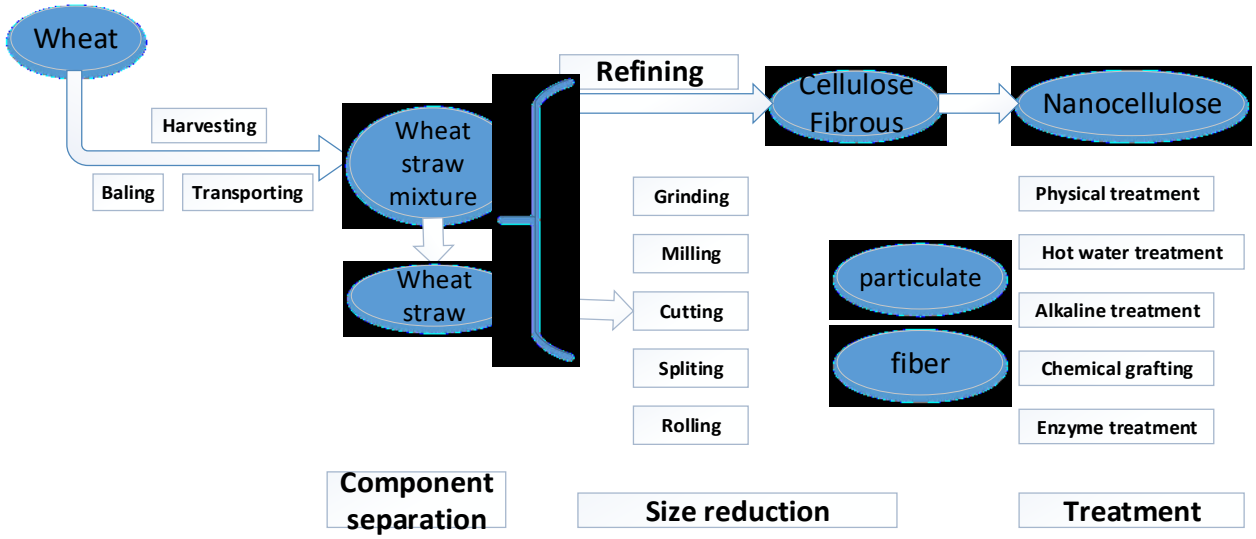

Figure 2.6 Schematic presentation of wheat straw processes

These methods can be used either alone or in combination. The steps below are specifically the common methods for wheat straw processing and pretreatments:

1) Component separation
2) Size reduction
3) Hot-water treatment
4) Alkaline treatment
5) Refining process
6) Chemical grafting

The results show that processing and treatment significantly influence the fiber form, structure, surface morphology, chemical composition thus impact the performance of final products. This emphasizes the need to have control over the processing and manufacturing process (Hollertz 2014). It should also be noted that the increased consumption of energy and cost might be resulted from the processing and treatment.

Separation of the stems from the original plant source is an important step to ensure the high quality of fibers for reinforcing use in composite. This step involves stem collection and removal of the others as much as possible. Some coarse but effective separation methods are to separate by weight difference (blowing) to avoid time-consuming and cost-adding. Or even, sometimes for some low-requirement cases, this step is skipped without taking off the other parts. Component separation is often not carried out for large-scale process because of cost and labor involved (Sun 2010b).

Size reduction is mainly a physical process where wheat straw is disrupted by mechanical force, which may be followed by screening for partition or blowing away plant residues, which have a high content of silica. milling, grinding, cutting and splitting reduce wheat straw particle size, and increases bulk density and accessible surface area and roughness, which improves the efficiency of subsequent processing by decreasing transportation costs, improving flow properties, and minimizing heat and mass transfer limitations (Volynets and Dahman 2011).

It should be noted that physical processings change structural and surface properties of wheat straw and thereby influence the mechanical bonding with polymers. Physical treatments do not extensively change the chemical composition of the fibers. Therefore, the interface is generally enhanced via an increased mechanical bonding between the fiber and the polymer resin (Faruk et al. 2012).

Processed wheat straw is a discontinuous material, in the form of either fiber or particle, according to its length-to-diameter (l/d) ratio know as aspect ratio. The particulate fillers, such as straw flour, enhance the tensile and flexural moduli of the composite with little effect on the composite strength. Whereas straw fibers with higher aspect ratios contribute to an increase in the strength and moduli of composite (R. M Rowell et al. 1997).

The alkaline treatment breaks up the protective outer layer (comprised of waxes) of the straw, disrupts the hydrogen bonding in the network structure, and solubilizes lignin and hemicellulose. The effects on the fiber are 1) increased surface roughness and 2) incremented amount of active hydroxyl groups exposed on the fiber surface (Franco and Valadez-González 2005). Both are beneficial to interfacial adhesion promotion, either by better mechanical interlocking or by increasing the number of possible reaction sites. It was concluded from literature that mechanical property improvements of composite upon alkylation were correlated with a change of the morphological and chemical structures in microfibrils of the fiber (Pereira et al. 2015). On the other hand, application of alkaline treatment increases the pH of the wheat straw-polyester binder system, which negatively affects the curing process of thermoset by reducing the reaction rate (Sam-Brew 2017) (Khalfallah, Marcel, et al. 2014).

The alkaline treatment proved its effectiveness for component removing, fiber modification and surface modification. It was reported that even silicon dioxide can be chemically dissolved with a low-concentration sodium hydroxide solution (Zhang et al. 2004). The effect of alkali treatment on the wetting ability of sisal–epoxy composites was examined (Bisanda 2000). Treatment of sisal fiber in a 0.5 N solution of sodium hydroxide resulted in more rigid composites with lower porosity and higher density. The treatment improved the adhesion characteristics, due to improved work of adhesion because it increases the surface tension and surface roughness. The resulting composites showed improvements in the compressive strength and water resistance. It was also discovered that the removal of intra-crystalline and inter-crystalline lignin and other waxy surface substances by the alkali substantially increases the possibility for mechanical interlocking and chemical bonding (Bisanda 2000).

Hot water could be used as a method to separate water-soluble hemicelluloses from the cell wall of straw. Hot water treatment is an economic chemical treatment on wheat straw in papermaking industry, bio-oil production and fiber reinforced composite. The simple setup and low cost are its advantages. The hot-water treatment on wheat straw can remove simple hydrocarbons called hot water-soluble

extracts, including free fatty acids (25.8–48.4%), waxes (9.4–27.0%) and others (Zhang et al. 2004) (Sun et al. 2003).

Wheat straw is made up of bundles of fibers (or agglomeration of elementary fibers). These bundles can be broken down mechanically or chemically to achieve the fineness required. The degree of this breakdown, in turn, dictates their end use. This process is called refining for fiber extraction as shown in Figure 2.7.

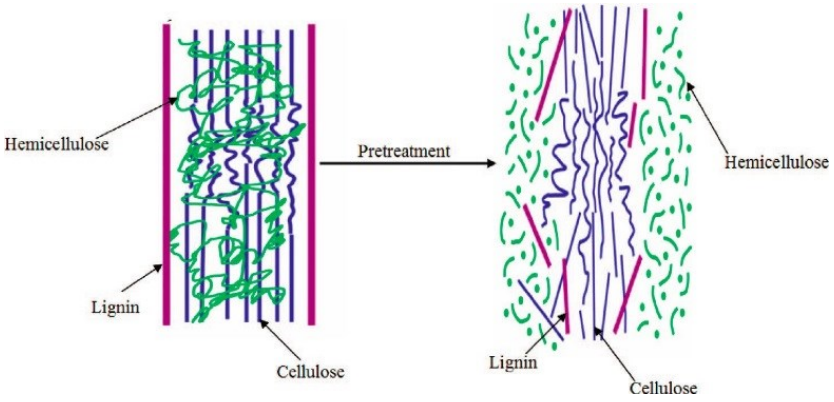

Figure 2.7 Refining process of natural fiber (Hsu et al. 1980)

Similar to pulping process for wood, wheat straw refining is carried out for generation of wheat straw fiber mostly for papermaking industry. Refining essentially is a combination of chemical, thermal and mechanical processes. During refining, waxes are removed by organic solvent extraction with acetone or ethanol; alkali extraction is then used to dissolve or partially dissolve lignin and pectin. Eventually, pressurized refining of wheat straw under appropriate processing conditions disintegrates the straw material and generates fiber bundles and fiber of sufficient quality (Sauter 1996). However, the refining process requires high energy (Mo et al. 2005).

Poor compatibility with synthetic binders calls for the surface modification on wheat straw, thereby an effective control is achieved over the fiber-polymer interface by increasing surface wettability. The basic principle of chemical modifications for compatibility improvement is introducing a third material that has properties intermediate chemically between the fiber and binder. In addition, reports indicate that it is possible to reduce the amount of moisture absorbed in natural fibers and composites by using compatibilizers or by acetylation of hydroxyl groups present in the fiber (Chestee et al. 2017) (Rowell et al. 1986).

Some commonly used chemical methods involving coupling agents are silanization, acetylation, benzoylation, isocynadate, mathacrylate. For example silane can be introduced to supply much more amine functionality that can possibly react with the resin in the interphase. Acetylation is another method of modifying the surface of natural fibers and making them more hydrophobic through the introduction of an acetyl functional group into an organic compound. The main idea of acetylation is to coat the –OH groups of fibers which are responsible for their hydrophilic character with molecules that have a more hydrophobic nature. Maleic anhydride (MAH) treatment is not only used to modify fiber surface but also the polymeric matrix to achieve better interfacial bonding in between fiber and matrix and improved mechanical properties in composites. Meanwhile, some researchers apply peroxide treatments on natural fibers due to its simplicity and relatively good mechanical properties (Ali et al. 2016). Grafting chemical species on to the fiber surface has also been reported to improve the interaction between the fibers and matrix. Although grafting can improve the properties of the composite to a significant extent, this process increases the material cost of system. The use of dispersing agents and/or coupling agents (Peças et al. 2018) (Bledzki et al. 1996) is a cheaper route to improve properties and makes more practical sense for high volume, low cost composite systems. The use of dispersing or coupling agents can change the molecular morphology of the polymer chains both at the fiber-polymer interphase and also in the bulk matrix phase.

There may be multiple strategies and steps involved in processing wheat straw. The processing and treatments have significant effects on quality of fiber and resultant composites. Production of composite requires the wheat straw raw material processed for suitable feedstock. It is often necessary to introduce treatment for wheat straw to ensure an enhanced adhesion with polymeric resins. Treatments change fiber characteristics and morphology to improve the bond between the polymeric resins and wheat straw by chemical and physical means (Gauthier et al. 2003). It is well known that incompatibility with polymeric resins has been one of the deficiencies associated with wheat straw restricting the use in production of polymer composites. The root cause of poor compatibility lies in present of wax and ash/silica existing in the cuticular layer of the epidermis. The outer thin waxy and silica layer surrounding the straw stem inhibits sufficient direct contact between the binder and the straw fibers (Yasin et al. 2010), lowers the wettability of wheat straw with water based resins and poses a problem in the production of straw-based composite boards. Additionally, wax and ash degrade the mechanical and electrical properties of the composite, increase equipment and tool wear, and require more resin to

maintain the required properties. Separating wax and ash from the produced fiber materials improves the wetting of water-based resins but also increases swelling effect.

Although the improved compatibility and mechanical properties are achieved/attained through processing and treatment, the applied physical and chemical methods boost the risk for fiber degradation and consecutively to augmentation in the processing cost. For example, the process and treatments performed to separate and isolate the individual fibers are always detrimental to the integrity of the fibers as their natural characters (Célino et al. 2013). Also, it should be noted that any processing and treatments of wheat straw raw material would also affect the production cost and energy and could cause environmental impact (Thielemans and Wool 2004).

Therefore, the selection of method for straw treatment should take into account the application requirements and economic consideration.

2.3.4 Use of Wheat Straw in Polymer Composites

Because of increasing concerns on forest utilization and global climate change, in the recent past 20 years studies have been carried on to investigate the viability of using wheat straw as an alternative to other nature fibers used in composites. Driven by increased environmental and health concerns, wheat straw based composites have diversified their applications into packaging, building/construction and automotive engineering by replacing the petroleum derived conventional reinforcing materials, glass fiber and other plant fibers (Pervaiz and Sain 2004) (Wolcott and Smith 2004). MDF (medium density fiber board), particleboard, and car panels manufactured with wheat straw have been successfully developed in multiple applications, such as furniture and automotive industry.

As an agricultural residue, wheat straw offers a great promise and new challenges as a replacement for wood and other natural fiber products. Rice straw and wheat straw can be easily crushed to chips or particles, which are similar to wood particle or fiber, and may be used as substitutes for wood-based raw materials (Yang et al. 2003). Wheat straw, for example, offers desirable geometric and mechanical attributes for replacement of wood in cement-bonded particleboard (Soroushian et al. 2004). Rice straw-wood particle composite boards and rice straw-waste tire particle composite boards are successfully manufactured as insulation boards, using the method used in the wood-based panel industry (H.S. Yang et al. 2004). It was found that tensile and flexural properties of the agro-residue-filled composites showed that they could be used as an alternative to wood-fiber-filled composites (Panthapulakkal and Sain 2006).

Other main attractive applications for straw are bio-based products, such as wood-based materials, biodegradable plastics, and sorbents. Since the 1980s, depletion of the world's forests has steadily forced up the price of wood and wood-based materials (Sun and Sun 2002). In recent years, it has been difficult to obtain solid woods, and this causes problems for wood-based industry (Sun 2010b).

2.3.5 Research Problems and Challenges

The structure of wheat straw fiber is morphologically different and more complex than that of wood (Robson and Hague 1993) or bast fibers (hemp, kenaf). Straw fibers are relatively shorter and smaller, with reduced mechanical properties compared with wood fibers (Rexen 1975) (Grigoriou 2000). The bulk density of straw particles is one-third lower than typical wood particles (Grigoriou 2000). In general, the chemical composition of wheat straw is similar to that of wood, containing cellulose, hemicellulose, lignin, and a certain percentage of extractives. The major difference in chemical composition between the two materials is the high content of silica and wax in wheat straw, which are mainly located on the surface layer (Rowell 1992). Wheat straw also has lower cellulose and higher lignin and hemicellulose contents than typical softwood species (Markessini et al. 1997).

Limited commercial attempts have been made to manufacture wheat straw panels in Canada (Cooper and Balatinecz 1999). Urea formaldehyde (UF) adhesive is the most commonly used binder in wood composite manufacturing in many countries. More than 90% of particleboards are bonded with UF resin, which creates strong bonds (Dalen and Shorma 1996) (Luo and Yang 2010). Urea However, in the case of wheat straw, UF exhibits several problems in achieving the desired standards for the physical and mechanical properties of panels due to the high silica and wax content, as well as the high pH and acid buffering capacity of wheat straw (Sauter 1996) (Hague et al. 1998). The most important of the parameters listed above is the layer of wax on the wheat straw surface, which inhibits adhesion with the UF binder. Poor bonding of particles adversely affects all of the basic properties of the final product. Currently, there is little information on the properties of UF-bonded wheat straw particleboard panels manufactured using acetic anhydride and steam-treated raw materials (Bekhta et al. 2013). Moreover, resin systems like urea formaldehyde or phenol formaldehyde are in the process of being discontinued in Canada and other parts of the world because of the toxicity concerns related to formaldehyde. Therefore, new binder systems are required to replace these two well stablished binders in the composites industry.

As mentioned previously, the layer of wax and silica on the surface of the straw creates problems for achieving good bonding with adhesives (Schmidt et al. 2011). However, recent studies with straw have revealed that bonding quality can be improved by treating straw with different chemicals and enzymatic methods that enhance surface wettability and increase the surface free radical concentration (R. M. Rowell et al. 1997) (Loxton and Hague 1996) (Gomez-Bueso et al. 2000) (Karr and Sun 2000) (Han et al. 2001) (Schmidt et al. 2011) (Zhang et al. 2003).

The criteria for appropriateness of wheat straw for certain application relies on understanding its structure and how it interacts with the binders. The main criterion for justifying the wheat straw based composites in various fields of applications is its low cost and lightweight, in additional to the biological benefits. The adequate raw material availability facilitates their utilization as a replacement for more expensive wood and other fibers. Aside from the economic perspectives, the appropriateness of a fiber for composite purposes is driven by its attributes.

1. Mechanical Properties

When used as composite reinforcement, essentially natural fibers are expected to provide reinforcing "strength and stiffness" to final composite products. However, wheat straw has relatively low strength but acceptable (Reddy and Yang 2007) compared to wood and bast fibers. Therefore, the evaluation and improvement of straw for composite applications is a field that requires further research to enable a suitable technology for manufacturing straw pressboards. More specifically, the literature review has identified that the mechanical properties are highly dependent on the surface characteristics and the nature of interaction of straw and binders. Wheat straw as agro-residue has the potential to be utilized as reinforcement in pressboard composites if additional research is carried out.

2. Hydrophilic and Hydrophobic Nature of Straw

It is well known wheat straw lacks adhesion to major polymeric resins due to incompatibility (Shankar et al. 2014). Epidemic cuticular layer comprised of cutin embedded in wax layer. Hence the external surface of the straw has a hydrophobic characteristic. All the plant fibers have an affinity for water in their internal cellular structure. This strong affinity produces swelling of the fibers connected with the uptake of water, which facilitates dyeing in watery solutions, but also weaken the strength. The internal surface of the straw is hydrophilic. The moisture content of the fibers is dependent on the content of non-crystalline parts and the void content of the fibers. Overall, the

hydrophilic nature of natural fibers influences the mechanical properties. The equilibrium moisture content of some natural fibers is demonstrated in previous study (Rowell 2008).

The hydrophilic-hydrophobic nature of the straw poses a major problem for utilization as reinforcement in composites. The moisture content of the fibers is dependent on the content of non-crystalline parts and the void content of the fibers. Absorption of moisture causing swelling of the fibers has been a major drawback of natural fibers, which leads to a weak bond at the fiber/resin interface in the composites. Abdul Khalil et al. (Khalil et al. 2008) remarked that loss in fiber strength results in high impact loss, which is mainly due to the swelling of cell wall structures.

The literature review has elucidated that in order to improve the bonding between the straw and the resin binder a few strategies can be used: 1) removal of the water sorption into the reinforcing fibers before incorporating them in the composites; 2) reduction of void content by compressing; and 3) wetting and dispersion of resin binder on the surface of the straw. However, there is still a significant gap in the literature addressing the hydrophilic-hydrophobic nature of wheat straw and the relevance of this parameter in manufacturing pressboards. Although several surface treatments to modifying the conditions on the surface of fibers are reported in the literature, there is not specific study on wheat straw that correlates the type of treatment, its effect on binder compatibility and finally on the properties of the pressboard.

3. Thermal Degradation

The sensitivity of wheat straw to thermal heat decomposition constitutes another possible limitation for using natural fibers in composites (Faruk et al. 2012). The elevated temperatures are normally needed either to soften (thermoplastic) or to cure (thermosetting) the binder resins for manufacture of wheat straw composites. The thermal heat causes chemical dehydration of wheat straw followed by degradation. Natural fibers with cellulose and lignin are reported to have color changes at 180°C and significant weight losses (~70%) between 220°C and 300°C (Szcześniak et al. 2008). The cellulose insulation in transformers degrades with time at rates which depends on the temperature, moisture content, oxygen and acids in the insulation system (Sanghi 2003).

2.4 Nanocellulose and Nanocomposite

Nanocellulose can be extracted from the various starting source materials. Cellulose nanofibrils (CNF) are nano-scale fibrils with high aspect ratio, and their width varies from 50 to 500 nm (being

several micrometers in length) and are formed as a result of cellulose chain-stacking, induced by hydrogen bonds (Hoeng et al. 2016). These nanofibers which consist of both crystalline and amorphous domains, can be produced by liberating the fibrils from the integral microfiber bundles through vigorous mechanical fibrillation processes (Habibi et al. 2010) (Turbak et al. 1983). By far, many reviews have discussed their exceptional characteristics, such as biodegradability, excellent mechanical properties, high surface area, light weight, etc (Moon et al. 2011) (Lavoine et al. 2012) (Siró and Plackett 2010). So far, researchers have used CNF as reinforcing agents in different composites such as hybrid plastics, papers and thin packaging films. For instance, the use of CNF in the papermaking wet-end results in papers with higher strength (Mörseburg and Chinga-Carrasco 2009). CNF was used as binder in particleboard, fiberboard and laminates (Christensen et al. 1981) (Joseleau et al. 2012) (Reising et al. 2012); Nanocellulose was also employed as a binder for natural fibers (Tayeb et al. 2018).

Polymer nanocomposites have received great deal of interests among the scientific and industrial communities in recent years (Lee et al. 2005). Cellulose nanocomposites are manufactured using different processes, and these processes affect the composite properties, such as the dispersion, distribution and alignment of the reinforcing phase. Thus, the research and development of the manufacturing process of celluloses nanocomposites is an essential part of the development of cellulose nanocomposites. The processing of nanocomposites initially involved solvent casting of water-soluble or water-dispersive polymers, which were mixed with cellulose nanomaterials (Favier, Canova, et al. 1995) (Favier, Chanzy, et al. 1995) (Mathew and Dufresne 2002) (Oksman et al. 2016), because both nanofibers and nanocrystals are easily dispersed in water.

2.5 Polymeric Binder

The main role of a binder in pressboard composites is to connect the dispersed phase (fibers or particles) and to allow transfer of stress. High mechanical performance of the composite is expected through effective stress transfer in case of a strong fiber-polymer adhesion (Güven et al. 2016) (Faruk et al. 2012) (Mohanty et al. 2001). The mechanical performance of composites is compromised with a weaker interfacial strength, when delimitation and/or void formation occurs.

Generally, the interfacial adhesion within a composite material can be ascribed to mechanical interlocking and chemical bonding (Matthews, F. L. Rawlings 1994). Mechanical interlocking has less influence on the mechanical performance of composite compared to chemical bonding. Chemical

bonding occurs when there are chemical groups on the fiber surface and on the binder that can react to form bonds and as a consequence the resulting interfacial strength depends on the type and the amount of the bonds. Both covalent bonding and hydrogen boding at the interfacial region are prevalent in the thermoset-lignocellulosic composites. This is because lignocellulosic hydroxyl (–OH) groups could serve as reaction sites with various functional groups in the thermoset system (Yasin et al. 2010).

For the effective bonding to occur, fiber and binder must first be brought into intimate contact. Whether binder disperses on surface of binder is related to compatibility of the fiber-polymer complex, which are controlled by the surface energies of the materials and reflected and measured by wettability. Therefore wettability can be regarded as an essential precursor to bonding. Insufficient fiber wetting results in lack of bonding at interface, such as defects, voids and delamination, which act as stress concentrators and lead to mechanical failure (Chen et al. 2006). The fiber wettability has been approved to affect the toughness, tensile and flexural strength of composites (Wu and Dzenis 2006).

In production of wheat straw reinforced composites, a strong adhesion at the interface is required for an effective transfer of stress and load distribution throughout the interface so as to take advantage of the high modulus of the fiber (Mohanty et al. 2005). Appropriate polymeric binder selection is a key to a sufficient interaction in composite production for enhanced mechanical property and water resistance (Halvarsson 2010). Additionally, the composites' shape, surface appearance, environmental tolerance and overall durability are affected by binder, whereas the wheat straw reinforcement carries most of the structural loads, thus providing macroscopic stiffness and strength.

2.5.1 Types of Binder

Themoplastic Binders

Thermoplastics are characterized by their ability to soften and regain flow characteristics upon heating from solid state (Halvarsson et al. 2008). Upon heating, the relative weak intermolecular forces, such as Van der Waals and hydrogen bonds, holding molecules together are temporarily broken allowing molecular maneuverability. When thermoplastics are used in production of composite, the fibers are mixed in with the molten polymer, and the composite is then shaped into the desired form at high temperature (Thielemans and Wool 2004).

Wheat straw has been used for making composites with polypropylene (Amirpouyan Sardashti 2015) (Hornsby et al. 1997a) (Panthapulakkal and Sain 2006), polyethylene (Panthapulakkal and Sain 2007),

polyester (White and Ansell 1983), polyvinyl acetate, polyurethane (Borda et al. 2004), poly (3-hydroxybutyrate-co-3-hydroxyvalearate) (Avella et al. 2000) and Novolac resin (Patil et al. 2000).

Polyamide 6 is one of common engineering thermoplastics and has higher modulus and service temperature than commodity thermoplastics due to its intra-molecular hydrogen bonding. Polyamide 6 (see its structure in Figure 2.8) is capable of forming hydrogen bonding with cellulose fibers, which make better compatibility between them (Xu 2008). The SEM images of fracture surfaces indicated efficient bonding occurred in polyamide-wood fiber composite materials (McHenry and Stachurski 2003). However, due to its high processing temperature polyamide 6 has been restricted in natural fiber composites. Early studies on cellulose fiber reinforced polyamide 6 were generally discouraging. Severe thermal degradation occurred with cellulosic material when polyamide 6 was used, which led to poor reinforcing ability (Klason et al. 1984).

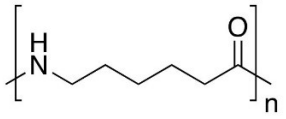

Figure 2.8 Chemical structure of polyamide 6

Techniques having been explored in processing polyamide 6 with natural fibers include treatments (alkaline treatment) on natural fibers (Santos et al. 2007) (Jacobson et al. 2001), low temperature (210°C) used in compounding (Dweiri and Azhari 2004) at 225–235°C (Santos et al. 2007), multiple heating zone extruders was used to reduce the fiber degradation by avoiding unnecessary heating (Jacobson et al. 2001). The use of compression molding can lower the chance of thermal and mechanical degradations at a cost of diminished mechanical properties (compounding effect and formation of voids). Plasticizers were used (Xu 2008) to facilitate the flow of polyamide. The addition of halide salts was conducted to reduce the melting point of polyamides (Zhang et al. 2009) (Misra et al. 2004) combinations of halide salts and plasticizers/lubricant agents were also investigated (Xu 2008) (Amintowlieh et al. 2012). The overall objective of those findings reported in the literature was to reduce processing temperature, reduce the extruder mechanical shear force or reduce the fiber residence time during processing in order to minimize thermal degradation while facilitating processing.

Thermoset Binders

Contrary to thermoplastics, the thermoset resins irreversibly form covalent bonds during curing to a highly cross-linked three-dimensional network structure. The thermosets therefore have stronger

binding ability and lower water absorption while offering higher thermal stability at low cost compared to thermoplastic binders (Godavarti 2005). These cross-linked structures are highly solvent resistant, tough, and creep resistant. The fiber loading can be as high as 80%, but the composite part is unable to be reshaped after polymerization (Thielemans and Wool 2004).

Epoxies, formaldehyde based resins, and polyester have been used as thermoset binders and are reportedly the most widely used resins for natural fiber reinforced polymer composites. Low cost, low cure temperatures, water or partly water solubility, resistance to microorganisms, excellent hardness, lack of color, and resistance to abrasion are some of the good quality properties. However, the formaldehyde resin has the ability to release formaldehyde even after the curing. The emission of formaldehyde from urea-formaldehyde or phenol-formaldehyde resins and end-products has been of major health concerns and been argued for several years (Baumann et al. 2000) (Sharp 2004) (Roffael et al. 2007) (Halvarsson 2010). The stringent regulation of formaldehyde-containing products and limited petrochemical resources have promoted the development of novel alternative binder resins with improved properties and environmental friendliness (Halvarsson 2010). Therefore, the use of these common thermoset resins as binders is not engaging.

Polyester Binder–Acrodur

Acrodur is a series of thermosetting polyester solutions commercially supplied by BASF. Acrodur are aqueous acrylic resins comprised of polycarboxylic acid and polyalcohol shown in Figure 2.9 and are free of phenyl and formaldehyde. The backbone of the polycarboxylic acid can be modified with a latex component to form dispersions. At temperature above 130°C, the polycarboxylic aid groups react with polyalcohol to form polyester or latex-modified polyester in case of the dispersion. Under this temperature the resin exhibits thermoplastic properties and confers the prepreg materials very good storage stability. After the curing process, the material has thermoset properties: it is hydrophobic, resistant, and tough to wear. Acrodur resins can help reduce or eliminate the formaldehyde that otherwise would be emitted into the air (Anderson et al. 2005).

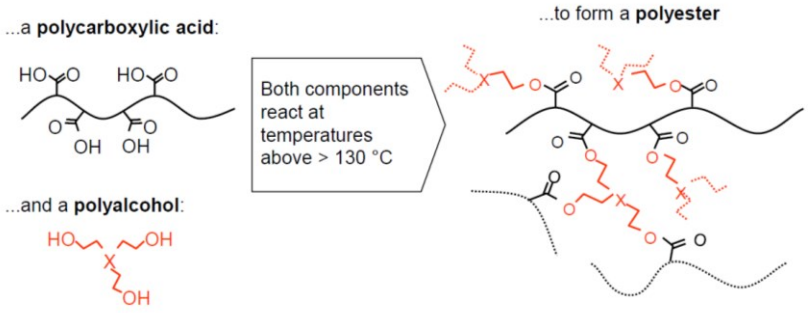

Figure 2.9 Chemical composition of Acrodur solution (Karbstein et al.)

In production of Acrodur composite, reinforcing fibers are impregnated in resin solution with low viscosity and after removal of water the pre-polymers react in situ into a crosslinked structure. A wide range of composite properties is adjustable by varying the ratio between the pre-polymers with a cross-linking agent and/or introducing latex component (Mohanty et al. 2005).

Acrodur is said to deliver a remarkable list of benefits for natural fiber composite production. It works for natural fibers, and it cures at low curing temperature and with short heating time. Acrodur resin has the ability to form hydrogen and covalent bonds with the hydroxyl groups present in cellulose through the formation of ester groups and the composite produced is more hydrophobic. When a good fiber–matrix adhesion is achieved, the path of wicking water molecules is tortuous due to better fiber–matrix integrity. The combination of thorough wet-out, with mechanical and chemical bonding (Liang et al. 2013), permits composites with very high fiber amounts and heat and water resistance. Acrodur also eliminates the hydrocarbon solvents and volatile organic compound (VOC) emissions that commonly devolve during crosslinking and subsequent part service life (Nordmann et al. 2010).

The main application areas of Acrodur so far are passenger and truck vehicle panels and components. For example, approximately 5–10 kg bast fibers can be used in a single vehicle. In the furniture industry Acrodur has also been used with non-woven mats of bast fibers for manufacturing chairs and tables (Karbstein et al.).

Acrodur has gained popularity in the automotive and furniture industries where it's currently being used in combination with natural fibers, including wood, kenaf, sisal, flax, jute, coir and hemp, ramie fiber, soy bean flour or the combination of some of these fibers (Khalfallah, Abbès, et al. 2014) for various reinforcement applications because of its excellent bonding properties (Sam-Brew 2017)

(BASF SE 2011) (Medina et al. 2008) (Akampumuza et al. 2017) (Chen et al. 2005) (Liang et al. 2013) (Ummartyotin and Sain 2014) (Reck and Turk 1999) (Sam-Brew 2017) (Islam and Miao 2013).

The literature review was unable to find any research investigating the use of Acrodur and wheat straw in pressboard composites.

The cure reaction of Acrodur occurs as a combination of chemical kinetics and diffusion. The curing reaction between the polyalcohol hydroxyl (–OH) groups and the polyacrylic carboxylic acid (–COOH) groups involves condensation step growth polymerization with acid anhydride as the intermediate. During the curing process at elevated temperature, no catalysts (initiators) or an accelerator is required. According to the literature (Gerst et al. 2009), when the temperature rises above 130°C the cure reaction starts. As the reaction takes place, the amount of crosslinking increases and finally the three-demensinal network forms. The H_2O as byproduct is produced.

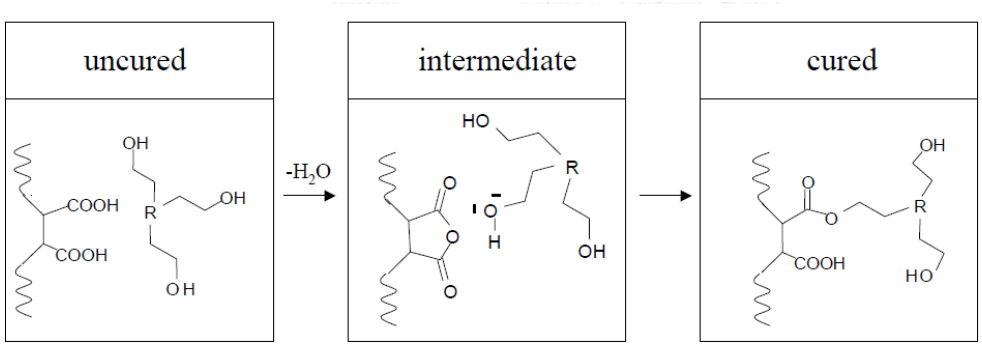

Figure 2.10 Cure reaction of Acrodur (Gerst et al. 2009)

The reaction mechanism is shown in Figure 2.10. At higher temperatures, the anhydride ring is formed followed by a nucleophilic attack of the hydroxyl group. This reaction is acid catalyzed, since the reaction velocity sharply decreases at pH values above 5. In general, no other additional catalysts are needed (Gerst et al. 2009).

The curing kinetics of Acrodur resins has not been studied extensively up to date. The curing behavior of Acrodur DS 3530 curing behavior was investigated by Khalfallas with DSC analysis for optimization of Acrodur-hemp composite production. The ultimate heat of reaction ($\Delta H_{Acrodur}$) was determined to be 140 ± 4 J/g. The glass transition temperature of cured Acrodur was observed at 65°C. The composite matrix curing yield was estimated to be 72% at 170°C for 3 min (Khalfallah, Abbès, et al. 2014). Sam-Brew investigated the thermal behavior of the Acrodur 950L and three impregnated

natural fibers (wood, hemp and flax) (Sam-Brew 2017). No obvious heat absorptions due to crosslinking reaction were observed over the whole heating range of 50°C to 200°C for neat Acrodur. However, exothermic peaks representing the curing reaction took place at higher temperatures between 140°C and 200°C for impregnated fibers. No significant effect of fiber type on curing peak temperatures was found in his study (Sam-Brew 2017).

The use of wheat straw in composites implies a restriction about the choice of the binders. Binder selection is limited by the temperature at which wheat straw degrades.

1) Wheat straw is thermally unstable above 200°C, although under some circumstances it is possible for wheat straw to be processed at higher temperature for a short period of time (Summerscales et al. 2010a).
2) Poor compatibility results in low adhesive strength and low loading level of wheat straw. The ineffective wetting of wheat straw with the water-based polyester resin leads to a poor interfacial adhesion, thus effective load distribution is not achieved and the mechanical properties of the composites will be impaired (Hodzic and Shanks 2013). One alternative for obtaining good compatibility between natural fibers and a resin is to use more polar thermoplastic resins, such as polyamide (Le Digabel et al. 2004), or a polar thermosetting polyester.

2.6 Manufacturing Pressboard

2.6.1 Compression Molding

Compression molding is a method of molding in which the molding material is first placed in an open mold cavity. The mold is closed with a top force or plug member, then pressure is applied to force the material into contact with all mold areas, while heat and pressure are maintained until the molding material has cured (solidified) or dispersed evenly. Compression molding is very popular in the manufacture of natural fiber composites because of high volume productivity, its high reproducibility and short cycle time. An additional advantage of compression molding is its ability to mold large parts with simple geometry (flat). Also, it is one of the lowest cost molding methods compared with other methods such as transfer molding and injection molding. Moreover it wastes relatively little material, giving it an advantage when working with expensive compounds. However, compression molding often provides poor product consistency and difficulty in controlling flashing.

As an example, the thermosets compression process uses mats made of natural fibers impregnated with resins. As shown in Figure 2.11, the fiber mats are sprayed with resin and compressed into their final contour in a hot mold. Due to the air-permeability the parts can be dried in a vacuum process (Jacobs 2006) or vacuum can be used to assist the molding. This process is transferable to a variety of natural fiber mats or thermoset systems.

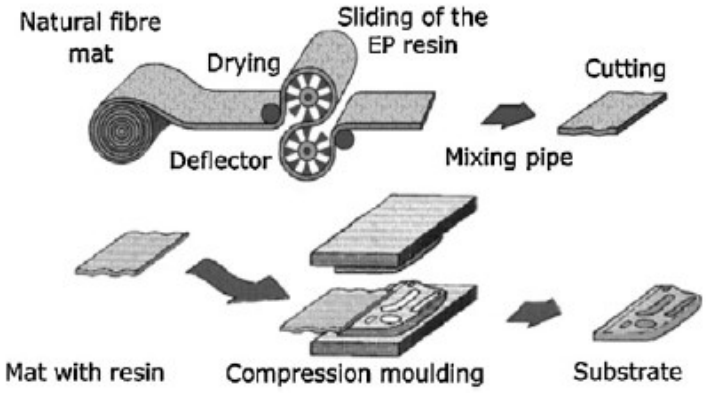

Figure 2.11 Thermoset mat compression molding process (Jacobs 2006)

2.6.2 Production of Pressboard

The first step is to conduct any pre-treatment on the natural fiber treated and then create a mat, which can be hand-laid, non-woven or woven depending on the type and size of fiber. The mat is then impregnated with polymer binder. Before the formed mats are transferred into the hot press, they go through a pre-pressing stage designed to reduce the thickness of the mat by removing as much air as possible necessary to reduce the operations cycle time and to facilitate the heat transfer at hotpress stage. Hot pressing of the pressboard can be conducted in a hydraulically operated press. The hot pressing cycle consists of a complex mix of operation parameters ranging from temperature, pressure, resident time, and aeration times (also known as venting or burping), combined with formulation parameters of the type of resin and the size of wheat straw being used.

The press temperatures employed are normally dependent either on softening temperature of thermoplastics or on the curing behavior for thermosets being used. The heat activates the transformation of resin while pressures compacts the materials. The hotpress cycle time is dependent on heat transfer to ensure the thermoplastics achieves its desired flow (after melting) or the thermosets completes curing. Normally a few minutes (2–15 minutes) for pressboards with thickness of about 3

mm are needed. This is referred to as the hotpressing period and is based on the resins curing kinetics or melting temperature. During the hotpressing period, decompression is conducted for a few seconds for a couple of times to de-gas pressurized vapors within the pressboard. This is essential to prevent delamination potentially caused by blows or blisters once the press opens and the internal gas pressure within the pressboard is higher than tis bond strength. The gas accumulating within the pressboard can be from residual moisture or produced as a by-products of resin curing.

2.7 Factors Influencing Pressboard Properties

The reinforcing fiber, polymer resin, and fiber matrix adhesion are influential factors having profound effects on composite properties, specifically including fiber type, resin type, the ratio between them. The fiber length (length distribution) and its geometry also play a decisive role in composites. Usually, most mechanical properties of a fiber can be enhanced by increasing the aspect ratio (Liu et al. 2007) and orientation could lead to anisotropy. It should be noted that application of intensive shear force processing during mixing could result in reduction of fiber length in the final composite. However the improved fiber dispersion may result in improved composite properties (R. M Rowell et al. 1997).

The limiting processing temperatures when using lignocellulosic materials with thermoplastics is important in determining processing techniques. High processing temperatures (200°C) that reduces melt viscosity and facilitates good mixing cannot be used (except for short periods) because high temperatures lead to thermal degradation of the natural fibers (R. M Rowell et al. 1997). Higher fiber content improves the impact strength. Unfortunately, increased fiber content increases the water uptake (Bledzki et al. 2008). Moreover, the composite's ductility can be affected.

The even dispersion and distribution of polymer binder in the natural fibers, especially for nanocellulose filler in small quantities (<5%), contributes to the quality of adhesion and imparts significant influence to properties of composites. A good stress transfer can be maximized by improving the interaction and adhesion between the two phases and also by maximizing the length of the fibers retained in the final composite (Bigg et al. 1988).

Fiber drying before processing is a relevant step. Zhang et al. (Zhang et al. 2014) and Davies and Bruce (Davies and Bruce 1998) among others showed that water absorption of composite reinforced with cellulose based fibers result in a reduction in mechanical strength and modulus, due to degradation of fiber matrix interface caused by moisture aborted (Khalfallah, Abbès, et al. 2014). However, the effect of moisture was controversial. It was reported by Masseteau et al. that adhesion quality between

fiber and matrix (epoxy) was better in humid compared to dry environments (Masseteau et al. 2014). The enhancing effect of moisture was attributed to increased energy of adhesion.

2.7.1 Parameter Determination of Compression Molding

An investigation on Acrodur composite was conducted by Islam and Miao (Islam and Miao 2013) to produce optimized flax fabric reinforced Acrodur biocomposites by varying the ratio between Acrodur solution and dispersion (3:1, 3:2, 1:1), relative humidity (0%, 40%, 60% and 80%), curing time and temperature (160°C for 20min, 180°C for 10min, and 200°C for 5min). The results of those authors indicated that the best mechanical properties were obtained with processing conditions of (1) Acrodur solution to dispersion ratio of 3:1, (2) curing temperature of 160°C and (3) curing time of 20 min, (4) relative humidity of 40%. Bubbles were observed on the plate's surface when press time was reduced (Islam and Miao 2013). The needle-punched mats of hemp and kenaf were impregnated with Acrodur (20–25%) and compression molded at 200°C, under different pressures (Medina et al. 2008).

Compression molding on Acrodur was conducted with attached vacuum by Medina (Medina et al. 2008). The benefits associated were that equipped with a vacuum chamber the press permits to achieve very short cycle times, due to the fact that the residual moisture and the condensation products of the polymer's chemical reaction were removed very fast by evacuation. Otherwise, trapped air or moisture would lead to bubbly surface or delaminated structure and seriously deteriorate the composite quality. The pressboards manufactured under vacuum conditions showed optically a better surface and a more homogenous surface, where the fibers were better covered with the matrix. The odor during the compression were noticeably reduced due to the direct evacuation of vapors or volatiles. (Medina et al. 2008).

The hot-pressing time had a significant effect on the flexural properties and density of both the kenaf fiber/soy flour composites and kenaf fiber/Acrodur resin composites. As the hot-pressing time increased (from 10 to 20 minutes), the flexural properties and density decreased for the other two composites with Acrodur resin. With 28 wt % Acrodur resin (on the basis of 100% solid content) as a binder and with the biocomposites hot-pressed for 10 min, the swelling thickness and water absorption of the composites were reduced by 55 and 64%, and the flexural strength and modulus were improved by 72 and 188%, respectively (Liang et al. 2013).

The moisture content of the mat was less than 15 wt % after impregnation. The mat was hot-pressed under a pressure of 5 MPa and at a temperature of 150°C. Three pressing times were used: 10, 15, and

20 min. However the flexural strength and modulus and density of the kenaf fiber/soy flour composites decreased as the hot-pressing time increased. This might have been due to irreversible acid-catalyzed depolymerization and the reversible crosslinking of cellulose molecules (Yang and Qian 2001) (Kang et al. 1998).

2.8 Summary of Research Gaps and Challenges

The research on wheat straw and its composites is still in the early stages and the utilization of wheat straw has been restricted mostly in high volume, relatively low-tech and non- or semi-load bearing applications. For example, the use of wheat straw have been restricted due to its inferior mechanical property, especially compared to the pressboard made with wood fiber or bast fibers.

The development of the straw pressboards with improved properties is still facing challenges. Wheat straw as reinforcement presents some features that interfere the final properties of composite pressboard. Wheat straw cab be an appropriate alternative reinforcement for polymer composites but it does expose some deficiencies emerging from its inherent nature. In addition, there are also some less explored aspects and gaps in the literature, such as the electric performance, thermal conductivity and acoustic insulation properties of wheat straw-based composites. The technology for effective manufacturing of wheat straw-binder pressboard is not well known yet. This lack of knowledge and understanding precludes the manufacturing of wheat straw based pressboards and the development of wheat straw pressboards with acceptable final properties.

The primary research challenges in this literature review include:

a) Poor understanding of effects of treatments on wettability of hydrophilic binders, which controls interfacial affinity between wheat straw and synthetic binders;

b) The lack of information about the cure reaction for Acrodur, specifically the correlation of time and temperature with the curing conversion;

c) The lack of knowledge about the adhesion strength of Acrodur and wheat straw; and

d) Poor understanding about the effects of the factors affecting the manufacturing process, such as wheat straw size, treatment of wheat straw, formulation, incorporation of CNF, compression temperature, time and pressure.

Chapter 3
Surface Treatment and Effect Evaluation

3.1 Introduction

The poor interfacial adhesion caused by the incompatibility between wheat straw and polymers has been one of the impediments that deter the widespread utilization of wheat straw in polymer composites, especially when water based resins are applied (John and van Reen 1995) (Sauter 1996). For example, the poor properties of urea formaldehyde-bonded straw boards were related to the interface characteristics of binder and straw (Liu et al. 2003). The treatments on wheat straw are required to improve the compatibility between binder and straw by removing the hydrophobic wax-cutin layer contributing significantly to the ineffective wetting of binder on the fiber surface.

Interface and Compatibility

Wheat straw is comprised mostly of stems, leaves and a small amount of others. The stem is surrounded by the lower part of leaf called sheath as shown in Figure 3.1. The characteristics of four surfaces vary due to the different chemical composition and morphology. The exterior of wheat straw exposes to the surroundings and exerts protection functions, on which lies a layer of hard shell called epidermis, comprised of the cuticle, a thin waterproof layer comprised of cutin embedded in waxes. The waxes are collective name of a complex mixture of nonpolar lipids (Hansen et al. 2013). Wheat straw is also rich in ash, most of which is presented on the surface of stems and leaves. Silica (SiO_2) constitutes 65–70% of the total ash content (Xu 2010).

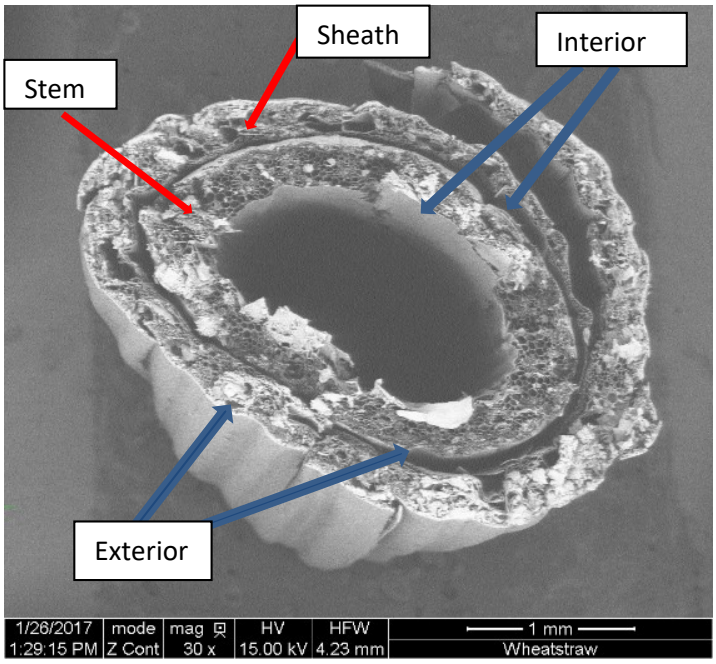

Figure 3.1 SEM image (taken by author) showing wheat stem surrounded by a sheath

Four surfaces behave differently at the fiber-binder interfacial adhesion, due to the different chemical and structural features as summarized in Table 3.1. It is evident that the relative high levels of silica and wax are mainly located on the surface of wheat straw (Harper and Lynch 1981) (Mo et al. 2005), except stem interior.

Table 3.1 Surface features of Stem and sheath (Atik and Ates 2012) (Liu et al. 2005) (Singh et al. 2011)

Anatomic part	Surface	Chemical composition	Structural feature	Comments
Stem	Exterior	Ash, wax	a waxy silica layer, dense packed	significantly different
	Interior	Cellulose	a very porous structure	
Sheath	Exterior	Ash, wax	dense waxy epidermis	almost the same
	Interior	Ash, wax	dense waxy epidermis	

In wheat straw based composites, the surface properties of reinforcement exert a significant influence on the interfacial adhesion between the fiber and binder and interferes with the moisture absorption, which ultimately dictates the structure and properties of the composites (Hansen et al. 2013). Due to the presence of impermeable wax-cutin layer acting as a barrier to bonding (Markessini et al. 1997)

(Han et al. 1998), the framework of cellulose and hemicellulose becomes inaccessible for polymer binder, especially for aqueous binder solutions or dispersions. The high silica content of wheat straw is also considered a primary limiting factor for its electrical use in addition to the physically inhibiting effect. It was reported that this layer gave rise to problems in achieving the desired standards for the physical and mechanical properties of composites (Yahya et al. 2017). For example, Sauter and Hague reported the layer of wax on the wheat straw surface inhibited adhesion with the UF binder (Sauter 1996) (Hague et al. 1998).

Treatment and Wettability

Treatments were reported to alter hydration nature and roughness of the fiber surface and increasing the surface free radical concentration (Han and Rowell 1997) (Loxton and Hague 1996) (Singh et al. 2011). Size-reduction such as milling is considered as physical treatment and contributes somewhat to removing undesired components by screening out generated cell fragments, dust, and fines that are rich in silica (White and Ansell 1983) (Jones and Milne 1963) (Inglesby et al. 2005).

Alkaline treatment or mercerization is one of the mostly used chemical methods for modifying natural fibers and has been proved as an effective tool for improvement of interfacial adhesion and mechanical properties in composite production (Islam et al. 2009) (Franco and Valadez-González 2005). Alkaline treatment was reported to not only remove noncellulosics from natural fibers, including a certain amount of simple hydrocarbons (cutin and waxes) and SiO_2, but also partially dissolves lignin and/or hemicellulose. The improved interfacial bonding and composite mechanical properties were illustrated in previous studies (Herrera-Franco and Valadez-Gonzalez 2005) (Valadez-Gonzalez et al. 1999) (Islam and Pickering 2007). Disadvantages associated with alkaline treatment are destructive fiber quality caused by harshness of alkaline treatment (Yahya et al. 2017), and the water and energy consumption and pollution of toxic wastes.

Hot-water treatment is capable to remove the extractable fraction from cellulosic fibers (Mustajoki et al. 2010), and its removal efficiency iss a function of treating time (Zhang et al. 2004). The water-soluble substances from wheat straw mainly include lipophilic extractives such as free fatty acids, waxes, and others (Sun et al. 2003). It was also reported that minor amounts of low molecular weight hemicelluloses and lignin were easily dissolved in hot water (Sun 2010c) (Sun 2010a). Wheat straw was reported to be treated by hot-water in previous studies (Ullah et al. 2018) (Bekhta et al. 2013). In comparison to alkaline treatment, hot-water treatment is considered a less harsh and less expensive

approach for modification of natural fibers, because less degradation of fiber is created due to its milder condition under which hot-water treatment is performed.

Thomas Young Equation in Equation 3.1 defines contact angle as an angle θ formed (shown in Figure 3.2) when equilibrium of a drop resting on a plane solid surface under the action of three surface tensions:

γ_{LV} at the interface of the liquid and vapor phases,

γ_{SL} at the interface of the solid and the liquid, and

γ_{SV} at the interface of the solid and vapor.

Small contact angles ($\theta \ll 90°$) correspond to high wettability, while large contact angles ($\theta \gg 90°$) correspond to low wettability. The contact angle is a useful inverse measure of spreadability or wettability. The contact angle of wheat straw surfaces can be measured to quantitatively reflect the differences in surface chemistry and morphology (Oliveira et al. 2010) induced by the treatment. The measured contact angle is called the "apparent" contact angle used to describe the overall effects of surface morphology and surface chemistry on wettability.

$$\gamma_{SV} - \gamma_{SL} = \gamma_{LV} \cos\theta \qquad 3.1$$

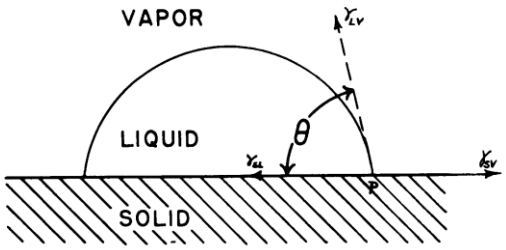

Figure 3.2 Contact angles formed by sessile liquid drops on a solid surface (Zisman 2009)

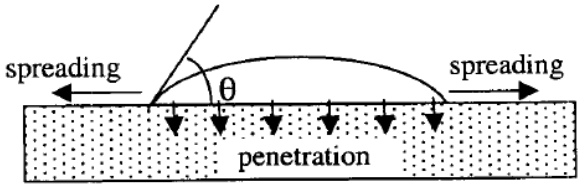

Figure 3.3 Adhesive wetting on a porous material surface (Shi and Gardner 2001)

When a liquid drop is placed on a porous surface, in addition to formation of contact angle, however, the liquid also spreads over a solid surface and penetrates into porous solid substrate as shown in Figure 3.3. The adhesive spreading and penetrating are also important indices for evaluating natural fiber based material adhesion. In 2001, Shi and Gardner developed a wetting model to describe the dynamic contact angle process on wood surface. A parameter (*K*) was introduced in this model to quantify the liquid penetration and spreading during the liquid wetting process (Shi and Gardner 2001). The final expression of the wetting model is:

$$\theta = \frac{\theta_i \cdot \theta_e}{\theta_i + (\theta_e - \theta_i)\, exp\left[K\left(\frac{\theta_e}{\theta_e - \theta_i}\right)t\right]} \qquad 3.2$$

in which, θ_i, represents the initial contact angle, θ_e, represents equilibrium contact angle. *K* is then a constant referred to the intrinsic relative contact angle decrease rate.

Due to the porous and rough features of naturally occurred wheat straw surface similar to wood, the liquid spreads and penetrates at the same time, which results in the fact that the contact angle changes as a function of time. When the model developed by Shi and Gardner is applied on wheat straw, the physical meaning of the *K-value* represents how fast the liquid spreads and penetrates into the porous structure of wheat straw (Liu et al. 2003). Therefore, in addition to simple comparison of contact angles, which is unable to fully describe the behavior of liquid on porous surface, the spreading and penetrating are also considered as indices for evaluating wetting process. The measurement of contact angle and its rate of change with time can give an insight into the wetting process and wettability and is suitable to evaluate the effect of surface treatments.

Instead of only examination of the instantaneous or equilibrium contact angles (Herczeg 1965) (Chen 1970), researchers measured the contact angle change as a function of time in liquid wetting studies (Maldas and Kamdem 1998) (Scheikl and Dunky 1998). Dynamic adhesive wettability of wood was studied by Shi and Gardner (Shi and Gardner 2001). The surface properties including wettability were reported by Gardner (Shi and Gardner 2001) on wood and by Liu (Liu et al. 2003) on wheat straw. In Liu's study, the wettability of what straw treated by a 0.6% NaOH solution was investigated using urea-formaldehyde (UF), phenol-formaldehyde (PF), and polymeric diphenylmethane diisocyanate (PMDI) resins (Liu et al. 2003). However, Liu did not separate the stem and sheath, neither did he investigate the wettability using water-based Acrodur.

Structural variations can extensively impact the mechanical properties of the fiber and thereby the mechanical properties of the composite (Valadez-Gonzalez et al. 1999). The morphology of a surface, in addition to chemistry, plays a vital role in interfacial adhesion not only in affecting the wetting process of binder but also in forming mechanical interlocking build up on the uneven fiber surface. The structure feature of wheat straw was observed by Liu using SEM (Liu et al. 2003), the was cuticle composed mostly of cutin and waxes and silica cells were observed on epidermis of wheat straw while in the interior surface were parenchyma cells observed. The parenchyma cells are distributed throughout the basic parenchyma tissues, which are thinner, deformed, and fragile. The shape and dimension of the parenchyma cell vary with straw species (Wu 1991).

Thermal Stability and Kinetics

The thermal degradation of lignin, a complex three-dimensional polymer has been reported to occur over a wider range, from as low as 180°C to 900°C. The decomposition temperature range of chemical components of natural fibers are advised in Table 3.2. Investigating the thermal properties of wheat straw is important in evaluating its potential use in the processing of composites at elevated temperatures above 200°C. The knowledge of the thermal degradation of the natural fibers and the determination of the temperature at which the largest loss of mass is revealed, are helpful in determining the processing parameters during the production processes (Masłowski et al. 2018).

Table 3.2 Decomposition temperature range of chemical components of natural fibers

Chemical component	Degradation temperature°C *	Degradation temperature°C **
Cellulose	315–400	250–440
Hemicellulose	220–315	150–360
Lignin	160 to 900	180–900, 300–900

*(H. Yang et al. 2007)

**(Lee and Fasina 2008) (Carrier et al. 2011) (Naik et al. 2010) (Yang et al. 2006) (García et al. 2013)

The degree of conversion (denoted as α) is the extent of the thermal degradation reaction of wheat straw fiber and it is defined as the change in the amount of reactant (weight of wheat straw fiber) as a function of time according to Equation 3.3 below.

$$\alpha = \frac{\Delta m_{total} - \Delta m_{residual}}{\Delta m_{total}} \qquad 3.3$$

where Δm_{total} is total mass loss within the range of interest, $\Delta m_{residual}$ is the residual mass loss obtained from TGA analysis or other methods.

Flynn, Wall, and Ozawa have developed a method to determine the activation energy as a kinetic parameter of the thermal degradation of a material (Ozawa 1986). Equation 3.4 below shows the common activation energy calculation method known as Ozawa-Flynn-Wall (OFW) method.

$$\log \beta \approx 0.457 \left(\frac{-E_a}{RT}\right) + \log\left(\frac{AE_a}{R}\right) - \log f(\alpha) - 2.315 \qquad 3.4$$

Taking a plot of log β versus -1/RT at a constant conversion (multiple βs) yields a line with a slope of 0.4567Ea, thus the activation energy can be determined for any conversion.

3.2 Research Objectives and Approach

The effects of hot-water and NaOH treatments were investigated in terms of wettability, surface morphology as well as thermal stability. More specifically, the contact angle measurement, volume changing rated determination, the morphology observation and TGA analysis were utilized to evaluate the performance of the treatments. In addition, the evaluation of binder absorption is very important in identifying the locations where the binder is distributed most. By knowing the location of binder will help to determine how much binder is needed and the mechanism of binder reinforcement of straw or interface.

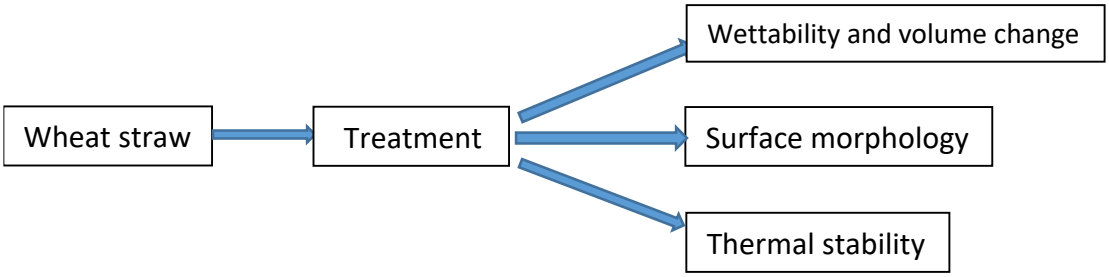

Figure 3.4 Strategy of treatment on wheat straw and the effect evaluation

The research approach for treatment on wheat straw and the effect evaluation is shown in Figure 3.4. Firstly, wheat straw undergoes the three treatments; secondly, the wettability is evaluated by applying model and quantitatively obtaining parameter *K* using a contact angle measuring apparatus; next, the structural features of the wheat straw surface are observed before and after treatments using a scanning

electron microscope (SEM); and, finally, the thermal degradation temperatures and activation energy of wheat straw before and after treatment are evaluated using TGA.

3.3 Materials and Methods

3.3.1 Materials

The wheat straw used in this chapter was collected from one of 2018 freshly harvested wheat straw bale obtained from an AC Mountain, soft white winter variety wheat, cultivated in Woodrill farms in Ontario, Canada and was supplied by Omtec Inc.. The wheat straw samples were randomly selected from a bag of wheat straw raw material as described above. After the leave blades and the nodes were cut off, the internodes (stem and leave sheath) of around 10–15cm were cut into three (3) equal-length pieces, according to the method shown in Figure 3.5, to generate 3 specimens near to each other, to eliminate the effects of the sources other than treatments. The resultant pieces are shown in Figure 3.6 (a), which were subjected to three treatments. The assumption made here is that the three pieces of wheat straw from the same sample have the very similar chemical composition and surface structure and are considered as "the same surface".

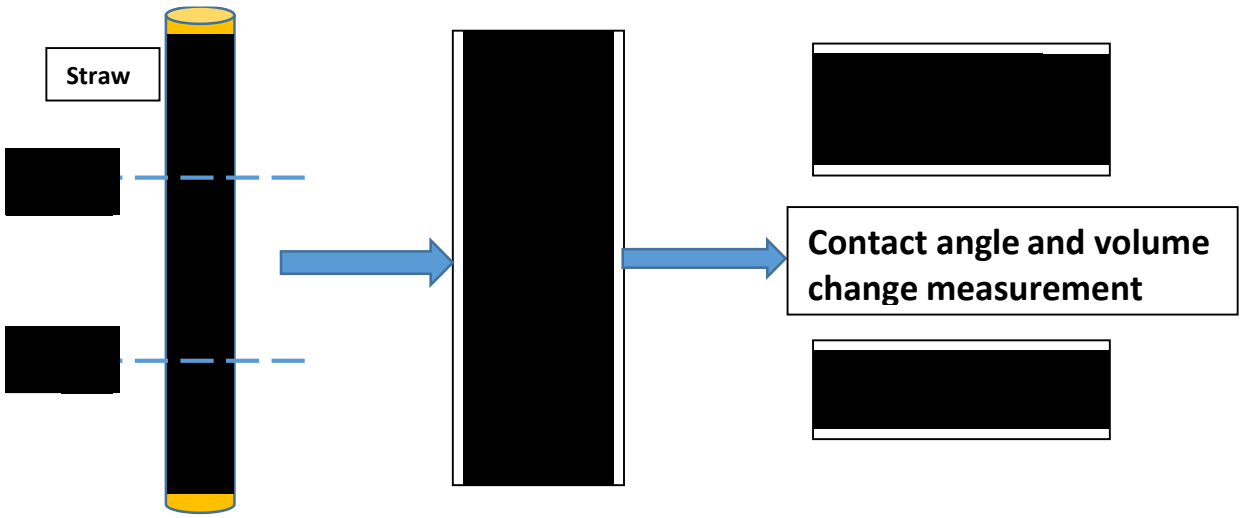

Figure 3.5 Methodology of sample preparation for treatment and contact angle measurement

Sodium hydroxide used was from Sigma-Aldrich company (ACS reagent, >=97.0%, pellets). DI water is de-ionized water prepared at University of Waterloo.

Two testing media for contact angle measurement, 1:1 diluted Acrodur DS3530 solution and de-ionized water, were evaluated in the wetting experiment. The Acrodur DS3530 was obtained from BASF with high wet-out of natural fibers. (Stewart 2010)

The de-ionized water was prepared at University of Waterloo facility.

3.3.2 Treatments

Prepared wheat stem and sheath samples were soaked in 3 wt. % NaOH aqueous solution at straw/solution mass ratio of 1 : 2 at room temperature for 24 hours as shown in Figure 3.6 (b). Next the treated samples were subsequently washed with running tap water followed by distilled water until no alkali was present in the wash water.

Hot water treatment was conducted by boiling wheat straw samples, including both stem and sheath, in deionized (DI) water at temperature of 100°C for 2 hours as shown in Figure 3.6 (c).

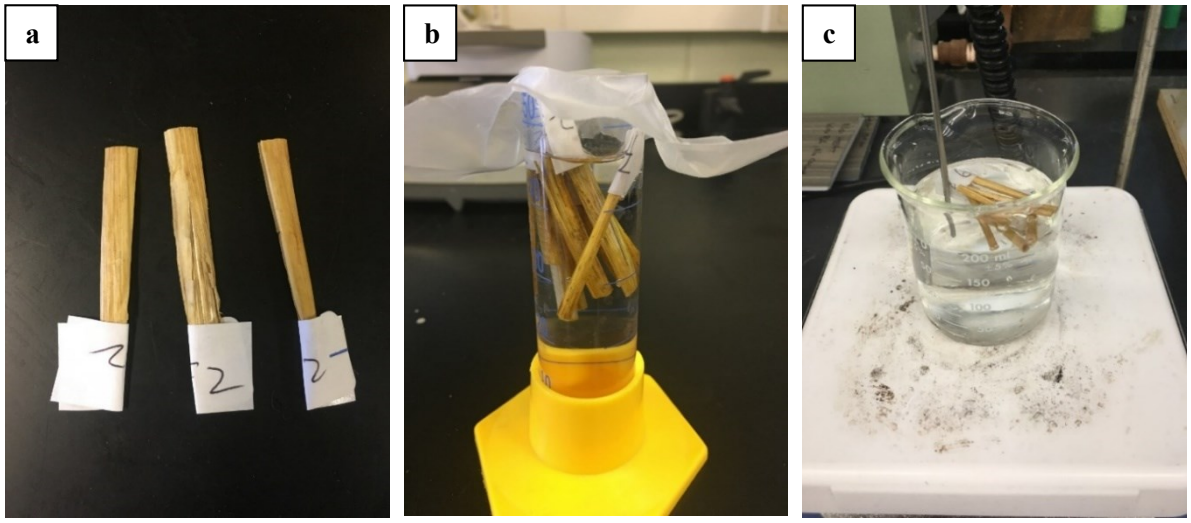

Figure 3.6 Wheat straw samples before treatment (a) and during NaOH (b) and hot-water (c) treatment

3.3.3 Measurements

Wheat straw samples (both sheath and stem) were cut longitudinally with a knife and spread carefully to expose both exterior and interior. Then the spread specimens were mounted onto clean glass slides using double-sided tape shown in Figure 3.7 as the examples. The samples were exposed at room temperature allowing absorbed moisture to evaporate until the water content equilibrates.

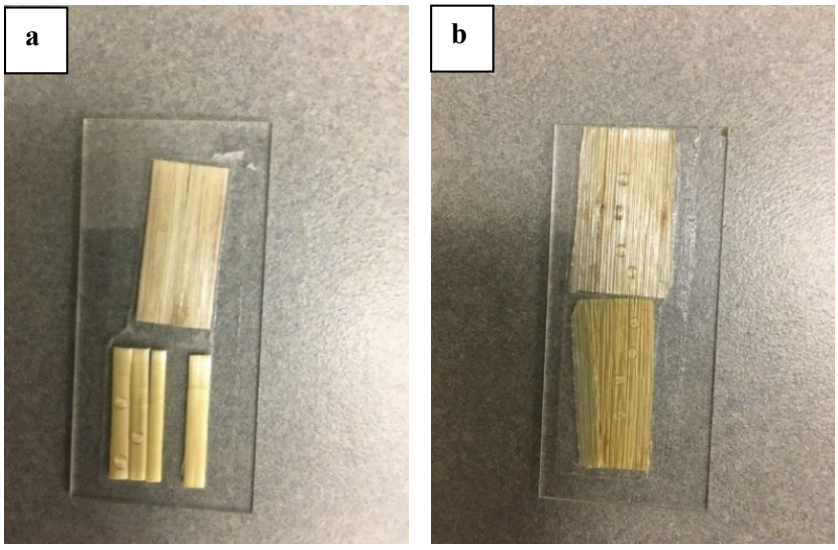

Figure 3.7 Specimens for contact angle measurement: interior and exterior of water treated stem (a) and sheath (b)

Two anatomic parts of wheat straw, stem and sheath, before and after the above mentioned treatments were examined. The contact angle and volume change were measured on the both exterior and interior of stem and sheath.

The contact angles were determined by the sessile drop method with VCA Optima (VCA-2500XE video contact angle system). A custom-made moisture chamber was used to keep sample inside for wetting experiment. The purpose was to eliminate the effect of moisture evaluation. The measurement was conducted at room temperature. A drop of liquid of around 2 μL was deposited on the specimens' surface with a micrometric syringe. A sequence of images was recorded with a mounted video camera at the rate of image per 3 seconds starting immediately after the moment of drop deposition, as the drop shape changed as time elapsed.

Scanning electron microscopy (SEM) was used to observe the microstructure and the surface morphology of Exterior and interior surfaces of wheat straw samples before and after treatments. The instrument used was a Quanta 250 FEG Scanning Electron Microscope. The samples were coated with gold to provide about 200 A˚ gold layer thickness using a vacuum sputter coater.

The thermogravimetric analysis (TGA) of the wheat straw was conducted using a TA Instruments Q500 TGA under non-isothermal conditions. The test was performed on wheat straw samples before and after the treatments under either air or nitrogen atmosphere. The samples weight is monitored as a

function of the temperature increased from 35 to 800°C using a heating rate of 10°C/min. The Ozawa-Flynn-Wall method uses the multiple heating rates. The different heating rates used were 5, 10, 25, 40, and 50°C/min and the temperature range covered in these experiments was from 35 to 650°C.

3.4 Results and Discussions

3.4.1 Wettability and Binder Absorption

The effects of three treatments, two surfaces of two wheat anatomic parts on the wettability of two testing media were investigated by comparing the initial contact angles and *K-value*s representing the rate of contact angle change due to spreading and penetration. The three treatments were non-treatment, alkaline treatment and hot-water treatment. Two wheat anatomic parts were wheat stem and sheath. Two surfaces were exterior and interior. Two testing media were DI water and diluted Acrodur DS3530 solution.

Table 3.3 24 combinations of two anatomic part, two surfaces, two testing media and three treatments

Treatment	Straw part	Surface	Testing medium
Non-treatment	Stem	Exterior	DI water
			Acrodur DS3530
		Interior	DI water
			Acrodur DS3530
	Sheath	Exterior	DI water
			Acrodur DS3530
		Interior	DI water
			Acrodur DS3530
Alkaline Treatment	Stem	Exterior	DI water
			Acrodur DS3530
		Interior	DI water
			Acrodur DS3530
	Sheath	Exterior	DI water
			Acrodur DS3530
		Interior	DI water
			Acrodur DS3530
Hot-water treatment	Stem	Exterior	DI water
			Acrodur DS3530
		Interior	DI water
			Acrodur DS3530
	Sheath	Exterior	DI water
			Acrodur DS3530
		Interior	DI water
			Acrodur DS3530

The wetting experiments were conducted on the contact angle change as a function of time for two anatomic parts, two surfaces, two testing media and three treatments. So 24 combinations of these factors were tested as shown in Table 3.3. 6–8 specimens for each sample were tested, and 2–5 locations for each specimen were measure depending on the size of the surface area. It normally took 1–10 min for a measurement depending on how fast liquid drop shape changed.

The recorded images were processed and analyzed using VCA Optima. The angles were determined by utilizing the software. The representative images are shown in Figure 8.1 in Appendix A, which shows the same trend of contact angle decreasing as a function of time. As observed, the contact angle starting at 0 second was 98.00°, after 6 minutes, dropped to 87.60°. The information obtained through software processing is representatively shown in Table 3.4. It is seen from this table that the left and right contact angles of each drop shape were obtained every 3 seconds through image analysis changing as a function of time, as well as the width, height and volume of droplet, and contact area with the surface.

Table 3.4 Typical date sheet (of first 27 sec) for wetting experiment processed with VCA optima; Substrate: untreated stem exterior; testing medium: Acrodur 3530

Capture_time	Left_angle	Right_angle	Width	Height	Area	Volume
second	degree	degree	mm	mm	mm^2	µL
0	98.0	96.5	1.798	0.982	2.54	1.773
3	94.0	94.6	1.827	0.975	2.621	1.766
6	94.7	95.1	1.834	0.967	2.641	1.775
9	94.9	94.9	1.834	0.967	2.641	1.775
12	94.9	94.0	1.841	0.956	2.661	1.76
15	94.8	94.9	1.841	0.943	2.661	1.74
18	93.8	92.6	1.862	0.934	2.723	1.738
21	92.1	91.1	1.862	0.926	2.723	1.699
24	93.1	92.4	1.862	0.936	2.723	1.735
27	93.1	91.8	1.862	0.943	2.723	1.743

The measured contact angles in the graph of Figure 3.8 (a and b) also indicated that the contact angle were changing as a function of treatment time. It is seen from Figure 3.8 (c) that the width of contact between the sessile drop and the solid surface increased first and remained as time elapses, and this increase is due to liquid spreading. It is also seen from Figure 3.8 (d) that the drop volume decreases as a function of time. The volume decrease is due to primarily liquid penetration into the porous structure

of the wheat straw surface, which confirms that the contact angle changing as a function of time was caused by both liquid spreading and penetration into the substrate. This observation is in agreement with that of Liu (Liu et al. 2003).

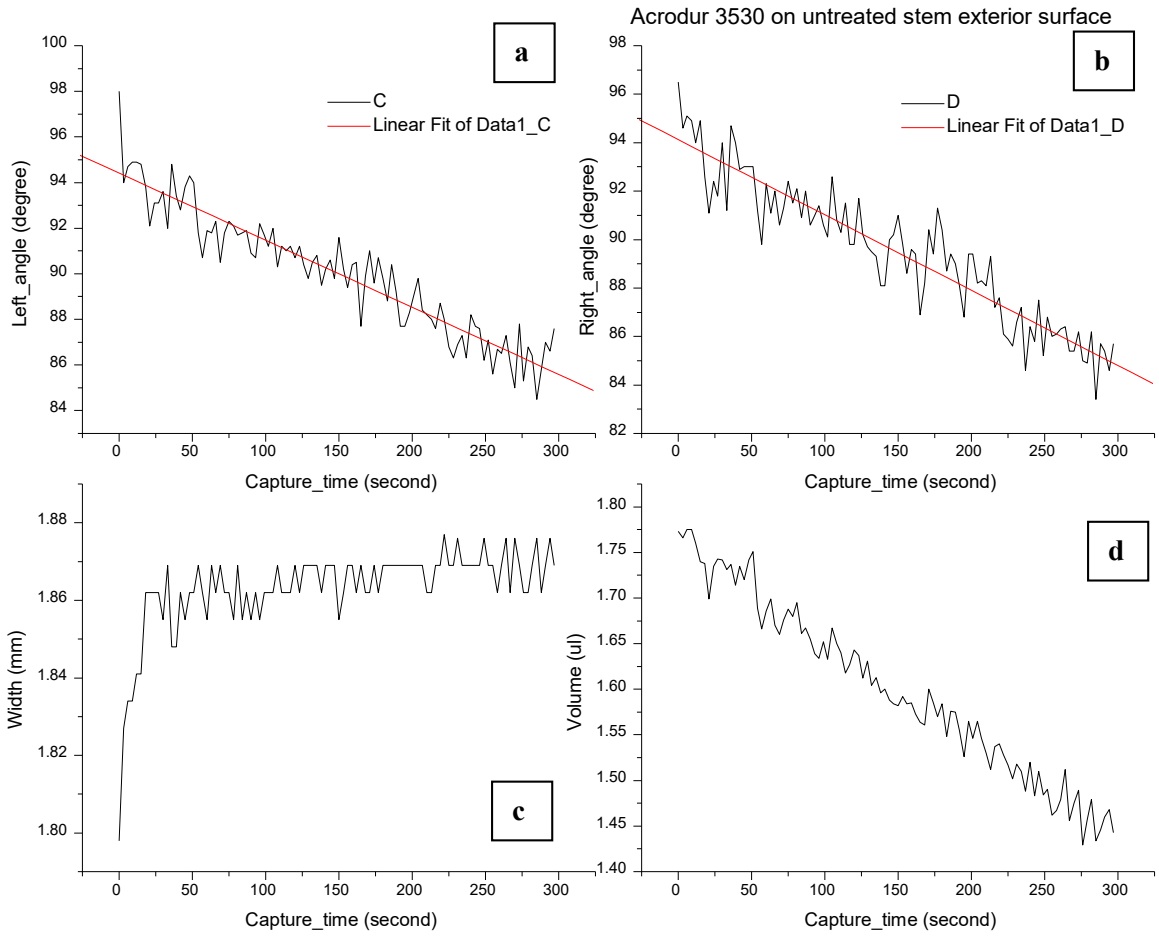

Figure 3.8 Left and right contact angles (a and b), as well as width (c) and volume (d) of droplet as a function of time; Substrate: untreated stem exterior; testing medium: Acrodur 3530

It should be note that a significant amount of data scatter was found in the experimental results. The great variations were attributed to the presence of naturally occurring random fiber flaws and the lack of uniformity in the surface characteristics along and across each specimen, as well as operator errors in determination of baseline and manual fit of droplet boundary using software. Therefore, to eliminate the bias of variation induced by surface features of wheat straw, the apparent initial contact angle was

introduced and the apparent initial contact angle of a specific liquid-solid pair was calculated as such. The data points of first 27 seconds were averaged to obtain the initial contact angle for left and right sides. Then the right and left contact angles were averaged for each drop as shown in Figure 3.9. This initial contact angles were obtained by averaging of initial contact angles of all the 5–8 specimens from the same surface-liquid system.

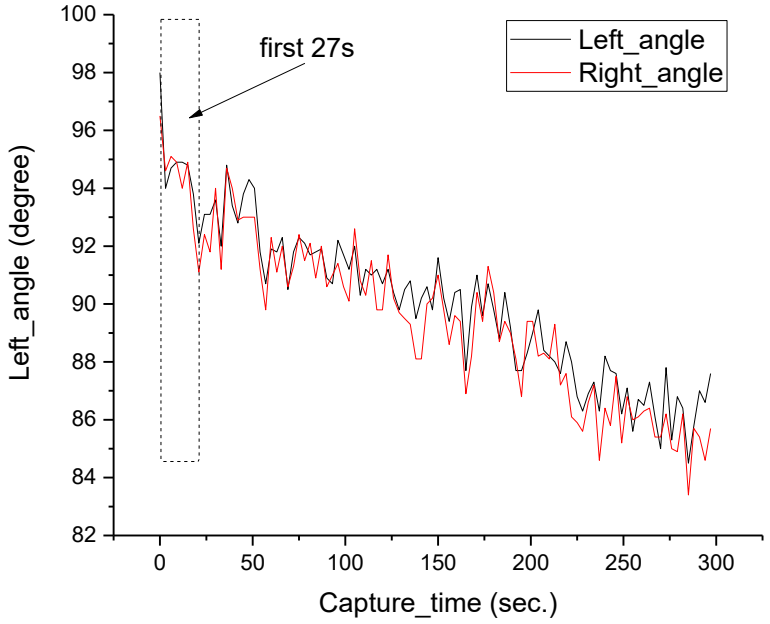

Figure 3.9 Determination of initial contact angle

Substrate: untreated stem ex; Test medium: Acrodur 3530

The wetting model described in Equation 3.2 was applied to these experimental data. The Marquardt-Levenberg algorithm was used to obtain the penetration/spreading constant (*K-value*) that provides the best fit between the equation and the data (Marquardt 1963). The *K-value* of wetting process for each combination of liquid-solid was calculated. The averaged contact angle data of each solid-liquid system was used to plot the relationship of contact angle versus time and the wetting model fit.

As observed from Figure 3.8 (d), the volume of the liquid droplet also changed as a function time. This was mainly attributed to the penetration of liquid into the porous structure of wheat straw. The

volume changing rate in unit of μL/s was obtained by establishing a trendline of the data points of first 27 seconds as shown in Figure 3.10.

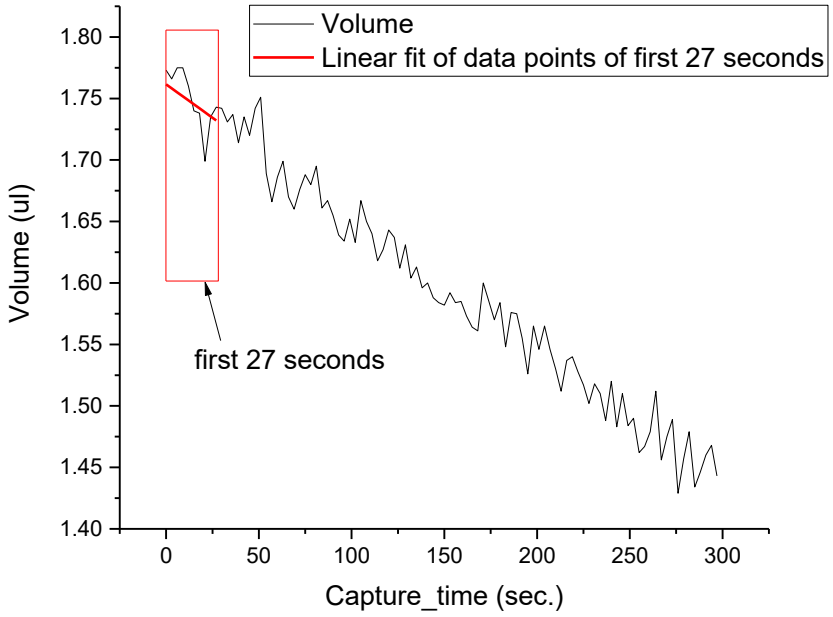

Figure 3.10 Determination of volume change as a function of time

Substrate: untreated stem ex; Test medium: Acrodur 3530

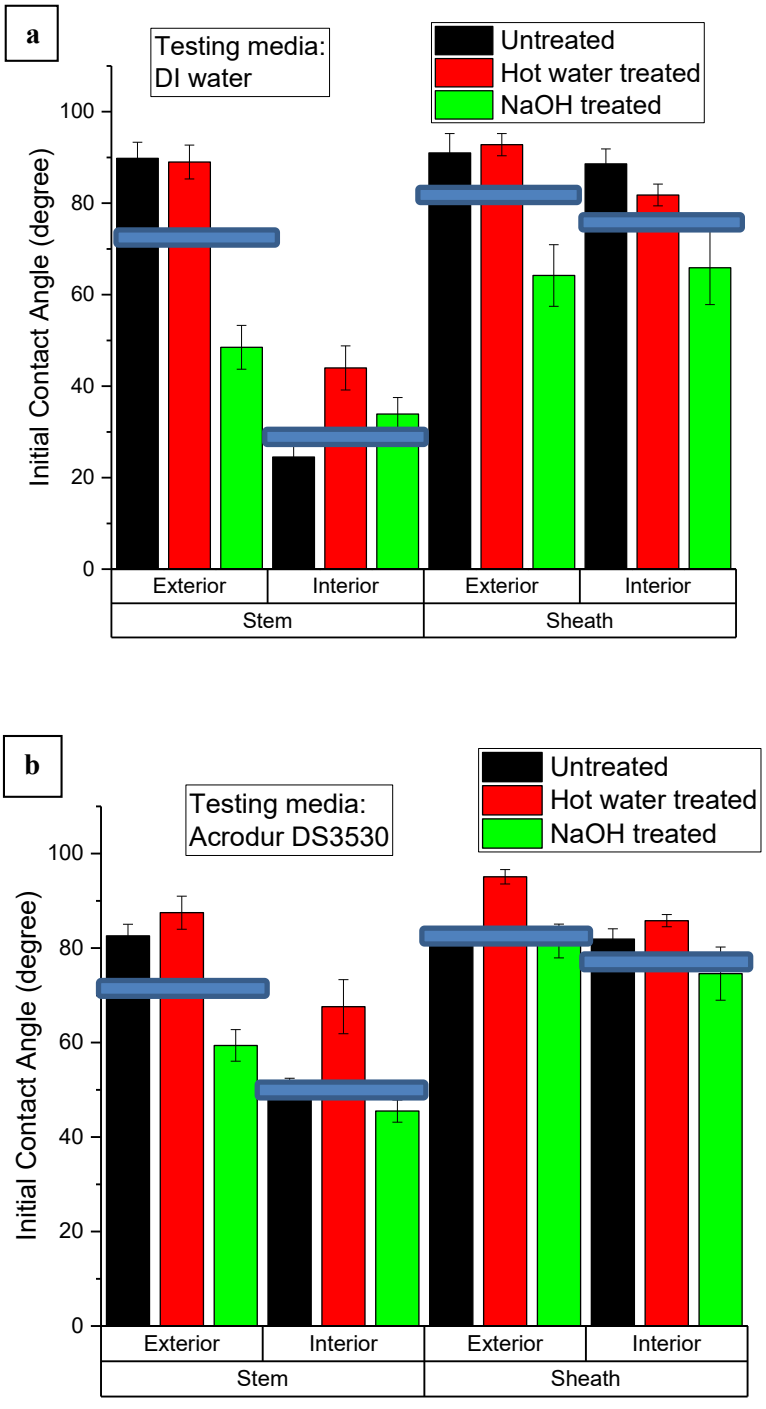

Figure 3.11 Initial contact angle graphs with DI water (a) and Acrodur (b) as testing media; Blue horizontal bars identify the average of three measured initial contact angles on the same surface

Table 8.1 in Appendix A shows the pooled mean of apparent initial contact angles for each liquid-surface pair calculated by averaging first-27-second data point using the method mentioned previously in 3.4.1. Then the averages of first-27-second data of 2–5 locations for each specimen, 6–8 specimens for each sample were averaged to obtain "grand mean" or "pooled mean", which is the mean of the means of several subsamples.

The bar graphs in Figure 3.11 compare the effects of three treatments, of two anatomic parts, of two surfaces, and of two media, on wettability, as group for easy comparison. It is seen from Figure 3.11 that, for untreated samples, the contact angles of the interior surface of the stem were smaller than those on the exterior surface for the same test media. Both Acrodur DS3530 and DI water had initial contact angles in range of ~82–90° on untreated stem exterior, whereas the contact angles on untreated stem interior are much lower, being 24° for DI water and 49° for Acrodur DS3530, respectively. However, both sheath interior and exterior of untreated wheat straw did not show much differences in measured contact angles, which were in range of 80–91° and comparable to those on stem exterior. This demonstrates that the behavior of the stem interior was quite different from those on other three surfaces. This phenomenon is connected to the surface chemical compositions and anatomical structure, which conforms to their biological functions of protecting plant or of transporting nutrients (White and Ansell 1983). As known, the presence of waxes and cutin on exterior of stem and both exterior and interior of sheath results in the more hydrophobic feature, which is consistent to the greater contact angles measured in this experiment. On the other hand, the absence of cuticle layers, richness of cellulose, and loose structure displayed on stem interior give rise to hydrophilic characteristic, leading to low contact angles.

After hot water treatment, both Acrodur DS3530 and DI water contact angles on sheath interior and exterior, and stem exterior changed slightly and remained in the same range as on untreated ones. Surprisingly, hot water treatment increased the contact angles on the stem interior to 44° and 67° for hot water treated and NaOH treated wheat straw, respectively. This might be caused by removing the impurities and dust on the surfaces.

NaOH treatment showed significant effect on sheath interior and exterior, and stem exterior. The DI water contact angles dropped to 48° for stem exterior, which was the largest change, and 64° and 65° respectively for sheath interior and exterior. The Acrodur contact angles on these three surfaces dropped

significantly too. The contact angle of the NaOH treated surfaces can reach values as low as around 50°, as compared to around 90° before the treatment. This indicates that NaOH treatment was an effective method for improving the wettability of wheat straw surfaces. NaOH treatment achieved the same effect on stem interior, whereas the contact angle increase was observed but not as much as the hot water treated did. The optical observation also showed the smooth surface seen on the exterior surface disappears and porous structure appears, this phenomenon called chemical etching was observed in Liu's study (Liu et al. 2003) of alkane treatment on wheat straw.

For two test media, DI water and Acrdour DS3530, there was not significant difference found on same surfaces of untreated or treated. It can be attributed to the similar surface tension of both media because Acrodur DS3530 is water based solution containing 50% water.

The above "pooled" comparison method can provide an overall comparison for all the surface-liquid systems, but it could be misleading for some occasions. The reasons for that are: 1) the significant variations due to the heterogeneity exists among different specimens of the same sample, and even among the different locations on the same piece of specimen, although the steps were taken during material preparation to ensure representative and homogenous test samples. As was to be expected, smaller variations were noted within the clean stem exterior samples compared with the other surfaces. The stem interior samples were expected to exhibit a relatively larger within group variation compared to the other biomass types because of its more heterogeneous plant part composition of wood and bark from stems and branches, as well as foliage. 2) Not all the initial contact angles were measurable. The contact angles on some surfaces became immeasurable, which led to missing data points. Most of missing data points are caused by the fact that liquid spreads and penetrates too fast to be recorded.

"Paired comparison" of initial contact angle was conducted as described in Appendix A, in addition to pooled comparison to eliminate the deviation from sample, because the specimens for three treatments were from the piece of straw.

The measurement of both contact angle and its rate of change with time can provide more information on the wettability and is suitable to evaluate the effect of different surface treatments. The simulation of experimental data with model described by Equation 3.2 was used to plot contact angle changes as a function of time. By using a nonlinear parameter simulation technique, parameter K was obtained from experimental data. The software Origin was used for model fitting and calculation of the penetration-spreading constants (*K-value*s) of all the samples. To obtain K-value for a particular

liquid/solid system, a nonlinear curve-fitting method was used to fit the empirical data in model. The experimental data of the contact angles for DI water and Acrodur DS3530 solution on untreated, NaOH treated and hot-water treated wheat straw surfaces was fit to Equation 3.2. The equation was applied to the experiment data. The *K-value*, and the R^2 value of the constant were calculated based on curve-fitting results by using statistical analysis method associated with Origin software. The parameter adj. R-square represents how good the model was fit with data (goodness of fit). The greater adj. R-square is, the better the fit of the experimental curve indicates.

Figure 3.12 and Figure 3.13 representatively demonstrate the experimental data and the model fit of the contact angle decrease as a function of time for the different wheat straw surfaces and two testing media systems. The model fit results for other samples can be found in Appendix B. It is seen from Figure 3.12 that the fitted curve well captured the trend in the experimental data as well as smoothed out the noise presented in experimental data, which illustrates that the wetting model provided a good fit to the experimental data. It is confirmed by the adj. R-squared of 0.97 and 0.91 for left and right contact angle of sample #6, respectively, compared to less fitting of 0.81 and 0.71for sample #1 in Table 8.5 in Appendix A. Therefore, the developed wetting model could accurately describe the adhesive wetting process on the wheat straw surface. However, poor model fit was noticed on stem interior, the reason for which is that the model was developed suitable for wood structure, which does not show porous structure like stem interior, whereas the structure of stem exterior, and sheath interior and exterior is more like that of wood.

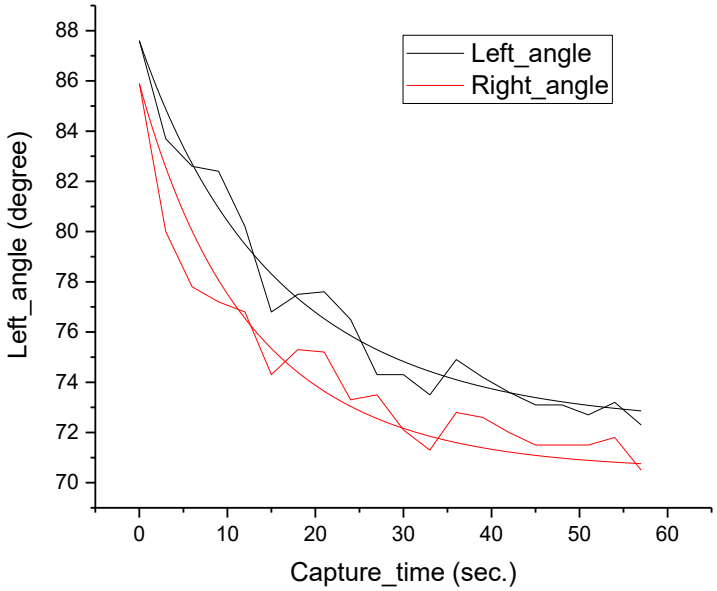

Figure 3.12 Model fit with experimental data from NaOH treated-sheath exterior-Acrodur DS3530 sample #6

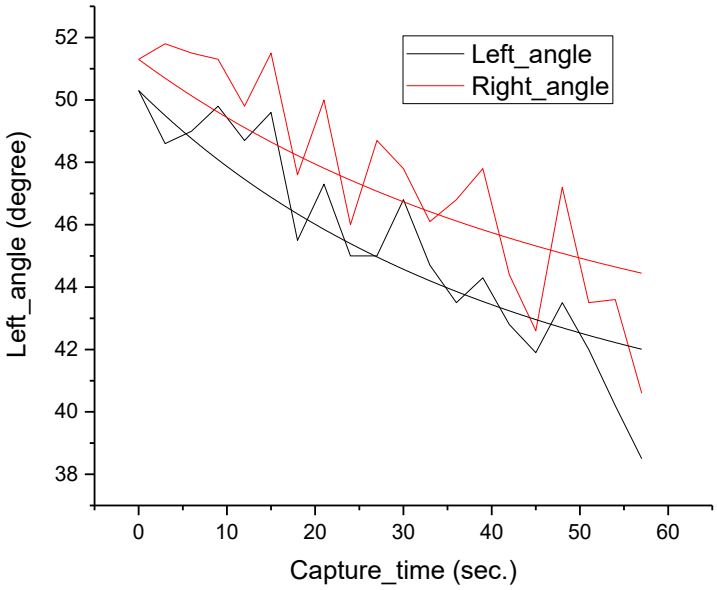

Figure 3.13 Model fit with experimental data from NaOH treated-sheath exterior-Acrodur DS3530 sample #1

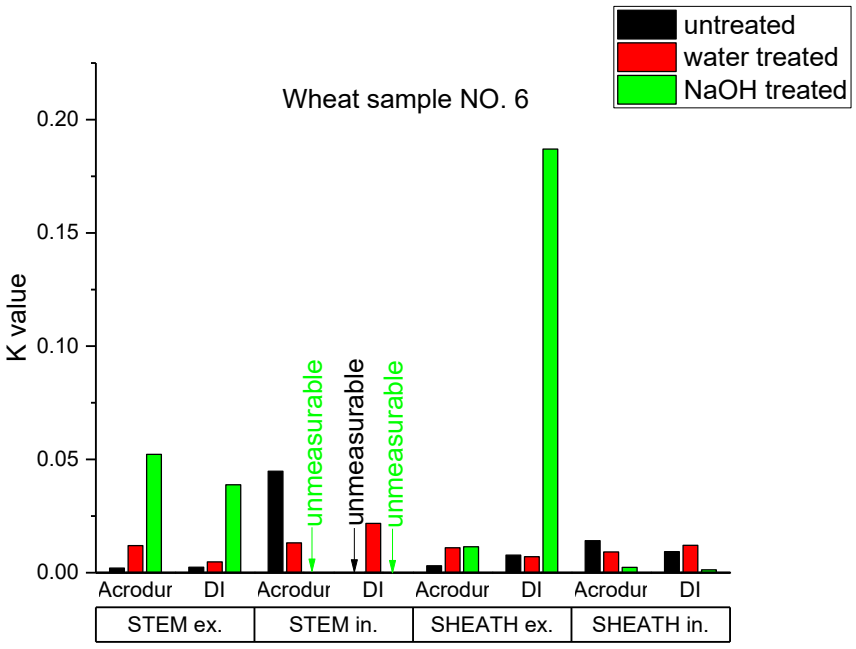

Figure 3.14 *K-value* result for sample #6

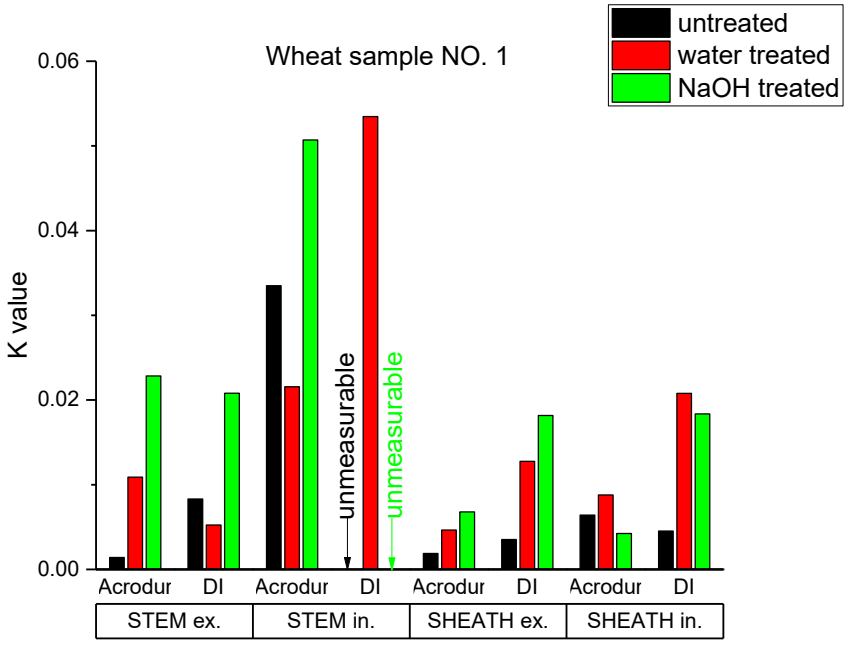

Figure 3.15 *K-value* result for sample #1

Based on *K-value* results obtained from model fitting, the wettability of two liquids for the different wheat straw surfaces, whether treated or not, are discussed below separately. The bar graphs of constant *K-value* for sample #6 and #1 are shown in Figure 3.14 and Figure 3.15. It should be noted that some of *K-value*s were unavailable because the liquid shape changed so fast that contact angles became unmeasurable or too few data points obtained to form a curve. The *K-value*s became infinity for these cases, meaning the liquid changing rate is very high.

The same trend was found for these two samples. The *K-value* of the stem interior was higher than that of the other three surfaces for both DI water and Acrodur DS3530 on the untreated wheat straw. That is, both testing media spread and penetrated much faster on stem interior than on the other three surfaces, mainly due to the porous structure of stem interior. This is in conformity to the results of initial contact angles in previous sections.

The alkali treatment apparently had an effect on the contact angles of the two liquid media on either the exterior or interior surfaces of stem and sheath. The *K-value* of DI water and Acrodur DS3530 on the NaOH treated wheat stem was much greater than that of the untreated surface. For example, for stem exterior, the *K-value* increased by several times, whereas the *K-value* even increased to infinity for stem interior. This proved that the spreading and penetration of DI water and Acrodur DS3530 on the NaOH treated stem surface were substantially improved. On the other hand, NaOH treated sheath of both sample #1 and #6 exhibited slightly increased *K-value* on exterior, and decreased K-value on interior. As discussed above, the structure of the stem interior is different. After treating the exterior surface with NaOH, the chemical etching was more obvious on the exterior surface than on the interior surface. Thus, the etched exterior surface was likely to accelerate the adsorption of DI water or Acrodur DS3530 and then increased the spreading and penetrating rate. Therefore, the increase of *K-value* induced by NaOH treated can be contributed to removal of surface hydrophobic wax-cutin layer as well as roughness resulted from destructive effect of the chemical etching. Previous publication (Liu et al. 2003) showed that NaOH treated wheat straw substantially improved the wettability of the three water-based resins. The spreading and penetrating abilities of the three resins improved very quickly. He concluded that alkali treatment could be effective in improving the wettability of the wheat straw surface.

In contrast, hot-water treatment exhibited the same influence on *K-value* as NaOH treatment but with smaller magnitude. For example, the *K-value* of Acrodur DS3530 on hot-water treated stem exterior

is just around half or less than half of that on NaOH treated one. This demonstrates that hot-water treatment increases wettability of wheat straw by extracting water-soluble.

The paired comparisons of contact angle along with *K-value* for other samples (#2, #4, #7, and #8) are attached in Appendix B.

During the measurement of contact angle with sessile drop measurement on impermeable surfaces the volume of the liquid droplet may be subjected to minor changes due to evaporation. On porous surfaces that can absorb the liquid the volume of the droplet is subjected to more noticeable changes. This is the case observed here for wheat straw, whereas the volume of the droplet changed significantly due to absorption of water or Acrodur into the porous structure of wheat straw.

The change in the volume of the droplet was measured as a function of time and the rate of volume change was calculated in units of μL/s. The bar graphs in Figure 3.16 compare the effects of three treatments, of two anatomic parts, of two surfaces, and of two media (DI water and Acrodur) on liquid volume changing rate. It should be noted the logarithmic ($\log_{10}$) scale is used in these graphs to illustrate the significant difference in volume changing rates.

It is seen from Figure 3.16 that, for four surfaces, the volume changing rate on the interior surface of the stem were much larger (more than 100 times) than those on the other three surfaces for both Acrodur DS3530 and DI water. Three other surfaces did not show much differences in volume changing rate, with the volume changing rate being in the range of 10^{-3}–10^{-2} μL/s. This demonstrates that the absorption on the stem interior was quite different from those on other three surfaces. This phenomenon is connected to the surface chemical compositions (waxes and cutin) and anatomical structure (White and Ansell 1983) and is in a good agreement with the results of contact angle comparisons. The loose structure and hydrophilic characteristics displayed on stem interior gave rise to a significant amount of liquid absorbed.

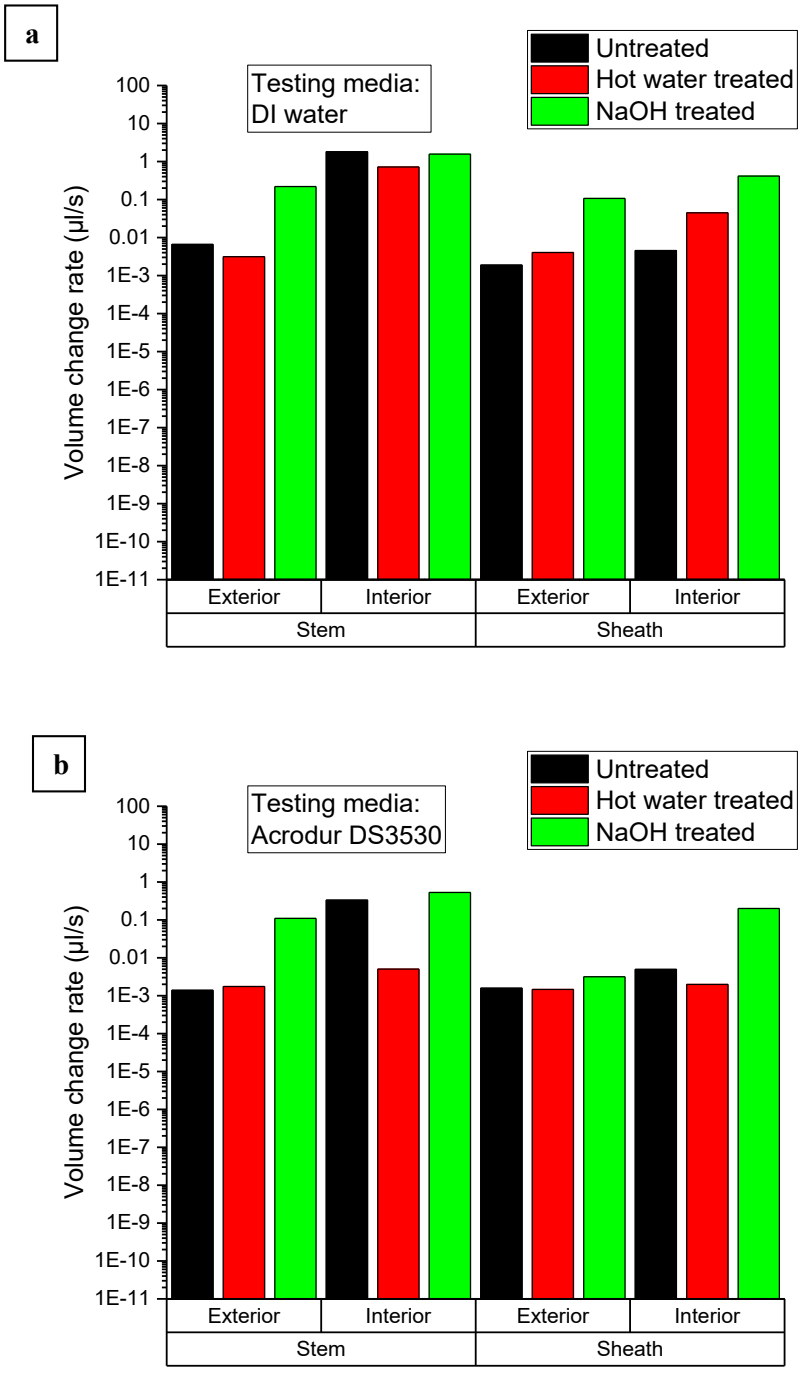

Figure 3.16 Rate of volume change (µL/s) of DI water (a) and Acrodur (b) during contact angle measurement

NaOH treated samples showed significantly increased (10–100 times) volume changing rates on all four surfaces (interior and exterior of stem and sheath) and both testing media. This can be related to the removal of non-cellulosic matters and exposure of the porous structure on wheat straw. This corroborated well with the results of optical observation reported in Section 3.4.2 where the roughness and cleanness on NaOH treated surfaces were discussed. This indicates that NaOH treatment was an effective method for greatly enhancing of the absorption water or binder inside the wheat straw structure.

After hot water treatment, the volume changing rate on sheath interior and exterior, and stem exterior increased slightly or remained in the same range as those observed on the untreated ones. Surprisingly, hot water treatment decreased the volume changing rate on the stem interior. This might be caused by removing the impurities and dust on the surfaces.

For two test media, DI water generally showed higher volume changing rates than Acrdour DS3530. This can be attributed to the relatively high viscosity of Acrodur DS3530.

In summary, two treatments were applied to the four wheat straw surfaces. The contact angle of DI water and Acrdour DS3530 solution was measured on these four surfaces before and after treatments. The wetting process on the four wheat straw surfaces was described by using a dynamic wetting model. The wetting model could be used to accurately describe contact angle changes as a function of time, except on stem interior. The constant *K-value* in the model was obtained and used to quantify the spreading and penetrating rate of the liquid-solid surface system.

The smaller contact angles, higher *K-value*s and fast absorption on stem interior, and similar wetting behavior exhibited on the other three surfaces, i.e., stem exterior, sheath interior and exterior, were attributed to the differences in surface morphology and surface chemistry, i.e. porous structure and less waxy materials on stem interior. The volume changing rate results demonstrate that the testing media were mostly absorbed in the wheat straw sample when exposed to stem interior.

Two test media, DI water and Acrdour DS3530, demonstrated slight difference on same surfaces of untreated or treated. It was attributed to the similar surface tension of both media because Acrodur DS3530 is a solution containing 50% water.

NaOH treatment showed significant influence on wetting process of DI water and Acrodur DS3530, implied by decreased contact angles and increased *K-values* for all the surfaces. Whereas, hot-water

treatment exhibited same effect on wettability as alkali treatment but with less magnitude. This indicates that alkali treatment was a more effective method for improving the wettability of wheat straw surfaces than hot water treatment.

It was also concluded by volume changing rate results that the testing media (DI water and Acrodur DS3530) were mostly absorbed in the wheat straw samples when exposed to stem interior and the other three surfaces when NaOH treatment was applied. Therefore, this study demonstrates that the absorption of binder inside the wheat straw itself can be explored as a venue for further reinforcing the straw by curing the binder inside it.

3.4.2 Surface Morphology

The effect of the alkali and hot-water treatments on the morphology of wheat straw was investigated with the assistance of scanning electron microscopy (SEM). It is well-known that the wheat straw contains waxes and silica (Harper and Lynch 1981) (Mo et al. 2005) in addition to other non-cellulosic matters. The removal of these non-cellulosic components leads to the structural change. It is important to study the morphological changes on the wheat straw fiber as the structural variations can extensively affect the mechanical and morphological properties of the fiber and thereby the mechanical properties of the composite (Herrera-Franco and Valadez-Gonzalez 2005) (Mwaikambo and Ansell 2002) (Islam et al. 2010). The interior and exterior of the untreated, NaOH treated and hot-water treated wheat stem and sheath were examined using SEM at various magnifications. Representative SEM photomicrographs at 200 magnification illustrating the morphology of wheat straw surfaces before and after treatments are depicted in Figure 3.17–Figure 3.22. The SEM images at 500 and higher magnifications were also taken for each surface shown in Figure 8.18–Figure 8.23 in Appendix C.

Micrographs of outer and inner surfaces of untreated wheat straw stem are shown in Figure 3.17 (a and b) respectively. The outer layer of stem named epidermis is rich in cellulose covered by a layer of silica of approximately 1% according to Liu (Liu et al. 2003) and wax. This outermost layer of silica and wax gives a smooth appearance to the epidermis surface as it can be seen in Figure 3.17 (a). The outer layer presented some cracks and debris as shown in image. Further observation showed that there were cuticles and stomas in the exterior surface.

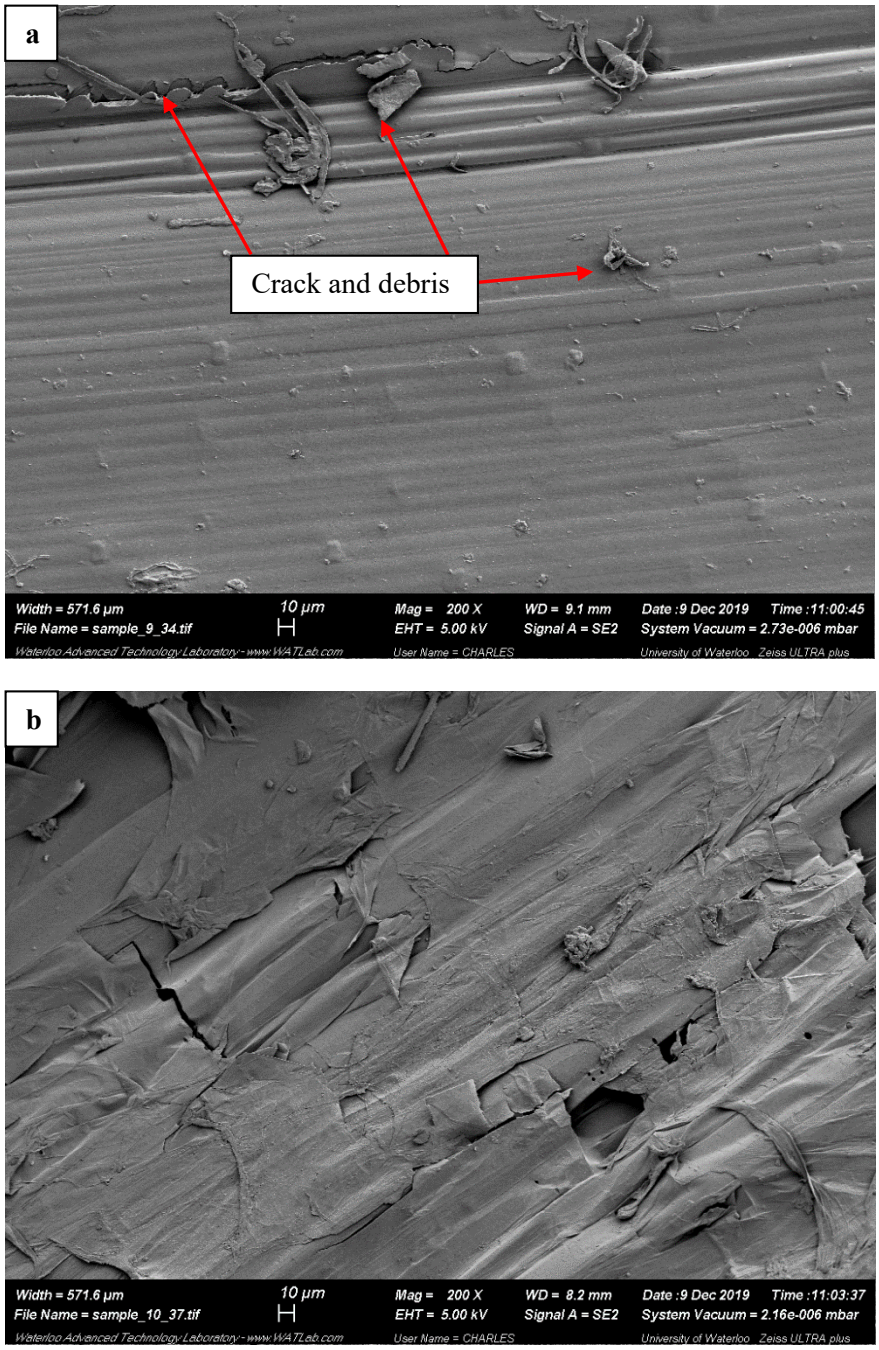

Figure 3.17 Exterior (a) and interior (b) of untreated wheat stem

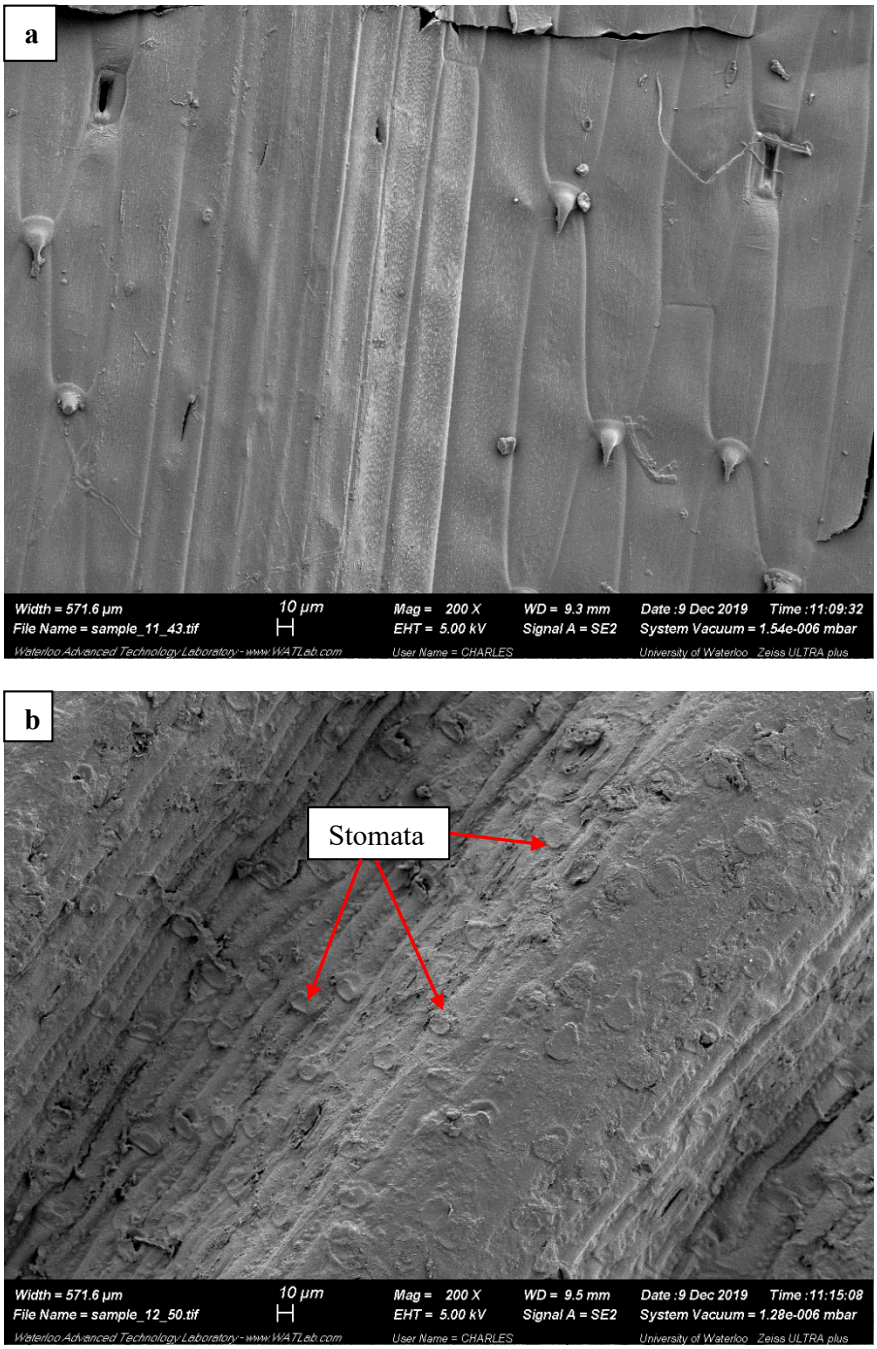

Figure 3.18 Exterior (a) and interior (b) of untreated wheat sheath

In contrast, the inner breakage structures of the stem produced a very coarse surface mainly because of the inner porosity of loose structure of stem, which was observed in Figure 3.17 (b). The inner tissues are comprised of cellulose microfibrils bonded together by an amorphous matrix of lignin and

hemicellulose (Hornsby et al. 1997a) (Hornsby et al. 1997b). On the inner surface of wheat straw stem was no smooth appearance observed, representing the absence of silica and waxes. The tissue of the interior surface consisted mainly of parenchyma cells. It was observed that there were parenchyma cells in the interior surface, as shown in Figure 3.17 (b). The parenchyma cells are distributed throughout the basic parenchyma tissues, which are thinner, deformed, and fragile. These parenchyma cells were not closely arrayed and did not form cuticle. It seems that the inner layers are either peeled off or broken into smaller pieces.

Figure 3.18 (a and b) show the exterior and interior of sheath before treatment. The smooth feature was observed on exterior, which was similar with that of stem exterior. It was noticeable that on the surfaces were the stomata for gas exchange as shown in images.

The images of exterior and interior surfaces of NaOH treated wheat stem are shown in Figure 3.19 (a and b). If comparing Figure 3.19 (a) with Figure 3.17 (a) and Figure 3.19 (b) with Figure 3.19 (b), it is evident from the micrographs that the stem treated with NaOH exhibited considerably cleaner surfaces with the roughness showing coarser fiber texture on exterior in comparison with untreated stem. The small rugged canals on exterior surfaces was due to this phenomenon known as "chemical etching" (Liu et al. 2003), which caused the cuticle either partially visible or entirely absent under SEM. The exterior surface of NaOH-treated wheat straw appeared to be chemically etched. Little changes were observed on the interior surface after NaOH treatment shown in Figure 3.19 (b).

Figure 3.20 (a and b) show the surfaces of wheat sheath after alkaline treatment. The same changes were found on both sides of sheath as that on exterior of stem treated with NaOH. The appearance of smoother surface with deeper inter-fibular disintegration of the bundle were a result of removal of non-cellulosic material suggested by literatures (Shen et al. 2011) (Liu et al. 2003).

Several authors have reported similar findings for alkaline treatment on different plant fibers. Rougher fiber surface after alkali treatment was observed in the case of sisal (Mwaikambo and Ansell 2002), hemp (Feng et al. 2008), and wheat straw (Liu et al. 2005) (Vedoy 2012). These authors argued that the removal of hemicellulose, lignin, wax and silica caused the exposure of the cellulose microfibrils and thereby rougher surface texture. In addition, the presence of white spots at the surfaces of the wheat stem and sheath seen in Figure 3.19 (a) and Figure 3.20 was attributed to be the residue of the partially removed silica layer by Vedoy (Vedoy 2012).

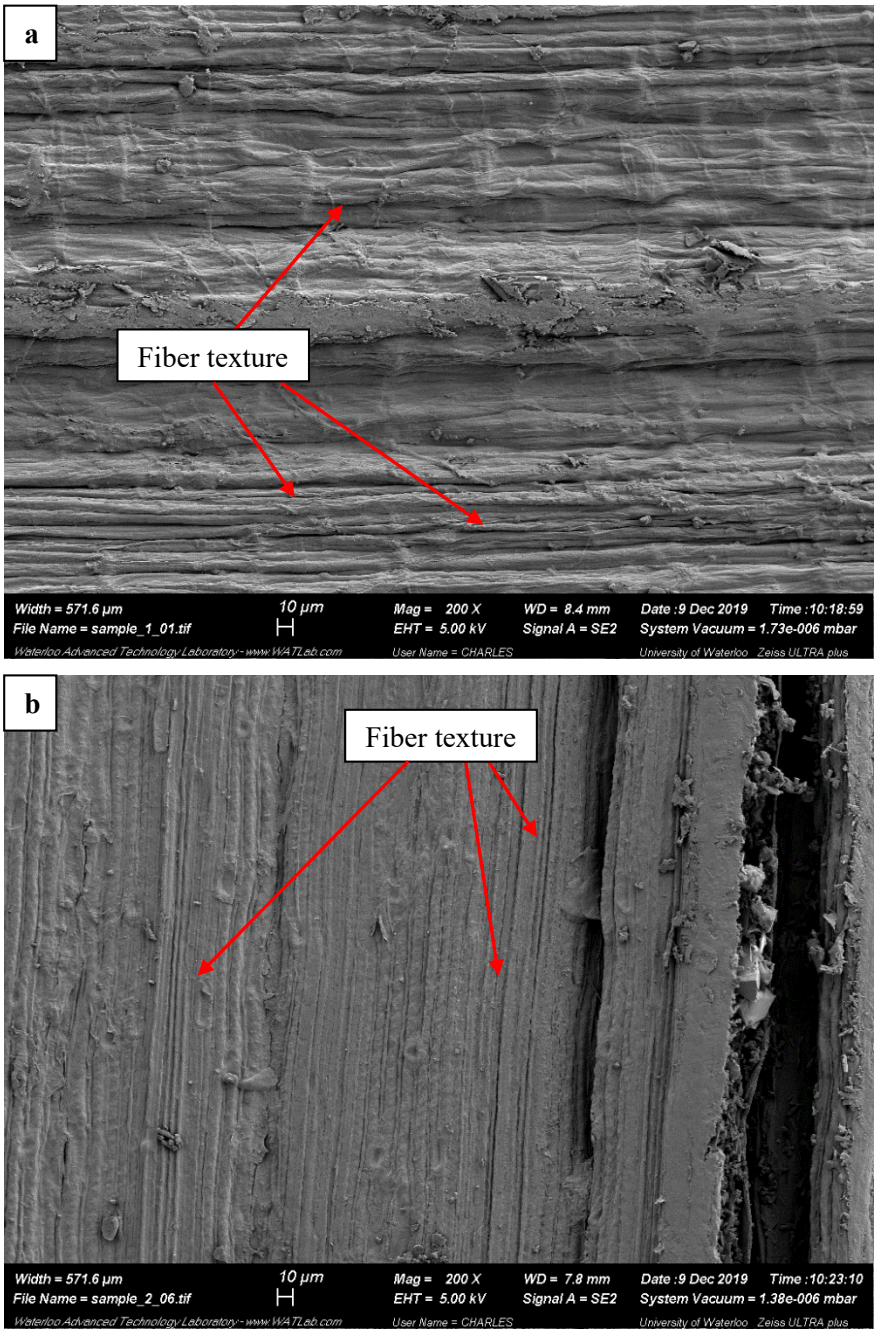

Figure 3.19 Exterior (a) and interior (b) of NaOH treated wheat stem

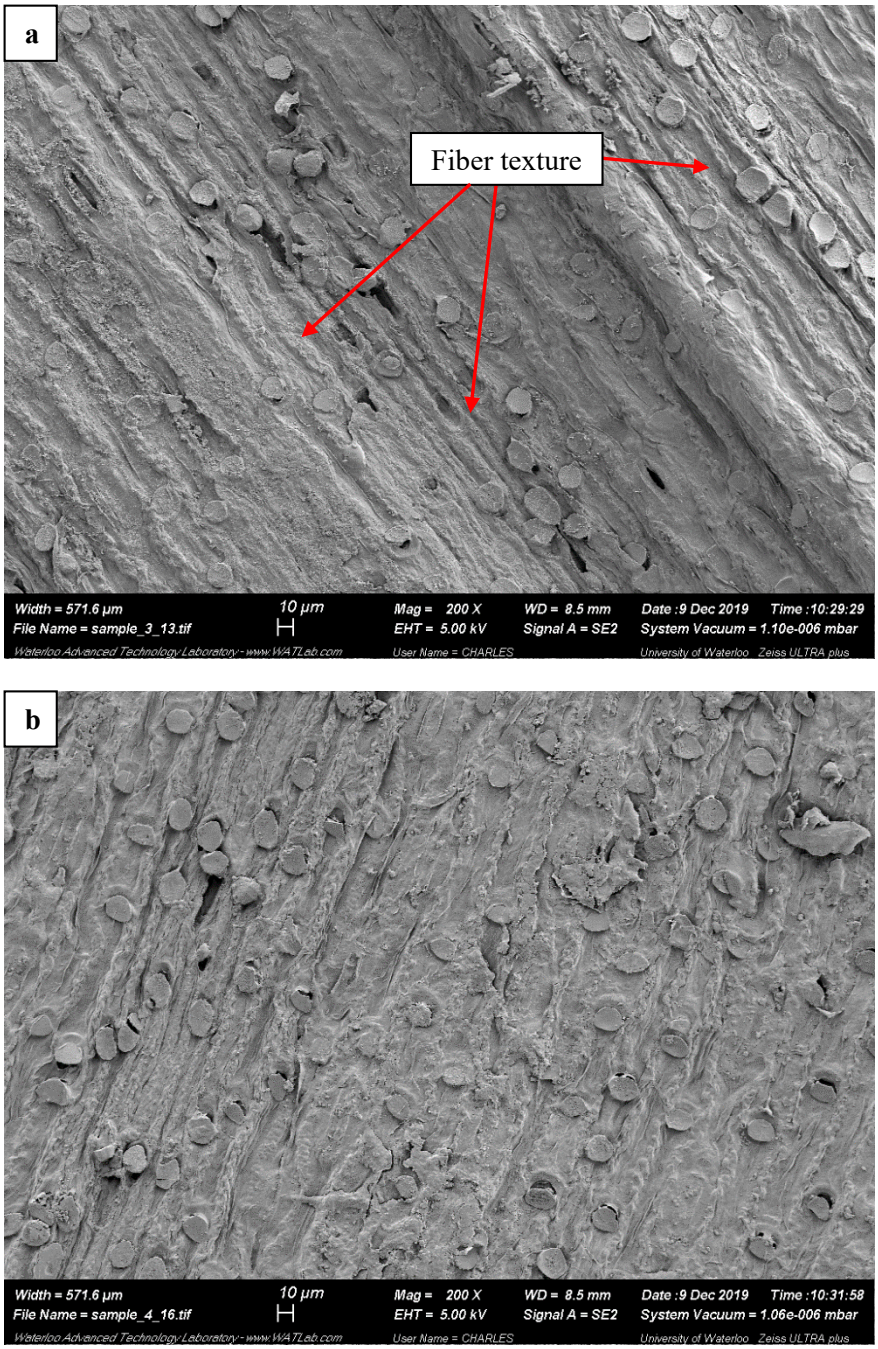

Figure 3.20 Exterior (a) and interior (b) of NaOH treated wheat sheath

It was also widely reported that a coarser surface can induce both better mechanical interlocking and bonding reaction between fiber and polymer. The improved bonding reaction is due to the removal of the surface impurities and exposure of the fiber hydroxyl groups to the polymer matrix whereas the

coarser surface is responsible for inducing more fiber-polymer interpenetration at the surface (Herrera-Franco and Valadez-Gonzalez 2005) (Mwaikambo and Ansell 2002) (Islam et al. 2010).

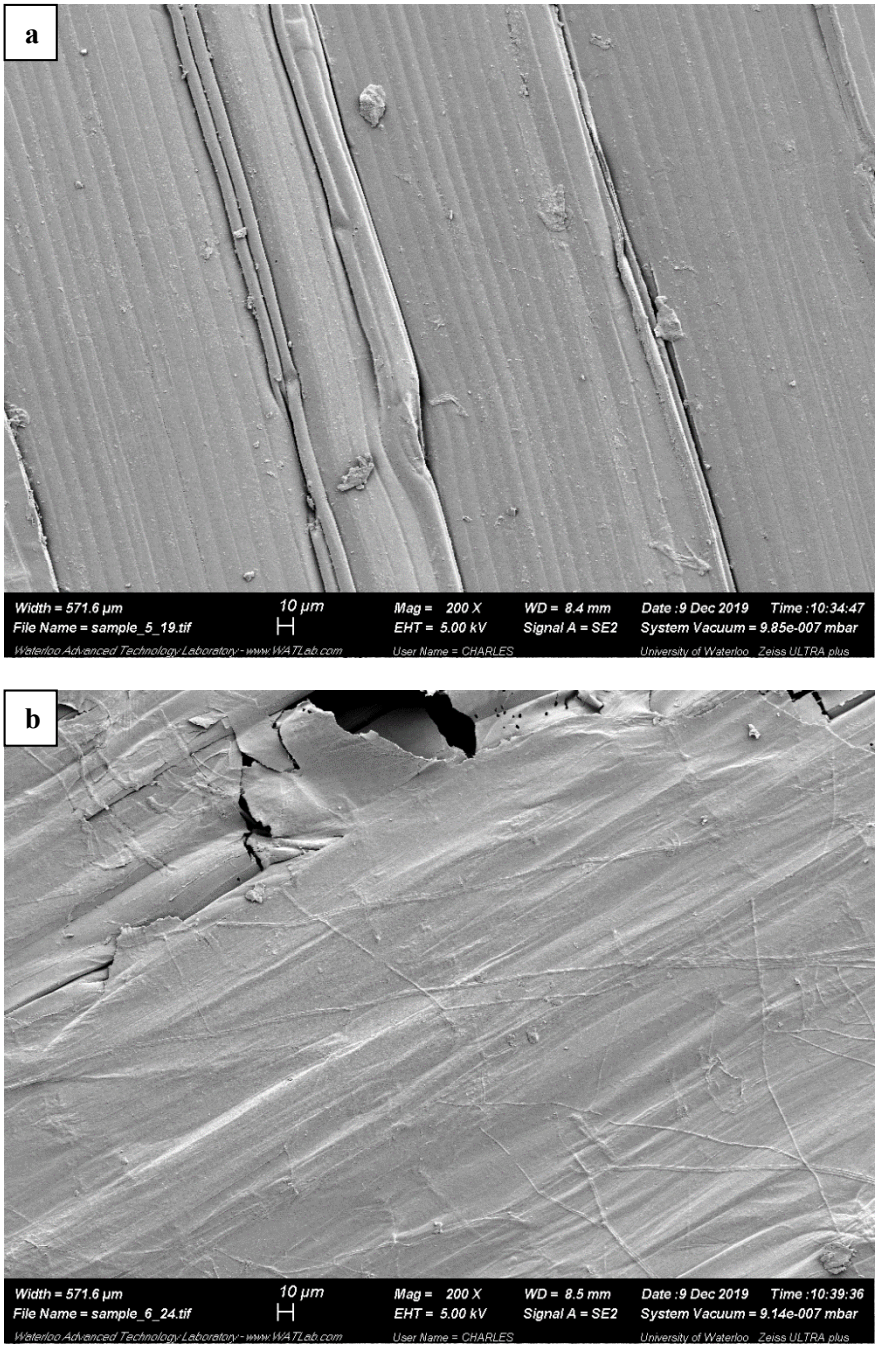

Figure 3.21 Exterior (a) and interior (b) of hot-water treated wheat stem

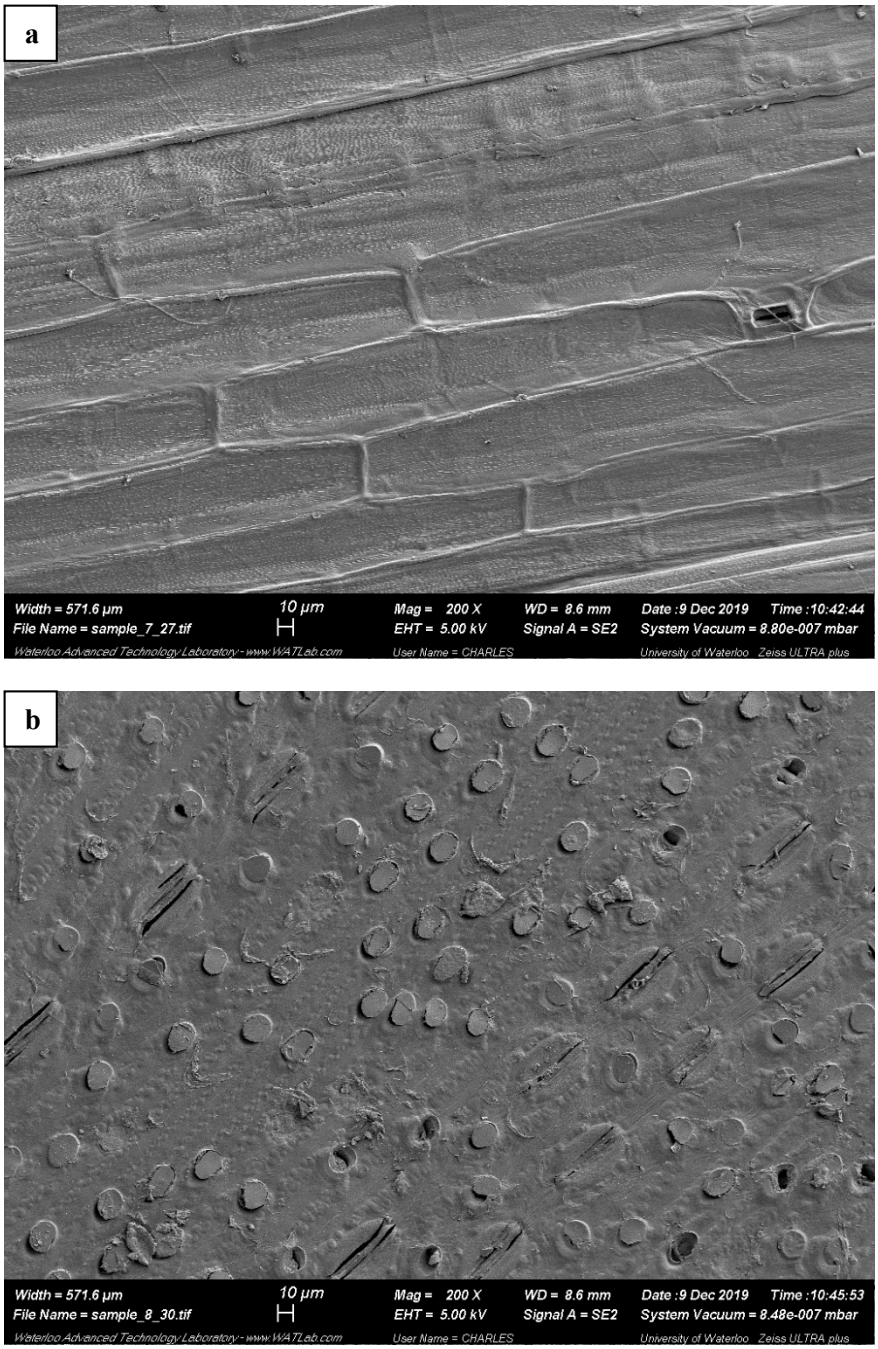

Figure 3.22 Exterior (a) and interior (b) of hot-water treated wheat sheath

Similar morphological features in the images of the alkali treated wheat straw samples are observed in the micrographs of hot-water treated wheat straw samples. The surface texture of hot-water treated wheat straw in Figure 3.21 and Figure 3.22 seems not as coarse as in the case of alkaline treated wheat

straw. Cracks and cellulose fibers are also visible. Figure 3.21 (a and b) and Figure 3.22 (a and b) demonstrate that the treatment with hot water was not sufficient to remove all of the non-cellulosic materials from the sample surfaces, because only the water soluble fractions were extracted.

In summary, the morphological features (e.g., exposure of cellulose fibers, fibrillation, etc.) observed for alkaline and hot-water treated wheat straw samples correspond well with the removal of non-cellulosic material (especially surface waxes, hemicellulose and lignin). It can be concluded from the micrographs of wheat straw before and after the treatments: 1) The morphological features, such as cleanliness and appearance of fiber texture on stem exterior and sheath exterior and interior after NaOH treatment were due to removal of non-cellulosic components, including waxes and silica, which not only exposed the hydrophilic cellulose framework, but also changed the surface morphology and led to structural disruption observed. Both increased hydrophilicity and roughness contribute to improvement of wettability. 2) In comparison, the treatment in boiling water for 2 hour did not exhibit as significant changes on surface structure as NaOH treatment. Two conclusions are in agreement with the effects of treatments on wettability described in previous part.

3.4.3 Thermal Stability

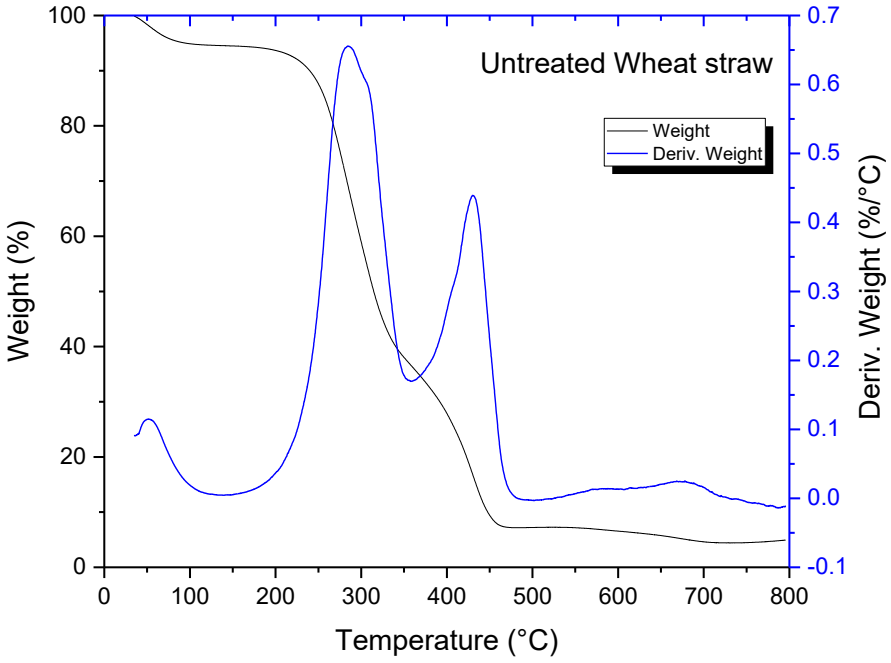

Figure 3.23 TGA and DTG thermographs of untreated wheat straw in air

According to the TGA and DTG curves of the wheat straw samples in air before the treatments in Figure 3.23, it is evident that the DTG curves showed two prominent weight loss peaks and two relatively flat regions, i.e., to say the heating process of wheat straw can be divided into four different stages, in agreement with the previous studies (H. Yang et al. 2004) (Raveendran et al. 1996).

I. The first stage — drying (<200°C) mainly showed that wheat samples lost surface moisture accompanied with slight decline in mass, accounting for an around 6% degradation of the sample. The mass loss from room temperature to about 180°C can be attributed to the loss of water and lower molecular mass volatiles, which is consistent with moisture content results shown in chapter 6 and 7.

II. The second stage — devolatilization (200–350°C) was the foremost stage of biomass pyrolysis, where volatiles resulted from the thermal decompositions of cellulose and hemicelluloses were removed, and the weight loss was prominent and reached up to 60% or so. With the increase in temperature, the DTG values increased sharply and then reduced rapidly after reaching the maximum at 284–288°C as shown in the figure. It is inferred that the large weight loss peak is mainly caused by cellulose pyrolysis, in consistence with the previous studies (Wu et al. 2014).

III. The third stage was the slow combustion stage (350–480°C), where loss of heavier hydrocarbons and lignin occurred, and the total weight loss only had 20% or less. With the increase in temperature, the changing situation of DTG presented the same trend with the second stage, whereas the maximal weight loss rate was smaller.

IV. The fourth stage (>480°C) was the carbonization stage, where the residual combustion (ash) occurred. The TGA values were basically unchanged, and the DTG values were very close to zero, which demonstrated that the thermal cracking of three chemical components had completed after 480°C. The slightly higher residual mass of around 1.84% could be attributed to wheat straw having a significantly higher percentage of the more thermally stable lignin and incombustible ash.

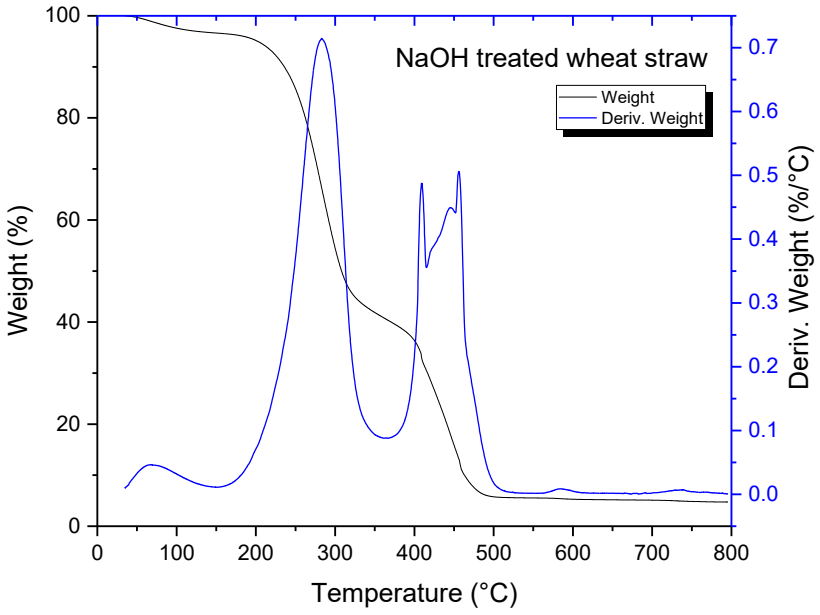

Figure 3.24 TGA and DTG thermographs of NaOH treated wheat straw in air

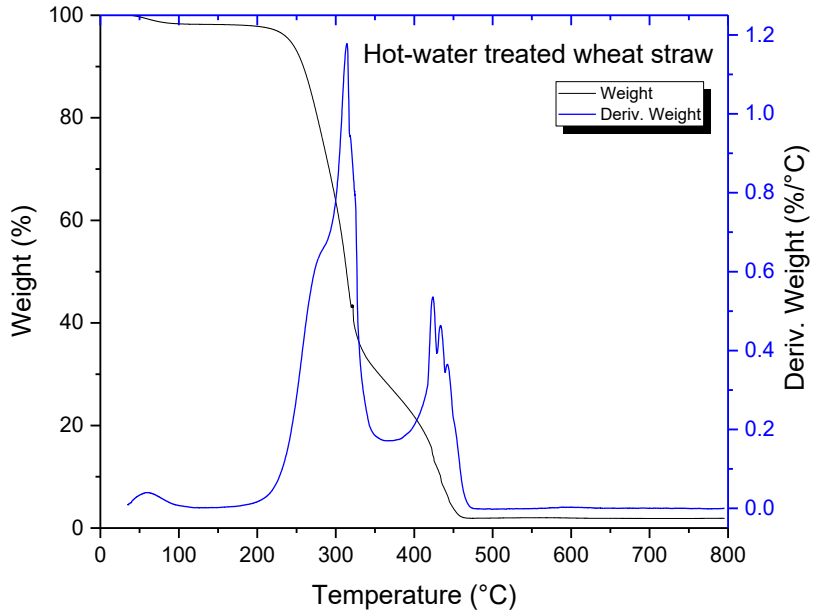

Figure 3.25 TGA and DTG thermographs of hot-water treated wheat straw in air

The TGA and DTG curves of NaOH treated and hot-water treated wheat straw in Figure 3.24 and Figure 3.25 exhibit the same trend as that of untreated one, except for the minor shifts onset and peak temperatures, indicating thermal stability change after the treatments.

It is seen in Figure 3.24 that NaOH treatment caused a slight decrease in onset and peak temperatures for wheat straw. The onset temperature dropped from 239°C to 226°C, while the main decomposition temperature decreased from 284°C to 276°C for NaOH treated wheat straw. This may be a result of presence of a lower order of cellulose structure after strong alkaline solution treatment.

In Figure 3.25, the onset of degradation of hot-water treated wheat straw was improved compared with untreated ones, which implies the improved thermal stability. The increased thermal stability can be explained by the removal of water-insoluble chemicals by water extraction process, which affects the main decomposition of wheat straw. Wheat straw prepared by hot-water process also shifted peak degradation temperature from 290 to 314°C. The increase of temperature maximum indicates a lower diffusion of the degradation products which in turn indicates that the crystallinity of the cellulose structure was not affected by the hot water treatment.

The onset temperatures of degradation, peak temperature, degradation rate, and residual weight after 600°C for three treated wheat straw samples are tabulated below in Table 3.5. The onset temperatures of degradation of wheat straw were 239°C, 226°C and 248°C respectively for non-treatment, NaOH treatment and hot-water treatment, indicating the suitability of wheat straw for processing under these temperatures. Consequently, these results indicate that composites utilizing hot-water treated wheat straw could suffer less thermal degradation during the composite fabrication process than composites using alkali and untreated wheat straw samples. Compared to results in literature, it was observed by Vedoy (Vedoy 2012), alkaline treatment increased 2% weight loss temperature from 238 to 246°C.

Table 3.5 Degradation characteristics of wheat straw in air

Treatment	T_{Onset} (5%) of degradation (°C)	Peak temperature	Rate of degradation (wt.%/min)	Residue after 600°C (%)
Non treatment	240	284	2.18	1.84%
Hot-water	249	314	2.22	0.00%
NaOH	226	277	2.21	0.60%

The plots for the TGA of untreated wheat straw fibers in both air and nitrogen at heating rates of 5, 10, 25, 40, and 50°C/minute are presented in Figure 8.24, of NaOH treated and hot-water treated wheat

straw in nitrogen in Figure 8.25 and Figure 8.26 in Appendix D. It is seen that the mass of the wheat straw decreases in mass as the temperature increases. It is also seen that the TGA curve shifts toward the higher temperature region with the increase in heating rate, namely, the degradation temperature increased upon reaching the same weight loss, which is known as heat-transfer-lag effect (Navarro et al. 2009). In comparison between two atmospheres, it is observed that the onset of degradation for samples heated in air occurs slightly earlier than that in nitrogen. For example, 20°C/min in air has an onset of 268°C with the onset 2°C higher for nitrogen. The explanation is that in nitrogen, the degradation rate is much lower than in oxidative atmosphere as the lack of oxygen is likely hindering some oxidation of the material.

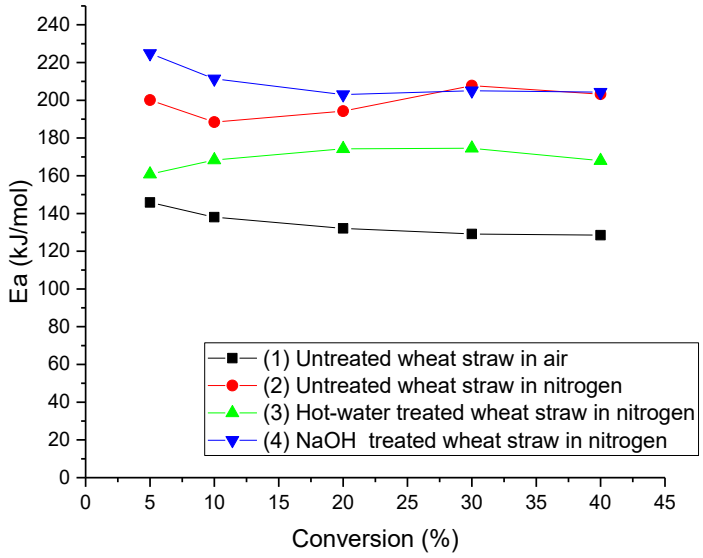

Figure 3.26 Thermal degradation activation energy of untreated wheat straw in air (1) and in nitrogen (2), hot-water treated (3) and NaOH treated (4) wheat straw in nitrogen

The Ozawa-Flynn-Wall (OFW) method (Ozawa 1965) (Flynn and Wall 1966) was used to estimate the activation energy of thermal decomposition. The OFW method is one of the so-called model-free methods that allow calculation of activation energy by using minimal a priori information about a system under study. The data required for application of this method is obtained from TGA curves. For wheat straw conversions of 5, 10, 20, 30 and 40% were used to complete the OFW analysis. The region of 5% to 40% was chosen as it is in second region described above where the initial majority of mass

loss occurs and is of most interest to the current study. Processing wheat straw with a polymer binder typically requires temperatures at or below the onset of degradation temperature and it can be assumed that mass loss comes primarily from second region during processing.

It can be seen that the untreated wheat straw exhibited higher activation energy in nitrogen than in air; this difference is around 64 kJ/mol in average. This is understandable as a nitrogen atmosphere is less favorable to oxidization than oxygen rich air. The activation energy varied greatly depending on the treatment applied on wheat straw samples. In nitrogen atmosphere, NaOH treated wheat straw showed the highest activation energy followed by untreated, hot-water treated. The activation energies varied from 209.72 to 169.20 kJ/mol for NaOH treated and hot-water treated wheat straw respectively.

The activation energy–conversion relationship and degradation temperatures are tabulated in Table 8.6 in Appendix D for each conversion value in both air and nitrogen, in which 5% conversion is used to quantify the onset. This data is also plotted in Figure 3.26 up to a conversion of 40%. The main focus of this work is to better understand the onset of thermal degradation, therefore the conversions investigated here are limited to 40%. The log β versus 1/RT plots for determining the activation energy are included in Appendix D.

In summary, the alkaline treatment significantly decreased the onset degradation temperature of wheat straw while hot-water treatment showed a little impact on it. The explanations can be found in that removal of non-cellulosic components was accompanied by structure change of wheat straw and /or transformation of cellulose crystalline structure caused by harsh alkaline treatment.

Since the thermal degradation of wheat straw is a very complex process, the objective of this study was not to elucidate the elementary steps of the reaction mechanism. The objective of the chemical kinetics study was to establish a method for identification and selection of treatment of wheat straw with superior thermal stability necessary for compounding and manufacturing with polymers. In this way, it may be possible to develop methods to prevent or minimize the thermal degradation of wheat straw and expand its use toward engineering thermoplastics with processing temperatures above 220℃ and thermosets.

3.5 Conclusion

Two relative cost-effective surface treatments, alkaline and hot-water treatments, were applied on wheat stem and sheath, and the effects of treatment were evaluated in terms of wettability, binder

absorption, surface morphology and thermal stability. NaOH treatment showed significant influence on wettability of DI water and Acrodur DS3530, implied by decreased contact angles, increased *K-value*s and increased volume changing rates for all the surfaces. Whereas, hot-water treatment exhibited same effect on wettability as alkali treatment but with less magnitude. The increased wettability and binder absorption of wheat straw after the treatments was ascribed to removal of non-cellulosic materials, especially the waxes and silica on the surface, and increased roughness porous structure. This was confirmed by the surface morphology of wheat straw samples before and after the treatments observed using the SEM microscope. NaOH treatment created cleanliness and appearance of fiber texture on stem exterior and sheath exterior and interior. However, the alkaline treatment considerably decreased the onset degradation temperature of wheat straw while hot-water treatment shifted the onset degradation temperature to a slightly lower level.

Overall, the results confirmed that alkaline treatment was an effective method for surface modification of wheat straw for increased surface wettability, binder absorption, surface morphology change, however it may cause destructive structure change, while a decrease of onset degradation temperature was found on NaOH treated samples. Whereas, hot-water treatment illustrated relatively low effects on onset temperature of wheat straw thermal decomposition, and on wettability and morphology.

Chapter 4
Kinetics of Acrodur Cure Reaction

4.1 Introduction

A family of polyester resins, Acrodur, cures at elevated temperatures to form rigid, three-dimensional network, which provides adhesion strength and integrates the materials. However, the existing literature regarding cure condition of Acrodur is scarce and the cure condition varied widely throughout the literature with the cure temperature and time altering in a big range from 130°C, or 150°C, up to 220°C and the time from less than one minute to 20 minutes, respectively (Reck and Turk 1999) (Gerst et al. 2009) (Medina et al. 2008). Neither optimum combinations of temperature and time were reported, nor was level of cure correlated to the curing conditions. Due to controversy and inadequacy in determination of cure condition, there is therefore a need in putting efforts in optimization of the manufacturing process of composites involving Acrodur resins according to specific application requirements. As shown in Figure 4.1, upon curing at temperatures of above 130°C as stated, these reactive oligomers and monomers react and the ester bonds are formed due to the condensation reaction between the acrylic acid copolymer and the multiple hydroxyl groups of crosslinker.

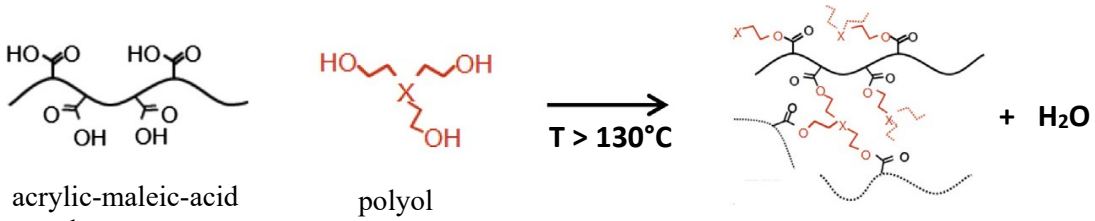

acrylic-maleic-acid copolymer

polyol

Figure 4.1 Crosslinking reaction of Acrodur solution (Gerst et al. 2009)

The properties of thermosetting material gradually change during the course of thermoset curing, as illustrated schematically in Figure 4.2. In early stage the reaction is chemical controlled, where larger and branched molecules were produced. As the reaction proceeds, the material increases in viscosity, and eventually crosslinks. As a result, the material loses the ability to flow or dissolve due to the increased glass transition temperature (T_g).

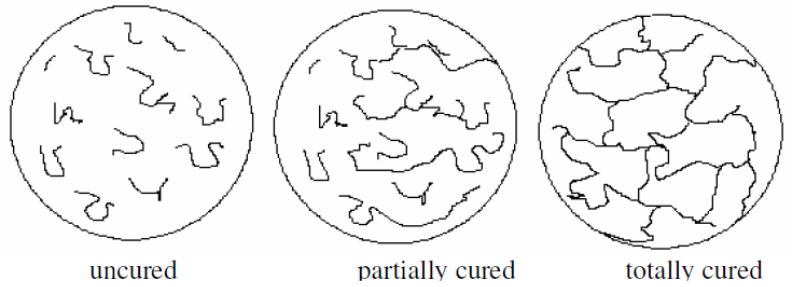

Figure 4.2 Schematic representation of curing stages

There are many factors that can affect the rate of a chemical reaction. Among these factors, temperature and concentration are the two parameters that have an impact on all the chemical reactions, whereas pressure can only influence certain types of reactions that involve the gaseous reactants or products. In the condensed phase kinetics, the conversion is used more commonly than the concentration, as shown in Equation 4.1.

$$\frac{d\alpha}{dt} = k(T)f(\alpha) \qquad 4.1$$

Although the formulation of the Acordur samples are predetermined and the components in products are at fixed ratio, the incorporation of other components, such wheat straw reinforcing fibers, or cellulose nanofibril (CNF), can affect the cure behavior by the hydroxyl groups existing in the cellulose and hemicellulose which can react with Acrodur through condensation reaction (Liang et al. 2013).

The preferred crosslinking temperatures were reported by Eichner etc. to be from 180 to 200°C in order to achieve high production rates, although it crosslinks at a temperature as low as 130°C (Eichner et al. 2005). Reck and Turk (Reck and Turk 1999) reported the temperature during compression molding should be at least 200°C with cycle times less than 60 seconds. They also reported that the influence of press time on the flexural modulus is much less pronounced than that of temperature. The same curing condition of about 200°C for less than one minute was adopted by Gerst to complete Acrodur cure reaction (Gerst et al. 2009). Curfman proposed the preferable curing temperature is about 205°C or higher (Curfman 2011). Khalfllah cured Acrodur at 170°C for 3 minutes to a curing conversion of 72% (Khalfallah, Abbès, et al. 2014). Acrodur-flax composites were cured at 170°C for 180 seconds in a study conducted by Rasyid (Rasyid et al. 2016). The processing times of less than one minutes were reached during the compression molding of three- dimensional components with a high forming degree by Medina (Medina et al. 2008). It can be concluded from above mentioned literature that the temperature ranges of 170°C or 180°C to 200°C or 220°C for less than one minute to a few

minutes was the preferred curing condition for Acrodur, and that longer reaction times are usually needed at lower temperatures.

The so-called irreversible reactions can be considered as a special situation where the backward reaction rate is negligible (Li 2017). The reaction rate of Acrodur esterification can be described in Equation 4.2, which has a corresponding back reaction that also has an associated rate as in Equation 4.3.

$$\frac{d\alpha}{dt}_{forward} = k(T)_{forward} f(\alpha_{reactant}) \qquad 4.2$$

$$\frac{d\alpha}{dt}_{backward} = k(T)_{backward} f(\alpha_{product}) \qquad 4.3$$

Due to the occurrence of by-product water evaporation, the pressure can also be one affecting factor that shifts reaction equilibrium of Acrodur polyesterification. The relationship between the rate constant and the pressure of product gas has been experimentally confirmed by several workers (Beruto et al. 1980) (Zawadzki and Bretsznajder 1938) (Reading et al. 1991).

Differential Scanning Calorimetry (DSC)

Conversion–temperature or time relationship can be established by measure ΔH or $\Delta H_{residual}$, using either Equation 4.4 or 4.5 as follows:

$$\alpha = \frac{1}{\Delta H_{total}} \int_0^t \frac{dH}{dt} dt \qquad 4.4$$

$$\alpha = \frac{\Delta H_{total} - \Delta H_{residual}}{\Delta H_{total}} \qquad 4.5$$

where, α, is conversion degree or reacted fraction, ΔH_{total} is the total amount of heat consumed over the entire reaction. $\Delta H_{residual}$ is residual enthalpy. The Equation 4.5 is usually used for postcure of incompletely cured products. The relationship between enthalpy and time/temperature obtained from DSC measurement based on either equation above servers as the experimental input in kinetic study, thus the kinetic parameter, activation energy, can be calculated.

When the samples are measured in high pressure crucibles the endothermic vaporization peak of the volatile side-products is completely suppressed. Transitions with a distinct loss of weight can only be observed in open pan mode.

When open pan mode is applied, it is assumed that the residual water trapped in the Acrodur resin has been completely removed before the material is entering the cure temperature region. The water

evaporated in the cure temperature region is solely and exclusively generated from the cure reaction as by-product. And it is further assumed that the byproduct water evaporates instantly and completely as soon as it is produced in the cure temperature region. Based on the assumptions made above, the heat flow measured by DSC during the range of temperature/time is net enthalpy of both cure reaction and water vaporization. This combined heat is called apparent heat. The apparent heat is proportional to the conversion as a measure of degree of cure, because both cure reaction and heat of water evaporation are related to advancement of the cure reaction. It is assumed that inclusion of water evaporation heat does not affect the conversion calculation.

Another example of interfering events is thermal degradation. The thermal degradation, if which cannot be isolated due to concurrence, could spoil the study. The thermal degradation can possible be isolated and interpreted with assistance of more information and techniques, such as, based on separation of temperature regimes that thermal degradation occurs in.

Thermal Gravimetric Analysis (TGA)

The ester bond formation is accompanied by the loss of a water molecule, as illustrated in Figure 4.1, where it is seen the conversion of components of Acrodur to polyester eliminates one water molecule and creates one crosslink. The one-to-one relationship between mass loss and conversion leads to the TGA degree of conversion is illustrated in Equation 4.6 and 4.7, as analogies of Equation 4.4 and 4.5, respectively. In this manner the conversion vs. time/temperature curves can be constructed, which is used as input for kinetic study.

$$\alpha = \frac{\Delta m_t}{\Delta m_{total}} \qquad 4.6$$

$$\alpha = \frac{\Delta m_{total} - \Delta m_{residual}}{\Delta m_{total}} \qquad 4.7$$

where, α, is conversion degree or reacted fraction, Δm_{total} is the total amount of mass loss over the entire reaction. Δm_t is mass loss up to time, and $\Delta m_{residual}$ is residual mass loss. The Equation 4.7 is usually used for postcure of incompletely cured products.

In summary, DSC and TGA measure the enthalpy involved or mass loss of cure reaction, which provides the experimental input to completely study the progress of cure, to calculate the kinetics parameters, and to observe the effects that the formulation, temperature and time, and pressure, when gaseous matters involved, have on the curing behavior of thermosets.

Friedman Iso-conversional Method

Once the relationship between conversion (α) and temperature or time has been established using the experimental data obtained from the DSC or TGA measurements according to the Equation 4.4, 4.5, 4.6, and 4.7, the kinetic parameters of the cure reaction can be calculated using kinetic analysis.

Two principle equations associated with kinetics are referred to as the rate equation (Equation 4.1) and the Arrhenius equation (Equation 4.8). The rate of a reaction (dα/dt) in condensed state is usually describe as a result of two functions independent of each other: the *k*(T) function, which depends solely on the temperature T and follows the Arrhenius law, and the $f(\alpha)$ function which depends on the conversion degree and is related to the mechanism of the reaction. Equation 4.9 is obtained by combining equation 4.1 and 4.8.

$$k(T) = \mathrm{A}\, exp\left(\frac{-E_a}{RT}\right) \qquad 4.8$$

$$\frac{d\alpha}{dt} = \mathrm{A}\, exp\left(\frac{-E_a}{RT}\right) \mathrm{f}(\alpha) \qquad 4.9$$

where Ea is the activation energy, A is the pre-exponential factor, R refers to the universal gas constant, and T corresponds to the absolute temperature. Based on Equation 4.8, the reaction rate always increases with temperature, and temperature dependence shows very strong nonlinearity, i.e., a small change of temperature will lead to a significant change of reaction rate.

Two major kinetic analysis approaches are model fitting and model-free methods. The first approach is based on fitting of kinetic data to assumed reaction models, whereas model-free iso-conversional methods were developed to describe the thermoset cure processes when models are unknown. The main implication of equation 4.8 is that the reaction rate at a constant conversion degree is only a function of temperature, and this is the basic assumption of the so-called iso-conversional methods. One of the model-free iso-conversional methods developed by Friedman (Friedman 2007), also known as differential method, derives from taking the logarithmic form of Equation 4.9, shown as Equation 4.10:

$$\ln\left(\frac{d\alpha}{dt}\right) = \ln A - \frac{E_a}{RT} + \ln \mathrm{f}(\alpha) \qquad 4.10$$

To determine the corresponding activation energy and pre-exponential factor at each degree of cure, a plot of ln (dα/dt) vs. 1/T should be drawn at each degree of cure. The resulting slope is proportional to the activation energy, Ea, and the intercept is proportional to the pre-exponential factor, A. Friedman method allows one to obtain at each given conversion the activation energy, Ea, which is independent

of the reaction model (Friedman 2007). The pre-exponential factor can also be evaluated independently of the reaction model. This helps in avoiding the problems that originate from the uncertainty of the reaction model and allows determining the dependence of the activation energy on the conversion.

By doing this analysis, the relationship between the activation energy and degree of cure can be quantified to provide extra information about the change in kinetics throughout the reaction. The activation energy is constant for a single step reaction. For a multistep kinetics the dependence of the activation energy (Ea) with conversion (α) reflects the variation in relative contribution of single steps to the overall reaction rate. The shape of this dependence is indicative of the reaction mechanism (Vyazovkin et al. 1992). The model-free kinetics have been investigated successfully and extensively on other thermosetting resins cures such as epoxy's (Hardis et al. 2013) (Sbirrazzuoli and Vyazovkin 2002). It has been demonstrated that this type of analysis allows one not only to obtain consistent results from isothermal and non-isothermal date, but also to get important clues about the cure mechanisms (Sbirrazzuoli and Vyazovkin 2002).

The α value can be obtained from an experiment performed under constant temperature (for isothermal conditions) or from an experiment performed at a given heating rate (for non-isothermal conditions). Isothermal measurements involve maintaining the sample at a fixed temperature for various time intervals, whereas dynamic measurements involve heating the sample at a constant rate over a desired temperature range. For non-isothermal mode, by substituting β = dT/dt (the heating rate in non-isothermal methods), this expression can be written in the logarithmic form as in Equation 4.11:

$$\ln\left(\beta \frac{d\alpha}{dT}\right) = \ln A - \frac{E_a}{RT} + \ln f(\alpha) \qquad 4.11$$

The non-isothermal methods are the most commonly used for performing the kinetics analysis of solid state cure reactions because the dynamic thermoanalysis method has some advantages over isothermal method as it can better capture the kinetic data both at the start and end of a reaction, and complex reaction mechanisms can be more easily interpreted by a comparison of measurements at different heating rates (Daniel-da-Silva et al. 2010). However, in practice, the production of wheat straw-Acrodur composites, wheat straw impregnated with Acrodur is subject to the preset temperatures and pressures in compression molding process. Therefore, isothermal mode is a good cure simulation of compression molding conditions of Acrodur and wheat straw-Acrodur composites.

4.2 Research Objectives and Approach

The objective of this work is to undertake a systematic study on kinetics of Acrodur cure. Acrodur was firstly characterized by DSC and TGA, using both isothermal and non-isothermal methods, under hermetic or non-hermetic conditions. The relationship of the conversion (degree of curing) was then established with temperature or time. Friedman iso-conversional method was used to determine the kinetic parameters of the Acrodur cure reaction. The cure behavior of Acrodur DS3530 and 950L was compared. The effects of inclusion of cellulose nanofibril (CNF) and natural fiber wheat straw on Acrodur cure were also assessed. The objective here is to quantify kinetic parameters and characterize time–temperature dependent cure behavior, thus providing a guiding tool for optimization of cure conditions in terms of physical properties, process time and energy consumed, which ultimately affect both the cost and the quality of the final products.

4.3 Materials and Methods

4.3.1 Materials

Three thermosetting Acrodur binders investigated in this kinetic study were Acrodur DS3530, cellulose nanofibril reinforced Acrodur DS3530 and Acrodur 950L, denoted throughout this chapter as **Thermoset #1**, **#2**, and **#3**, respectively. All the Acrodur samples were provided by BASF, and the **Thermoset #2** was prepared at Suzano facility by mechanically mixing less than 5% cellulose nanofibril (CNF) in **Thermoset #1**.

The sample preparation for thermal analyses was conducted on uncured **Thermoset #1**, **#2** and **#3** by placing the Acrodur solutions on an aluminum foil and removing the water at temperature of 80ºC until the weight was constant, in order to avoid the interfering of residual water. The temperature of 80°C is much lower than stated cure starting temperature 130ºC, which ensured no crosslink reaction was initiated during drying. A series of the pre-cured Acrodur samples were prepared by heating uncured **Thermoset #1**, **#2** and **#3** at different temperatures, i.e. 180°C, 200°C, and 220°C, for 12 minutes. The uncured and pre-cured **Thermoset #1** samples are shown in Figure 4.3, where the images (a, b and c) are different form of **Thermoset #1** before curing, corresponding to solution, chunk of solid and ground powder. Unless otherwise stated, the uncured **Thermoset #1** refers to the sample in solid form across this chapter. After curing at a series of temperatures for 12 minutes, the pre-cured **Thermoset #1** exhibits a very low density as shown in Figure 4.3 (d and e) due to high porosity created

by volatiles. The non-isothermally cured **Thermoset #1** from powder form up to 400°C is displayed as image (f), which is seen to cure in a single piece. The uncured **Thermoset #2** and **Thermoset #3** solution before drying are shown in Figure 4.4.

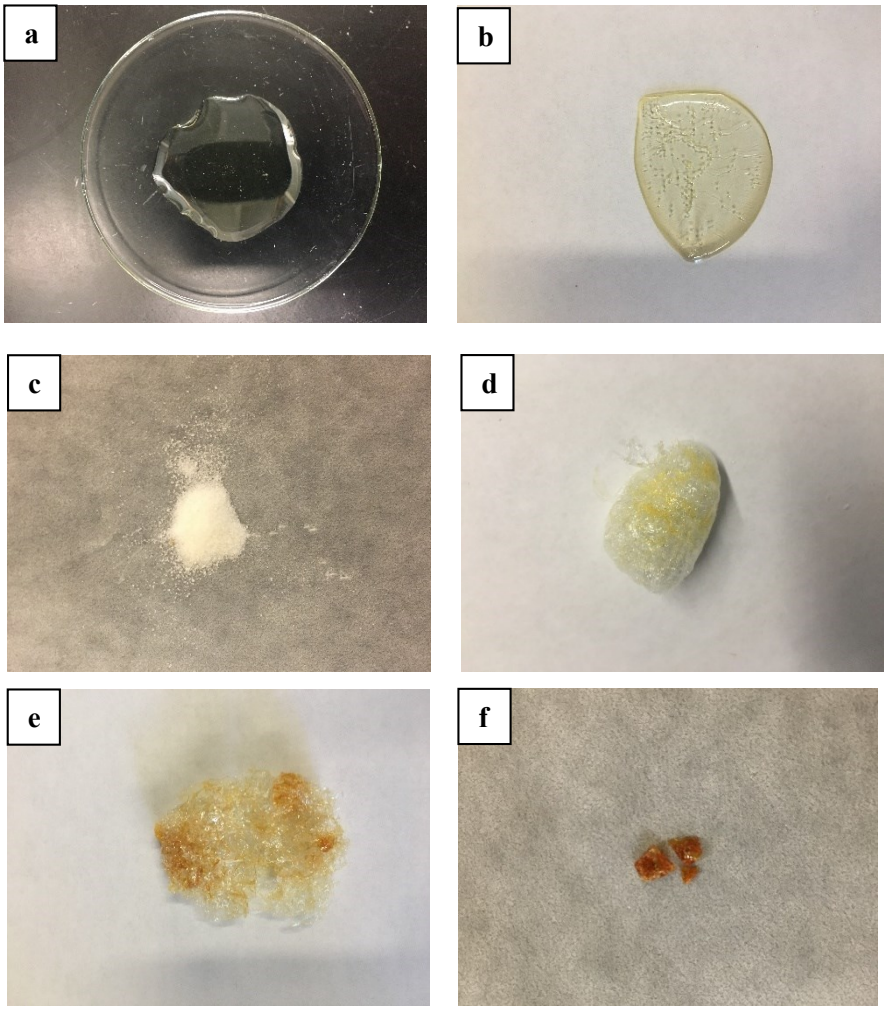

Figure 4.3 **Thermoset #1** solution (a), uncured **Thermoset #1** dried at 80°C (b) (c) and pre-cured **Thermoset #1** at 180°C (d) and at 200°C (e), and **Thermoset #1** cured up to 400°C (f)

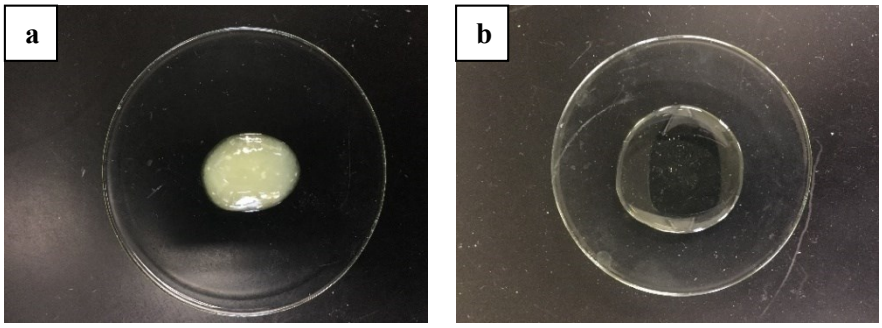

Figure 4.4 **Thermoset #2** solution (a) and **Thermoset #3** solution (b)

To evaluate the effects of incorporation of wheat straw, as well as three treatments of wheat straw on Acrodur curing, the prepregs containing wheat straw and 40% **Thermoset #1** were prepared. The wheat straw used was hammer milled particles (#2), on which two treatments, i.e. hot-water and NaOH treatment, were applied separately using the same methods described in Chapter 3. The NaOH treatment was conducted by soaking wheat straw in 3 % NaOH aqueous solution at straw/solution mass ratio of 1:2 at room temperature for 24 hours. Hot-water treatment was applied by boiling wheat straw in deionized (DI) water at temperature of 100°C for 2 hours. The treated wheat straw was then washed and vacuum-dried at 60–80°C to a moisture level of below 10 %. Then untreated and treated wheat straw samples were impregnated with 20% and 40% **Thermoset #1**. The pregregs of wheat straw-20% or 40% **Thermoset #1** are shown in Figure 4.5. The above prepared uncured and pre-cured Acrodur binders, and the prepregs were used for both TGA and DSC measurements.

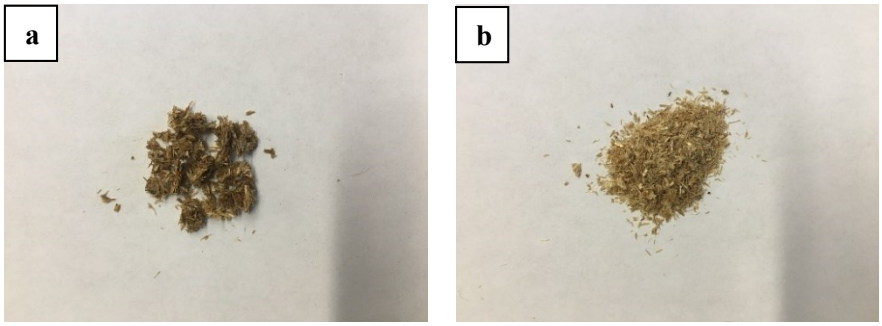

Figure 4.5 Prepreg of wheat straw #2-40% **Thermoset #1** (a) and prepreg of NaOH treated wheat straw #2-40% **Thermoset #1** (b)

4.3.2 Differential Scanning Calorimetry (DSC) Measurement

The DSC experiments were carried out in nitrogen atmosphere using TA instruments Q2000, while the static nitrogen flow was kept 50 mL/min. An empty DSC pan was used as a reference to balance the heat capacity of the sample pan. The samples with sizes ranging from 5 to 10 mg were placed in Tzero aluminum pans. The samples were either hermetically closed with lids or closed with non-hermetical lids (namely, hermetic pan or standard pan). When it is hermetically sealed, the Tzero hermetic pans hold maximum 300 kPa (3 bar), whereas the standard aluminum pans are unable to retain the sample during the experiment, due to expansion of formed water product. The heat flow was measured as function of the temperature and time for the samples. DSC measurements were conducted in three scanning modes, single scanning rate mode, the dynamic mode and isothermal mode, as follows.

4.3.2.1 DSC Experiment #1: Non-isothermal Method at Single Heating Rate

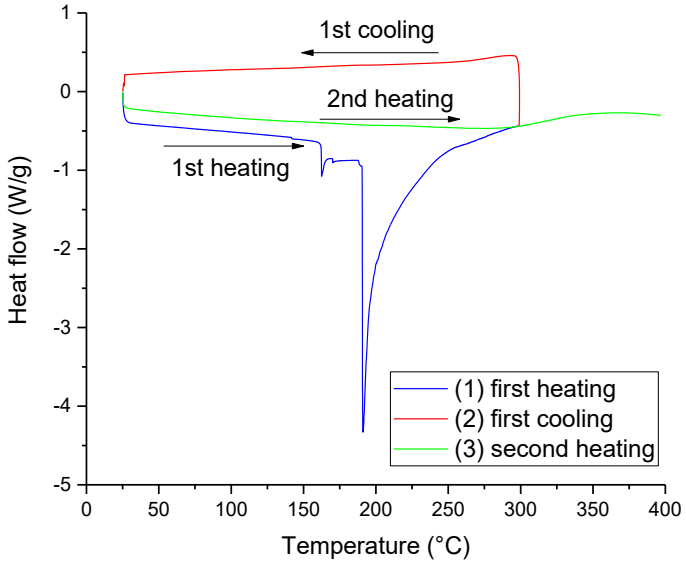

Figure 4.6 Illustrative example of DSC scanning profile

All the uncured and pre-cured Acrodur samples, including **Thermoset #1**, **#2**, and **#3**, the untreated and treated wheat straw-**Thermoset #1** prepregs, were heated from 25 to 300°C at a heating rate of 10°C /min followed by a cooling cycle at rate of 10°C /min. Then the second heating was applied to

measure the residual enthalpy. An illustrative example of DSC scanning profile is shown in Figure 4.46 where first heating, first cooling and second heating are encompassed.

4.3.2.2 DSC Experiment #2: MDSC Measurement

As learn previously, the T_g increases as the reaction proceeds. To carry out such investigations by DSC, the jump ΔCp in the specific heat at the glass transition must be of sufficient magnitude ($\Delta Cp=Cp1 - Cpg$, where Cp1and Cpg are the heat capacities in the liquid state and the glassy state, respectively). However, a low ΔCp value is characteristic of a fully cured thermosetting resin (Grenet et al. 2000). In some cases, the T_g is undetectable possibly due to mask of other thermal events.

The Modulated Differential Scanning Calorimetry (MDSC) was useful in this case. In MDSC, a sinusoidal modulation (oscillation) is overlaid on the conventional linear heating ramp to yield a heating profile in which the average sample temperature still continuously increases with time but not in a linear fashion. The net effect of imposing this more complex heating profile on the sample is the same as if two experiments were run simultaneously on the material – one experiment at the traditional linear (average) heating rate and one at a sinusoidal (instantaneous) heating rate. MDSC can be used to determine the evolution of the glass transition temperature (T_g) with the extent of the reaction and the T_g of the fully cured system, $T_{g\infty}$. By comparison to conventional DSC, the MDSC data reveals the complexity of the glass transition behavior, such as overlapping peaks, of the sample which can be transformed into meaningful information (Grenet et al. 2000).

The uncured **Thermoset #1** sample was placed in either a hermetic aluminum pan or a pan with a non-hermetic lid, and MDSC experiments were carried out in nitrogen atmosphere. The amplitude and the period of the oscillation during MDSC experiments were 2°C and 50 seconds, respectively. The average heating rate was varied between 1 or 3°C /min.

4.3.2.3 DSC Experiment #3: Non-isothermal Method at A Series of Heating Rates

Non-isothermal experiments on uncured **Thermoset #1** samples in hermetic pans were conducted at 5, 10, 15, 20 and 25°C /min from 25°C up to 300°C for the first heating and 25 to 400°C for the second heating at a constant rate of 10°C/min. In addition, the uncured **Thermoset #1** samples were also scanned in aluminum pans with non-hermetic lid, and with pierced lid, for non-isothermal analysis in the same temperature range at the same heating rates.

4.3.2.4 DSC Experiment #4: Isothermal Method at A Series of Temperatures

To simulate the compression molding conditions in practice, the Acrodur and prepreg samples both in hermetically sealed pans or in pans with a non-hermetic lid were scanned using isothermal scanning mode. The samples were first examined while curing temperature was kept isothermal at varied reaction time, and then the residual cure enthalpy was determined in the second heating at 10°C/min heating rate (also called postcuring). Heating profiles of isothermal DSC scans on uncured **Thermoset #1** and corresponding time are illustrated in Table 4.1 and Table 4.2 for hermetic and non-hermetic mode, respectively.

Table 4.1 Heating profiles of isothermal DSC measurement (in hermetic mode)

Isothermal temperature (°C)	Isothermal duration (minute)
130	5,10,15,20,30,40,50
140	5,10,15,20,30
150	5,10,15,20
160	5,10,15,20
170	2,4,6,8,10
180	2,4,6,8,10
190	2,4,6,8,10
200	2,4,6,8,10

Table 4.2 Heating profiles of isothermal DSC measurement (in non-hermetic mode)

Isothermal temperature (°C)	Isothermal duration (minute)
130	30,60,90,120
140	30,60,90,120
150	10,20,40,60
160	10,20,30,40
170	5,10,20,25
180	2,4,6,8
190	1,2,3,4
200	1,2,3

4.3.3 Thermogravimetric Analysis (TGA) Measurement

The TGA measurements were conducted using TA Instruments Q500. Sample sizes ranging from 10 to 20 mg were heated in TGA furnace from 35 to 650°C in nitrogen atmosphere. The mass loss of the samples was measured as function of the temperature and time. TGA scans were conducted in three scanning modes, i.e. single scanning rate mode, the dynamic mode and isothermal mode, as follows.

4.3.3.1 TGA Experiment #1: Non-isothermal Method at Single Heating Rate

The uncured, pre-cured **Thermoset #1**, **#2**, and **#3** samples, the untreated and treated wheat straw, and the wheat straw-**Thermoset #1** prepreg samples were heated from 35 to 650°C at a heating rate of 10°C /min in nitrogen atmosphere.

4.3.3.2 TGA Experiment #2: Non-isothermal Method at A Series of Heating Rates

Non-isothermal experiments on uncured **Thermoset #1** and prepregs of wheat straw-**Thermoset #1** were conducted at 5, 10, 15, 20 and 25°C /min from 35°C up to 650°C.

4.3.3.3 TGA Experiment #3: Isothermal Method at A Series of Temperatures

In isothermal TGA mode, the **Thermoset #1** samples were kept isothermally for a fixed time span of 5 minutes at 130, 140, 150, 160, 170, 180, 190, and 200°C, then the samples were heated at 10°C/min in the TGA furnace until 650°C.

4.4 Results and Discussions

Presented in this section are the results of fundamental kinetic study on cure reaction of thermosetting Acrodur in three heating modes, i.e. single scanning heating rate, non-isothermal method at a series of heating rates, and isothermal heating at a series of temperatures for varying times. The thermal curves of conversion versus temperature or time can be constructed from experimental data measured by both TGA and DSC. The TGA and DSC experimental data obtained using the dynamic methods were analyzed using model-free iso-conversional method—Friedman method to investigate the dependence of the activation energy with the degree of conversion. The TGA and DSC experimental data obtained by isothermal method were used to simulate the compression molding conditions and to structure the conversion–time plots. The baselines were determined by structuring a straight line between two points set as starting and ending points for area integration. The determination of baseline was arbitrary and operator-determined but the effort was exerted trying to be consistent for all the comparisons as much as possible and reasonable, at least within the comparisons.

4.4.1 Thermoset #1

4.4.1.1 Non-isothermal Method at Single Heating Rate

4.4.1.1.1 TGA Experiment #1

Presented in Figure 4.7 are the complied TGA thermographs at 10°C/min heating rate for uncured, and pre-cured **Thermoset #1** samples. It is seen that the thermal profiles of the **Thermoset #1** in Figure 4.7 consist of three distinct stages, except a minor mass loss below 150°C attributed to the evaporation of residual free moisture and probably lower molecular mass volatiles. The first peak occurred in the range of 130–275°C, whereas the second in the range of 275–380°C, and 380–500°C for the third. The latter two were considered to connect to the sample degradation and of no special interest in this chapter.

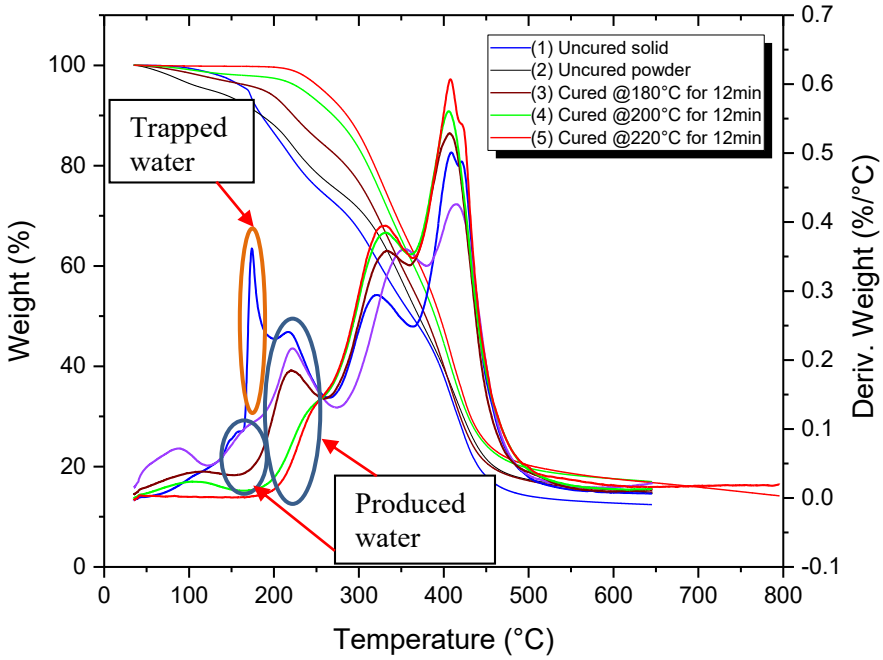

Figure 4.7 TGA thermographs of **Thermoset #1**, uncured solid (1) and uncured powder (2), pre-cured for 12minutes at 180°C (3), 200°C (4), and 220°C (5)

The weight loss within the temperature regime of 130–275°C was considered curing-related and of significant interest. The first peak for both uncured and pre-cured **Thermoset #1** was in the same temperature range of 150–275°C, however, the shapes of first peak were quite different upon a close look. The curve of uncured sample of bulky solid displayed a complex shape indicated as curve (1) in Figure 4.7. By zooming in this temperature regime, a small bump of minor magnitude was observed at low temperature (around 150°C), immediately followed by a sharp intense peak. This sharp peak suggested that the rate of weight loss of the uncured **Thermoset #1** started increasing significantly as

the temperatures were elevated to this point, reached a maximum in the vicinity of 175°C. Then a broad peak of considerable magnitude developed starting at 200°C, centered at approximate 218°C and ended at 265°C. The uncured powder **Thermoset #1** exhibited different TGA curve shown in curve (2). The only difference is that the sharp peak at 175°C is not seen.

On the other hand, in the thermograph of pre-cured **Thermoset #1**, the weight loss signal at 175°C disappeared, and only one single peak corresponding to the peak at 218°C appeared in this range. The peak position shifted slightly to higher temperatures and the corresponding areas, representing the mass loss, became smaller as the pre-cured temperature increased from 180°C to 200°C and then to 220°C, as demonstrated in Table 4.5, which summarizes the residual mass loss represented by the area under the DTA curves within the cure-related temperature regime for uncured and pre-cured samples. For the area integration, an arbitrary initial weight of resin was chosen from the TGA data at a temperature around 140°C after residual water has been removed. Further examination of the rate curves showed that the major curing related weight loss process appeared to begin after 140°C.

Table 4.3 Peak temperature and residual mass loss of uncured and pre-cured **Thermoset #1**

Thermoset #1	T_{peak} (°C)	$\Delta m_{residual}$ (%)
Uncured solid	220	23.29
Uncured powder	222	20.02
Cured at 180°C for 12min	220	12.89
Cured at 200°C for 12min	239	6.78
Cured at 220°C for 12min	242	5.30

So the difference in thermographs between uncured samples in two forms, i.e. the sharp peak in curve (1) indicated by the orange oval at range of 150–195°C implicates that it is possibly connected to the trapped moisture due to lagging effect of heat transfer and encapsulating effect caused by chunk of solid samples. The peak in range of 123–189°C in curve (2) disappeared in pre-cured sample (3), (4), and (5) and is connected to crosslinking. The weight loss should be derived from water evaporation produced via the curing reaction that causes the Acrodur to crosslink into a network solid. The origin of the peak at 210°C could also be derived from the polymerization reaction, probably with different mechanism. The whole range of 130 – 275°C is consistent with the publications that stated cure temperature range from 150–220°C (Rasyid et al. 2016) (Reck and Turk 1999) (Khalfallah, Marcel, et al. 2014). It was reported that cured Acrodur DS3530 (**Thermoset #1**) resists thermal deformation at

180°C (Khalfallah, Abbès, et al. 2014). The overlapping of peaks of trapped and produced moisture is problematic limiting further investigations of the cure main peak.

4.4.1.1.2 DSC Experiment #1 in Hermetic Mode

A series of DSC measurements with hermetic and non-hermetic modes were performed parallel to TGA measurement. The DSC signals in the same temperature range were analyzed and generally related to TGA thermographs.

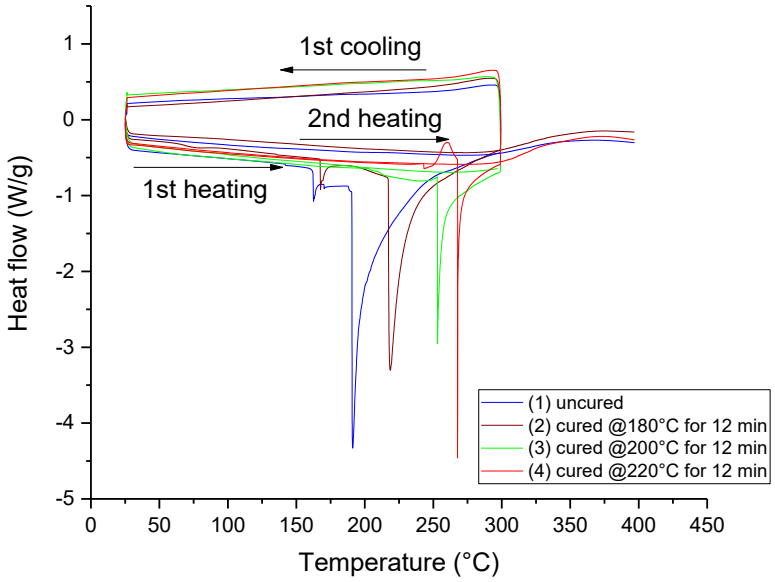

Figure 4.8 DSC thermographs of **Thermoset #1**, in hermetic mode, uncured (1), pre-cured for 12minutes at 180°C (2), 200°C (3), and 220°C (4)

The DSC thermographs at 10°C/min heating rate of the same samples investigated in 4.4.1.1.1 are presented in Figure 4.8. This figure shows three scanning curves for each heating rate: 1st heating, 1st cooling and 2nd heating. The thermal events of interest are seen on the 1st heating containing several peaks.

The curves of the 1st cooling and 2nd heating did not contain peaks. This indicates that no significant endothermic or exothermic events were observe during cooling or 2nd heating. It is possible in some cases to observe the glass transition temperature as a step change (not as a peak) in the DSC curve. However, no obvious transition that could be clearly attributed to T_g was observed here. The 2nd heating

curve shows a very shallow and wide transition centered at around 300°C. This transition could be attributed to some postcure reaction that may become relevant when the temperature is raised above the upper limit of the 1st heating, or to the onset of thermal degradation.

It is seen that the DSC thermograph of uncured sample for the first scan showed two endothermic regions. It should be noted that no the weak endothermic signals appeared at below 100°C that is related to the remaining water because the closed system prevents the moisture evaporation. A step down endothermic signal and baseline tilted toward endothermic direction were observed starting from the temperature of around 150°C, which could be connected to the glass transition of samples. A sharp distinct endothermic peak appeared right after and erupted out at the temperatures of 200°C, proceeding into the broad endothermic signal from this temperature up to 250°C or even higher to 300°C with a long trailing, where the curve leveled off the baseline. Similar to TGA analysis, the abrupt peak within this temperature region for uncured **Thermoset #1** can be regarded as a combination of two peaks, starting with a sharp intense peak pointing out at 200°C followed by a broad peak that is overlapping with it. However, the overlapping became in a greater extent for DSC than for TGA. The same trends were observed for three pre-cured samples, where the step down signals, sharp peaks as well as overlapped broad peaks shifted to higher temperatures as the pre-cure temperature increased from 180°C to 200°C and to 220°C. The appearance of post reaction peak for pre-cured samples indicated that the Acrodur reaction in temperature range of interest had not gone to completion due to either low temperatures or short heating times. The peak position and post-reaction enthalpy changed as a function of conversion. The integration of the peak using a linear baseline yields a value for the heat of cure or postcure.

Table 4.4 Characteristic temperatures and cure enthalpy of **Thermoset #1** in hermetic mode

Thermoset #1	T_{Peak} (°C)	ΔH_{total} (J/g)
Uncured	191	320
Cured at 180°C for 12 min	240	215
Cured at 200°C for 12 min	253	83
Cured at 220°C for 12 min	268	55

The temperature regime from 150 to 300°C was considered to cover the all the cure reaction related signals possibly combined with other thermal activities that occurs within this region. By examining

the temperature range, the heat of reaction or post-reaction was estimated by integrating the area of the second DSC peak of uncured or pre-cured **Thermoset #1** samples.

The curing characteristics peak temperatures and reaction heat, for uncured and pre-cured **Thermoset #1** are shown in Table 4.4. Observed was the position of second peaks at 191, 240, 253 and 268°C, respectively, for uncured and pre-cured **Thermoset #1** samples. The ultimate heat of reaction ($\Delta H_{Acrodur}$ = 320 ± 32 J/g in this case) was estimated by integrating the area of the second DSC peak of uncured **Thermoset #1**. For each pre-cured **Thermoset #1** sample, a post-reaction peak was observed and evaluated as shown in Table 4.4. As seen, the peak temperature shifted to higher position with decreased postcure enthalpy.

4.4.1.1.3 DSC Experiment #1 in Non-hermetic Mode

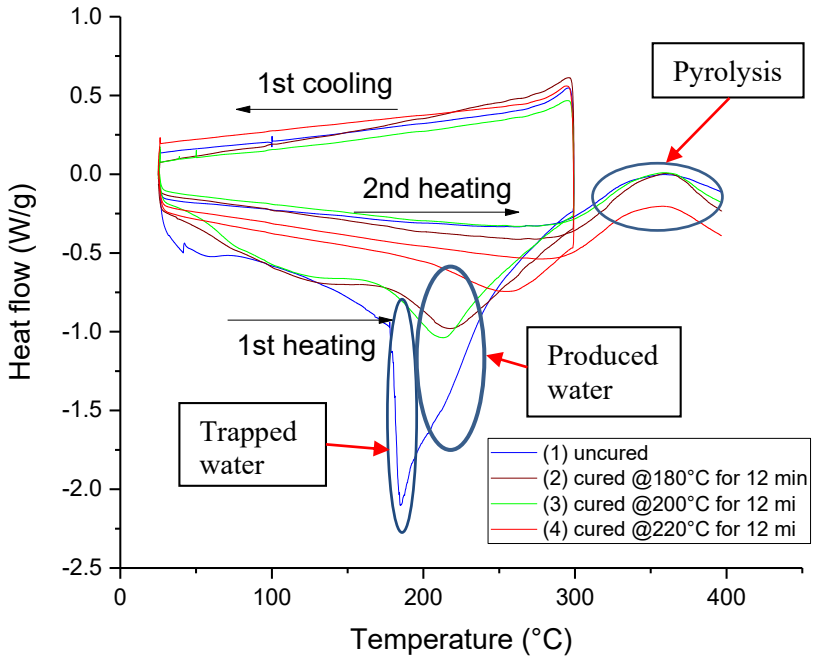

Figure 4.9 DSC thermographs of **Thermoset #1**, in non-hermetic mode, uncured (1), pre-cured for 12minutes at 180°C (2), 200°C (3), and 220°C (4)

Displayed in Figure 4.9 are the DSC thermographs in non-hermetic mode at 10°C/min of uncured and pre-cured **Thermoset #1**, which were the same samples as in the section 4.4.1.1.1 and 4.4.1.1.2.

The DSC curves of non-hermetic mode are quite different from those in hermetic mode. Unlike in hermetic pan mode, besides the peak below 150°C corresponding to contained moisture, only one big peak was observed and the cure reaction at higher temperature region. The observation is in good agreement with the findings from TGA analysis seen from previous section 4.4.1.1.1. In addition, it is observed that in non-hermetic mode that the cure peak started earlier at a lower temperatures and developed into a broad peak, associated with a baseline tilted toward endothermic direction. The endotherm shift to lower temperature was related to the fact that by removing the produced water from the system in open pan mode, as long as the product is produced, the esterification reaction is moving forward easily. Therefore, cure took place at lower temperatures and the broad peak indicates that the reaction kept happening within the course. The shift of baseline in endothermic direction is attributed to the increasing heat absorption of the sample as result of water evaporation. In addition, the DSC curves of second heating cycle shifting toward exothermic direction at above 300°C, indicated by blue oval in Figure 4.9, confirmed that the pyrolysis (thermal degradation) of material started at this temperature, which is in consistence with TGA results. Also, no softening below 300°C was discovered for second heating until the degradation happens which centered at 350°C, suggesting the cured **Thermoset #1** is rather stiff and strong below 300°C and is capable of keeping its integrity.

In contrast, the flat baseline in hermetic mode was observed at the beginning of temperature increase indicating that no mass loss appeared. Therefore, the cure reaction had not taken place until it reached the point indicated by a sharp peak shooting out at 200°C for uncured sample, when the reaction abruptly started accompanied by high rate of water evaporation. This observation of a higher onset and peak temperatures suggested that it was more difficult for the curing reaction to start when the system operated in hermetic mode, and it can be inferred that the removal of water by-product helped moving the cure reaction forward.

Table 4.5 Characteristic temperatures and cure enthalpy of **Thermoset #1** in non-hermetic mode

Thermoset #1	T_{Peak} (°C)	ΔH_{total} (J/g)
Uncured	185	209
Cured at 180°C for 12 min	217	66
Cured at 200°C for 12 min	213	86
Cured at 220°C for 12 min	257	55

Same as in last section, the curing characteristics peak temperatures and reaction heat, for uncured and pre-cured **Thermoset #1** are shown in Table 4.5. The same trend is seen that the peak temperature shifted to higher position with decreased cure or postcure enthalpy from uncured to precured sample, and from samples precured at low temperature to high.

4.4.1.1.4 DSC Experiment #2: MDSC

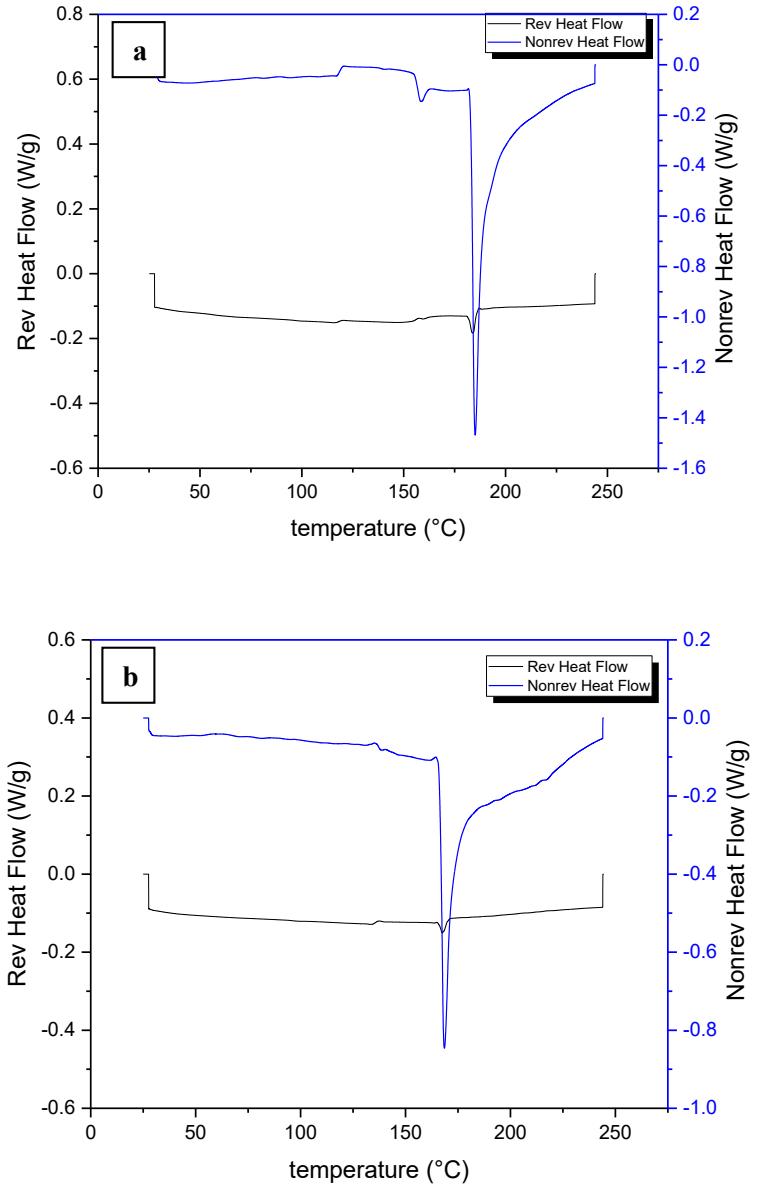

Figure 4.10 MDSC thermographs of **Thermoset #1** in hermetic (a) and non-hermetic (b) modes

The glass transition temperature of completely cured Acrodur was not detected with conventional DSC. It might be because of the overlapping of post-curing and glass transition in 250–300°C temperature region, or weak signal of transition, or no glass transition at all for Acrodur due to fully crosslinked structure with little mobility. The temperature modulated DSC was useful in this case. MDSC was used in order to detect the glass transition temperature of fully cured Acrodur, $T_{g\infty}$.

Figure 4.10 displays the MDSC thermograph in both hermetic and non-hermetic modes. By comparison to conventional DSC, the MDSC data, by separating the heat flow signal into reversible and non-reversible ones, the potential glass transition could be shown in reversible heat capacity signal. The glass transition can be observable by MDSC as step increase in heat capacity. There was no clear evidence that the glass transition happened in first heating, while no glass transition signal was observed below 250°C for the second heating. It may be attributed to no mobility of chains due to high crosslinking level. This observation is in agreement with the investigation reported by Gerst (Gerst et al. 2009) of no softening at 180°C and that made by Reck & Turk (Reck and Turk 1999) that once cured, Acrodur has no softening point and there is virtually no decrease in their modulus with increasing test temperatures (up to 220–230°C).

To clearly identify reaction peaks and cure temperature region, the thermographs of DSC (in both hermetic and non-hermetic modes) and of TGA of uncured **Thermoset #1** at the same of 10°C/min heating rate are superimposed in Figure 4.11.

By zooming in temperature region of 130 to 300°C, it is observed that both DSC and TGA thermographs were loosely consistent with each other, and the major peak in the DSC thermograph roughly corresponded to the temperature range where the major weight loss was found to occur. The weak endothermic signal below130°C was not connected with the polymerization reaction. The step down signal in hermetic DSC graph could be considered to correspond to first peak cure in TGA thermal curves. The broad peak from 200 to 300°C is comprised of two overlapping peaks for uncured **Thermoset #1**, whereas only the peak corresponding to 210°C appears for pre-cured samples. The difference may justify that the peak overlapped at lower temperature region could be first step cure, followed by the second step cure when some monomers or oligomers are still trapped within cross-linked matrix and may further diffuse and react, due to their lower mobility.

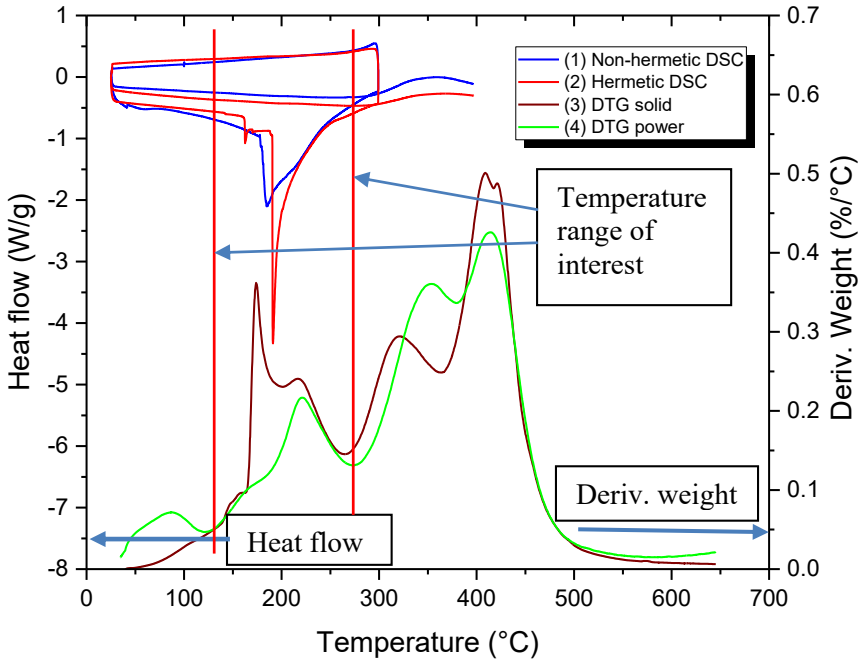

Figure 4.11 Superimposed DSC and TGA thermographs of uncured **Thermoset #1,** DSC in non-hermetic (1) and non-hermetic (2), and DTG solid (3) and powder (4)

The cure reaction is considered to take place mainly in the interval from approximately 130 to 300°C, possibly with coexistence of other thermal activities at lower temperature region, such as the evaporation of trapped moisture and small molecules. The overlapping peaks in TGA and DSC indicated the complexity of cure reaction, which leads to difficulty of suitable peaks isolation. Therefore, the whole temperature regime was chosen to for cure analysis. The uncertainty of existence of other thermal activities can be reflected in evolution of the activation energy with conversion in later sections.

4.4.1.2 Non-isothermal Method at A Series of Heating Rates

Non-isothermal experiments on uncured samples were conducted at 5, 10, 15, 20 and 25°C/min. Based on the temperature regime determined for cure reaction obtained from the DSC and TGA scans in previous section 4.4.1.1, the dynamic kinetic analyses were performed in the temperature range of 150–300°C for iso-conversion investigations. The straight baselines were established from onset of cure peak up to 300°C to quantify the areas above the endothermic curves for DSC analysis or under

DTA curves for TGA analysis. These data were further processed to obtain the fractional conversion (α) and the rate of reaction. The Friedman method was employed to obtain the evolution of the activation energy with the extent of the reaction. These calculations and all analyses and comparisons were performed using Origin software. The complexity of the reaction behavior of the Acrodur cure is reflected by the non-constant activation energy, which can be transformed into meaningful information to depict reaction mechanisms.

4.4.1.2.1 TGA Experiment #2 in Solid

The non-isothermal cure behavior of **Thermoset #1** was investigated by TGA within the temperature region of room temperature to 650°C at five different heating rates. Figure 4.12 shows the resultant TGA thermographs recorded at 5, 10, 15, 20, and 25°C /min.

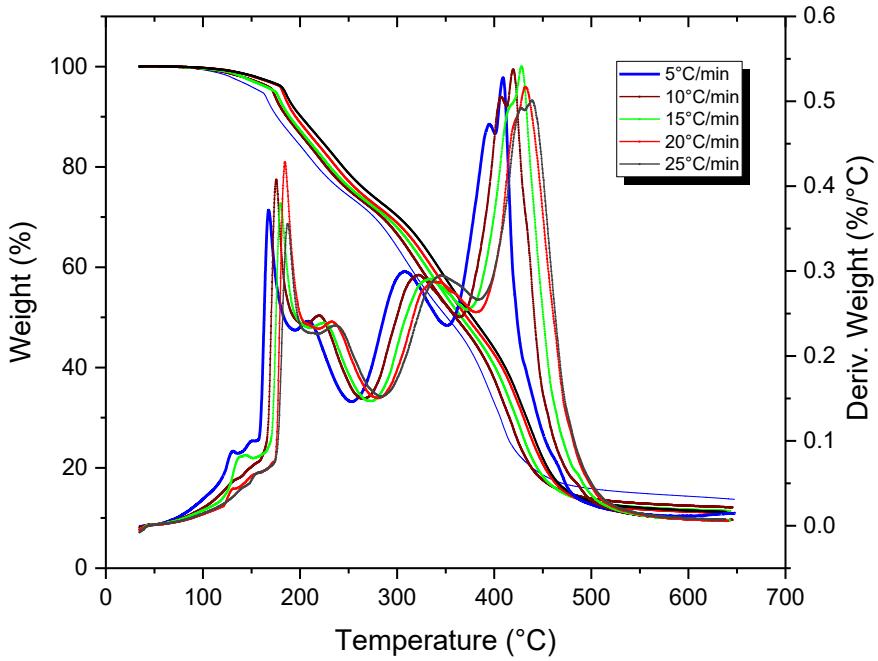

Figure 4.12 Non-isothermal TGA thermographs of **Thermoset #1** at a series of heating rates

It is seen that TGA curves for all of the rates followed the same general shape. Based on discussion in 4.4.1.1, the cure reaction is determined to occur in the temperature region starting around 150°C to nearly 300°C.

The degree of conversion is the fraction of Acrodur cured at time t (min) and is proportional to mass loss in comparison to the total mass loss within curing temperature regime, call the relative extents of cure. The analysis was normalized by determination of the weight at onset temperature of around 150°C as arbitrary initial weight. The weight fractions of **Thermoset #1** were calculated on a basis of the overall weight loss within this region. From the TGA curves, the values of the degree of cure reaction (α), ranging from 0 (completely uncured) to 1 (fully cured), at various heating rates can be calculated using Equation 4.4.

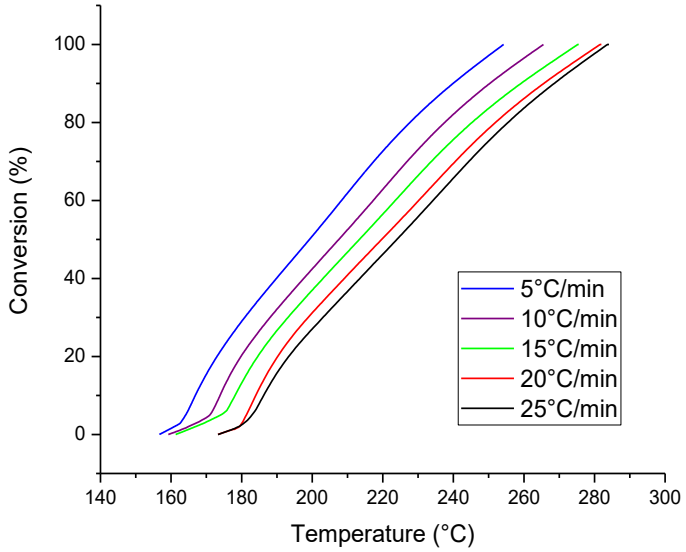

Figure 4.13 Fractional conversion of the reaction of **Thermoset #1** as a function of temperature at a series of heating rates

Figure 4.13 gives the evolution of the extent of the reaction at different heating rates as a function of the temperature. All the curves display similar sigmoidal shapes. Note that the curves were displaced to higher temperatures with increased heating rate. Increasing heating rate resulted in a curing process that was slower (reached later) and required a higher temperature to reach same conversion because the heat transfer is not as effective as they were for lower heating rates, as a result of mass transfer limitations of sample size. The highest overall rates of cure were observed to be around 0.4%/min at temperature of around 200°C.

The Friedman method was performed to calculate kinetic parameter of the curing reaction, activation energy (E_a). As discussed previously, $f(\alpha)$ is assumed to be constant for constant values of α, according to iso-conversional methods. Based on Equation 4.6, consequently, at a given relative conversion, the Ea can be calculated from the slope of the plot of ln (dα/dt) vs. 1/T for a set of heating rates. Therefore, a dozen values of α were selected, ranging from 0.05 to 0.95, at equal intervals. The values of $\Delta m_t/\Delta m_{total}$ and T were determined for each α for each TGA experiment. Plots of ln[$\Delta m_t/\Delta m_{total}$] versus 1/T are shown for each value of α in Figure 8.31, where the straight lines were obtained from least squares treatments of the data. The slope of each line is equal to –Ea/R, while the intercept is ln [A$f(\alpha)$]. As indicated in Figure 8.31 in Appendix E, the reaction with a higher Ea has a steeper slope; the reaction rate is thus very sensitive to temperature change. In contrast, the reaction with a lower Ea is less sensitive to a temperature change. Wherein, the Ea value is applied to represent the different degree of curing reaction, and the variation of Ea along the course of conversion to represent the reaction complexity.

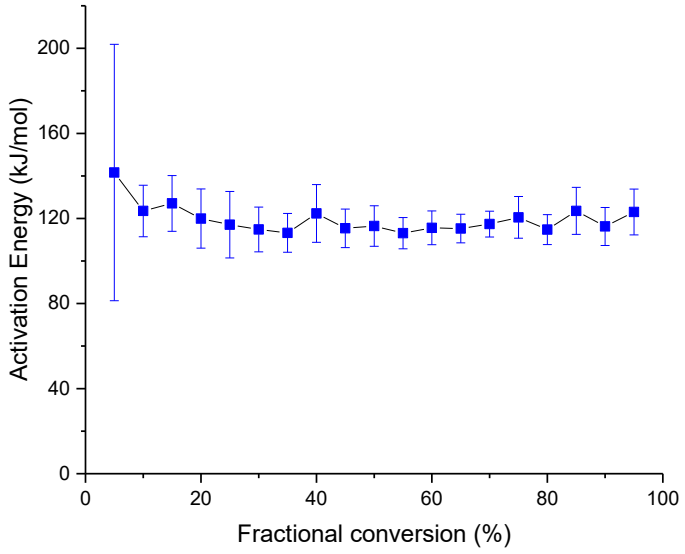

Figure 4.14 Dependence of activation energy with the extent of isothermal TGA cure of **Thermoset #1**

The values of Ea is plotted as functions of α in Figure 4.14. As known, determination of the activation energy was based on this combined heat involved in the temperature regime, called apparent heat, the activation energy is called apparent activation energy. The error bars calculated using student's T

distribution indicate that 68% possibility of activation energy falling in this range. It is observed that the activation energy starts at 142 kJ/mol at 5% conversion with 43% uncertainty. Then the activation energy slight decreased from 127 to 113 kJ/mol at 35% conversion, then increased to 122 kJ/mol followed by a gradual decrease. Overall, the activation energy holds steady in the range of 113–127 kJ/mol with an error of approximate 10% until 95% conversion. Nevertheless, the difference between the maximum (127 kJ/mol) and minimum (113 kJ/mol) is quite small.

Although DSC and TGA are unable distinguish the multiple reactions and transitions from measured signals, by examining the progress of estimated Ea as function of conversion, it is possible to extract the cure information reflecting cure behavior and mechanisms. The apparent activation energy is steady between 113–127 kJ/mol with a small variation, which reveals the simplicity of the reaction indicating that the reaction in this temperature regime might be single-step process with one mechanism. Data at very low conversion was subject to large error due to inconsistent behavior caused by heat transfer lagging effect and TGA baseline uncertainty caused by the interference of trapped moisture or low molecular weight moieties.

The TGA curves revealed important overlapping of the cure peak located within the temperature regime of 130–275°C with an extra peak, which is believed be attributed to evaporation process of trapped moisture. The overlapping of peaks makes it difficult to determine the enthalpy for each individual transition and prevents further analysis of the main polyesterification.

From the discussion offered above it is clear that several events were happening in the temperature range of interest 100 – 300^{o}C. The process of peak deconvolution was conducted on DTG curves using Origin software. The process started by creation of a simple baseline. The baseline subtraction was then performed to simplify the process of curve fitting the events happening during Acrodur curing. Three peaks were assigned corresponding to surface trapped moisture (1), trapped moisture (2) and cure. The weight loss accounted for around 32% of the total loss.

Figure 8.32 in Appendix E shows how the TGA experimental data curve of **Thermoset #1** at 5°C/min rate, as an example, was deconvoluted into individual peaks. Peaks 5, 4, and 3 corresponded to weight loss contribution of 4.37%, 3.29%, and 24.39%, respectively. The devolution method and statistics are presented in Table 8.7 in Appendix E, whereas the Table 8.8 in Appendix E presents the analysis of variance (ANOVA) for curve fitting. The Levenberg-Marquardt algorithm was employed to fit a Gaussian model to a set of measured data points by minimizing the sum of the squares of the

differences between the data points and the function. The values 0.98 of both R-square and adjusted R-square indicated that the Gaussian model described the experimental data well, although minor discrepancy was noticed as shown in Figure 8.32. The deconvolution results of the DTA curves for other heating rates are attached in Appendix E.

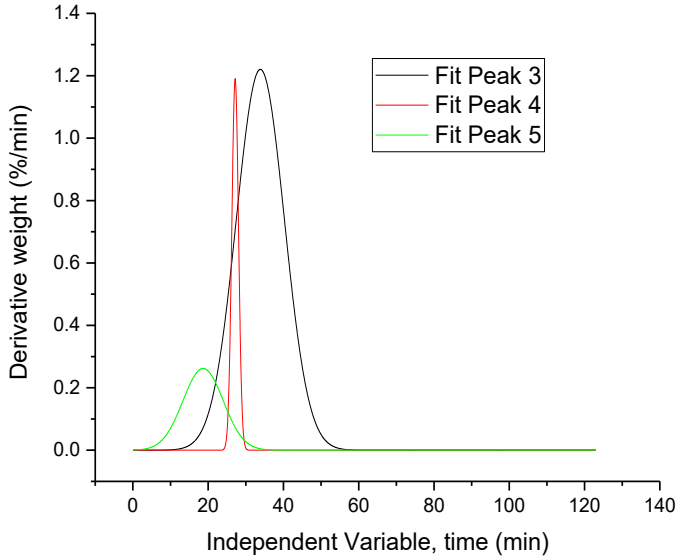

Figure 4.15 Three individual peaks within the temperature region

The peaks obtained from the deconvolution within the temperature region of interest were extracted and processed. Three peaks, that is peak 5, 4, and 3, appeared in the temperature regime of 100–300°C and were selected, as shown in Figure 4.15. The relative contribution of each peak to weight loss are listed in Table 4.6 based on the area under each curve. The assignment of these peaks 5, 4 and 3 were made according to the previous observations made using TGA and DSC.

Table 4.6 Relative weight loss contribution of fit peaks of interest

Peak	Corresponding activity	T_{peak} (°C)	Relative contribution
Peak 5	Moisture evaporation	128	13.63%
Peak 4	Moisture evaporation	171	10.25%
Peak 3	Cure	204	76.10%

Considering the complexity of the experimental curves and the uncertainty inherent to this process, two processing methods were applied for peak deconvolution. In **method #1** (single-peak-cure) only peak 3 was considered to be connected to cure reaction; whereas in **method #2** (triple-peak-cure) three peaks were taken into account for cure reaction.

The superimposed peaks and the fractional conversion as a function of temperature for **method #1** are presented in Figure 4.16 and Figure 4.17. The activation energy at a series of degrees of conversions were determined as the slop of ln (dα/dt) vs. 1/T at different heating rates, as shown in Figure 8.36 in Appendix E. The variation of activation energy as a function of conversion is illustrated in Figure 4.18. As seen, the activation energy for single-peak curing method holds rather steady at around 134–139 kJ/mol with small uncertainty across all conversions. The error bars were quite low in magnitude, because of the deconvolution process removing the signals from other events co-existing during the thermal analysis.

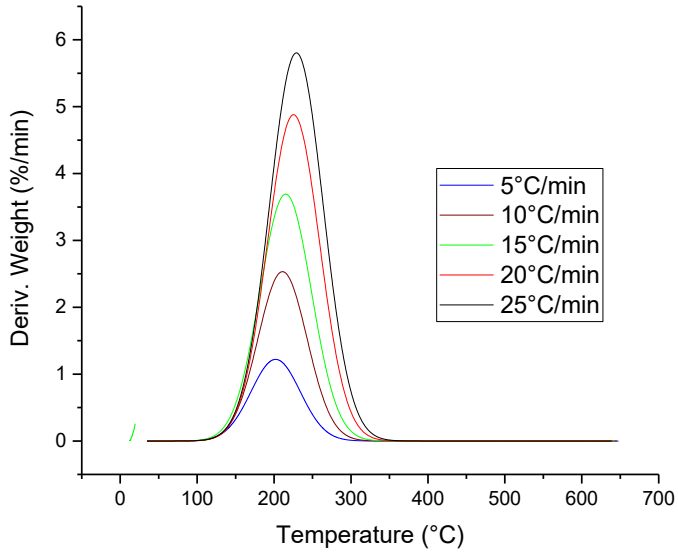

Figure 4.16 Superimposed DTG peaks at a series of heating rates, for single-peak-cure

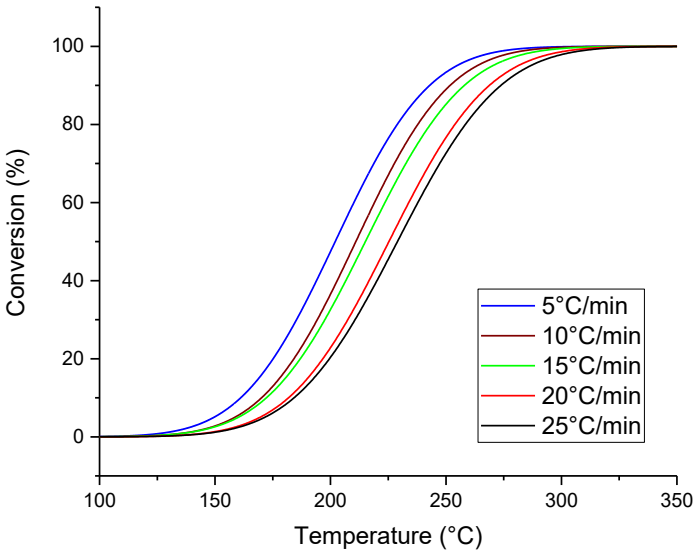

Figure 4.17 Fractional conversion of the reaction of **Thermoset #1** as a function of temperature at a series of heating rates, for single-peak-cure

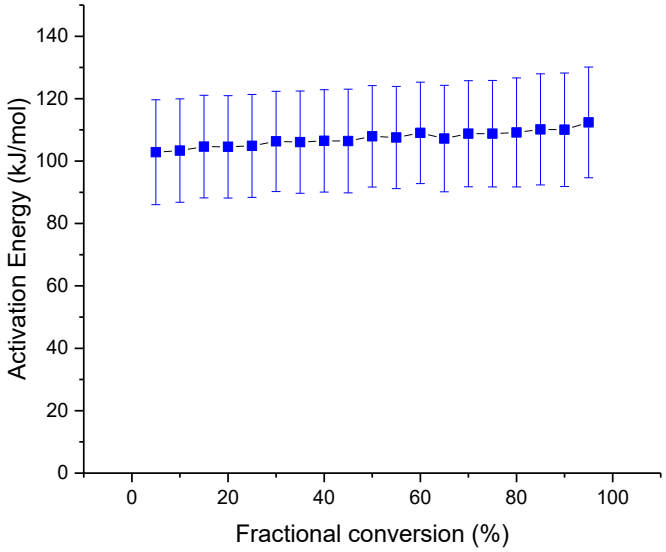

Figure 4.18 Dependence of activation energy with the extent of non-isothermal TGA cure of **Thermoset #1**, for single-peak-cure

For the triple-peak-cure **method #2**, the conversion as a function of temperature and the activation energy as function of conversion are shown in Figure 4.19 and Figure 4.20, respectively. It is observed that the activation energy started at low value of 79 kJ/mod and jumped to 143 kJ/mol at a conversion of 20%, then fell down to 91 kJ/mol at a conversion of 35%, followed by a gradual increase to 100 and 108 kJ/mol at 40% and 45% conversion, respectively, then held steady at around 110 kJ/mol until the end of conversion. Compared to single-peak-cure method, the variation of activation energy at a conversion below 35% reflected the complexation of the process, which is obvious when the three peaks were combined. Also the error bars were still quite small. For both methods the activation energy was observed to increase with increasing relative conversion, suggesting that the esterification proceeded with more difficult for the polymer to cure as conversion increased.

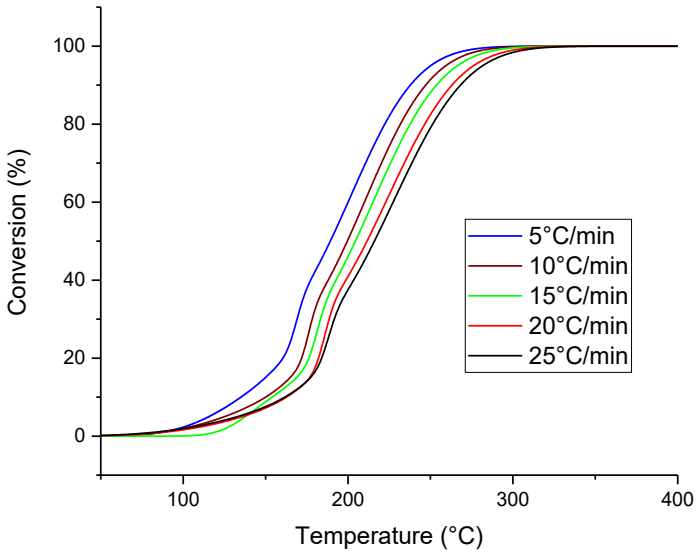

Figure 4.19 Fractional conversion of the reaction of **Thermoset #1** as a function of temperature at a series of heating rates, for triple-peak-cure

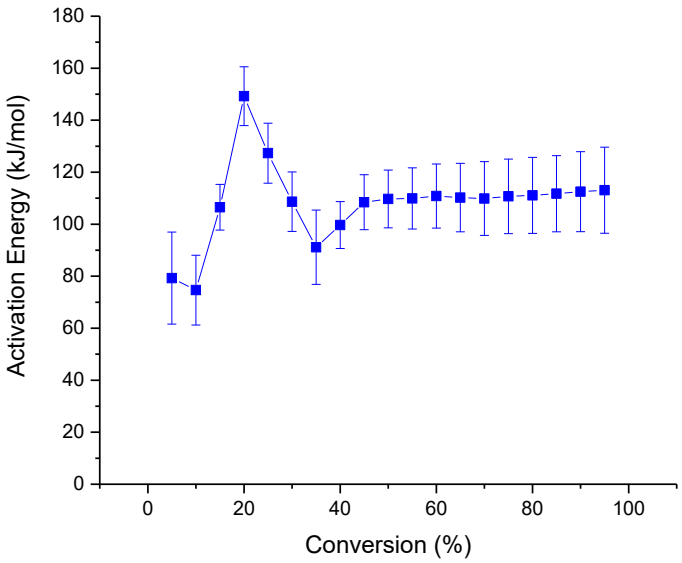

Figure 4.20 Dependence of activation energy with the extent of isothermal TGA cure of **Thermoset #1**, for triple-peak-cure

The deconvolution was repeated in order to separate overlapping TGA peaks and to determine the contribution of individual peaks. It made it possible to quantitatively analyze the individual steps in the curing process. This is helpful to better understand the fundamental properties of Acrodur cure reaction when associated with other thermal activities at lower temperatures. However, the introduction of subjective errors in the isolation and determination of peaks was unavoidable when the operator subjectively presumes and creates the criterion for isolation of superimposed peaks. Therefore, to minimize any contribution of subjective assumptions the analysis was based only on determination of temperature regions for the cure reaction, without presuming any criterion for isolation of peaks. The temperature plays a role in the curing reaction and proper temperature ranges for those events were previously identified with assistance of both DSC and TGA techniques. Therefore, the uncertainty in the analysis by deconvolution was minimized.

In summary, the curing process of Acrodur was discovered to be accompanied by evident overlapping of other events. Application of deconvoluation helped to isolate the events from each other but it is inevitable to introduce non-subject errors.

4.4.1.2.2 TGA Experiment #2 in Powder

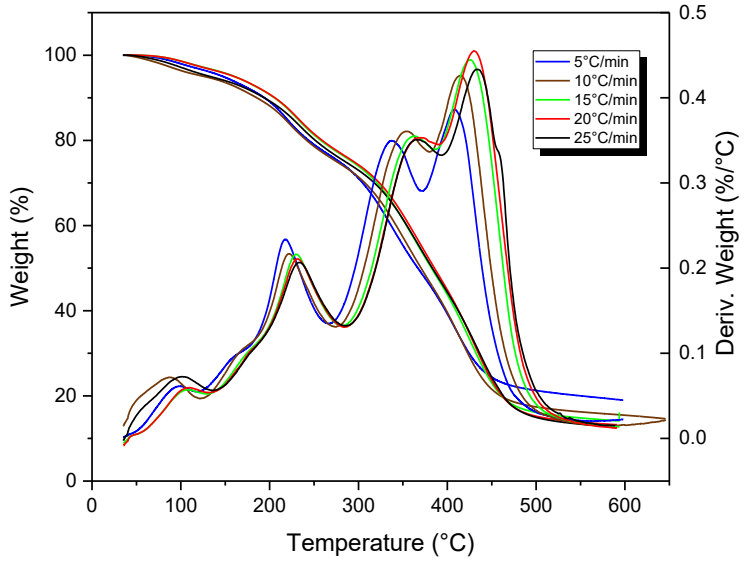

Figure 4.21 Non-isothermal TGA thermographs of **Thermoset #1** powder at a series of heating rates

The non-isothermal cure behavior of **Thermoset #1** powder was also investigated by TGA within the temperature region of room temperature to 650°C at five different heating rates. Figure 4.21 shows the resulting TGA thermographs recorded at 5, 10, 15, 20, and 25°C /min. As discussed previously, two main peaks exist in 130–275°C temperature regime, as shown in Figure 4.21, corresponding to weight loss of 4.90% ± 0.43% and 15.12% ± 0.48% on the base of total weight, and are believed to be related to the cure reaction. These values were quite consistent for all five heating rates. Based on the TGA experiments with five heating rates, the activation energy of **Thermoset #1** powder was determined as the slope of ln (dα/dt) as function of 1/T as shown in Figure 8.37 in Appendix E. The dependence of activation energy with conversion is illustrated in Figure 4.22. It is seen that the activation energy started from low value at 125 kJ/mol and increased to the maximum of 198 kJ/mold at 30% conversion followed by a steady trend around 180 kJ/mol.

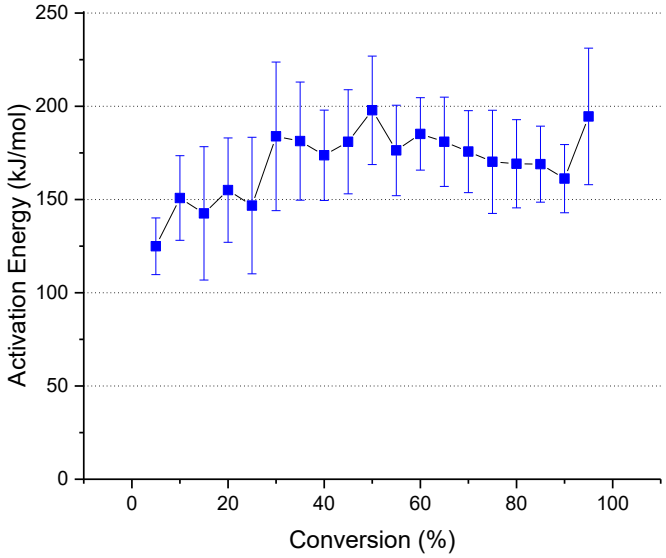

Figure 4.22 Dependence of activation energy with the extent of isothermal TGA cure of **Thermoset #1** powder

The observed trend was probably the result of the reactions of a process encompassing both chemical and diffusion kinetics. The kinetics of such reactions can be described using a diffusion control function. The actual reaction rate can be expressed as a product of the reaction rate of the chemically controlled reaction and the diffusion function. Two mechanisms may lead to the varied activation energies involved in course of curing. The variation of the activation energy can be ascribed to the increase in viscosity of the product as the degree of conversion increases. Similar behavior was observed for curing of isocyanate polymer (He and Yan 2005) (Daniel-da-Silva et al. 2010).

4.4.1.2.3 DSC Experiment #3 in Hermetic Mode

The non-isothermal cure behavior of **Thermoset #1** was investigated in hermetic pans using DSC. Figure 4.23 shows the DSC thermographs recorded at heating rates of 5, 10, 15, and 20°C/min. It is seen that the DSC thermographs were almost identical in shape for the different heating rates. The heat absorption appeared from 150°C to 300°C. The upper limit of 300°C for the 1st heating curve was chosen to prevent including thermal degradation. It also appeared that as the heating rate increased, the peak of cure reaction was delayed and shifted to higher temperatures.

The onset temperature, the peak temperature and reaction enthalpy of the endothermic peak of **Thermoset #1** at different heating rates were measured from the DSC curves and are shown in Table 4.7. The peak temperature was observed to shift to higher temperatures when the heating rate was increased. It was also found that the enthalpy value varied among various heating rates but for most heating rates its value was about 300 J/g (with exception at 5°C/min).

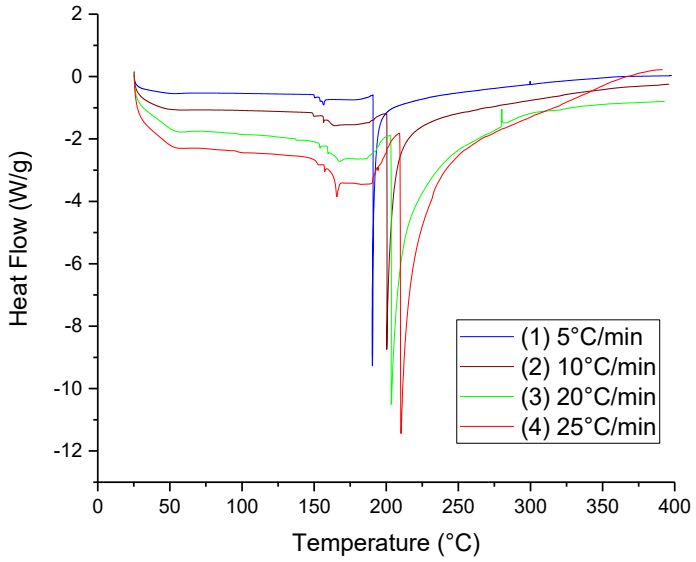

Figure 4.23 Dynamic DSC curves for the reaction of **Thermoset #1** at a series of heating rates, in hermetic mode

Table 4.7 Peak temperature and enthalpy of cure reaction of **Thermoset #1** at a series of heating rates, in hermetic mode

Heating rate, β (°C/min)	T_{Peak} (°C)	ΔH_{total} (J/g)
5	190	303
10	199	325
20	204	339
25	210	322

The degree of conversion is the fraction of Acrodur cured at time t (min) and it is proportional to enthalpy absorbed by sample within the curing temperature regime. This is also called the relative

extents of cure. From the DSC curves, the values of the degree of cure reaction (α) at various heating rates can be integrated by using equation 4.4. As discussed previously, according to iso-conversional methods f (α) is assumed to be constant for constant values of α. Based on Equation 4.10, consequently, at a given relative conversion, the Ea can be calculated from the slope of the plot of ln (dα/dt) vs. 1/T for a set of heating rates. Therefore, a dozen values of α were selected, ranging from 0.05 to 0.95, at equal intervals. Values of $\int_0^t \frac{dH}{dt} dt / \Delta H_{total}$ and T were determined for each α for each DSC experiment. Plots of ln $[\int_0^t \frac{dH}{dt} dt / \Delta H_{total}]$ versus 1/T are shown for each value of α in Figure 8.38 in Appendix E, where the straight lines were obtained from least squares treatments of the data. The slope of each line is equal to -Ea/R, while the intercept is ln [Af(α)].

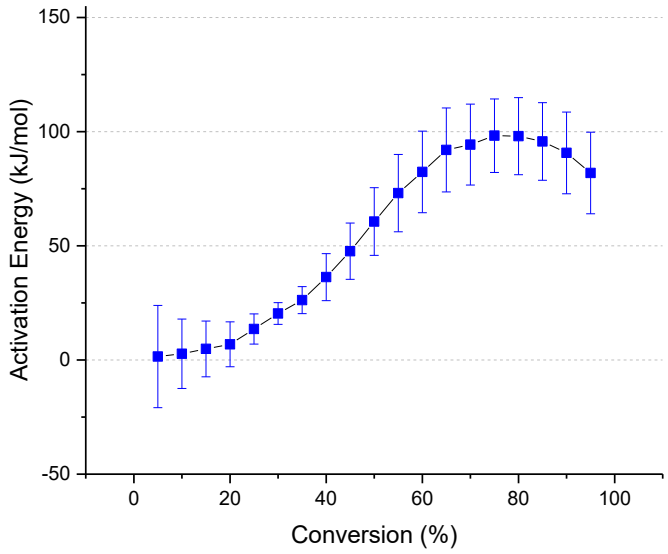

Figure 4.24 Dependence of Ea with the conversion of non-isothermal DSC cure of **Thermoset #1**

The values of apparent activation energy, Ea, is plotted as functions of α in Figure 4.24. The apparent activation energy increased from near 0 to 98 kJ/mol at 75% conversion with the large variation at low conversion, and then started to drop gradually to 82 kJ/mol. Data at very low conversions is subject to large errors due to DSC baseline uncertainties and a low signal-to-noise ratio. Ea increased with increasing relative conversion, suggesting that as the esterification proceeded it was more difficult for the polymer to cure. The shape of the DSC trace revealed the complexity of the reaction, indicating that the reaction in this temperature regime is a complex process that might combines more than one

mechanisms. The change in the activation energy suggests that parallel reactions are likely taking place simultaneously or the mechanism of reaction is changing. Similar to results of TGA, as indicated in Figure 8.38, the reaction with a higher Ea had a steeper slope; the reaction rate is thus very sensitive to temperature change. In contrast, the reaction with a lower Ea is less sensitive to a temperature change.

As learned from TGA analysis, there are two peaks overlapping, possibly representing two mechanisms. However, the peaks are overlapped to great extent in the DSC thermographs and there is no clear way to isolate such peaks. In this case, an approach to force deconvolution could result in misinterpretation of experimental dada. Therefore, DSC signals were analyzed as a whole, meaning inclusion of thermal evaporation.

It should be noted, although hermetic pans were used, which hold up to maximum 3 bar, depending on the amount of sample that was examined and how well the lids were closed, it is possible the vapor burst off the lid leading to loss of mass. To ensure that mass is constant, the sample was placed in a hermetically sealed pan and the weight was measured before and after each DSC experiment.

4.4.1.2.4 DSC Experiment #3 in Non-hermetic Mode

The **Thermoset #1** was also investigated non-isothermally in non-hermetic mode at four or five different heating rates. Figure 4.25 shows the resultant DSC thermographs recorded at 5, 10, 15, and 25°C /min for pans closed with non-hermetic lid. The figure shows three scanning curves for each heating rate: 1st heating, 1st cooling and 2nd heating. The thermal events of interest are seen on the 1st heating containing several peaks. The same trend is found as in non-hermetic mode in Figure 4.15, while the difference mainly lies in the shape the cure peaks. The peaks were much broader with a tilted baseline. The heat absorption started at 150°C and proceeded to around 250°C. It is noted that the increasing heating rates shifted the peak to higher temperatures.

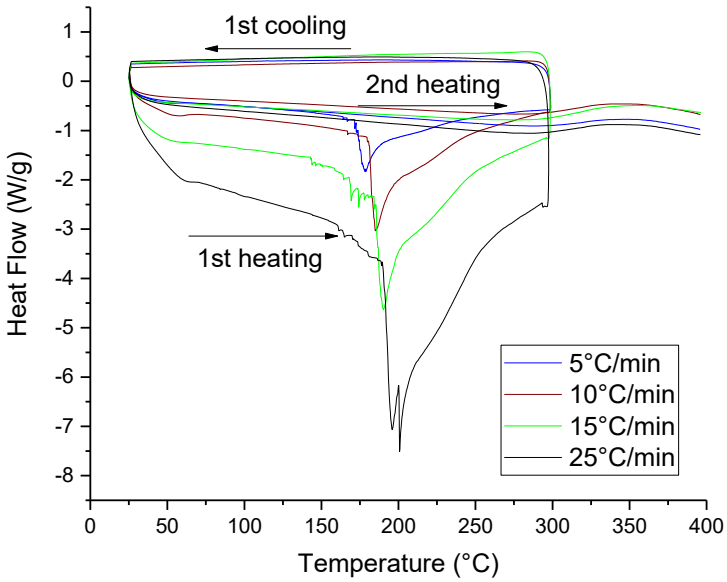

Figure 4.25 Dynamic DSC curves of **Thermoset #1** at a series of heating rates, in non-hermetic mode

The peak temperature and reaction enthalpy of the endothermic peak of **Thermoset #1** at different heating rates were extracted from the DSC curves as shown in Table 4.8. The extracted data reflects the reactivity, the temperature of maximum cure rate, and the amount of energy involved. In open pan mode, the total enthalpy is due to the value of cure enthalpy and the water (by-product) evaporation enthalpy.

Figure 4.26 gives the development of the extent of the reaction at different heating rates as a function of temperature. All the curves have similar sigmoidal shapes.

Table 4.8 Peak temperature of **Thermoset #1** reaction at a series of heating rates, ini non-hermetic mode

Heating rate, β (°C/min)	T_{Peak} (°C)	ΔH_{total} (J/g)
5	178	307
10	185	303
15	190	308
25	196	292

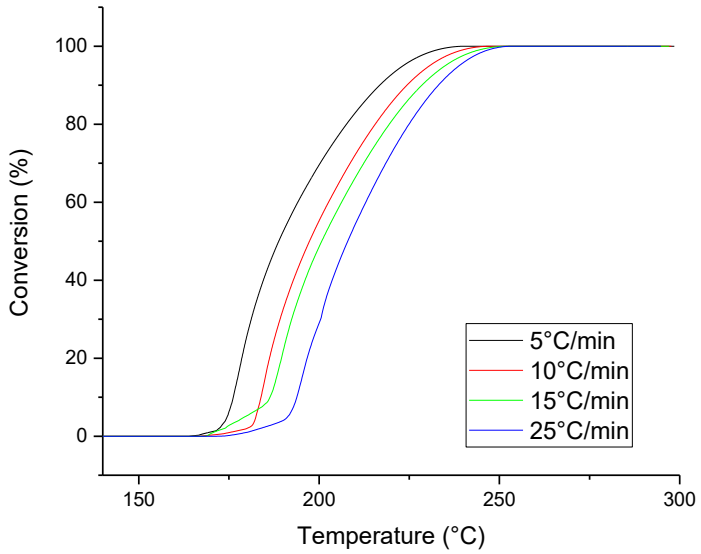

Figure 4.26 Fractional conversion of **Thermoset #1** as a function of temperature at a series of heating rates, in non-hermetic mode

The Freidman mothed was applied by producing the plots of ln (dα/dt) versus 1/T for each value of α shown in Figure 8.39 in Appendix E. The values of Ea were plotted as a function of α in Figure 4.27. The apparent activation energy varied from 105 to 232 kJ/mol. Ea increased with increasing relative conversion suggesting that as the esterification proceeded it was more difficult for the polymer to cure. The DSC curves and the dependence of Ea with the conversion are in agreement with each other and their shapes revealed the complexity of the reaction indicating that in this temperature region this is a complex process that might combines more than one mechanisms or that parallel reactions take place simultaneously.

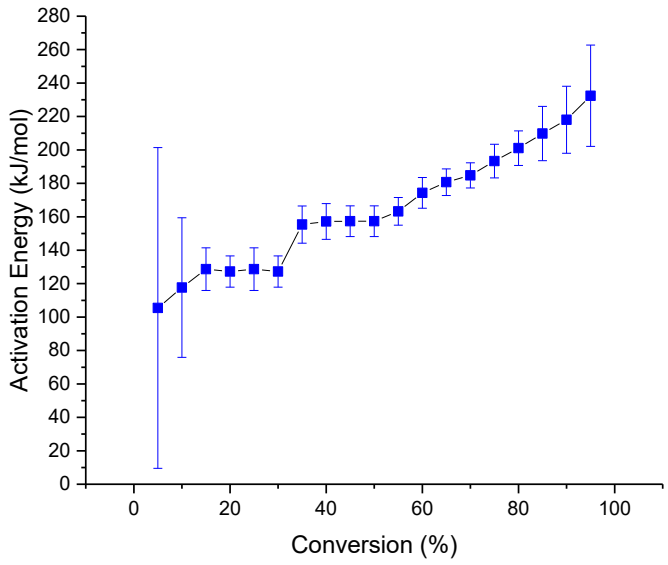

Figure 4.27 Dependence of activation energy on the extent of the reaction of **Thermoset #1**, in non-hermetic mode

The non-hermetic mode is not as accurate as hermetic mode because the mass loss during the measurement due to water evaporation creates a complication for two reasons: the contributions of the enthalpy of evaporation and the changes in the weight that is used in the calculation of heat of reaction (assumed constant in other calculations). Moreover, the appropriate determination of the onset and end points of the data range played a more important role due to complexity of thermal events.

It is also necessary to consider thermal lag effects resulting from a poor heat transfer when the chunks of solid samples were used. This effect was eliminated by using ground power samples which were evenly placed in the DSC pans.

The sample **Thermoset #1** powder was investigated using non-hermetic mode for activation energy estimation as shown in Figure 4.28. Table 4.9 displays the onset and peak temperatures and enthalpy involved in the temperature regime of interest. The slope of ln (dα/dt) as a function of conversion is illustrated in Figure 8.40 in Appendix E. As seen in Figure 4.29, the activation energy gradually increased from 149 kJ/mol to 291 kJ/mol as the cure reaction progressed. The activation energy tended to increase with the extent of the reaction, which indicated that the more energy was required at latter portion of conversion. The increase in Ea as the reaction proceeds under non-isothermal conditions

might be a consequence of the contribution of secondary reactions that may occur at higher temperatures, such as vitrification, which led to the difficulty of molecule mobility as a result of increased degree of crosslinking. The finding is in consistence with the results in TGA analysis of **Thermoset #1** powder.

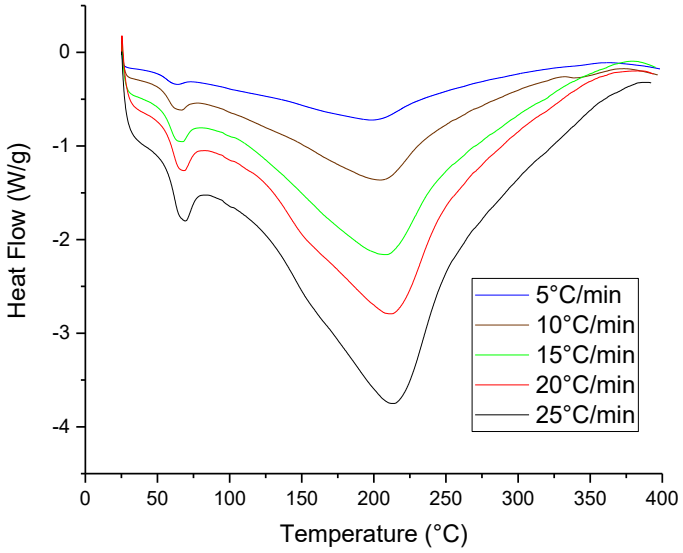

Figure 4.28 Dynamic DSC curves of **Thermoset #1** powder at a series of heating rates, in non-hermetic mode

Table 4.9 Onset and peak temperature and enthalpy of cure reaction of **Thermoset #1** powder at a series of heating rates, in non-hermetic mode

Heating rate, β (°C/min)	T_{Onset} (°C)	T_{Peak} (°C)	ΔH_{total} (J/g)
5	151	199	95
10	156	205	97
15	160	209	110
20	168	214	106
25	167	215	118

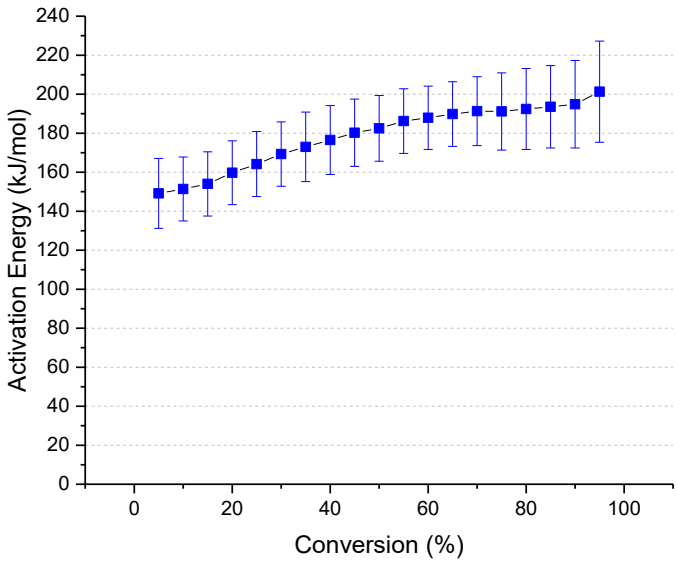

Figure 4.29 Dependence of Ea with the extent of non-isothermal DSC cure of **Thermoset #1** powder

4.4.1.2.5 Discussions

The model-free iso-conversional method was successfully applied to non-isothermal DSC and TGA data of Acrodur curing, in both hermetic modes and in both solid and powder forms. The method yielded a dependence of the effective activation energy on the extent of cure. The shape of the DSC and TGA traces revealed the complexity of the reaction, indicating that the reaction in this temperature regime is a complex process that might combine more than one mechanisms. The resulting Ea values derived from both TGA and DSC did reflect changes in the reaction mechanism and kinetics with the temperature and extent of conversion, suggesting that multiple reactions took place during the process. The variation in the values of activation energy may be related to uncertainty of determination of temperature range studied. A nonlinearity of Arrhenius plot normally resulting from the temperature dependence of reaction mechanism can also contribute to the large uncertainty as a consequence.

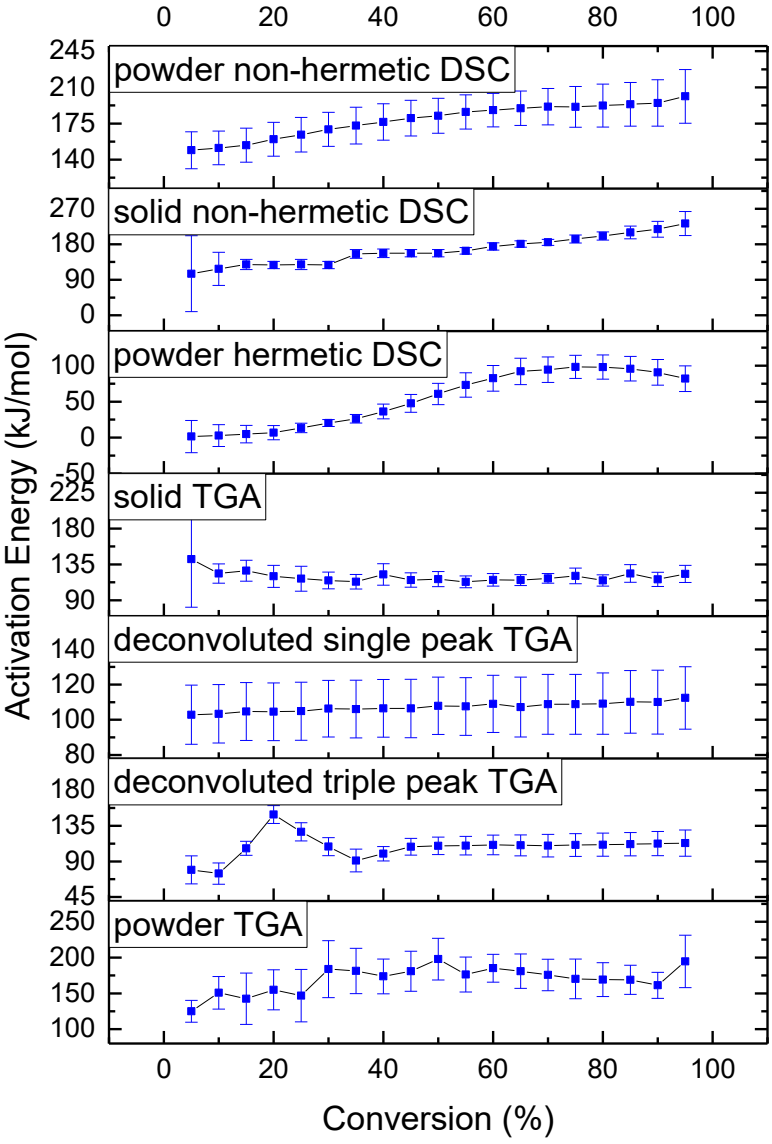

Figure 4.30 Comparison of activation energy of **Thermoset #1** from different methods

The activation energies Ea obtained from the combinations of two techniques of DSC and TGA, two modes of hermetic and non-hermetic, and two forms of solid and powder are plotted in Figure 4.30 and correlated with each other. As shown in Figure 4.30, the differences in the activation energy varied significantly with variable uncertainty. However, it is apparent that the DSC derived activation energy showed the agreement in following the same or similar increasing trend. **Thermoset #1** exhibited a

higher activation energy at high conversion than at low conversion in the curing process. This meant that more heat was needed to cure at high molecular weight. On the other hand, the activation energy obtained from TGA measurements remained relatively steady and exhibited slight increasing intendancy during the whole course of curing, except for deconvolution of single-peak-cure analysis. The discrepancies of activation energies obtained from DSC and TGA experiments are likely to be derived from the techniques used and also to the selection of the onset and the end point selected of the range of interest.

In conclusion, the shape of the DSC and TGA curves revealed the complexity of the reaction, indicating that the reaction in this temperature regime was a complex process that might combined more than one mechanisms. The resulting values estimated from both TGA and DSC did reflect changes in the reaction mechanism and kinetics with the temperature and extent of conversion, suggesting that multiple reactions took place during the process.

4.4.1.2.5.1 Two Possible Mechanisms

The cure of Acrodur is a condensed phase reaction, which typically include more than a single reaction step (Vyazovkin 2000) (Vyazovkin 2015). If a process involves more than one step, the activation energy Ea is typically found to vary with conversion (α) and/or temperature (Vyazovkin 2016). Therefore, it is no wonder that variable estimated activation energy was observed in the kinetic study of Acrodur cure. The overall increasing trend of activation energy as function of conversion is noticeable in Figure 4.30 with the exceptions. This, in turn, revealed the complexation of the Acrodur cure.

The activation energy remains relatively constant at low level up to around 40% conversion. Beyond 40% conversion the Ea values raised. This behavior is attributed to high crosslinking which reduces the molecular mobility and the process changes from being kinetically controlled to diffusion controlled. The activation energy required to achieve 100% conversion of **Thermoset #1** is more than that required below 40% conversion, depending on the thermal analysis technique used (TGA or DSC), analysis condition (hermetic or non-hermetic), and sample form (solid or powder). The higher activation energy is the more sensitive the reaction is to temperature. This implies that the temperature must reach a certain threshold to let the reaction occur. This is true for this case and was confirmed by the isothermal experiments. It was concluded that the assumption of the validity of a single-step equation when restricted to a given α value holds for complex reactions that combine both the chemically controlled

part of the reaction and the diffusion-controlled part, in agreement with the kinetic study conducted by Sbirrazzuoli (Sbirrazzuoli 2019).

4.4.1.2.5.2 Effect of Pressure

Esterification is a well-known process, from which the esters of carboxylic acids can be produced. Esterification is a reversible reaction limited by the low equilibrium conversion and has been performed with excess alcohol and/or by continuous removal of water to shift the equilibrium conversion (Scott 1995). The differences in cure behavior between the hermetic and non-hermetic curves, and solid and powder samples can be very informative. Figure 4.31 demonstrates the DSC thermographs obtained in hermetic and non-hermetic modes with two sample forms, i.e., solid Figure 4.31 (a) and powder Figure 4.31 (b), respectively. It is apparent that the pressure showed significant influence on cure behavior by controlling the removal of vapor phased water. When the system was closed (hermetic mode), the reaction started and reached maximum rate at higher temperatures than when the system was open (non-hermetic mode). It is reported that the reverse reaction no matter involving gaseous phase or not, does not affect the activation energy, and the height of the reaction energy barrier is constant (Lesnikovich and Levchik 1985). However, the value of pre-exponential factor A grows with supersaturation (pressure due to present of gaseous molecule) since it affects the nucleation rate (Prodan et al. 1976) (Pysiak and Glinka 1981). This contributes to the change in reaction rate.

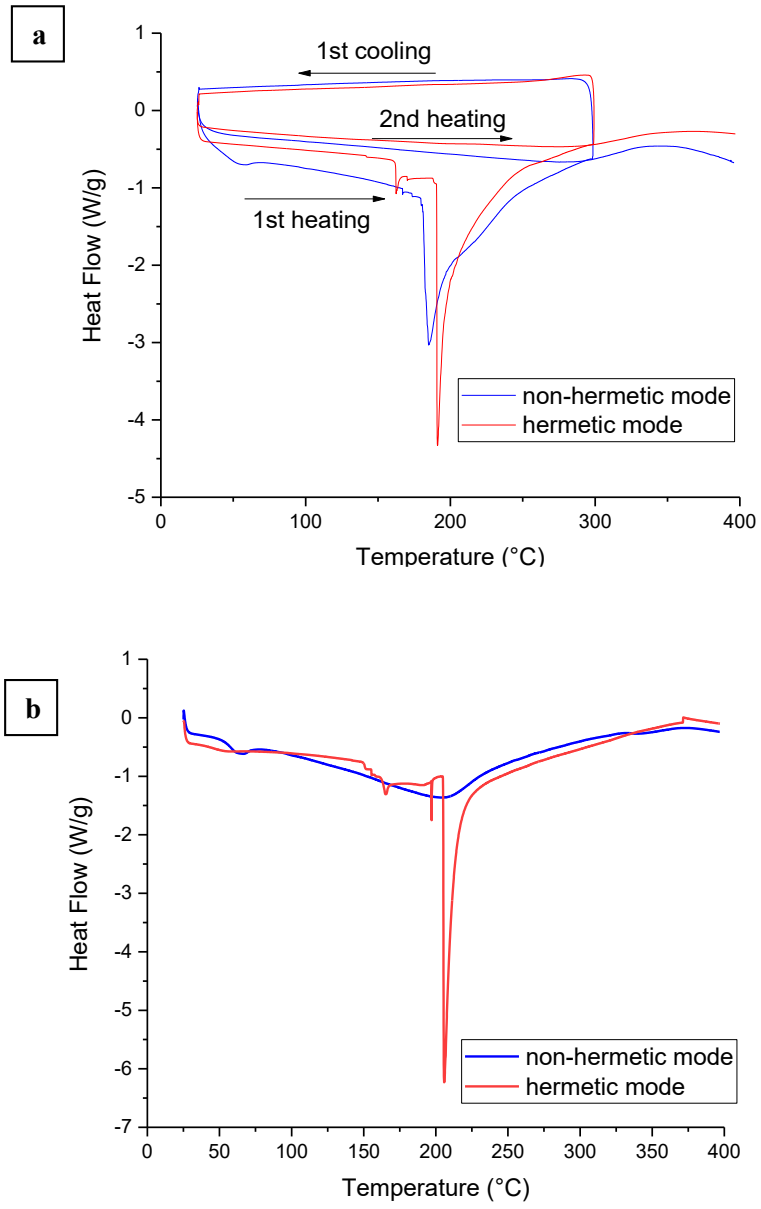

Figure 4.31 DSC comparison of **Thermoset #1** solid (a) and powder (b) between non-hermetic and hermitic modes (10°C/min)

In practice, the composite prepreg is compression molded in the mold during about 10 minutes with 2–3 times of aeration. Therefore, the condition is more like the combination of two methods, which would be equivalent to alternating hermetically sealed pan and pan with regular lid (non-hermetic). When the composite pregreg is compressed, it is equivalent to hermetic mode because the water

produced is retained in the material. When the compression is released, it is more like open pan mode when the water vapor leaves the system freely. So the whole compression molding process is considered as a successful alternation of compression and ventilation steps.

Therefore, it is really necessary that a few times the ventilation (burping) be performed during the compression molding. By removing the product water when ventilation is applied, the cure reaction goes forward faster. Additionally, the controlled release of moisture also contributes to avoiding formation of blister and delamination of pressboards caused by burst and retention of water vapor.

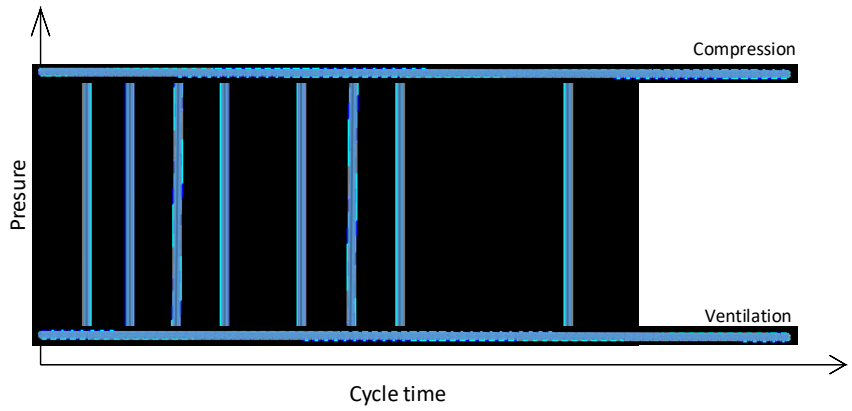

Figure 4.32 Compression and ventilation steps alternating in compression molding

4.4.1.2.5.3 Effect of Particle Size (Sample Form)

It is known that reaction rate has to do with the particle size of the solid material. The size of a solid shows the effect on the reaction rate by changing surface area and hence on the effective contact area. Therefore, the more finely divided the solid is, the faster the reaction happens, because the powdered solid has a greater surface area and higher free energy of the surface than the single lump. This contributes to the reduction of the barrier effect and facilitates the collision between the reactants as well as the release of gaseous products (Tamhankar and Doraiswamy 1979).

The solid sample showed the similar effect on cure behavior as shown in Figure 4.31 (a), where with non-hermetic pan, the solid sample exhibited the similar curve shape as hermetic mode. On the contrary, the impact of pressure was more significant for powder sample as seen in Figure 4.31 (b). When non-hermetic pan was used, the thermograph of the powder sample completely changed it shape. The sharp peak disappeared and became a broad peak. As known, the cure reaction of Acrodur is an addition-by-elimination solid-solid reaction, wherein the solid reactants react to give a solid product, and in addition

a gaseous product is involved. Therefore, it is controlled by the simultaneous influence of reaction and diffusion. In a solid-solid reaction, the immobile product layer formed may offer a barrier to the progress of the reaction (Tamhankar and Doraiswamy 1979).

4.4.1.3 Isothermal Method at A Series of Temperatures

The study of **Thermoset #1** was carried under isothermal condition using TGA and DSC to complement the studies as variable temperatures (scanning). These conditions (temperature and time) were set to approximate the compression molding conditions of the prepreg containing **Thermoset #1**, where the temperature of press platens is meant to be constant for a certain time to cure the prepreg. In this section, the cure behavior of **Thermoset #1** was investigated isothermally. The isothermal measurements were performed at equal intervals of 10°C between 130 and 200°C for the first heating. Before starting each experiment, the samples were completely uncured (0%). The heating stages were applied. The first heating stage was used to study the effect of constant temperatures for curing the samples, without necessarily achieving full conversion. Therefore, the fist isothermal state is expected to provide a certain degree of curing (conversion) depending on the combination of temperature and time. The second heating was applied to ensure the resin is fully cured (100%). The enthalpy measured in second stage is the residual heat from the first heating. The second stage is called postcuring. Measurement of the endotherm in the second heating indicated that the sample was not fully cured in the first heating. The residual enthalpy method (measurement of the enthalpy on the second stage) is a favorable method because it is simple and provides a more reliable way to determine the baseline. By quantifying the residual heat in postcuring, the degree of cure is easily determined according to Equation 4.5 and the relation of conversion with t (time) or T (temperature) was constructed.

4.4.1.3.1 TGA Experiment #3 for 5 Minutes

A series of TGA measurements of **Thermoset #1** were performed isothermally at a temperature in the range of 130–200°C using the interval of 10°C, i.e. 130, 140, 150, 160, 170, 180, 190, 200°C for a time of 5 minutes. The samples were then heated at 10°C/min up to 650°C to measure the residual mass loss. The second heating completely cured **Thermoset #1** and the mass loss measured was residual mass loss from the first isothermal heating.

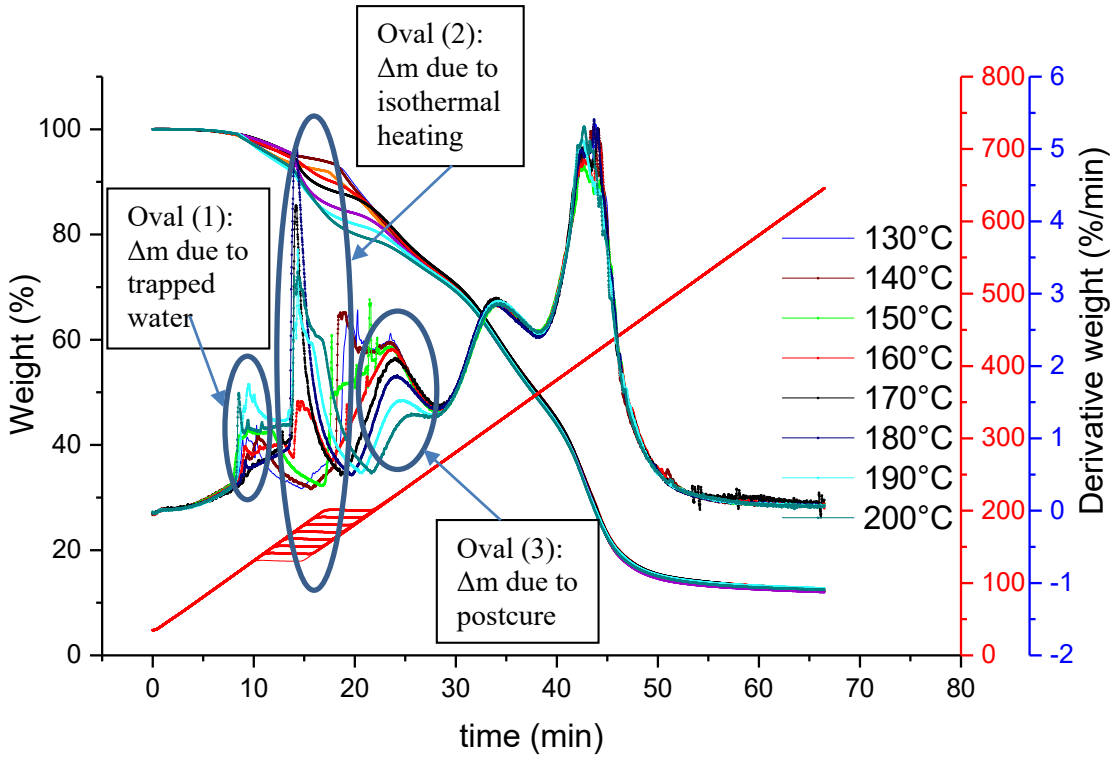

Figure 4.33 A series of TGA (time derivative) curves at 10°C/min of **Thermoset #1** cured isothermally at different temperatures for 5 minutes

* Left axis is weight % (black), first right axis is temperature (inner, red) and second right axis is derivative weight with time (outer, blue)

Isothermal TGA curves obtained at each pre-determined temperature from 130 to 200°C for fixed curing duration of 5 minutes are given in Figure 4.33. It should be noted that DTG signal was based on time, and the TGA and DTG curves were plotted against time, instead of temperature as other plots, for better demonstrating of isothermal process. It is followed by Table 4.10 that summarizes the first isothermal and residual weight loss for each temperature. The conversion (α) was calculated using Equation 4.4, where $\Delta m_{total} = \Delta m_{iso} + \Delta m_{residual}$. Figure 4.34 shows the obtained conversion – isothermal temperature relationship Experiment #3 for 5 minutes.

Table 4.10 Residual weight loss and conversion for isothermal TGA curing of **Thermoset #1** for 5 minutes

T_{iso} (°C)	$\Delta m_{moisture}$ (%)	Δm_{iso} (%)	$\Delta m_{residual}$ (%)	α (%)
	Blue oval (1)	Blue oval (2)	Blue oval (3)	
Reference			20.52	
130	6.38	0	22.24	0
140	5.65	0	22.13	0
150	0	7.40	20.16	0
160	4.42	4.46	16.74	15.67
170	3.49	7.68	14.68	28.44
180	3.29	11.52	12.21	40.47
190	6.63	10.91	9.63	53.06
200	6.3	13.77	7.48	63.53

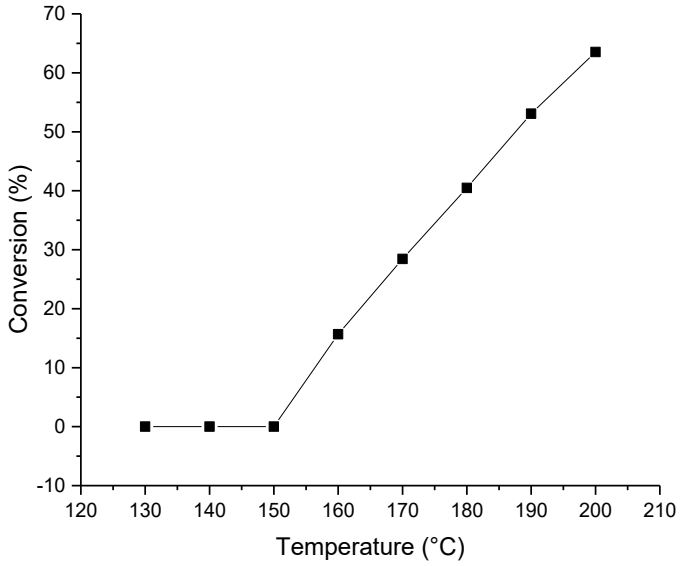

Figure 4.34 TGA conversion –temperature relationship of **Thermoset #1** cured isothermally for 5 minutes

For this system the low temperature region when the weight loss started was 112°C, which was related to residual moisture peak corresponding to blue oval (1) in Figure 4.33. The temperature of 264°C was where the peaks for all isothermal temperatures met. The two decomposition peaks were located above 300°C. The mass loss within the initial temperature region accounted for 26.80% with

standard deviation 0.61% by averaging all the temperatures tested. The small standard deviation indicated the experimental data held steady. The 26.80% mass loss mainly encompassed the mass loss due to residual moisture from surrounding and to curing induced water.

Mass loss associated with evaporating of residual water indicated in Figure 4.33 by blue oval (1) was estimated to be 6.28 ± 0.60% by averaging. By excluding the residual water of 6.28±0.60% from ovaerall mass loss of 26.80%, the mass loss associated with evaporating of residual water was successfully isolated, and the Δm_{total} was obtained at 20.52%. Then the conversion was obtained by dividing residual mass loss corresponding to blue oval (3) in Figure 4.33 by Δm_{total} of 20. 52%, representing all weight loss due to the cure combined with thermal weight loss of unknown, possibly thermal degradation.

At low temperatures, such as 130, 140 and 150°C, at isothermal stage, only one peak was observed and the weight loss was mainly connected to residual moisture leaving the system. The moisture is assumed to have evaporated before entering the curing temperature region. The sample isothermally cured for 5 minute at 160°C showed a combination of weight loss of both residual water and produced water, respectively, represented by two peaks appearing in this region, with the mass loss of Δm_{water} of 4.42% and Δm_{cure} of 4.46% respectively. The residual moisture could leave the system at higher temperature which is overlapping with cure reaction, might be related to free moisture or trapped moisture. The sample isothermally cured for 5 minute at 180°C showed a small residual mass loss ($\Delta m_{residual}$ = 12.21%) that from Equation 4.7 converts to 40% cure. And the residual mass loss of the sample isothermally cured 5 minute at 190°C and 200°C translates to α = 53% and 64% conversion, respectively.

From TGA analysis, it is deduced that under the condition of TGA heating (non-hermetic), the cure of **Thermoset #1** started at 160°C. To be more precise, the temperature of 160°C was sufficiently high to make the cure reaction happen effectively and be observed. The fastest reaction rate of 4.18%/°C and 5.09 %/°C was observed at 170°C and 172°C for isothermal temperature of 170°C and 180°C, respectively. The results from isothermal TGA measurements indicated the cure reaction was initiated at 160°C and reached its maximum of reaction rate in the narrow interval of 170–173.6°C. This provides a guideline for the selection of temperatures for curing this resin in the compression molding. This also suggests that the press platen during the pressing operation must be set to temperatures above 160°C, or that at least the temperature of 172–175°C is required to cure **Thermoset #1**.

4.4.1.3.2 DSC Experiment #4 for 10 Minutes in Hermetic Mode

A series of DSC measurements of **Thermoset #1** cured isothermally in the range of 130–200°C at the intervals of 10°C, i.e. 130, 140, 150, 160, 170, 180, 190, 200°C for a course of 10 minutes. The cured samples were cooled to a room temperature. Then the samples were heated at 10°C/min up to 300°C to measure the residual reaction enthalpy. The thermographs of isothermal first heating cycle for **Thermoset #1** sample are superimposed in Figure 4.35 as a function of time. It should be noted that the endothermal peak associated to cure reaction was only observed for experiments above 180°C, as indicated by blue ovals in Figure 4.35. The second heating was conducted until 300°C to completely cure **Thermoset #1** and to avoid thermal degradations above such temperature. The curves are shown in Figure 4.36**. T**he enthalpy measured in the second heating (post-curing) was considered to be the residual (incomplete) heat of first isothermal curing remaining. This residual heat was obtained by integrating the peak area.

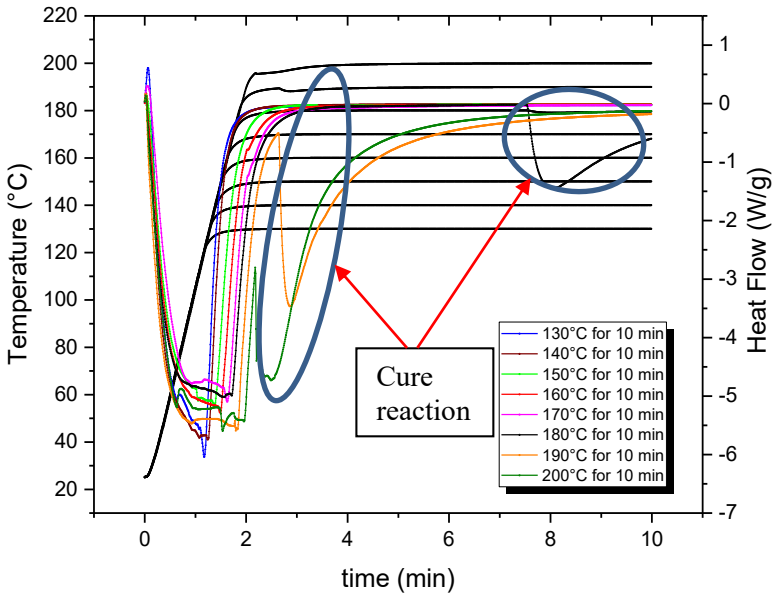

Figure 4.35 First heating cycle of **Thermoset #1** isothermally at temperatures of 130–200°C for 10 minutes

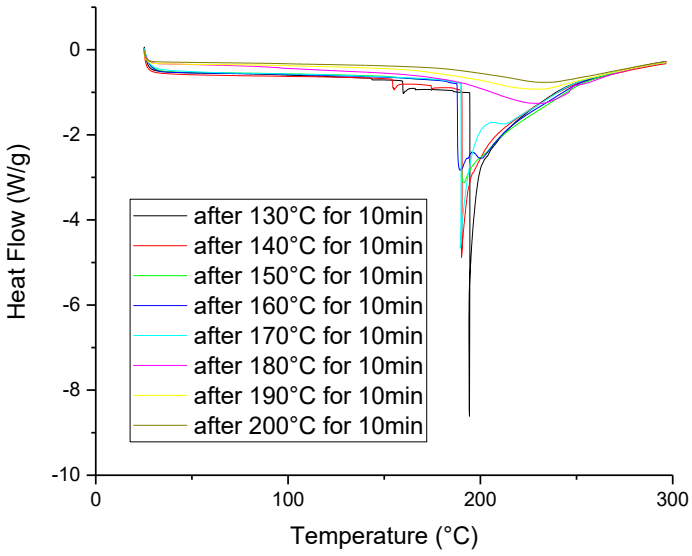

Figure 4.36 Second heating cycle obtained at 10°C/min of **Thermoset #1** cured isothermally

Table 4.11 Residual heat for isothermal DSC curing of **Thermoset #1** for 10 minutes and conversion calculated for the first isothermal heating

T_{iso} (°C)	$\Delta H_{Residual}$ (J/g)	α (%)
Reference	275	
130	294	0
140	314	0
150	367	0
160	359	0
170	318	0
180	63	81
190	45	86
200	40	88

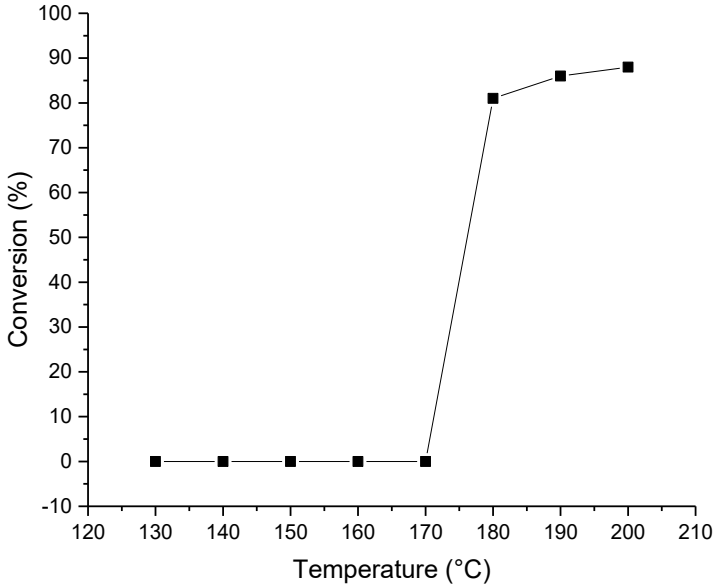

Figure 4.37 DSC conversion –temperature relationship of **Thermoset #1** cured isothermally for 10 minutes

The "Reference ΔH_{total}" was calculated as 275 J/g by averaging of measurements obtained at 130°C. The residual heat and conversion degree calculated based on the "Reference ΔH_{total}" for each set of temperature and time are presented in Table 4.11 and Figure 4.37. It is noticed that the residual exothermic heat decreased with increasing cure temperature. The conversion of the samples at these different isothermal curing temperatures was, as expected, found to increase with the increase of temperature. It is observed that the time of 10 min for temperatures 180, 190, and 200°C led to 81%, 86% and 88% of conversion, respectively. Moreover, for the isothermal heating at 200°C, the cure reaction was considered to be very close to completion for a course of 10 minutes. That is, after cured at 200°C for 10 min, the conversion practically reached completion and the heat flow measure after the second heating was very little. Thus, it could be considered that the combination of 200°C and 10min is enough to fully cure **Thermoset #1**.

4.4.1.3.3 DSC Experiment #4 in Isothermal Conditions and in Hermetic Mode

Thermoset #1 samples were analyzed in hermetic pans subjected to isothermal heating for selected temperatures in the range 130–200°C using the interval of 10°C. During these experiments the samples

became cured partially or fully depending on heating temperature and the extent of time. An example of temperature profile as a function of time for isothermal cure at 130°C is shown in Figure 4.38. Subsequently, after the first heating the samples were cooled to 25°C and then subjected to a second heating with temperature scanning from 25°C to 300°C at 10°C /min heating rate. The enthalpy determined from the area of the exothermic peak in the temperature region during the second heating represent the residual enthalpy, $\Delta H_{residual}$. The temperature range used in the second heating ensured the resin was 100% cured by the end of the cycle.

Isothermal DSC heat flow curves obtained at 130,140 150, 160,170,180,190, and 200°C for varied curing durations are given in Figure 8.42, Figure 8.43, Figure 8.44, Figure 8.45, Figure 8.46, Figure 8.47, Figure 8.48 and Figure 8.49, respectively. Table 8.14 to Table 8.21 summarize the characteristic temperature and residual heat corresponding to heating durations for each temperature and conversion.

After being heated at isothermal condition for certain times, the residual endothermic peaks were observed during dynamic cycle as shown in Figure 8.42 in Appendix E as an examples at 130°C. As discussed, the endothermal signals were a result of the reactivity of the residual functions that have not reacted during the isothermal period. By measuring the $\Delta H_{residual}$ and comparing it to ΔH_{total}, the amount of cure occurring during isothermal heating is known and suggested by $\Delta H_{total} - \Delta H_{residual}$. When cure reaction started in first heating, then conversion (α) at different time with respect to Acrodur cured different temperatures was calculated from Equation 4.5: $\alpha\ (\%)=100 - \Delta H_{residual}/\Delta H_{total}$. The data at very low conversions is subject to large errors due to the uncertainties in TGA baseline determination caused by run-to-run variation (inconsistency), reflected by variation of total reaction heat measured by different heating rates. Therefore, the average of reaction heat, ΔH_{total} of 332J/g, was obtain by averaging the reaction heat measured at 130°C, at which the cure reaction is not triggered or the heat involved in isothermal cycle is negligible.

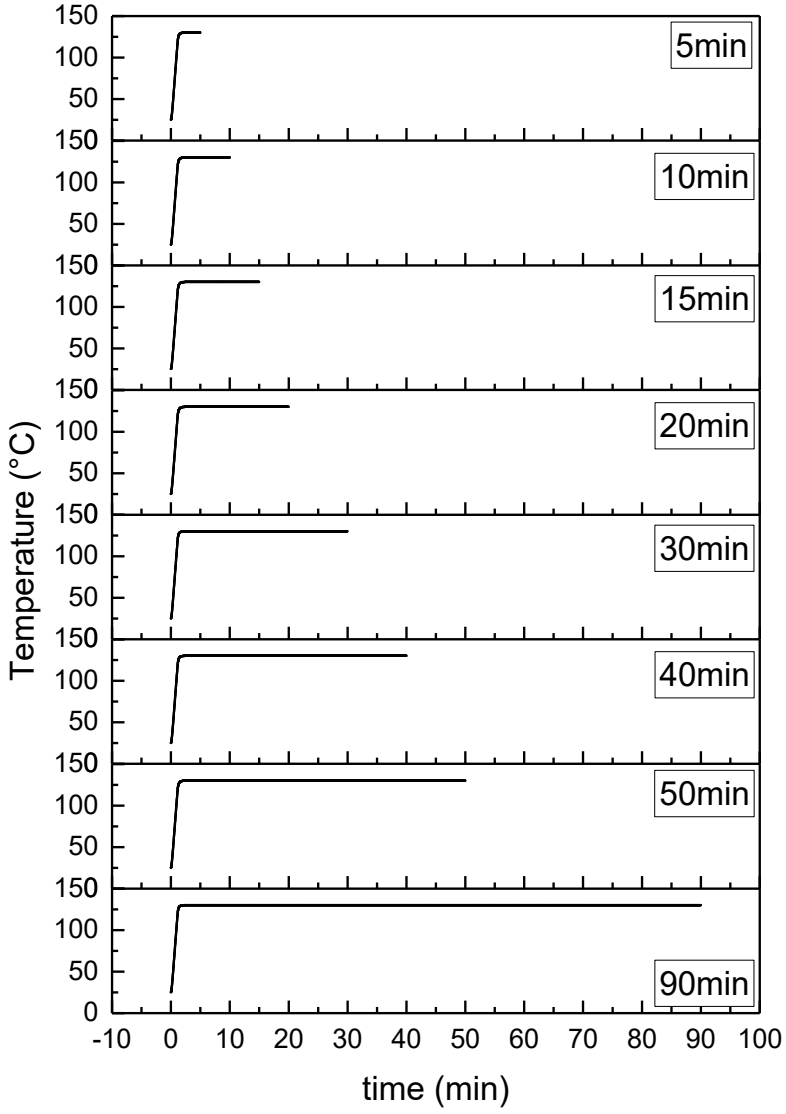

Figure 4.38 Representative illustration of isothermal curing (first heating) at 130°C for various times

Based on the determination of enthalpy and the observation of the shape of postcuring peak, it is reasonable to deduce that the cure reaction is considered to have not started when the onset and peak temperatures of postcuring peaks were the same, and vice versa.

It was observed that the isothermal curing temperatures below 180°C for tested durations, did not make detectable differences in residual heat measured in second heating. That is, for T_{iso} <180°C, no evidence of an endothermic reaction was observed during isothermal heating cycle. This fact can be interpreted in at least two different ways: either the enthalpy of the reaction is too weak to be detected, or there is no reaction during the experimental time. From the above observation, it was induced that the temperatures below 180°C, basically, are not sufficiently high to provide the energy and to cure **Thermoset #1**, at the last for the longest time investigate here. As shown through in Figure 8.42 to Figure 8.49 in Appendix E, corresponding to isothermal temperature of 130–200°C.

When the temperature was selected to be 180°C or above the isothermal process in first heating showed the effect on residual heat measured in the second heating, as shown in Figure 8.47 in Appendix E. The differences in endotherm intensity were observed across Figure 8.47, Figure 8.48 and Figure 8.49 in Appendix E, which were related to cure (esterification) reactions having taken place in first heating cycle. It can be seen that the conversion degree increased with reaction time. It took less than 4 minutes at 180°C and 190°C, and around less than 2 minutes at 200°C for **Thermoset #1** to cure to a satisfactory level. It can be concluded that there is a threshold temperature of at least 180°C, to trigger the cure reaction of **Thermoset #1**.

The conversion versus time plots for isothermally cured **Thermoset #1** at 170, 180, 190, and 200°C are shown in Figure 4.39 to illustrate the progress of curing of **Thermoset #1** in terms of the conversion (degree of curing). It should be noticed: 1) a series of curves that are parallel for the first 80% of cure; and 2) the highest temperature curves are at the shortest times. The optimum heating time corresponding to a given temperature can be determined by observing conversion-time curves in Figure 4.39. The optimum heating time can be determined by observing when the endothermic reaction peak is complete. The results show that with increasing time at certain temperature (degree of curing), the enthalpy of the post-curing reaction decreased. It is observed that the conversion increased rapidly to 80% after 2 or 4 minutes but beyond that increases more slowly toward 90%.

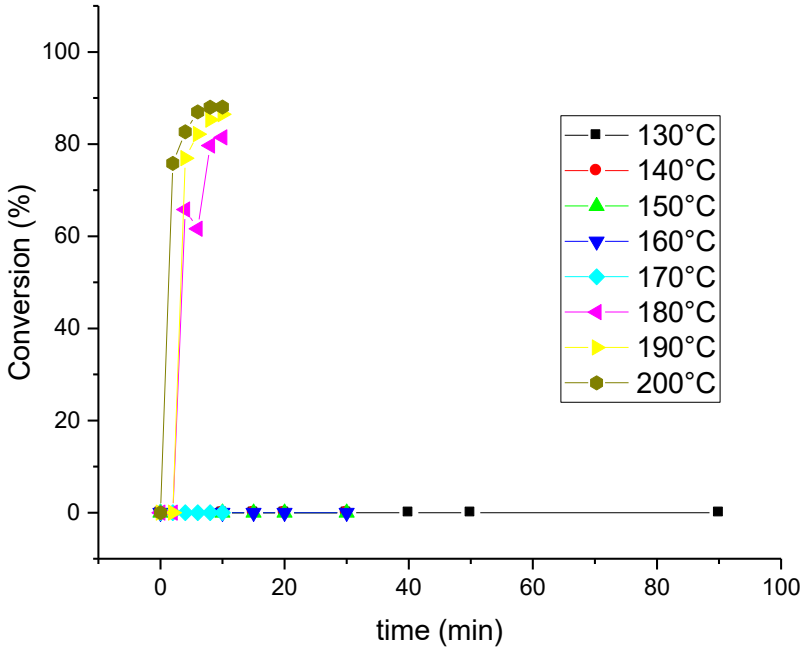

Figure 4.39 Conversion extent for different reaction temperatures as a function of reaction time, in hermetic mode

4.4.1.3.4 DSC Experiment #4 for Various Times in Non-hermetic Mode

The same series of isothermal DSC scanning as described in 4.3.1.3.2 were conducted under non-hermetic condition. **Thermoset #1** samples were initially subjected to isothermal heating for various times in the range of 130–200°C using the interval of 10°C at 130, 140, 150, 160, 170, 180, 190, and 200°C for varying curing durations; results are shown in Figure 8.50, Figure 8.51, Figure 8.52, Figure 8.53, Figure 8.54, Figure 8.55, Figure 8.56 and Figure 8.57 in Appendix E, respectively. The endothermal signals in the temperature region during the second heating represent the residual curing reaction. Table 8.22 to Table 8.29 in Appendix E summarize the residual heat measured in the second heating corresponding to several times for each temperature and the calculated conversion (degree of curing).

The residual endothermic peaks were observed during second heating for all samples. As discussed, the endothermal signals were a result of the reactivity of the residual functional groups that did not

react during the first isothermal period. By measuring the $\Delta H_{residual}$ and comparing it to ΔH_{total}, the amount of cure occurring during isothermal heating can be calculated by ΔH_{total} - $\Delta H_{residual}$. The conversion (α) at different times with respect to different temperatures was calculated from Equation 4.5: $\alpha\ (\%) = 100 - \Delta H_{residual}/\Delta H_{total}$. The average of reaction heat, ΔH_{total} of 180 J/g was obtain by averaging the reaction heat measured non-isothermally at heating rates of 10 and 15°C/min.

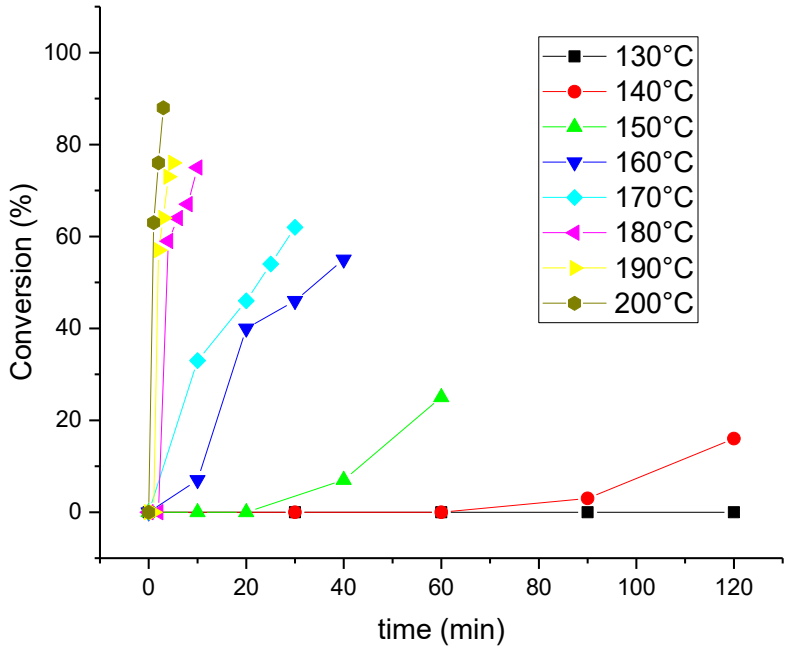

Figure 4.40 Conversion extent for different reaction temperatures as a function of reaction time, in non-hermetic mode

The conversion versus time plots for isothermally cured **Thermoset #1** for all the tested temperatures are shown in Figure 4.40 to illustrate the conversion (degree of curing). It is observed that as the isothermal temperature increased the higher degree of cure was achieved with short times, and longer reaction times were needed at lower temperatures. For example, isothermally at 130 and 140°C for 120 minutes, no or a little curing was measured; when the temperature increased to 150, 160, and 170°C, the conversion was measured at 30 to 60% within 30–60 minutes; with further increase in the temperature to 180, 190 and 200°C at least 80% of conversion was measured within minutes. The optimum heating time can be determined by observing when endothermic reaction peak was complete.

It is seen the degree of cure of more than 80% can be achieved in a few minutes at 180°C. It took less than 2 minutes at 200°C for **Thermoset #1** in non-hermetic condition to cure to a high degree of conversion. This is in agreement with the finding conducted by Gerst (Gerst et al. 2009), where the curing reaction was completed in less than one minute at curing temperatures of about 200°C.

It should be noticed that compared to isothermal cure in hermetic mode in 4.4.1.3.3, the non-hermetic condition significantly dropped the "threshold temperature" for significant curing from 180 to 150°C. This is significantly meaningful for optimization of compression molding conditions and energy saving.

As already noted, these investigations with DSC and TGA estimated 90% as the highest conversion achieved for the conditions evaluated here.

4.4.1.3.5 Discussion

The samples were cured isothermally in the first heating using isothermal DSC and TGA followed by the measurement of the residual heat (for DSC) or mass loss (for TGA) in the second heating. This information provided the experimental input to completely study the progress of cure and thereby to optimize the compression molding parameters in pressboard manufacture. A correlation for the evolution of conversion with temperature and time, conversion = f(time and temperature) was constructed based on DSC or TGA experimental data.

4.4.1.3.5.1 Effect of Temperature and Time

The isothermal results showed that the cure reaction of **Thermoset #1** is more sensitive to temperature than to time for the scope of the intervals studies. Only when the temperature was above a certain level (threshold) the reaction rate increased significantly. It was observed that in hermetic mode, below 180°C, the ten minutes' exposure to 170°C displayed a little effect on the cure conversion. On the other hand, when the temperature reached the "temperature threshold", the cure reaction was complete within 10 minutes. Higher temperatures required a shorter time. The same observation was made on non-hermetic mode, where the difference was the "temperature threshold" shifted to low temperatures.

It can be seen that the conversion degree increased with reaction time when temperatures were above 180°C for hermetic mode and above 150°C for non-hermetic mode. The heating times of less than 10 minutes were considered sufficiently long for fully curing samples when the system was sealed (hermetic mode). The high sensitivity to temperature is characterized by high activation energies. This

is in good agreement with non-isothermal results, indicating that the temperature dependence of cure reaction is a more intrinsic feature. The same observation of critical temperature was found in a study (Guenthner et al. 2011), where cure characteristics of tri-cyanate ester was investigated.

4.4.1.4 Discussions

Based on the reaction heat or mass loss of cure measured by isothermal and non-isothermal DSC and TGA, the cure reaction of **Thermoset #1** was investigated and characterized, in terms of onset and peak temperatures, and cure conversion as a function of temperature or time, and kinetic activation energy. Both DSC and TGA results were compared and evaluated. TGA is more reliable than DSC because of uncertainty of hermetic condition as well as the heat due to water vapor expansion.

In comparison of TGA and DSC results, the cure reaction of **Thermoset #1** was observed starting from low temperatures of 158–175°C, and reached its maximum rate of 169–187°C from TGA thermographs, followed by non-hermetic DSC of 178–196°C peak temperature and then by hermetic DSC of 184–206°C, depending on the heating rates. The isothermal cure profiles provided further information in terms of duration and enthalpy of the cure reaction, indicating that the reaction is dependent on temperatures greater than 160°C for TGA and 180°C for DSC.

It is inferred that the cure reaction of **Thermoset #1** was initiated above 160°C, particularly from 180°C, reached the fastest rate at around 200°C. This temperature range is within the temperature range for cure Acrodur stated in literatures mentioned in introduction.

Cure was also found dependent on whether the produced water was hold in the system or free to release. When the system is open, the cure reaction initiated at lower temperatures of around 150°C and with faster reaction rates. The differences of onset and peak temperatures between three results can find explanations in the non-hermetic or hermetic lids preventing the water leaving the system freely compared to completely open system of TGA measurements.

Two step curing can be proposed, due to the monomers, and oligomers, are usually more susceptible to thermal (and oxidative) degradation than the fully cured thermoset, resulting in a discolored final product that cannot achieve the maximum expected performance. A temperature that is too high or curing that is too fast may create stresses and other non-ideal properties in the material, or even decompose the resin.

4.4.1.5 **Selection of Curing Profile for Compression Molding**

The non-isothermal and isothermal results provide a guiding tool for optimization of the compression molding parameters in pressboard manufacture. Based on the inference that Acrodur curing is more sensitive to temperature than to time, the higher temperatures can cure the resin in a shorter time, with higher conversion degree. It is proposed that the heating profile of the temperature above 160 ºC or 170 ºC for 10min is sufficient to completely cure the Acrodur sample. Higher temperatures require shorter time, such as the temperature of 180 ºC cures **Thermoset #1** in 4 minutes, 200 ºC within 2 minutes. It might be an option to use higher temperatures, for example 200ºC, which would completely cure in the fastest rate, however the possibility of thermal degradation increases on the surface of composites due to lagging effect of heat transfer.

4.4.2 Thermoset #2

Thermoset #2 is cellulose nanofibril (CNF) reinforced Acrodur DS3530 (**Thermoset #1**), with CNF content of less than 5%. The objective of this part is to evaluate the effect of addition CNF on thermal behavior of Acrodur DS3530.

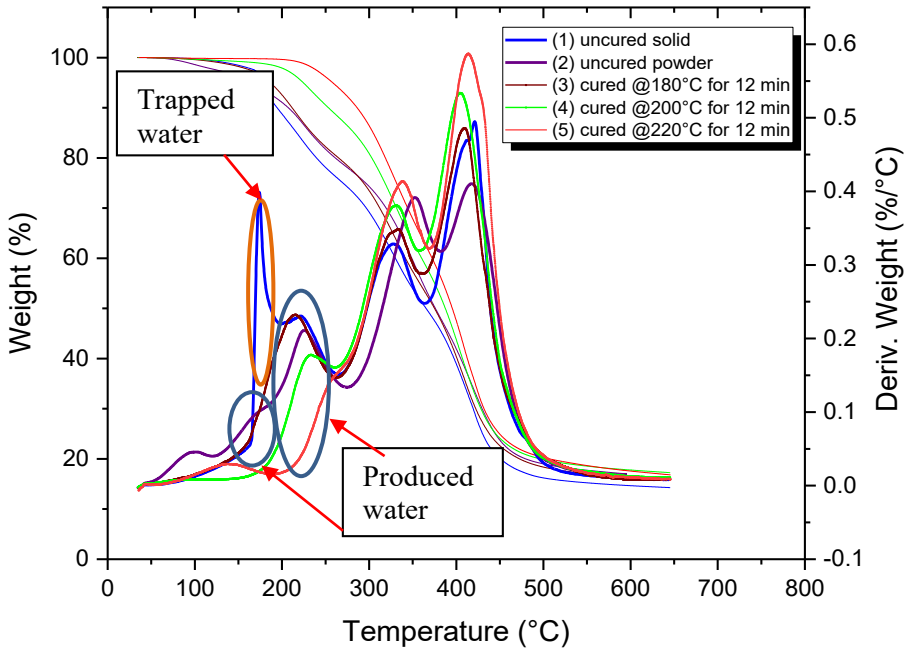

Figure 4.41 TGA thermographs of **Thermoset #2**, uncured solid (1) and powder (2), pre-cured for 12minutes at 180°C (3), 200°C (4), and 220°C (5)

4.4.2.1 TGA and DSC Experiment #1

The TGA thermographs of uncured and pre-cured **Thermoset #2** are presented in Figure 4.41, where the similar trend was found as in 4.4.1.1 for **Thermoset #1**. The residual mass loss decreased as the pre-cure temperature increased. The sharp peak at 175° in curve (1) of Figure 4.41 is attributed to the trapped water, while the overlapped peak centered at around 210°C is connected to cure reaction.

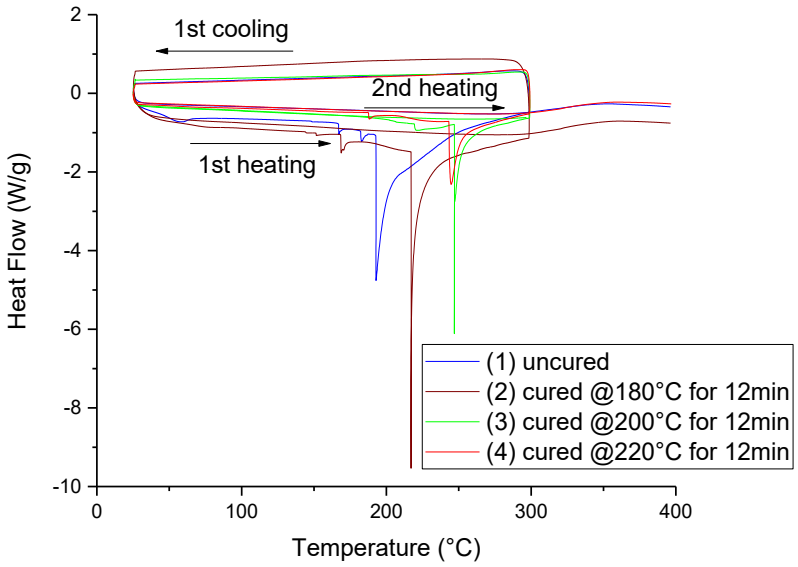

Figure 4.42 DSC thermographs of **Thermoset #2**, in hermetic mode, uncured (1), pre-cured for 12minutes at 180°C (2), 200°C (3), and 220°C (4)

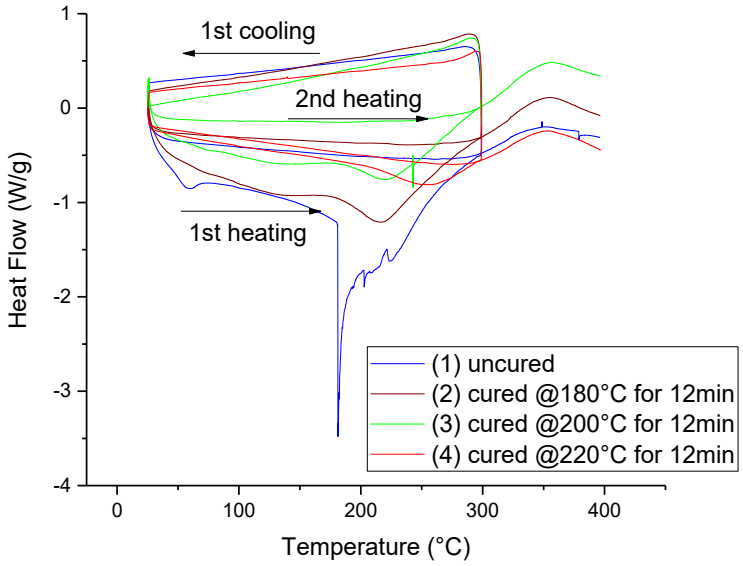

Figure 4.43 DSC thermographs of **Thermoset #2**, in non-hermetic mode, uncured (1), pre-cured for 12minutes at 180°C (2), 200°C (3), and 220°C (4)

Presented in Figure 4.42 and Figure 4.43 are the complied DSC thermographs at 10°C/min heating rate for uncured, and pre-cured **Thermoset #2** in hermetic and non-hermetic modes, respectively. Similar to those of **Thermoset #1**, the DSC thermographs in hermetic mode for the first scan showed two endothermic regions, except the one below 100°C related to the remaining moisture. A combined step-down/endothermic transition was observed at higher temperature region ranging from 150 to 250°C for first heating, which could be connected with the trapped water of samples. A sharp distinct endothermic peak popped out at even higher temperatures ranging from 200 to 275°C, proceeding into the broad endothermic signal from this temperature up to 300°C with a long trailing. This temperature region from 150 to 300°C was considered to cover the all the cure reaction related signals possibly combined with other thermal activities that occurred within this region. By examining the the temperature range from 150 to 300°C, the heat of reaction or post-reaction was estimated by integrating the area of the second DSC peak of uncured or pre-cured **Thermoset #2**.

The DSC thermographs of non-hermetic mode were characterized by tilted baseline due to the reduced total weight. Similarly, the peaks in first heating related to free and trapped moisture, and cure reaction were observed in Figure 4.43.

In comparison with those of **Thermoset #1**, the onset and peak temperatures of **Thermoset #2** for both hermetic and non-hermetic modes were at the small temperature range. The curing behavior of the CNF modified system are considered the same as that of **Thermoset #1**. This implies that the interaction between CNF and the carboxylic acid groups of **Thermoset #1** that was expected was not significant to exhibit the effect on cure reaction of **Thermoset #1**.

4.4.2.2 TGA Experiment #3 in Solid

Similar to **Thermoset #1**, the kinetics of **Thermoset #2** curing were investigated by non-isothermal TGA at five different heating rates. Figure 4.44 shows the TGA thermographs recorded at 5, 10, 15, 20, and 25°C /min. The curves reveal that, the starting and peak temperatures of curing reaction of the **Thermoset #2** were decreased by 2°C and 4°C, respectively, for heating rate of 10°C /min.

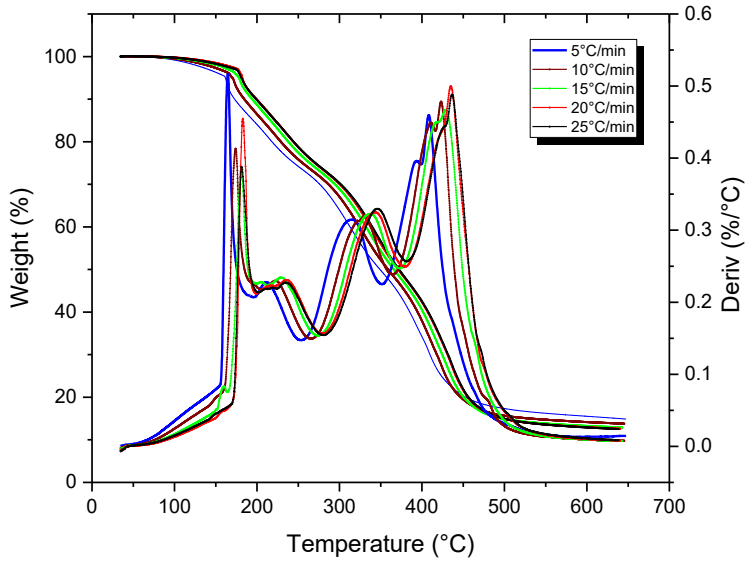

Figure 4.44 Non-isothermal TGA curves of **Thermoset #2** solid at a series of heating rates

To evaluate possible effects of incorporation of CNF on the curing behavior of **Thermoset #2**, the Friedman's method was applied to calculate the activation energy Ea of the curing reaction. The variation of conversion as a function temperature is illustrated in Figure 4.45. The Ea value of curing reaction could be obtained by plotting ln $[\Delta m_t/\Delta m_{total}]$ versus 1/T for each value of α in Figure 8.58 in Appendix E. The values of Ea were plotted as functions of α in Figure 4.46. The variation of Ea

along the course of conversion is interpreted as the result of a complex reaction mechanism where multiple reactions are likely to compete or as a result of diffusion effects.

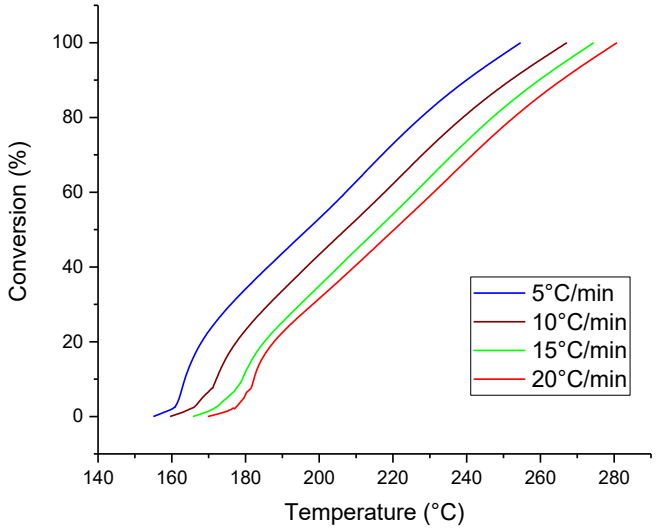

Figure 4.45 Fractional conversion (degree of curing) of the reaction of **Thermoset #2** solid as a function of temperature at a series of heating rates

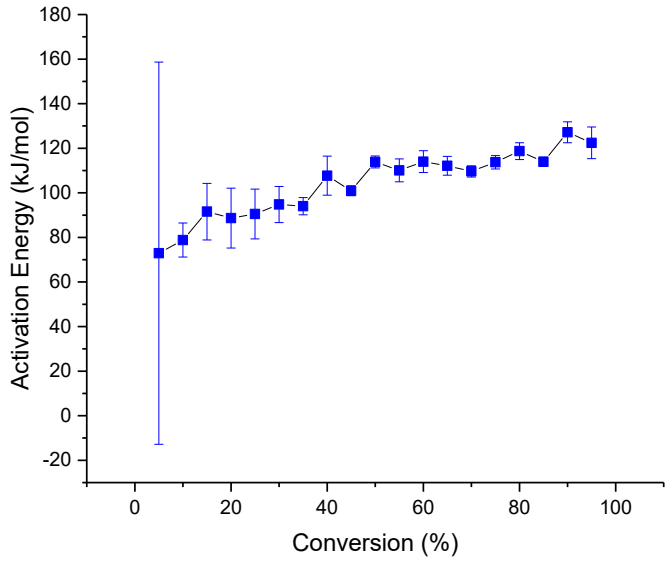

Figure 4.46 Dependence of activation energy with the extent of isothermal TGA cure of **Thermoset #2** solid

Figure 4.46 shows that the activation energy of **Thermoset #2** steadily increased from 73 to maximum 127 kJ/mol at 90% conversion as the conversion progressed. The large variation in activation energy at the 5% conversion may be the attributed to uncertainty in the determination of the onset point in TGA thermographs. The Ea value of **Thermoset #2** is less than that of **Thermoset #1** largely, which demonstrates that the addition of less than 5% of CNF had the effect on the cure reaction of Acrodur DS3530 (**Thermoset #1**) by requiring lower energy.

Therefore, it is concluded that the addition of CNF to the formulation of **Thermoset #1** influenced cure kinetics. **Thermoset #1** with less CNF required a lower energy (lower activation energy) to initial the polymerization. At the same degree of conversion, the activation energy decreased with addition of CNF. The presence of the hydroxyl functional groups on the surface of CNF may be the reason for the effect on the curing reaction. This behavior observed here is in agreement of other reports in the literature (Xie et al. 2004). The inclusion of 5% of CNF in **Thermoset #1** conferred the benefits including lower activation energy.

4.4.2.3 TGA Experiment #3 in Powder

Thermoset #2 in form of powder was also investigated non-isothermally using TGA at five heating rates. The resulting thermographs, the ln (dα/dt) vs 1/T, and the resulting activation energy as a function of conversion are shown in Figure 4.47, Figure 8.59 and Figure 4.48, respectively. Two main peaks exist in 130–275°C temperature regime, as shown in Figure 4.47, were attributed to the cure reaction. Based on the TGA experiments with five heating rates, the activation energy of **Thermoset #2** powder was determined as the slope of ln (dα/dt) as function of 1/T as shown in Figure 8.59 in Appendix E. The dependence of activation energy with conversion is illustrated in Figure 4.48. It is seen that the activation energy was blow 140 kJ/mol for first 20% conversion and increased and kept relatively steady between 165–183 kJ/mol.

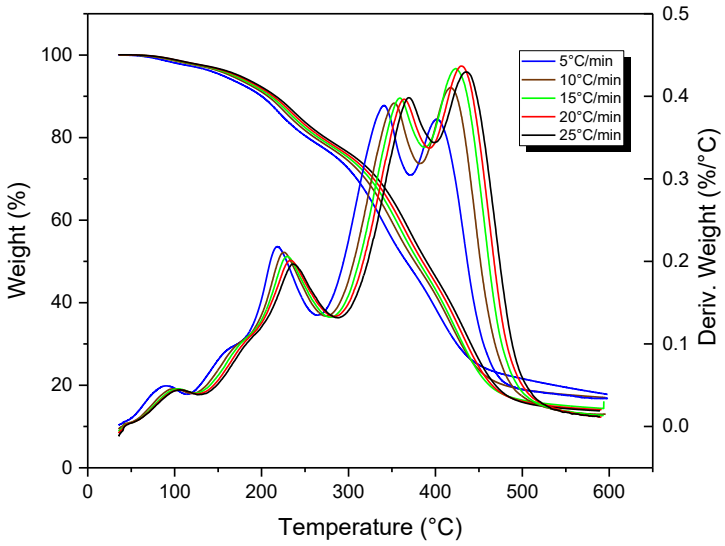

Figure 4.47 Non-isothermal TGA curves of **Thermoset #2** powder at a series of heating rates

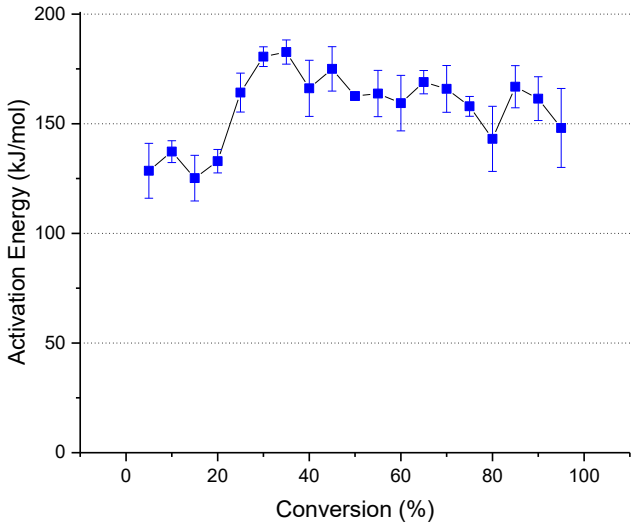

Figure 4.48 Dependence of activation energy with the extent of isothermal TGA cure of **Thermoset #2** powder

4.4.2.4 DSC Experiment #3 in Hermetic Mode

The non-isothermal cure behavior of **Thermoset #2** was investigated using DSC in hermetic mode. Figure 4.49 shows the DSC thermographs recorded at heating rates of 5, 10, 15, and 25°C/min. It is seen that the DSC thermographs were almost identical in shape for the different heating rates. The heat absorption appeared from 150°C to 300°C. It is also observed that as the heating rate increased, the peak of cure reaction was delayed and shifted to higher temperatures.

The peak temperature and reaction enthalpy of the endothermic peak of **Thermoset #2** at different heating rates were measured from the DSC curves and are shown in Table 4.12. The peak temperature was observed to shift to higher temperatures when the heating rate was increased. It was also found that the enthalpy value varied among various heating rates.

Following the same procedure as for **Thermoset #1**, the plots of ln $[\int_0^t \frac{dH}{dt} dt / \Delta H_{total}]$ versus 1/T of **Thermoset #2** are shown for each value of α in Figure 8.60 in Appendix E. The slope of each line is equal to -Ea/R. The values of apparent activation energy, Ea, obtained from the slop of each straight line in Figure 8.60 is plotted as functions of α in Figure 4.50.

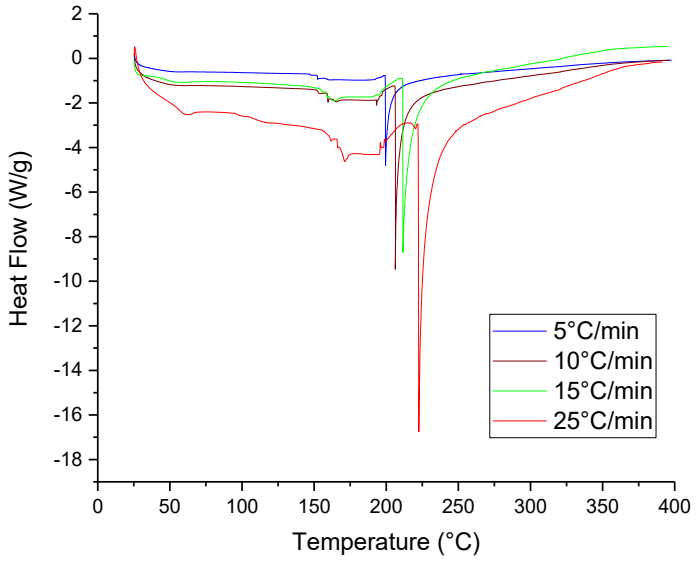

Figure 4.49 Dynamic DSC curves for the reaction of **Thermoset #2** powder at different heating rate, in hermetic mode

Table 4.12 Peak temperature and enthalpy of cure reaction of **Thermoset #2** powder at a series of heating rates, in hermetic mode

Heating rate, β (°C/min)	T_{Peak} (°C)	ΔH_{total} (J/g)
5	200	279
10	206	259
15	212	232
25	223	214

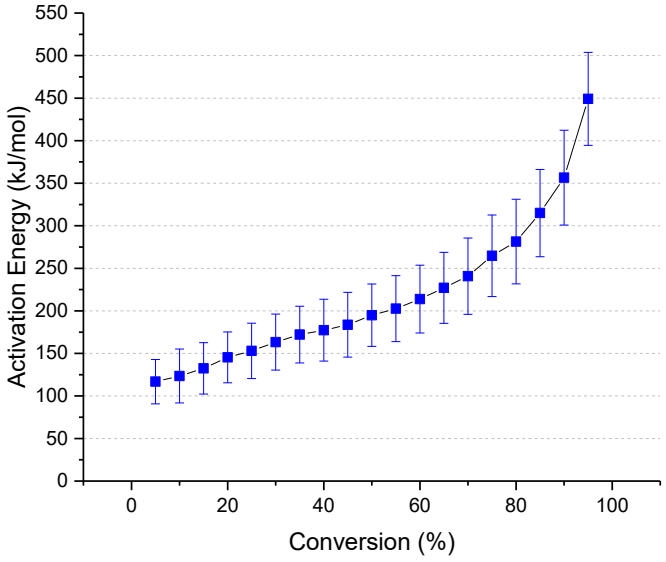

Figure 4.50 Dependence of activation energy with the extent of non-isothermal DSC cure of **Thermoset #2** powder

The apparent activation energy followed a simple increasing trend from 117 to 240 kJ/mol at 70% conversion, then the trend accelerated to 449 kJ/mol at 95% conversion. The overall variation was constant at low level. This increasing trend of Ea suggests that as the esterification proceeded it was more difficult for the polymer to cure, with two or more mechanisms involved.

4.4.2.5 DSC Experiment #3 in Non-hermetic Mode

Thermoset #2 was also investigated non-isothermally using DSC in non-hermetic mode at various heating rates in two forms, i.e. solid and powder. The DSC thermographs of **Thermoset #2** solid are shown in Figure 4.51 while the peak temperature and reaction enthalpy for each heating rate are tabulated in Table 4.13. According to the iso-conversion method, the resulting activation energy as a function of conversion is presented in Figure 4.52, which illustrates the activation energy started from 109 kJ/mol and increased to maximum 240 kJ/mol at 50% conversion followed by variation around 200 kJ/mol for the conversion up to 95%.

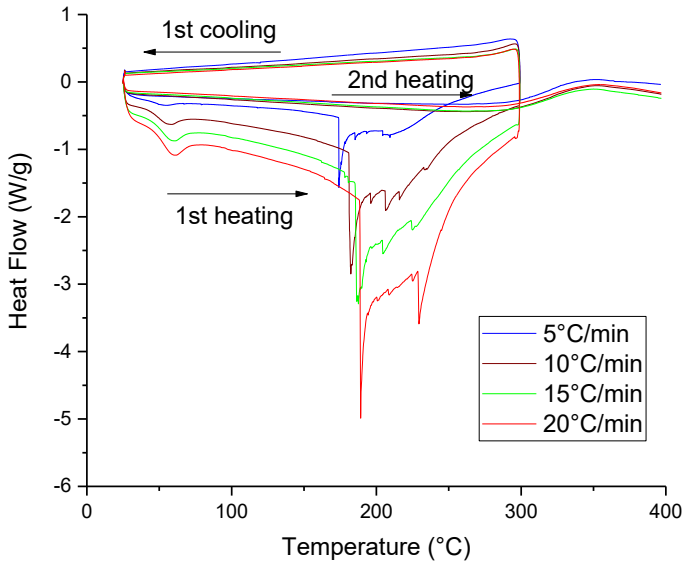

Figure 4.51 Dynamic DSC curves of **Thermoset #2** solid at a series of heating rates in non-hermetic mode

Table 4.13 Peak temperature and enthalpy of cure reaction of **Thermoset #2** solid at a series of heating rates, in non-hermetic mode

Heating rate, β (°C/min)	T_{Peak} (°C)	ΔH_{total} (J/g)
5	174	214
10	182	256
15	188	217
20	189	249

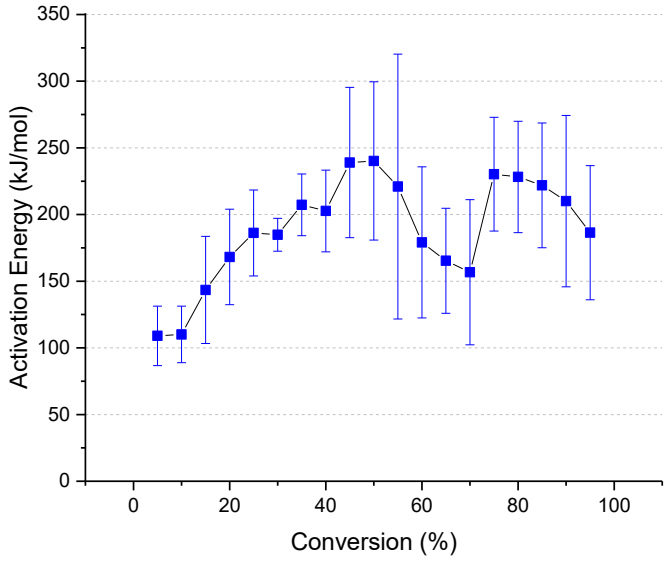

Figure 4.52 Dependence of activation energy with the extent of non-isothermal DSC cure of **Thermoset #2** solid

The thermographs, ln (dα/dt) vs 1/T plots, and variation of activation energy are illustrated in Figure 4.53, Figure 8.61 in Appendix E and Figure 4.54, respectively, for the **Thermoset #2** samples in form of powder. Table 4.14 presents the peak temperature and reaction enthalpy involved for each heating rate. The estimated activation energy in Figure 4.54 varied following an increasing trend from lowest 124 kJ/mol at 5% conversion up to 304 kJ/mol at 95%. It is also seen that the uncertainty associated with activation energy became larger as the cure reaction progressed.

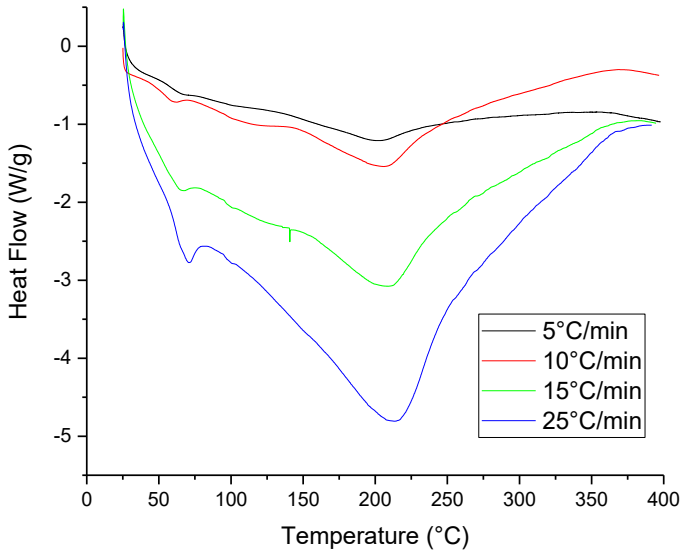

Figure 4.53 Dynamic DSC curves of **Thermoset #2** power at a series of heating rates in non-hermetic mode

Table 4.14 Peak temperature and enthalpy of cure reaction of **Thermoset #2** powder at a series of heating rates, in non-hermetic mode

Heating rate, β (°C/min)	T_{onset} (°C)	T_{Peak} (°C)	ΔH_{total} (J/g)
5	144	199	137
10	149	205	124
15	158	208	112
25	163	214	114

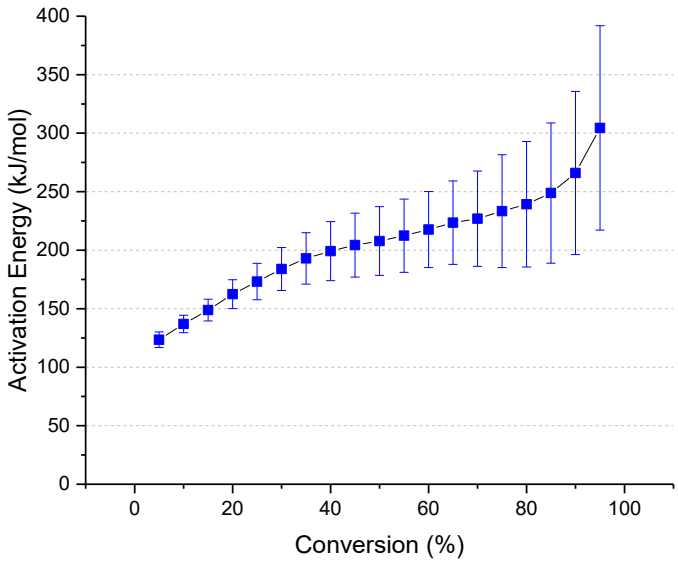

Figure 4.54 Dependence of activation energy with the extent of isothermal DSC cure of **Thermoset #2** powder

The similar effect of sample form is recognized in thermographs of **Thermoset #2** as discussed in 4.4.1.2.5.2 for **Thermoset #1**. In comparison of the thermographs of both solid and powder forms, the sharp peaks appearing in solid sample thermographs indicate the reaction started abruptly at a certain temperature, whereas the onset temperature and broad peaks for powder samples demonstrate the earlier start of cure reaction and the reaction progressed at much smoother rates. This makes sense because the powder form is more homogeneous and the higher surface-volume ratio facilitate the reaction progress. On the other hand, the bulky solid is associated with the lagging effect of heat transfer and water evaporation. The gradual reaction progress also contributes to accurate identification of onset and endset of reaction curves, which led to lower uncertainty in activation energy estimation.

4.4.2.6 Discussions

The model-free iso-conversional method was successfully applied to non-isothermal DSC and TGA data of **Thermoset #2** curing. The activation energies Ea obtained from the combinations of two techniques of DSC and TGA, two modes of hermetic and non-hermetic, and two forms of solid and powder are plotted in Figure 4.55 and correlated with each other.

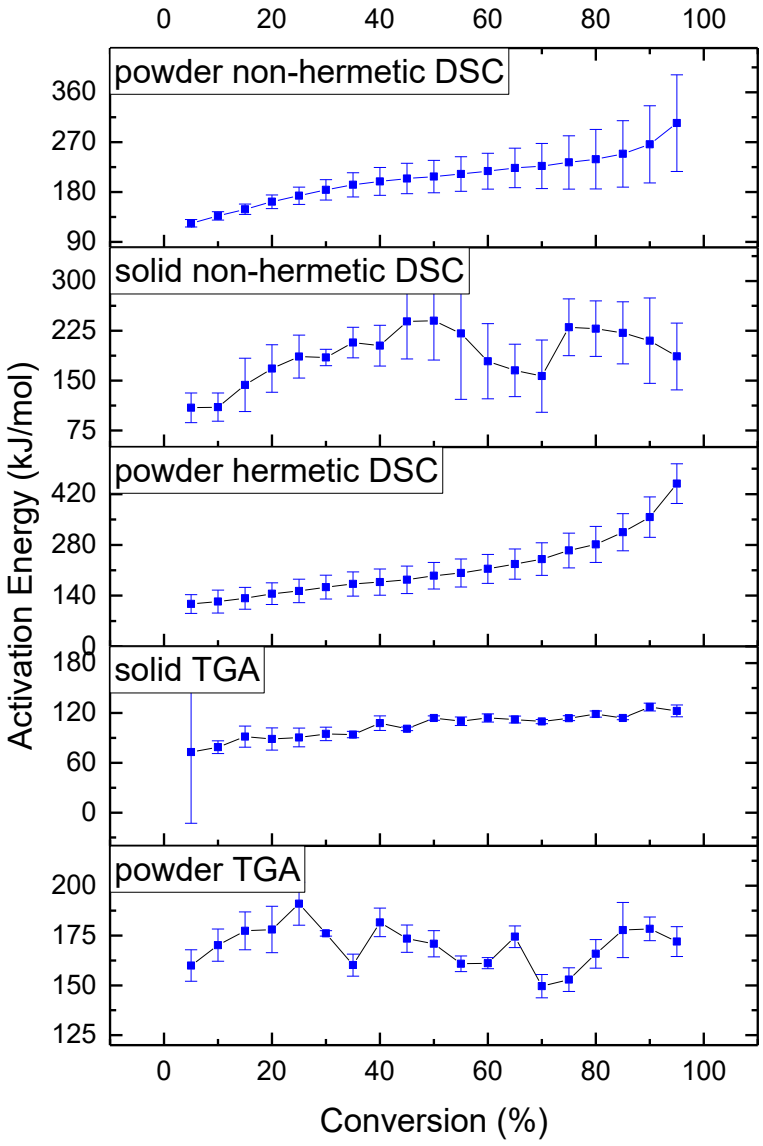

Figure 4.55 Comparison of activation energy of **Thermoset #2** from different thermal analysis methods

As shown in Figure 4.55, the differences in the activation energy varied significantly with variable uncertainty. However, it is apparent that the DSC derived activation energy showed the agreement in following the same or similar increasing trend. **Thermoset #2** generally exhibited a higher activation energy at high conversion than at low conversion in the curing process. This meant that more heat was

needed to cure at high molecular weight, suggesting that multiple reactions occurred during the process. On the other hand, the activation energy obtained from TGA measurements remained relatively steady and exhibited slight increasing intendancy during the whole course of curing. The discrepancies of activation energies obtained from DSC and TGA experiments are likely to be derived from the techniques used and also to the selection of the onset and the end point selected of the range of interest. The variation in the values of activation energy can be attributed to the uncertainty of determination of temperature range studied and/or the temperature dependence of reaction mechanism.

4.4.3 Thermoset #3

Thermoset #3 is thermosetting Acrodur 950L with higher viscosity than Acrodur DS3530 (**Thermoset #1**) due to its higher molecular weight of approximate 80,000g/mol. The objective of this part is to investigate and compare the cure behavior of **Thermoset #3** with **Thermoset #1** and **#2**.

4.4.3.1 TGA and DSC Experiment #1

Similar to 4.4.1.1 and 4.4.1.5, where **Thermoset #1** and **#2** are investigated, the TGA and DSC thermographs of uncured and pre-cured **Thermoset #3** are presented in Figure 4.54, Figure 4.57 and Figure 4.58, with the latter two corresponding to hermetic and non-hermetic modes. The similar trend observed here was found as in 4.4.1.1 and 4.4.2.1 for **Thermoset #1** and **#2**. The measured residual mass loss and enthalpy reduced as the pre-cure temperature increased. The sharp peak at 175° in TGA curve (1) is attributed to the trapped water, while the overlapped peak centered at around 210°C is connected to cure reaction. Follow the same procedure, the assignment of thermographs peaks was conducted corresponding to trapped water and cure reaction. The temperature regime of interest was determined to be from around 150 to 300°C.

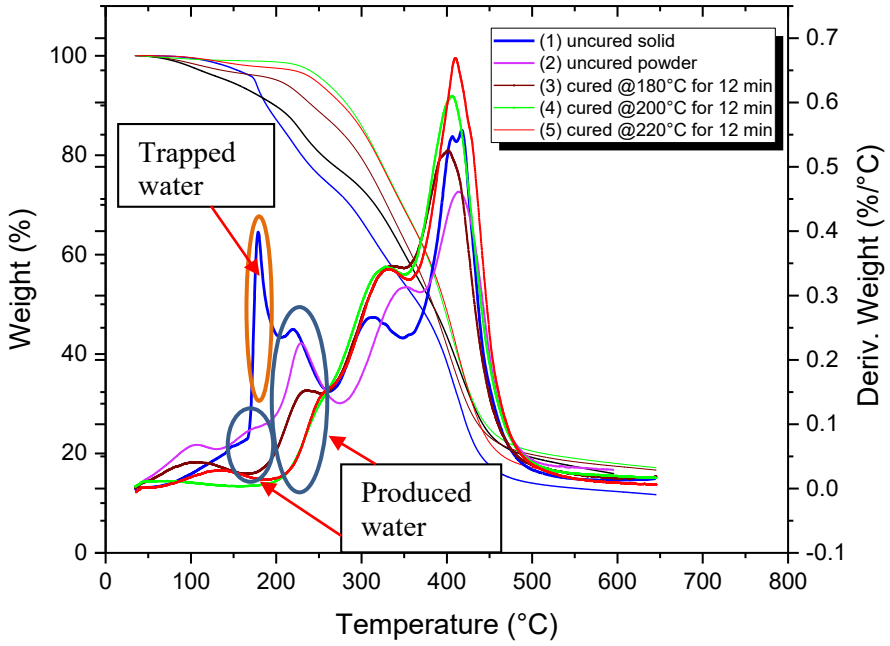

Figure 4.56 TGA thermographs of **Thermoset #3**, uncured solid (1) and powder (2), pre-cured for 12minutes at 180°C (3), 200°C (4), and 220°C (5)

Similar to those of **Thermoset #1**, two endothermic regions except the one related to the remaining moisture were found in the DSC thermographs. The temperature region ranging from 150 to 250°C for first heating could be connected with the trapped water of samples. A sharp distinct endothermic peak followed by broad endothermic signal was observed at the temperatures region of 200 to 300°C. This temperature region from 150 to 300°C was of the most interest. The heat of reaction or post-reaction was estimated by integrating the area of the second DSC peak of uncured or pre-cured **Thermoset #3**. The DSC thermographs of non-hermetic mode were characterized by tilted baseline due to the reduced total weight. Similarly, the peaks in first heating related to free and trapped moisture, and cure reaction were observed in Figure 4.58.

The onset and peak temperatures of **Thermoset #3** for both hermetic and non-hermetic modes were in the same temperature range with those of **Thermoset #1** and **#2**. It is implied that the curing behavior was not changed significantly by increased molecular weight of **Thermoset #3**.

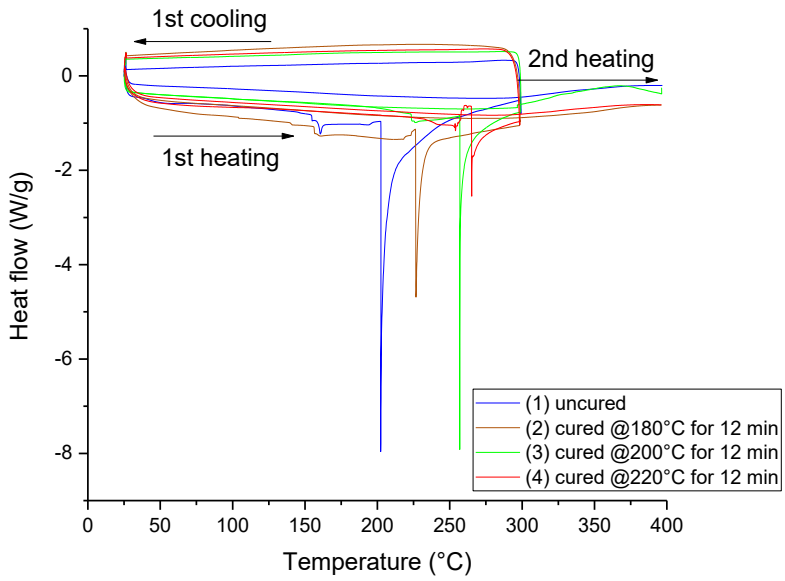

Figure 4.57 DSC thermographs of **Thermoset #3**, in hermetic mode, uncured (1), pre-cured for 12minutes at 180°C (2), 200°C (3), and 220°C (4)

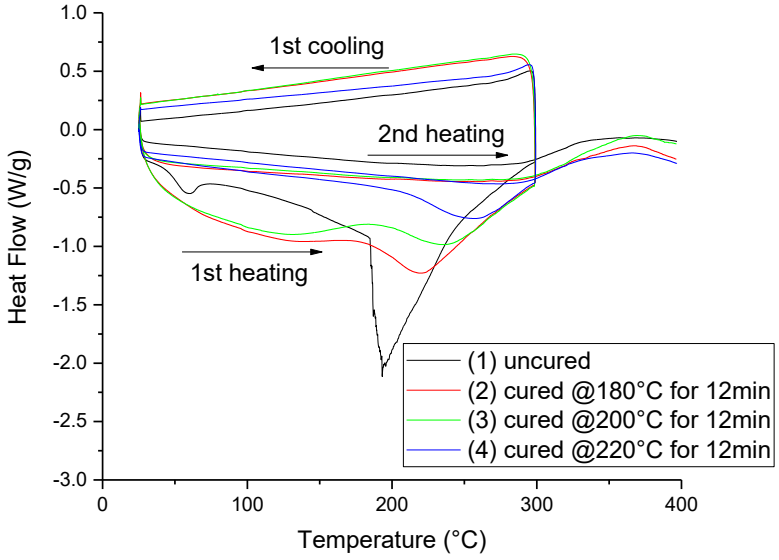

Figure 4.58 DSC thermographs of **Thermoset #3**, in non-hermetic mode, uncured (1), pre-cured for 12minutes at 180°C (2), 200°C (3), and 220°C (4)

4.4.3.2 TGA Experiment #3 in Solid

From a series dynamic TGA experiments carried out at five different heating rates, the curing behavior of **Thermoset #3** was investigated, and activation energy was estimated using Friedman method. **Thermoset #3** was investigated non-isothermally using TGA at five heating rates. The thermographs, the ln (dα/dt) vs 1/T, and resultant activation energy as a function of conversion are shown in Figure 4.59, Figure 8.62 in Appendix E and Figure 4.60, respectively. The obtained activation energy in Figure 4.60 followed a gradual increasing trend from 120 kJ/mol to 160 kJ/mol, except for 10% conversion, where the activation energy jumped sharply to 163 kJ/mol with high level of uncertainty. The increasing trend of Ea indicates that more than one mechanism can be involved in this temperature region, which is in agreement with the findings of **Thermoset #1** and **#2**.

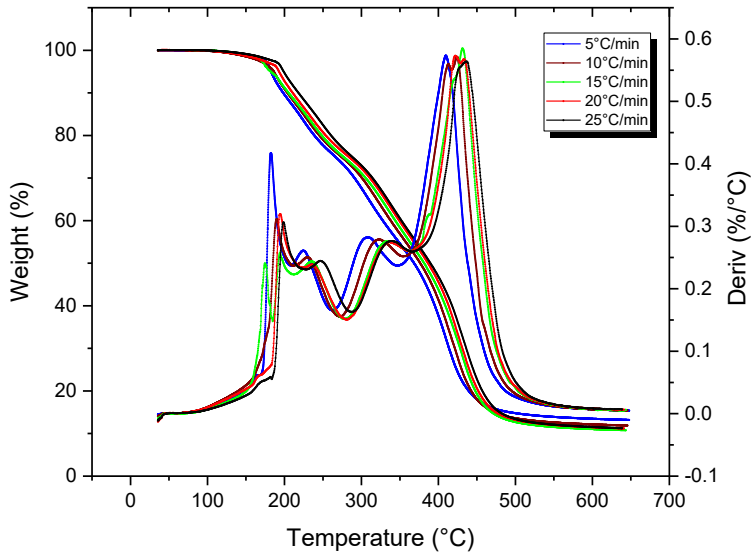

Figure 4.59 Non-isothermal TGA curves of **Thermoset #3** solid at a series of heating rates

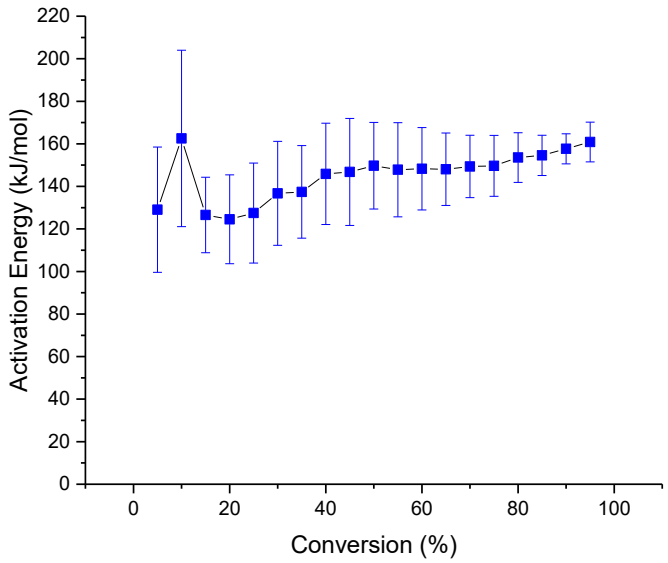

Figure 4.60 Dependence of activation energy with the extent of isothermal TGA cure of **Thermoset #3** solid

4.4.3.3 TGA Experiment #3 in Powder

Thermoset #3 in form of powder was also investigated non-isothermally using TGA at five heating rates. The thermographs, the ln (dα/dt) vs 1/T, and the resulting activation energy as a function of conversion are shown in Figure 4.61, Figure 8.63 in Appendix E and Figure 4.62, respectively. The activation energy in Figure 4.62 increased from 85 kJ/mol to maximum 193 kJ/mol at 40% conversion, then fluctuated between 150 and 200 kJ/mol to the cure reaction completion.

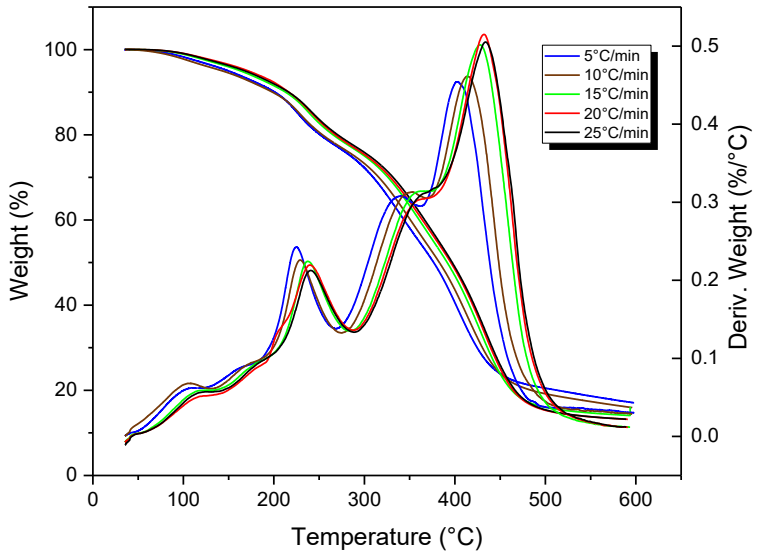

Figure 4.61 Non-isothermal TGA curves of **Thermoset #3** powder at a series of heating rates

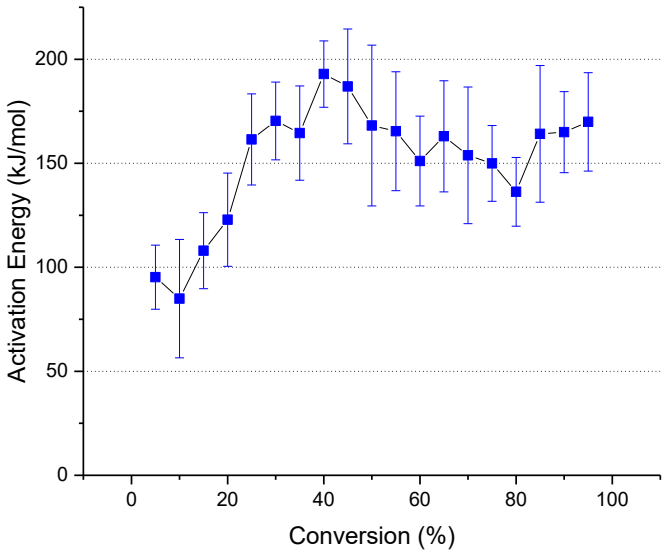

Figure 4.62 Dependence of activation energy with the extent of isothermal TGA cure of **Thermoset #3** powder

4.4.3.4 DSC Experiment #3 in Hermetic Mode

The non-isothermal cure behavior of **Thermoset #3** was investigated using DSC in hermetic mode. Figure 4.63 shows the DSC thermographs recorded at heating rates of 5, 10, 15, and 25°C/min. It is seen that the DSC thermographs were almost identical in shape for the different heating rates. The heat absorption appeared from 150°C to 300°C. It is also observed that as the heating rate increased, the peak of cure reaction was delayed and shifted to higher temperatures.

The peak temperature and reaction enthalpy of the endothermic peak of **Thermoset #2** at different heating rates were measured from the DSC curves and are shown in Table 4.15. The peak temperature was observed to shift to higher temperatures when the heating rate was increased. It was also found that the enthalpy value varied among various heating rates.

Following the same procedure as for **Thermoset #1** and **#2**, the plots of ln $[\int_0^t \frac{dH}{dt} dt / \Delta H_{total}]$ versus 1/T of **Thermoset #2** are shown for each value of α in Figure 8.64 in Appendix E. The slope of each line is equal to -Ea/R. The values of apparent activation energy, Ea, is plotted as functions of α in Figure 4.64. The gradual increasing trend was observed in Figure 4.64 from 75 kJ/mol to 126 kJ/mol accompanied by increased activation energy uncertainty. The increasing trend of Ea indicates that more than one mechanism can be involved in this temperature region, which is in agreement with the findings of **Thermoset #1** and **#2**. The large error bars reveal the uncertainty were associated with determination of the baselines and/or non-linearity of ln (dα/dt) as a function of 1/T caused by temperature dependence of reaction mechanism.

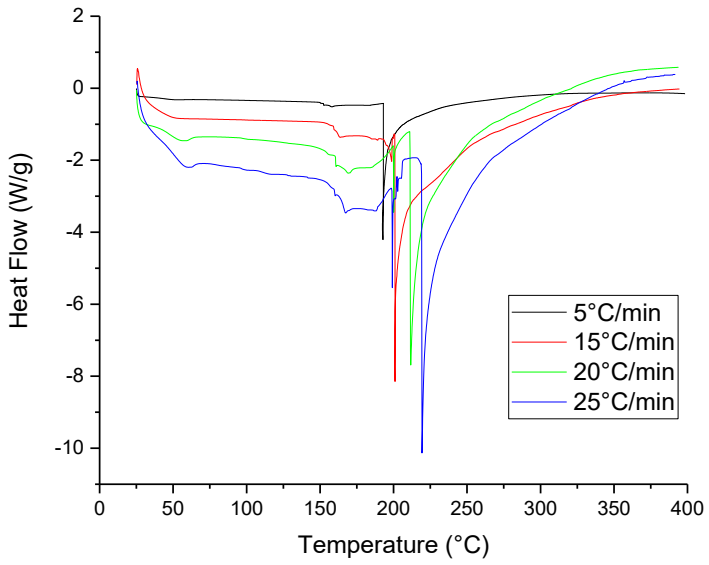

Figure 4.63 Dynamic DSC curves for the reaction of **Thermoset #3** powder at different heating rate, in hermetic mode

Table 4.15 Peak temperature and enthalpy of cure reaction of **Thermoset #3** powder at a series of heating rates, in hermetic mode

β (°C/min)	T_{onset} (°C)	T_{Peak} (°C)	ΔH_{total} (J/g)
5	193	193	289
15	201	201	247
20	211	212	221
25	219	219	218

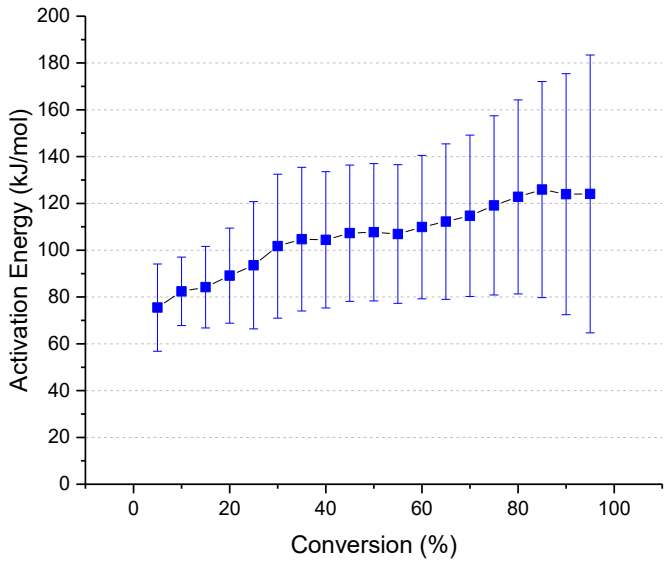

Figure 4.64 Dependence of activation energy with the extent of non-isothermal DSC cure of **Thermoset #3** powder

4.4.3.5 DSC Experiment #3 in Non-hermetic Mode

The same as in 4.4.2.5 for **Thermoset #2**, **Thermoset #3** was also investigated non-isothermally using DSC in non-hermetic mode at four heating rates. The DSC thermographs of **Thermoset #3** solid are shown in Figure 4.65 while the peak temperature and reaction enthalpy for each heating rate are tabulated in Table 4.16. With the iso-conversion method applied, the resulting activation energy as a function of conversion is presented in Figure 4.66, which illustrates the activation energy started from 125 kJ/mol and decreased to maximum 76 kJ/mol at 20% conversion followed by a steady increase to around 174 kJ/mol for the conversion up to 95%. The increasing trend of Ea indicates that more than one mechanism can be involved in this temperature region.

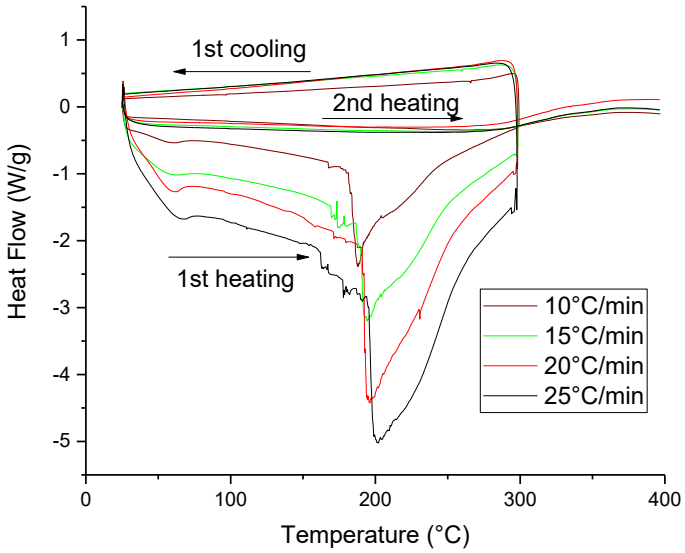

Figure 4.65 Dynamic DSC curves of **Thermoset #3** solid at a series of heating rates in non-hermetic mode

Table 4.16 Peak temperature and enthalpy of cure reaction of **Thermoset #3** solid at a series of heating rates, in non-hermetic mode

Heating rate, β (°C/min)	T_{Peak} (°C)	ΔH_{total} (J/g)
10	188	214
15	194	195
20	196	227
25	202	195

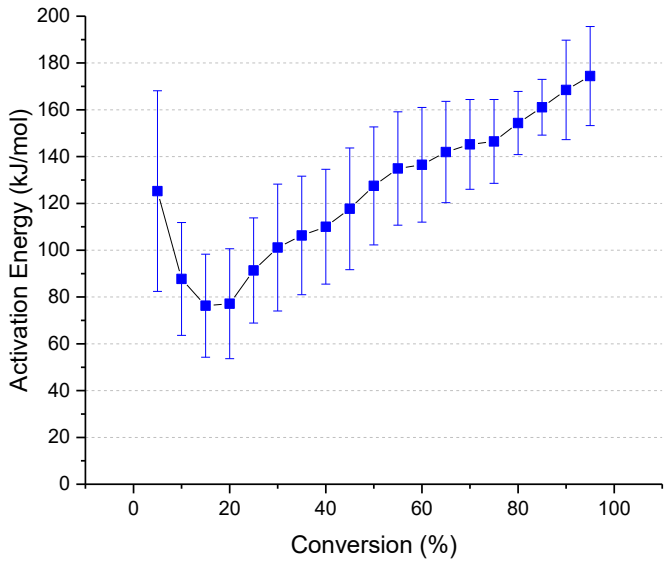

Figure 4.66 Dependence of activation energy with the extent of non-isothermal DSC cure of **Thermoset #3** solid

The thermographs of **Thermoset #3** powder, ln (dα/dt) vs 1/T plots, and the resulting dependence of activation energy on the conversion is illustrated in Figure 4.67, Figure 8.65 in Appendix E and Figure 4.68, respectively. Table 4.17 presents the peak temperature and reaction enthalpy involved for each heating rate. The estimated activation energy in Figure 4.68 varied following an increasing trend from lowest 93 kJ/mol at 5% conversion to 147 kJ/mol at 50%. Then activation energy started to drop gradually to 125 kJ/mol at 95%. The uncertainty associated with activation energy was relatively small compared to the results from other methods and sample form.

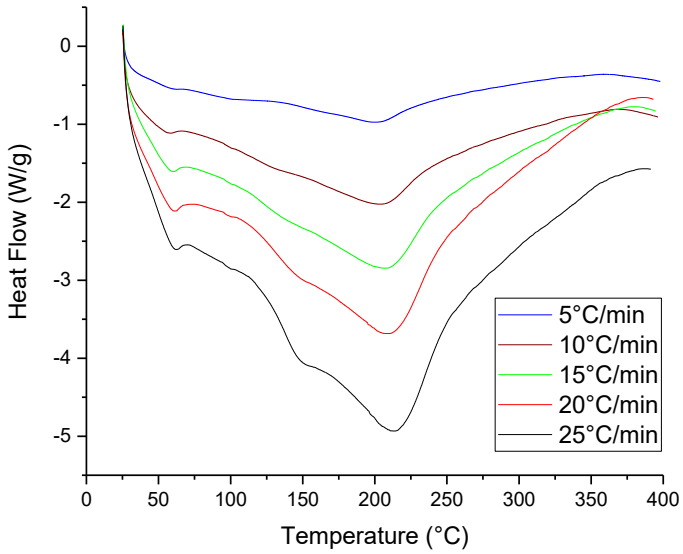

Figure 4.67 Dynamic DSC curves of **Thermoset #3** power at a series of heating rates in non-hermetic mode

Table 4.17 Peak temperature and enthalpy of cure reaction of **Thermoset #3** powder at a series of heating rates, in non-hermetic mode

Heating rate, β (°C/min)	T_{onset} (°C)	T_{Peak} (°C)	ΔH_{total} (J/g)
5	138	199	112
10	153	205	113
15	159	210	108
20	170	211	113
25	176	216	118

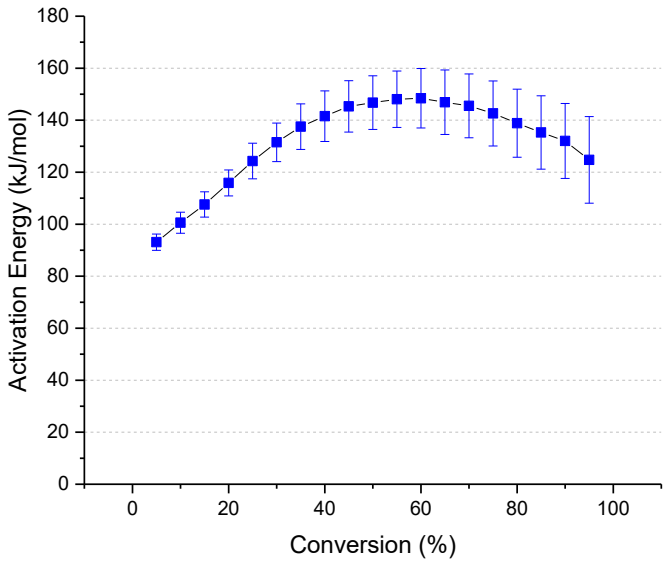

Figure 4.68 Dependence of activation energy with the extent of non-isothermal DSC cure of **Thermoset #3** powder

4.4.3.6 Discussions

Similarly, the model-free iso-conversional method was applied to non-isothermal DSC and TGA data of **Thermoset #3** curing. The activation energies Ea obtained from the combinations of two techniques of DSC and TGA, two modes of hermetic and non-hermetic, and two forms of solid and powder are plotted in Figure 4.69 and correlated with each other.

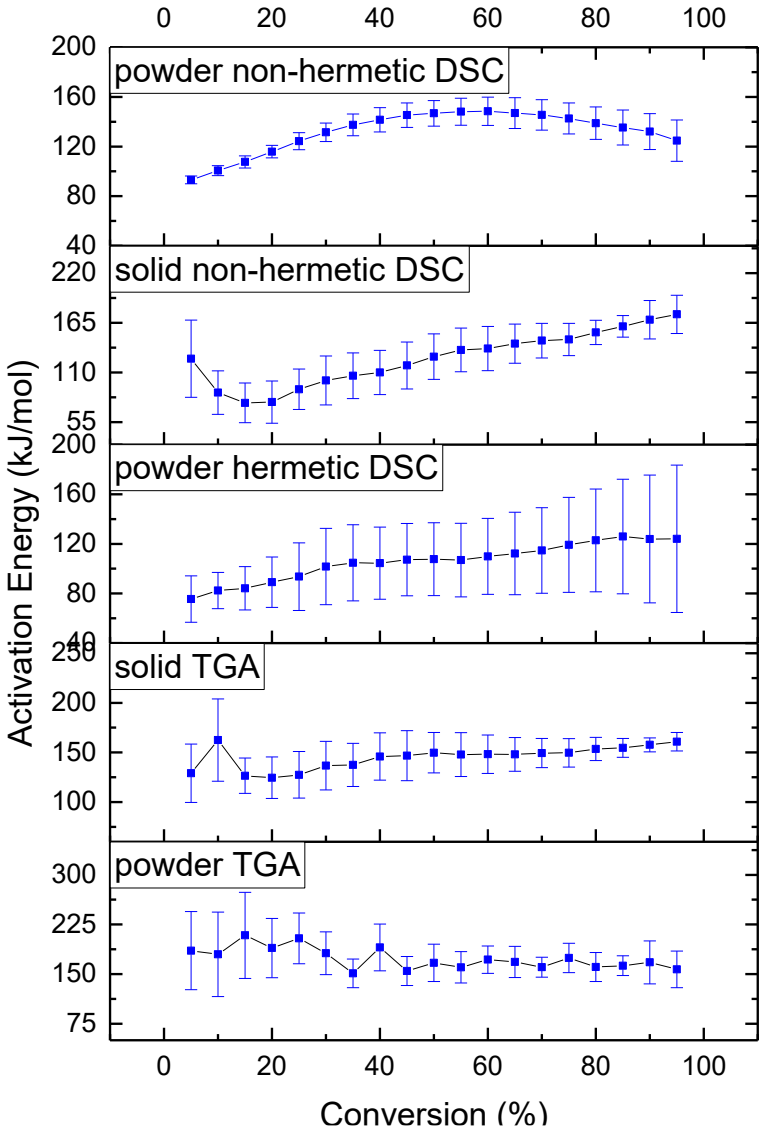

Figure 4.69 Comparison of activation energy of **Thermoset #3** from different methods

As shown in Figure 4.69, the differences in the activation energy varied significantly with variable uncertainty. However, it is clear that the DSC derived activation energy followed the same or similar increasing trend. **Thermoset #3** generally exhibited a higher activation energy at high conversion than at low conversion in the curing process. This indicates that more heat was required to cure at high molecular weight, suggesting that multiple reactions took place at different stages. On the other hand, the activation energy obtained from TGA measurements remained relatively steady and exhibited slight increasing intendancy during the whole course of curing. This is in a good agreement with the

observations from **Thermoset #1** and **#2**. The discrepancies of activation energies obtained from DSC and TGA experiments are likely to be derived from the techniques used and also to the selection of the onset and the end point selected of the range of interest. The variation in the values of activation energy can be attributed to the uncertainty of determination of temperature range studied and/or the temperature dependence of reaction mechanism.

4.4.4 Prepreg (Semi-finished Composite)

In order to understand the effects of incorporation of wheat straw on Acrodur cure reaction, the thermal behavior of the prepregs, which is semi-finished composites containing wheat straw and **Thermoset #1** before curing, was investigated using hermetic DSC. The effect of three treatments of wheat straw, two wheat straw sizes, and two binder concentrations were investigated and evaluated by comparing the onset and peak temperatures and the reaction heat (ΔH) involved in composite cure reaction. The activation energy of the prepregs was also calculated using both TGA and DSC dynamic methods.

4.4.4.1 DSC experiment #1 in Hermetic Mode

Typical DSC curves of untreated wheat straw #1 (size) reinforced **Thermoset #1** composite at 10°C/min from 25°C to 400°C are shown in Figure 4.70 as a representative illustration. The curves (2), (3) and (4) were the prepregs containing untreated, hot-water treated and NaOH treated wheat straw, respectively, while the curve (1) was obtained from neat **Thermoset #1**. As seen, the shape of curves is very similar to that of neat **Thermoset #1** in general, which suggests that the cure reaction of **Thermoset #1** played a dominant role in the prepreg's thermal behavior. The first step down endothermal peak can be linked to softening transition of polymer material. The second peak around 210°C corresponded to the cure reaction of **Thermoset #1**. It should also be noticed that, in hermetic mode, the onset and peak of cure reaction coincided at the same temperatures. It is evident in Figure 4.70 that, in comparison to the neat **Thermoset #1**, for which the onset (peak) temperature was located at 200°C and the enthalpy involved in cure reaction was 295 J/g, the onset (peak) temperatures for the prepregs shifted to higher values signifying slower cure rates at beginning. This was expected because the incorporation of wheat straw lowered the concentration of reaction components of **Thermoset #1**.

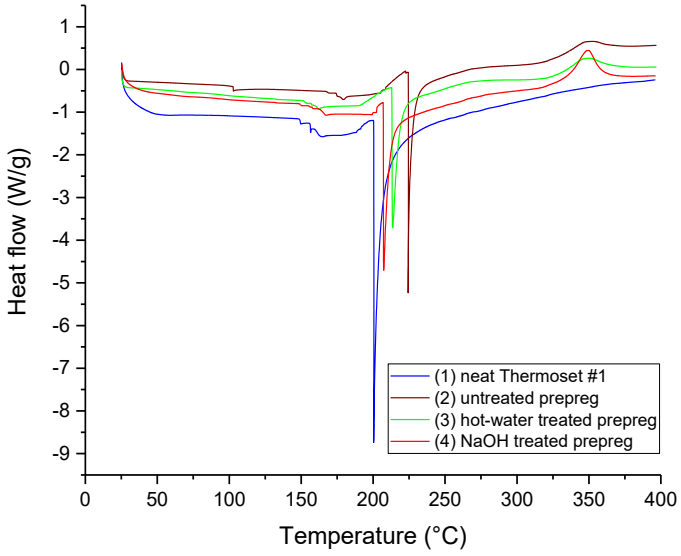

Figure 4.70 DSC thermographs of prepregs of untreated (1), hot-water treated (2), and NaOH treated (3) with 40% **Thermoset #1**

To investigate the effect of wheat straw size, treatment, and concentration of **Thermoset #1**, a replicated 2×2×3 factorial experimental design was performed, corresponding to the varying factors, i.e. two levels of wheat size, fiber (#1) and particle (#2), three treatments (non-treatment, hot-water treatment, and NaOH treatment), and two binder loading levels (20% and 40%). Three or four replicates were scanned using DSC at the same condition for each sample. The onset (peak) temperature and enthalpy were the responses as in this factorial experimental design.

The onset temperature is a temperature where the cure reaction starts. The onset temperature indicates that starting temperature of the cure reaction, and speaks to the reactivity of the sample (Sam-Brew 2017). The peak temperature obtained from the peak of the exothermic reaction indicates the temperature at which the cure rate reaches a maximum. The reaction heat represented by the area above the curve defines the amount of energy absorbed during the reaction and speaks to the chemical bond formation between the resin molecules during cure reaction (Sam-Brew 2017).

Base on the factorial experimental design, the variation in onset (peak) temperature and enthalpy within the prepreg sample were mainly attributed to three factors: 1) reinforcement size; 2) the treatment applied to wheat straw; and 3) binder concentration. However, the error might be derived from the

inconsistence of experiments, such as, if the hermetic lid was seal well or not, which determined how much pressure the pan holds until it bursts (maximum 3 bars). The purpose of three or four replicated experiments was to randomize and to separate the error.

The average of the onset (peak) temperatures and enthalpy of 3 or 4 replicates are illustrated in Table 8.30 in Appendix E. The analysis of variance was conducted and the ANOVA is shown in Table 8.31 in Appendix E. The raw data for all the replicates is attached in Appendix F. Base on the ANOVA, a significant difference (at 0.95 confident level) was observed in onset (peak) temperature between all three treatments, two wheat straw sizes, and two binder concentrations. The binder concentration exhibited the most significant effect on both onset (peak) temperatures and involved reaction enthalpy. The effect of wheat straw size was also significant on both responses, while the treatment affected the least significantly the onset (peak) temperatures, and its effect on the heat was insignificant statistically.

The reactivity of **Thermoset #1** in the presence of the wheat straw is studied by the onset and peak temperatures, and enthalpy involved. First, two levels of binder loading, 20% and 40% were examined. The higher binder loading level displayed lower onset (peak) temperatures (221 vs 127°C) and higher cure enthalpy (127 vs 156 J/g).

The prepregs containing wheat straw #2 showed slightly higher onset (peak) temperature (216 vs 219°C) and cure heat (136 vs 144 J/g) than those with wheat straw #1. That is that smaller size wheat straw delayed the initiation of cure reaction and maximum reaction rate arrived later. This suggests that the smaller size needed higher temperature and took long time for cure reaction.

With respect to the wheat straw with different treatments, based on the values in Table 8.30, the lower onset (peak) temperature value of 214°C for the NaOH treated samples indicates an early start of curing of the **Thermoset #1** resin in the presence of the NaOH treated wheat straw, followed by the hot-water treated (217°C) and the untreated (222°C) wheat straw. The higher temperature observed in the untreated samples indicates the reaction started and reached maximum rate latest.

4.4.4.2 TGA and DSC Experiment #3 of Prepreg (Untreated Straw #2-40% **Thermoset #1**) in Non-hermetic Mode

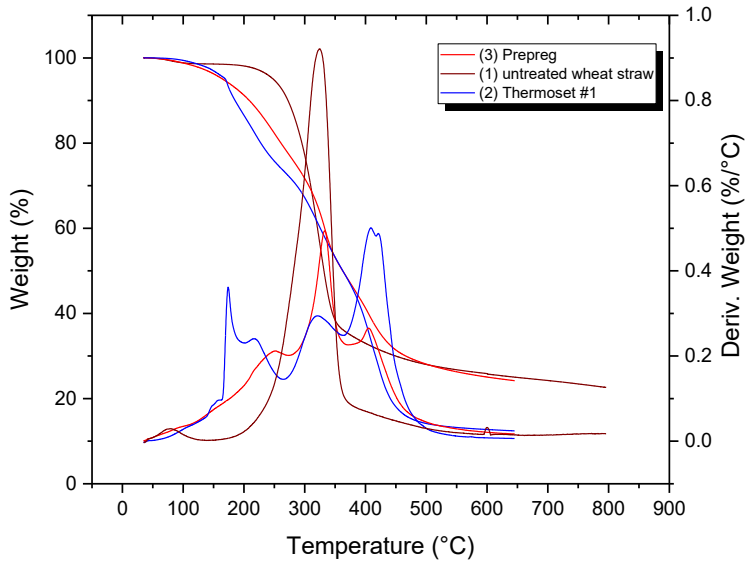

Figure 4.71 TGA thermographs of untreated wheat straw (1), **Thermoset #1** (2) and prepreg (3) containing 40% **Thermoset #1**

A very weak mass loss corresponding to cure reaction was observed in Figure 4.71 within the cure temperature regime of 150–275°C for the prepregs. The cure signal is too weak because of the effect of addition of wheat straw or non-homogeneity of the sample. In addition, when the pressure was not applied, the impregnated wheat straw exhibited a loose structure without a compression force. The reactivate components in the composite were too far apart and it is difficult to react with each other.

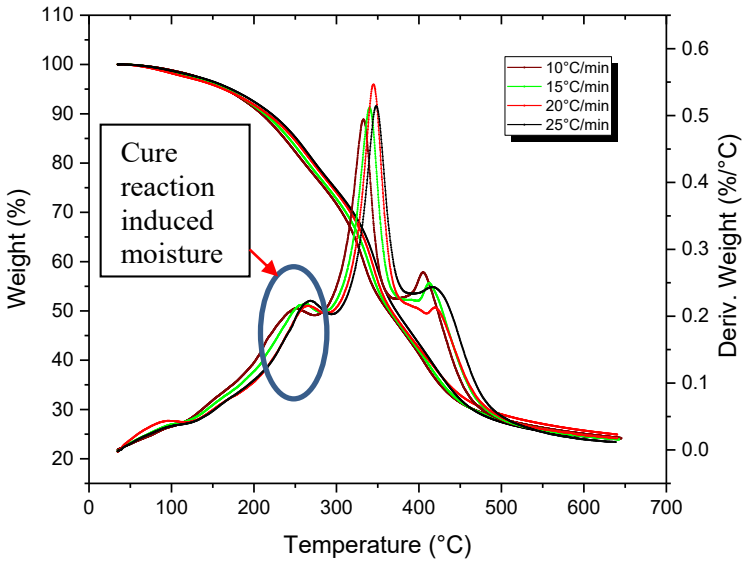

Figure 4.72 Non-isothermal TGA thermographs of the prepregs of untreated wheat straw at a series of heating rates

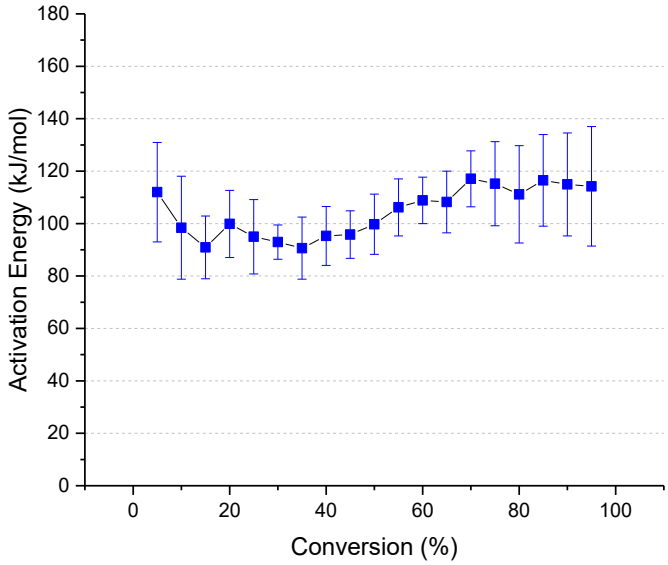

Figure 4.73 Dependence of activation energy with the extent of isothermal TGA cure of prepregs of untreated wheat straw and 40% **Thermoset #1**

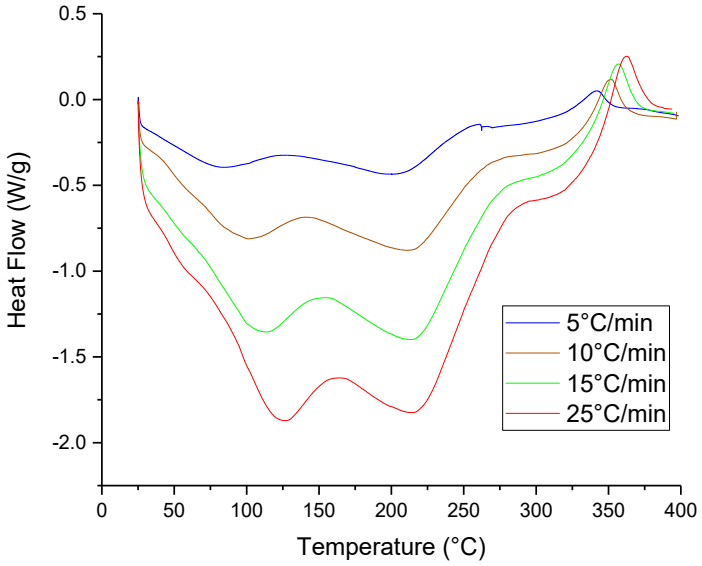

Figure 4.74 Non-isothermal DSC of the prepregs of untreated wheat straw and 40% **Thermoset #1** at a series of heating rates, in non-hermetic mode

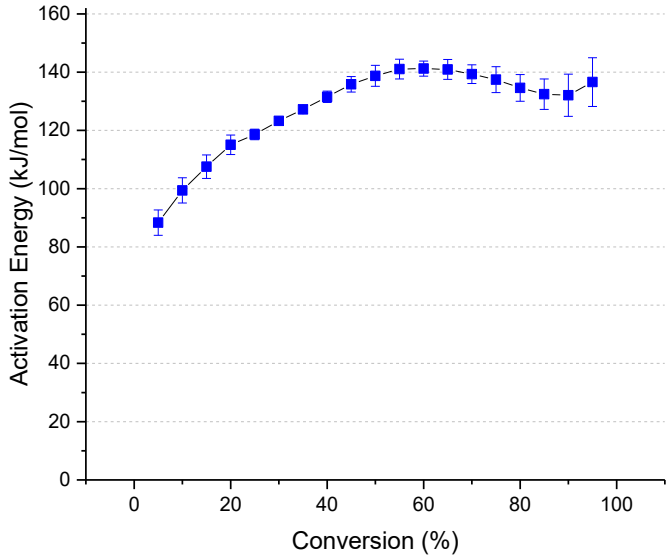

Figure 4.75 Dependence of activation energy with the extent of isothermal DSC cure of prepregs of untreated wheat straw and 40% **Thermoset #1** in non-hermetic mode

It can be referred from TGA and DSC of the prepreg of 40% of **Thermoset #1** and wheat straw #2 in Figure 4.72 and Figure 4.74 that the cure reaction shifted to higher temperature range of around 220–250°C due to the addition of wheat straw, which exerted the effect by lowering the concentration of reactive components in the Acrodur binder.

4.4.4.3 Discussion

The experimental studies by means of TGA and DSC were performed to evaluate the effects of loading of wheat straw of three treatments and two particle sizes on cure reaction of the prepregs containing polyester binder (**Thermoset #1**) and wheat straw in terms of onset and peak temperatures, and enthalpy, as well as activation energy. The variations of **Thermoset #1**'s characteristic temperatures and enthalpy were measured and compared for the samples with wheat straw of three treatments, two size, two loading levels.

4.4.5 Comparison of Three Acrodur Binders and Prepreg

The effect of binder type, i.e., **Thermoset #1**, **#2** and **#3**, corresponding to Acrodur DS3530, CNF reinforced Acrodur DS3530 and 950L can be evaluated by comparison of the onset and peak temperatures and reaction enthalpy of **Thermoset #1**, **#2** and **#3**.

In TGA curves of the samples either in solid or powder form, the onset and peak temperatures are almost the same at around 175°C for trapped moisture, and at around 210°C for cure reaction, as shown in Figure 4.76, Figure 4.77. The mass loss in studied temperature range is around 22% for all three samples. It is also observed the onset and peak temperature in DSC thermographs in Figure 4.78 for three samples in powder form were in the same range, except for DSC thermographs in hermetic mode, where the peak temperature of **Thermoset #3** was found slightly lower than that of **Thermoset #1** and **#2** as shown in Figure 4.79 and in Table 4.18. The overall observation implies there was no significant difference in cure behavior of **Thermoset #1**, **#2** and **#3** under tested conditions. It is concluded that **Thermoset #1**, **#2** and **#3** behaved non-isothermally the same in the temperature range of 150–300°C.

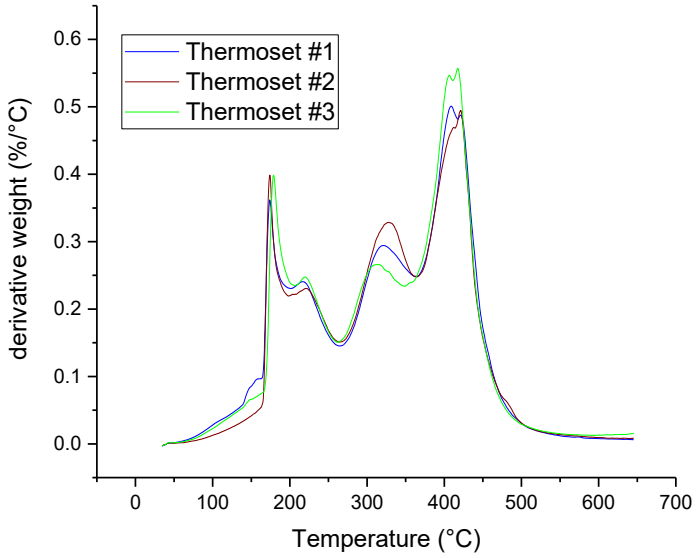

Figure 4.76 DTG thermographs of **Thermoset #1, #2, and #3** solid

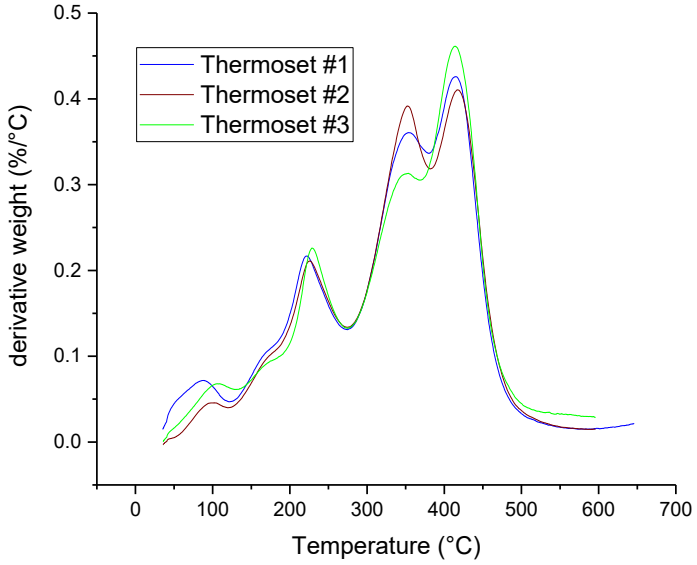

Figure 4.77 DTG thermographs of **Thermoset #1, #2, and #3** powder

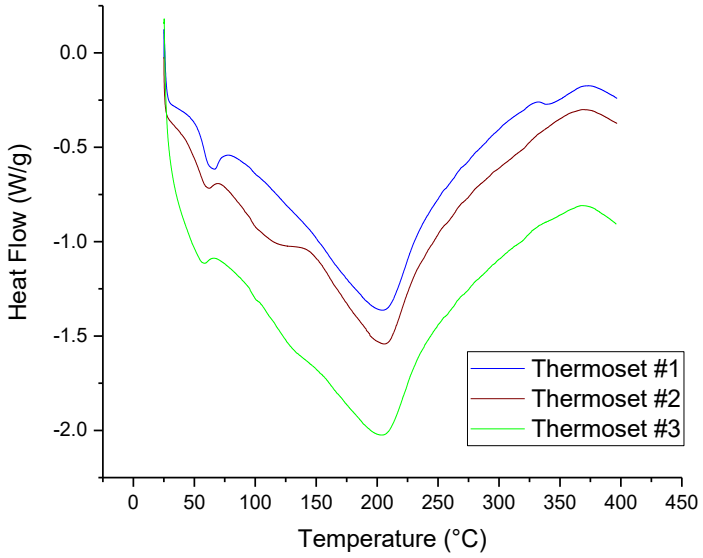

Figure 4.78 DSC thermographs of **Thermoset #1, #2, and #3** powder in non-hermetic mode

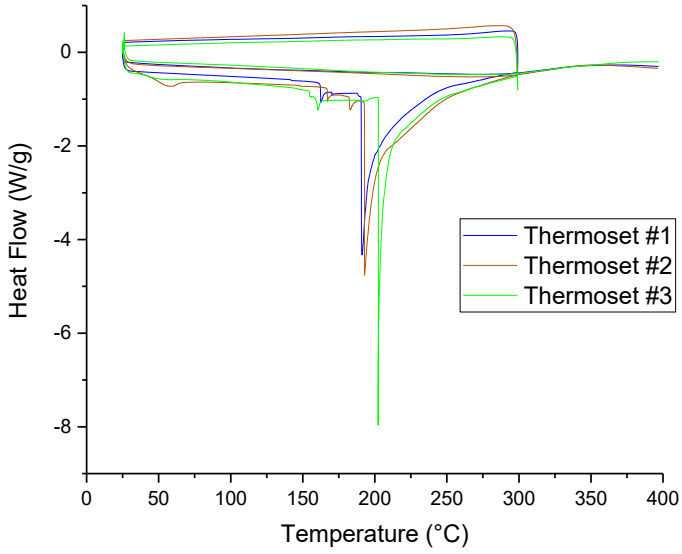

Figure 4.79 DSC thermographs of **Thermoset #1, #2, and #3** solid in hermetic mode

Table 4.18 Parallel comparison of peak (onset) temperature and reaction enthalpy between **Thermoset #1, #2, and #3**

Sample	T_{peak} (°C)	Enthalpy (J/g)
Thermoset #1	191	257
Thermoset #2	193	315
Thermoset #3	202	242

In addition to onset and peak temperatures, the three types of Acrodur binders and the pregregs comprised of 40% **Thermoset #1** were also investigated and compared in terms of the dependence of activation energy with the conversion. Figure 4.80 demonstrates the variation of activation energy obtain from the sample in form of powder studied under non-hermetic condition as a function of the degree of cure reaction. It is observed that the three Acrodur binders, i.e. **Thermoset #1**, **#2**, and **#3**, and the prepreg exhibited the similar increasing trend of Ea with the conversion. They all started at low value of Ea, then the activation energy increased until the conversion reached 50–60%. For the latter portion of conversion, the increasing rate became small, except for **Thermoset #3**. The changing activation energy as a function of the conversion reflected the fact that the reaction mechanism may change as the cure reaction progressed. It required more energy at the latter portion of the conversion than at the beginning. This can be attributed to the chemical controlled reaction at low conversion and diffusion controlled reaction at high conversion.

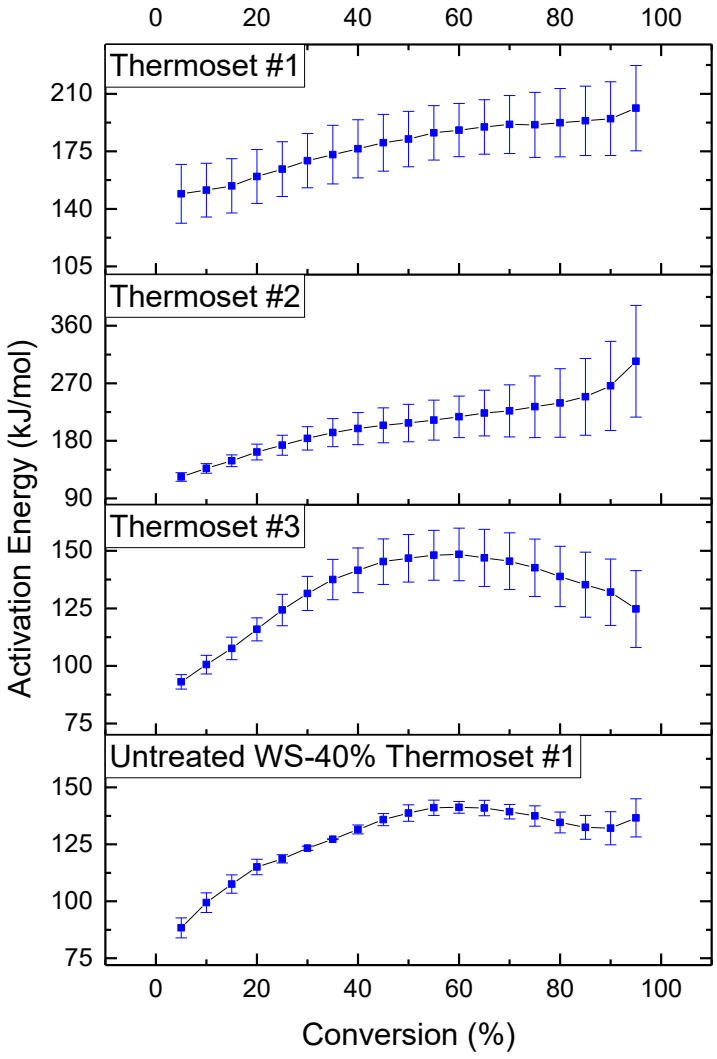

Figure 4.80 Activation energy of **Thermoset #1**, **#2**, and **#3** powder and prepreg containing 40% **Thermoset #1** from DSC measurement in non-hermetic mode

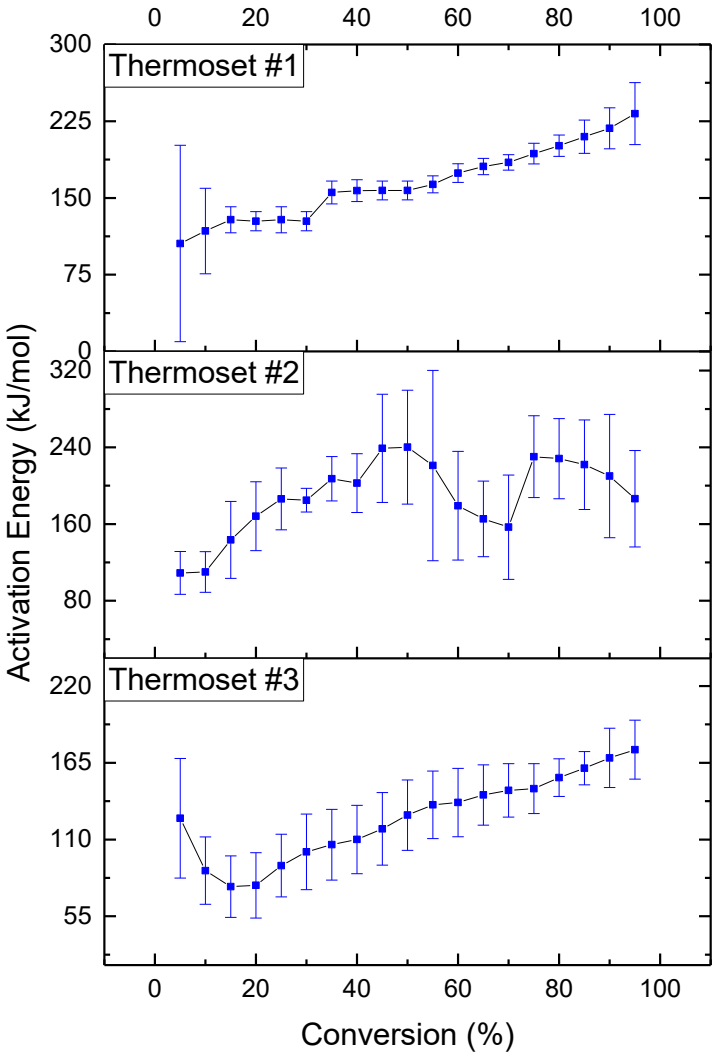

Figure 4.81 Activation energy of **Thermoset #1**, **#2**, and **#3** solid from DSC measurement in non-hermetic mode

The samples in solid form were also investigated using non-hermetic DSC. Although the overall increasing trend can be identified, the dependence of activation energy on the conversion became complicated, which was suggested by the combined increasing and decreasing trend during the curing process were observed in Figure 4.81. The explanation can be found in the solid lump samples that complicated the process by slowing down the diffusion of the reactants even at low conversion.

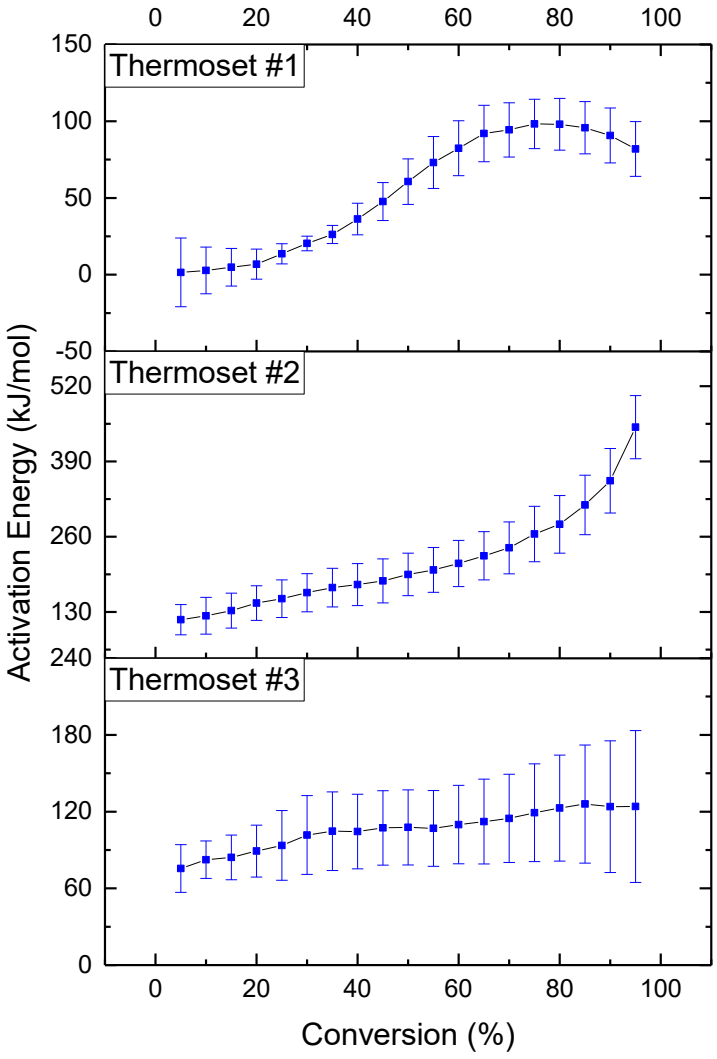

Figure 4.82 Activation energy of **Thermoset #1**, **#2**, and **#3** powder from DSC measurement in hermetic mode

The simple increasing relationship of activation energy and the conversion was found in **Thermoset #1**, **#2**, and **#3** powder that were analyzed using DSC in hermetic mode, as shown in Figure 4.82. It is inferred that under hermetic condition, three binders exhibited apparently combined mechanisms along the conversion, which is in agreement with that under non-hermetic condition.

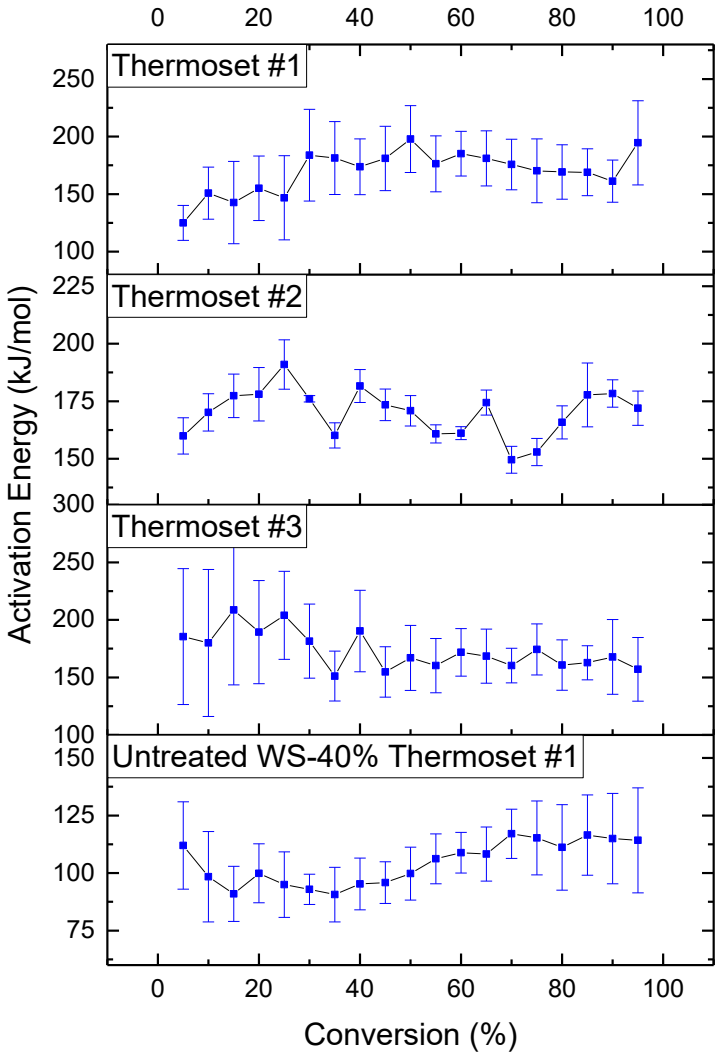

Figure 4.83 Activation energy of **Thermoset #1**, **#2**, and **#3** powder and prepreg containing 40% **Thermoset #1** from TGA measurement

The relationship of activation energy with the conversion obtained from TGA analysis is shown in Figure 4.83 and Figure 4.84 corresponding to the sample form of powder and solid respectively.

As seen in Figure 4.83, the variation of activation energy was relatively small and no apparent increasing trend was noticeable. The prepreg also demonstrated the same trend as neat Acrodur binders. Similarly, the solid samples in Figure 4.84 followed the same relatively steady trend, except the

extraordinary large uncertainties associated at low conversion of below 10%. This can be related to the interference of trapped moisture due to hindering effect of the big sample size.

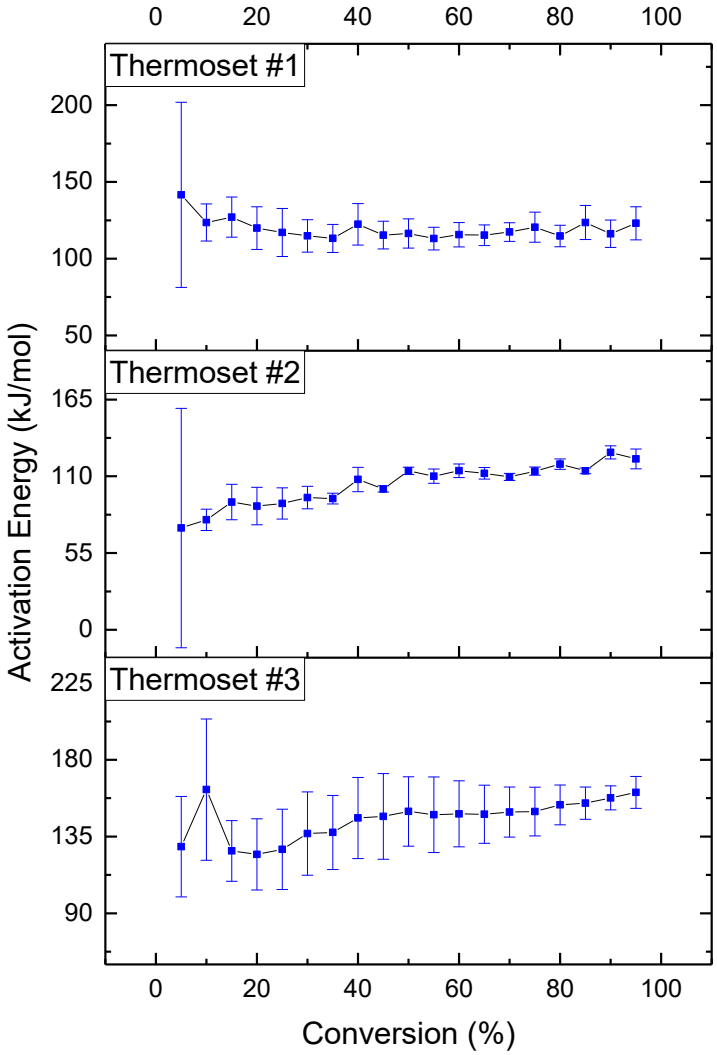

Figure 4.84 Activation energy of **Thermoset #1**, **#2**, and **#3** solid from TGA measurement

Based on the above comparison, it is evident the dependence of activation energy on the conversion differed between two analytical techniques. The evident increasing tendency was found in Figure 4.80, Figure 4.81 and Figure 4.82 that the DSC was used, whereas the activation energy obtained using TGA showed low variation and hold relatively steady during the whole process. The difference can be

explained by the fact that the TGA curves demonstrated relatively clear temperatures for the onset and termination points. This is attributed to the characteristics of two analytical techniques, because TGA is a completely open system, with assistant of purge gas, the moisture and other gaseous matters were carried away instantaneously as soon as they were produced. However, in DSC analysis, the pans and lids with limited volume were used that restricted the free removal of the moisture and other gaseous matters.

4.5 Summary of Findings

In this work, the cure kinetics and the effects of the parameters on cure behavior of three thermosetting Acrodur binders, i.e. **Thermoset #1**, **#2** and **#3,** and the prepregs containing wheat straw-**Thermoset #1** were characterized isothermally and non-isothermally by means of two complementary thermal analyses (TGA and DSC). Both non-isothermal and isothermal heating profiles for DSC were carried out with both hermetic and non-hermetic modes. The examined parameters were temperature and time, pressure, two binder forms (powder and solid), addition of less than 5% CNF, addition of wheat straw of two sizes (fiber and particle), three treatments, and two loading levels (20% and 40%).

The characteristic temperatures, mass loss (for TGA), enthalpy (for DSC), and conversion independence of temperature or time, were determined and characterized. The relationship between degree of conversion (curing) and temperature and time for isothermal TGA and DSC was established. The dependence of the effective activation energy on the extent of cure was yielded by applying model-free isoconversional method for different experimental condition. The results from TGA and DSC were compared and correlated.

A good knowledge of the curing kinetics and curing cycle (how fast, how long at given temperature, how much of degree of curing) can provide a guideline for the production of Acrodur based composites and allow for the control of the degree of curing of the materials, and optimize the cure condition. Based on the results, the suitable cure temperatures and time can also be selected to cure the material to a desired extent of crosslinking and to avoid high temperatures at which undesirable side reactions or degradation may occur.

Analysis of the dependence of activation energy on the conversion allowed for better understanding the complex curing processes that may include different chemical reactions or a chemical reaction complicated by a mass transfer processes such as evaporation of water. Moreover, the curing process

can also be accompanied by vitrification, or thermal degradation. The tentative explanations were proposed to explain the kinetic of curings.

Since no previous systematic studies using calorimetry to investigate the cure kinetics of Acrodur or Acrodur based composites were found in the literature, no references are available for comparing the results of this chapter with. Based on the results presented here and discussed previously, the conclusions can be drawn as following.

1. The relationship of temperature-time-conversion was established based on isothermal TGA and DSC studies. The Acrodur cure at isothermal condition was observed starting from 150°C for non-hermetic mode and from 170°C for hermetic. These temperatures are considered the "threshold temperatures" for Acrodur cure reaction. Below these threshold temperatures, crosslinking did not happen during the reaction times evaluated here. Above the threshold temperatures, crosslinking increased as the higher temperature and the heating time increased.
2. The combination of temperature above 170°C for at least 5 minutes led to the degree of crosslinking reaching nearly full conversion. Thus, it could be considered that 170°C is a high enough temperature to fully cure **Thermoset #1** under practical compression molding condition.
3. The thermal degradation of Acrodur was observed above 300°C.
4. No softening of fully cured Acrodur ($T_{g\infty}$) was observed below 300°C in either regular DSC or modulated–temperature DSC curves.
5. The impacts of pressure on the cure reaction was revealed by the change of thermographs shape, and onset (peak) temperature. It is observed that the reaction occurred earlier (at lower temperatures) and smoother in non-hermetic mode than in hermetic mode.
6. The DSC and TGA results were compared and evaluated. The TGA results are considered more reliable than DSC due to the relatively clear determination of temperature intervals (onset and termination points) necessary for data analysis. Moreover, analysis of the DSC data was further complicated by the difficulty in exclusion and isolation of interfering events, such as trapped water evaporation. This is the case under the hermetic condition as well as the heat due to water vapor expansion.
7. The smaller size (powder form) of the binders is preferable for the cure reaction than the solid form, mainly because powder sample eliminated the diffusion controlling step at low

conversion. Therefore, from this perspective, a good dispersion of binder on wheat straw can contributed to a faster and smoother cure reaction.

8. The cure behavior of three binder types, **Thermoset** #1, **#2** and **#3** were compared, and the effect of incorporation of CNF in **Thermoset #1** was determined. No significant differences among the cure behavior of **Thermoset** #1, **#2** and **#3** were noticed in term of onset (peak) temperature.

9. The effect of adding natural fiber wheat straw was evaluated, with regard to two sizes and three treatments, two loading levels. The onset (peak) temperatures of the prepregs were investigated using DSC hermetic. The results indicate that addition of what straw shifted the onset and peak temperature to higher level. This implies the need to increase platen temperatures during production of pressboard for the prepregs to ensure efficient bonding of the **Thermoset #1** resin with the wheat straw. The higher binder loading level (40%) displayed lower onset (peak) temperatures (221 vs 127°C) than 20% loading. The smaller size (straw particle) needed higher temperature 219°C than straw fiber at 216°C. The NaOH treated samples demonstrated an early start of curing of the **Thermoset #1**, followed by the hot-water treated (217°C) and the untreated (222°C) straw.

10. It can be concluded based on the above discussion that, for production of composite pressboards, the press platen during the pressing operation must be set to temperatures above 170°C for 5–10 minutes for neat Acrodur, and around 220°C for the prepregs to guarantee temperatures in the mat exceed this temperature and ensure effective bonding of the binders, without inducing serious thermal degradation of wheat straw and Acrdour. The aeration step during compression is necessary to ventilate the contained and produced moisture and this allow the cure reaction move forward.

11. The activation energy was estimated using isoconversional method from both TGA and DSC experimental data of various conditions, i.e., two sample forms, hermetic and non-hermetic modes. The deconvolution of TGA curves was also conducted.

12. The values of activation energy varied significantly among the thermal analysis techniques, two sample forms, hermetic and non-hermetic modes. Great levels of the variation of activation energy obtained from difference techniques and conditions were connected to the uncertainties associated to the combination of multiple processes due to uncertainty in determination of onset and termination points of the baseline. For example, trapped moisture evaporation overlapping

at starting phase of cure and diffusion process or thermal degradation overlapping at ending phase.

Despite the significant variation of the activation energy for the Acrodur cure reaction, a consistent pattern was observed and the overall increasing trend in dependence of activation energy on conversion manifested the multiple steps were involved in the tested temperature range. This is in agreement with the statement that the complex reaction mechanism normally associated with condensed phase reactions (Sbirrazzuoli 2019). The interpretation of the dependence of activation energy values upon the conversion may provide useful mechanistic clues. The activation energy remained relatively low up to around 40–60% conversion. Beyond 40–60% conversion the Ea values raised. The tentative explanation was proposed to explain the kinetic of cure. This behavior was attributed to the developed high crosslinking which reduced the molecular mobility and the process changes from being kinetically controlled to diffusion controlled.

Chapter 5
Lap Adhesion

5.1 Introduction

The mechanical properties of fiber-polymer composites do not only depend on the individual characteristics of fiber and polymer, but also on the interfacial adhesion. The adhesion at the interface of reinforcing fibers plays a critical role in determining the integrity of the composites. The applied stress is efficiently transferred only if the adhesion between the fiber and the polymer is well-established. The effects of fiber-polymer adhesion on mechanical properties has been intensively demonstrated in previous studies. It was reported that fiber-polymer adhesion directly influences the mechanical performance of the composites, especially strength, which is significantly increased if fiber polymer adhesion is improved (Nyström et al. 2007) (Arbelaiz et al. 2005) (Keener et al. 2004).

The main factors that affect the joint strength of bonded joints are the properties of the adherend surface and adhesive and the stress concentrations that depend on the joint geometry (Kairouz and Matthews 1993), i.e. surface characteristics, adherend and adhesive thickness, and overlap. The adhesion strength is generally stated in terms of lap shear strength. Lap shear strength is the ability of a material to resist lateral forces that cause the internal structure of the material to slide against itself.

The lap shear strength is reported as the failure stress in the adhesive, which is calculated as a ratio of the maximum load applied to the surface area over which it was applied, given by Equation 5.1:

$$\tau = \frac{P}{bl} \qquad 5.1$$

where P is the applied load, b the width of the joint, l the length of the joint, τ the adhesive shear stress.

In a single lap joint configuration, the adherend may undergo bending under load due to its asymmetry which results in the development of considerable peel stress at the overlap ends (Campilho et al. 2013). The shear stress also peaks at the same locations because of gradual adherend straining along the overlap (Campilho et al. 2007). In addition, it does not give a true measure of the shear strength due to adherend bending and induced peel loads (Campilho 2016).

Several mechanisms can be responsible for the failure of the material, which can be grouped into failure of adherend (delamination, failure of the fibres, etc.), failure at the interface adhesive /adherend, and failure of the adhesive (cohesive failure of adhesive). Demonstrated in Figure 5.1 are the typical

failures that could happen during this test. It is not always easy to identify failure mode. Sometimes mixed failure modes — any combination of two or more of the six classes of failure mode defined above — can happen. This should include percentages when more than one failure mode occurs.

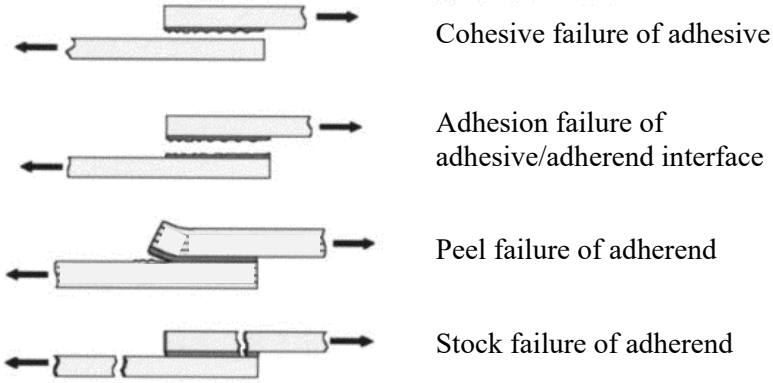

Figure 5.1 Representation of failure modes of adhesive joints under shearing force (Hart-Smith 1973)

5.2 Research Objectives and Approach

This chapter is intended to provide further insights in the development of wheat straw based thermoset composite pressboards. The goal is to evaluate the interfacial strength between straw and the binder Acrodur. The hypothesis to be evaluated here is if the thermoset Acrodur cured under typical compression molding conditions is capable of providing sufficient adhesion at interface of wheat straw. The specific objective is to prepare and to evaluate lap joints with straw and Acrodur and then measure the strength. More specifically, single lap bonded specimens of straw were prepared and the single lap shear strength was measured to investigate the influences of binder concentration, and two types of surfaces of straw stem on the failure mode and the strength of bonded joints.

5.3 Materials and Methods

The wheat straw samples used in this chapter were collected from one of freshly harvested wheat straw bales in 2018 that were obtained from an AC Mountain, soft white winter variety wheat, cultivated in Woodrill farms in Ontario, Canada and supplied by Omtec Inc.. The wheat straw samples were selected from a bag of wheat straw raw material. After the leave blades and sheaths and the nodes were cut off, only wheat stems were chosen for the test because sheaths were thin and weak. Straws

containing natural defects or damage occurring during harvest or transportation were excluded. Samples were randomly selected from the set of straws containing no visual damage or defects. The unopened (without longitudinal cut) stems were used except for two interior-interior specimens. In this case, the stems of around 10–15cm were cut open (longitudinal direction) and flattened.

The adhesives used in this chapter were Acrodur DS3530 solutions in Figure 5.2 (a) and cellulose nanofibril reinforced Acrodur DS3530. Acrodur DS3530 is a thermoset acrylic based polyester solution. The CNF-Acrodur DS3530 was prepared by mixing around 5% cellulose nanofibril in a solution of Acrodur DS3530 shown in Figure 5.2 (b).

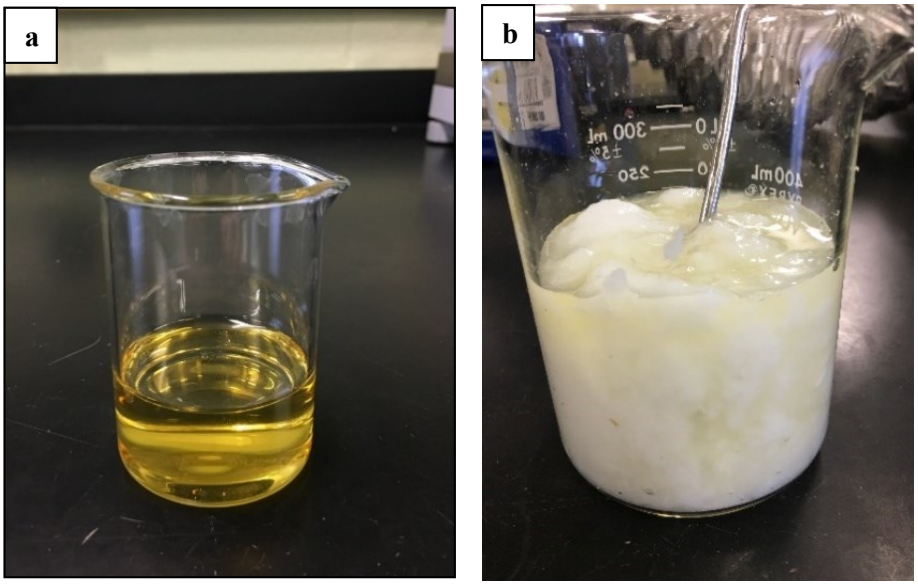

Figure 5.2 Acrodur DS3530 solution (a) and cellulose nanofibril solution (b)

The selected wheat stems were dried in oven at 50°C prior to impregnation of adhesive. Acrodur DS3530 or CNF-Acrodur DS3530 solution were diluted with deionized water at a ratio of 1:1. Then the diluted Acrodur DS3530 or CNF-Acrodur DS3530 solutions were sprayed slowly onto the stems while being stirred in an orbital mixer. Four levels of Acrodur DS3530 were used for sample preparation: 50%, 20%, 5% and 2%, while only 5% of CNF-Acrodur DS3530 was applied. For binder contents as low as 5% and 2%, the distribution of binder became critical for effective adhesion. Lower concentrations by adding more DI water were used to ensure effective binder distribution on wheat straw.

Once impregnated, the excess water was removed by drying in a convection oven at 50°C to achieve the moisture content of less than 10%. After drying, two samples of impregnated stems were then overlapped manually along stem direction (grain direction) and placed in between two aluminum plates.

The plates were compressed in hydraulic press with the temperature controlled at 170°C for 5–7 minutes for curing the adhesive. The compression force used was 20,000 lb. Using a compression force of 25.000 lb had shown to damage the straw, because the force might be too high. The representative examples of the specimens manufactured are shown in Figure 5.3 (a).

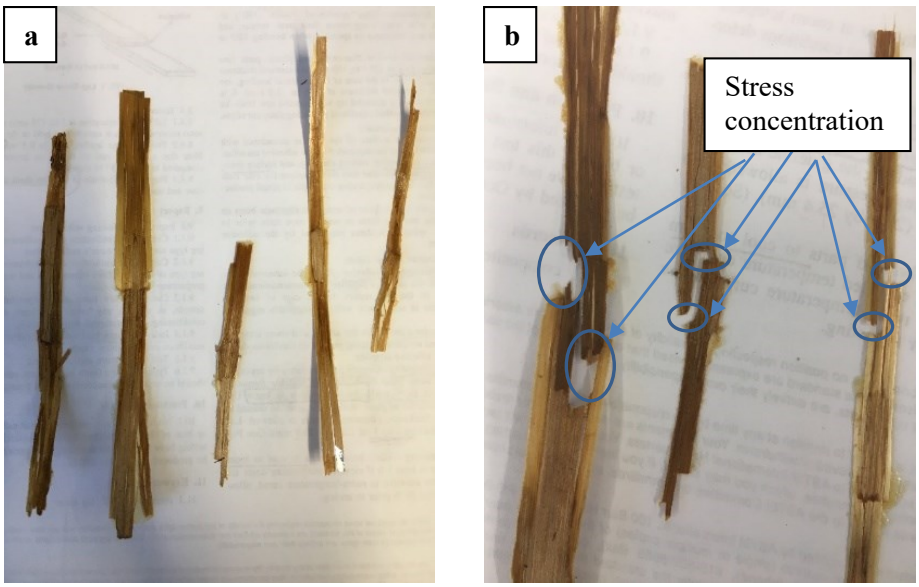

Figure 5.3 Representative examples of the specimens before (a) and after (b) test

In this study, the test procedure described in ASTM D5868 (2005) was adopted for this specific system of polyester binder and wheat stem. The dimension requirement for adherend is not practical for naturally occurring wheat straw, due to the presence of random fiber flaw and lack of uniformity of wheat straw characteristics, compared with those of manmade materials. Therefore it may not be feasible to limit test specimen geometry to that is called for in ASTM D5868, although it was known that the single lap joint is quite sensitive to changes in geometrical parameters (Ferreira et al. 2005).

Single-lap shear strength was measured for wheat straw joints bonded with different concentrations of Acrodur DS3530 cured at 170°C, under 20,000lb of force for 5–7 minutes. The lap shear strength test was conducted at room temperature on the compression cured samples using a Test Resources Universal Test Machine (Test Resources Inc., Shakopee, MN, USA). Firstly, the area in the bonding area was measured in square meters. Force was applied to the specimen until failure. A crosshead rate of 1.3mm/min was used. Both load at failure and type of joint failure were recorded. The adhesion strength was calculated by $\tau=P/bl$ given in Equation 5.1. For irregular geometry of natural fibers, an approximation method of square/rectangle was used.

5.4 Results and Discussions

Table 5.1 and Table 5.2 present the measurement of adhesion strength based on the maximum load for all configurations for Acrodur DS3530 and CNF-Acrodur DS3530 as well as the mode of failure. In this table, ex and in denote the "exterior" and "interior" surfaces of stem, respectively.

Table 5.1 Acrodur DS3530 adhesion strength and failure mode

Acrodur DS3530	Lap Surface	Area (m^2) Approx.	Max Load (N)	Stress (Pa)	Failure mode
50%	unspecified	0.010425	65.68	6,300	Stock break failure
50%	unspecified	0.007378	29.55	4,006	Stock break failure
20%	Ex-ex	0.022509	35.96	1,598	Stock break+ 5% adhesive failure
20%	Ex-in	0.006368	42.77	6,716	Adhesive failure
20%	Ex-in		N.A.		Stock break failure
20%	Ex-in		N.A.		Stock break failure
5%	Ex-ex		N.A.		Weak bond/tore open
5%	In-in	0.010893	5.42	498	Stock break failure
5%	Ex-in	0.011238	4.83	430	Stock break failure
5%	Ex-ex	0.023298	54.22	2,327	Stock break failure
5%	Ex-ex	0.006722	15.99	2,379	Stock break with unopened structure
2%	Ex-ex	0.006427	Low		Stock break failure
2%	Ex-ex	0.004349	Low		Stock break failure
2%	In-in	0.009015	102.54	11,374	50% stock break-50% adhesive mixed failure
2%	Ex-ex	0.007237	28.46	3,932	Stock break failure
2%	Ex-ex	0.007261	N.A.	Impaired specimen from compression molding	

It was observed from Figure 5.3 (b), the failures occurred mostly on stem edges of the overlap, which is in agreement with the locations of high stress concentration. Some of the variations in the results were attributed to the presence of naturally occurring lack of uniformity in the surfaces. This variation is inherent to the nature of most natural materials. The most common mode of failure was stock failure, for all the binder concentrations. The non-stock failure was found to be a half-half mixed failure on interior-interior adhesion. This demonstrates that the weak point was the stem itself instead of adhesion at the interface. Therefore, it is reasonable to consider that this measured the "tensile strength" of the stem and not adhesion strength. It was concluded that addition of 2% Acrodur DS3530 was able to

provide sufficient adhesion for holding two pieces of wheat straw together. It was further concluded that the combination of temperature of 170°C and pressure of 20,000lb of force was sufficient for curing Acrodur DS3530 and that as low as 2% of this adhesive was able to provide sufficient bond strength to prevent adhesive failure.

The effect the nature of adherend surface and its structure is likely to play an important role in production of wheat straw-Acrodur composite. It was observed that during sample preparation the stem exterior did not hold liquid very well due to smoothness of the surface and consequently Acrodur DS3530 solution did not wet the surface of the stem as effectively as in the case of the interior stem surface. On the other hand, the porous structure and roughness of the stem interior surface absorbed the solution of adhesive thus contributing to bond formation as well as strengthening wheat straw itself. This become important when wheat straw is considered the weak point. This can be one of possible reasons why the only non-stock failure was observed on interior-interior adhesion. In addition, with a short time for impregnation, the reduced amount of adhesive solution going into the wheat straw and preferentially stayed on the surface of the stem to provide improved adhesion. On the other hand, a longer impregnation time allowed penetration of binder into the stem structure. As a consequence, the stem penetration of the binder under the surface of the stem is likely to have contributed to increasing the strength of the stem tissue near the surface.

Table 5.2 CNF-Acrodur DS3530 adhesion strength and failure mode

CNF-Acrodur DS3530	Lap Surface	Area (m2) Approx.	Max Load (N)	Stress (Pa)	Failure mode
4.85%	Ex-ex	0.006426	9.254	1,440	Stock break failure
4.85%	Ex-ex	0.006041	7.001	1,159	Stock break failure
4.85%	Ex-ex	0.005937	4.337	731	Stock break failure
4.85%	In-in	0.010655	Impaired specimen from compression molding		
4.85%	Ex-ex	0.007497	Impaired specimen from compression molding		
4.85%	Ex-ex	0.006291	Impaired specimen from compression molding		

By considering other observations with respect of production of wheat straw-Acrodur pressboard, that at least 20%–40% Acrodur DS3530 had to be used to provide sufficient adhesion, the explanation can be found in the fact that when wheat fiber size is small, the specific surface area became large therefore requiring more adhesive to fill the interface formed by gaps and pores among the straw stems.

Table 5.2 shows that the specimens with 4.85% of CNF-Acrodur DS3530 as binder resulted in "stock failure" the same as Acrodur DS3530. The stress values in Pa decreased compared to that of specimens using Acrdoru DS3530 as binder. The results did not demonstrate the reinforcing effect of addition of nanofiller as observed in literature (Lee et al. 2014) (Chakrabarty and Teramoto 2018). This can be attributed primarily to weak strength of the adherend wheat straw and to agglomeration of CNF fibers in Acrodur DS3530 solution.

5.5 Conclusion

The single-lap shear strength of the wheat straw joints adhered with 2%, 5%, 20% and 50% of thermoset Acrodur DS3530 was found to solely depend on strength of wheat straw itself. The failure occurred dominantly as "stock failure", suggesting that the failure strength of wheat straw bonded joint was not always proportionate to adhesion strength of adhesive due to the weakness of substrates, wheat straw for this case. The failure was found to be more related to adherend-straw and not the adhesive (binder). Therefore, the tested strength can be interpreted as the "tensile strength" of wheat straw, not bond strength. Other factors not investigated here, like existence of natural defects, irregular geometry, thermal degradation due to exposure to high temperatures, structural damage from compression, binder distribution on the surface or penetration, could also contribute to straw (adherend) failure.

The conclusions made in this chapter can provide a valuable baseline for controlling distribution of binder, amount and concentration of binder, size of fiber and compression molding conditions (temperature and force) relevant to the production of wheat straw-Acrodur pressboard.

Chapter 6
Wheat Straw–Polyamide 6 Pressboard

6.1 Introduction

Polyamide 6 is one of commonly used engineering polymers because of its balance of processability, strength, durability, and thermal stability that it imparts to the composites when used as matrix. Polyamide 6 is regarded as an alternative of most thermoplastic resins for obtaining good compatibility with natural fibers (Le Digabel et al. 2004) because of its polar characteristic.

However, the high processing temperature of polyamide 6 has been an obstacle limiting natural fibers reinforcing efficiency in polyamide 6 composites with natural fibers. Cellulose fibers normally have a thermal degradation temperature in the range of 200–250°C. The common belief is that natural fiber is only suitable for low melting temperature (under 180°C) commodity thermoplastics such as PE, PP, PVC and PS (Xu 2008). Particular focuses in previous research were either on reducing the processing temperatures of polyamide 6 by adding additives, or on modifying the natural fibers to increase their thermal stability. Wheat straw is thermally unstable above 220°C, although under some circumstances it is possible for wheat straw to be processed at slightly higher temperatures for a short period of time. Limited work has been reported on the use of wheat straw with polyamide 6 at high temperatures of above 220°C.

6.2 Research Objectives and Approach

The main goal of this chapter is to develop an effective method for manufacturing wheat straw-thermoplastic polyamide 6 composite pressboards with improved mechanical, dielectric and other properties. The methodology of Design of Experiment was employed for this purpose. The effects of parameters of formulation and compression molding condition on the mechanical properties of the resultant pressboards were evaluated, and the parameters were optimized based on the factorial experimental design.

Specific Objectives:

The specific objectives of this research are:

1) to evaluate effect of formulation on properties,

2) to evaluate effect of processing conditions on properties,

3) to identify suitable conditions for wheat straw-polyamide 6 pressboard manufacturing, and

4) to identify challenges that still need additional work.

This chapter was intended to focus on how the wheat straw – polyamide 6 composite pressboards were fabricated from raw materials. This chapter first describes how wheat straw and polyamide 6 were used in this research as well as the processing methods performed on wheat straw raw material. Within the framework of this research, wheat straw of two sizes were examined. Polyamide 6 in two forms was selected as thermoplastic binder. The physical and thermal characterizations were conducted on both wheat straw and polyamide 6 to evaluate size, density, moisture content, chemical composition, thermal stability and others parameters. The thermal studies of wheat straw and polyamide 6 using thermogravimetric analysis (TGA) and differential scanning calorimetry (DSC), provided the information of the effective processing temperatures for pressboard production.

The wheat straw – polyamide 6 pressboards were next manufactured using compression molding technology. The compression molding was carried out in a way, to control heat, pressure and time applied to the composite. The detailed manufacturing procedures used for wheat straw-polyamide 6 pressboard manufacture is described in the following section.

At last, the performance of the resultant pressboards was evaluated mainly in terms of mechanical and electrical properties. The property tests were performed on the manufactured pressboards as per the American Society for Testing and Materials (ASTM) standards. The chapter ends with the process of data analysis and the evaluation of the pressboard properties against those specified and currently used in the industries. More specifically, the effects of wheat straw size, binder geometry, and compression molding conditions on mechanical properties of the pressboards were investigated and evaluated in terms of flexural property.

The parameters in the formulation and in the compression molding exerted significant influences on the performance of the composite pressboard. The improvement of mechanical property combined with other properties can be achieved by varying those parameters. The parameters investigated in this chapter are summarized in Table 6.1, corresponding to formulation and production stages, respectively.

Table 6.1 Parameters at formulation and production stages

Formulation stage		Production stage
Wheat straw	**Binder**	**Compression molding**
Wheat straw fiber (#1)	Polyamide 6 powder	Fiber orientation
Wheat straw stem (3–4cm) (#3)	Polyamide 6 fiber	Mixing method
		Compression temperature
		Compression pressure
		Compression resident time
		Aerorating time

6.3 Materials and Methods

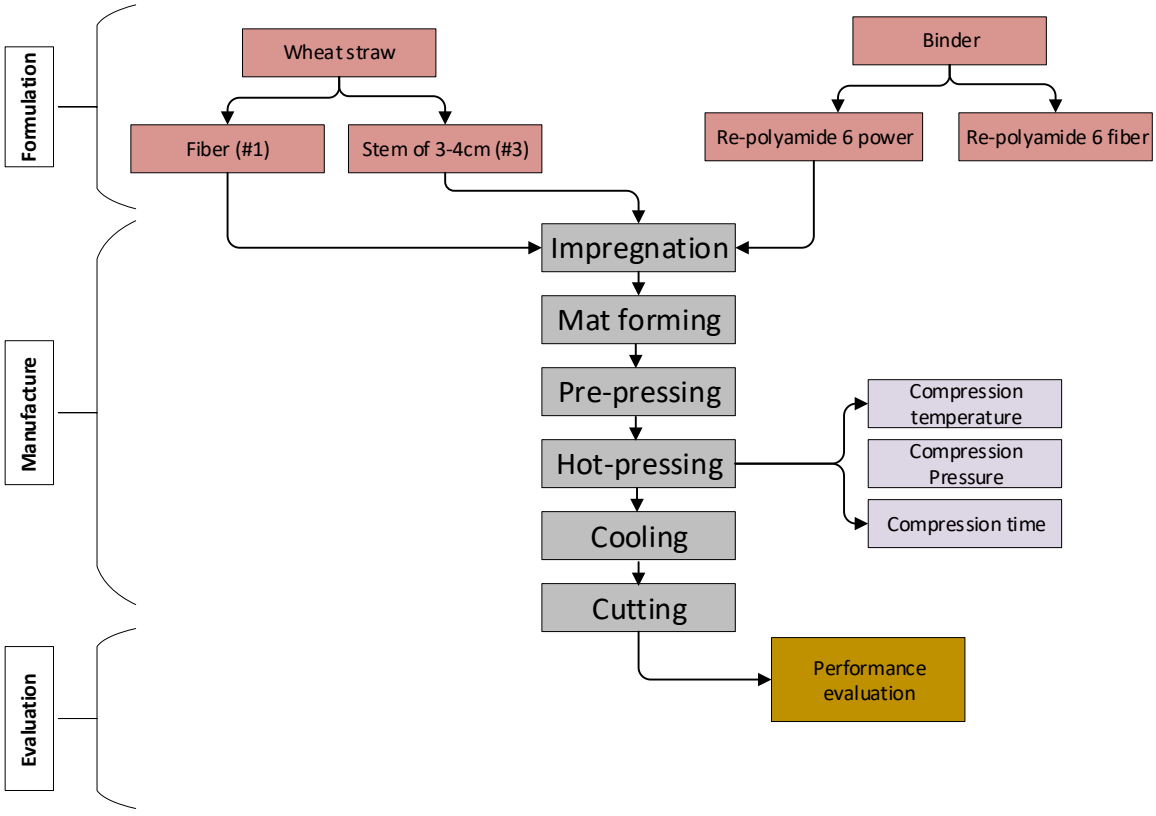

Figure 6.1 Flowchart of wheat straw-polyamide 6 composite pressboard production

The overall workflow of the method is presented in Figure 6.1, which is comprised of three stages. i.e. formulation, manufacture and evaluation. Firstly, the raw material – wheat straw and binder polyamide 6 – were prepared and formulated; secondly, the composite pressboards were produced using compression molding method; finally, the mechanical and other properties were investigated and evaluated. The experimental processes will be described in detail in later section.

6.3.1 Materials

Wheat straw used in this work were supplied by Omtec, Mississauga, ON, Canada. The raw material was obtained from an AC Mountain, soft white winter variety wheat, cultivated in Woodrill farms in Ontario, Canada. After stored under dry, cold condition, the raw material was first fed to a flywheel by end cutter to reduce their sizes approximately to 3–5 cm. The cut wheat straw was then fed to a directly coupled, rotary hammer mill for grinding. The ground wheat straw was screened through three sieves with mesh opening sizes of 4.6, 1.19, and 0.5 mm, sequentially. The small particles and dusts created during processing removed by a vacuum system and subsequent screen separation. After sieving, oversized (on 4.6 mm screen) and undersized (through 0.5 mm screen) residues were discarded. The ground wheat straw between mesh opening sizes of 4.6–1.19 mm was collected and labelled #1; the particle through the 1.19–0.5 mm sieve was collected and labelled #2. Figure 6.2 (a and b) shows the visual appearance of the wheat straw samples #1 and #2. Both wheat straw fiber and particle used in this project were characterized as discontinuous due to their length-to-diameter (l/d) ratio and do not have any preferential stress direction.

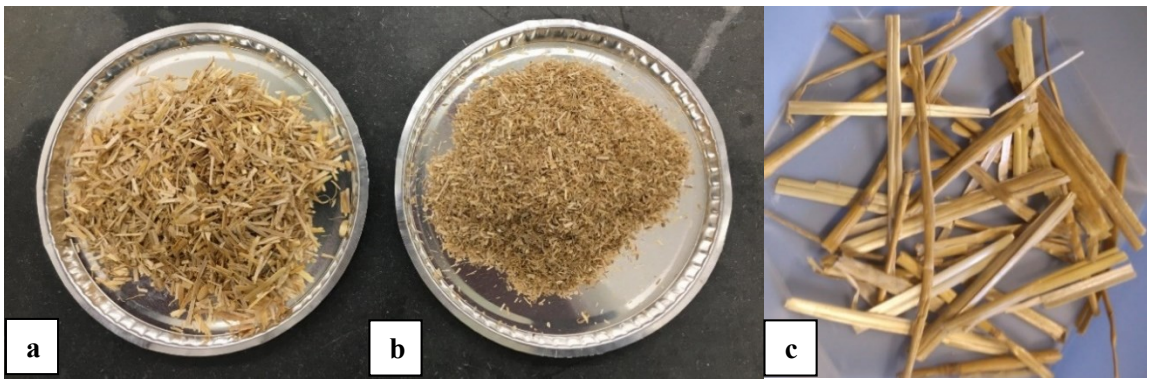

Figure 6.2 Wheat straw fiber (#1) (a), particle (#2) (b) and wheat stem (#3) (c)

It is generally accepted that fiber strength and stiffness are greatest along the fiber axis or longitudinal direction where lays the highly oriented crystalline cellulose structure (Bos et al. 2002). To explore the

potential of use of long wheat stem in composite and take advantage of long aspect ratio (longer stress transfer effect), the work presented here also involved incorporation of aligned or unidirectional wheat stem of 3–4 cm in length (shown in Figure 6.2 (c)) within the composite pressboards. The long wheat stems (#3) were selectively separated to obtain entirely stem parts with leaves, grains and nodes excluded manually. The selected stems were cut into 3–4 cm in length. The long stems could be further processed by splitting longitudinally with purpose of exposure more surface area and reduction of inter anti-compression force.

The milled wheat straw, either fiber (very short) or particle (flour), is the most preferable choice for large-scale production due to the high availability, ease handling, the higher bulk density and the free flowing nature when manufacturing complex parts of isotropic nature (AL-Oqla and Sapuan 2014). On the other hand, the long stem is incorporated for better reinforcing effect by long-distance stress transfer.

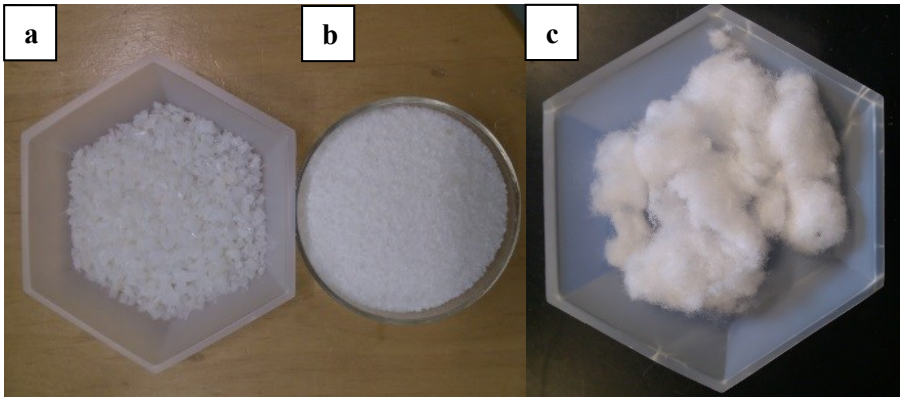

Figure 6.3 Recycled-polyamide 6 pellet before (a) and after (b) grinding and polyamide 6 fiber (c)

The polyamide 6 used was recycled from industrial waste. The use of recycled polyamide 6 contribute to the cost reduction of overall production. The recycled polyamide 6 in form of pellet shown in Figure 6.3 (a and b) was provided by Kal-Polymers Inc. It was recycled and reprocessed to the form of pellets in color of clear or white. The recycled polyamide 6 pellet received was then ground to obtain the powder with particle size of less than 0.1 mm (Figure 6.3 (b)). Polyamide 6 fiber shown in Figure 6.3 (c) is a byproduct of yarn production supplied by Firestone Textiles Company, Woodstock, ON. Recycled polyamide 6 fiber was also employed in this work and expected to get entangled with wheat straw fibers for better dispersion.

A correlation between the composite thickness and the resin content established experimentally by other authors indicated that the percentage of the resin contained in the composite was proportional to its thickness (Khalfallah, Abbès, et al. 2014). In their case, the least amount of resin was required to obtain a good distribution of the resin over the natural fiber reinforcement. Therefore, the optimal fiber/resin ratio should be found to avoid the presence of blisters and to control the quality of the pressboard in terms of density, visual aspect and mechanical properties. The weight fraction of wheat straw was determined as the dry wheat straw mass ($M_{wheat\ straw}$) over the polyamide 6 mass ($M_{polyamide\ 6}$) plus the dry wheat straw mass ($M_{wheat\ straw}$) as in Equation 6.1

$$M_f = \frac{M_{wheat\ straw}}{M_{wheat\ straw} + M_{polyamide\ 6}} \qquad 6.1$$

6.3.2 Characterization Methods

Wheat straw and polyamide 6 were characterized with respect to the physical, chemical and thermal properties and surface morphology. The instrument and characterization procedures are described as follows.

The bulk density of wheat straw was measured for the wheat straw #1 and #2 by weighing the weight of materials of known volume. The wheat straw samples were freely poured into a box of known volume without compaction. The densities were calculated by dividing mass by volume.

The particle size and the aspect ratio of the wheat straw (#1 and #2) were measured using optical microscopy. The stereomicroscope Leica MZ6 (Type DFG 290, Leica Microsystems Ltd.) was used for image generation and acquisition. The images of the particles were taken using a digital camera with the stereomicroscope at a magnification of 63X. The images taken were then analyzed using an image processing software program called ImageJ (National Institutes of Health Image). The number of particles in each image is counted using the software. This program provides the dimensions of the particle by drawing the best fitting ellipse around the particle. From this ellipse, the major and minor axis is drawn to obtain the length and width of the particle being measured. The aspect ratio is calculated as the ratio of length and width.

Moisture content analysis was performed according to ASTM method 2654 to quantify the water content in wheat straw and polyamide 6. The moisture contents of the wheat straw and polyamide 6

before and after drying were determined using the OHAUS MB45 Moisture Analyzer at a constant temperature of 110°C.

Melt flow index (MFI) measures how easy the melt thermoplastics flow and is considered as an indirect measurement of molecular weight and viscosity. The measurement of MFI was conducted using MFI Dynisco Polymer Test D4001DE (Alpha Technologies) according to the procedure described in ASTM D1238. The MFI values for recycled polyamide 6 pellet was obtained at 230℃ with 2.16kg of weight.

The Fourier transform infrared (FTIR) analysis was carried out using a Bruker Tensor 27 FTIR analyzer. The polyamide 6 samples were grounding to a fine powder and mixed with potassium bromide (KBr). This mixture was compressed into thin discs using a hydraulic press. These discs were used to obtain the infrared spectrum in the spectral range of 400–4000 cm^{-1}. Thirty-two (32) scans per sample were collected with spectral resolution of 4 cm^{-1}. Baseline correction was performed for all samples spectra using OPUS program.

TGA of wheat straw and polyamide 6 was performed using a Q500 series from TA Instruments. The samples were submitted to a constant heating rate of 10°C/min ranging from 35 to 800°C under air atmosphere.

DSC analyses were performed on both wheat straw and polyamide 6 using Q2000 TA instrument. The oven dried wheat straw samples of 5–10 mg hermetically sealed in the T-zero pans were heated from 35°C to 250°C at a rate of 10°C /min. The polyamide 6 samples of 5–10 mg hermetically sealed in the T-zero pans was heated in 3 cycles. In the first cycle, the samples were heated from 35° C to 300°C at a rate of 10°C/min. This was done to remove the thermal history of the samples. In the second cycle, the samples were cooled from 300°C to 35°C at 10°C/min. In cycle 3, the samples were heated from 35°C to 300°C at the same rate. Cycle 2 and 3 were used to analyze the samples for their thermal properties.

6.3.3 Manufacturing Method

The production process involved the use of hydraulic press and a custom-designed pressing mold set. The custom-designed pressing mold sets used for production of pressboard consist of square mold, a flat plate and a solid plunger. One set was made of steel and the other was made of aluminum for better

heat transfer during hot-pressing. The mold is a square and the inner side of mold is 11.6 cm, therefore the area of molded pressboards is 134.56 cm^2.

Wheat straw-polyamide 6 composite pressboards were manufactured with varying parameters using the following procedure. The manufacturing procedure followed steps: 1) preparation of material; 2) wheat straw impregnated with polyamide 6; 3) pre-press to reduce the volume of composite; 4) hot press to form and maintain the final profile of the pressboard; and 5) pressboard de-molded and cooled.

A full factorial design of experiment was designed and utilized to evaluate the effect of different factors on the response: the flexural strength of the pressboards obtained from the compression molding process conducted according to the parameters set based on DOE. A linear model was developed and the adequacy of the model was checked by the normal probability distribution and the residual plots.

Specifically, five sequential sets of experiments using full 2^3 factorial design were conducted, where three parameters were examined at a time, and two levels for each parameter were chosen and denoted by "-" (low) and "+" (high). All the other parameters were kept constant. The flexural strength of resultant pressboards was measured as the response. This experiment design allows evaluating the effect of each variable (also referred to as factor) as well as the interactions between these variables on the response variables, i.e., flexural strength and modulus.

Table 6.2 Formulation and compression molding parameters and their levels

	Parameter		Level
Wheat straw	Fiber #1	Variable	50–90% (balance of others)
	Stem #3	Variable	0, 10%, 30%
	Split Stem #3	Variable	10%, 30%
Binder	PA6 powder	Variable	10%, 20%, 30%,
	PA6 fiber	Variable	20%
Compression molding condition	Force (lbf)	Variable	20,000, 30,000, 40,000
	Temperature(°C)	fixed	221℃, 227℃
	Holding time (min)	fixed	3, 3.5, 4 min
	Aeration	fixed	2–3 times

By combining formulation and compression molding parameters, the parameters to be examined in this chapter and their corresponding levels are illustrated in Table 6.2. Based on the results of materials characterization, the operation temperature for production of wheat straw with polyamide 6 binder

pressboard was determined to be 221 or 227℃. The heating time of less than 5 minutes was consider long enough for melting the polymer and avoiding serious decomposition of reinforcing fibers. The compression force was determined at 3 levels, i.e. 20,000, 30,000, and 40,000lbf. It should be noted that the force in unit of lbf was used for easy expression of the compression molding pressure, because throughout the thesis the area of all the pressboards molded has been the same being 134.56 cm^2 (20.88 square inch). Therefore, the pressures are 957.85, 1436.78 and 1915.70 psi, respectively for 20,000, 30,000, and 40,000lbf.

Although moisture within the composite is reported to have plasticizing effect on mobility of polyamide 6 (Amintowlieh et al. 2012), the moisture evaporation at the operation temperature could cause the blast (sudden release of accumulated pressures) and lead to voids in the pressboard. The voids in the pressboard are weak points which lead to failure. Therefore, the moisture content was fixed below 10% before going into the hot press.

The initial screening of parameters included specifically the wheat straw size, #1 and #3 (split or not), polyamide 6 form (fiber and pellet), fiber orientation and compression molding parameters, including pressure, temperature, time, as shown in Table 6.2. After first a few preliminary experiments, some parameters had been applied and evaluated but due to their poor performances in improvement of flexural properties, these variables were excluded and greyed out in Table 6.2. For example, both polyamide 6 powder and fiber were used in production of wheat straw-polyamide 6 composite pressboards. However, only the results for the polyamide 6 powder were presented, because the polyamide 6 fiber tended to entangle and did not allow a good dispersion prior to melting. This may have contributed to a loss of integrity of pressboard. The other parameters screened out included because of their non-significant effects, split wheat stem, fiber orientation, temperature of 227℃, holding time longer than 5 minutes. The temperature above 227℃ showed clear evidence of burning and significant amount of sample losses. Therefore, it was concluded that the processing temperature must not exceed 227℃. Fiber orientation affects the properties of the composites. The best mechanical properties can generally be obtained for composites when the fiber is aligned parallel to the direction of the applied load (Herrera-Franco and Valadez-Gonzalez 2005) (Norman and Robertson 2003). However, the poor effect of incorporation of aligned wheat stem led to the exclusion of this parameter.

Table 6.3 Factors and levels for five sets of experiments (1st to 5th, corresponding to Experiment #1to #5)

	Experiment #01		Experiment #02		Experiment #03		Experiment #04		Experiment #05	
Factors	Low	High	Low	High	Low	High	Low	High	Low	High
A: force (lbf)	20000	30000	20000	30000	30000	40000	20000	40000	20000	40000
B: PA 6 (%)	10	20	10	30	20	30	10	30	10	30
C: stem (%)	0	10	0	30	20	30	10	30	10	30

The variables to be examined in five sets of factorial experiments (Experiment from 1st to 5th) were determined as binder content, inclusion of #3, and compression molding force, with temperature and time fixed at 221℃ and 3.5 minutes. The variables and their levels are listed in Table 6.3. These upper and lower levels of the variables as well as non-variable value were determined based on preliminary experiments.

Take the Experiment #02 as an example, three variables were studied using two levels for each variable according to Table 8.33 in Appendix G, where three factors examined were: force (A), binder content (B), and incorporation of wheat straw stem with length of 30–40 mm (C). Two levels for each factor were chosen denoted by "-" (low) and "+" (high). Based on the results of the first experiment, the values of binder content and wheat stem content were increased. All the other factors were kept the constant to ensure that responses respond only to the change by selected factors. The temperature was fixed at 221℃ and holding time was 3 minutes.

Table 8.34 in Appendix G shows the design matrix for Experiment #02, which covers all eight combinations of the three factors investigated. In this table, the factors were coded to eliminate the correlation between them. The "-1" and "1" denote "low" and "high" levels of a factor, respectively, in variable levels corresponding to A, B, C columns. All eight combinations of parameters were labeled in the first column, denoting the combination represented by the last three columns. For example, run **a** is made at the "high" level for factor **A**, and at the `low' of the other two factors. It should also be noted from "run order" column in Table 8.34 that the experiments were performed at random order during all the Experiment sets in order to eliminate biases in response caused by trends in errors or other independent variables.

6.3.3.1 Production of Wheat Straw – Polyamide 6 Composite Pressboard

The pressboards were prepared according to the procedure described in this section for properties evaluations. The detailed procedure of manufacturing wheat straw – polyamide 6 composite pressboard is described as following in Table 6.4:

Table 6.4 Manufacturing process of wheat straw-polyamide 6 composite pressboard

Step	Parameter or Technique used
Formulation	Dry and weigh
Resination	Sprinkle impregnation
Mat formation	Manual dry laid-up
Pre-press	At 25,000–30,000 lbf
Hot press	At 20000, 30000, 40000 lbf, 221°C/ aeration
Cool down	At room temperature

1) **Formulation**: The weight of wheat straw for each pressboard was fixed at 32g on dry weight, which makes the target board thickness of approximately 3 mm. Two sizes of wheat straw, fiber (#1) and stem (#3), as described in section 6.1, were examined. The milled wheat straw fiber (#1) and cut stems (#3) were dried in a vacuum oven at 60–80°C for 4 hours to moisture content of below 10%. Two types of polyamide 6 impregnated with wheat straw were recycle polyamide 6 powder and polyamide 6 fiber. Polyamide 6 of both powder and fiber were dried for 1 hour. Based on the dry weight of wheat straw, the amount of polyamide 6 applied was accurately weighed and formulated. The formulation varied as a variables according to the experimental design summarized in Table 6.3.

2) **Impregnation and mat forming**: Manual dry laid-up method was used for mat formation. The wheat straw mats were formed in an open-ended mold with a close fitting plunger using hand layup method, where layers of wheat straw fibers were evenly placed in the mold, alternating with layers of polyamide 6 using hand sprinkling method, with both faces (top and bottom) being wheat straw. When stems of 3–4 cm were included, the stems were distributed in core and face aligned or randomly oriented.

3) **Pre-press**: The plunger was fitted in the mold and pressed onto the composite with a force of 15,000 lbf for 60 seconds for pre-press (cold-press at room temperature) in hydraulic press (Model3853-0, S/N 12000-937 CARVER, INC. shown in Figure 6.10 (a)). Pre-press reduces

the volume and thickness of the mat and increases the homogeneity and density of the formed mats. The resultant mats were a flat non-woven structure, consisting of polyamide 6 distributed in wheat straw fibers.

4) **Hot-press**: The pre-pressed mat then underwent compression molding process, where the platens were heated up to the set temperature. An aluminum plate and plunger set were then used in compression molding for better heat conductivity. Initially no pressure was applied, when composite was in the hot press; a slight contact was made between the plunger and the platens of the hot press to allow for effective heat transfer. The composite material was allowed to sit in between platens and then the set compression force was applied to the composite. Next, the force was released for 2 or 3 times to allow produced gas to escape, and then the set force applied, for a total time of 3.5 minutes in the hot press. Aluminum foils were used on both sides of mat for easy removal of pressboard from the mold.

5) **Cooling-down**: The pressboard was carefully removed from the mold after compression molding and cooled down at room temperature. The area of pressboards was measured 11.6 by 11.6 cm (4.57 inch) with around 3 mm thickness.

Figure 6.4 represents two examples of the produced wheat straw –polyamide 6 pressboards, without (a) or with stem of 3–4cm (b) incorporated.

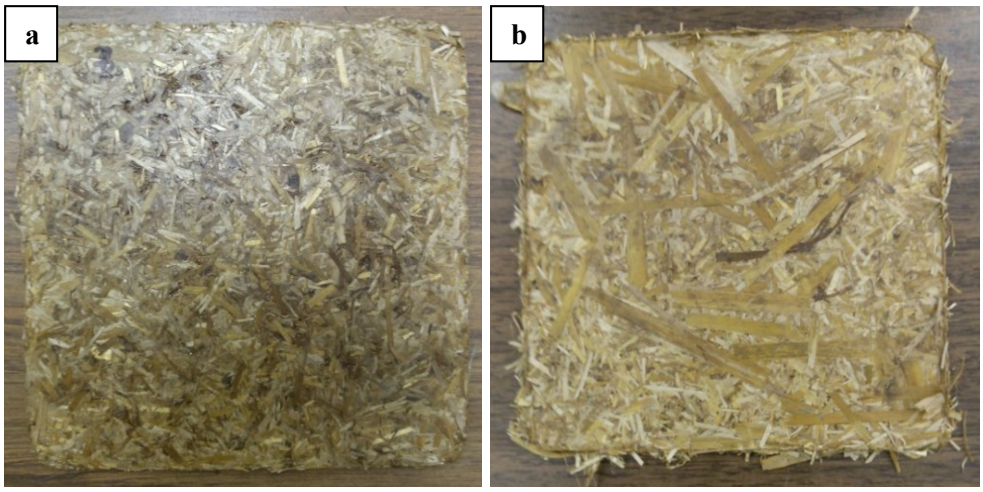

Figure 6.4 Illustrative examples of wheat straw-polyamide 6 pressboard without (a) or with stem of 3–4cm (b) incorporated

6.3.4 Evaluation Methods

The flexural properties are important for the structural applications, where the materials endure more flexural stresses. The plain rectangular bars were cut from the pressboard samples. The central areas of pressboards were preferred to eliminate edge effects. Thicknesses were measured individually using caliper. The specimens were 75 mm long, 15 mm wide and 3 mm thick. The specimens were cut using a Mastercraft 120V 9-inch bandsaw model no. 055-6748-6. At least eight specimens were measured for each combination of processing conditions and formulations. Figure 6.5 shows the specimens cut from wheat straw-polyamide 6 fiber composite pressboards as illustrative examples.

The flexural strength and modulus of the wheat straw –polymer composite pressboard were tested using a Testresources Universal Test Machine (Test Resources Inc., Shakopee, MN, USA), in accordance with the procedure described in ASTM D 790. A three-point bending setup was used, with a span of 50 mm and a crosshead speed of 1.3 mm/min. The flexural strength and flexural modulus were determined. All testings of mechanical properties were performed at room temperature.

Figure 6.5 Specimens from wheat straw-polyamide 6 pressboard

The maximum stress and flexural modulus were calculated by Equation 6.2 and 6.3, where L is the support span (50mm), b is the width, d is the thickness, P is the maximum load, and m is the slope of the initial straight line portion of the load-deflection curve.

$$S = \frac{3PL}{2bd^3} \qquad 6.2$$

$$E = \frac{L^3 m}{4bd^3} \qquad 6.3$$

The dielectric breakdown voltage through the thickness of a test specimen was measured in accordance with ASTM D149-09, method A: short-time test. For the short-time method, voltage is applied across the two electrodes and raised from zero to dielectric breakdown at a uniform rate. Breakdown is when an electrical burn-through punctures the sample, or decomposition occurs in the specimen.

Figure 6.6 Wheat straw-polyamide 6 pressboard specimens for dielectric test

Dielectric Testing was conducted at room temperature according to the following procedures: The alternating 60 hz voltage is applied on opposite faces of specimens as shown in Figure 8.68 in Appendix G. The voltage was increased from zero or from a level well below the breakdown voltage of specimens, until dielectric failure of the test specimen occurs. The rate-to-rise was 2,222 V/s. Dielectric failure was determined by an increase in conductance over 20 mA. Dielectric breakdown voltage, n, is the potential difference, at which dielectric failure occurs in an electrical insulating material located between two electrodes, Dielectric strength was calculated by dividing the breakdown voltage by thickness.

6.4 Results and Discussions

6.4.1 Material Characterization

Table 6.5–Table 6.8 present information on the physical and chemical properties of wheat straw and polyamide 6 used in this chapter. Bulk density and moisture content of wheat straw are presented in Table 6.5. It is seen the small size (#2) exhibited higher density than wheat straw fiber (#1).

Table 6.5 Bulk density of wheat straw

Sample	Bulk density (kg/m^3)	Moisture content	
		As received	After drying
Wheat straw fiber (#1)	75.48 (1.57*)	6.97%	2.87%
Wheat straw particle (#2)	92.53 (0.91*)	6.25%	4.33%
Wheat Straw stem (3–4cm) (#3)	N.A.	6.20%	4.12%

*Values in parenthesis are standard deviations

Component analysis was conducted as follows. On dry weight basis, weight fractions of different parts (internode, node, leaf, and head were present in the wheat straw raw material as received at 61%, 5%, 20% and 13.6% respectively. The leaves (including sheaths) and nodes fraction were removed from stems for pressboard production because of their high silica content.

Table 6.6 Particle size analysis of wheat straw fiber as received

Particle Length	Fiber (#1)	Particle Length	Particle (#2)
<10.00 mm	99%	<3.00 mm	99%
Aspect Ratio		Aspect Ratio	
<25	99%	<25	99%
<10	89%	<10	92%
<5	64%	<5	72%

The collected wheat straw fiber #1 was analyzed regarding particle size and aspect ratio. The particle length and aspect ratio were presented in Table 6.6 for both wheat straw #1 and #2. The result of MFI of polyamide 6 shown in Table. 6.2 indicates that the recycled polyamide 6 pellets at 230℃ obtained sufficient mobility to flow within composite because MFI in the range of 20 g/10min is considered suitable for molding applications.

Table 6.7 MFI and moisture content of polyamide 6

Sample	MFI
Polyamide 6 pellet	20.2 g/10min
Polyamide 6 fiber	23.1g/10min

Table 6.8 Moisture content results of wheat straw and recycled polyamide 6

Sample	As received	After drying
Polyamide 6 powder	1.54%	0.67%
Polyamide 6 fiber	3.71%	1.41%

Figure 6.7 shows a FTIR spectrum of recycled polyamide 6. Table 6.9 presented below is a compilation of measured values of peak wavelengths found in recycled polyamide 6 sample.

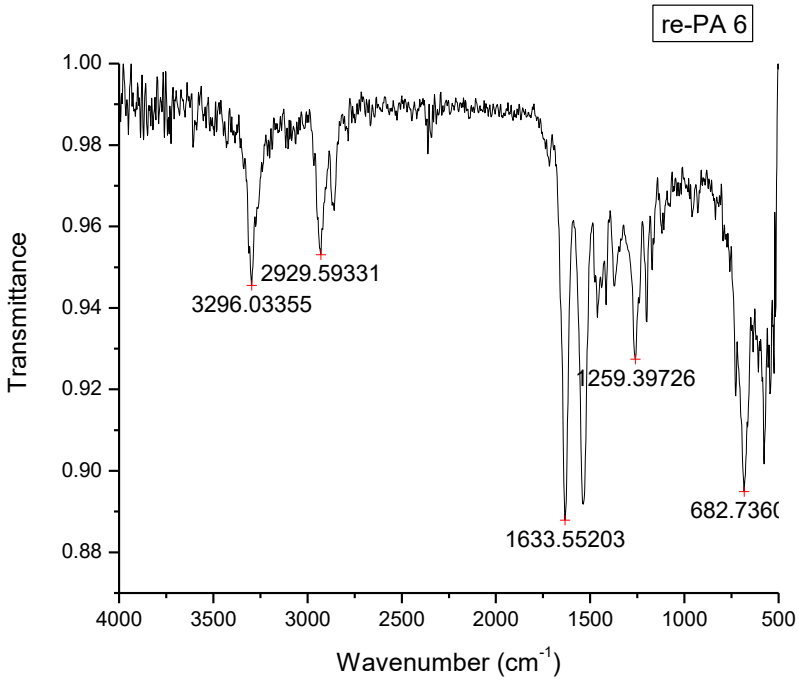

Figure 6.7 FTIR spectrum of recycled polyamide 6 pellet

Table 6.9 Assignment of FTIR spectrum of polyamide 6 pellet

Wave number (cm^{-1})	Assignment
3296.03	N–H stretching
2929.59	CH2 stretching
1633.55	Amide I stretching
1539.00	Amide II stretching
1259.40	Amide III stretching
682.74	C–C bending and deformation

The TGA thermograph and the derivative thermogravimetry (DTG) curves on recycled polyamide 6 are shown in Figure 6.8 (a) and (b) for pellet and fiber form, respectively. The onset and peak

temperatures of thermal degradation were observed at 380°C and 415°C for polyamide 6 pellet, and 370°C and 475°C for polyamide 6 fiber.

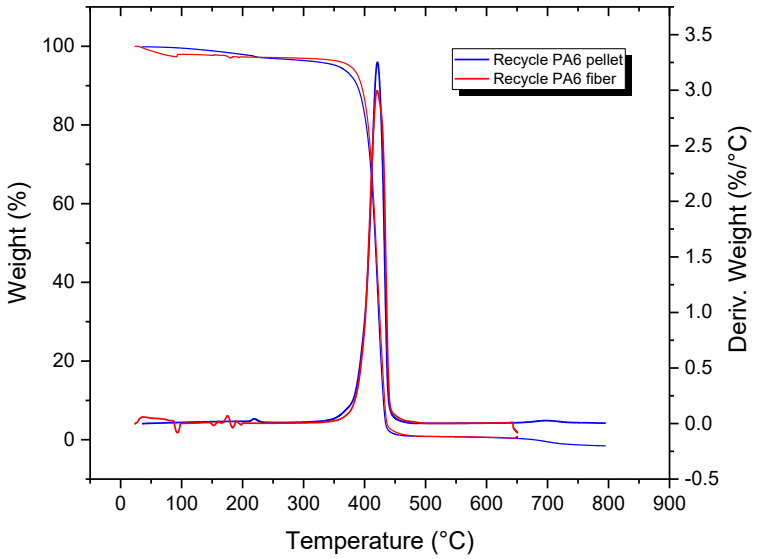

Figure 6.8 TGA thermograph of polyamide 6 pellet (1) and fiber (2)

The DSC thermographs of polyamide 6 in Figure 6.9 (a) and (b) show the peak at 219°C indicating its melting point. DSC analysis did not show the evidence of the impurities existing in the recycled polyamide 6.

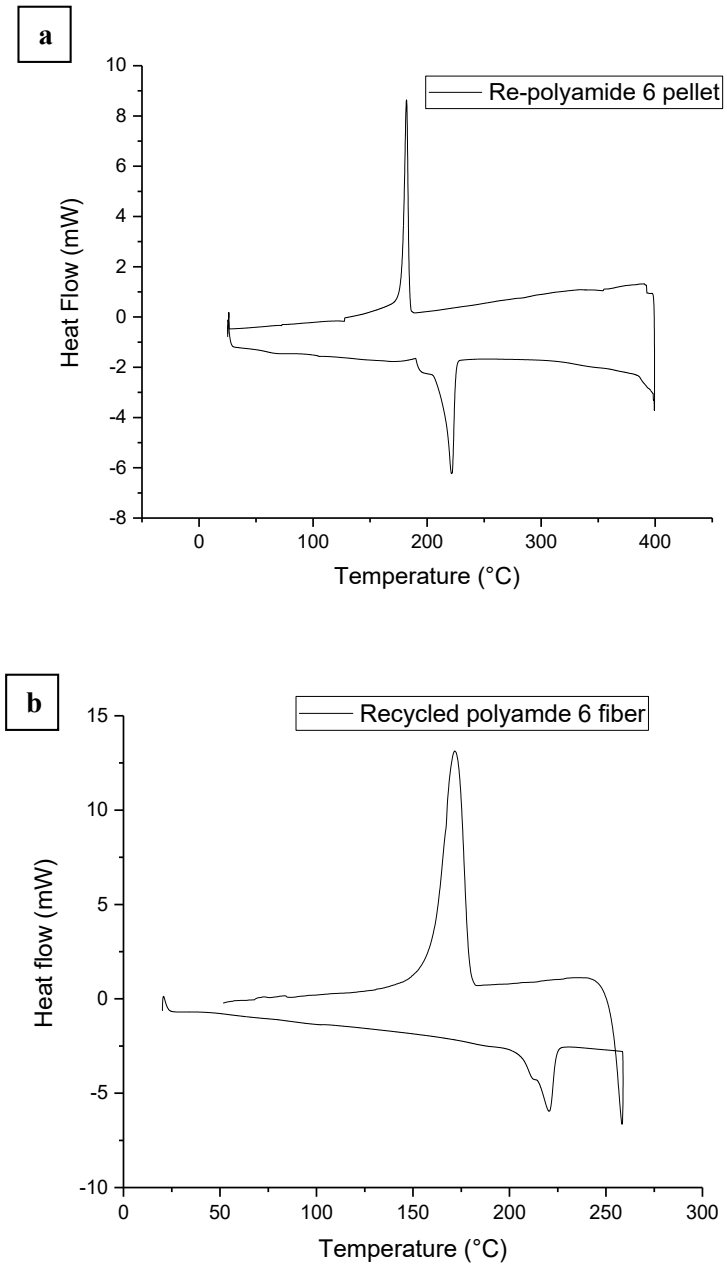

Figure 6.9 DSC thermographs of polyamide 6 pellet (a) and polyamide 6 fiber (b)

The production process was carried out with composite formulations and compression molding conditions as parameters. The properties of final wheat straw-binder composite pressboards are the overall reflection of these parameters. In this section, the effects of compression molding parameters

and composite formulations on mechanical and dielectric properties of final pressboards were investigated. The relationships of processing parameters and mechanical and dielectric properties are evaluated and discussed.

6.4.1.1 TGA of Wheat Straw

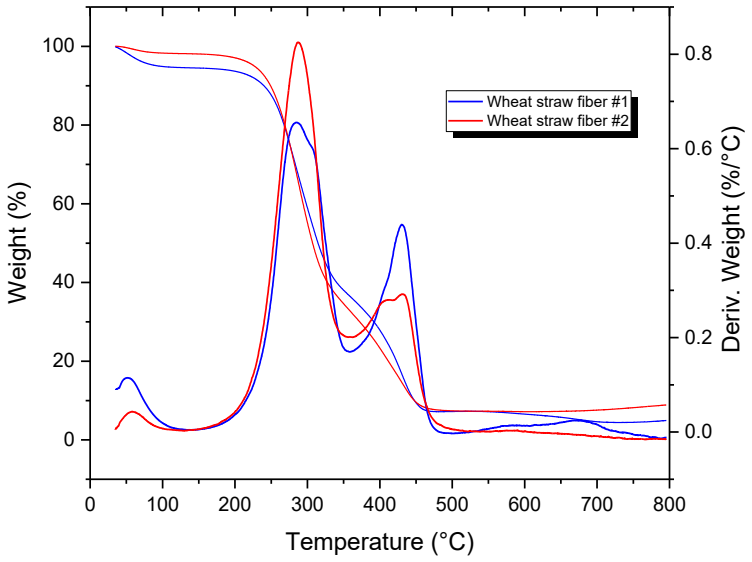

Figure 6.10 TGA thermograph of wheat straw fiber (a) and particle (b)

The thermal stability of wheat straw has been discussed in section 3.4.3. The TGA thermographs are shown in Figure 6.10. TGA analysis of wheat straw in Table 6.10 shows the degradation of wheat straw starts at 221°C.

The non-isothermal TGA results from chapter 3 (3.6) shows that the 1% mass loss of wheat straw happens at 200~226 ℃, and 5% mass loss of wheat straw happened at 240~273℃ with activation energy Ea =134.71(kJ/mol) in air. Therefore, it is safe for process wheat straw at 221℃ for a short time of a few minutes without causing serious decomposition.

Table 6.10 TGA analysis of wheat straw

Wheat straw	Fiber (#1)	Particle (#2)	Comments
First peak	51°C	58°C	
Mass loss	~8%	~4 %	Moisture evaporation
Onset (5%) of degradation (°C)	221°C	222°C	
Second peak	284°C	288°C	
Third peak	431°C	432°C	
Total degradation	~85%	~89%	Thermal degradation
Residue after 600°C (%)	6%	7%	Inorganic materials: ashes, silica

6.4.2 Flexural Property

The flexural strength of the pressboards produced according to the factorial design was measured as a response variable. The relationships between the parameters used in production of pressboards and flexural strength was established and evaluated for better understanding of the process and improvement of pressboard production.

The typical flexural stress–strain curve of wheat straw-polyamide 6 is shown in Figure 6.11. All the composite specimens tested were found to have similar stress–strain curves shape. It is seen that the pressboard breaks more with “brittle fracture” than “ductile”.

Flexural strength is defined as the maximum flexural stress supported by a specimen during a flexural test and represents the material ability to resist deformation under load. Flexural strength is an important parameter when selecting the correct material to design parts for different applications (e.g., automotive, furniture). All the wheat straw-polyamide 6 composite samples were broken during testing and, therefore the flexural stress at break became the flexural strength of the material.

The flexural modulus is obtained from the inclination of the elastic region of strain-stress curve and describes the ability of a material to resist bending when force is applied. Different industries (e.g., aerospace, automotive, construction, etc) use this property to select the correct materials for designing parts which must support loads without flexing. Therefore, the desirable flexural modulus will depend on the type application.

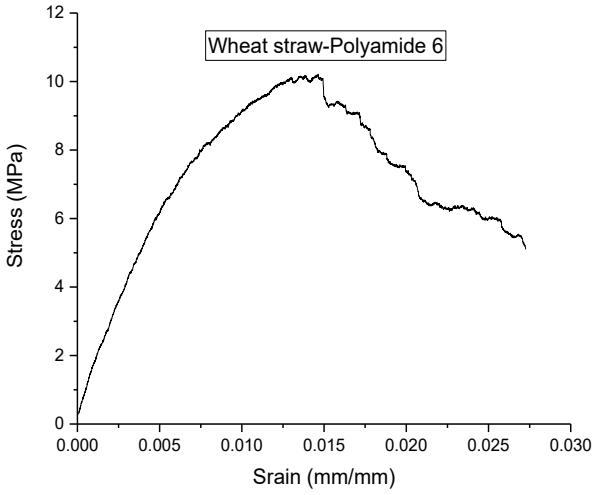

Figure 6.11 A typical flexural stress–strain curve of wheat straw-polyamide 6 (straw fiber, 10% stem and 30% polyamide 6, molded at 221°C and 40,000 lbf for 3.5 minutes)

6.4.2.1 Flexural Strength and Modulus

The five experiments were conducted based on a 2^3 full factorial design in Table 6.3. The flexural properties were measured and summarized in Table 8.35 Appendix and Table 8.36 Appendix, and in Figure 6.12 and Figure 6.13 respectively, in terms of flexural strength and flexural modulus.

It is seen that the overall flexural performance of these composites prepared here was poor if compared with other composites. For flexural strength, only 3 out of 40 were above 20 MPa, while 32 of 40 were below or slightly above 10 MPa. The maximum flexural strength of 26.2 MPa were obtained at formulation of 30% polyamide 6 powder, 30% stem of 3–4cm, and 40% wheat straw #1, and at compression molding condition of 30,000 lbf, 221°C for 3.5 minutes, which also exhibited relatively high flexural modules of 1,076 MPa.

The wheat straw base composites have been reported in previous studies of our group (Vedoy 2012). In his study, the wheat straw –polyamide composites were prepared at 235°C during extrusion and at 240–250°C during injection molding. It was reported that the polyamide 6 with addition of 15% wheat straw achieved the average 110 MPa in flexural strength and highest 2,690 MPa in flexural modulus, with different sizes (mid and large) and treatments (alkali and silane) (Vedoy 2012).

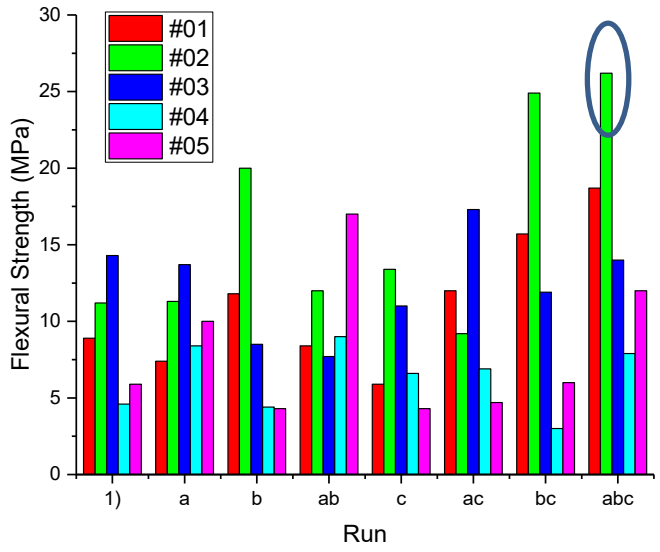

Figure 6.12 Flexural strength of wheat straw-polyamide 6 pressboards for Experiment #01–#05

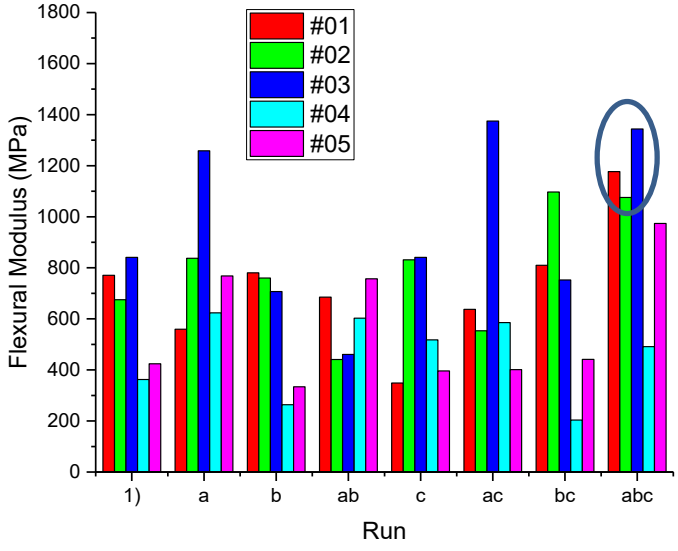

Figure 6.13 Flexural modulus of wheat straw-polyamide 6 pressboards for Experiment #01–#05

The poor performance compared to the results from other studies was attributed to low content and poor distribution of polyamide 6, which led to the weak interfacial bonding between the fiber and the matrix. The lack of binder become more critical when fiber content increased above 50%. In this case, the total interfacial area between matrix and fiber becomes bigger and micro-spaces (voids) between fiber and matrix may be formed. As a consequence of these voids between fiber and matrix, poor stress transfer and brittleness could occur.

6.4.2.2 Data Analysis of DOE

The wheat straw-polyamide pressboards fabricated in Experiment #02 were measured and given in Table 8.37 in Appendix G. The flexural strength results were utilized to perform the statistical analysis, where the influence of the three factors, i.e. force (A), polyamide 6 content (B), and incorporation of wheat stem (C), on the flexural strength and modulus was investigated.

A full-term linear regression model expressed in Equation 6.3 was used to fit the experimental data. The model parameters and effects were calculated based on Equation 6.3 and 6.4. The analysis of variance (ANOVA) table was summarized in Table 8.38 in Appendix G. The ANOVA indicated that the main factors B was significant, whereas the factor A and C is not affecting the response. In addition, the interactions between the factors were also insignificant for the response.

$$y = \beta_0 + \beta_1 A + \beta_2 B + \beta_3 C + \beta_4 AB + \beta_5 AC + \beta_6 BC + \beta_7 ABC + \varepsilon \quad (6.3)$$

$$(Effect_i) = 2 \times \beta_i \quad (6.4)$$

The normal probability plot of effects shown in Figure 8.69 in Appendix G was used to confirm the specification of significant effects. The normal probability plot of effects indicated that a straight line was yielded by small effects which were distributed around zero. It is reasonable to conclude that those effects falling along a straight line were resulted from random variation about the mean and not due to any significant effects of the variables. The effect of factor B deviated from this line greatly indicating that the flexural strength was positively influenced by the factor B. As shown in

Figure 8.70 in Appendix G, with a rise in polyamide 6 content from low level to high, the effect was reflected in the average respond (flexural strength) increasing from 12.08 MPa to 21.78 MPa. No interaction of any two factors was found to deviate the straight line, indicating no significant interaction effects on the response. As an example, shown in Figure 8.71 in Appendix G is the interaction between

factor B and C. Two lines are parallel to each other due to the non-significant interaction between these two factors.

With the most influential parameters revealed, Equation 6.5 was developed by reducing the linear model to consist only factor B. By substituting the parameters, the model became Equation 6.6.

$$y = \beta_0 + \beta_2 B \qquad 6.5$$

$$\hat{y} = 16.925 + 4.85B \qquad 6.6$$

The response can be predicted for different values of factors by applying established model (Equation 6.6), By subtracting the real response (from experiment) by predicted ones (from model) residuals was estimated. Figure 8.72 in Appendix G shows calculated predicted response and residuals. Then the adequacy of the new model was checked by checking the residual distribution. Unequivocally, it was concluded from Figure 8.72 that the error is roughly following a normal distribution and the above model can meet the criteria that the model is adequate to describe the experimental data. The DOE analysis and data for NNP of effect, interaction of factor B and C, and NNP of residue can be found in Appendix G.

In conclusion, according to the statistical analysis results (normal probability plot and Anova), factor B shows a positive and significant effect on response, while none of the other factors or factors interaction studied during Experiment #02 were affecting the flexural strength of produced pressboards. Therefore, in order to maximize the flexural strength, higher level of polyamide 6 should be employed for production of wheat straw pressboards.

Consequently, further experiments were conduct using the factors and levels suggested by Experiment #02. However, the results did not meet the expectation as suggested by the results of Experiment #02. The higher content of polyamide 6 led to softened binder squeezed out of the mold or the delaminated pressboards due to peeling off. This effect was getting worse especially when higher compression force of 40,000 lbf was applied. The explanation was proposed that the poor interaction between fiber and binder due to incompatibility. The difficulty was that the compression mold design for high content of polyamide 6, which is not suitable, due to the limitation of manufacturing method and high processing temperature of polyamide 6.

6.4.3 Dielectric Property

The dielectric strength was calculated by dividing the measured breakdown voltage by the thickness of the sample and expressed in kV/mm. A higher dielectric strength represents a better quality of insulator. The results of wheat straw–polyamide 6 composite pressboard are shown in Table 6.11. The dielectric strength in oil is 6.65 kV/mm, which is slightly higher than 5.20 kV/mm in air. Both dielectric strength were far lower than the pressboards made with Kraft softwood commercially (26.46 kV/mm) or in the laboratories (18.06–21.26 kV/mm) (Myers and Hettwer 1993).

Table 6.11 Dielectric strength wheat straw-polyamide 6 composite pressboard

		Dielectric strength (kV/mm)	
Wheat straw	Binder	In Air	In Oil
Untreated #1	30% Polyamide 6	5.20	6.65

6.5 Conclusion

In this chapter, the flexural properties of produced wheat straw –polyamide 6 pressboards were measured according to ASTM to estimate the effects of three factors, i.e. compression molding force, polyamide 6 content and wheat stem of 3–4cm content. The overall experiment was conducted based on a 2^3 full factorial. The validity of experiment was guaranteed by randomization. The model parameters and effects was used to calculate based on a full linear regression model. The significant factors and interactions were determined by normal possibility plot. The parameter ranges were adjusted accordingly to previous statistical analysis. However, the further adjustment did not improve the flexural strength as expected. The explanation can be the errors introduced during productions because of poor control of temperature and destruction of pressboard due to peeling off. The best overall result of flexural strength was 26.2 MPa from the Experiment #02. The corresponding flexural modulus was 1,076 MPa. The pressboards were manufactured with 40% wheat straw #1, 30% wheat stem (#3), and 30% polyamide 6 power, at 30,000 lbf, 221°C for 3 minutes. No evidence that incorporation of wheat straw stem of 3–4cm improved the flexural strength and modulus was noticed.

Chapter 7
Wheat Straw–Acrodur Pressboard

In this chapter, the wheat straw–Acordur composite pressboards were prepared when the knowledge gained in previous chapters was applied and the mechanical and other properties were measured and evaluated for the influence of the formulation and manufacturing factors.

7.1 Introduction

Currently, there is no information in the open literature on manufacturing or the properties of wheat straw-Acrodur pressboard. The goal of this chapter is to develop an effective method for manufacturing wheat straw-Acrodur composite pressboards with improved mechanical, dielectric and other properties. The research objective is to evaluate the effects of wheat straw size and treatment, different binder, and compression molding conditions on the performance of the straw pressboards. The performance-enhancing characteristics of the wheat straw pressboards will add value to wheat straw based products and help expand them into new markets. However, to achieve this goal it is necessary to improve the optimal formulation and manufacturing parameters affecting the performance of the pressboards.

Heat-curable aqueous acrylic based Acrodur is a series of thermosetting polyester solutions or suspensions commercially supplied by BASF, comprised of a modified polycarboxylic acid and a polyol (as cross-linking agent), and 50% of water was used as solvent media. Acrodur was developed as an alternative to the phenol-formaldehyde resin and other thermosetting binders (Wötzel et al. 1999) frequently used for binding fiber mats, thus avoiding emission of volatiles (like formaldehyde) from the resin into the atmosphere.

According to the literature the thermosetting Acrodur is said to deliver several benefits to pressboard composites. Firstly, it works for natural fibers, due to the chemical polarity and low viscosity. Liang et al. (Liang et al. 2013) and Medina et al. (Medina et al. 2008) reported also that Acrodur exhibits a good adhesion with natural fibers (hemp and kenaf). The effective bondability with natural fibers was attributed to its compatibility with cellulose and strong bonding ability to form effective fibers–matrix integrity. The formation of ester linkages between the carboxyl groups of Acrodur and the hydroxyl groups of the cellulosic fiber was observed by Liang (Liang et al. 2013) through FTIR spectra. In addition, it cures at relatively low curing temperatures and with short heating time, typically less than 10 minutes was reported. Thirdly, it is beneficial for people and environment as the only byproduct of

curing is water. No authors have reported the investigation of Acrodur as a binder for wheat straw based composites.

In addition to thermosetting Acrodur, Acrodur 4444X, was developed as a thermoplastic binder for nonwoven composite applications. Acrodur 4444X is an aqueous suspension. Acrodur 4444X allows for various processing options, such as hot or cold press. Combination of compression and back-injection molding has further potential for design and strength/weight performance (Karbstein and Weed 2015). Acrodur 4444X has not been found in literature to be used with natural fibers in composite applications. Various studies have proven the ability of Acrodur to satisfactorily bond with natural fibers (agricultural crops and plant residues). As two common thermosetting Acrodur, DS3530 and 950L have been used with kenaf (Liang et al. 2013), flax (Islam and Miao 2013) (Liang et al. 2013), jute-sisal fiber mixture (Reck and Turk 1999), hemp and kenaf (Medina et al. 2008) in application of automotive and others, bamboo (Böck 2014), wood (Reck and Turk 1999), cotton-sisal (Kalbe 2011).

Nanocellulose due to its excellent reinforcing effect has received a great deal of attention from scientific and industrial communities in the past decades. The cellulose nanofibril, also known as CNF, is a fibrous material with a width of 4–20 nm, L/D > 100 (Lee et al. 2014). Producing CNF from cell walls of higher plants means peeling off the microfibrils with mechanical forces, leading to the destruction and breakage of microfibrils (Mondal 2017) (Chakrabarty and Teramoto 2018) (Lee et al. 2014).

When CNF is mixed with heat-curable Acrodur DS3530, chemical groups of carboxylic acids react not only with the chemical groups of polyols but also are expected to react with hydroxyl groups on the surface of CNF to form a crosslinked network. As a result, CNF is integrally incorporated into the network and the reinforcement of nanocellulose in the composite is expected, which lead to enhanced interfacial adhesion of wheat straw composite. Another benefit is that adding nanocellulose additive in Acrodur solution or suspension can also increase the binder viscosity (Mondal 2017) and potentially lead to improved mechanical strength of composite (Lee et al. 2014) (Chakrabarty and Teramoto 2018). CNF has been used with various polymeric matrices , such as polyolefins (Boldizar et al. 1987), natural starch from potato (Dufresne et al. 2000), phenol–formaldehyde resin (Nakagaito and Yano 2004), melamine formaldehyde (Nakagaito and Yano 2004) . The properties of some CNF reinforced polymer nanocomposites increased significantly even when the amount of CNF was smaller than 10 vol.%. The matrices for these high performance CNF model nanocomposites were PLLA (poly-L-lactic acid)

(Jonoobi et al. 2010), regenerated cellulose (Pullawan et al. 2010), and polyvinyl alcohol (Lu et al. 2008).

The effects of hot-water and NaOH treatments of wheat straw on wettability, surface morphology and thermal stability have been study in Chapter 3. The considerable enhancement on the wettability, surface morphology and thermal stability of wheat straw were achieved by using these two treatments. The increased wettability can provide better binder distribution. A coarser surface can induce both better mechanical interlocking and bonding reaction between fiber and polymer improving the mechanical properties of the composite (Mwaikambo and Ansell 2002) (Herrera-Franco and Valadez-Gonzalez 2005) (Islam and Pickering 2007). The improved bonding reaction is due to the removal of the surface impurities and exposure of the fiber hydroxyl groups to the polymer matrix whereas the coarser surface is responsible for inducing more fiber-polymer interpenetration at the surface. Thermal stability allows for wider temperature range for processing.

In this chapter, the knowledge gained in previous chapters and from the literature is applied to produce wheat straw –Acrodur composite pressboard. It is expected that, the improved wettability of the straw surface is beneficial to create an even distribution of binder. The high specific area and porous structure also assist in the formation of physical bonding, making the wheat straw fiber compatible to water based Acrodur solution. In order to verify this hypothesis, in this chapter, the potential to enhance the mechanical properties of wheat straw –Acrodur pressboard via application of two relatively cost-effective treatments was investigated. Two treatments, hot-water and NaOH treatments, were conducted on wheat straw. The untreated and treated wheat straw was impregnated with various Acrodur binders for pressboard production. The effects of the alkali and hot-water treatments on the straw fiber and mechanical properties of the composite pressboard were investigated.

7.2 Research Objectives and Approach

The chemical formulation is an essential part of development of wheat straw-based composite pressboard. Wheat straw-Acrodur composite is a material in which wheat straw is impregnated either with thermoplastic Acrodur (softens by heating and solidifies by cooling) or with thermosetting Acrodur (rigid three-dimensional network). The hypothesis that CNF additive can increase mechanical properties was also evaluated. Therefore, the primary factors in this regard are the composite constituents: wheat straw, Acrodur binder and CNF additive. Equally importantly, the manufacturing

technology and the manufacturing conditions also play a decisive role in determining the quality of the wheat straw –Acrodur composite pressboard.

The research goal reported in this chapter to prepare wheat straw–Acrodur pressboards using compression molding technology and knowledge obtained in previous chapters. It involved compression molding of the composite material in a confined mold, where chemical or physical changes were initiated by heat and the material solidified to its final shape when cooled down. Pressure is exerted to compress the material to form a desired shape and squeeze the resin to fill up the cavity until the resin is solidified after a certain period of time.

At the first stage, the composite components were selected based on the individual characteristics and availability, and the compatibility between wheat straw and binders. The second stage involved the selection of appropriate manufacture technology –compression molding and optimization of compression molding parameters. At the last stage, the performance of the produced pressboard was evaluated in terms of mechanical, dielectric and other properties.

Table 7.1 Parameters at formulation and production stage

Formulation stage		Production stage
Wheat straw	**Binder**	**Compression molding**
Wheat straw particle (#2)	**Thermoset #1**	Fiber orientation
Wheat straw fiber (#1)	**Thermoset #2**	Mixing method
Wheat straw #1/#2	**Thermoset #3**	Compression temperature
Hot-water treated wheat straw (#1 and #2)	**Thermoset #4**	Compression pressure
NaOH treated wheat straw (#1 and #2)	**Thermoplastic #5**	Compression resident time
		Aerating time

The motivation is to produce pressboards and then evaluate the improvement of mechanical property combined with other properties by varying the parameters of formulation and compression molding conditions. The parameters investigated in this chapter that exert influences on the performance of the composite pressboard are listed in Table 7.1, corresponding to formulation and production stages, respectively. Wheat straw of two sizes were treated and examined. The untreated and treated wheat straw was used as the reinforcing material in Acrodur composite with purpose of improving the interfacial compatibility between wheat straw and binder. Both thermosetting and thermoplastic

polyester solutions and suspension, Acrodur binders from BASF were used as binder, with or without cellulose nanofibril (CNF) as reinforcing additive. The compression molding was carried out in a way to control time, heat and pressure applied to the composite. At last, the performance of the resultant pressboards was evaluated mainly in terms of mechanical, electrical and other properties of interest, and the effects of these parameters on the properties of final products were analyzed and evaluated.

The objective of this chapter is to focus on how the composite pressboards were fabricated from raw materials. This chapter describes wheat straw, polymer binders and additive used in this research. It also includes detailed descriptions of the processing and treatments that were performed on wheat straw raw material to obtain the portions required for pressboard manufacture, and the physical and thermal characterizations were conducted to provide the insights into the behavior of the materials. The manufacturing procedures used for pressboard manufacture in this study differed among thermoplastic Acrodur, thermosetting Acrodur, and CNF reinforced Acrodur. The flexural properties were performed on the manufactured pressboards as per the American Society for Testing and Materials (ASTM) standards. At last, the effects of wheat straw sizes, the treatments on wheat straw, different Acrodur and compression molding conditions on mechanical properties of the pressboards were investigated and evaluated in terms of flexural property. The chapter ends with the process of data analysis and effect evaluation of the pressboard properties against those currently used in the industries.

7.3 Materials and Methods

Two sizes of wheat straw, fiber (#1) and particle (#2), as described in 6.3.1, were examined as reinforcement in this chapter.

Sodium hydroxide used for treatment was from Sigma-Aldrich company (ACS reagent, >=96.0%, pellets); DI water was de-ionized water prepared at University of Waterloo.

Two thermosetting Acrodur solutions used as binder were **Thermoset #1** and **Thermoset #3** (Figure 8.73 (a and c) in Appendix H). They are acrylic based polyester solutions. Acrodur DS 3530 resin is an aqueous solution of a modified poly (carboxylic acid) with a poly (hydric alcohol) as crosslinking component.

The third binder used was nanocellulose-reinforced **Thermoset #1** as shown in Figure 8.73 (b) in Appendix H, containing 3–5 wt. % of cellulose nanofibril (CNF). The CNF pulp was prepared mechanically with refiners from eucalyptus trees by Suzano Papel e Celulose and was chemically

pulped by the Kraft process and bleached. Then 3–5 wt. % of nanocellulose was dispersed in **Thermoset #1** using mechanical mixing at Suzano facility. The illustrative graph is showing in Figure 8.74 in Appendix H.

Table 7.2 Physical and chemical properties of **Thermoset #1, #2, #3, #4** and **Thermoplastic #5**

Binder system	Product	Polymer	Type	Density (g/cm^3)	pH	T_g (ºC)	Viscosity (mPa·s) (23 ºC)	Product key properties
Thermoset #1	Acrodur DS3530	Acrylic	Solution	approx. 1.21	3.5	-	150–300 M_W ≈ 12,000 g/mol	Hard, brittle, heat and water resistance
Thermoset #2	CNF-Acrodur DS3530							
Thermoset #3	Acrodur 950L	Acrylic	Solution	approx. 1.2	3.5	-	900–2500 M_W ≈ 80,000 g/mol	Hard, brittle, heat and water resistance
Thermoset #4	Acrodur DS3530/950L							
Thermoplastic #5	Acrodur 4444X	Styrene-acrylic	Dispersion	N.A.	3.5	97	50–300	Hard, visco-plastic

Sources: technical data sheet (Kalbe 2007) (Gerst et al. 2009)

The fourth Acrodur binder used was **Thermoplastic #5** shown in Figure 8.75 in Appendix H, which is the thermoplastic version of Acrodur newly developed in 2015 by BASF. **Thermoplastic #5** is a polystyrene-acrylic based polyester dispersion, however its chemical components and structure has not been disclosed by the supplier. Information on the physical and chemical properties of Acrodur binders used in this research is presented in Table 7.2. It should be noted that throughout this chapter, Acrodur DS3530, 950L, and 4444X are denoted as **thermoset #1**, **thermoset #3**, and **thermoplastic #5**, respectively. CNF-Acrodur DS3530 is denoted as **thermoset #2**.

Two sizes of wheat straw (#1 and #2) were treated separately with NaOH solution or hot water, while the untreated wheat straw was considered as control. As described in Chapter 3, the alkaline treatment was conducted in such a way where wheat straw was soaked in 3 wt. % NaOH aqueous solution at straw/solution mass ratio of 1:2 at room temperature for 24 hours (Figure 3.6 (b)). Hot-water treatment was applied by boiling wheat straw in deionized (DI) water at temperature of 100°C for 2 hours (Figure 3.6 (c)). The treated wheat straw was then washed using DI water and vacuum-dried at 60–80°C to a moisture level of below 10 %. The untreated and treated straw samples are shown in Figure 7.1.

Figure 7.1 Untreated (1) NaOH (2) and hot-water (3) treated wheat straw fiber and untreated (4) NaOH (5) and hot-water (6) treated wheat straw particle

7.3.1 Characterization Methods

The bulk density of treated wheat straw were measured according to the method described in section 6.3.2.

Moisture content analysis was performed using the OHAUS MB45 Moisture Analyzer. The samples were uniformly spread on an aluminum pan and placed on the analyzer where it was heated to 80ºC until the weight remained constant. WinWedge software is used to record the data in terms of percentage of moisture evaporated from the sample. The solid contents of Acrodur and CNF solution were determined by "solid content = 100% - moisture content".

The Fourier transform infrared (FTIR) analysis was performed on uncured and cured **Thermoset #1**, **#2**, and **#3**, and dried **Thermoplastic #5**, using the same instrument and the same procedure as described in 6.3.2 for polyamide 6 samples.

The TGA and DSC analysis of **Thermoset #1**, **#2**, and **#3** have been conducted and studied in detail in Chapter 4.

Thermoplastic #5 for the TGA and DSC analysis was prepared by removing the contained water at 80 ºC. Then TGA and DSC analysis were carried on the prepared samples, using the same instrument and the same procedure described in Chapter 4. The samples were subjected to a constant heating rate of 10°C/min ranging from 35 to 650°C under nitrogen atmosphere.

7.3.2 Manufacturing Method

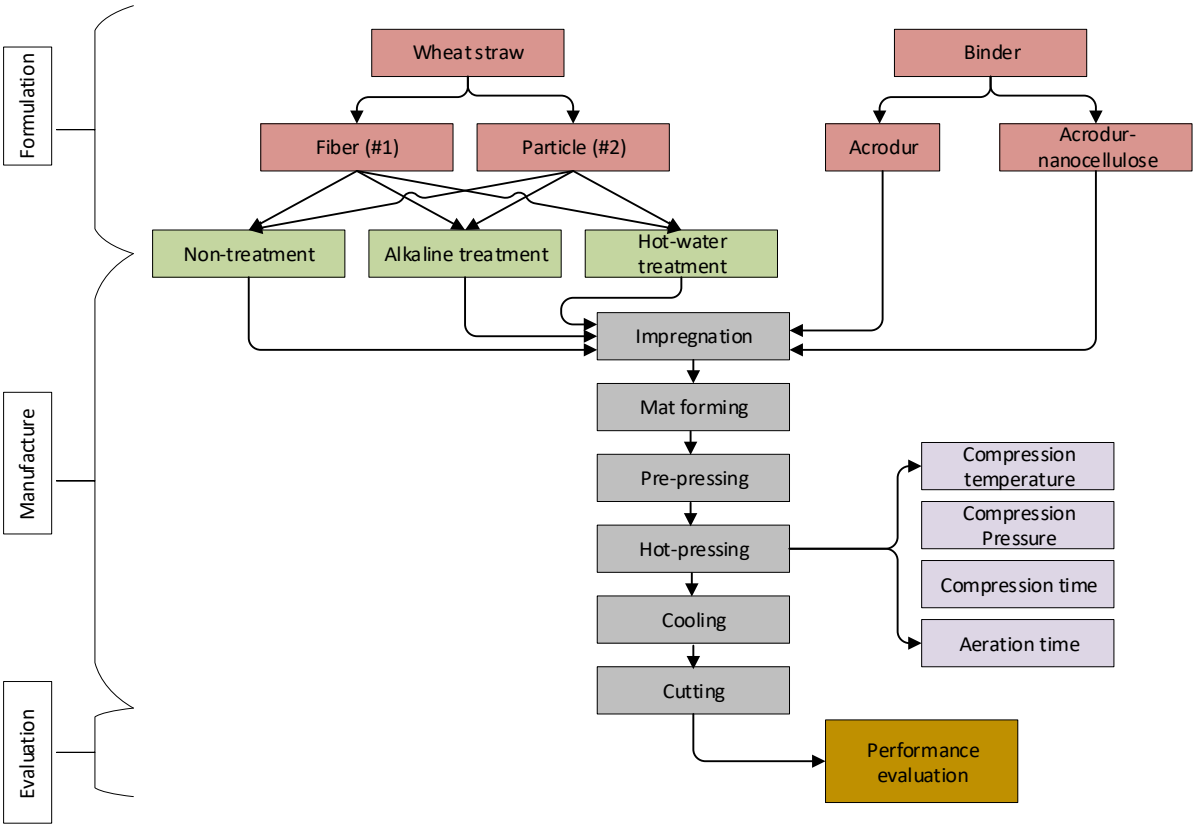

Figure 7.2 Flowchart of wheat straw-thermosetting Acrodur composite pressboard production

The wheat straw-Acrodur composite pressboards were manufactured with varying parameters as per following procedure. The production process involved the use of hydraulic press and a custom-designed pressing mold set consisting of a square mold, a flat plate and a solid plunger, described in the previous section (6.3.3).

The production of wheat straw-Acrodur composite pressboards involves several steps, which are summarized in the flow diagram shown in Figure 7.2. At first stage, untreated or treated wheat straw is

formulated with Acrodur binders; at second stage, the pressboards are fabricated via compression molding of the composite; at last stage, the properties of resultant pressboard are examined and evaluated. The detailed illustration is presented in subsequent sections.

Pressure is exerted on the composite material not only to bring the wheat straw fibers close enough for physical or chemical bonding to occur, but also to help the resin infuse into the inner structure of wheat straw. However, high pressures could lead to the damaging of the hollow fibers structure and organization. There is a critical pressure (maximum) existing that can be applied for improving the mechanical properties before damaging the structure of the reinforcing fibers.

As mention earlier, for easy expression and because of the conserved pressboard area, the force in unit of lbf is used. Although the pressure used for hopressing varied widely in literature, two levels of force 30,000 and 45,000 lbf were selected for this study, corresponding to 1,436.8 and 2,155.7 psi. These levels were selected based on the capability of the hydraulic press and other values reported in the literature.

Table 7.3 Formulation and compression molding parameters and their levels for **Thermoset #1**, **#2** and **#3**

	Parameter		**Level**
Wheat straw	Fiber #1	Variable	Untreated, NaOH treated, hot-water treated
	Particle #2	Variable	Untreated, NaOH treated, hot-water treated
	Fiber #1/ particle #2		
Binder	**Thermoset #1**	Variable	10%, 20%, 40%, 60%
	Thermoset #3	Variable	20%, 40%
	Thermoset #2	Variable	20%, 40%
Compression molding condition	Force (lbf)	Variable	30,000, 45,000
	Temperature (°C)	Variable	170 –190, 200
	Holding time (min)	fixed	10–15
	Aeration	fixed	2–3 times

Table 7.4 Formulation and compression molding parameters and their levels for **Thermoplastic #5**

	Parameter		**Level**
Wheat straw	Fiber #1	Variable	Untreated, NaOH treated, hot-water treated
	Particle #2	Variable	Untreated, NaOH treated, hot-water treated
Binder	**Thermoplastic #5**	Variable	20%, 40%
Compression molding condition	Force (lbf)	fixed	45,000 (pressure: 2155.17psi)
	Temperature (°C)	Variable	120 or 200
	Holding time (min)	fixed	3–10
	Aeration	fixed	0 times

The wheat straw-Acrodur composite pressboards were manufactured with varying parameters as in Table 7.5 followed by detailed procedure.

Table 7.5 Manufacturing process of wheat straw-Acrodur composite pressboard

Step	Parameter or Technique used
Formulation	Dry and weigh
Impregnation	Spray impregnation
Drying	Convection oven, at 50°C
Mat formation	Hand layup
Pre-press	At 25,000–45,000 lbf
Hot press	At 30000, 45000 lbf, 170–200°C/ aeration
Cool down	At room temperature

1. **Formulation:** The weight of wheat straw for each pressboard was fixed at 32g on dry weight, which makes the target board thickness of approximately 3 mm. Wheat straw of both sizes was dried in a convection oven first to remove the moisture to facilitate the wetting process during resin impregnation. The required amount of dried wheat straw was weighed and added to the mixer bowl for impregnation. Based on the dry weight of wheat straw and solid content of Acrodur solution (Table 7.7), the amount of Acrodur was applied. The weight fraction of wheat straw was determined as the dry wheat straw mass ($M_{wheat\ straw}$) over the Acrodur solution solid content mass ($M_{Acrodur}$) and the dry wheat straw mass ($M_{wheat\ straw}$):

$$M_f = M_{wheat\ straw}/(M_{wheat\ straw} + M_{Acrodur}) \quad 7.1$$

2. **Resin impregnation:** To allow smooth resin flow and penetration into the wheat straw, the viscosity of Acrodur was lowered by mixing with deionized water at a ratio of 1:1. Then diluted Acrodur solution (50:50) was sprayed using squeeze bottle slowly onto the wheat straw while being stirred (called the method of "spay-while-stirring"). An orbital bowl mixer (KitchenAid mixer) was used to improve the mixing efficiency, allowing better wetting of Acrodur by spreading over the surface or into the structure of straw. Impregnation of Acrodur is considered effective when the solution spreads over the surface of wheat straw and penetrates into the cracks, cell lumen, and even cell walls. Wheat straw stems of 3–4cm can be incorporated hopefully for a better reinforcing effect. Once impregnated, the excess water was removed in convection over at 50°C to achieve residual moisture of less than 10%.

3. **Mat-formation and pre-press:** After drying, impregnated wheat straw was then evenly laid manually as per hand layup process and spread to loose composite mats in the mold. Then the mats were pre-pressed in the mold using the hydraulic press to reduce the mat thickness and to ensure contact between the particles. The pre-pressed mats held their shape mainly by physical interactions when the mold was removed. The images in Figure 7.3 show the mat in the mold before pre-press (a) and after pre-press (b).

Figure 7.3 Wheat straw-Acrodur mat before (a) and after pre-press (b)

4. **Hot-press:** The pre-pressed mats were subsequently hot-pressed at various temperatures and pressures between two platens with temperature controlling unit. Prior to hot pressing, two

glass fiber reinforced Teflon sheets were used on both sides of the mats to prevent direct contact between the mold plates and the impregnated wheat straw and to allow for easy removal of the final board after pressing. Aluminum plate and plunger were employed in hot pressing for better heat transfer. The mats were then placed into the hydraulic press and compressed using the compression molding parameters shown in Table 7.4. The heat cured the binder and caused a series of physical and chemical changes to the pressurized composite, which consolidate and harden the final product. Compression time of less than 10 minutes was used, which was dependent on observation of the amount of released water vapor. The residual and produced moisture was vaporized during the heating stage. A de-gassing time during hot pressing is necessary to release entrained steam and air to avoid delamination of the pressboard.

5. **De-mold and cool:** Once the resin had cured the mold was opened and lifted to allow de-molding. At last, the composite pressboards are removed from the mold for cooling at room temperature. Depending on selected press parameters different thickness and densities of the pressboards are produced. The finished composite pressboards were cut into testing specimens using a saw blade for mechanical and other tests. Figure 7.4 presents an example of resultant wheat straw-**Thermoset #1** pressboard.

Figure 7.4 Illustrative example of wheat straw-thermosetting Acrodur pressboard

7.3.3 Evaluation Methods

The manufactured pressboards were evaluated in terms of mechanical and electrical properties, as well as some other relevant physical and thermal properties.

The wheat straw-Acrodur pressboard specimens for flexural properties measurement were prepared and measured using the same instrument and same procedure described in Chapter 6.

The pressboards made with wheat straw-**Thermoset #1** were used for dielectric strength measurement. To examine the effect of washing process after treatments, the half of wheat straw sample was washed thoroughly using distilled water, and the other half did not go through wash process. The specimen preparation method and dielectric strength measurement method were the same as described in 6.3.4. The same equipment was used for the measurement. The breakdown voltages were measured and recorded.

The pressboard samples were prepared by immersing the liquid nitrogen and breaking into small pieces using pliers. The specimens were prepared by being coated with gold to provide about 200 A˚ gold layer thickness using a vacuum sputter coater. The instrument used was a Quanta 250 FEG Scanning Electron Microscope.

7.4 Results and Discussions

7.4.1 Material Characterization

Table 7.6 Bulk density of treated wheat straw

Wheat straw	Bulk density (kg/m^3)	Moisture content (after drying)
NaOH treated Fiber (#1)	61.92 (0.15*)	3.31%
Hot-water treated Fiber (#1)	56.31 (0.68*)	4.11%
NaOH treated particle (#2)	66.21 (0.44*)	5.81%
Hot-water treated particle (#2)	70.28 (0.66*)	3.63%

*Values in parenthesis are standard deviations

The Bulk density and moisture content results of treated wheat straw #1 and #2 are shown in Table 7.6. It is seen that, compared to untreated wheat straw, both alkali and hot-water treatment decreased the bulk density of both sizes wheat straw. The explanation is that the treatments had removed water soluble component and part of hemicelluloses, which creates the porous structure. The solid content

results of Acrodur are shown in Table 7.7. All the Acrodur samples have approximate 50% of solid content.

Table 7.7 Moisture content and solid content of **Thermoset #1**, **#2**, **#3**, **Thermoplastic #5** and CNF solution

	Moisture content	Solid content
Thermoset #1	42.12%	56.88%
Thermoset #2	46.17%	52.83%
Thermoset #3	39.41%	60.59%
Thermoplastic #5	49.66%	50.34%
Nanocellulose 480	96.35%	2.65%

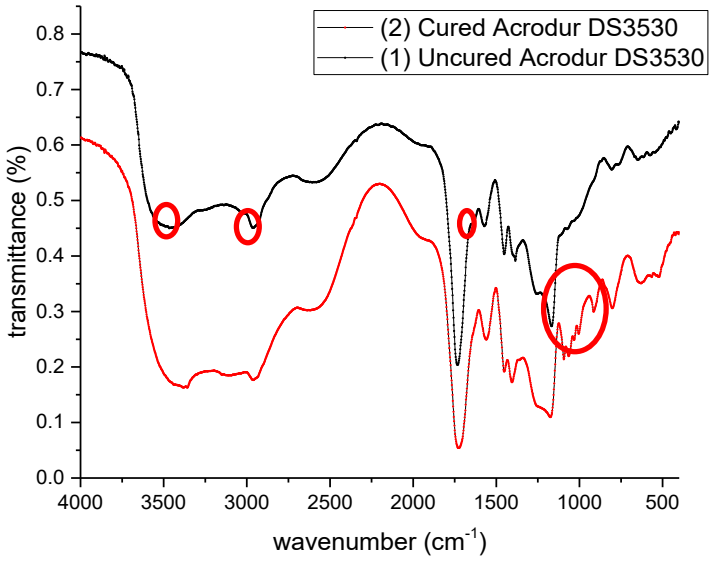

Figure 7.5 Fourier transform Infrared spectra of **Thermoset #1** before and after curing

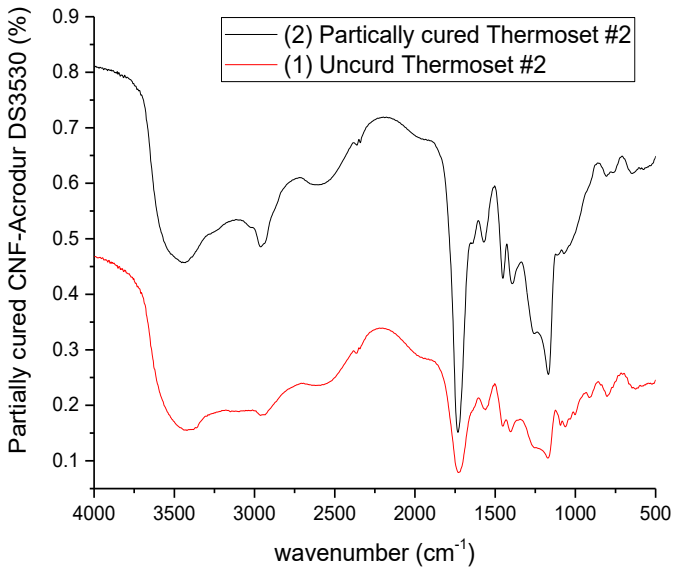

Figure 7.6 Fourier transform Infrared spectra of **Thermoset #2** before and after curing

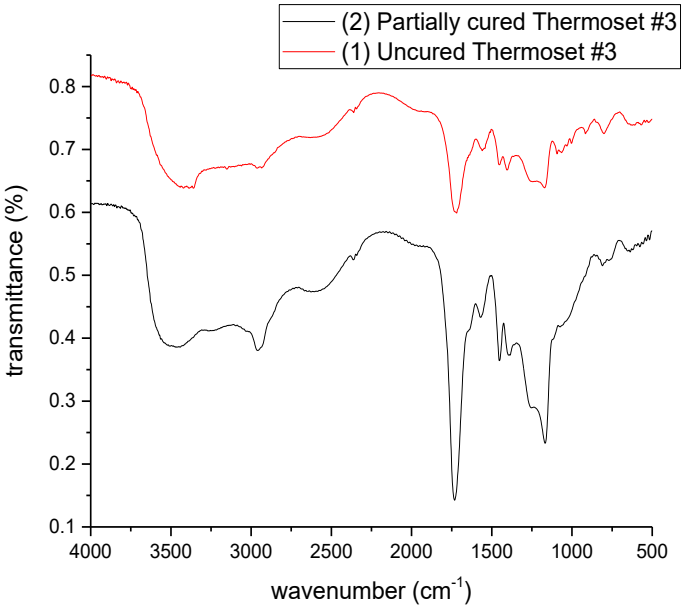

Figure 7.7 Fourier transform Infrared spectra of **Thermoset #3** before and after curing

Determination of the structural properties of Acrodur before and after curing. The FTIR spectra of **Thermoset #1**, **#2** and **#3** are showing in Figure 7.5, Figure 7.6, and Figure 7.7, respectively. The characteristic bands of the FTIR spectra of the samples studied are listed in Table 7.8. The functional group regions were selected and compared to the literature (Ummartyotin and Sain 2014) (Liang et al. 2013) (Rasyid et al. 2019).

Table 7.8 Assignment of FTIR spectra of **Thermoset #1**, **#2** and **#3**

Wave number (cm^{-1})	Assignment
3500–3000	O–H stretching (–OH of alcoholic and carboxylic)
2900–2800	CH_2 or CH_3 stretching
1740,1720	C = O ester stretching
1720, 1641. 1560	C=O stretching (COO–)
1398	C=O bending (COO–)
1360	C–H and O–H bend
1260–1000	C–OH

In the case of uncured **Thermoset #1**, **#2** and **#3**, as shown in curve (1) of Figure 7.5, Figure 7.6, and Figure 7.7, the O–H stretch broad peak centered at around 3500 cm^{-1} and C–O stretching vibration of hydroxyl at 1260–1000 cm^{-1} could be attributed to the presence of polyalcohol. OH stretch in the 3200–2900 cm^{-1} region centered near 3000 cm^{-1} and C=O stretch at 1720 cm^{-1} could be linked to the presence of polycarboxylic groups. No absorption associated with CNF is observed in FTIR spectrum of **Thermoset #2**, which can be attributed to low concentration of CNF.

The FTIR spectra of partially cured **Thermoset #1**, **#2** and **#3** are displayed in curve (2) of Figure 7.5, Figure 7.6, and Figure 7.7. After curing, it is supposed that intensity reduction of the–OH group characteristic band at 3500 cm^{-1} (Ummartyotin and Sain 2014), should be observed due to the crosslinking reaction of both compounds to form polyester. There is a slight decrease in the intensity of the O–H stretch broad peak centered at 3300 cm^{-1} in my spectra. The disappearance of peak C–O stretching vibration at 1260 cm^{-1} corresponding to the reduction of polyalcohol content is not observed clearly. The bands at 1560 cm^{-1} and 1398 cm^{-1} attributed to carboxylate stretching and bending vibrations of a carboxylate is supposed to reduce in width and intensity (Liang et al. 2013), due to chemical reactions occurred after curing, which is not clear in my spectra. The presence of polyester is not identified in my spectra by the appearance of C=O stretching vibration at 1720 cm^{-1} coexisted with

C–O stretching vibration peak of ester group at 1160 cm^{-1} (Rasyid et al. 2019) (Liang et al. 2013). These expected observations are not present in the spectra of partially cured samples can be ascribed to the low level of cure density at 180°C for 10 minutes.

The FTIR spectrum of **Thermoplastic #5** is present in Figure 7.8. The characteristic bands of the FTIR spectrum are listed in Table 7.9. It can be seen the typical peaks of aromatic hydrocarbons and the acrylic ester bonds. The peaks at 3061 cm^{-1} and 3027 cm^{-1} are the characteristic absorption stretching vibrations of C–H in benzene rings. The characteristic benzene double bound absorption peak is detected at 1602 cm^{-1}. The peak at 841 cm^{-1} is ascribed to the C=O in butyl acrylate, and those at 2958 cm^{-1} and 3083 cm^{-1} are the C–H structure key stretching vibration peaks of CH_3 and CH_2, respectively. The stretching vibrating peaks of acrylates arising from C=O are observed at 1732 cm^{-1} (Chen et al. 2015) (Wan et al. 2008). The FTIR spectrum reveal **Thermoplastic #5** is comprised of aromatic and acrylic ester groups, which is in consistence with the BASF data sheet of one of thermoplastic Acrodur, stating Acrodur DS3558 is comprised of styrene-acrylate dispersion modified with polycarboxylic acid and a polyol as the crosslinking agent.

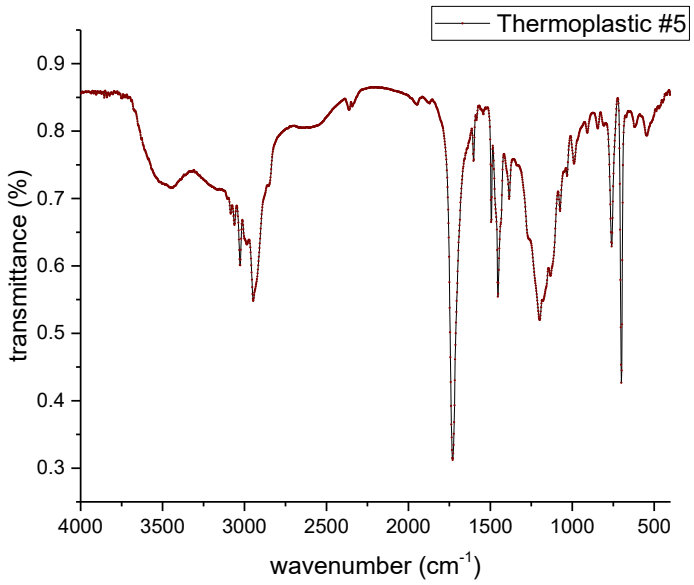

Figure 7.8 Fourier transform Infrared spectra of **Thermoplastic #5**

Table 7.9 Assignment of FTIR spectrum of **Thermoplastic #5**

Wave number (cm^{-1})	Assignment
3440	O–H stretching of hydroxyl groups
3030	C–H aromatic of benzene
2958 - 3083	CH_2 or CH_3 stretching
1732	C=O for acrylate stretching ester
2900	C–H aliphatic of acrylate
1602	C=C of benzene
1067, 1029	C–H in plane bending of benzene
841	C=O in butyl acrylate
761	Benzene substitution

The thermal stability of treated wheat straw has been discussed in section 3.4.3 of Chapter 3. The results show the onset temperature of 5% thermal degradation is 249°C and 226°C for hot-water treated and NaOH treated wheat straw, respectively. The activation energy is 169.20 and 209.72 kJ/mol, respectively for hot-water treated and NaOH treated wheat straw. This indicates both hot-water treated and NaOH treated wheat straw can withstand the processing temperature up to 200°C without severe thermal decomposition triggered.

The cure reaction and thermal stability of Acrodur binders was investigated using TGA in Chapter 4. The TGA thermographs for uncured **Thermoset #1**, **#2** and **#3** are shown in Figure 7.9. It can be seen from the thermographs that the degradation profiles of the **Thermoset #1**, **#2** and **#3** are very similar, consisting of three distinct stages, except the minor loss of mass due to the evaporation of residual moisture. The first peak occurred in the range of 150–265°C (peak at approx. 210°C), the second in the range of 265–380°C, and 380–480°C for the third. The first peak is considered mainly for cure reaction of Acrodur combined with a small peak of the starting of the decomposition of lower boiling point components (i.e. CO, CO_2, CH_4, ethylene and acetylene) by polyester at 180°C. (Braun and Levin 1986) This range is in a good agreement to DSC analysis and data sheet from BASF. The mass loss must be due to the water as by-product of the reaction leaving the system. The second and third peaks are at 325°C and 410°C, which can be attributed to cured Acrodur's thermal degradations. The second degradation stage may be due to decomposition of polyester leading to the formation of volatile products and the third degradation stage is due to oxidation of volatile and charred products. The TGA thermographs indicate that **Thermoset #1**, **#2** and **#3** are more thermally stable than wheat

straw, therefore, incorporation with **Thermoset #1**, **#2** and **#3** provides protecting barrier for wheat straw from thermal decomposition.

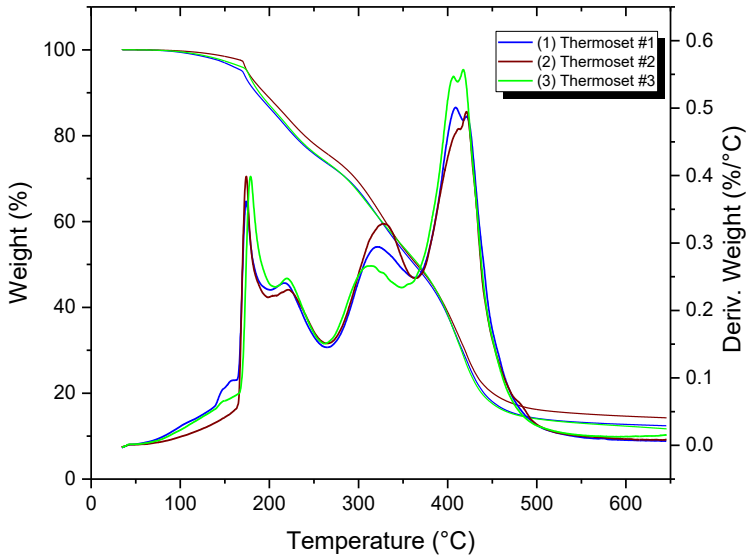

Figure 7.9 TGA thermographs of uncured **Thermoset #1** (1), **#2** (2), and **#3** (3)

Table 7.10 Thermal degradation data of **Thermoset #1** at 10°C/min in a nitrogen atmosphere

	First peak	Mass loss	Second peak	Mass loss	Third peak	Mass loss
Thermoset #1	217°C	22%	319°C	26%	412°C	34%
Thermoset #2	223°C	21%	328°C	25%	420°C	34%
Thermoset #3	222°C	22%	311°C	20%	412°C	40%
Annotation	Induced water evaporation and minor thermal degradation		Thermal decomposition of cured Acrodur		Oxidation of volatile and charred products	

The TGA thermograph of CNF is shown in Figure 7.10. It is seen that initial degradation temperature of CNF is at 215°C, and peak position is at 329°C, which is slightly higher than wheat straw. Figure 7.10 shows that the thermal decomposition peak with maximum weight loss for CNF appeared at 330°C, which is in consistence with the temperature region of 330.00–332.74°C stated in the literature (Yahya et al. 2015)

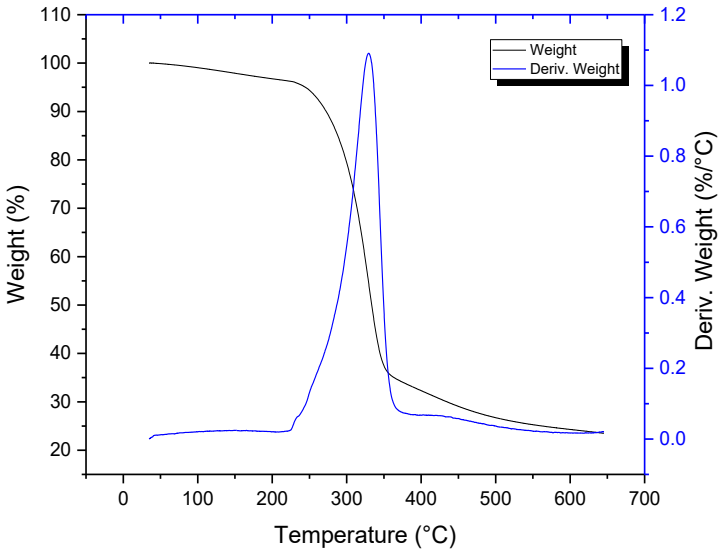

Figure 7.10 TGA thermograph of dried CNF

The DSC thermalgraphs of **Thermoset #1**, **#2**, and **#3** were analyzed in Chapter 4. It was concluded that the cure reaction for these three Acrodur binders occurs at temperature range of 150–220°C. The higher temperatures are, the faster the crosslinking happens in thermosetting Acrodur. As a result, the effective curing of **Thermoset #1**, **#2**, and **#3** occurs in the temperature range of 170–200°C for less than 10 minutes.

The DSC analysis of **Thermoset #2** was described in Chapter 4. The same phenomena were found in the DSC thermographs of **Thermoset #2** with **Thermoset #1**, which indicates that curing reaction occurs for these two Acrodur and lead to crosslinked solid at this temperature range. It has been concluded that the curing reaction for **Thermoset #2** occurs at temperature above 130°C. The higher temperatures are, the faster the crosslinking happens in thermosetting Acrodur. As a result, the effective curing of **Thermoset #2** occurs in the temperature range of 170–190°C for less than 10 minutes.

TGA and DSC thermographs of **Thermoplastic #5** are shown in Figure 7.11. Unlike **Thermoset #1** or **#2** or **#3**, **Thermoplastic #5** is a type of thermoplastic polymer in suspension. The significant weight drop for **Thermoplastic #5** occurs at around 415°C, which is much higher than thermal degradation temperature of wheat straw. The first softening point (T_g) of around 100°C in agreement with BASF document (Karbstein and Weed 2015), and the second softening temperature appears at around 200°C,

which provides the guideline for selection of processing temperature. The emergence of two softening temperatures can be attributed to two kinds of polymer segments in polymer chain.

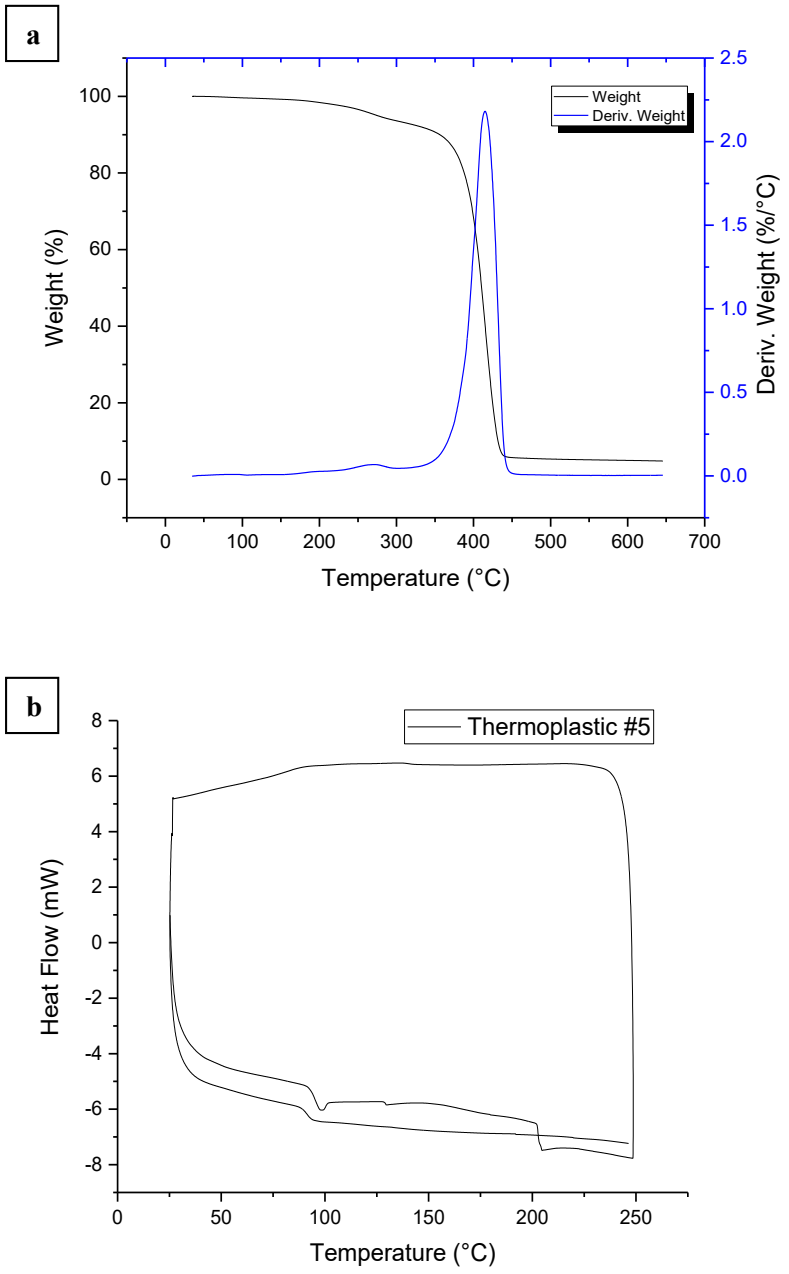

Figure 7.11 TGA (a) and DSC (b) of **Thermoplastic #5**

7.4.2 Flexural Property

A typical flexural stress–strain curve obtained from the flexural testing of wheat straw-Acrodur composite pressboard is shown in Figure 7.12. All the wheat straw-Acrodur composite pressboards were broken during testing, and all the composite samples tested were found to have similar stress–strain curve shapes. As seen, the curve starts with a linear elastic region, where the stress increases proportionally to the strain and the slope is flexural modulus. Then the curve enters a brief region of formation of internal crack and then fractures. The stress–strain characteristics indicate that the wheat straw-Acrodur pressboards are brittle materials, and there is little or no plasticity. The flexural property results are presented in following subsections organized according to the type of binder.

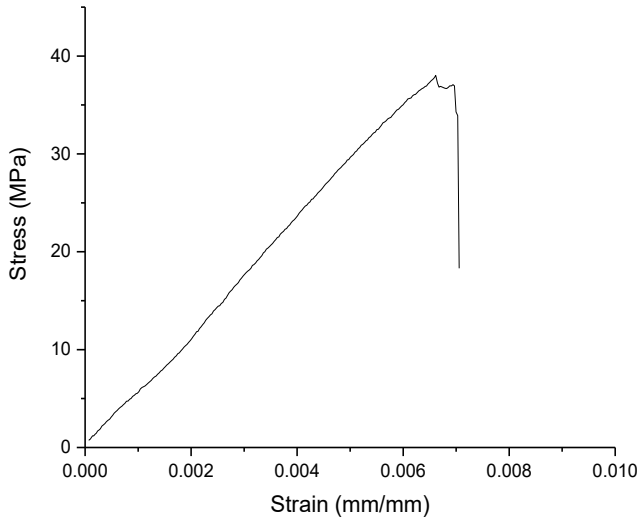

Figure 7.12 A typical flexural stress–strain curve of wheat straw-Acrodur pressboards (straw fiber and 40% **Thermoset #1** molded at 200°C and 45000 lbf for 10 minutes)

7.4.2.1 Thermoset #1

Thermoset #1 is Acrodur DS3530 in form of solution with low molecular weight and viscosity compared to **Thermoset #3**, Acrodur 950L.

7.4.2.1.1 Molded at 30,000 lbf, 170–190°C

The flexural results of the pressboards manufactured with untreated wheat straw and **Thermoset #1** at 170–190°C, 30,000lbf for 10 minutes are presented in Table 7.11. It is seen that the pressboards made with wheat straw particle (#2) showed better flexural properties than that with wheat straw fibers (#1). And the flexural properties were improved with higher binder content (40%). The pressboards with 20% **Thermoset #1** exhibited poor flexural strength and modulus. However, with 40% binder content, the flexural properties were improved significantly and reached its highest of 21.4 MPa and 3128 MPa in flexural strength and modulus, respectively.

Table 7.11 Flexural strength and modulus of wheat straw-**Thermoset #1** composite pressboard; Hot press condition: F = 30,000 lbf, T = 170–190°C, time = 10 min

Treatment	Wheat straw	**Thermoset #1**	Flexural Strength (MPa)	Flexural Modulus (MPa)
Untreated	#1	20%	12.4	2,562
Untreated	#1	40%	16.6	1,642
Untreated	#2	20%	13.2	2,622
Untreated	#2	40%	21.4	3,128

The flexural results of the pressboards manufactured with untreated wheat straw-**Thermoset #1** are presented in first portion of Table 7.12. The compression molding conditions were the same as that in Table 7.11, except the force increased from 30,000 to 45,000 lbf. The significant effect of higher pressure was observed on flexural properties. The application of 45,000lbf of force improved the flexural strength from 21.4 MPa to an average of 35.9 MPa. The highest of 38.6 MPa was achieved with mixed wheat straw #1 and #2, at 20% binder content, which is amazingly an improvement of 80%. At the same time, the flexural moduli increased dramatically as well, with an average of 5,838 MPa and the highest of 6,233 MPa, which nearly doubted the value obtained with force 30,000 lbf. It should also be noted that this increase was achieved with lower resin content, thus representing a potential cost savings.

Table 7.12 also encompasses the results of hot-water treated and NaOH treated wheat straw. As observed, hot-water treatment slightly increased the flexural strength and modulus to the highest of 39.6 MPa and 6,767 MPa, respectively. On the other hand, compared to untreated and hot-water treated wheat straw, the flexural properties of NaOH treated wheat straw was more sensitive to binder content.

The 10% binder content showed very poor flexural properties due to lack of binder. With higher binder content, flexural properties increased and reached to the highest of 39.7 MPa and 6,876 MPa at 40% **Thermoset #1**, although further pushing the binder up to 60% did not exhibit expected effect, indicating the optimal **Thermoset #1** content for wheat straw pressboard is around 40%.

Table 7.12 Flexural strength and modulus of wheat straw-**Thermoset #1** composite pressboard; Hot press condition: F = 45,000 lbf, T = 170–190°C, time = 10 min

Treatment	Wheat Straw	**Thermoset #1**	Flexural Strength (MPa)	Flexural Modulus (MPa)
Untreated	#1	20%	34.5	5,789
Untreated	#1	40%	36.3	5,694
Untreated	#1&2	20%	38.6	5,494
Untreated	#1&2	40%	35.0	6,233
Untreated	#2	20%	36.2	6,092
Untreated	#2	40%	34.9	5,723
Hot-water treated	#1	20%	36.9	4,917
Hot-water treated	#1	40%	32.8	3,835
Hot-water treated	#2	20%	39.6	6,767
Hot-water treated	#2	40%	36.2	5,482
NaOH treated	#1	20%	16.5	3,121
NaOH treated	#1	40%	27.2	3,444
NaOH treated	#1&2	40%	28.2	4,946
NaOH treated	#2	10%	2.1	286
NaOH treated	#2	20%	16.9	4,004
NaOH treated	#2	40%	39.7	6,876
NaOH treated	#2	60%	36.0	6,353

Overall, the increase of force from 30,000 to 45,000 lbf exhibited a profound influence on flexural properties with 80% and 100% improvements realized in flexural strength and modulus, respectively. The effect of resin content was weakened by increased force. The treatments realized 2% and 10% improvement respectively in flexural strength and modulus. The mixture of two size of wheat straw #1 and #2 exhibited a small positive effect on flexural properties.

7.4.2.1.2 Molded at 45,000 lbf, 200°C

The flexural results of the pressboards manufactured at higher temperature of 200°C and force of 45,000lbf are presented in Table 7.13. The results show that higher compression molding temperature did not improve the flexural properties of pressboard with hot water and NaOH treated wheat straw, but in fact a decrease was observed. The untreated wheat straw particle #2 illustrated a slight improvement at both 20% and 40% binder content. The best results obtained were 43.1 MPa and 7,981MPa, respectively for flexural strength and modulus, corresponding to 11.6% and 28.0% improvement compared to pressboard made at 170–190°C.

The optimized value for the maximum flexural strength of nonwoven flax fiber reinforced Acrodur biocomposites was found at 25% moisture content, 170°C curing temperature and 180 seconds curing time. Maximum flexural strength and modulus of 44.83 MPa and 4.70GPa were attained. This is in agreement with other literature that concluded that curing temperature significantly affects the strength of nonwoven flax fiber reinforced Acrodur biocomposites, followed by the moisture content and curing time (Rasyid et al. 2016).

Table 7.13 Flexural strength and modulus of wheat straw-**Thermoset #1** composite pressboard; Hot press condition: F = 45,000 lbf, T = 200°C, time = 5–7 min

Treatment	Wheat Straw	**Thermoset #1**	Flexural Strength (MPa)	Flexural Modulus (MPa)
Untreated	#1	20%	33.4	5,117
Untreated	#1	40%	33.8	5,517
Untreated	#2	20%	43.1	7,981
Untreated	#2	40%	39.5	6,889
Hot-water treated	#1	20%	17.9	3,138
Hot-water treated	#1	40%	27.9	4,588
Hot-water treated	#2	20%	21.2	3,602
Hot-water treated	#2	40%	31.5	5,525
NaOH treated	#1	20%	18.2	3,803
NaOH treated	#1	40%	30.5	5,937
NaOH treated	#2	20%	22.2	5,131
NaOH treated	#2	40%	33.1	6,476

Thermoset #2 is comprised of less than 5% cellulose nanofibril (CNF) and **Thermoset #1**. It is expected that the incorporation of CNF will lead to an addition mechanism of reinforcing of composites. The flexural results of the pressboards manufactured with untreated wheat straw and **Thermoset #2** at 170–190°C, 30,000lbf for 10 minutes are presented in Table 7.14. It is noticeable that the pressboards made with wheat straw particle showed better flexural properties than that with wheat straw fibers. And the flexural properties were improved with higher binder content (40%). The pressboards with 20% **Thermoset #2** exhibited extremely poor flexural strength and modulus. However, with increased binder content, the flexural strength was improved significantly and reached its highest of 25.7 MPa.

Table 7.14 Flexural strength and modulus of wheat straw-**Thermoset #2** composite pressboard; Hot press condition: F = 30,000 lbf, T = 170–190°C, time = 10 min

Treatment	Wheat Straw	**Thermoset #2**	Flexural Strength (MPa)	Flexural Modulus (MPa)
Untreated	#1	20%	5.3	1,197
Untreated	#1	40%	10.5	1,814
Untreated	#2	20%	5.3	1,120
Untreated	#2	40%	25.7	2,892

Table 7.15 presents the flexural property results of **Thermoset #2** at force of 45,000 lbf. Firstly, the comparison between pressboards made at higher compression force of 45,000 lbf (Table 7.15) and 30,000 lbf (Table 7.14) depict once again that the force plays a significant role in determining the flexural properties of the pressboard. Secondly, the same phenomenon was noticed that NaOH treated wheat straw was more susceptible to the binder level. The biggest gap of 19.1 MPa vs 41.4 MPa, in flexural strength was found on pressboard made with 20% and 40% of **Thermoset #2** with NaOH treated wheat straw #2. Thirdly, compared to the second best result of 41.4 MPa in flexural strength, the best result was 49.1 MPa achieved by the pressboard made with untreated wheat straw #2 at 40% **Thermoset #2**. And for the same pressboard, the flexural modulus reached 9,083 MPa. In summary, the addition of CNF to **Thermoset #1** accomplished a 13.9% and 13.8% rise for flexural strength and modulus respectively, from the best result of pressboards made with binder **Thermoset #1**. This fact indicated that reinforcing effect of CNF was demonstrated positively.

Table 7.15 Flexural strength and modulus of wheat straw-**Thermoset #2** composite pressboard; Hot press condition: F = 45,000 lbf, T = 170–190°C, time = 10 min

Treatment	Wheat straw	**Thermoset #2**	Flexural Strength (MPa)	Flexural Modulus (MPa)
Untreated	#1	20%	33.4	6,236
Untreated	#1	40%	35.8	5,950
Untreated	#1&2	20%	38.7	5,690
Untreated	#1&2	40%	38.0	6,191
Untreated	#2	20%	36.1	6,239
Untreated	#2	40%	49.1	9,083
Hot-water treated	#1	20%	30.8	5,545
Hot-water treated	#1	40%	30.7	4,874
Hot-water treated	#2	20%	32.8	6,473
Hot-water treated	#2	40%	38.7	5,582
NaOH treated	#1	20%	19.4	3,759
NaOH treated	#1	40%	36.5	5,986
NaOH treated	#2	20%	19.1	4,270
NaOH treated	#2	40%	41.4	6,656

Thermoset #3 is Acrodur 950L in form of solution, with high molecular weight and viscosity. The flexural property results for the pressboards made with another thermosetting resin, **Thermoset #3**, are displayed in Table 7.16. The flexural strength and moduli are generally comparable to but at the lower end of that of pressboards made with **Thermoset #1** or **Thermoset #2**, with an average for untreated wheat straw of 33.62 MPa against 35.92 MPa for **Thermoset #1** and 38.52 MPa for **Thermoset #2**. The same trend was found in the comparison of hot-water treated wheat straw, with an average of 31.6 MPa against 36.34 MPa and 33.3 MPa, respectively for **Thermoset #1** and **Thermoset #2**. However, an exception was observed for NaOH treated wheat straw. The pressboard made with NaOH treated wheat straw #1 and 20% **Thermoset #3** stood out of others, with flexural strength of 59.8 MPa and modulus of 7,081 MPa. No reasonable explanations were found.

Table 7.16 Flexural strength and modulus of wheat straw-**Thermoset #3** composite pressboard; Hot press condition: F = 45,000 lbf, T = 170–190°C, time = 10 min

Treatment	Wheat Straw	**Thermoset #3**	Flexural Strength (MPa)	Flexural Modulus (MPa)
Untreated	#1	20%	28.4	4,240
Untreated	#1	40%	30.3	3,686
Untreated	#1&2	20%	37.6	5,416
Untreated	#1&2	40%	34.1	4,844
Untreated	#2	20%	39.2	6,273
Untreated	#2	40%	32.1	4,729
Hot-water treated	#1	20%	35.1	5,279
Hot-water treated	#1	40%	26.3	4,227
Hot-water treated	#2	20%	35.3	4,931
Hot-water treated	#2	40%	29.7	4,474
NaOH treated	#1	20%	59.8	7,081
NaOH treated	#1	40%	37	5,505
NaOH treated	#2	20%	N.A**	N.A.**
NaOH treated	#2	40%	40.5	5,514
NaOH treated-Hot-water treated (2:1)	#2	40%	39.5	5,868

***The results were unavailable due to the poor quality of produced pressboard*

Thermoset #4 is a mixture of **Thermoset #1** and **#3** at ratio of 1:1. The pressboards made with mixture binder (**Thermoset #1** and **#3**) were measured and the results were presented in Table 7.17. No significant effects were observed on flexural properties. The average of 35.3 MPa was found for untreated wheat straw, which is in the same range as other thermoplastic Acrodur binders.

Table 7.17 Flexural strength and modulus of wheat straw-**Thermoset #4** composite pressboard; Hot press condition: F = 45,000 lbf, T = 170–190°C, time = 10 min

Treatment	Wheat Straw	**Thermoset #4**	Flexural Strength (MPa)	Flexural Modulus (MPa)
Untreated	#1&2	20%	38.9	5,870
Untreated	#1&2	40%	31.6	4,310

Table 7.18 Flexural strength and modulus of wheat straw-**Thermoplastic #5** composite pressboard; Hot press condition: F = 45,000 lbf, T = 120°C, time = 5–7 min

Treatment	Wheat Straw	**Thermoplastic #5**	Flexural Strength (MPa)	Flexural Modulus (MPa)
Untreated	#1	20%	35.3	2,715
Untreated	#1	40%	38.5	2,368
Untreated	#2	20%	36.8	3,961
Untreated	#2	40%	35.9	4,011

Table 7.19 Flexural strength and modulus of wheat straw-**Thermoplastic #5** composite pressboard; Hot press condition: F = 45,000 lbf, T = 200°C, time = 10 min

Treatment	Wheat Straw	**Thermoplastic #5**	Flexural Strength (MPa)	Flexural Modulus (MPa)
Untreated	#1	20%	39.5	5,808
Untreated	#1	40%	N/A**	N/A**
Untreated	#1&2	20%	40.9	4,920
Untreated	#1&2	40%	29.3	6,161
Untreated	#2	20%	47.0	6,818
Untreated	#2	40%	25.4	3,974
Hot-water treated	#1	20%	43.2	6,445
Hot-water treated	#1	40%	30.1	4,578
Hot-water treated	#2	20%	48.9	5,725
Hot-water treated	#2	40%	26.2	4,263
NaOH treated	#1	20%	59.1	6,814
NaOH treated	#1	40%	32.5	3,897
NaOH treated	#2	20%	63.0	6,439
NaOH treated	#2	40%	41.0	4,678

***The results were unavailable due to the poor quality of produced pressboard*

Thermoplastic #5 is Acrodur 4444X in form of suspension. As the only thermoplastic Acrodur binder, the results of **Thermoplastic #5** are shown in Table 7.18 and Table 7.19, corresponding to two compression molding temperatures used. The pressboards made at 120°C (Table 7.18) exhibited an

average of 36.6 MPa for untreated wheat straw, with no significant difference found for two binder levels. On the other hand, the flexural properties of the pressboards made at 200°C displayed an adverse behavior, which is that the flexural properties dropped as the binder content increased. For some cases, the wheat straw with 40% **Thermoplastic #5** was unable to produce the pressboards that can be measured for flexural test. However, with just 20% **Thermoplastic #5**, the wheat straw was held together so well that an average of flexural strength and modulus was achieved at 48.7 MPa and 6,138 MPa, respectively. The overall best results were 63.0 MPa for flexural strength achieved by the pressboard made with NaOH treated wheat straw #2 and 20% **Thermoplastic #5**, and 6818 MPa for flexural modulus obtained from the pressboard made with untreated wheat straw and 20% **Thermoplastic #5**.

Summary

The hypothesis that the composite formulation and compression molding conditions influence flexural properties of wheat straw-Acrodur pressboard was proposed at beginning of this chapter. This hypothesis was tested by measurement the flexural properties of wheat straw –Acrodur composite pressboards manufactured using the compression molding process. The flexural strength and modulus were investigated as a function of the composite formulation and compression molding conditions.

The characteristics of the composite pressboards displayed clearly the dependence on the molding parameters, i.e. force, temperature and time. To clearly identify the effects of the parameters examined, and due to the complexion of comparisons, the results were put together, and the inter-comparisons of different parameters levels were made for individual parameter using bar charts.

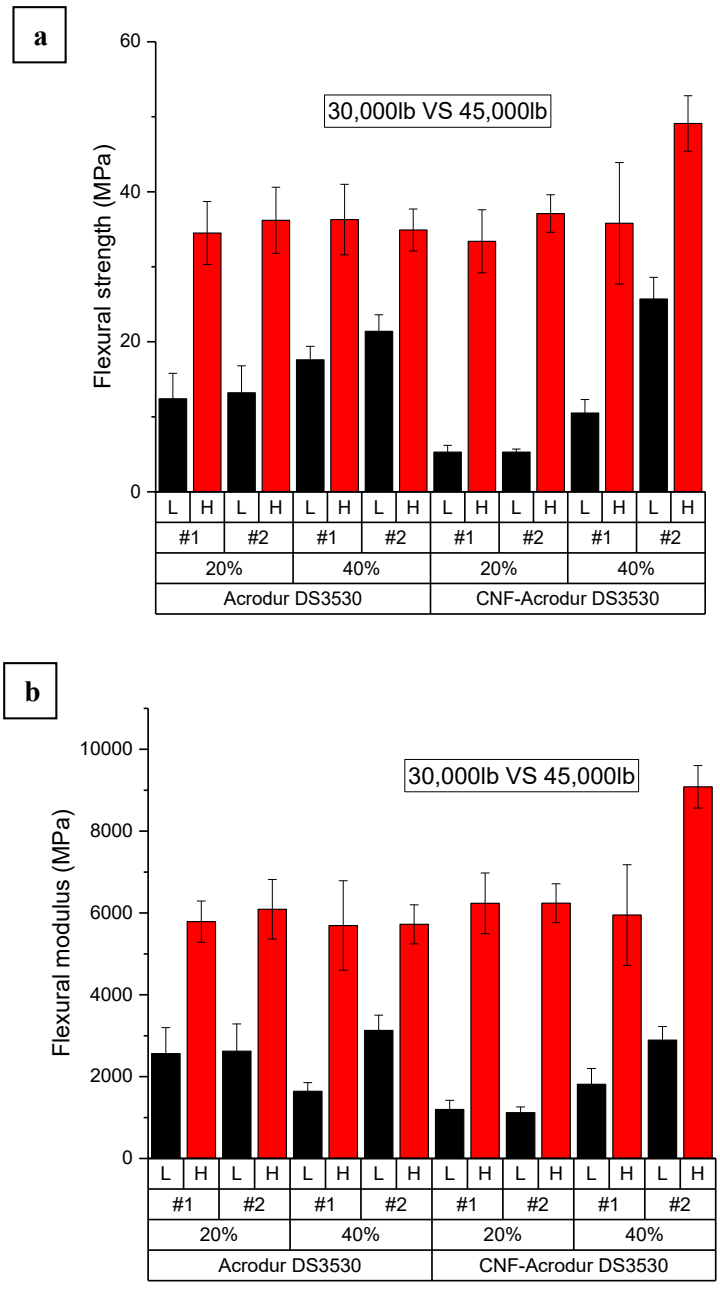

Figure 7.13 Flexural strength (a) and modulus (b) comparison between two levels of force (L–low, H–high)

* 30,000 lbf in black, 45,000 lbf in red; #1 and #2 are types of straw, 20% and 40% are binder contents

It was studied that two press molding forces (30,000 and 45,000lbf) were carried out to compare the dependence of the mechanical properties of wheat straw-Acrodur composite pressboards on the process force. The comparisons were made between two force levels, 30,000 and 45,000lbf, denoted in Figure 7.13 as “low” and “high”, respectively. The binders used in this comparison were **Thermoset #1** and **Thermoset #2**. Two levels of binder content were involved. Two sizes of untreated wheat straw were denoted as #1, #2 in the graphs. Figure 7.13 illustrates the flexural properties of the composites depending on the manufacturing force. As noted, the higher values of flexural properties were recognized at higher molding force, 45,000 lbf. It was seen that the averages flexural strength and modulus of pressboards increased remarkably from 16.2 to 35.5 MPa, and 2,489 to 5,825 MPa, respectively, as compression molding force increased, by comparing the results where **Thermoset #1** was used. The same trend was found in comparison of pressboards made with **Thermoset #2**. The effect of force was more profound in this case. The flexural strength and modulus were increased by 332% and 392% respectively by comparing the averages.

The increased flexural properties at higher pressure/force can be attributed to the enhanced interactions between binder and wheat straw fibers due to reduced distance as well as the increased density caused by well compressed composite structure.

It is known from the literature that the mechanical properties are a result of improved integrity and the changes of board density. The positive relationship between density and mechanical properties has been reported by Liang (Liang et al. 2013). It was reported (Khalfallah, Abbès, et al. 2014) that the Young’s modulus increases with increasing density. However, there is a critical pressure that damages the structure of fibers and impair its mechanical reinforcing effect. Although the pressures of 1,500 psi was reported to cause the damage to natural fibers (Medina et al. 2008) (Behzad and Sain 2005) and consequently a negative effect on the mechanical properties can be found, the force as high as 45,000 lbf still achieved improvement in flexural strength and modulus. It can be inferred that 45,000 lbf has not reached the maximum pressure which can be applied for improving the mechanical properties before damaging the structure of the fibers. Due to limitation of the laboratory hydraulic press setup, whose force capability is 50,000 lbf, the answer to the “maximum effective pressure” question is still unknown yet.

For future work, a pressing higher than 45,000 lbf can be suggested until a negative effect on mechanical properties is observed. This can serve as a reference for the upper limit of pressure applied

on the wheat straw. It should be recognized that the process parameters are to be optimized depending on the use. It should be always taken into account that for avoiding fiber damage a manufacturing pressure of less than maximum pressure should be chosen.

The compression molding temperature along with resident time has significant influence on quality of wheat straw-Acrodur composite pressboards, by sufficiently curing the thermosetting binder and not thermally degrading the reinforcing fibers. Based on the kinetic analysis results of Acrodur cure reaction in Chapter 4, two temperature levels, 170–190°C and 200°C, were applied for production of wheat straw-thermosetting **Thermoset #1** composite pressboards. The hypothesis made was that the higher crosslinking density at 200°C increases the integrity of pressboard and leads to improved mechanical properties.

Figure 7.14 did show that, for most cases, the hypothesis was positively supported by the experimental results because the flexural properties at 200°C were found to be higher than or at least at the same level as that at 170–190°C. However, the effect of high temperature on flexural properties was minor. Oppositely, the results of hot-water treated wheat straw exposed a clear but negative dependence of flexural properties on compression molding temperature, shown as blue circle in Figure 7.14. The flexural strength dropped when the high temperature was employed. The greatest drop occurred to hot-water treated wheat straw with 20% **Thermoset #1**, where the decreases in flexural strength from 36.9 to 17.9 MPa (51% decrease), and from 39.6 to 21.2 MPa (46% decrease) were for wheat straw #1 and #2.

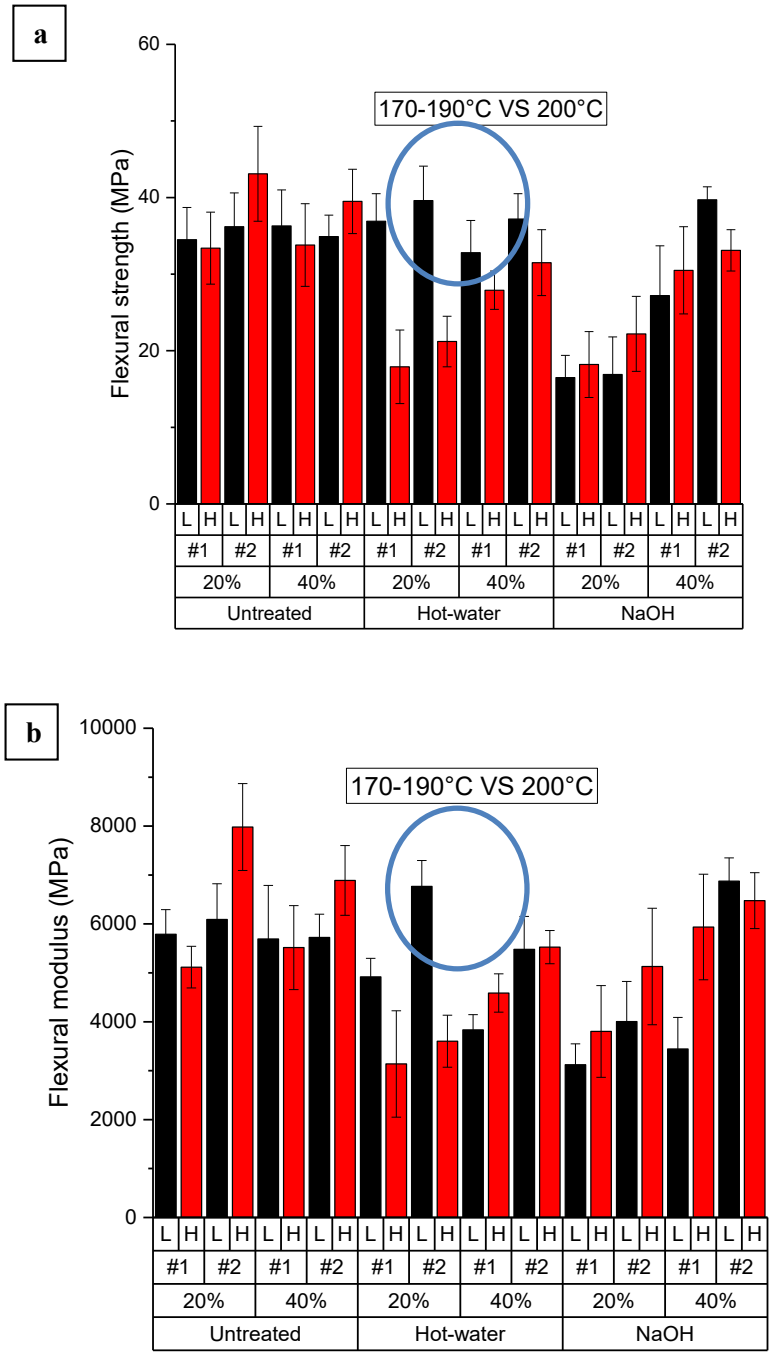

Figure 7.14 Flexural strength (a) and modulus (b) comparison between two temperature levels (H–high, L–low) for **Thermoset # 1** pressboards

As discussed earlier, the temperature should be controlled to be high enough to activate the cure reaction of Acrodur and maintain a fast curing rate, but to be below the temperatures, where serious thermal degradation is invoked. It is inferred that 170–190°C was an optimal range for hot pressing of **Thermoset #1**, which cured the binder to a good crosslinking level and achieved the optimal mechanical strength and modulus. It is noticed that the surface of pressboards compressed at 170–190°C for 10 minutes exhibited a light-reflecting character of continuous phase of the binder formed from cure reaction shown in Figure 7.15, although a slight discoloration became noticeable on the surface for the pressboards. It is a tradeoff that compromises wheat straw and achieves better percolation of binder, because the curing reaction is more sensitive to temperature and thermal degradation of wheat straw is slow (negligible) and acceptable as long as time resident time is monitored and well-controlled.

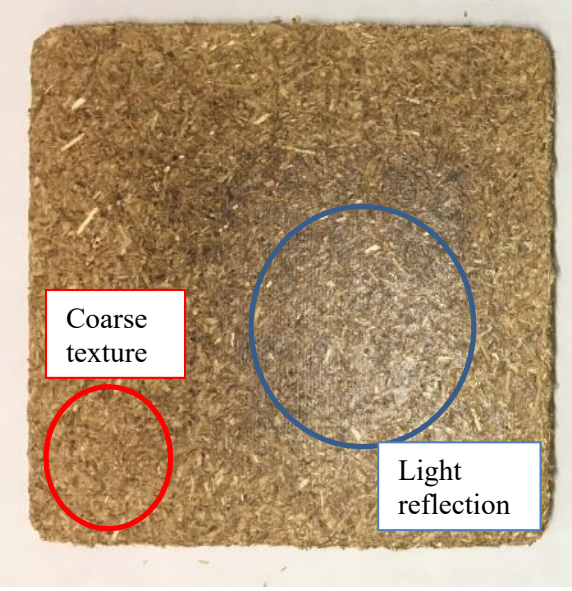

Figure 7.15 Formation of binder continuous phase

On the other hand, 200°C did not further improve mechanical properties significantly. The reasons might be the thermal decomposition caused on wheat straw and Acrodur. This explanation finds the supports from the observation of the appearance of pressboard made at 200°C for 5–7 minutes. The much darker color appeared on the surfaces of the pressboards, which were at direct contact to the hearting platens.

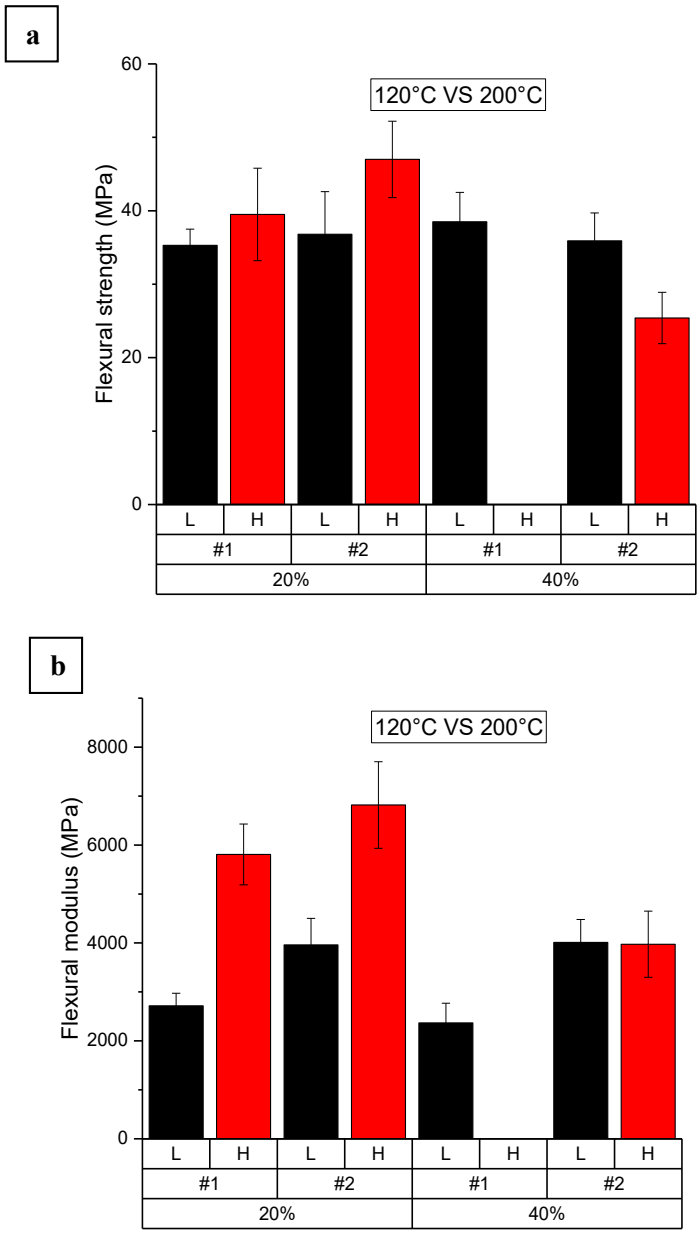

Figure 7.16 Flexural strength (a) and modulus (b) comparison between two temperature levels for the pressboards made with **Thermoplastic #5**

*A missing data point due to unavailability of pressboard

In case of **Thermoplastic #5**, the applied temperature was observed to be positively correlated at 20% binder content, and negatively correlated at 40% binder content, to the flexural properties of resultant pressboards. Two temperature levels were used for wheat straw-**Thermoplastic #5**

composites, where hot press temperature 120°C was just above reported and experimentally verified softening point (97°C) of **Thermoplastic #5**. For pressboards manufactured at 120°C, the flexural strength was at the same level of 35.3–38.5 MPa no matter the binder weight fraction changed from 20% to 40%. However, for the pressboards made at 200°C, there were significant drops in flexural strength when binder content increased from 20% to 40%. The pressboard made using wheat straw #1 and 40% binder could not even be produced successfully due to the high flowability of composite out of the mold, which is indicated by a missing bar (data point) in Figure 7.16.

The comparison between the pressboards made at two temperatures in Figure 7.16 revealed that the higher flexural strength and modulus were achieved at high temperature, the maximum reaching 46.0 MPa and 6,818 MPa for wheat straw #2 at 20% binder fraction, even though the color change of the pressboards became noticeable at the pressboard surfaces. The explanation for the opposite effects of temperature on the mechanical properties at different binder levels can be that the temperature just above softening temperature for **Thermoplastic #5** is not high enough to allow the binder gaining sufficient mobility to distribute and disperse well in wheat straw. Whereas at 200°C the good distribution and dispersion of binder was achieved at low concentration of 20%, which then led to more homogeneous and improved adhesion throughout the composite material. However, as binder level increased, the composite mobility achieved at high temperature was too high to be controlled and caused pressboard failure.

In composite the binder serves as adhesive and provides the adhesion at the interface to hold the individual fibers together and to achieve the integrity of composite pressboards. The pressboards were prepared with different levels of binder and measured. The independence of flexural properties on binder content was established from the experimental results. It is generally observed that, for two binder levels of 20% and 40%, the pressboards made with higher binder content had predominantly exhibited higher values, if not slightly lower, in flexural strength and modulus for different compression molding forces, different temperatures, and different combinations of two wheat straw sizes, and three treatments, and **Thermoset #1**, **#2**, and **#3**, with scarce exceptions shown as blue circle in the graphs.

The examples of independence of flexural strength and modulus on Acrodur content level are displayed for the occasions of different combinations of other parameters as follows:

1. compressed at low force (30,000 lbf) and low temperature (170–190°C) in Figure 7.17;
2. compressed at high force (45,000 lbf) and low temperature (170–190°C) in Figure 7.18;

3. compressed at high force (45,000 lbf) and high temperature (200°C) in Figure 7.19;
4. for **Thermoset #1** and **Thermoset #2** in Figure 7.17;
5. for three treatments in Figure 7.18 and Figure 7.19.

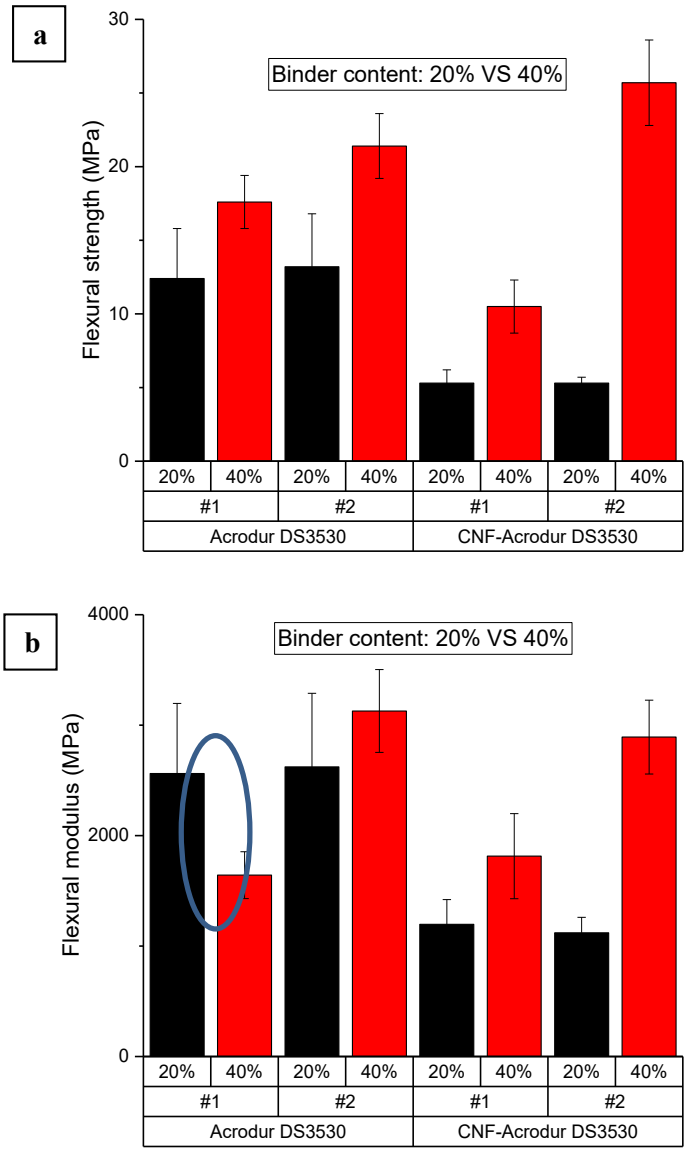

Figure 7.17 Flexural strength (a) and modulus (b) comparison between two binder content levels for the pressboards made with untreated wheat straw at F = 30,000 lbf, T = 170–190°C, time = 10 min

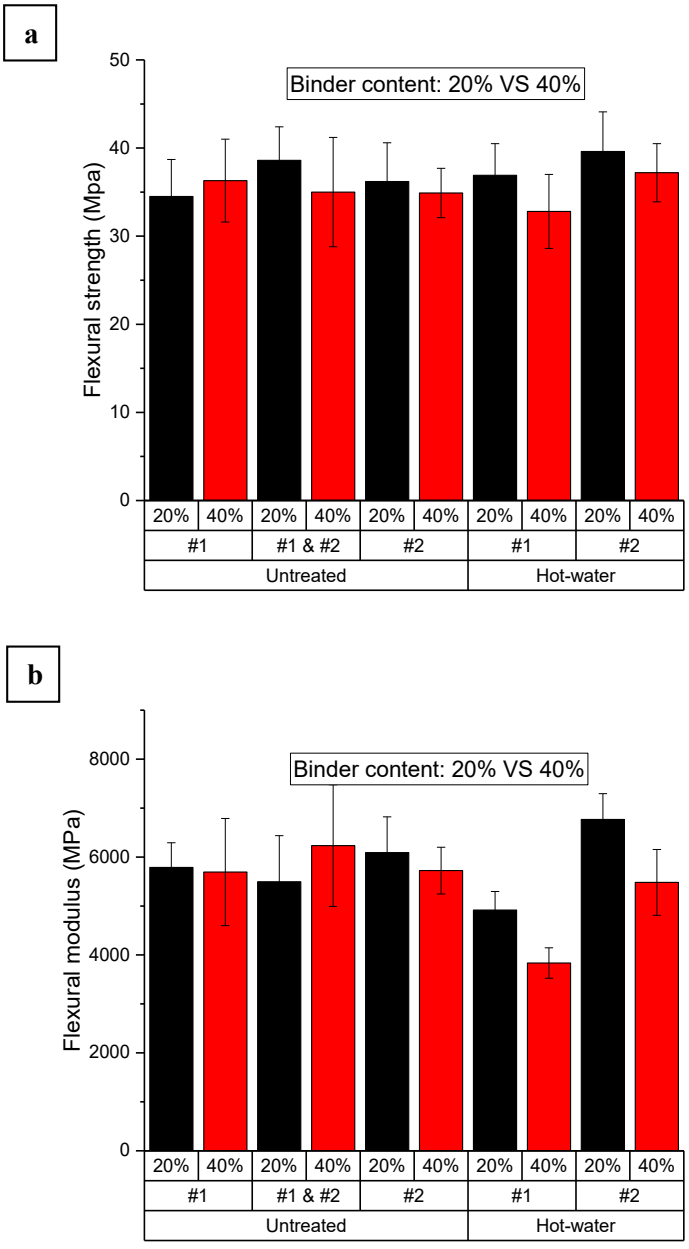

Figure 7.18 Flexural strength (a) and modulus (b) comparison between two binder content levels for the pressboards made with **Thermoset #1** at F = 45,000 lbf, T = 170–190°C, time = 10 min

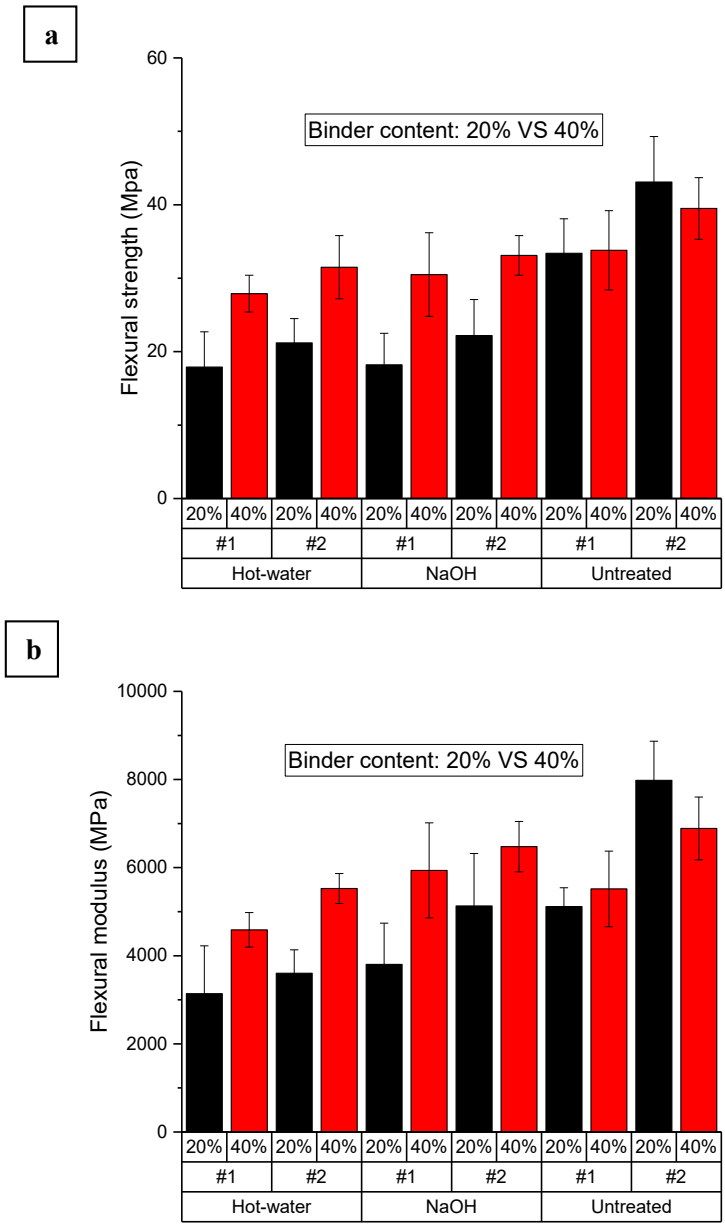

Figure 7.19 Flexural strength (a) and modulus (b) comparison between two binder content levels for the pressboards made with **Thermoset #1** at F = 45,000 lbf, T = 200°C, time = 10 min

To further investigate the correlation of binder content with mechanical properties in an extended range, four levels of **Thermoset #1**, 10%, 20%, 40% and 60%, were impregnated with NaOH treated wheat straw #2. It is seen from the results shown in Figure 7.20 that both flexural strength and modulus exhibited a positive relationship with binder content and reach a maximum at 40 % of binder. The

extremely low mechanical properties for the 10% binder were attributed to the lack of adhesion. When more binder was impregnated, it resulted in a significant increase of flexural strength and modulus, until the 60% binder did not exhibit improvement in mechanical properties and slight drop was observed.

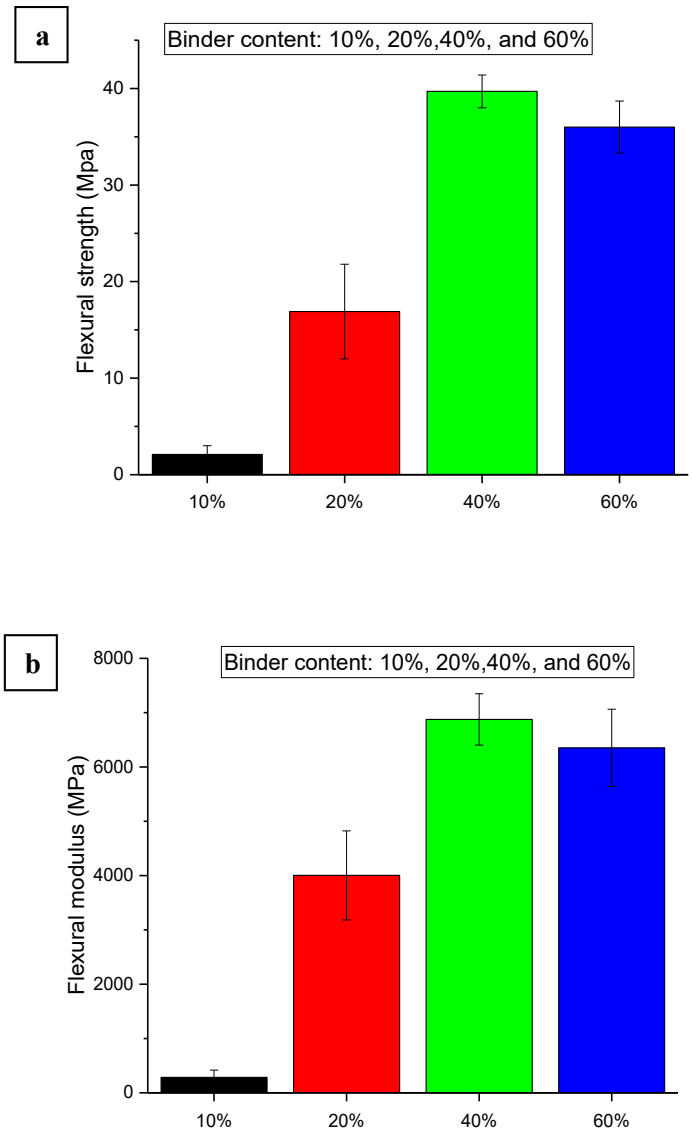

Figure 7.20 Flexural strength (a) and modulus (b) comparison between four binder content levels for the pressboards made with NaOH treated wheat straw #2-**Thermoset #1** at F = 45,000 lbf, T = 170–190°C, time = 10 min

This is in agreement with observations reported by Sardashti (Sardashti 2009) on polypropylene-straw composites, where the flexural strength dropped about 28% with the addition of 30% of wheat straw. A further decrease of 46% on the flexural strength of the composite happened when the wheat straw content is increased to 50%. This reduction in the flexural strength is attributed to the weak interfacial bonding between the fiber and the matrix due to the lack of binder. Yang et al. (H.S. Yang et al. 2007) reported that the poor interfacial bonding became more noticeable as the fiber content increased, because the total interfacial area between matrix and fiber becomes bigger and microspaces (voids) between fiber and matrix may be formed. As a consequence of these voids between fiber and matrix, poor stress transfer and brittleness could occur.

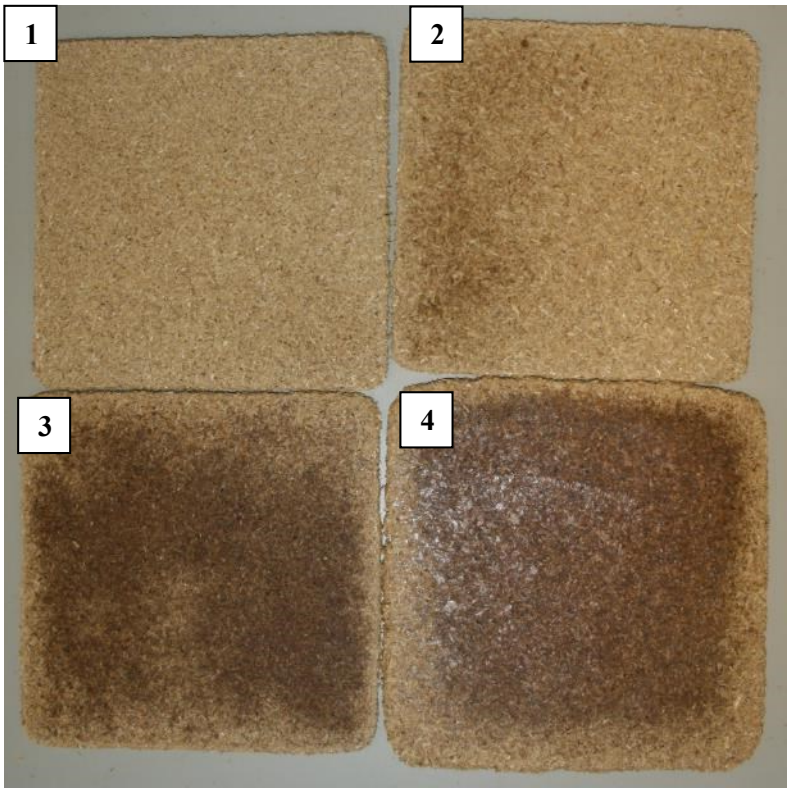

Figure 7.21 Surface appearance of NaOH treated wheat straw-**Thermoset #1** pressboard with binder content of 10, 20, 40, and 60% from (1) to (4)

With an assistance of observation of surface morphology in Figure 7.21, it was recognized that 10% or 20% of **Thermoset #1** appeared not sufficient to fully wet the NaOH treated wheat straw particle (#2). In Figure 7.21, it is seen that, from left, pressboards appeared “dry” due to lack of binder and showed somewhat flaky face layers porous/rough surface, to right in contrast, a thin layer of continuous

hard-rigid polymer was formed on the surface with the wheat straw buried in. The “lack of binder” effect became more conspicuous in this case, because the particles (#2) have high surface area/volume ratio compared to fibers (#1). In addition, alkaline treatment created porous structure on wheat straw by removing waxes, silica and small organic molecules. The pressboards manufactured with higher binder content showed optically a better surface in Figure 7.21 (3 and 4), where the fibers are better covered with the binder.

It should also be noted that, however, to counteract the negative effect that binder lack due to high specific area has on pressboard strength properties, more resin is incorporated during pressboard manufacture further increasing costs. The higher binder content used, the more likely blisters and delamination occur due to trapped water vapor inside. The bubbly surface indicated the trapped water vapor inside the cured material as shown in Figure 7.22 (a and b). Also wheat straw aggregation as seen after impregnated with high **Thermoset #1** content (60%) shown in Figure 7.22 (c).

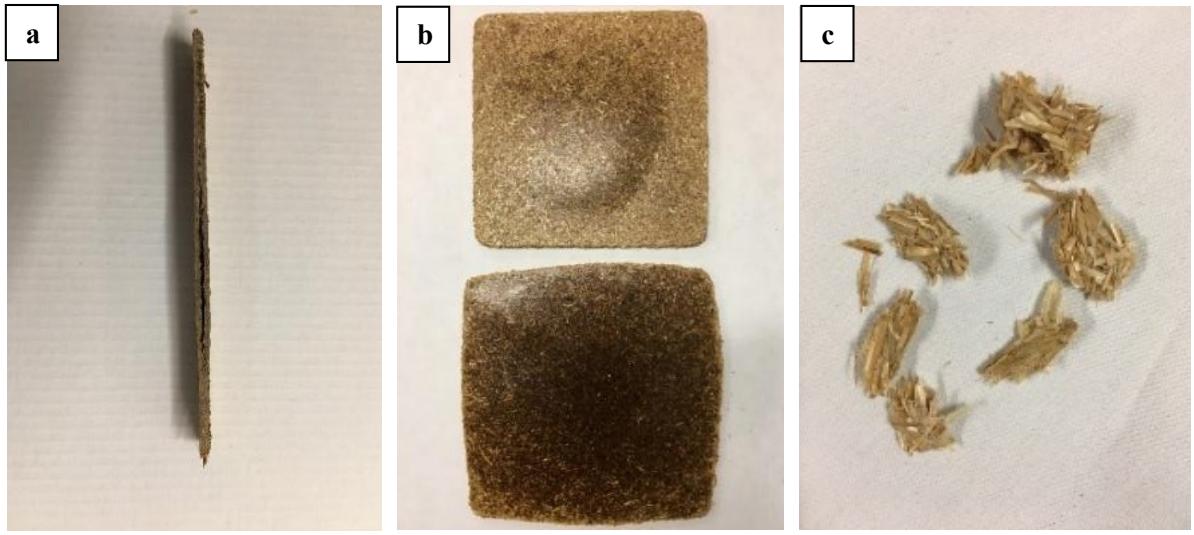

Figure 7.22 Illustrative example of delaminated pressboard

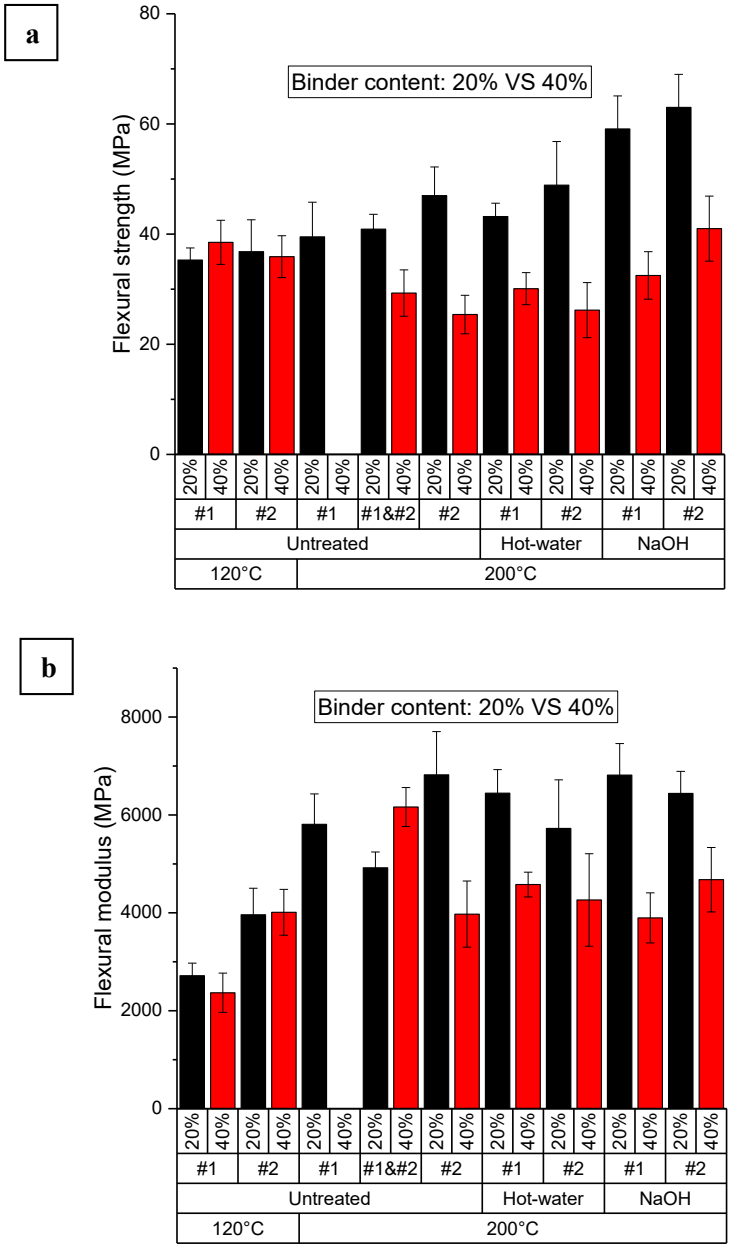

Figure 7.23 Flexural strength (a) and modulus (b) comparison between two binder content levels for the pressboards made with **Thermoplastic #5** at F = 45,000 lbf, T = 120 or 200°C, time = 10 min

One exception is **Thermoplastic #5** at 200°C in Figure 7.23, as previously discussed, where high binder content caused overmuch flowability at high temperature and led to pressboard failure. On the contrary, at low temperature, the mobility of composite was well-controlled.

In summary, the binder transfers stress from the matrix to the fiber and plays an important role in determining the mechanical and other properties. The good flexural strength of wheat straw-Acrodur composite pressboards can not only be attributed to very high distribution of the binder between the fibers in the composite, but also to the good adhesion between wheat straw and Acrodur, which is confirmed by the assistance of SEM analysis of pressboards in 7.4.5. There is a critical binder content level that provides sufficient and effective adhesion for composite. Below that, the adhesion is insufficient for formation of integrity of pressboards. From the observation, the critical binder content for wheat straw-**Thermoset #1** is above 40%, although it was reported that Acrodur permits composites with very high loading levels, as high as 70% or even 90%.

7.4.2.1.3 Effect of Wheat Straw Size (#1, #2, Hybrid #1 and #2)

Flexural properties of wheat straw-Acrodur composite pressboards were found to be influenced by fiber size and geometry. It was observed from almost all formulations and conditions that #2 exhibited higher values or at least at the same level as #1, except for a few occasions. As an example, it is distinctly suggested from Figure 7.24, where the pressboards were manufactured using **Thermoset #1** at 45,000 lbf, 200°C for 10minutes, that the flexural performance of the pressboards made with #2 surpassed those with #1 within the same treatments, when three treatments were applied. Also shown in Figure 7.25, for four Acrodur binders, i.e. **Thermoset #1, #2, #3**, and **Thermoplastic #5**, the pressboards fabricated with #2 exhibited slightly higher values in flexural strength and modulus. It should be noted that the largest variation between flexural properties of #1 and #2 occurred to the pressboards using 40% **Thermoset #2**. The flexural strength and modulus increased by 37.1% from 35.8 to 49.1 MPa, and by 52.7% from 5,950 to 9,083 MPa, respectively. The flexural modulus of 9,083 MPa is actually the best for overall results.

The hybrid effect on the flexural properties of wheat straw fiber (#1) and particle (#2) at 1:1 ratio was evaluated as a function of binder type and weight fraction. And the flexural performance of hybrid wheats straw #1 and #2 mixture was in between that of two components sizes or at the same level.

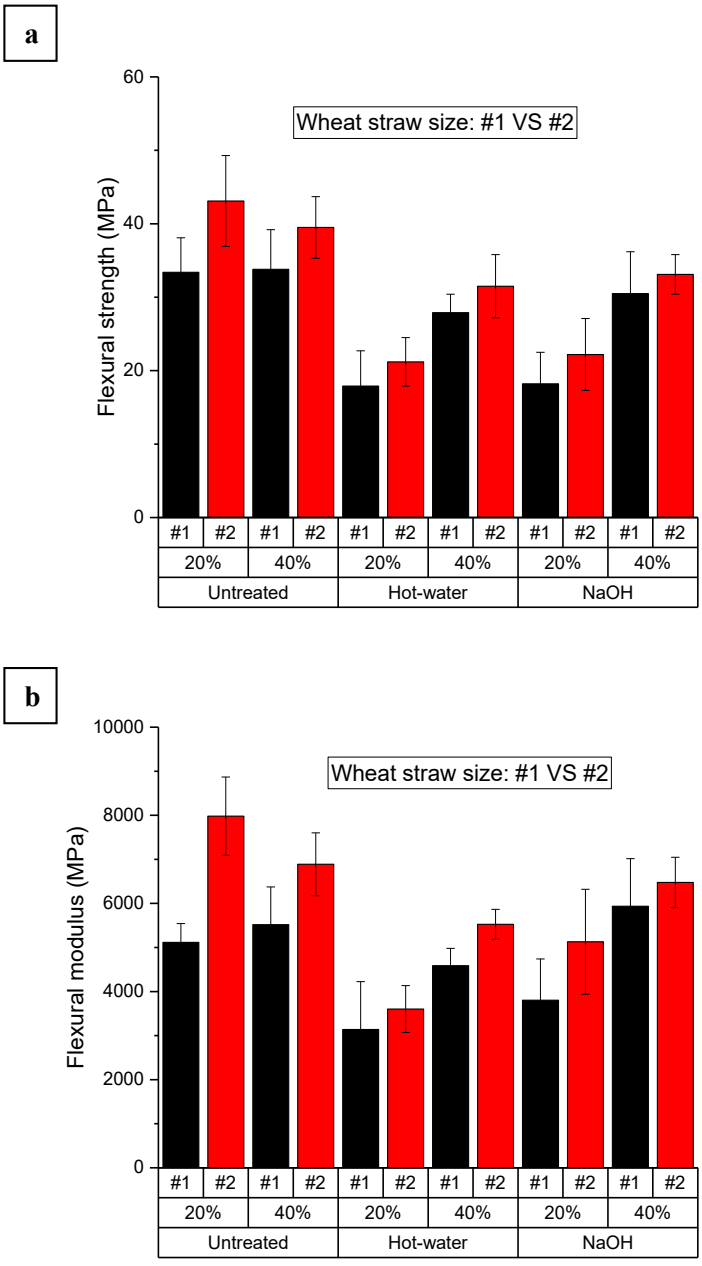

Figure 7.24 Flexural strength (a) and modulus (b) comparison of two wheat straw sizes (#1 and #2) for three treatments; pressboards made with **Thermoset #1** at F = 45,000 lbf, T = 200°C, time = 10 min

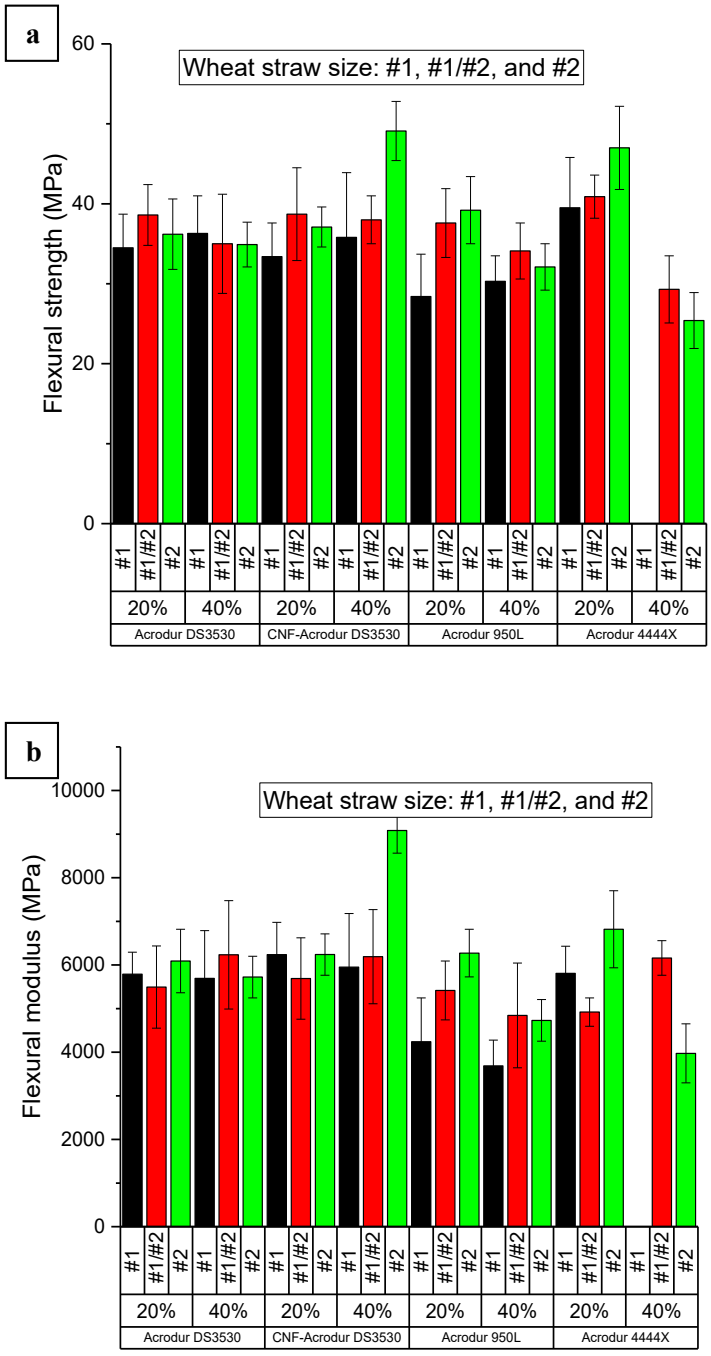

Figure 7.25 Flexural strength (a) and modulus (b) comparison of two untreated wheat straw sizes (#1 and #2) and mixture of #1 and #2 at 1:1 ratio

It is known that the higher aspect ratio owned by wheat straw #1 than particle (#2) is capable to impart more effective stress transfer. However, the observation that the strength reinforcing effect of wheat straw fiber #1 was not as good as that of #2 has been proven by the experimental results. The observation can be justified by the fact that wheat straw particles were milled severely and the waxy/ silica layer on the surface was destroyed, which gave rise to the smaller size and more hydrophilic cellulose structure exposed. Due to the smaller size and good shapeability, particle (#2) tends to pack themselves better during compression molding process, and the pressboard made with wheat straw #2 have a very homogeneous composite structure with few pores and higher density. In addition, the high specific area of smaller size of particles (#2) allows for better resin penetration and wetting, which was approved in Chapter 3. Acrodur monomers penetrated in particle structure, and instead, the binder tends to fill up the space between fibers (#1). Both high packing density and well binder distribution play more important role in determining integrity of composite pressboards than aspect ratio of fiber and lead to improved mechanical properties. However, because of high specific area of particle, the requirement of binder becomes critical for achievement of effective bonding.

The complementary effect of wheat straw #1 and #2 was expected because the hybridization of two sizes and geometry of wheat straw allows small particles to fill up the space between fibers and achieve higher composite density while taking advantage of long aspect ratio of fibers. However, the results showed that no evident hybrid effect was observed on the flexural properties. This indicates the interactions between two sizes were uncertain.

7.4.2.1.4 Effect of Treatment of Wheat Straw

It was proven in Chapter 3 that the treatments change the surface wettability and morphology of wheat straw. To further evaluate the effectiveness of the treatments on mechanical performance of wheat straw-Acrodur composites and to establish the relationship of the treatments and the mechanical properties of resultant pressboards, the non-treated, hot-water treated and NaOH treated wheat straw were used in the production of composite pressboards and their flexural properties were investigated as a function of three wheat straw treatments.

The flexural strength and modulus results were averaged within three treatments for overall treatment comparison. At the same time, due to existence of large variations, the maximum values were also used for the comparison.

Flexural properties of wheat straw-Acrodur composite pressboards were found to be influenced by wheat straw treatment methods. However, there were no simple and evident trends found in Figure 7.26. It was manifested that both hot-water and NaOH treatments induced the fall in the flexural properties of the pressboards made with **Thermoset #1** at two temperature levels, and **Thermoset #2**. The degradation effect of NaOH treatment is larger in magnitude than hot-water treatment for the pressboards made with **Thermoset #1** and **Thermoset #2** at low temperature level (170–190°C), and is at the same level for **Thermoset #1** at 200°C. Similar to this case, it was reported by Vedoy that the composites prepared with alkaline treated wheat straw samples have flexural modulus similar to the one prepared with untreated wheat straw (Vedoy 2012).

On the other hand, the opposite trend was recognized for **Thermoset #3** and **Thermoplastic #5**. The flexural properties increased when the treatments were applied, whereas NaOH treatment attained much more significant effect than hot-water treatment, which was mediocre. The NaOH treated wheat straw-**Thermoset #3** composite pressboards at low binder content of 20% surprisingly achieved 59.8 MPa in flexural strength, which was a 110% increase from corresponding untreated wheat straw and is the second best for overall results.

The same trend was found on the pressboards made with **Thermoplastic #5**. Hot-water treatment did not alter much the flexural property of composite pressboard; NaOH treatment stunningly improved the flexural strength to 63.0 MPa at low binder content of 20%, representing the overall best result. This can be attributed to better wettability and binder absorption effectively created by NaOH treatment.

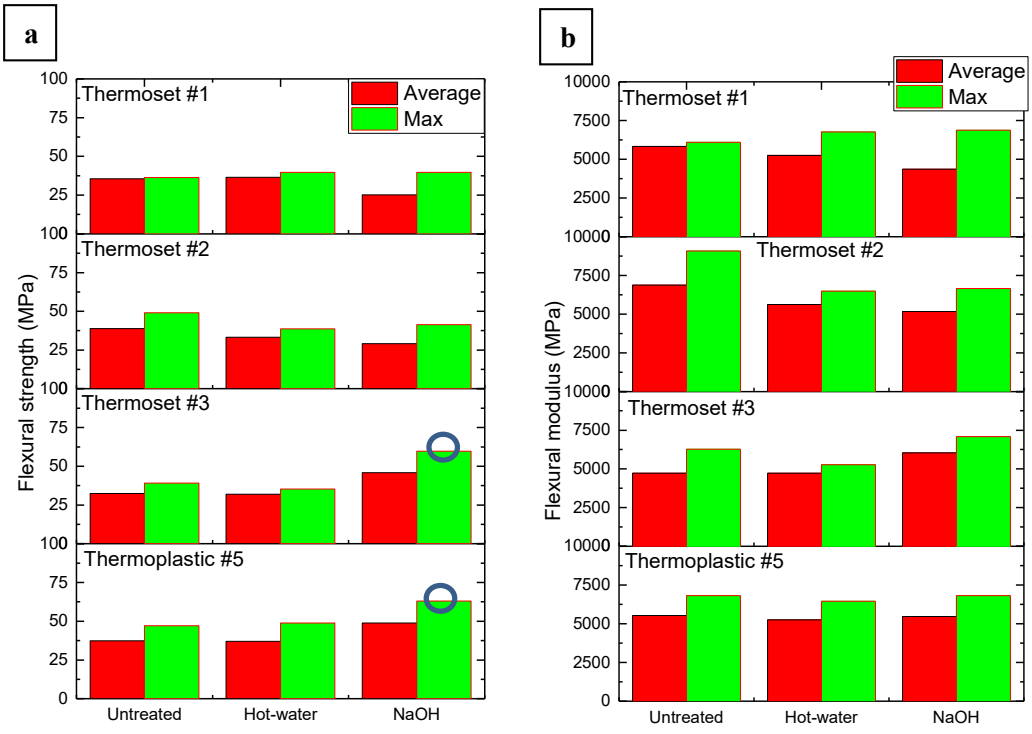

Figure 7.26 Flexural strength (a) and modulus (b) comparison of three treatments, for four Acrodur binders

As learned from Chapter 3, the treatments increase wettability and create the porous structure on wheat straw, by removing non-cellulosic components from wheat straw, which facilitates the binder diffusion and hence enhance the strength, However, on the other hand, structure disruption was observed due to harshness of treatments, especially for NaOH treatment. It was reported that alkaline treatment lessens fiber quality and leads to destructive transformation at the fiber surface (Liu et al. 2018). Therefore, the drop in flexural properties for the pressboards made with NaOH treated wheat straw-**Thermoset #1**/**Thermoset #2** can be attributed to destructive structure caused by the treatments and the lack of binder. This has been validated from the morphology observations in Figure 7.21. As for the distinct behavior found between **Thermoset #1** and **Thermoset #3**, it might be attributed to different chemical composition and higher molecular weight of **Thermoset #3**. With regard to **Thermoplastic #5**, whose chemical composition is not disclosed yet, it is inferred that its thermoplastic characteristic plays a role in determining the interaction with NaOH treated samples.

Figure 7.27 Discoloration of wheat straw-**Thermoset #2** composite pressboard, untreated, hot-water treated, and NaOH treated from (1) to (3)

In addition, the effect of hot-water and NaOH treatment on thermal stability of wheat straw was examined in Chapter 3. Although the onset degradation temperature for NaOH treated wheat straw is lower than untreated ones, the decreased discoloring of pressboards as shown in Figure 7.27 is noticed. From this image, it is seen that the pressboard specimen made of untreated wheat straw showed the darkest color compared to the other two on the right, which is attributed to removal of non-cellulosic components from wheat straw and probably to high thermal resistance of Acrodur as well.

Although the best results were obtained from NaOH treated samples, it should be recognized that the increased production cost and the pollution of NaOH treatment counteracts the benefits. In addition, more resin is required due to high specific area created by NaOH treatment, indicating another weakness.

Firstly, when Acrodur binders were used for production of wheat straw base pressboards, it achieved much high flexural strength and modulus than the wheat straw-polyamide 6 pressboards. Compared to the maximum of 26.2 MPa and 1,075 MPa for flexural strength and modulus for composites with polyamide 6, respectively, the Acordur binders accomplished superior fulfillments which more than doubted the flexural strength of polyamide 6 composites and gained exceptionally eight times of maximum modulus.

Secondly, within Acrodur binders, similar to 7.4.2.1.4, both the average and maximum were used for comparisons. Figure 7.28 encompasses the comparisons of the flexural strength and modulus of the pressboards manufactured with **Thermoset #1** (at two temperature levels), **Thermoset #2**, **Thermoset #3** and **Thermoplastic #5**, for three treatments.

The flexural strength and modulus of pressboards manufactured with untreated wheat straw and four different Acrodur binders are presented in top portion of Figure 7.28. It is clearly indicated that the **Thermoset #1** and **#3** composite pressboard showed similar strength properties in the range of 30–40 MPa. **Thermoplastic #5** composite pressboards exhibited relative high flexural strength of close or above 40 MPa at low binder fraction, except for those made with high binder content. In comparison, **Thermoset #2** composite pressboard have the highest flexural strength. Such a trend can be attributed to the chemical composition and molecular size in the binder, which affects the binder distribution and adhesion formation.

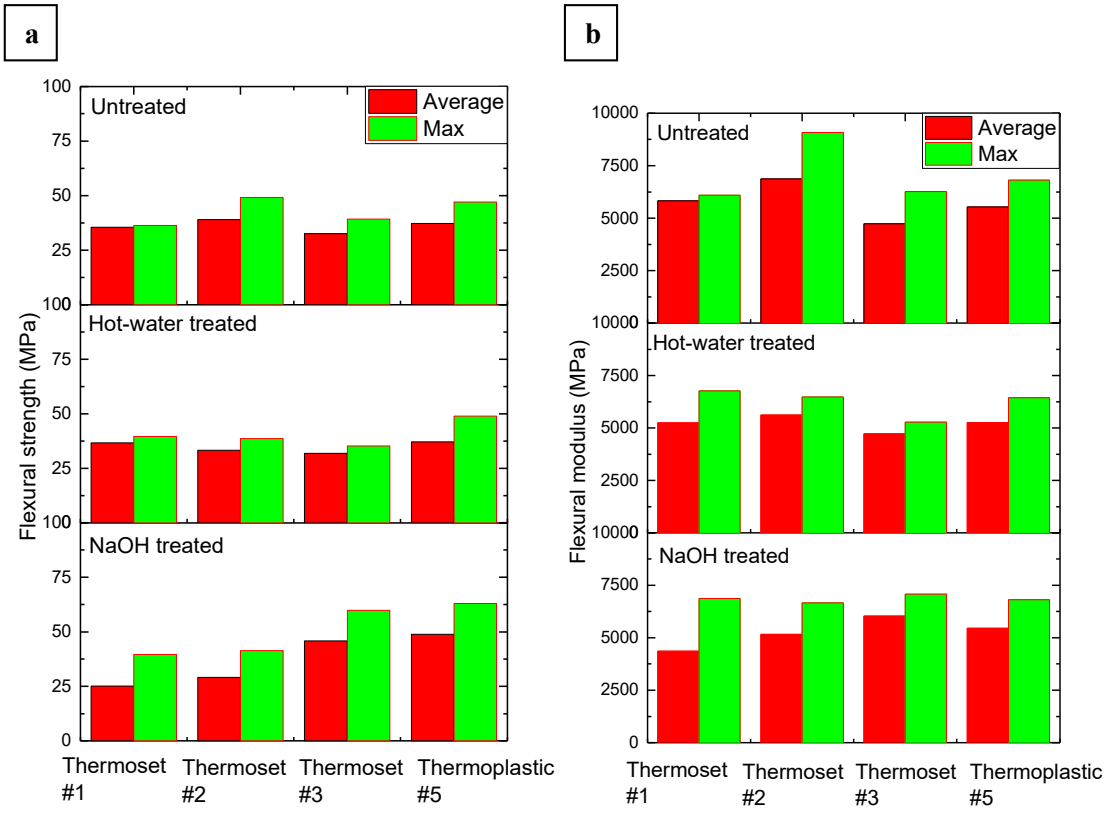

Figure 7.28 Flexural strength (a) and modulus (b) comparison of four Acrodur binders, for three treatments

As for hot-water treated samples, shown in mid portion of Figure 7.28, thermosetting Acrodur resins exhibited similar flexural behavior, and the flexural strength and modulus were in the same range of around 30 MPa, while **Thermoplastic #5** gave rise to an 48.9 MPa in flexural strength.

As for NaOH treated wheat straw, Both **Thermoset #3** and **Thermoplastic #5** fulfilled the record breaking 59.8 and 63.0 MPa, respectively, whereas the other binders were much lower in flexural performance.

The reinforcement of nanocellulose in the composite is expected due to CNF integrally incorporated into the network. To test the hypothesis, the wheat straw-**Thermoset #2** pressboards were prepared and measured the flexural properties. Also observed in Figure 7.28 by comparing **Thermoset #1** and **Thermoset #2**, the pressboards made with 40 % **Thermoset #2** and untreated wheat straw particle (#2) achieved a significant improvement in flexural property, where 41% and 59% increases were observed respectively for strength and modulus, compared to that of **Thermoset #1**. On the other hand, the reinforcing effect of CNF was minimal for wheat straw fiber #1 or wheat straw particle #2 at low binder content. The increased ultimate strength of **Thermoset #2** composites as reinforcing effect of CNF was at cost of compromising plasticity in these nanocomposites, which is supported by the fracture surface of brittle failure of wheat straw-**Thermoset #2** composite pressboards in 7.4.5.

Both **Thermoset #1** and **#3** are thermosetting acrylic based monomers solutions. They start curing at elevated temperatures via the esterification reaction of hydroxyl acids and polyols. The difference between them is the difference in the molecular weight and viscosity because of the chain length. No evident effect of hybridization of **Thermoset #1** and **#3** was found from the experimental results in Figure 7.29.

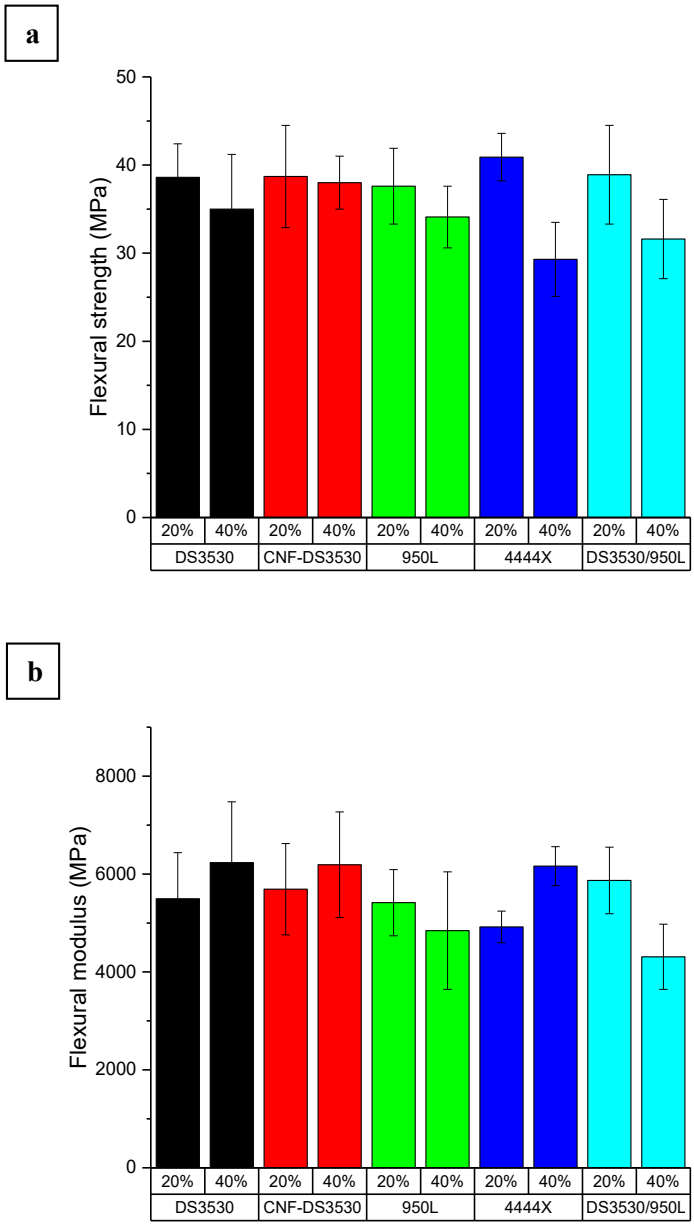

Figure 7.29 Flexural strength (a) and modulus (b) comparison of five Acrodur binders, pressboards made with untreated wheat straw #1/#2; F = 45,000 lbf, T = 170–190°C for Thermoset binders, T = 200°C for **Thermoplastic #5**, time = 10 min

7.4.2.2 Comparison with Previous Studies and Benchmarks

There have been studies reported concerning the composites made with thermosetting or thermoplastic Acrodur. The flexural strength and modulus were reported in a BASF document (Karbstein and Weed 2015) to be 44 MPa and 5164MPa respectively for the composes made with 75% loading of natural fiber and 25% thermoplastic Acrodur. With higher fiber loading level of 80%, my results accomplished an increase by 43% and 32% in flexural strength and modulus, respectively. It was reported by Islam and Miao (Islam and Miao 2013) that mixture of **Thermoset #1** and **#3** at ratio of 3:1 showed the best result with flax was cured at 160°C for 20 minutes. The best tensile properties were reported 50.0± 3.6 MPa, 4400± 250MPa, which were along fiber direction, in term of tensile strength and modulus. In comparison with these their results, the pressboards made with **Thermoset #4** achieved a 33% improvement in flexural modulus. Flexural strength and modulus of Acrodur–kenaf were reported in Liang's study (Liang et al. 2013) to be slightly less than 50 MPa, and 7000MPa respectively. Although the tensile strength and modulus of a single kenaf fiber can be as high as 11.9 and 60.0 GPa, respectively (Bolton 1994) (Karnani et al. 1997), the use of wheat straw of inferior mechanical property in this thesis accomplished much better flexural strength and modulus. It was reported by Amini and Tajvidi that adding CNC of 2, 5, 6% to **Thermoset #1** increased flexural modulus of natural fiber composites significantly up to 970 MPa, while it did not significantly affect flexural strength values (Amini and Tajvidi 2016). In comparison with their best result, a **nine-fold** increase in flexural modules was accomplished here by addition less than 5% CNF, which is astonishing. At the same time, the flexural strength was increased significantly. Reck and Turk (Reck and Turk 1999) investigated the use of jute-sisal fiber mat mixture in Acrodur resin and obtained flexural strength and modulus as high as 62 MPa and 5 GPa, respectively. The flexural strength value is close to my best results, while as the flexural modulus is 26% lower than my second best result.

Medina et al. (Medina et al. 2008) also reported highest flexural strength and modulus of 94 MPa and 8 GPa from NafacrylV—a combination of hemp and kenaf fiber mat processed using the foulard system and cured under vacuum. The final Young's modulus value of 3 layers of uni-direction flax tapes – Acrodur composites was 18 ± 1 GPa obtained by Khalfallah (Khalfallah, Abbès, et al. 2014). Those results are much higher than the results from this chapter. The reasons can be attributed to, 1) better mechanical and other properties of the natural fibers they used; 2) the high-end industrial equipment used with vacuum chamber; as well as 3) fiber alignment in composites.

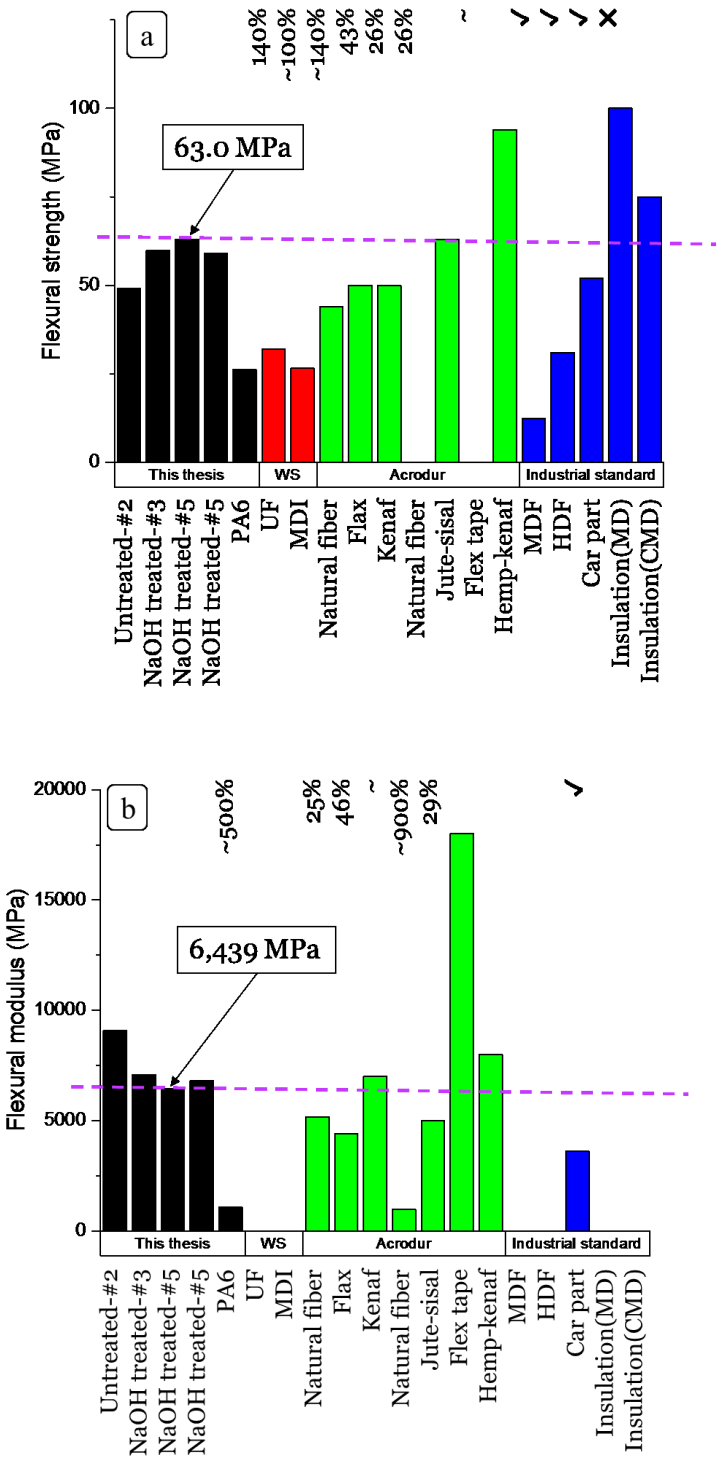

Figure 7.30 Comparison to previous studies and industrial benchmarks

According to ANSI/AHA A 208.1 and ANSI/AHA A 135, the requirements are 12.41 MPa in MOR (modulus of rupture for the natural fiber particleboards (medium density board), and 23.5 MPa for hardboards (high density board). The pressboards made in this thesis all exceed the requirements for particleboards and hardboards.

The standards for car board in automotive use are 52 MPa (ISO 527) for tensile strength and 3600 MPa (ISO 178) for flexural modulus. The results in this thesis successfully fulfill the requirements for automotive industrial use.

The tensile strength standards for insulation pressboards used in powder transformer described in IEC (International Electrotechnical Commission) 60641-3-1 are ≥ 100 MPa in machine direction and ≥ 75 MPa for across machine direction. The results in this thesis are close to the tensile standard in across machine direction.

The comparison with previous studies and industrial benchmarks was summarized in Figure 7.30.

7.4.2.3 Summary of Findings

Within the framework of this research work, the mechanical and morphological properties of wheat straw reinforced Acrodur composites independence of the composite formulation and manufacturing conditions were investigated, analyzed and evaluated. It can be concluded as follows.

1. Overall Acrodur showed better performance than polyamide 6.
2. All the pressboards exhibited brittle fracture behavior. This is attributed high fiber contents.
3. Wheat straw particle (#2) achieved higher flexural strength and modulus than straw fiber (#1).
4. Hybridization of two sizes (#1 and #2) of wheat straw yielded mediocre effects on mechanical properties.
5. Flexural strength and modulus were generally found to increase with binder level.
6. Flexural strength and modulus were generally found to increase with applied force level during compression molding.
7. The positive experimental evidences showed that the NaOH treatment led to the enhanced flexural characteristics, especialy for **Thermoset #3** and **Thermoplastic #5**. This was

attributed to the improved wettiblity and binder absorption of treated straw due to the removal of non-cellulosic components.

8. Hot-water treatment only exhibited the positive effect on the pressboard made with **Thermoplastic #5** and the effect was not evident as NaOH treatment. It may be because hot-water treatment showed little impact on removal of hemicellulose or lignin on the surface.
9. Addition of CNF in **Thermoset #1** solution exhibited significant enhancement effect on mechanical properties for untreated wheat straw.
10. Wheat straw composite pressboards based on **Thermoplastic #5** at low level displayed the highest flexural strengths compared to the composites based on other Acrodur binders
11. The flexural properties reached at a maximum of 63.1 MPa and 6,439 MPa, which was from the board made with NaOH treated wheat straw particulate, and 20% **Thermoplastic #5**, molded at 45,000 lbf and 200°C for 10 minutes.
12. Only of the best results was at 49.9 MPa and 9,083 MPa for flexural strength modulus, which was from the board made with untreated wheat straw particulate, and 40% **Thermoset #2**, compressed at 45,000 lbf and 170°C for 10 minutes.
13. Despite the benefits, the treatment on wheat straw increases the cost and generates byproducts. Therefore, direct use of untreated wheat straw incorporated into binder resin is considered a good option.
14. No clear and simple dependence of mechanical properties on temperature was found as long as temperature is in within the recommended range.
15. Acrodur curing is more sensitive to temperature than to time. Thermal degradation of wheat is the same case. Therefore, the control of temperature is more critical.

7.4.3 Dielectric Property

The dielectric strength results of **Thermoset #1** based pressboards tested at 60 Hz in air and in oil are summarized in Table 7.20. Based on the treatments applied, they were divided into three subgroups, i.e. untreated, hot-water treated and NaOH treated. It was observed that the dielectric strength for most of samples are below 10 kV/mm, except a number of sample being above 10 kV/mm, with the highest dielectric strength being 16.88 kV/mm for hot-water treated wheat straw #2- 40% **thermoset #1**

composite pressboard. It is also observed that the dielectric strength was higher in oil than in air, which makes sense that immersing in the insulation oil increased dielectric breakdown voltage. On the other hand, no significant effects of size of wheat straw, binder content on dielectric strength were observed.

Table 7.20 Dielectric strength of wheat straw-**Thermoset #1** composite pressboard

				Dielectric strength (kV/mm)	
Treatment	Washing	Wheat straw	**Thermoset #1**	In Air	In Oil
Untreated	✗	#1	20%	4.47	9.26
Untreated	✗	#1	40%	4.74	6.29
Untreated	✗	#2	20%	4.36	9.68
Untreated	✗	#2	40%	4.86	8.25
Hot-water treated	✗	#1	20%	6.75	8.85
Hot-water treated	✗	#1	40%	5.10	6.72
Hot-water treated	✗	#2	20%	6.11	14.73
Hot-water treated	✗	#2	40%	6.64	16.88
NaOH treated	✗	#1	20%	8.04	8.55
NaOH treated	✗	#1	40%	6.71	6.29
NaOH treated	✗	#2	20%	6.36	6.85
NaOH treated	✗	#2	40%	6.69	8.93
Hot-water treated	✓	#1	20%	4.98	9.56
Hot-water treated	✓	#1	40%	5.59	11.68
Hot-water treated	✓	#2	20%	6.42	11.48
Hot-water treated	✓	#2	40%	8.12	9.96
NaOH treated	✓	#1	20%	4.94	8.06
NaOH treated	✓	#1	40%	6.45	11.48
NaOH treated	✓	#2	20%	5.06	10.00
NaOH treated	✓	#2	40%	4.50	6.58

The effect of different binders was evaluated by comparing the dielectric strength of **Thermoset #1** pressboards with that of polyamide 6 or **Thermoset #3** in Table 7.21. Both pressboards made with polyamide 6 or **Thermoset #3** showed lower dielectric strength than **Thermoset #1**, whereas the dielectric performance of **thermoset #3** was really poor, being the lowest overall.

Table 7.21 Dielectric strength of wheat straw-polyamide 6 or **Thermoset #3** composite pressboard

			Dielectric strength (kV/mm)	
Treatment	Wheat straw	Binder	In Air	In Oil
Untreated	#1	30% Polyamide 6	5.20	6.65
Untreated	#1	40% **Thermoset #3**	3.79	5.42

The effect of treatment was examined among untreated, hot-water and NaOH treated samples. It is seen from Table 7.20 that hot-water treatment improved the dielectric property of wheat straw–**Thermoset #1** composite pressboards, and slight decrease was found on NaOH treated samples. The explanations can be found in the change in chemical composition of both treatments. Both hot-water and NaOH treatments are known to change the chemical composition by removing noncellulosics from natural fibers (Islam et al. 2009) (Ullah et al. 2018), which contribute to the improvement of dielectric properties because cellulose is higher in insulating ability than other components. Due to harshness of NaOH treatment, its effectiveness on removal of noncellulosic matters is more prominent than hot-water treatment. However, the introduction of Na^+ in treatment process negatively alter the dielectric performance of wheat straw. The fact that alkaline treatment leaves Na+ on the fiber surface by reacting with free OH groups was reported by Biagiotti etc. (Biagiotti et al. 2004) and Maslowski etc. (Masłowski et al. 2018)

As discussed that introduction of Na^+ negatively affect the dielectric property of composites, the hypothesis was made that washing with distilled water could help to take away Na^+ ion. The comparison was made to check the effect of washing process. For NaOH treated sample, washing with distilled water boosted the dielectric performance, although the dielectric strength still is below hot-water treated ones. On the other hand, no significant effects were found on hot-water treated samples.

A comparison of dielectric strength to the commercial and experimentally manufactured pressboards was made. Two commercially available pressboards, called Calendered Kraft softwood and Press-dried Kraft softwood, are 26.92 and 29.46 kV/mm in dielectric strength (Myers and Hettwer 1993), which are much higher than that of the wheat straw based pressboards manufactured in our laboratory. However, it is comparable to the Experimental Kraft softwood pressboard and stay at the lower end of range 18.06–21.26 kV/mm (Myers and Hettwer 1993).

The dielectric strength of tested pressboards is below the requirement for pressboard for electrical purposes specified in IEC 60641-3-1(International Electrotechnical Committee IEC 60641-3-1) (Enanv et al. 2008), which states that the requirement for the insulation pressboards is dielectric strength ≥ 12 kV/mm in air and ≥ 45 kV/mm in oil. The main reason for that is probably the existence of non-cellulosic component in wheat straw, whereas only pure cellulose extracted from wood is used in the production of insulation pressboards in current technology (Prevost and Oommen 2006).

7.4.4 Binder Distribution

One of the major issues in development of composites is distribution and dispersion of polymeric binder on the reinforcing fibers. Owing to nature of the surface waxy and silica residues had an adverse effect on the wetting and adhesion, especially for boards manufactured with low loading levels of binder. This lack of binder dispersion can result in clumping and agglomeration of binder which lead to inferior mechanical properties. As learned from Chapter 3 the structural and chemical changes on the surface were expected between untreated and treated wheat straw (both stem and sheath), although structural and morphological changes were not noticeable on my SEM images. And these changes alter the wetting behavior of Acrodur solution on wheat straw surface. To examine the distribution and dispersion of binder on reinforcing wheat straw, and to evaluate the effect of treatments on binder distribution and dispersion, the FEI Quanta 250 FEG SEM was used for binder distribution analysis.

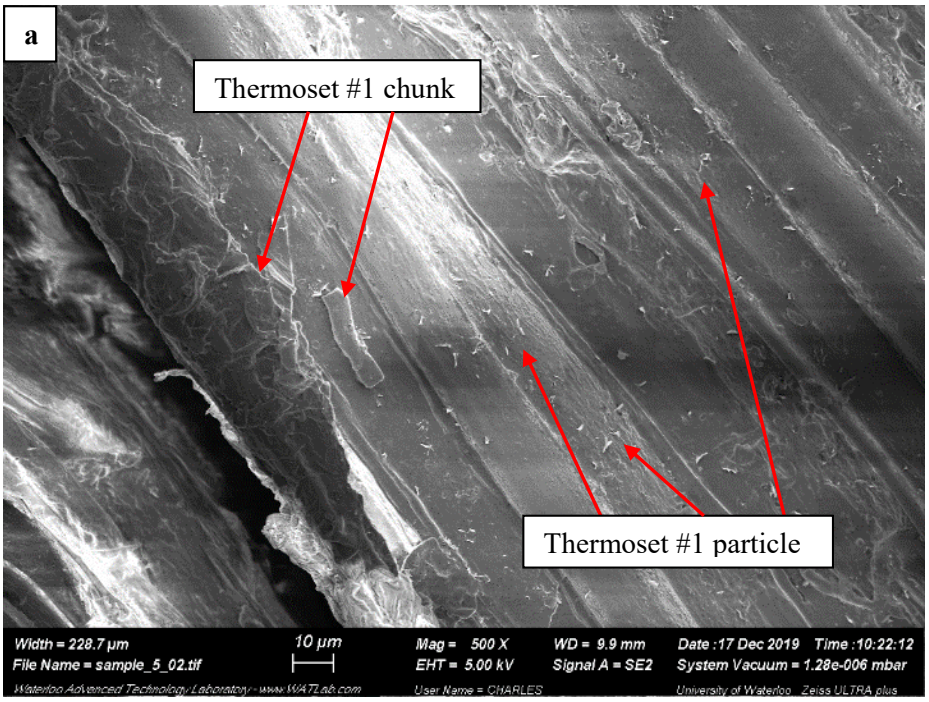
a
Thermoset #1 chunk
Thermoset #1 particle
Width = 228.7 µm
File Name = sample_5_02.tif
10 µm
Mag = 500 X
EHT = 5.00 kV
WD = 9.9 mm
Signal A = SE2
Date :17 Dec 2019 Time :10:22:12
System Vacuum = 1.28e-006 mbar
Waterloo Advanced Technology Laboratory - www.WATLab.com
User Name = CHARLES
University of Waterloo Zeiss ULTRA plus

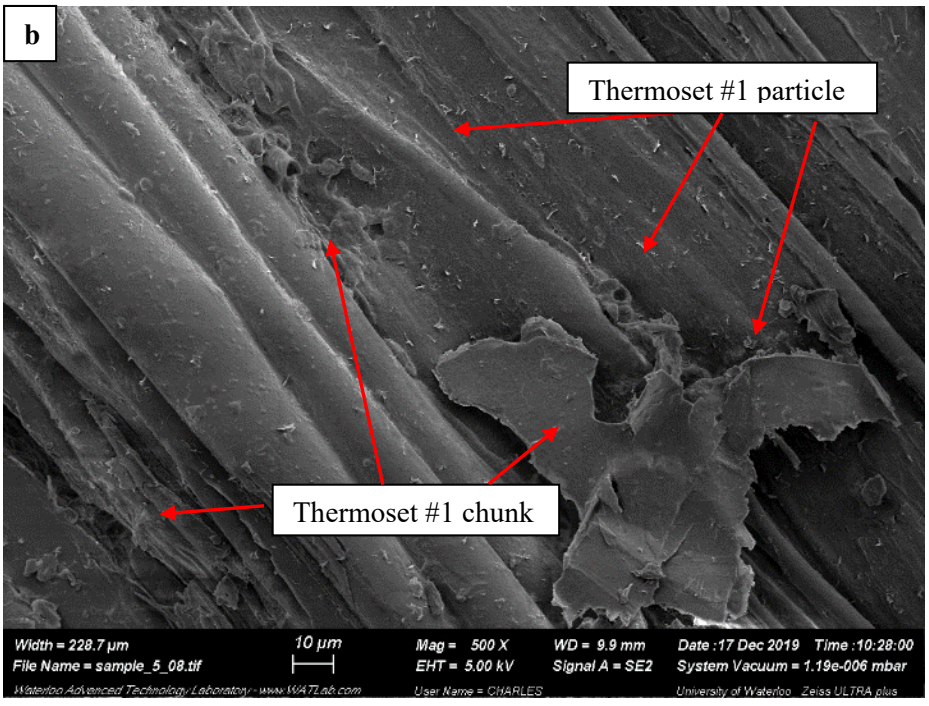
b
Thermoset #1 particle
Thermoset #1 chunk
Width = 228.7 µm
File Name = sample_5_08.tif
10 µm
Mag = 500 X
EHT = 5.00 kV
WD = 9.9 mm
Signal A = SE2
Date :17 Dec 2019 Time :10:28:00
System Vacuum = 1.19e-006 mbar
Waterloo Advanced Technology Laboratory - www.WATLab.com
User Name = CHARLES
University of Waterloo Zeiss ULTRA plus

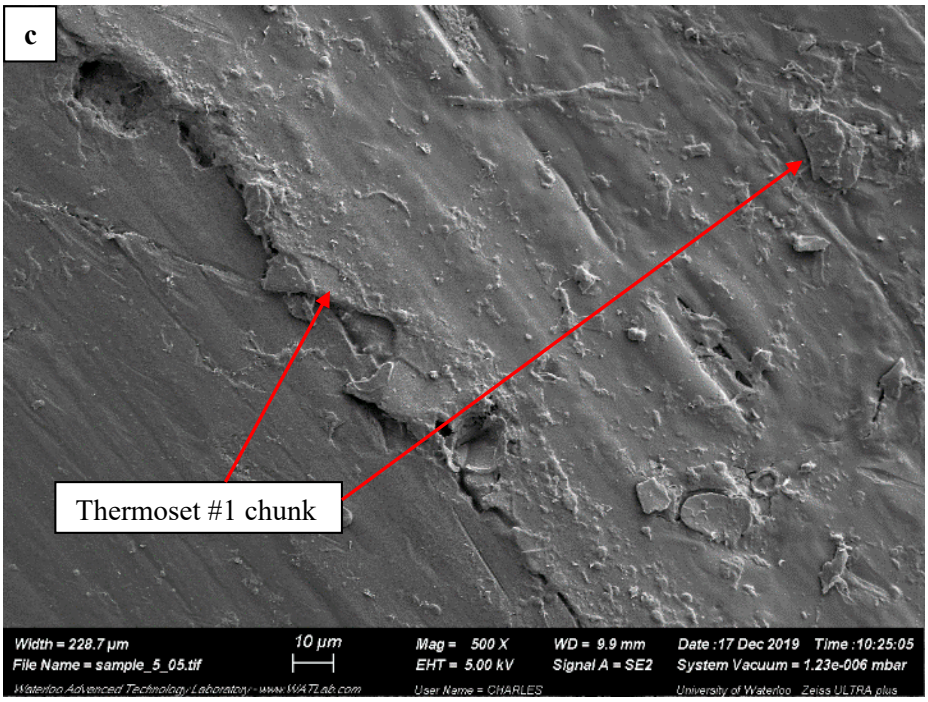

Figure 7.31 Binder dispersion on exterior (a) (b) and interior (c) of untreated wheat straw #1 impregnated with 40% **Thermoset #1**

Micrographs of untreated wheat straw #1 impregnated with 40% **Thermoset #1** are illustrated in Figure 7.31 (a, b and c). The smoothness of untreated wheat straw is visible in images (a and b) due to the existence of waxy layer on the surface, which is believed to be wheat stem exterior. It is also observed that **Thermoset #1** binder particles presented as white spots in images (a and b) were distributed well on stem exterior over a large area, whereas layers of **Thermoset #1** are also presented mostly on the edges of fibers with various thicknesses, because the cracks and roughness more likely hold the binder in place. In image (c) is only a big chunk layer of binder presented covering a large area.

Figure 7.32 (a and b) presents the SEM micrographs of untreated wheat straw #2 impregnated with 40% Thermoset #1. The inherent porosity of natural fibers is illustrated in image (a), where it seems like no binder is penetrated into. At higher magnification of 500 times, the rough structure on the fiber surface seems to be covered with a thin layer of binder.

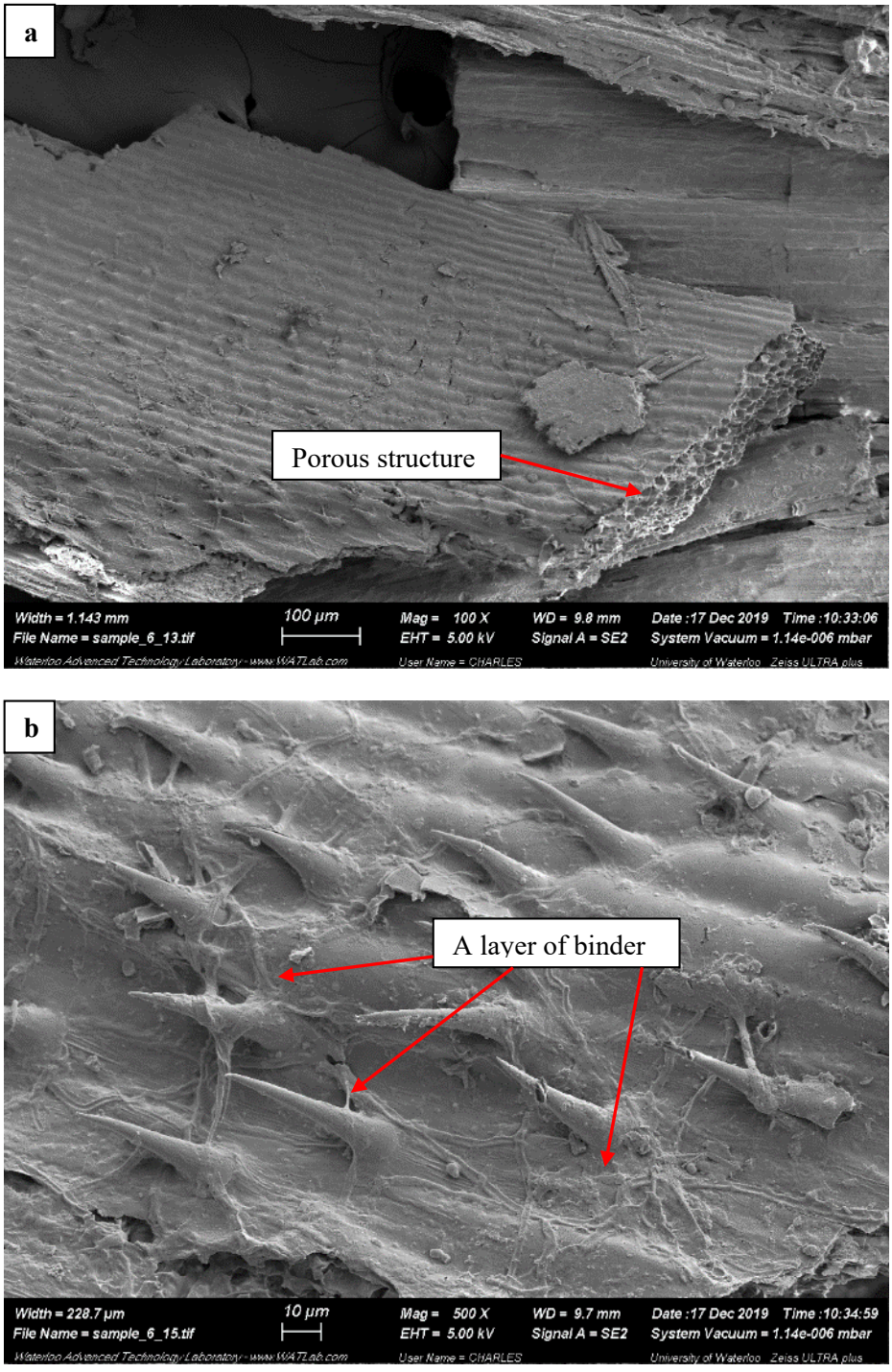

Figure 7.32 Porous structure (a) and well dispersed binder (b) on untreated wheat straw #2 impregnated with 40% **Thermoset #1**

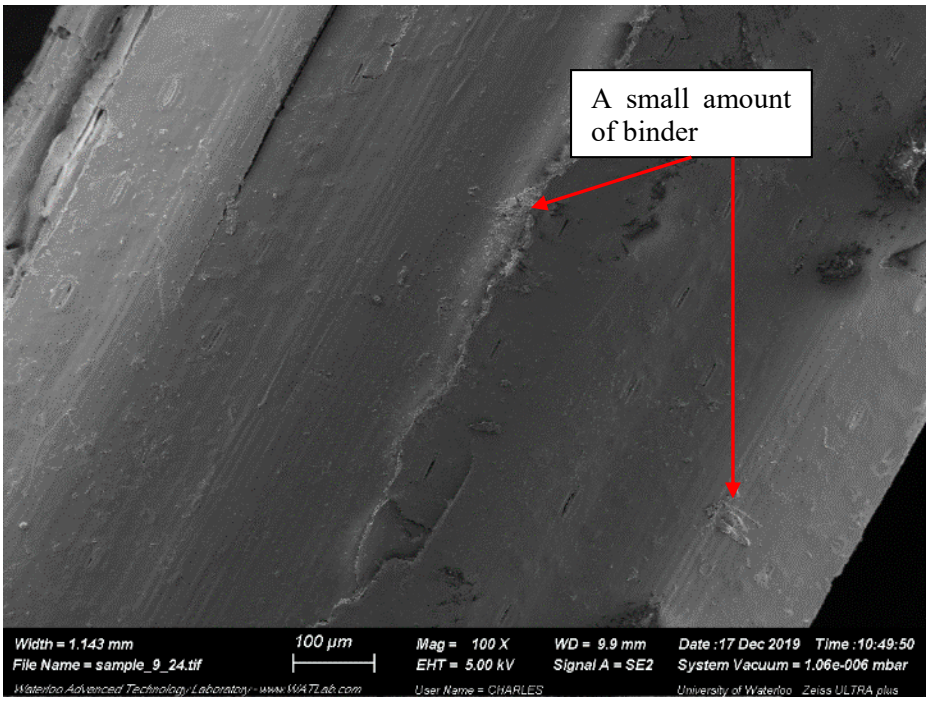

Figure 7.33 NaOH treated wheat straw #1 impregnated with 40% **Thermoset #1**

The micrograph of NaOH treated wheat straw #1 and # 2with 40% **Thermoset #1** is presented in Figure 7.33 and Figure 7.34, respectively. The stem exterior in Figure 7.33 is very smooth and clean. It does not show any evident features of NaOH treatment, just a small amount of binder is presented at cracks. On the contrary, on the #2 surface in Figure 7.34 (a and b), there present thin layers of binder. The reason might be wheat straw #2 shows more rough surfaces, which retain the binder.

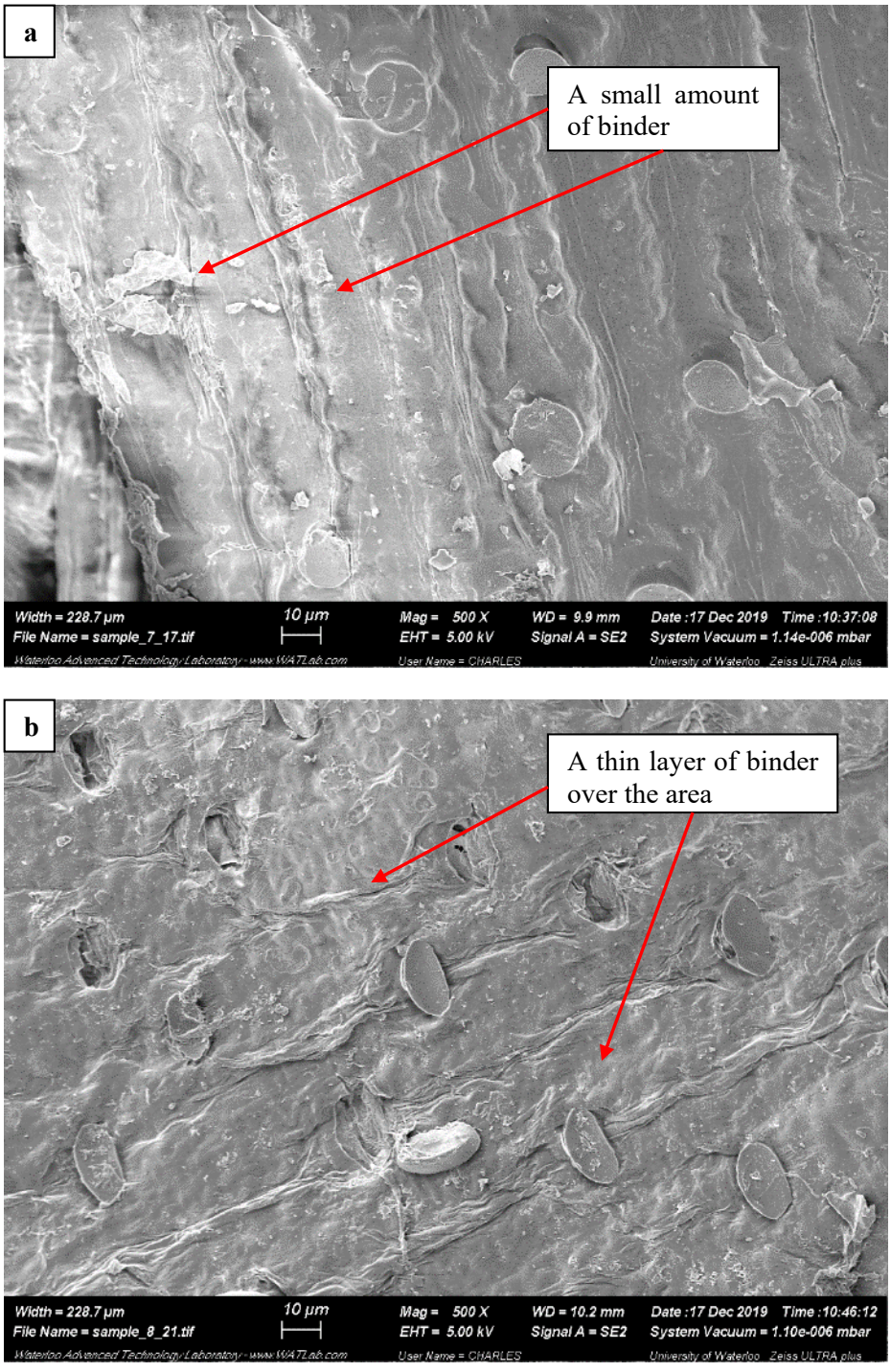

Figure 7.34 Binder dispersion (a) (b) on NaOH treated wheat straw #2 impregnated with 40% **Thermoset #1**

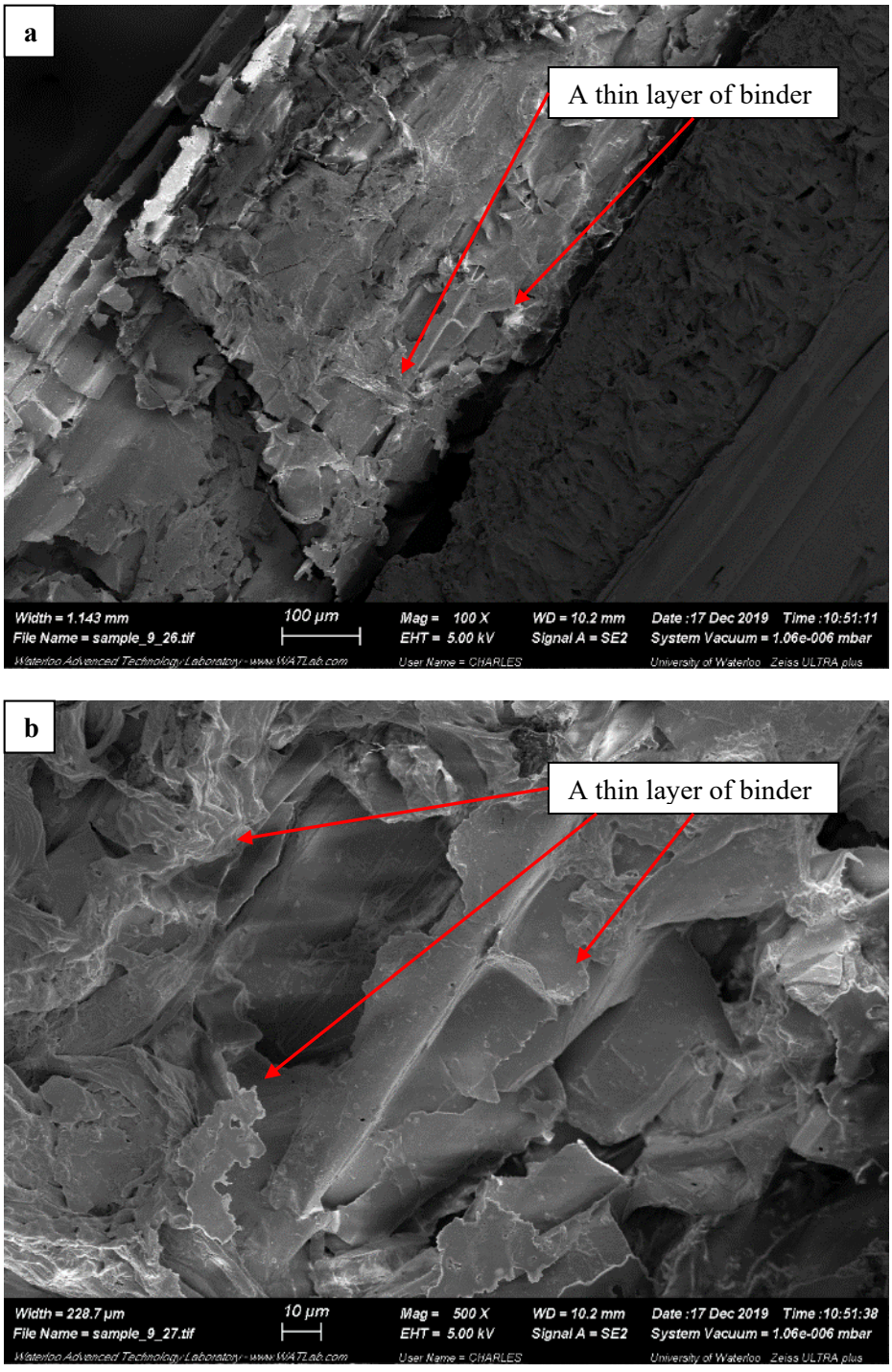

Figure 7.35 Binder dispersion (a) (b) on hot-water treated wheat straw #1 impregnated with 40% **Thermoset #1**

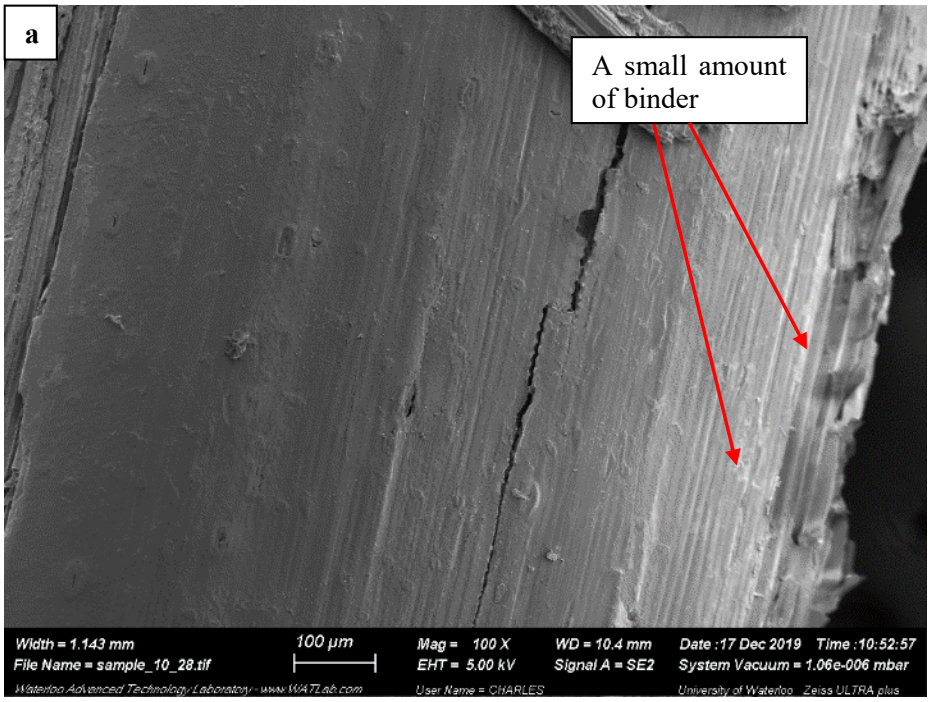
a
A small amount of binder
Width = 1.143 mm
File Name = sample_10_28.tif
100 µm
Mag = 100 X
EHT = 5.00 kV
WD = 10.4 mm
Signal A = SE2
Date :17 Dec 2019 Time :10:52:57
System Vacuum = 1.06e-006 mbar
Waterloo Advanced Technology Laboratory - www.WATLab.com
User Name = CHARLES
University of Waterloo Zeiss ULTRA plus

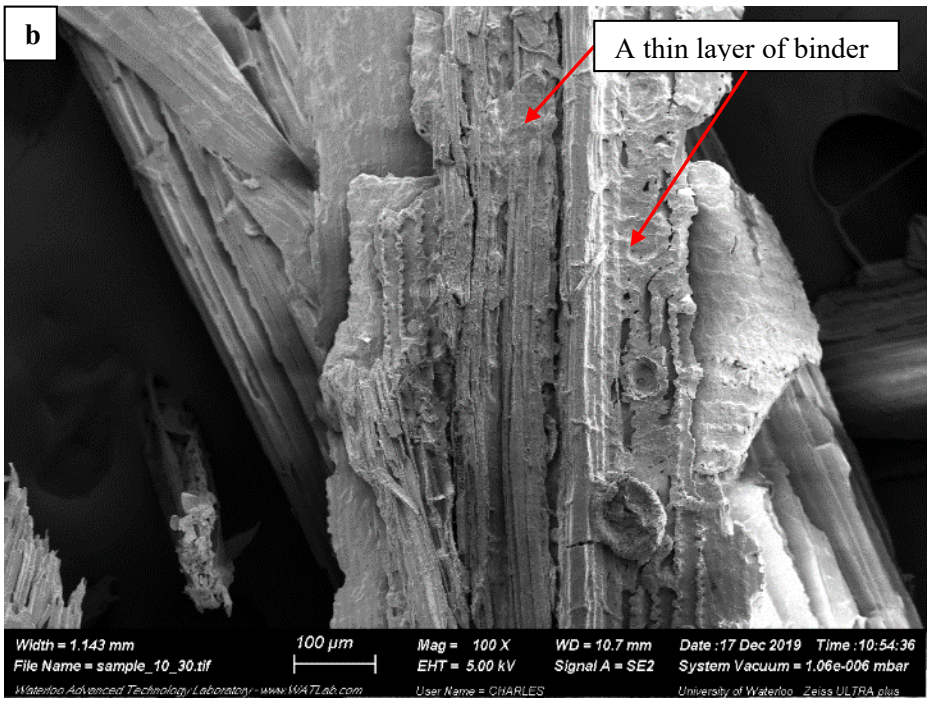
b
A thin layer of binder
Width = 1.143 mm
File Name = sample_10_30.tif
100 µm
Mag = 100 X
EHT = 5.00 kV
WD = 10.7 mm
Signal A = SE2
Date :17 Dec 2019 Time :10:54:36
System Vacuum = 1.06e-006 mbar
Waterloo Advanced Technology Laboratory - www.WATLab.com
User Name = CHARLES
University of Waterloo Zeiss ULTRA plus

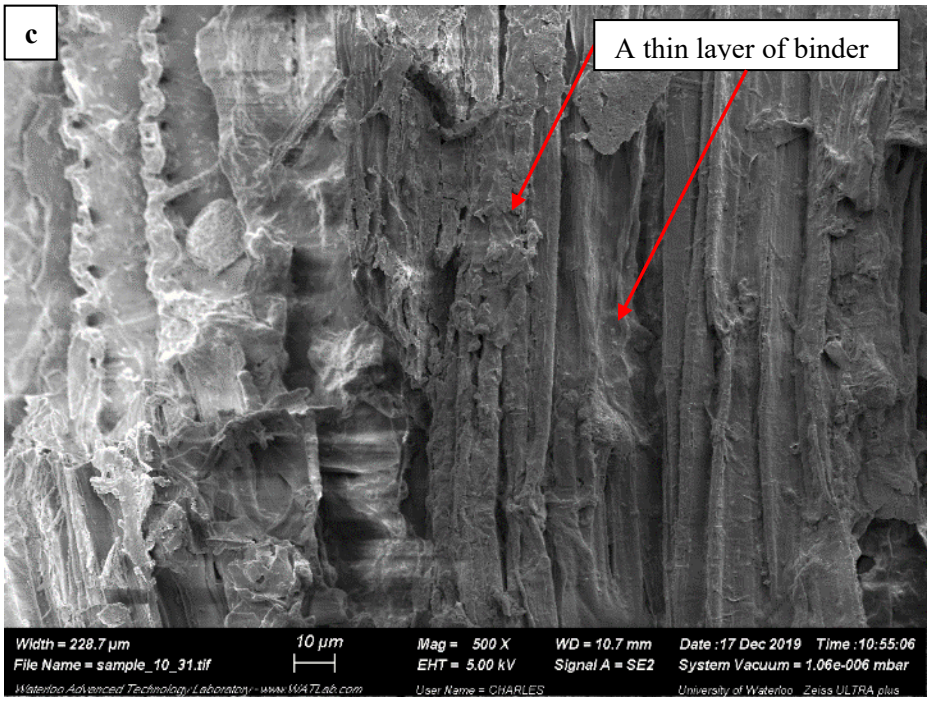

Figure 7.36 Binder dispersion on exterior (a) and interior (b) (c) of hot-water treated wheat straw #2 impregnated with 40% **Thermoset #1**

The surfaces in Figure 7.35 are believed to be interior of hot-water treated wheat straw #1, which feature the breakage of fiber tissues. The breakage and roughness are accompanied by the presence of a big amount of **Thermoset #1** over all the area. Therefore, it is reasonable to induce that the surface feature plays a more important role in determining the binder distribution than the treatments applied.

Figure 7.36 illustrates the surface features and binder distribution of hot-water treated wheat straw #2 with 40% **Thermoset #1**. The same observations are made on the wheat straw particles, where the smooth surface did not retain the binder as much as rough surfaces.

Overall, SEM micrographs clearly reveal uniform distribution of the polyester binders on the surface of reinforcing wheat straw at different loading levels of 20% and 40%. It can be inferred that impregnation of wheat straw using the spray-while-stirring method results in high prepreg quality in terms of binder distribution over the reinforcement. Water based solution of **Thermoset #1** exhibited a good affinity for binding with fibrous reinforcements because of its very low viscosity and its polar chemical composition. The wetting of the fiber surface by the binder is good since no air gap in the boundary surface is to be recognized. The 40% of binder loading can allow a good coverage of wheat

straw. No evidence was observed that the acrylic binder can penetrate and fill the micro-pores. It is evident that the binder is able to flow between fibers enhancing the specific surface area between wheat straw fibers. Hence, the Acrodur binder shows good adhesion to wheat straw. It could improve the mechanical properties of the final pressboard by enhancing the stress transfer between the fiber and the binder. The interior and exterior of wheat straw showed significant effect on binder distribution by affecting roughness and cracks. The smaller size (#2) of wheat straw affected the binder distribution by exposing more fracture and breakage of fiber. On the contrary, the effect of treatment is not significant to influence the binder distribution by altering the surface chemistry as expected, although the surface roughness of wheat straw was enhanced by the treatments.

7.4.5 Fracture Topography

The SEM images in low magnification can reveal overall dispersion, wetting, fracture characteristics and indications of fiber pull-out such as voids and spots. Images made in high magnification are useful to observe the quality of interface between filler and binder. Better fiber-binder adhesion usually is translated into enhanced mechanical properties. These images may also provide information about the fracture mechanisms such as crack propagation and load transfer between fiber and binder.

Figure 7.37 to Figure 7.46 show the SEM photomicrographs of fracture surface after cryogenic treatment in liquid nitrogen of composite pressboards with untreated or treated wheat straw and one of three types of binders at various loading levels.

Figure 7.37 and Figure 7.38 show the fracture surface SEM micrographs of the wheat straw-**Thermoset #1** composite pressboards at two binder loading levels of 20% and 40% respectively. The layered structure was observed in the cross sections of both 20% and 40% binder loading levels. The formation of layered structure of pressboards can be explained by the tendency of wheat straw fibers of high aspect ratio to spread transversely other than vertically under the pressure. The wetting of the fiber surface by the binder is very good since no air gap or free space in the boundary surface is to be recognized, suggesting a good compatibility of fiber and binder. In Figure 7.37 (a, b and c) the wheat straw fibers are closely packed, and **Thermoset #1** binder is observed in intimate contact with wheat straw. **Thermoset #1** tended to stay on the surface of untreated fibers and some penetrations of binder into micro pores of fiber were observed as shown in Figure 7.38 (a). The clean fracture surface of binder indicated its brittle feature. No obvious fiber pullouts are observed that indicates a sign of good fiber-binder adhesion. At higher binder loading level in Figure 7.38, the big chunks of binder started to

appear, which might indicate 40% **Thermoset #1** could be more than sufficient and reduction of binder can be an option.

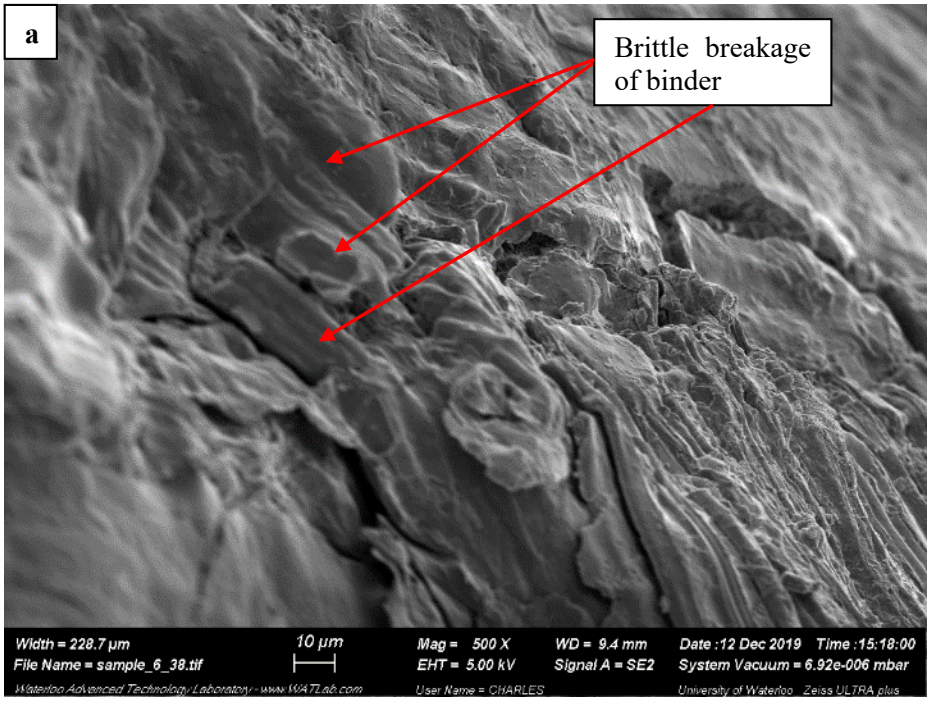

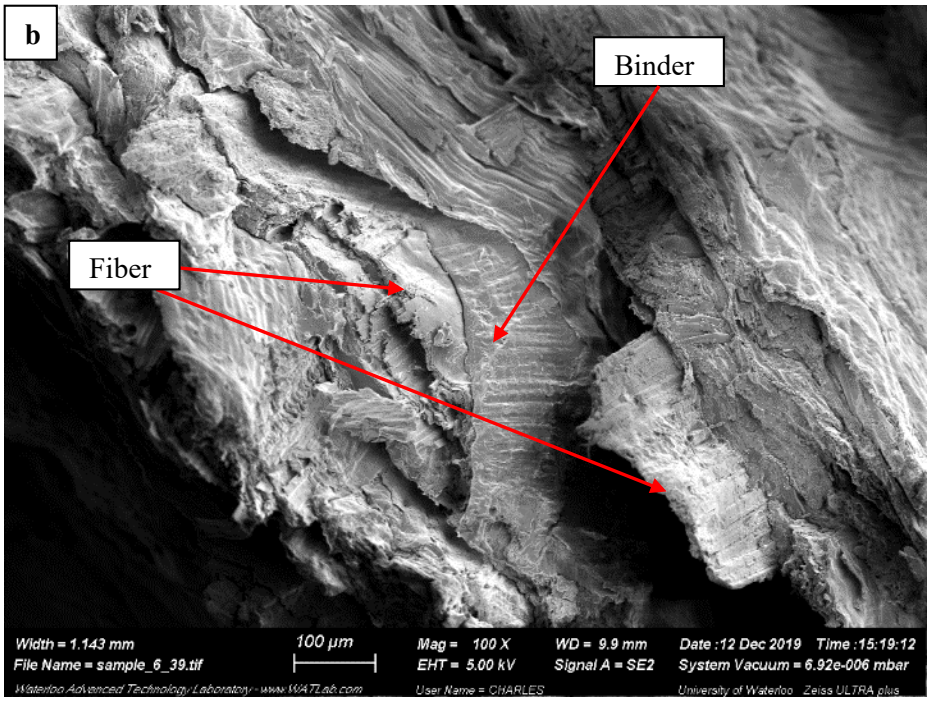

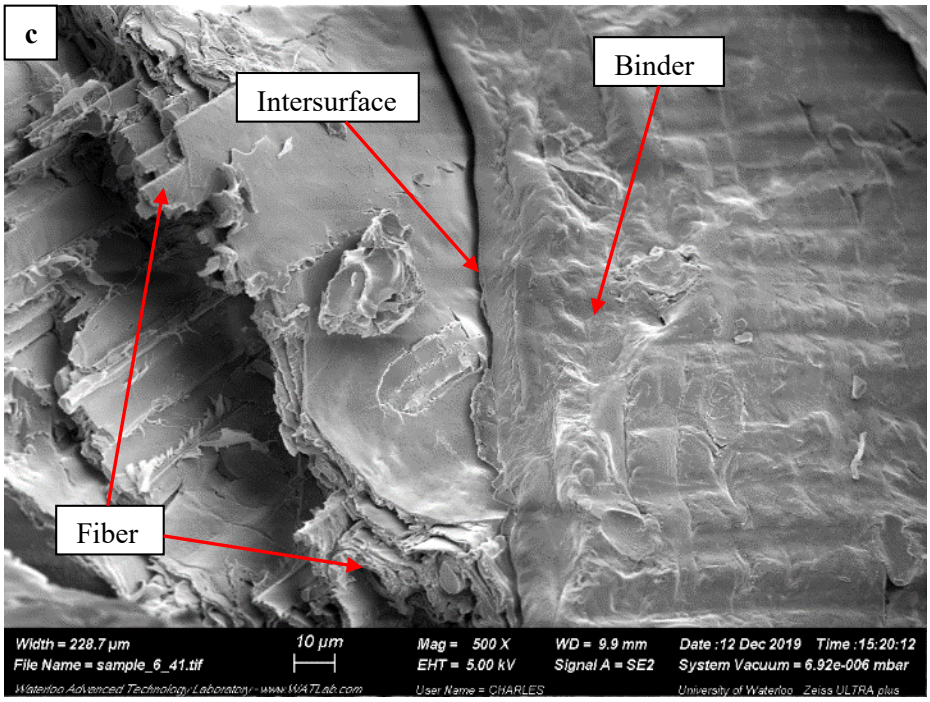

Figure 7.37 Binder breakage (a) and binder distribution (b) (c) on fracture surface of pressboard containing untreated wheat straw #2 and 20% **Thermoset #1**

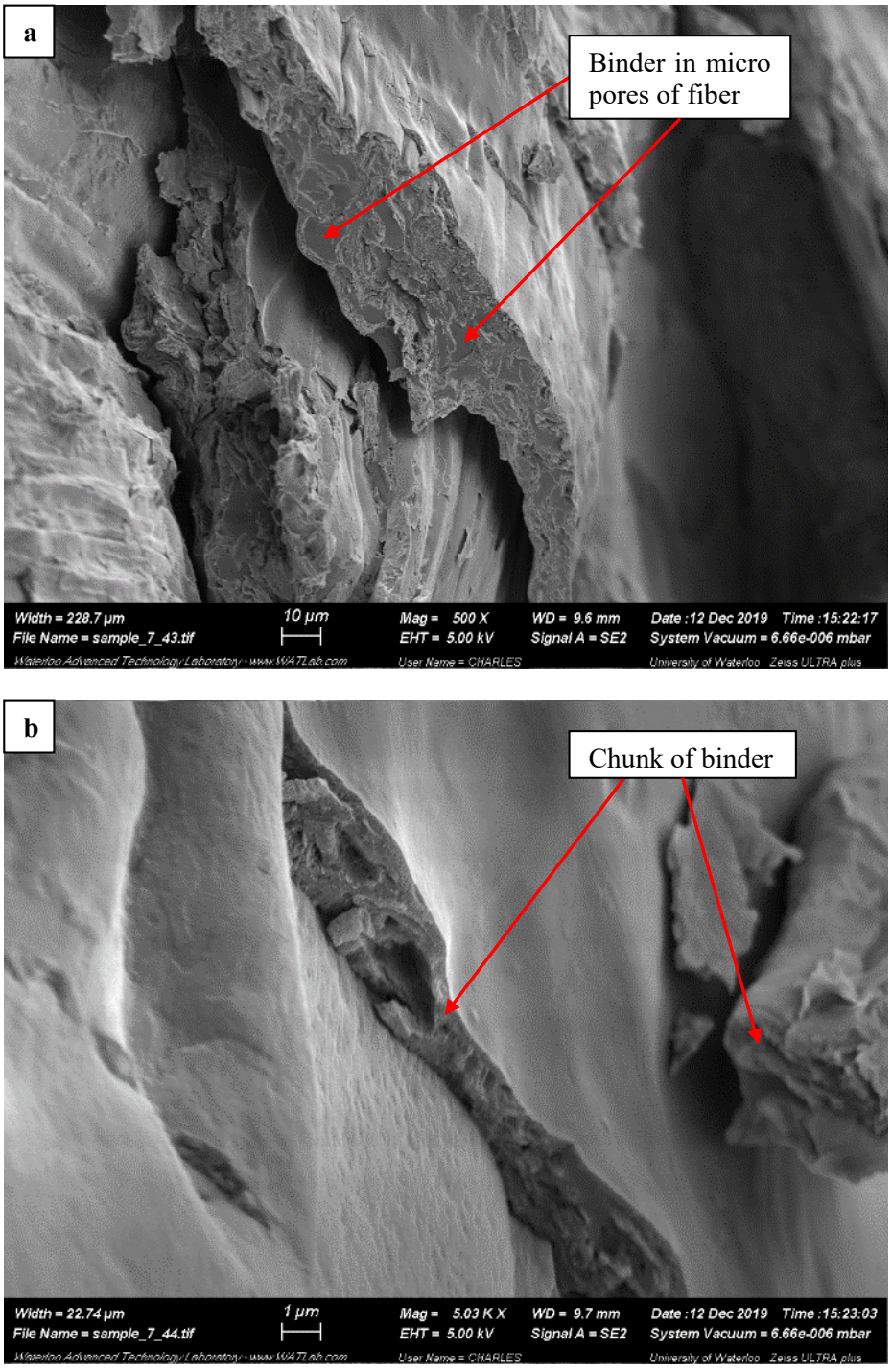

Figure 7.38 Penetration of binder (a) and poor dispersion of binder (b) on fracture surface of pressboard containing untreated wheat straw #2 and 40% **Thermoset #1**

The micrographs in Figure 7.39, Figure 7.40 and Figure 7.41 present the facture surfaces of pressboard of NaOH treated wheat straw at two binder levels of 20%, 40% and 60%, respectively. It is seen at lower binder level in Figure 7.39 that the fibers were well-packed and pressed. The layered structure of pressboard is still observed at cross section of fracture surface, where less binder and more fibers are presented. The gaps and voids appeared due to insufficient binder content. The wetting improvement effect of NaOH treatment is not apparent in comparison of untreated samples.

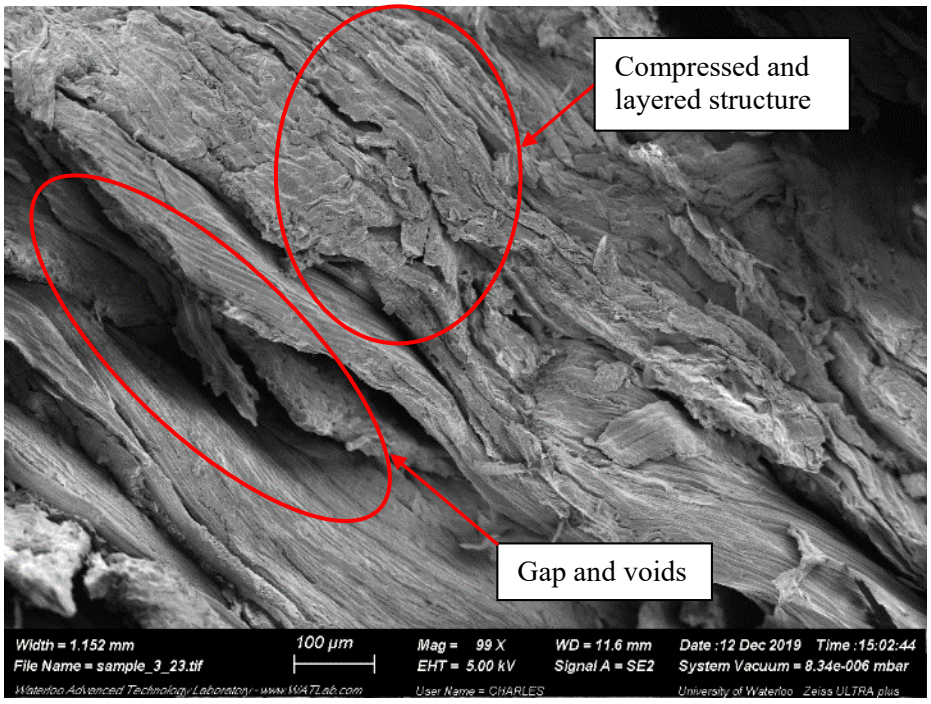

Figure 7.39 Fracture surface of pressboard containing NaOH treated wheat straw #2 and 20%

Thermoset #1

Figure 7.40 present the facture surface of pressboard with binder loading level increased to 40%. Figure 7.40 (a) shows that there was extensive longitudinal fiber breakage when the fiber was parallel to the fracture surface. In this case, the outer structural wall of the fiber was peeled off leaving the internal structure and microfibrils exposed. Fiber fragments indicate that fiber fracture occurs at the porous inner layer between the hard epidermis layers. In addition to more chances of seeing binder chunks, it is interesting to observe in Figure 7.40 (b and c) that the appearance of binder in porous structure of wheat straw fiber. The brittleness of facture indicates the binder breakage.

At even higher binder level of 60%, there are more chances in Figure 7.41 to observe chunks of binder and appearance of binder in the porous structure of wheat straw. This indicates that high level of binder loading led to poor level of distribution, and that increased binder might not effectively improve the adhesion between fibers. It suggests that 60% and even 40% is more than the appropriate binder loading level required.

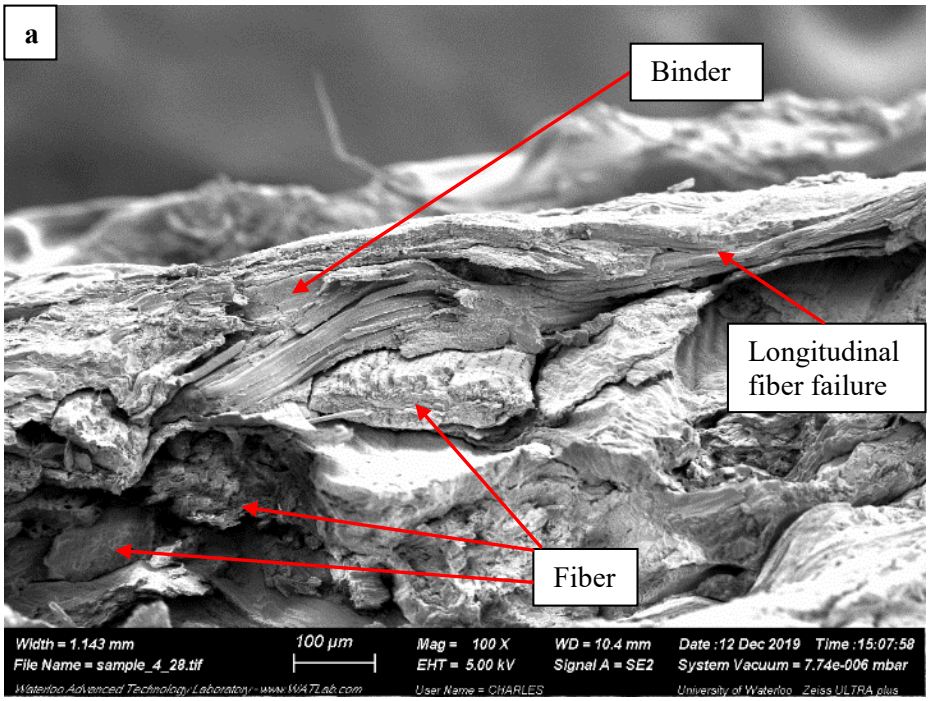

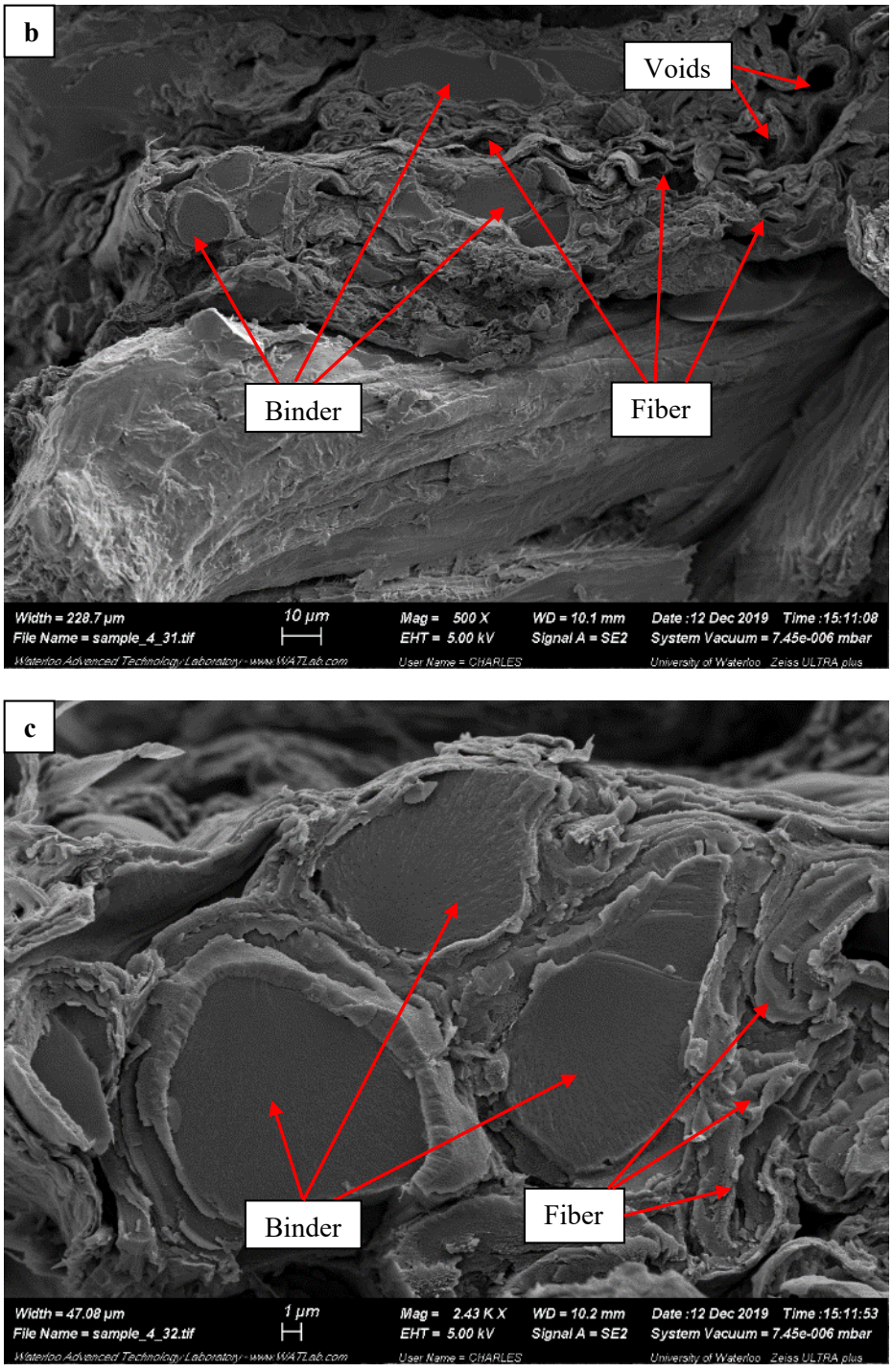

Figure 7.40 Brittle breakage of fiber (a) and binder (b) (c) on fracture surface of pressboard containing NaOH treated wheat straw #2 and 40% **Thermoset #1**

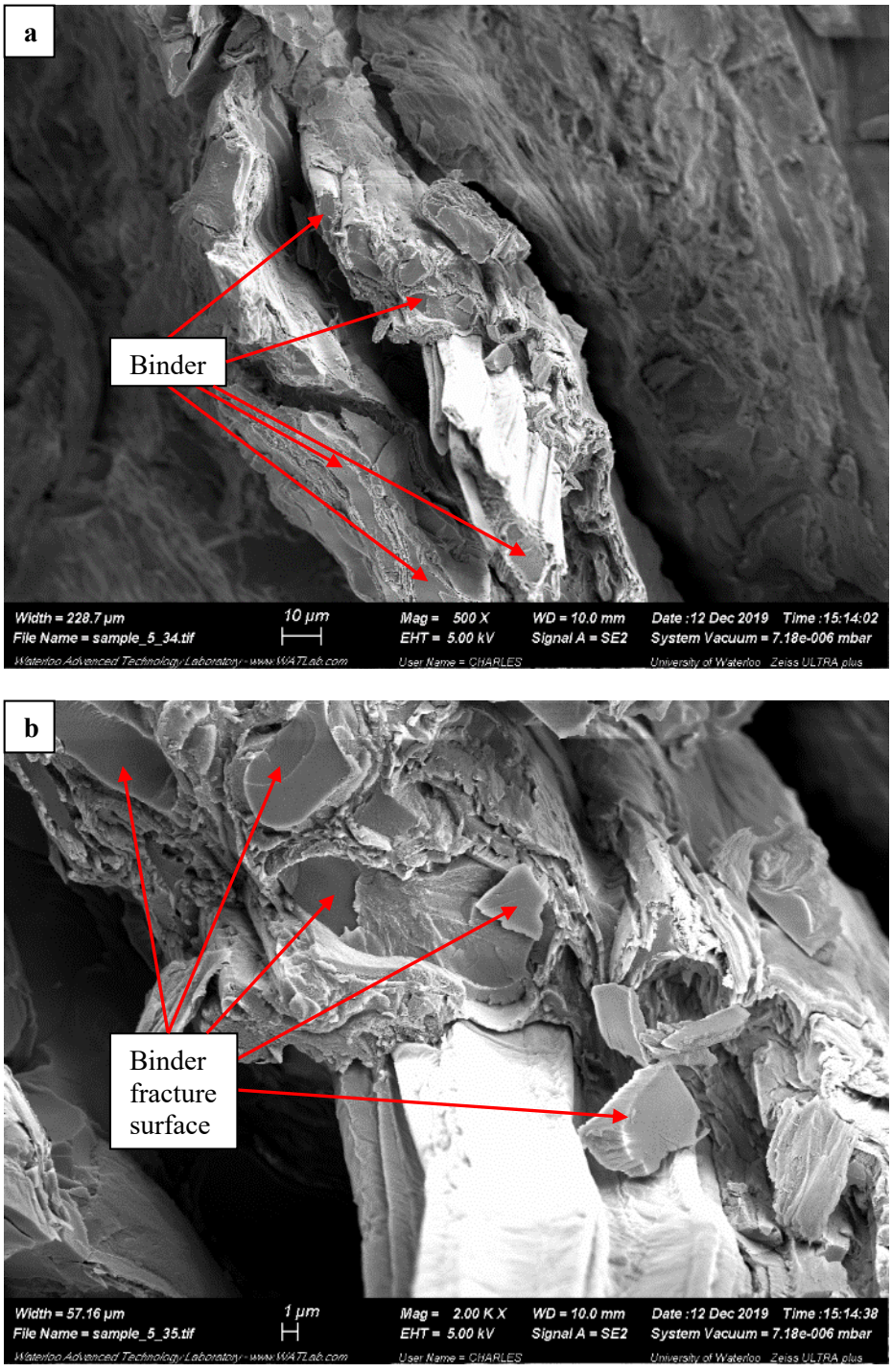

Figure 7.41 Penetration of binder (a) and brittle breakage of binder (b) on fracture surface of pressboard containing NaOH treated wheat straw #2 and 60% **Thermoset #1**

Figure 7.42 and Figure 7.43 present the micrographs of fracture surface of the pressboards containing **Thermoset #2** with untreated and NaOH treated wheat straw, respectively.

The layered structure is emphasized in Figure 7.42 (a), whereas the intimate interface between fiber and fibers are present in images (b and c). However, binder surfaces in images (b and c) bore the imprint of the wheat straw, which implies the weak bond at those spots.

No observation of CNF was made, which might be due to low concentration (less than 5% based on binder) of CNF. On the other hand, when NaOH treatment applied, the cracks at interfaces of fiber and binder appeared in Figure 7.43 (a and b). This indicates the NaOH treatment did not improve the interfacial adhesion as expected, on the contrary, it led to impaired interface.

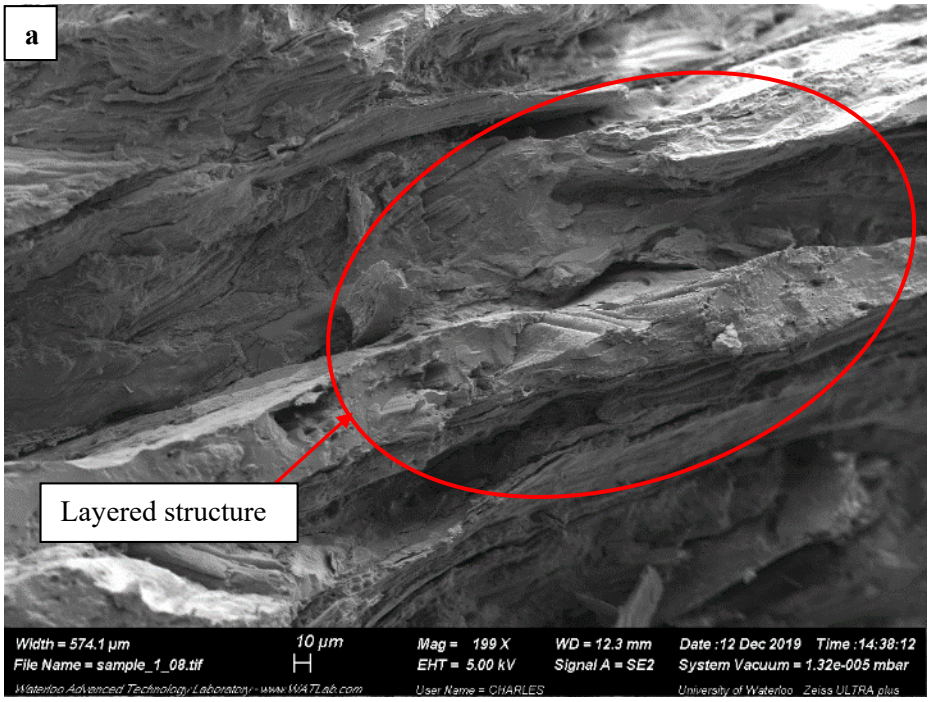

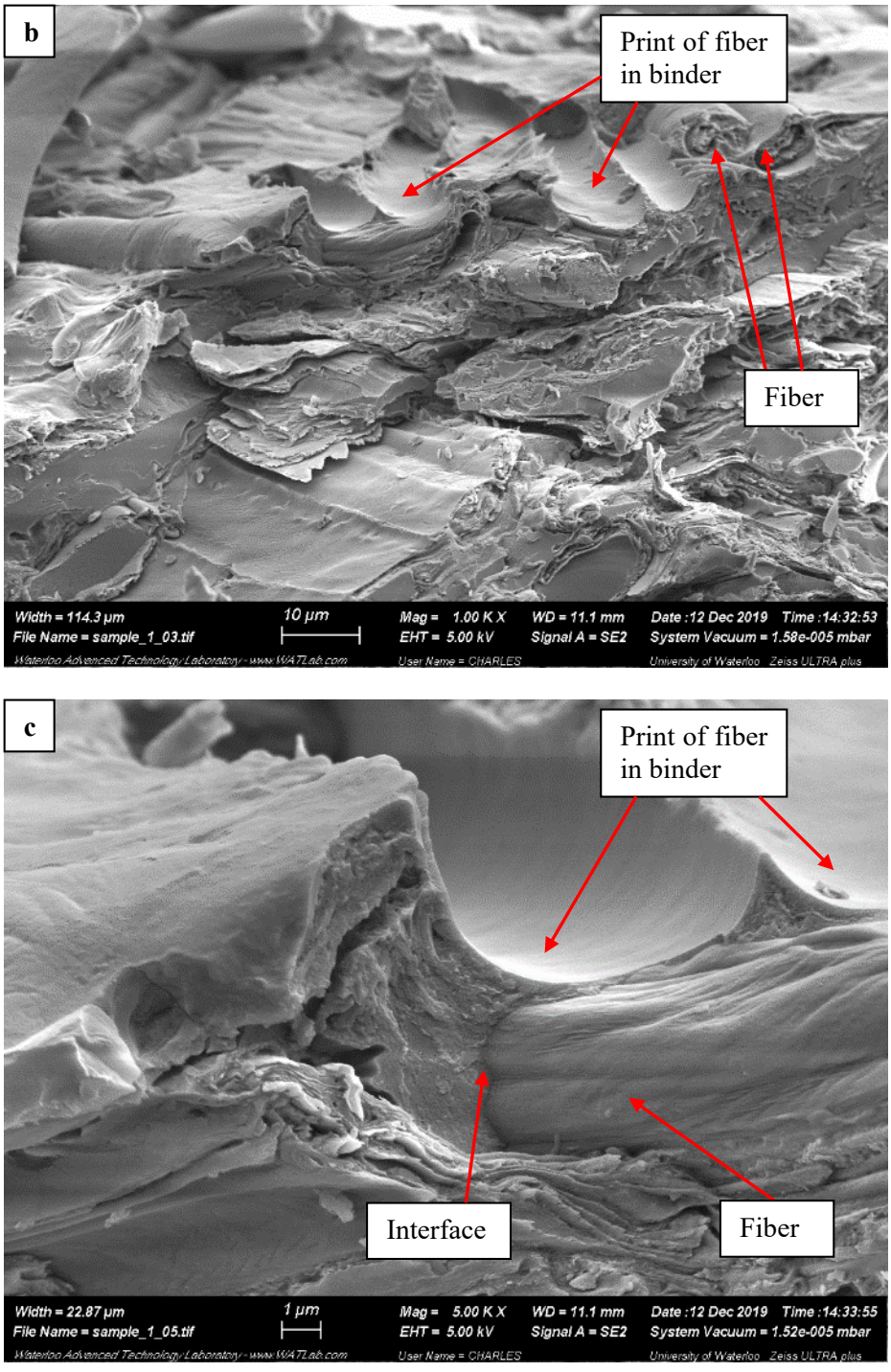

Figure 7.42 Layered structure (a), affinity between fiber and binder (b) (c) on fracture surface of pressboard containing untreated #2 and 40% **Thermoset #2**

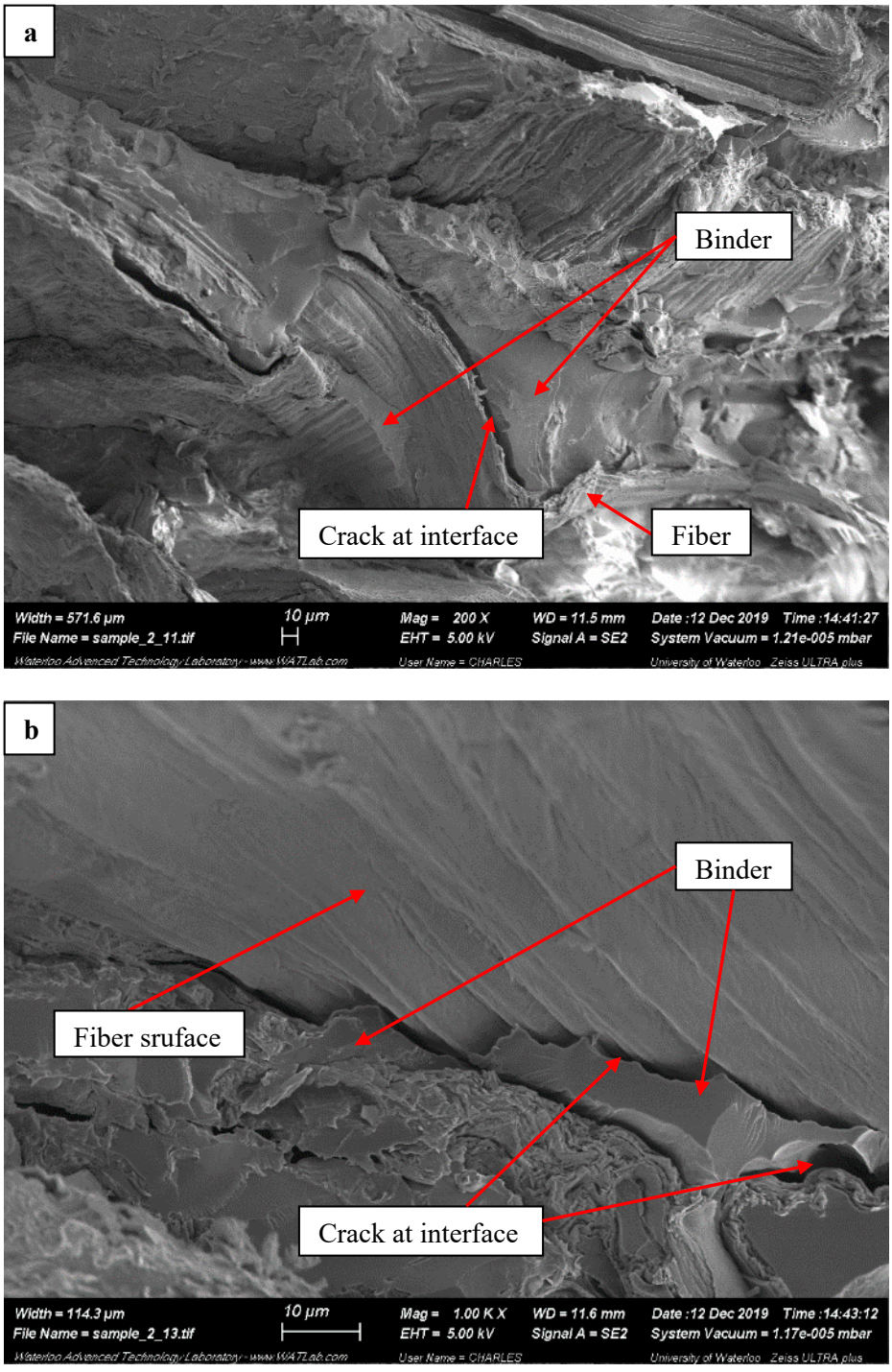

Figure 7.43 Cracks and separation of fiber and binder (a) (b) on fracture surface of pressboard containing NaOH treated #2 and 40% **Thermoset #2**

Figure 7.44, Figure 7.45 and Figure 7.46 illustrate the micrographs of fracture surface of the pressboards containing **Thermoplastic #5** with untreated, hot-water and NaOH treated wheat straw, respectively.

The layered structure is illustrated in Figure 7.44 (a), where the intimate interface between fiber and fibers are presented. The micro pores in structure of wheat straw remained unfilled as shown in Figure 7.44 (b), whereas in image (c) the binder is found at the interface of fibers.

In hot-water treated wheat straw-**Thermoplastic #5** pressboard in Figure 7.45 (a) the bubbly structure of **Thermoplastic #5** is observed, which is believed to be resulted from residual water upon heating. The intimate adhesion is observed from the images (a and b), whereas the more plastic breakage of binder is presented in the image (c).

The NaOH treated pressboards shown in Figure 7.46 exhibited effective adhesion at the interfaces, although in image (b) an unfilled microstructure of wheat straw is observed.

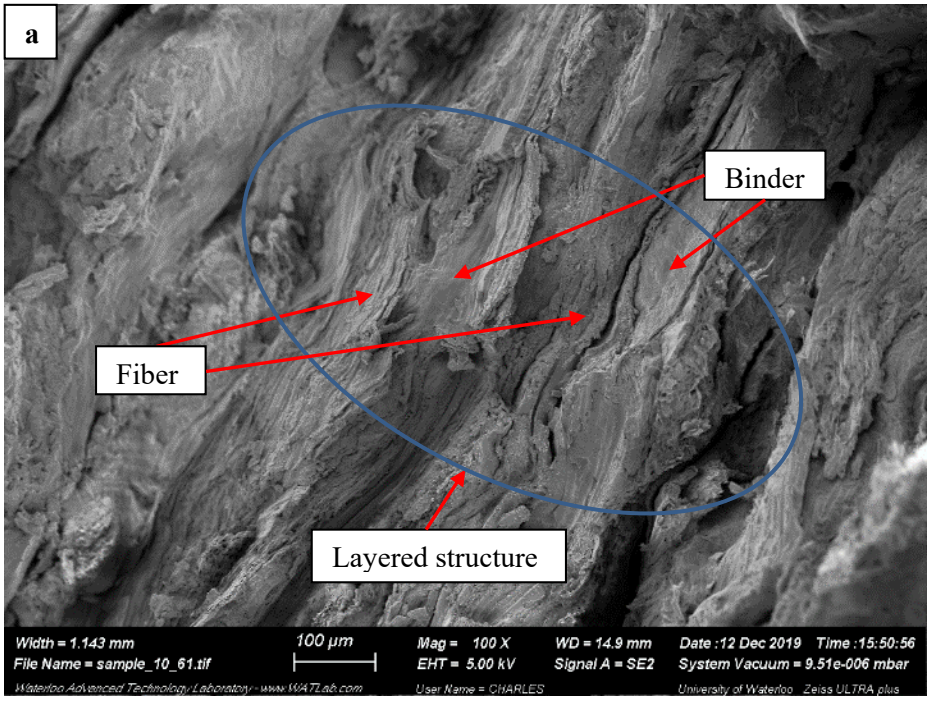

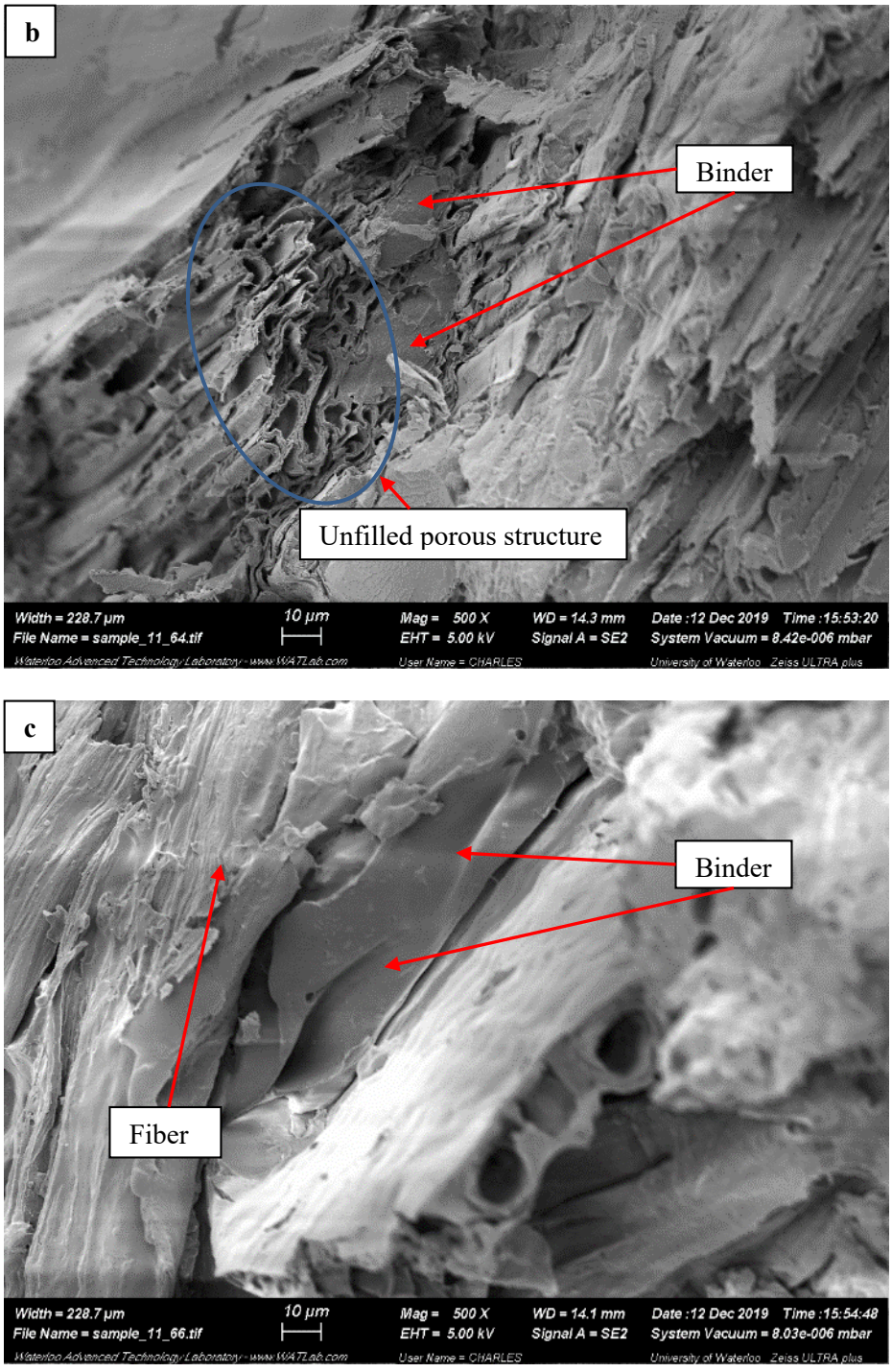

Figure 7.44 Layered structure (a), unfilled porsour structure of fiber (b) and binder existence between fibers (c) on fracture surface of pressboard containing untreated #2 and 20% **Thermoplastic #5**

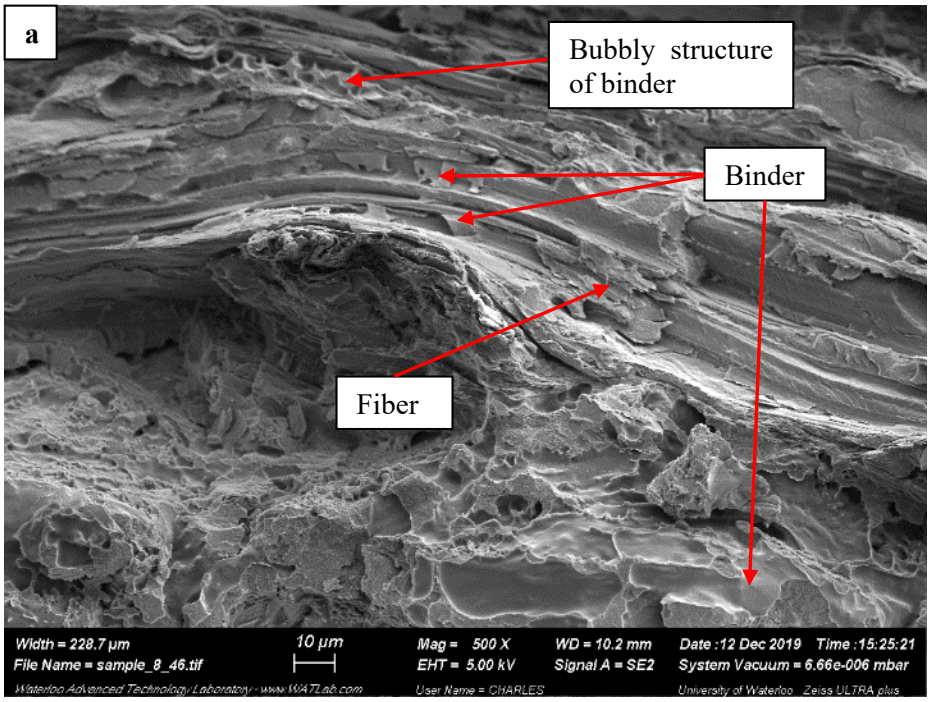
a
Bubbly structure of binder
Binder
Fiber
Width = 228.7 µm
File Name = sample_8_46.tif
10 µm
Mag = 500 X
EHT = 5.00 kV
WD = 10.2 mm
Signal A = SE2
Date :12 Dec 2019 Time :15:25:21
System Vacuum = 6.66e-006 mbar
Waterloo Advanced Technology Laboratory - www.WATLab.com
User Name = CHARLES
University of Waterloo Zeiss ULTRA plus

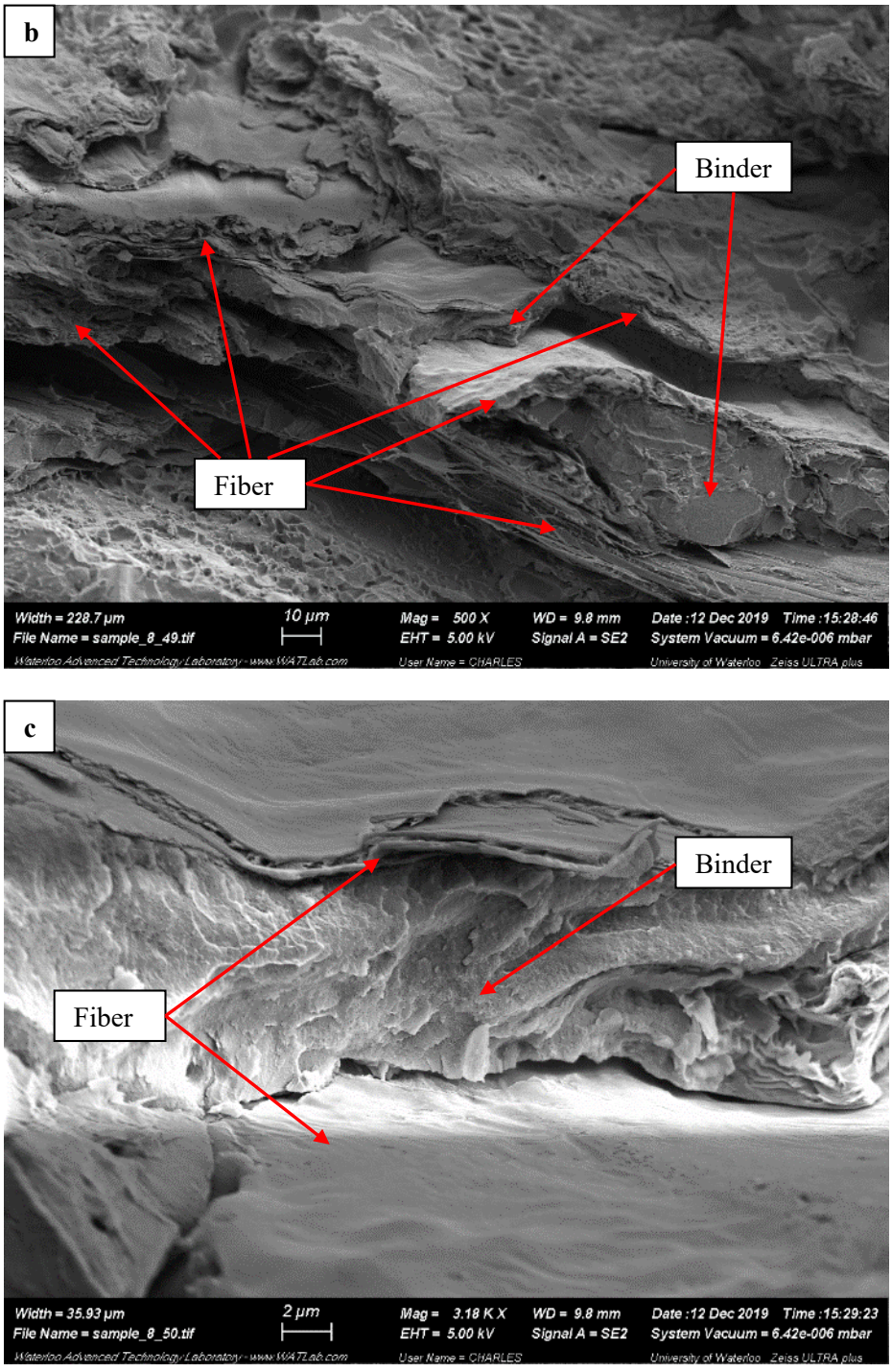

Figure 7.45 Structure of cured binder (a) and dispersion of binder (b) (c) on fracture surface of pressboard containing hot-water treated #2 and 20% **Thermoplastic #5**

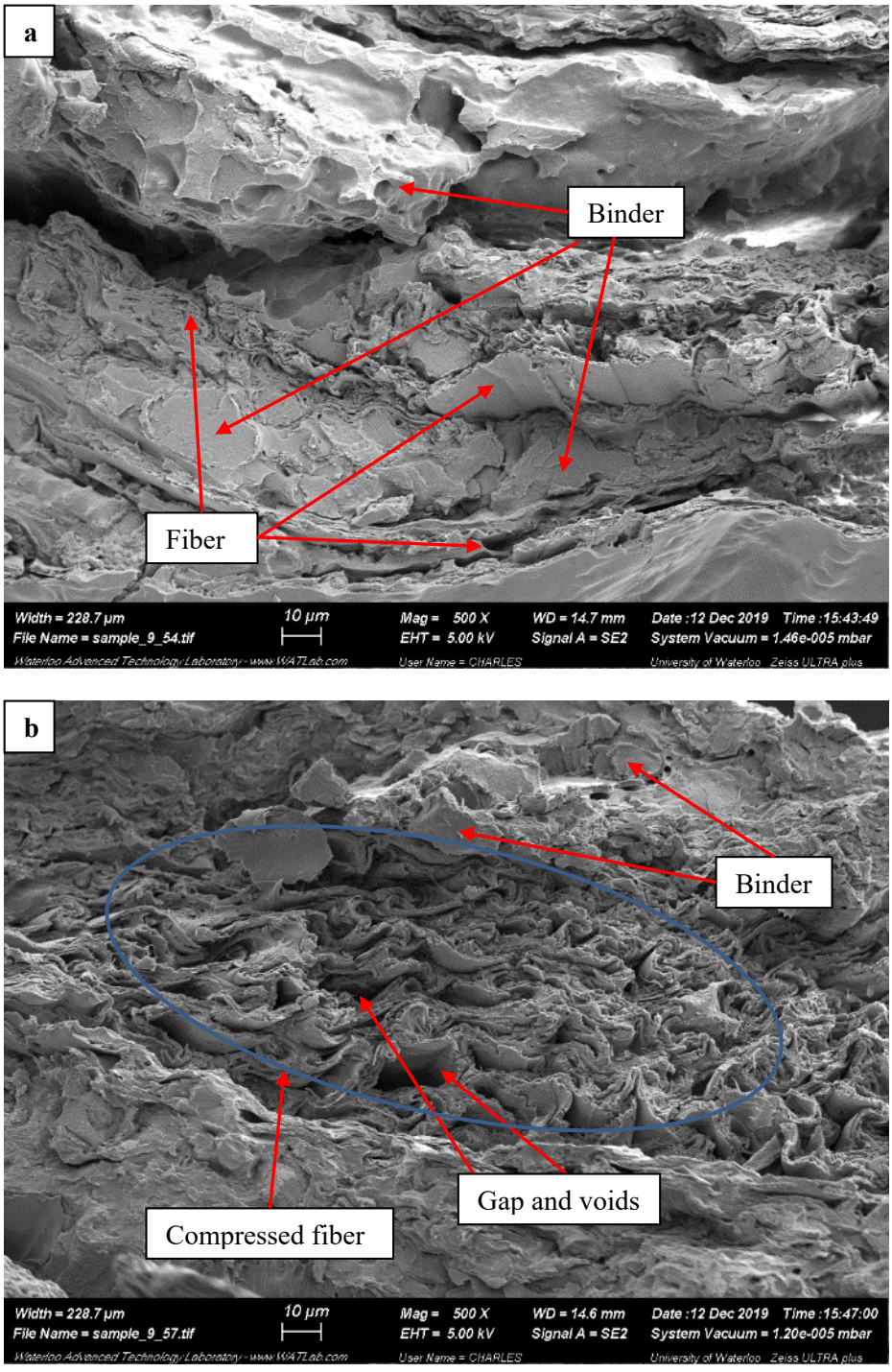

Figure 7.46 Binder dispersion (a) and unfilled voids in compressed fiber (b) on fracture surface of pressboard containing NaOH treated #2 and 20% **Thermoplastic #5**

Summary

The structure of composite pressboards was observed in all combinations of wheat straw and binder systems. The compaction of the material in composite pressboards was formed due to the manufacturing pressure. This compaction results in reduction of distance between the fibers and consequently in an increment of density. No fiber damages were observed in pressboard made at maximum compression force of 45,000 lbf.

The good adhesion of fiber-polymer was evident. The contribution of binder-reinforcement interfacial failure to the overall composite failure mechanism was very little. The investigations of fracture surfaces of composites with the electron scanning microscope showed that more simultaneous failures of the fiber and binder were observed at the fracture surface of the composite pressboards. The materials show a smooth fracture, more dominated by simultaneous breakage of fiber and binder than by interfacial failure indicated by fiber pull-out or clear "mold" marks on binder. No clear evidences of failure were observed occurring at the binder-reinforcement interface in the majority of pressboards studied. In some cases even a fiber fracture in longitudinal direction can be found in Figure 7.40 (a). This indicates a good adhesion between fiber and binder since fracture does not occur along the interface between them but inside the fiber. The load transfer from the binder into the fiber is ensured. Another indication of good fiber-matrix adhesion is observed in most of images. As examples, Figure 7.40 (c), Figure 7.41 (b), Figure 7.42 (c) and Figure 7.45 (a) show that there is no visible space in the interface matrix-fiber. These observations indicate very good adhesion between wheat straw and the Acrodur binders.

The good adhesion between wheat straw fiber and Acrodur can be attributed to inherent compatibility, low viscosity which facilitates wetting and distribution and thereby justifies the improved flexural properties of the wheat straw-Acrodur composites in comparison with wheat straw-polyamide 6 or other binders as discussed previously.

The properties cured Acrodur binders exhibit are directly related to the microstructure. The higher cross-linking density, the more rigid the molecular network becomes. The microstructural characteristics results in inherent brittleness of the material, which are exhibited at fraction surfaces of pressboard containing **Thermoset #1** and **#2** in SEM micrographs. The rigidness of the molecular network after crosslinking is responsible for the brittle behavior of these composites. On the contrary,

Thermoplastic #5 exhibited plastic feature indicated by plastic deformation at the fracture, which increases the toughness of adhesion.

Furthermore, it was expected that the NaOH and hot-water treatments could improve the interfacial bonding between fiber and polymer binder by enhancing the compatibility. NaOH and hot-water treatments can alter surface chemistry and increase surface roughness at different extent. Therefore, both treatments can potentially improve the adhesion fiber-matrix. However, it seems that the fiber treatment (e.g., hot-water and NaOH treatments) did not affect the interfacial bonding between wheat straw and three types of binders. From images previously presented, it appears that the binder-fiber interface of the treated wheat straw composite pressboard is similar to the one presented by the pressboards containing untreated wheat straw. This corresponds well with the flexural strength results which indicate that no further increment on the flexural strength was observed for composites using the NaOH or hot-water treated wheat straw.

In summary, all the wheat straw-Acrodur composite pressboard showed good wetting of the fiber by the binder, good binder distribution on the fibers and strong fiber-binder interaction, no matter whether the treatments were applied. Overall, very few voids and fiber pull-outs were observed. Neither the wheat straw treatment nor addition of CNF significantly affect the interfacial bonding between wheat straw and Acrodur binders.

7.5 Conclusion

The study presented in this chapter is based on efforts to improve the mechanical and other properties of wheat straw-Acrodur composite pressboards. The chapter covers the use of treatments on wheat straw and five Acrodur binders to enhance pressboard strength properties and contains a detailed experiment procedure. The knowledge obtained in Chapter 3 is applied to treat the wheat straw raw materials. The results of kinetic study of Acordur cure reaction in Chapter 4 were employed to provide guideline for selection compression molding parameters for optimal properties of final products. The information collected in Chapter 5 was used to ensure right binder loading levels. The flexural and dielectric properties were measured. The effects of wheat straw size, treatments of wheat straw, binder type, addition of CNF, and compression molding condition (temperature, pressure and time) were systematically examined and evaluated. After a thorough discussion on the test results and evaluation on the parameters and effects of interest, and properties evaluation against previous results and pressboard standards, the major outcomes of the study and conclusions can be drawn as follows.

The primary results demonstrated that wheat straw –Acrodur composite pressboards can be used for load-bearing components by using effective Acrodur binders, appropriate treatments and processing technology and conditions. Flexural strength and modulus were significantly improved compared to previous wheat straw composites, and even to some Acrodur composites of other natural fibers with much higher mechanical properties. The fiber loading can be as high as 80%. The enhancement of **Thermoplastic #5** in the properties is remarkable. The mechanical properties are relatively satisfactory for automotive industrial and insulation of transformers. The dielectric strength is at the lower end of range of Kraft softwood based pressboards, and there is a room for further improvement for application of wheat straw in power transformer.

Chapter 8
Conclusion and Contribution

8.1 Conclusion

The knowledge created in this thesis is a contribution to the development of novel bioproducts. This thesis has successfully demonstrated how to select the formulation and the processing conditions to control the performance of the pressboard composites. This was possible because of the systematic approaches taken to investigate several phenomena controlling the process. Although it was not the scope of this thesis to directly determine an application for the pressboards, there are various potential applications of wheat straw based polymer composites that seem suitable. The potential applications may include car parts in automotive industry, insulation products in power transformer industries or boards or panels in the furniture, construction or packaging industries.

The knowledge gained from the study of chemical treatment of wheat straw, kinetics study of Acrodur curing, and study on the Acrodur adhesion strength measurement was applied and utilized in the production of wheat straw based composite pressboards. The main conclusions and the contributions of the study are highlighted as follows:

1) The effects of alkaline and hot-water treatments on the wettability of wheat straw were investigated. The results confirmed that alkaline treatment was an effective method for surface modification of wheat straw for increased surface wettability, binder absorption and surface morphology changes. The binder absorption in wheat straw reinforces the fiber itself. However alkaline treatment may cause destructive structural change. Moreover, a decrease of onset degradation temperature was observed on NaOH treated samples. The hot-water treatment resulted in moderately improved mechanical properties for some cases, which was attributed to the partial removal of water soluables. These findings were corroborated with the observations reported by other authors in wheat straw and other types of natural fibers (Herrera-Franco and Valadez-Gonzalez 2005) (Valadez-Gonzalez et al. 1999) (Islam and Pickering 2007) (Ullah et al. 2018) (Bekhta et al. 2013).

2) The cure kinetics of Acrodur and the prepegs were investigated isothermally and non-isothermally using TGA and DSC. The effects of temperature, time and pressure and the addition of CNF and wheat straw were evaluated. The characteristic temperatures, mass loss (for TGA), enthalpy (for DSC) were determined and characterized. The temperature–time dependence of the conversion was

established. The dependence of the effective activation energy on the extent of cure was yielded by applying model-free iso-conversional method for different experimental conditions, the treatment and size of wheat straw.

3) The optimal compression molding conditions were proposed for the production of the pressboards that contained Acrodur (**Thermoset #1**, **#2** and **#3**). The objective was to achieve fast curing rate with desired crosslinking level while avoiding thermal degradation. It was proposed that specifically for the production of composite pressboards, the press platen during the pressing operation must be set to temperatures above 170°C for 5–10 minutes for neat Acrodur, and above around 220°C for the prepregs to guarantee the temperatures in the mat exceed this temperature and ensure effective bonding of the binders. The aeration step during compression is necessary in order to release the contained moisture and the water produced, and this aeration also allows the cure reaction to reach high conversion.

4) Analysis of the dependence of activation energy on the conversion allowed to improve the understanding the complexity of the curing processes. These tentative explanations are proposed to explain the kinetic of cure reaction. The variation of activation energy may be explained by many factors: different chemical reactions, chemical reaction complicated by mass transfer processes associated with viscous relaxation or vitrification or thermal degradation.

5) For the first time, the dependences of Acrodur cure reaction on the temperature, time and pressure, the binder type and form with incorporation of CNF, incorporation of straw of different size, different treatment were investigated systematically. It is my hope that this kinetic study will provide a guideline for the production of Acrodur based composites and allow for the control of the degree of curing of the materials. This will permit optimization of the curing conditions thus providing a new perspective into the production of Acrodur based composites with optimized conditions.

6) The single-lap shear strength of the wheat straw joints adhered with 2%, 5%, 20% and 50% of thermoset Acrodur DS3530 was found to solely depend on strength of wheat straw itself. The dominant “stock failure” found on samples suggested that the failure was more related to weakness of wheat straw and not the adhesive (binder). Such conclusion can provide a valuable baseline for controlling distribution of binder, amount and concentration of binder, size of fiber and

compression molding conditions (temperature, force) relevant to the production of wheat straw-Acrodur pressboard.

7) The wheat straw based composite pressboards using thermoplastic polyamide 6 or thermosetting or thermoplastic Acrodur were manufactured. The flexural and dielectric properties were measured. The effects of wheat straw size, treatments of wheat straw, binder type, addition of CNF, and compression molding condition (temperature, pressure and time) were systematically examined and evaluated.

8) The best overall results of wheat straw-polyamide 6 pressboard was 26.2 and 1075.5 MPa for flexural strength and modulus respectively. The pressboards were manufactured with 40% wheat straw #1, 30% wheat stem (#3), and 30% polyamide 6 power, at 30,000 lbf, 221°C for 3 minutes. No evidence that incorporation of wheat straw stem of 3–4cm improved the flexural strength and modulus was noticed. The low strength can mainly be attributed to the poor compatibility between polyamide 6 and wheat straw and the thermal degradation caused by exposure to high temperature.

9) The flexural strength and modulus of wheat straw-Acrodur composite pressboards were significantly improved compared to the previous wheat straw composites, and even to some Acrodur composites of other natural fibers with much higher mechanical properties. The primary results demonstrated that wheat straw –Acrodur composite pressboards can be used for load-bearing components by using effective Acrodur binders, appropriate treatments and processing technology and conditions. The fiber loading can be as high as 80%.

10) The enhancement of **Thermoplastic #5** in the properties is remarkable. The mechanical properties are relatively satisfactory for automotive industrial and insulation of transformers. The best overall result for wheat straw-Acrodur pressboard was 63.0 and 6,439 MPa for flexural strength and modulus respectively. The pressboard was comprised of NaOH treated straw particle and 20% **Thermoplastic #5** and was compression molded at 200°C and 45,000 lbf for 10 minutes.

11) The best modulus was obtained from the pressboard with flexural strength and modulus being 49.1 and 9083 MPa respectively, formulated untreated straw particle and 40% **CNF-Thermoset #1** and compression molded at 170–190°C and 45,000 lbf for 10 minutes.

12) Compared to the results of the boards or panels comprised of either wheat straw or Acrodur in the previous literature (Karbstein and Weed 2015) (Islam and Miao 2013) (Liang et al. 2013) (Bolton

1994) (Karnani et al. 1997) (Amini and Tajvidi 2016) (Reck and Turk 1999) (Medina et al. 2008) (Khalfallah, Abbès, et al. 2014), the best results obtained here are at a higher level. For the potential applications, the average results obtained also exceed the requirements of medium density fiberboard and high density fiber board. According to ANSI/AHA A 208.1 and ANSI/AHA A 135, the minimum flexural strength for both are 12.41 and 23.5 MPa respectively. The best results of this project meet and exceed the standards for boards in automotive use of 52 MPa (ISO 527) for tensile strength and 3600 MPa (ISO 178) for flexural modulus.

13) However, the results were unable to fulfill the requirement for insulation pressboards used in powder transformer. According to IEC (International Electrotechnical Commission) 60641-3-1, the best result of 63 MPa flexural strength was below the requirement of (tensile) strength ≥ 100 in machine direction and ≥ 75 for across machine direction. And the dielectric strength was at the lower end of range of Kraft softwood based pressboards, and there was a room for further improvement for application of wheat straw in the power transformers.

8.2 Suggestions for Future Work

Effect of Moisture Content and pH - Due to the limited time, there were some experimental conditions, influencing factors or kinetic parameters were out the scope of this study. These parameters therefore deserve additional investigation. Some other factors that influence the cure reaction of Acrodur, such as relative humidity and pH, were not investigated in this study.

Model Fitting and Predictive Ability - There are three kinetic parameters that are activation energy, pre-exponential factor A, and model used to describe the reaction. To capture the full picture of cure reaction of Acrodur, three kinetic parameters (Ea, A, f(α) or g(α)) are needed to generate predictive thermal curves which can be used to assess the transition in terms of percent conversion, time, and temperature, and for its practical use for predicting the behavior of a substance over the range of experimental temperatures.

Improvement of Temperature Control and Application of Controlled Cooling - It is induced that the reaction rate is very sensitive to temperature, the temperature control is critical for the quality of experimental data. Therefore, temperature controlling is key criterion for evaluation of the compression molding process and thus affecting the quality of final products. However, the advantages of this procedure are inconsistence of pressboard quality due to lack of accurate control of compression

molding temperature due to the limitation of the equipment. It is believed that the product consistency and reproducibility can be significantly improved, if production process can be well-controlled.

Two-step Curing - Two step curing, i.e. first heating at lower temperature to increase thermal stability and second heating at relatively high temperature to cure the sample to desired extent of conversion, is beneficial to achieve fully developed properties at the same time of avoiding the thermal degradation.

Selection of Combination of Curing Temperature and Time According to Property Requirement - The results from kinetics study of Acrodur can be more useful in practical production of the Acrodur composites, which could either allow a reduction of the press time to a minimum without decreasing the performance of the cured material, or control degree of crosslink according to target applications.

Bibliography

Akampumuza O, Wambua PM, Ahmed A, Li W, Qin XH. 2017. Review of the applications of biocomposites in the automotive industry. Polym Compos. 38(11):2553–2569. doi:10.1002/pc.23847.

AL-Oqla FM, Sapuan SM. 2014. Natural fiber reinforced polymer composites in industrial applications: feasibility of date palm fibers for sustainable automotive industry. J Clean Prod. 66:347–354. doi:10.1016/j.jclepro.2013.10.050.

Ali A, Shaker K, Nawab Y, Jabbar M, Hussain T, Militky J, Baheti V. 2016. Hydrophobic treatment of natural fibers and their composites—a review. J Ind Text. 47(8):2153–2183. doi:10.1177/1528083716654468.

Amini E, Tajvidi M. 2016. Investigating the effect of adding cellulose nanocrystals (CNC) on the mechanical and thermal behavior of Acrodur biocomposites [PowerPoint Presentation]. University of Maine.

Amintowlieh Y, Sardashti A, Simon LC. 2012. Polyamide 6–wheat straw composites: effects of additives on physical and mechanical properties of the composite. Polym Compos.(36):1230–1241. doi:10.1002/pc.

Anderson A, Yung A, Tanaka T. 2005. Eco-friendly alternatives to wood-based particleboard.

Arbelaiz A, Fernández B, Ramos JA, Retegi A, Llano-Ponte R, Mondragon I. 2005. Mechanical properties of short flax fibre bundle/polypropylene composites: Influence of matrix/fibre modification, fibre content, water uptake and recycling. Compos Sci Technol. 65(10):1582–1592. doi:10.1016/j.compscitech.2005.01.008.

ASTM D5868: Standard test method for lap shear adhesion for fiber reinforced plastic (FRP). 2005.

Atik C, Ates S. 2012. Mass balance of silica in straw from the perspective of silica reduction in straw pulp. BioResources. 7(3):3274–3282.

Avella M, Rota G, Martuscelli E, Raimo M, Sadocco P, Elegir G, Riva R. 2000. Poly(3-hydroxybutyrate-co-3-hydroxyvalerate) and wheat straw fibre composites: thermal, mechanical properties and biodegradation behaviour. J Mater Sci. 35:829–836. doi:10.1023/A:1004773603516.

BASF SE. 2011. Acrodur - ecotechnology by BASF.

Baumann MGD, Lorenz L, Batterman S, Zhang GZ. 2000. Aldehyde emissions from particleboard and medium density fiberboard products. For Prod J. 50(9):75–82.

Behzad T, Sain M. 2005. Cure simulation of hemp fiber acrylic based composites during sheet molding process. Polym Polym Compos. 13(3):235–244.

Bekhta P, Korkut S, Hiziroglu S. 2013. Effect of pretreatment of raw material on properties of particleboard panels made from wheat straw. BioResources. 8(2000):4766–4774.

Beruto D, Barco L, Searcy AW, Spinolo G. 1980. Characterization of the porous CaO particles formed by decomposition of CaCO3 and Ca(OH)2 in vacuum. J Am Ceram Soc. 63(7-8):439–443. doi:10.1111/j.1151-2916.1980.tb10208.x.

Biagiotti J, Puglia D, Kenny JM. 2004. A review on natural fibre- based composites. part II. J Nat Fibers. 1(2):37–68. doi:10.1300/J395v01n03.

Bigg DM, Hiscock DF, Preston JR, Bradbury EJ. 1988. High performance thermoplastic matrix composites. J Thermoplast Compos Mater. 1(2):146–160. doi:10.1177/089270578800100203.

Bisanda ETN. 2000. The effect of alkali treatment on the adhesion characteristics of sisal fibres. Appl Compos Mater. 7(5):331–339. doi:10.1023/A:1026586023129.

Bledzki AK, Jaszkiewicz A, Murr M, Sperber VE, Lutzendgrf R, Reubmann T. 2008. Processing techniques for natural- and wood-fibre composites. In: Pickering KLBT, editor. Woodhead Publishing Series in Composites Science and Engineering. Woodhead Publishing. p. 163–192.

Bledzki AK, Reihmane S, Gassan J. 1996. Properties and modification methods for vegetable fibers for natural fiber composites. J Appl Polym Sci. 59(8):1329–1336. doi:10.1002/(SICI)1097-4628(19960222).

Böck F. 2014. Bambus als rohstoff - potenziale prozesstechnischer umsetzung. :30–35.

Boldizar A, Klason C, Kubát J, Näslund P, Sáha P. 1987. Prehydrolyzed cellulose as reinforcing filler for thermoplastics. Int J Polym Mater Polym Biomater. 11(4):229–262. doi:10.1080/00914038708078665.

Bolton AJ. 1994. Natural fibers for plastic reinforcement. Mater Technol. 9(1–2):12–20. doi:10.1080/10667857.1994.11785012.

Borda J, Tesléry B, Zsuga M. 2004. Biologically degradable fiber-reinforced urethane composites

from wheat straw. Polym Compos. 20:511–514. doi:10.1002/pc.10374.

Bos HL, Van Den Oever MJA, Peters OCJJ. 2002. Tensile and compressive properties of flax fibres for natural fibre reinforced composites. J Mater Sci. 37(8):1683–1692. doi:10.1023/A:1014925621252.

Braun E, Levin B. 1986. Polyesters: A review of the literature on products of combustion and toxicity. Fire Mater. 10:107–123. doi:10.1002/fam.810100304.

Brown A, Kolattukudy P. 1978. Mammalian utilization of cutin, the cuticular polyester of plants. J Agric Food Chem. 26:1263–1266. doi:10.1021/jf60219a055.

Campilho RDSG. 2016. Joint design in natural fiber composites. In: Campilho RDSG, editor. Natural fiber composites. p. 279.

Campilho RDSG, Banea MD, Neto JABP, Da Silva LFM. 2013. Modelling adhesive joints with cohesive zone models: Effect of the cohesive law shape of the adhesive layer. Int J Adhes Adhes. 44:48–56. doi:10.1016/j.ijadhadh.2013.02.006.

Campilho RDSG, de Moura MFSF, Domingues JJMS. 2007. Stress and failure analyses of scarf repaired CFRP laminates using a cohesive damage model. J Adhes Sci Technol. 21(9):855–870. doi:10.1163/156856107781061477.

Carrier M, Loppinet-Serani A, Denux D, Lasnier J-M, Ham-Pichavant F, Cansell F, Aymonier C. 2011. Thermogravimetric analysis as a new method to determine the lignocellulosic composition of biomass. Biomass and Bioenergy. 35(1):298–307. doi:10.1016/j.biombioe.2010.08.067.

Célino A, Fréour S, Jacquemin F, Casari P. 2013. The hygroscopic behavior of plant fibers: a review. Front Chem. 1(January):43. doi:10.3389/fchem.2013.00043.

Chakrabarty A, Teramoto Y. 2018. Recent advances in nanocellulose composites with polymers: a guide for choosing partners and how to incorporate them. Polymers (Basel). 10(5). doi:10.3390/polym10050517.

Chen CM. 1970. Effect of extractive removal on adhesion and wettability of some tropical woods. For Prod J. 20(1):36–41.

Chen P, Lu C, Yu Q, Gao Y, Li J, Li X. 2006. Influence of fiber wettability on the interfacial adhesion of continuous fiber-reinforced PPESK composite. J Appl Polym Sci. 102(3):2544–2551. doi:10.1002/app.24681.

Chen Y, Sun L, Chiparus O, Negulescu I, Yachmenev V, Warnock M. 2005. Kenaf/ramie composite for automotive headliner. J Polym Environ. 13(2):107–114. doi:10.1007/s10924-005-2942-z.

Chen Y, Zheng J, Li H, Zhang ZJ. 2015. The synthesis of styrene acrylate emulsion and its application in xerographic paper. J Polym Eng. 35(3):199–207. doi:10.1515/polyeng-2014-0058.

Chestee SS, Poddar P, Sheel TK, Mamunur Rashid M, Khan RA, Chowdhury AMS. 2017. Short jute fiber reinforced polypropylene composites: effect of nonhalogenated fire retardants. Bucio E, editor. Adv Chem. doi:10.1155/2017/1049513.

Christensen R, Robitschek P, Stone J. 1981. Formaldehyde emission from particleboard. Holz als Roh- und Werkst. 39(6):231–234. doi:10.1007/BF02606276.

Cooper PA, Balatinecz JJ. 1999. Looking beyond 2005: product developments required. In: Spelter BW, editor. Global Panel Based Conference, Kuala Lumpur. p. 90–108.

Curfman GE. 2011. Sunshade for vehicles. United States Pat. doi:US 2010/0311130 Al.

Dakar M. 2015. Challenges of ethannol production from lignocellulosic biomass. Katzen Int Inc Technol Eng.:1–45.

Dalen H, Shorma TD. 1996. The manufacture of particleboard from wheat straw. In: Wolcott MP, Miklosko LC, Lentz MT, editors. Proceedings of the 30th international particle-board/composite material Symposium, Washington State University, Pullman, WA. p. 191–196.

Daniel-da-Silva AL, Bordado JCM, Martín-Martínez JM. 2010. Use of isoconversional methods to analyze the cure kinetics of isocyanate-ended quasi-prepolymers with water. J Appl Polym Sci. 116(5):2658–2667. doi:10.1002/app.24914.

Davies GC, Bruce DM. 1998. Effect of environmental relative humidity and damage on the tensile properties of flax and nettle fibers. Text Res J. 68(9):623–629. doi:10.1177/004051759806800901.

Le Digabel F, Boquillon N, Dole P, Monties B, Averous L. 2004. Properties of thermoplastic composites based on wheat-straw lignocellulosic fillers. J Appl Polym Sci. 93(1):428–436. doi:10.1002/app.20426.

Dufresne A, Dupeyre D, Vignon MR. 2000. Cellulose microfibrils from potato tuber cells: processing and characterization of starch-cellulose microfibril composites. J Appl Polym Sci. 76(14):2080–2092. doi:10.1002/(SICI)1097-4628(20000628)76:14.

Dweiri R, Azhari CH. 2004. Thermal and flow property–morphology relationship of sugarcane bagasse fiber-filled polyamide 6 blends. J Appl Polym Sci. 92(6):3744–3754. doi:10.1002/app.20359.

Eichner L, Scheidhauer R, Kruesemann J, Lahm M, Dittrich R, Jungmann H. 2005. Process for producing semifinished products and moldings. United States Pat.

Enanv SIS, Medical H, Ab S, Bertling S. 2008. International Standard IEC 60641-3-1. 2004.

Eroğlu H, Deniz I. 1993. Predesilication of wheat straw with NaOH. Papier. 47(11):645–650.

Evans P. 1979. Chemical and physical aspects of the interaction of sodium hydroxide with the cell wall components of straw. In: Grossbard E, editor. Straw Decay and Its Effect on Disposal and Utilization, University of Research Ltd, Shambrook, Bedford. p. 187–197.

Faruk O, Bledzki AK, Fink HP, Sain M. 2012. Biocomposites reinforced with natural fibers: 2000-2010. Prog Polym Sci. 37(11):1552–1596. doi:10.1016/j.progpolymsci.2012.04.003.

Favier V, Canova GR, Cavaillé JY, Chanzy H, Dufresne A, Gauthier C. 1995. Nanocomposite materials from latex and cellulose whiskers. Polym Adv Technol. 6(5):351–355. doi:10.1002/pat.1995.220060514.

Favier V, Chanzy H, Cavaille JY. 1995. Polymer nanocomposites reinforced by cellulose whiskers. Macromolecules. 28(18):6365–6367. doi:10.1021/ma00122a053.

Feng X, Chen J, Zhang H. 2008. Effect of high temperature alkali cooking on the constituents, structure and thermal degradation of hemp fiber. 108(6):4058–4064.

Ferreira JM, Silva H, Costa JD, Richardson M. 2005. Stress analysis of lap joints involving natural fibre reinforced interface layers. Compos Part B Eng. 36(1):1–7. doi:10.1016/j.compositesb.2004.04.011.

Flynn JH, Wall LA. 1966. A quick, direct method for the determination of activation energy from thermogravimetric data. J Polym Sci Part B Polym Lett. 4(5):323–328. doi:10.1002/pol.1966.110040504.

Franco PH, Valadez-González A. 2005. Fiber-matrix adhesion in natural fiber composites. In: Natural fbers, biopolymers, and biocomposites. CRC Press.

Friedman HL. 2007. Kinetics of thermal degradation of char-forming plastics from thermogravimetry. Application to a phenolic plastic. J Polym Sci Part C Polym Symp. 6(1):183–195.

doi:10.1002/polc.5070060121.

García R, Pizarro C, Lavín AG, Bueno JL. 2013. Biomass proximate analysis using thermogravimetry. Bioresour Technol. 139:1–4. doi:10.1016/j.biortech.2013.03.197.

Gauthier A, Derenne S, Largeau C, Dupont L, Guillon E, Dumonceau J, Aplincourt M. 2003. Comparative study of ligno-cellulosic material from wheat straw and of pure and mixed standard compounds via solid state ^{13}C NMR spectroscopy, conventional pyrolysis and TMAH thermochemolysis. J Anal Appl Pyrolysis.:277–293. doi:10.1016/S0165-2370(02)00067-0.

Gerst M, Reck B, Nordmann G. 2009. Zero-emission acrylic thermoset technology.

Godavarti S. 2005. Thermoplastic wood fiber composites. In: Natural fibers, biopolymers, and biocomposites.

Gomez-Bueso J, Westin M, Torgilsson R, Olesen PO, Simonson R. 2000. Composites made from acetylated lignocellulosic fibers of different origin. part I: properties of dry-formed fiberboards. Holz als Roh- und Werkst. 58:9–14. doi:10.1007/s001070050378.

Gordon GL, Phillips MW. 1989. Degradation and utilization of cellulose and straw by three different anaerobic fungi from the ovine rumen. Appl Environ Microbiol. 55(7):1703–1710.

Grenet J, Marais S, Legras MT, Chevalier P, Saiter JM. 2000. DSC and TSDC study of unsaturated polyester resin: influence of the promoter content. J Therm Anal Calorim. 61(3):719–730. doi:10.1023/A:1010172408643.

Grigoriou AH. 2000. Straw-wood composites bonded with various adhesive systems. Wood Sci Technol. 34(4):355–365. doi:10.1007/s002260000055.

Guenthner AJ, Lamison KR, Davis MC, Cambrea LR, Yandek GR, Mabry JM. 2011. Cure characteristics of tricyanate ester high temperature composite resins. Report No. AFRL-RZ-ED-TP-2011-029. Air Force Research Laboratory (AFMC).

Güven O, Monteiro SN, Moura EAB, Drelich JW. 2016. Re-emerging field of lignocellulosic fiber–polymer composites and ionizing radiation technology in their formulation. Polym Rev. 56(4):702–736. doi:10.1080/15583724.2016.1176037.

Habibi Y, Lucia LA, Rojas OJ. 2010. Cellulose nanocrystals: chemistry, self-assembly, and applications. Chem Rev. 110(6):3479–3500. doi:10.1021/cr900339w.

Hague J, McLauchlin A, Quinney R. 1998. Agri-materials for panel products: a technical assessment of their viability. In: 32nd International Particleboard/Composite Materials, Symposium Proceedings. p. 151–159.

Halvarsson S. 2010. Manufacture of straw MDF and fibreboards. Mid Sweden University.

Halvarsson S, Edlund H, Norgren M. 2008. Properties of medium-density fibreboard (MDF) based on wheat straw and melamine modified urea formaldehyde (UMF) resin. Ind Crops Prod. 28(1):37–46. doi:10.1016/j.indcrop.2008.01.005.

Hamilton RJ. 1995. Waxes: chemistry, molecular biology and functions. The Oily Press, Dundee.

Han G, Umemura K, Zhang M, Honda T, Kawai S. 2001. Development of high-performance UF-bonded reed and wheat straw medium-density fiberboard. J Wood Sci. 47(5):350–355. doi:10.1007/BF00766784.

Han G, Zhang C, Zhang D, Umemura K, Kawai S. 1998. Upgrading of urea formaldehyde-bonded reed and wheat straw particleboards using silane coupling agents. Japan Wood Res Soc. 44:282–286. doi:10.1007/Bf00581308.

Han JS, Rowell JS. 1997. Chemical composition of fibers. In: Rowell RM, Young RA, Rowell JK, editors. Paper and composites from agro-based resources. Taylor & Francis Inc. p. 83–134.

Hansen MA, Hidayat BJ, Mogensen KK, Jeppesen MD, Jørgensen B, Johansen KS, Thygesen LG. 2013. Enzyme affinity to cell types in wheat straw (Triticum aestivum L.) before and after hydrothermal pretreatment. Biotechnol Biofuels. 6(1):54. doi:10.1186/1754-6834-6-54.

Hardis R, Jessop JLP, Peters FE, Kessler MR. 2013. Cure kinetics characterization and monitoring of an epoxy resin using DSC, Raman spectroscopy, and DEA. Compos Part A Appl Sci Manuf. 49:100–108. doi:10.1016/j.compositesa.2013.01.021.

Harper SHT, Lynch JM. 1981. The chemical components and decomposition of wheat straw leaves, internodes and nodes. J Sci Food Agric. 32(11):1057–1062. doi:10.1002/jsfa.2740321103.

Hart-Smith LJ. 1973. Adhesive bonded single lap joints (analytical solutions for static load carrying capacity). Report No. NASA-CR-112236. NASA, United States.

He G, Yan N. 2005. Effect of moisture content on curing kinetics of pMDI resin and wood mixtures. Int J Adhes Adhes. 25(5):450–455. doi:10.1016/j.ijadhadh.2004.12.002.

Herczeg A. 1965. Wettability of wood. For Prod. 15:499–505.

Herrera-Franco PJ, Valadez-Gonzalez A. 2005. A study of the mechanical properties of short natural fiber reinforced composites. Compos Part B Eng. 36(8):597–608. doi:10.1016/j.compositesb.2005.04.001.

Hodzic A, Shanks R. 2013. Natural fibre composites: materials, processes and properties. Hodzic A, Shanks R, editors. Woodhead Publishing, Elsevier.

Hoeng F, Denneulin A, Bras J. 2016. Use of nanocellulose in printed electronics: a review. Nanoscale. 8(27):13131–13154. doi:10.1039/C6NR03054H.

Hollertz R. 2014. Dielectric properties of wood fibre components relevant for electrical insulation applications. KTH Royal Institute of Technology.

Hornsby PR, Hinrichsen E, Tarverdi K. 1997a. Preparation and properties of polypropylene composites reinforced with wheat and flax straw fibres. part I: fibre characterization. J Mater Sci. 2:443–449. doi:10.1023/A:1018521920738.

Hornsby PR, Hinrichsen E, Tarverdi K. 1997b. Preparation and properties of polypropylene composites reinforced with wheat and flax straw fibres. part II: analysis of composite microstructure and mechanical properties. J Mater Sci. 32:1009–1015. doi:10.1023/A:1018578322498.

Hsu TA, Ladisch MR, Tsao GT. 1980. Alcohol from cellulose. Chem Technol; (United States).

Inglesby MK, Gray GM, Wood DF, Gregorski KS, Robertson RG, Sabellano GP. 2005. Surface characterization of untreated and solvent-extracted rice straw. Colloids Surfaces B Biointerfaces. 43(2):83–94. doi:10.1016/j.colsurfb.2005.03.014.

Islam MS, Miao M. 2013. Optimising processing conditions of flax fabric reinforced Acrodur biocomposites. J Compos Mater. 48(26):3281–3292. doi:10.1177/0021998313508995.

Islam MS, Pickering KL. 2007. Influence of alkali treatment on the interfacial bond strength of industrial hemp fibre reinforced epoxy composites: effect of variation from the ideal stoicheometric ratio of epoxy resin to curing agent. Adv Mater Res. 29–30:319–322. doi:10.4028/www.scientific.net/AMR.29-30.319.

Islam MS, Pickering KL, Foreman NJ. 2009. Influence of alkali fiber treatment and fiber processing on the mechanical properties of hemp/epoxy composites. J Appl Polym Sci. 119:3696–3711.

doi:10.1002/app.31335.

Islam MS, Pickering KL, Foreman NJ. 2010. Influence of alkali treatment on the interfacial and physico-mechanical properties of industrial hemp fibre reinforced polylactic acid composites. Compos Part A Appl Sci Manuf. 41(5):596–603. doi:10.1016/j.compositesa.2010.01.006.

Jacobs W. 2006. Is NF always the best material choice for a product? example: an automotive doorpanel. In: Proceedings of the 6th Global Wood and Natural Fibre Composites Symposium.

Jacobson R, Caulfield D, Sears K, Underwood J. 2001. Low temperature processing of ultra-pure cellulose fibers into nylon 6 and other thermoplastics. In: Sixth International Conference on Woodfiber-Plastic Composites. p. 127–133.

Jin S, Chen H. 2007. Fractionation of fibrous fraction from steam-exploded rice straw. Process Biochem. 42:188–192. doi:10.1016/j.procbio.2006.07.030.

John Z, van Reen R. 1995. The second forest: filling the wood source gap while creating the environmental performance board of the 21st century. Mater Sci.:225–231.

Jones LHP, Milne AA. 1963. Studies of silica in the oat plant. Plant Soil. 18(2):207–220. doi:10.1007/BF01347875.

Jonoobi M, Harun J, Mathew AP, Oksman K. 2010. Mechanical properties of cellulose nanofiber (CNF) reinforced polylactic acid (PLA) prepared by twin screw extrusion. Compos Sci Technol. 70(12):1742–1747. doi:10.1016/j.compscitech.2010.07.005.

Joseleau JP, Chevalier-Billosta V, Ruel K. 2012. Interaction between microfibrillar cellulose fines and fibers: influence on pulp qualities and paper sheet properties. Cellulose. 19(3):769–777. doi:10.1007/s10570-012-9693-5.

Kairouz KC, Matthews FL. 1993. Strength and failure modes of bonded single lap joints between cross-ply adherends. Composites. 24(6):475–484. doi:10.1016/0010-4361(93)90017-3.

Kalbe M. 2007. Acrodur: an acrylate based alternative to standard thermosets? [PowerPoint Presentation] BASF Inc.

Kalbe M. 2011. Fiber composite materials of construction, particularly for roof liner structures. United States Pat. doi:US 20100322867A1.

Kang IS, Yang CQ, Wei W, Lickfield GC. 1998. Mechanical strength of durable press finished cotton

fabrics. part I: effects of acid degradation and crosslinking of cellulose by polycarboxylic acids. Text Res J. 68(11):865–870. doi:10.1177/004051759806801112.

Karbstein H, Funk J, Norton J. Lightweight bio-composites with Acrodur resin technology. [PowerPoint Presentation] BASF Inc.

Karbstein H, Weed D. 2015. Acrodur natural fiber composites. [PowerPoint Presentation] BASF Inc.

Karnani R, Krishnan M, Narayan R. 1997. Biofiber-reinforced polypropylene composites. Polym Eng Sci. 37(2):476–483. doi:10.1002/pen.11691.

Karr GS, Sun XS. 2000. Strawboard from vapor phase acetylation of wheat straw. Ind Crops Prod. 11(1):31–41. doi:10.1016/S0926-6690(99)00031-X.

Keener TJ, Stuart RK, Brown TK. 2004. Maleated coupling agents for natural fibre composites. Compos Part A Appl Sci Manuf. 35(3):357–362. doi:10.1016/j.compositesa.2003.09.014.

Khalfallah M, Abbès B, Abbès F, Guo YQ, Marcel V, Duval A, Vanfleteren F, Rousseau F. 2014. Innovative flax tapes reinforced Acrodur biocomposites: a new alternative for automotive applications. Mater Des. 64:116–126. doi:10.1016/j.matdes.2014.07.029.

Khalfallah M, Marcel V, Duval A, Abbès B, Abbès F, Guo YQ, Vanfleteren F, Rousseau F. 2014. Flax/Acrodur sandwich panel: an innovative eco-material for automotive applications. Jec Compos. 51(89):73–78.

Khalil HPSA, Kang CW, Khairul A, Ridzuan R, Adawi TO. 2008. The effect of different laminations on mechanical and physical properties of hybrid composites. J Reinf Plast Compos. 28(9):1123–1137. doi:10.1177/0731684407087755.

Klason C, Kubat J, Stromvall H-E. 1984. The efficiency of cellulosic fillers in common thermoplastics. part 1: filling without processing aids or coupling agents. Int J Polym Mater Polym Biomater. 10:159–187. doi:10.1080/00914038508078651.

Klemm D, Heublein B, Fink HP, Bohn A. 2005. Cellulose: fascinating biopolymer and sustainable raw material. Angew Chemie - Int Ed. 44(22):3358–3393. doi:10.1002/anie.200460587.

Lavoine N, Desloges I, Dufresne A, Bras J. 2012. Microfibrillated cellulose – its barrier properties and applications in cellulosic materials: a review. Carbohydr Polym. 90(2):735–764. doi:10.1016/j.carbpol.2012.05.026.

Lee KY, Aitomäki Y, Berglund LA, Oksman K, Bismarck A. 2014. On the use of nanocellulose as reinforcement in polymer matrix composites. Compos Sci Technol. 105:15–27. doi:10.1016/j.compscitech.2014.08.032.

Lee LJ, Zeng C, Cao X, Han X, Shen J, Xu G. 2005. Polymer nanocomposite foams. Compos Sci Technol. 65(15):2344–2363. doi:10.1016/j.compscitech.2005.06.016.

Lee S-B, Fasina O. 2008. TG-FTIR analysis of switchgrass pyrolysis. J Anal Appl Pyrolysis. 86(1):39–43. doi:10.13031/2013.24697.

Lesnikovich AI, Levchik S V. 1985. Isoparametric kinetic relations for chemical transformations in condensed substances (analytical survey). II: reactions involving the participation of solid substances. J Therm Anal. 30(3):677–702. doi:10.1007/BF01913614.

Li S. 2017. Fundamentals of reaction kinetics. In: Li S, editor. Reaction Engineering. Boston: Butterworth-Heinemann. p. 25–93.

Liang K, Gao Q, Shi SQ. 2013. Kenaf fiber/soy protein based biocomposites modified with poly(carboxylic acid) resin. J Appl Polym Sci. 128(2):1213–1218. doi:10.1002/app.38330.

Liu R, Yu H, Huang Y. 2005. Structure and morphology of cellulose in wheat straw. Cellulose. 12(1):25–34. doi:10.1023/B:CELL.0000049346.28276.95.

Liu W, Drzal LT, Mohanty AK, Misra M. 2007. Influence of processing methods and fiber length on physical properties of kenaf fiber reinforced soy based biocomposites. Compos Part B Eng. 38(3):352–359. doi:10.1016/j.compositesb.2006.05.003.

Liu Z, Wang F, Wang X. 2003. Surface structure and dynamic adhesive wettability of wheat straw. 36(2).

Liu Z, Wang H, Hui L. 2018. Pulping and papermaking of non-wood fibers. In: Pulp and Paper Processing. Open access peer-reviewed Edited Volume. p. 3–32.

Loxton C, Hague J. 1996. Utilization of agricultural crop materials in panel products. In: Proceeding No. 7286: The Use of Recycled Wood and Paper in Building Applications, Forest Products Society, Madison, WI.

Lu J, Wang T, Drzal LT. 2008. Preparation and properties of microfibrillated cellulose polyvinyl alcohol composite materials. Compos Part A Appl Sci Manuf. 39(5):738–746.

doi:10.1016/j.compositesa.2008.02.003.

Luo P, Yang C. 2010. Utilization of wheat straw in manufacture of particleboard. Int Conf Challenges Environ Sci Comput Eng CESCE 2010. 2:52–54. doi:10.1109/CESCE.2010.195.

Maldas DC, Kamdem DP. 1998. Surface tension and wettability of CCA-treated red maple. Wood Fiber Sci. 30(4):368–373.

Markessini E, Roffael E, Rigal L. 1997. Panels from annual plant fibers bonded with urea-formaldehyde resins. In: Proceedings of the 31th International Particleboard/Composite Materials Symposium, Pullman, Washington. p. 147–160.

Marx-Figini M. 1971. Investigations on biosynthesis of cellulose DPw and yield of cellulose of the alga valonia in the presence of colchicine. Biochim Biophys Acta. 237:75–77. doi:10.1016/0304-4165(71)90031-6.

Masłowski M, Miedzianowska J, Strzelec K. 2018. Natural rubber composites filled with cereals straw modified with acetic and maleic anhydride: preparation and properties. J Polym Environ. 26(10):4141–4157. doi:10.1007/s10924-018-1285-5.

Masseteau B, Michaud F, Irle M, Roy A, Alise G. 2014. An evaluation of the effects of moisture content on the modulus of elasticity of a unidirectional flax fiber composite. Compos Part A Appl Sci Manuf. 60:32–37. doi:10.1016/j.compositesa.2014.01.011.

Mathew AP, Dufresne A. 2002. Morphological investigation of nanocomposites from sorbitol plasticized starch and tunicin whiskers. Biomacromolecules. 3(3):609–617. doi:10.1021/bm0101769.

Matthews, F. L. Rawlings RD. 1994. Composite materials: engineering and science. Woodhead Publishing, Elsevier.

McHenry E, Stachurski ZH. 2003. Composite materials based on wood and nylon fibre. Compos Part A Appl Sci Manuf. 34(2):171–181. doi:10.1016/S1359-835X(02)00211-7.

Medina L, Schledjewski R, Schlarb AK. 2008. Process related mechanical properties of press molded natural fiber reinforced polymers. Spec Issue 12th Eur Conf Compos Mater ECCM 2006. 69(9):1404–1411. doi:10.1016/j.compscitech.2008.09.017.

Misra M, Mohanty A, Tummala P, Drzal L. 2004. Injection molded biocomposites from natural fibers and modified polyamide. Annu Tech Conf - ANTEC, Conf Proc. 2:1603–1607.

Mo X, Wang D, Sun X. 2005. Straw-based biomass and biocomposites. In: Natural fibers, bopolymers, and bocomposites. CRC Press.

Mohanty AK, Misra M, Drzal LT. 2001. Surface modifications of natural fibers and performance of the resulting biocomposites: an overview. Compos Interfaces. 8(5):313–343. doi:10.1163/156855401753255422.

Mohanty AK, Misra M, Drzal LT. 2005. Natural fibers, biopolymers, and biocomposites. Mohanty AK, Misra M, Drzal LT, editors. CRC Press.

Le Moigne N, Otazaghine B, Corn S, Angellier-Coussy H, Bergeret A. 2018. Surfaces and interfaces in natural fibre reinforced composites fundamentals, modifications and characterization.

Mondal S. 2017. Review on nanocellulose polymer nanocomposites. Polym Plast Technol Eng.:1377–1391. doi:10.1080/03602559.2017.1381253.

Moon RJ, Martini A, Nairn J, Simonsen J, Youngblood J. 2011. Cellulose nanomaterials review: structure, properties and nanocomposites. Chem Soc Rev. 40(7):3941–3994. doi:10.1039/C0CS00108B.

Mörseburg K, Chinga-Carrasco G. 2009. Assessing the combined benefits of clay and nanofibrillated cellulose in layered TMP-based sheets. Cellulose. 16(5):795–806. doi:10.1007/s10570-009-9290-4.

Mustajoki S, Leponiemi A, Dahl O. 2010. Alkaline peroxide bleaching of hot water treated wheat straw. BioResources. 5(2):808–826.

Mwaikambo LY, Ansell MP. 2002. Chemical modification of hemp, sisal, jute, and kapok fibers by alkalization. J Appl Polym Sci. 84(12):2222–2234. doi:10.1002/app.10460.

Myers GC, Hettwer PF. 1993. Insulating pressboard for electrical transformers. Forrest Prod J. 43(August 1992):49–52.

Naik S, Goud V V, Rout PK, Jacobson K, Dalai AK. 2010. Characterization of Canadian biomass for alternative renewable biofuel. Renew Energy. 35(8):1624–1631. doi:10.1016/j.renene.2009.08.033.

Nakagaito AN, Yano H. 2004. The effect of morphological changes from pulp fiber towards nano-scale fibrillated cellulose on the mechanical properties of high-strength plant fiber based composites. Appl Phys A Mater Sci Process. 78(4):547–552. doi:10.1007/s00339-003-2453-5.

Navarro M V, Murillo R, Mastral AM, Puy N, Bartroli J. 2009. Application of the distributed

activation energy model to biomass and biomass constituents devolatilization. AIChE J. 55(10):2700–2715. doi:10.1002/aic.11848.

Nordmann G, Kalbe M, Reck B, Gerst M, Norton J. 2010. Eco-friendly acrylic copolymers offering clean manufacturing , reduced VOC emissions, excellent performance. BASF Corp.

Norman DA, Robertson RE. 2003. The effect of fiber orientation on the toughening of short fiber-reinforced polymers. J Appl Polym Sci. 90(10):2740–2751. doi:10.1002/app.12913.

Nyström B, Joffe R, Långström R. 2007. Microstructure and strength of injection molded natural fiber composites. J Reinf Plast Compos. 26(6):579–599. doi:10.1177/0731684407075536.

Oksman K, Aitomäki Y, Mathew AP, Siqueira G, Zhou Q, Butylina S, Tanpichai S, Zhou X, Hooshmand S. 2016. Review of the recent developments in cellulose nanocomposite processing. Compos Part A Appl Sci Manuf. 83:2–18. doi:10.1016/j.compositesa.2015.10.041.

Oliveira V, Nunes B, Vilar R. 2010. Wetting response of KrF laser ablated polyimide surfaces. Nucl Instruments Methods Phys Res Sect B Beam Interact with Mater Atoms. 268(10):1626–1630. doi:https://doi.org/10.1016/j.nimb.2010.03.006.

Ozawa T. 1965. A new method of analyzing thermogravimetric data. Bull Chem Soc Jpn. 38(11):1881–1886. doi:10.1246/bcsj.38.1881.

Ozawa T. 1986. Non-isothermal kinetics and generalized time. Thermochim Acta. 100(1):109–118. doi:10.1016/0040-6031(86)87053-8.

Panthapulakkal S, Sain M. 2006. Injection molded wheat straw and corn stem filled polypropylene composites. J Polym Environ. 14:265–272. doi:10.1007/s10924-006-0021-8.

Panthapulakkal S, Sain M. 2007. Agro-residue reinforced high-density polyethylene composites: fiber characterization and analysis of composite properties. Compos Part A Appl Sci Manuf. 38(6):1445–1454. doi:10.1016/j.compositesa.2007.01.015.

Patil Y, Gajre B, Dusane D, Chavan S, Mishra S. 2000. Effect of maleic anhydride treatment on steam and water absorption of wood polymer composites prepared from wheat straw, cane bagasse, and teak wood sawdust using Novolac as matrix. J Appl Polym Sci. 77:2963–2967. doi:10.1002/1097-4628(20000923)77:13.

Peças P, Carvalho H, Salman H, Leite M. 2018. Natural fibre composites and their applications: a

review. J Compos Sci. 2(4):66. doi:10.3390/jcs2040066.

Pereira HPF, Rosa MDF, Cioffi MOH, Benini KCC de C, Milanese AC, Voorwald HJC, Mulinari DR. 2015. Vegetal fibers in polymeric composites : a review. Polimeros. 25(1):9–22. doi:10.1590/0104-1428.1722.

Pervaiz M, Sain M. 2004. High performance natural fiber thermoplastics for automotive interior parts. In: SAE 2004 World Congress & Exhibition.

Pollitt E. 2018. Automotive Composites. Glob Hemp Inc.

Prevost TA, Oommen T V. 2006. Cellulose insulation in oil-filled power transformers: part I - history and development. IEEE Electr Insul Mag. 22(2):5–14. doi:10.1109/MEI.2006.1618996.

Prodan EA, Pavlyuchenko MM, Prodan SA. 1976. Development of thopochemical reactions.

Pullawan T, Wilkinson AN, Eichhorn SJ. 2010. Discrimination of matrix–fibre interactions in all-cellulose nanocomposites. Compos Sci Technol. 70(16):2325–2330. doi:10.1016/j.compscitech.2010.09.013.

Pysiak J, Glinka A. 1981. Thermal decomposition of basic aluminium potassium sulphate. part I. stages of decomposition. Thermochim Acta. 44(1):21–28. doi:10.1016/0040-6031(81)80267-5.

Ramaswamy GN, Ruff CG, Boyd CR. 1994. Effect of bacterial and chemical retting on kenaf fiber quality. Text Res J. 64(5):305–308. doi:10.1177/004051759406400507.

Ramesh M, Palanikumar K, Reddy KH. 2017. Plant fibre based bio-composites: sustainable and renewable green materials. Renew Sustain Energy Rev. 79(May):558–584. doi:10.1016/j.rser.2017.05.094.

Rasyid MFA, Salim MS, Akil HM, Ishak ZAM. 2016. Optimization of processing conditions via response surface methodology (RSM) of nonwoven flax fibre reinforced Acrodur biocomposites. Procedia Chem. 19:469–476. doi:10.1016/j.proche.2016.03.040.

Rasyid MFA, Salim MS, Akil HM, Karger-Kocsis J, Mohd Ishak ZA. 2019. Non-woven flax fibre reinforced acrylic based polyester composites: The effect of sodium silicate on mechanical, flammability and acoustic properties. Express Polym Lett. 13(6):553–564. doi:10.3144/expresspolymlett.2019.47.

Raveendran K, Ganesh A, Khilar KC. 1996. Pyrolysis characteristics of biomass and biomass

components. Fuel. 75(8):987–998. doi:10.1016/0016-2361(96)00030-0.

Reading M, Dollimore D, Whitehead R. 1991. The measurement of meaningful kinetic parameters for solid state decomposition reactions. J Therm Anal. 37(9):2165–2188. doi:10.1007/BF01905585.

Reck B, Turk J. 1999. Thermally curable aqueous acrylic resins - a new class of duroplastic binders for wood and natural fibers. Angew Makromol Chemie. 272(4754):5–10.

Reddy N, Yang Y. 2005a. Long natural cellulosic fibers from cornhusks: Structure and properties. AATCC Rev. 5:24–27.

Reddy N, Yang Y. 2005b. Properties and potential applications of natural cellulose fibers from cornhusks. Green Chem. 7(4):190–195. doi:10.1039/b415102j.

Reddy N, Yang Y. 2007. Preparation and Characterization of Long Natural Cellulose Fibers from Wheat Straw. Agric Food Chem. 2007(55):8570–8575.

Reising AR, Moon R, Youngblood J. 2012. Effect of particle alignment on mechanical properties of neat cellulose nanocrystal films. J Sci Technol For Prod Process. 2:32–41.

Rexen F. 1975. Stroh als rohstoffimaterial für spanplatten. Holz Zentralblatt. 101(34):471–472.

Robson D, Hague J. 1993. The properties of straw fibre. In: Straw, A Valuable Raw Material, Pira International Silsoe Research Institute Joint Conference, Leatherhead, UK. p. 3.

Roffael E, Dix B, Schneider T. 2007. Influence of pulping process on the emission of formaldehyde and volatile organic acids from pulps and medium density fibreboards (MDF). Holz als Roh- und Werkst. 65:145–148. doi:10.1007/s00107-006-0141-9.

Rowell RM. 1992. Opportunities for lignocellulosic materials and composites. In: Emerging technologies for materials and chemicals from biomass: Proceedings of symposium; 1990 August 26-31; Washington, DC. p. 12–27.

Rowell RM. 2008. Natural fibres: types and properties. In: Pickering KLBT, editor. Properties and Performance of Natural-Fibre Composites. Woodhead Publishing. p. 3–66.

Rowell RM, Han JS, Rowell JS. 2000. Characterization and factors effecting fiber properties. Nat Polym an Agrofibers Compos.:115–134.

Rowell RM, Sanadi AR, Caulfield DF, Jacobson RE. 1997. Utilization of natural fibers in plastic

vomposites: problems and opportunities. Lignocellul Compos.:23–51.

Rowell RM, Tillman AM, Simonson R. 1986. A simplified procedure for the acetylation of hardwood and softwood flaxes for flakeboard production. J Wood Chem Technol. 6(3):427–448. doi:10.1080/02773818608085236.

Rowell RM, Young RA, Rowell JK. 1997. Paper and composites from agro-based resources. CRC Lewis Publ Raton/New York/Tokyo.

Saheb DN, Jog JP. 1999. Natural fiber polymer composites: a review. Adv Polym Technol. 18(4):351–363. doi:10.1002/(SICI)1098-2329(199924)18.

Saka S, Goring D. 1988. The distribution of lignin in white birch wood as determined by bromination with TEM-EDXA. Holzforschung. 42:149–153. doi:10.1515/hfsg.1988.42.3.149.

Sam-Brew SA. 2017. The use of flax and hemp resource for particleboard. The University of British Columbia.

Sanghi R. 2003. Chemistry behind the life of a transformer. Resonance. 8(6):17–23. doi:10.1007/BF02837865.

Sangster AG, Hodson M. 1986. Silica in higher plants. Ciba Found Symp. 121:90–107. doi:10.1002/9780470513323.ch6.

Santos PA, Spinacé MAS, Fermoselli KKG, De Paoli MA. 2007. Polyamide-6/vegetal fiber composite prepared by extrusion and injection molding. Compos Part A Appl Sci Manuf. 38(12):2404–2411. doi:10.1016/j.compositesa.2007.08.011.

Sardashti A. 2009. Wheat Straw-Clay-Polypropylene Hybrid Composites. The University of Waterloo.

Sauter SL. 1996. Developing composites from wheat straw. In: Proceedings, 30th International Particleboard/Composite Materials Symposium.Washington State University, Washington, USA.

Sbirrazzuoli N. 2019. Advanced isoconversional kinetic analysis for the elucidation of complex reaction mechanisms: a new method for the identification of rate-limiting steps. Molecules. 24(9). doi:10.3390/molecules24091683.

Sbirrazzuoli N, Vyazovkin S. 2002. Learning about epoxy cure mechanisms from isoconversional analysis of DSC data. Thermochim Acta. 388(1–2):289–298. doi:10.1016/S0040-6031(02)00053-9.

Scheikl M, Dunky M. 1998. Measurement of dynamic and staue contact angles on wood for the determination of its surface tension and the penetration of liquids into the wood surface. Holzforschung. 52:89. doi:10.1515/hfsg.1998.52.1.89.

Schmidt A, Mallon S, Bjerre A, Hvilsted S, Lawther M. 2011. Comparison of the chemical properties of wheat straw and beech fibers following alkaline wet oxidation and laccase treatments. J Wood Chem Technol. 22(1):39–53. doi:10.1081/WCT-120004433.

Scott K. 1995. Separation of liquid mixtures/pervaporation. In: Scott K, editor. Handbook of Industrial Membranes. Elsevier Science. p. 331–351.

Shankar RS, Srinivasan SA, Shankar S, Rajasekar R, Kumar RN, Kumar PS. 2014. Review article on wheat flour/wheat bran/wheat husk based bio composites. Int J Sci Res Publ. 4(4):1–9.

Sharp JG. 2004. Formaldehyde – the big issue. In: Proceedings of the 8th European Panel Symposium, Llandudno, Wales, UK, October 13-15 2004, Llandudno. p. 21–25.

Shen J, Liu Z, Li J, Niu J. 2011. Wettability changes of wheat straw treated with chemicals and enzymes. J For Res. 22(1):107–110. doi:10.1007/s11676-011-0134-3.

Shi SQ, Gardner DJ. 2001. Dynamic adhesive wettability of wood. Wood Fiber Sci. 33(1):58–68.

Shuda M, Drzal L, Ray D, Mohanty A, Misra M. 2008. Natural-fiber composites in the automotive sector. In: Properties and Performance of Natural-Fibre Composites. Woodhead Publishing, Elsevier. p. 221–268.

Singh S, Dutt D, Tyagi CH. 2011. Complete characterization of wheat straw (Triticum aestivum PBW-343 L. Emend. Fiori & PAOL.) - a renewable source of fibres for pulp and paper making. BioResources. 6(1):154–177. doi:10.15376/biores.6.1.154-177.

Siró I, Plackett D. 2010. Microfibrillated cellulose and new nanocomposite materials: a review. Cellulose. 17(3):459–494. doi:10.1007/s10570-010-9405-y.

Soroushian P, Aouadi F, Chowdhury H, Nossoni A, Sarwar G. 2004. Cement-bonded straw board subjected to accelerated processing. Cem Concr Compos. 26:797–802. doi:10.1016/j.cemconcomp.2003.06.001.

Stewart R. 2010. Automotive composites offer lighter solutions. Reinf Plast. 54(2):22–28. doi:10.1016/S0034-3617(10)70061-8.

Summerscales J, Virk A, Hall W. 2010a. A review of bast fibres and their composites. part 1: fibres as reinforcements. Compos Part A Appl Sci Manuf. 44(1):132–139. doi:10.1016/j.compositesa.2012.08.018.

Summerscales J, Virk A, Hall W. 2010b. A review of bast fibres and their composites. part 2: composites. Compos Part A Appl Sci Manuf. 44(1):1336–1344. doi:10.1016/j.compositesa.2012.08.018.

Sun RC. 2010a. Hemicelluloses. In: Cereal straw as a resource for sustainable bomaterials and biofuels. Elsevier Science. p. 73–130.

Sun RC. 2010b. Introduction. In: Cereal straw as a resource for sustainable bomaterials and biofuels. Elsevier Science. p. 1–11.

Sun RC. 2010c. Extractives. In: Cereal straw as a resource for sustainable bomaterials and biofuels. Elsevier Science. p. 49–72.

Sun RC, Salisbury D, Tomkinson J. 2003. Isolation and characterization of hot water-soluble lipophilic extractives from wheat straw. part II: spectroscopic and thermal characterization. Wood Fiber Sci. 35(3):469–477.

Sun RC, Sun XF. 2002. Fractional and structural characterization of hemicelluloses isolated by alkali and alkaline peroxide from barley straw. Carbohydr Polym. 49:415–423. doi:10.1016/S0144-8617(01)00349-6.

Sun RC, Tomkinson J. 2004. Essential guides for isolation/purification of polysaccharides. Encycl Sep Sci.:4568–4574. doi:10.1016/b0-12-226770-2/07271-9.

Szcześniak L, Rachocki A, Tritt-Goc J. 2008. Glass transition temperature and thermal decomposition of cellulose powder. Cellulose. 15:445–451. doi:10.1007/s10570-007-9192-2.

Tamhankar SS, Doraiswamy LK. 1979. Analysis of solid-solid reactions : a review. AIChE J. 25(4):561–582.

Tayeb AH, Amini E, Ghasemi S, Tajvidi M. 2018. Cellulose nanomaterials-binding properties and applications: a review. Molecules. 23(10):1–24. doi:10.3390/molecules23102684.

Theander O, Aman P. 1984. Anatomical and chemical characteristics. In: Sundstol F, Owen E, editors. Straws and other fibrous byproducts as feed. Elsevier, Amsterdam. p. 45–78.

Thielemans W, Wool RP. 2004. Butyrated kraft lignin as compatibilizing agent for natural fiber reinforced thermoset composites. Compos Part A Appl Sci Manuf. 35(3):327–338. doi:10.1016/j.compositesa.2003.09.011.

Thygesen A, Oddershede J, Lilholt H, Thomsen AB, Ståhl K. 2005. On the determination of crystallinity and cellulose content in plant fibers. Cellulose. 12(6):563. doi:10.1007/s10570-005-9001-8.

Turbak AF, Snyder FW, Sandberg KR. 1983. Microfibrillated cellulose, a new cellulose product: properties, uses and commercial potential. J Appl Polym Sci Appl Polym Symp. 37.

Ullah S, Pakkanen H, Lehto J, Alén R. 2018. A comparable study on the hot-water treatment of wheat straw and okra stalk prior to delignification. Biomass Convers Biorefinery. 8(2):413–421. doi:10.1007/s13399-018-0306-x.

Ummartyotin S, Sain M. 2014. Preparation of a cellulose and water-based resin composite. Mater Lett. 123:70–74. doi:10.1016/j.matlet.2014.01.143.

Valadez-Gonzalez A, Cervantes-Uc JM, Olayo R, Herrera-Franco PJ. 1999. Effect of fiber surface treatment on the fiber-matrix bond strength of natural fiber reinforced composites. Compos Part B Eng. 30(3):309–320. doi:10.1016/S1359-8368(98)00054-7.

Vedoy DLR. 2012. Development of methodologies for improving thermal stability of plant fibers for application in thermoplastic composites. The University of Waterloo.

Volynets B, Dahman Y. 2011. Assessment of pretreatments and enzymatic hydrolysis of wheat straw as a sugar source for bioprocess industry. Energy Environ. 2(3):427–446.

Vyazovkin S. 2000. Kinetic concepts of thermally stimulated reactions in solids: a view from a historical perspective. Int Rev Phys Chem. 19(1):45–60. doi:10.1080/014423500229855.

Vyazovkin S. 2015. Isoconversional kinetics of thermally stimulated processes. Springer Science & Business Media.

Vyazovkin S. 2016. A time to search: finding the meaning of variable activation energy. Phys Chem Chem Phys. 18(28):18643–18656. doi:10.1039/c6cp02491b.

Vyazovkin S V, Goryachko VI, Lesnikovich AI. 1992. An approach to the solution of the inverse kinetic problem in the case of complex processes. part III: parallel independent reactions. Thermochim

Acta. 197(1):41–51. doi:https://doi.org/10.1016/0040-6031(92)87037-B.

Wan T, Hu ZW, Ma XL, Yao J, Lu K. 2008. Synthesis of silane monomer-modified styrene–acrylate microemulsion coatings by photopolymerization. Prog Org Coatings. 62(2):219–225. doi:10.1016/j.porgcoat.2007.11.006.

Wangaard FF. 1979. Wood: its structure and properties. University Park, Pa.

White NM, Ansell MP. 1983. Straw-reinforced polyester composites. J Mater Sci. 18(5):1549–1556.

Wolcott M, Smith P. 2004. Opportunities and challenges for wood-plastic composites in structural applications. Proc Prog Wood Fiber Plast Compos.:1–10.

Wötzel K, Wirth R, Flake M. 1999. Life cycle studies on hemp fibre reinforced components and ABS for automotive parts. Angew Makromol Chemie. 272(4763):121–127. doi:10.1002/(SICI)1522-9505(19991201)272:1.

Wu XF, Dzenis YA. 2006. Droplet on a fiber: geometrical shape and contact angle. Acta Mech. 185(3–4):215–225. doi:10.1007/s00707-006-0349-0.

Wu Y. 1991. The cellulose chemistry on plant. Light lndustry Publication.

Wu Z, Wang S, Zhao J, Chen L, Meng H. 2014. Synergistic effect on thermal behavior during co-pyrolysis of lignocellulosic biomass model components blend with bituminous coal. Bioresour Technol. 169:220–228. doi:https://doi.org/10.1016/j.biortech.2014.06.105.

Xie H, Liu B, Yuan Z, Shen J, Cheng R. 2004. Cure kinetics of carbon nanotube/tetrafunctional epoxy nanocomposites by isothermal differential scanning calorimetry. J Polym Sci Part B Polym Phys. 42:3701–3712. doi:10.1002/polb.20220.

Xu F. 2010. Structure , ultrastructure , and chemical composition. In: Cereal straw as a resource for sustainable biomaterials and biofuels. Elsevier Science. p. 9–47.

Xu X. 2008. Cellulose fiber reinforced nylon 6 or nylon 66 composites. Georgia Institute of Technology.

Yahya MB, Lee HV, Abd Hamid SB. 2015. Preparation of nanocellulose via transition metal salt-catalyzed hydrolysis pathway. BioResources. 10(4):7627–7639. doi:10.15376/biores.10.4.7627-7639.

Yahya MN, Daniel D, Chin VS, Kamarudin SH, Chuah L. 2017. The potential of natural fibres for

automotive sector - review. In: 2017 IOP Conf. Ser.: Mater. Sci. Eng. 252.

Yang C, Shen Z, Yu G, Wang J. 2008. Effect and aftereffect of γ radiation pretreatment on enzymatic hydrolysis of wheat straw. Bioresour Technol. 99:6240–6245. doi:10.1016/j.biortech.2007.12.008.

Yang CQ, Qian L. 2001. Mechanical strength of durable press finished cotton fabrics. part IV: abrasion resistance. Text Res J. 71(6):543–548. doi:10.1177/004051759806801112.

Yang H, Yan R, Chen H, Lee DH, Zheng C. 2007. Characteristics of hemicellulose, cellulose and lignin pyrolysis. Fuel. 86(12–13):1781–1788. doi:10.1016/j.fuel.2006.12.013.

Yang H, Yan R, Chen H, Zheng C, Lee DH, Liang DT. 2006. In-depth investigation of biomass pyrolysis based on three major components: hemicellulose, cellulose and lignin. Energy & Fuels. 20(1):388–393. doi:10.1021/ef0580117.

Yang H, Yan R, Chin T, Liang DT, Chen H, Zheng C. 2004. Thermogravimetric analysis−Fourier transform infrared analysis of palm oil waste pyrolysis. Energy and Fuels. 18(6):1814–1821. doi:10.1021/ef030193m.

Yang HS, Kim DJ, Kim HJ. 2003. Rice straw-wood particle composite for sound absorbing wooden construction materials. Bioresour Technol. 86:117–121. doi:10.1016/S0960-8524(02)00163-3.

Yang HS, Kim DJ, Lee YK, Kim HJ, Jeon JY, Kang CW. 2004. Possibility of using waste tire composites reinforced with rice straw as construction materials. Bioresour Technol. 95:61–65. doi:10.1016/j.biortech.2004.02.002.

Yang HS, Wolcott MP, Kim HS, Kim S, Kim HJ. 2007. Effect of different compatibilizing agents on the mechanical properties of lignocellulosic material filled polyethylene bio-composites. Compos Struct. 79(3), 369.

Yao F, Wu Q, Lei Y, Guo W, Xu Y. 2008. Thermal decomposition kinetics of natural fibers: Activation energy with dynamic thermogravimetric analysis. Polym Degrad Stab. 93(1):90–98. doi:10.1016/j.polymdegradstab.2007.10.012.

Yasin M, Bhutto AW, Bazmi AA, Karim S. 2010. Efficient utilization of rice-wheat straw to produce value-added composite products. Int J Chem Environ Eng. 1(2):136–143.

Zawadzki J, Bretsznajder S. 1938. Some remarks on the mechanism of reactions of the type: solid=solid + gas. Trans Faraday Soc. 34(0):951–959. doi:10.1039/TF9383400951.

Zhang C, Liu Y, Liu S, Li H, Huang K, Pan Q, Hua X, Hao C, Ma Q, Lv C, et al. 2009. Crystalline behaviors and phase transition during the manufacture of fine denier PA6 fibers. Sci China Ser B Chem. 52(11):1835. doi:10.1007/s11426-009-0242-5.

Zhang D, Milanovic NR, Zhang Y, Su F, Miao M. 2014. Effects of humidity conditions at fabrication on the interfacial shear strength of flax/unsaturated polyester composites. Compos Part B Eng. 60:186–192. doi:10.1016/j.compositesb.2013.12.031.

Zhang J, Xu X, Zhou D. 2004. Application of FTIR method in chemical analysis of hot- water treated wheat straw. Journa1 Nanjing For Univ Natura1 Sci Ed. 28:31–33.

Zhang Y, Lu X, Pizzi A, Delmotte L. 2003. Wheat straw particleboard bonding improvements by enzyme pretreatment. Holz als Roh - und Werkst. 61(1):49–54. doi:10.1007/s00107-002-0349-2.

Zisman WA. 2009. Relation of the equilibrium contact angle to liquid and solid constitution. Contact Angle, Wettability, Adhes. 43:1–51. doi:10.1021/ba-1964-0043.ch001.

Appendix A

Treatment and Wettibility

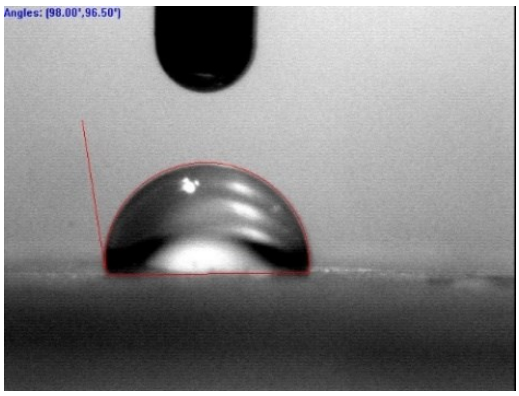

98.00°@0 sec

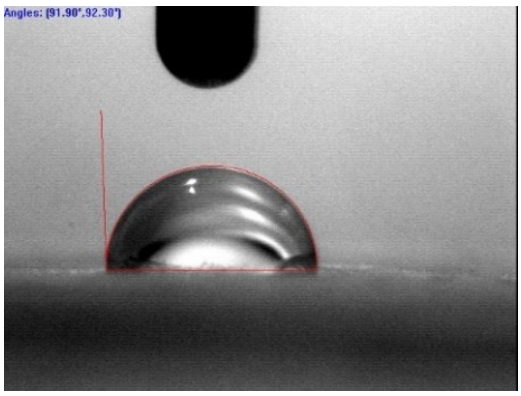

91.90°@60 sec

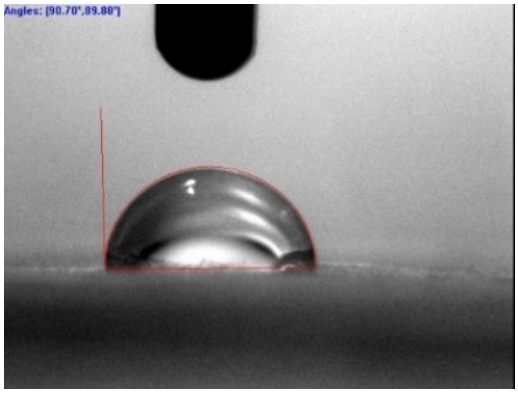

90.07°@120 sec

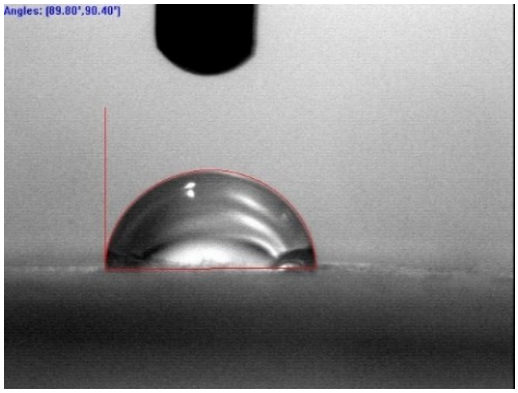

89.80°@180 sec

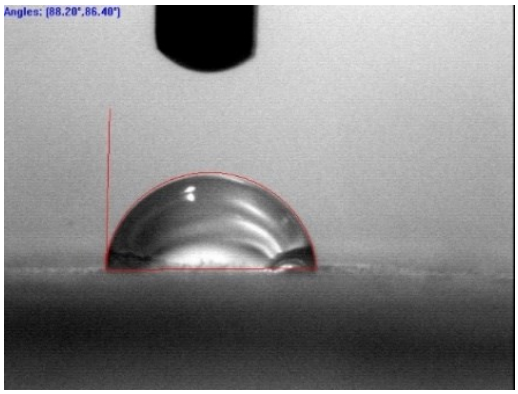

88.20°@240 sec

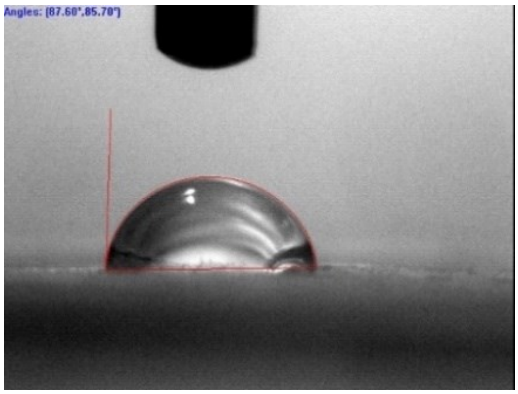

87.60°@300 sec

Figure 8.1 Contact angles measured at 0, 60, 120, 180, 240 and 300 seconds
Substrate: untreated stem exterior; testing medium: Acrodur 3530

Table 8.1 Apparent initial contact angle results (pooled mean)

Straw Part	Surface	Test Media	Initial Contact Angle (°, degree)		
			Untreated	Hot-water treated	NaOH treated
Stem	Exterior	DI water	89.8±3.53	89.0±3.71	48.5±4.80
		Acrodur DS3530	82.6±2.45	87.5±3.50	59.4±3.34
	Interior	DI water	24.5±5.92	44.0±4.82	33.9±3.61
		Acrodur DS3530	49.5±2.96	67.6±5.72	45.5±2.35
Sheath	Exterior	DI water	91.0±4.21	92.8±2.43	64.2±6.74
		Acrodur DS3530	81.0±2.79	95.1±1.52	81.5±3.58
	Interior	DI water	88.6±3.25	81.8±2.37	65.9±8.07
		Acrodur DS3530	81.9±2.20	85.8±1.29	74.6±5.62

Paired Comparison

To better compare the experiments and draw a more meaningful conclusion, a "paired" comparison method was introduced. The thought behind this method is that the comparison happens among the specimens from the same pieces of wheat straw and treated differently, therefore, the variations are mainly from the treatments as illustrated in Table 8.2.

Table 8.2 Comparison between "pooled" and "paired" comparison methods

	Pooled comparison	Paired comparison
Variation source	Treatment	Treatment
	Sample variation	

Figure 8.2, Figure 8.3, Figure 8.4 and Figure 8.5 representatively show the initial contact angles of sample #1, #3, #5 and #6 with treatments, anatomical parts, surfaces and testing media as parameters. The initial contact angle results for other samples are included in 0. The great variations are observed in sample to sample comparison. For example, for untreated stem exterior-DI water pair, the contact angles measured for sample #1, #3, #5 and #6 were 90.13°, 69.37°, 57.06°, and 86.62°, which represented the standard deviation as great as 20.37%. This is also justifying why doing "paired" comparison is more meaningful than "pooled" one by excluding the variations due to sample-to-sample difference.

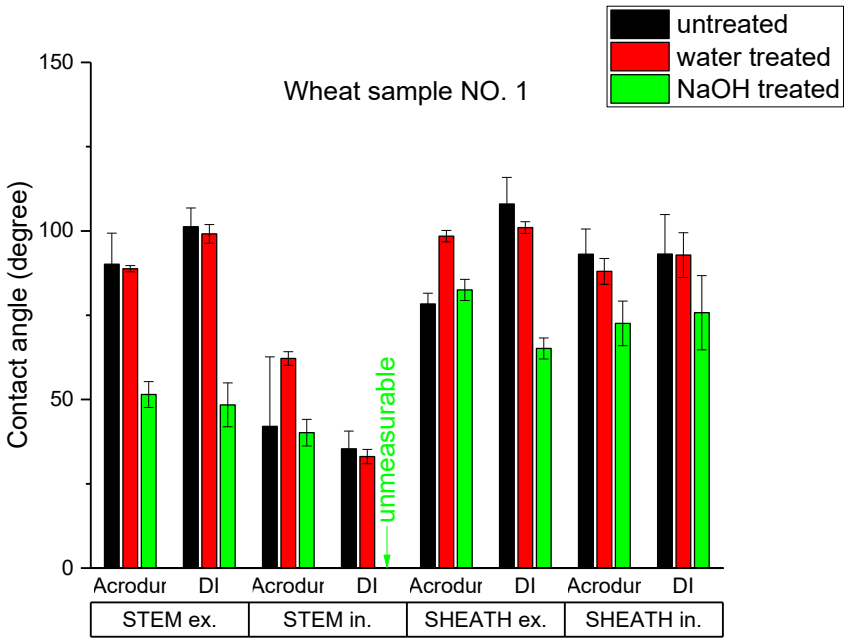

Figure 8.2 Contact angle comparison within sample #1

Within a single sample, the same trends as in the "pooled" results were found for the "paired' results. Stem interior displayed much smaller contact angle for these four samples than all other three surfaces. NaOH treatment significantly decreased the contact angles. Hot-water treatment didn't exhibit significant effect on wettability of four surfaces, while increased contact angle was attributed to washing off the impurities on the surface. Therefore, it is reasonable to conclude that NaOH solution is an effective treatment for wettability improvement of both Acrodur and DI on wheat straw. Still, the effect of two test media was found similar on each surface for all surfaces.

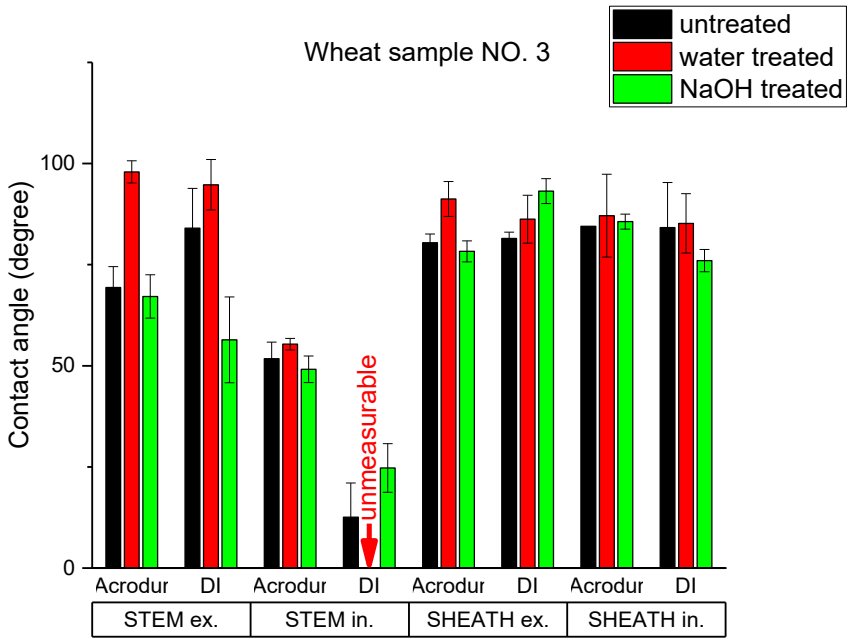

Figure 8.3 Contact angle comparison within sample #3

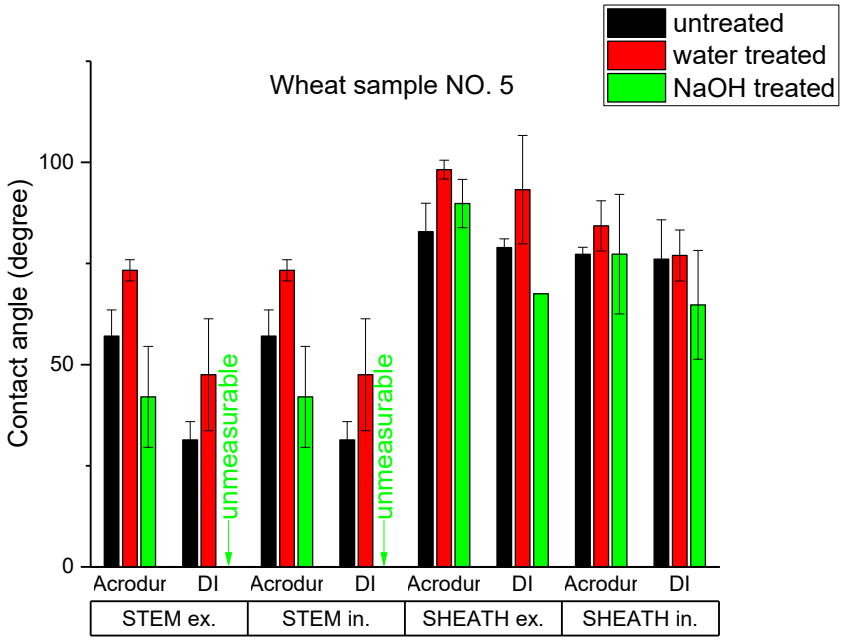

Figure 8.4 Contact angle comparison within sample #5

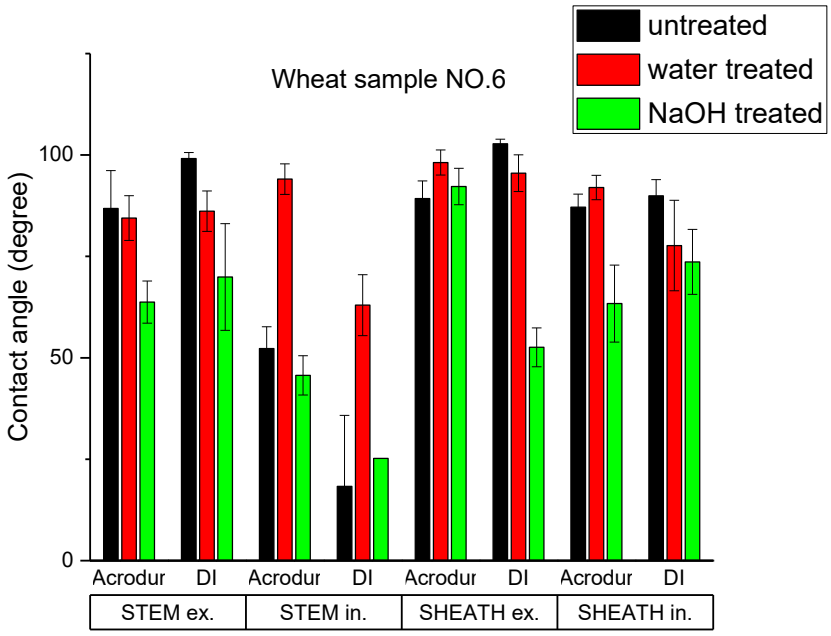

Figure 8.5 Contact angle comparison within sample #6

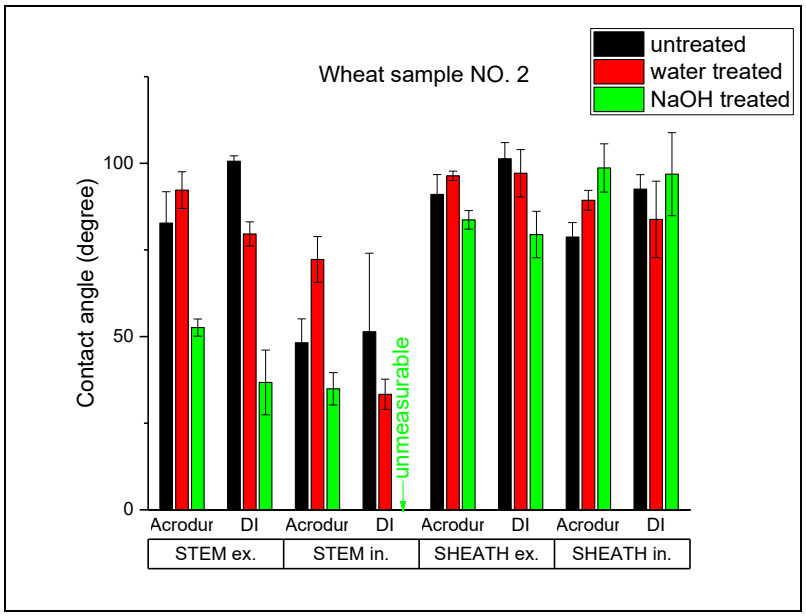

Figure 8.6 Contact angle comparison within sample #2

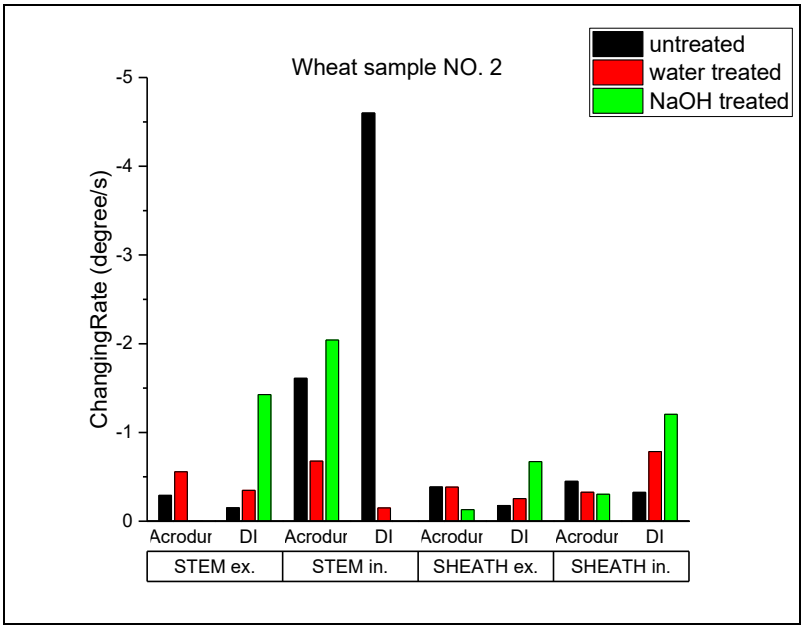

Figure 8.7 *K-value* result for sample # 2

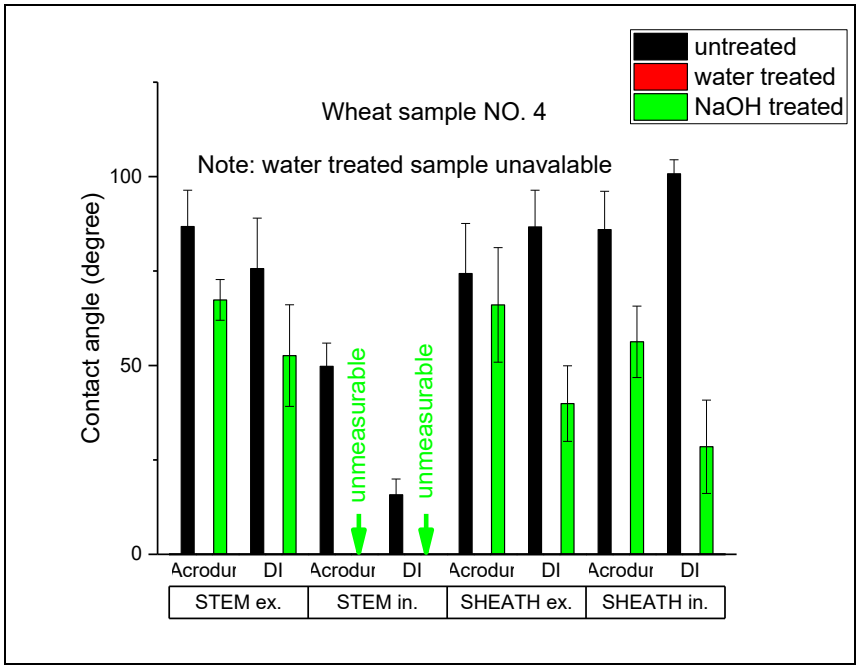

Figure 8.8 Contact angle comparison within sample #4

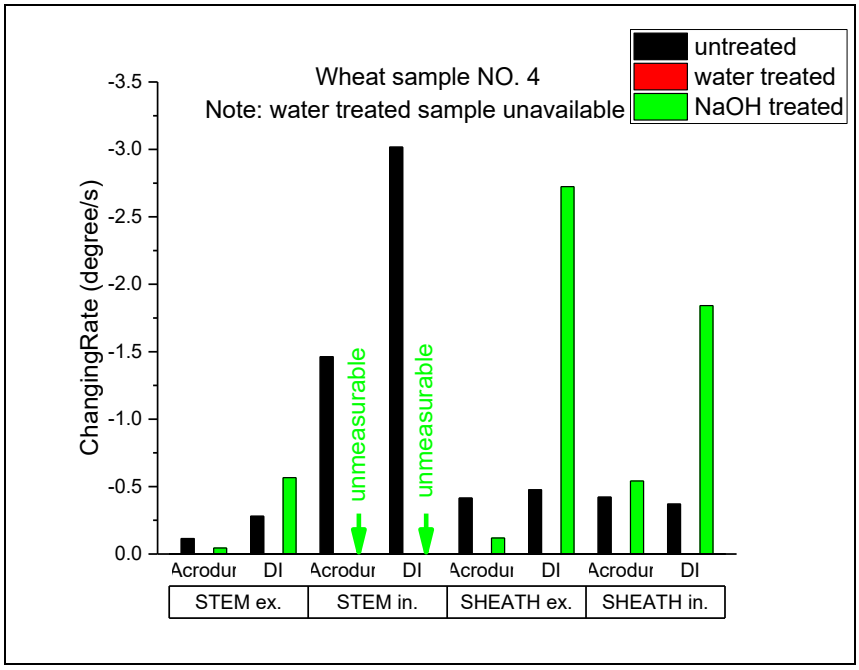

Figure 8.9 *K-value* result for sample # 4

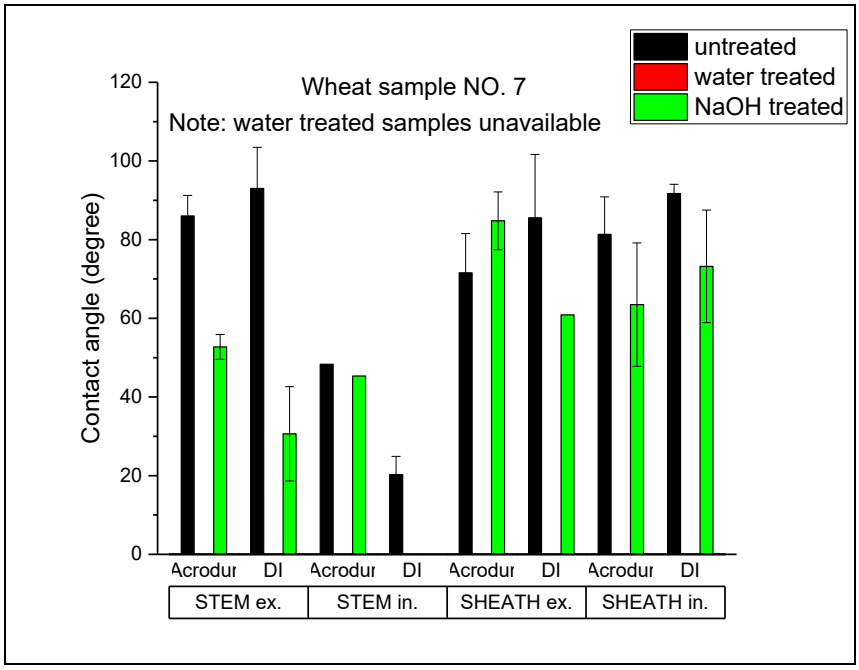

Figure 8.10 Contact angle comparison within sample #7

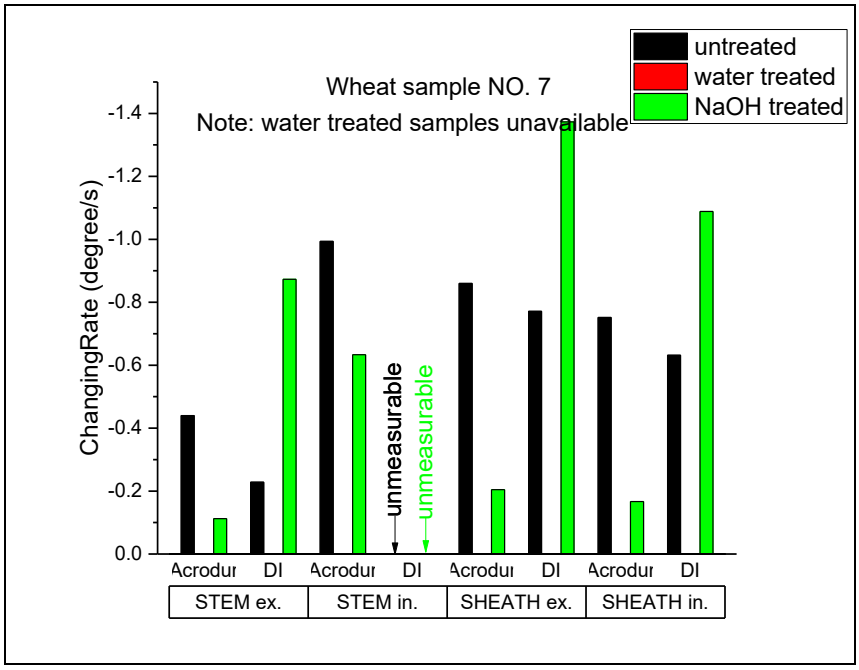

Figure 8.11 *K-value* result for sample # 7

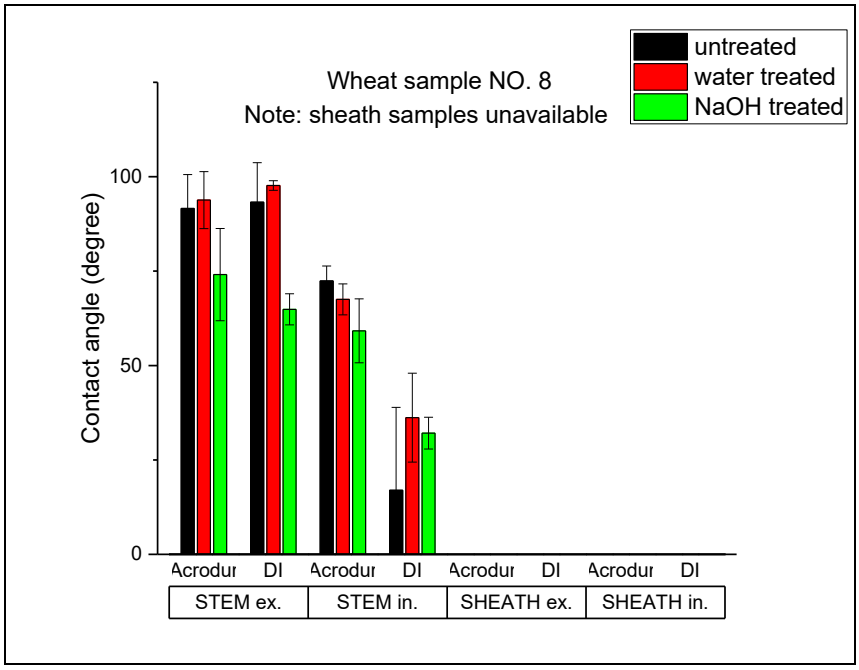

Figure 8.12 Contact angle comparison within sample #8

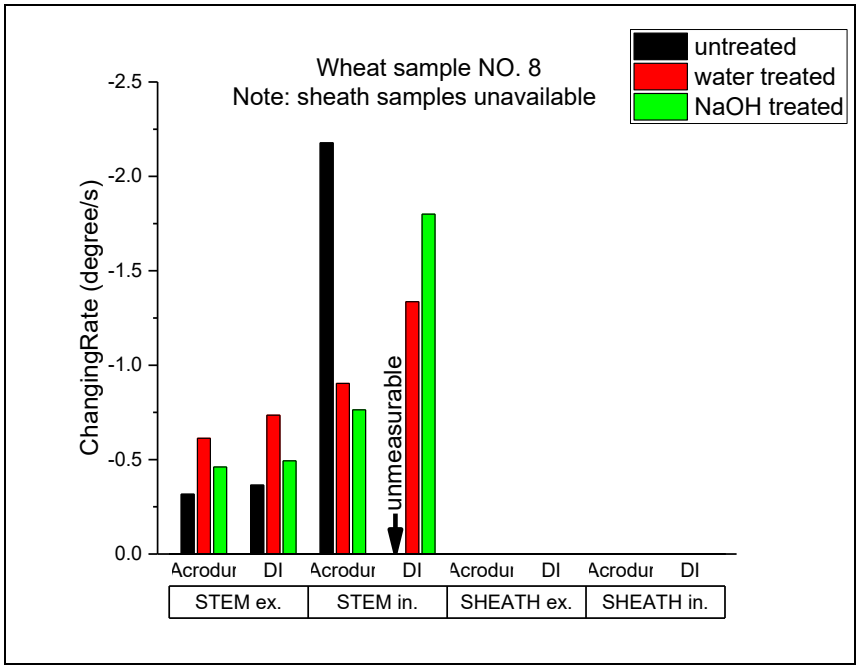

Figure 8.13 *K-value* result for sample # 8

Appendix B

Statistics for Model Fitting for Contact Angle

Table 8.3 Statistics of model fitting

	Contact_angle
Number of Points	20
Degrees of Freedom	19
Reduced Chi-Sqr	0.60277
Residual Sum of Squares	11.45271
R-Square(COD)	0.96847
Adj. R-Square	0.96847
Fit Status	Succeeded(100)

Table 8.4 ANOVA for contact angle fitting

	DF	Sum of Squares	Mean Square	F Value	Prob>F
Regression	1	118024.93729	118024.93729	195802.835	1
Residual	19	11.45271	0.60277		
Uncorrected Total	20	118036.39			
Corrected Total	19	363.2495			

Table 8.5 Model fit reports of NaOH treated-sheath exterior-Acrodur DS3530 sample #6 and #1

	Sample #6		Sample #1	
	Left contact angle	Right contact angle	Left contact angle	Right contact angle
Model	WettingModel (User)			
Equation	(qi*qe)/(qi+(qe-qi)*EXP(K*(qe/(qe-qi))*t))			
K	0.01159 ± 5.27897E-4	0.01493 ± 0.00106	0.00555 ± 5.38915E-4	0.00407 ± 5.5479E-4
qi	87.6	85.9	50.3	51.3
qe	72.3	70.5	38.5	40.6
Reduced Chi-Sqr	0.60277	1.22338	2.11628	3.20883
R-Square(COD)	0.96847	0.91257	0.81306	0.70936
Adj. R-Square	0.96847	0.91257	0.81306	0.70936

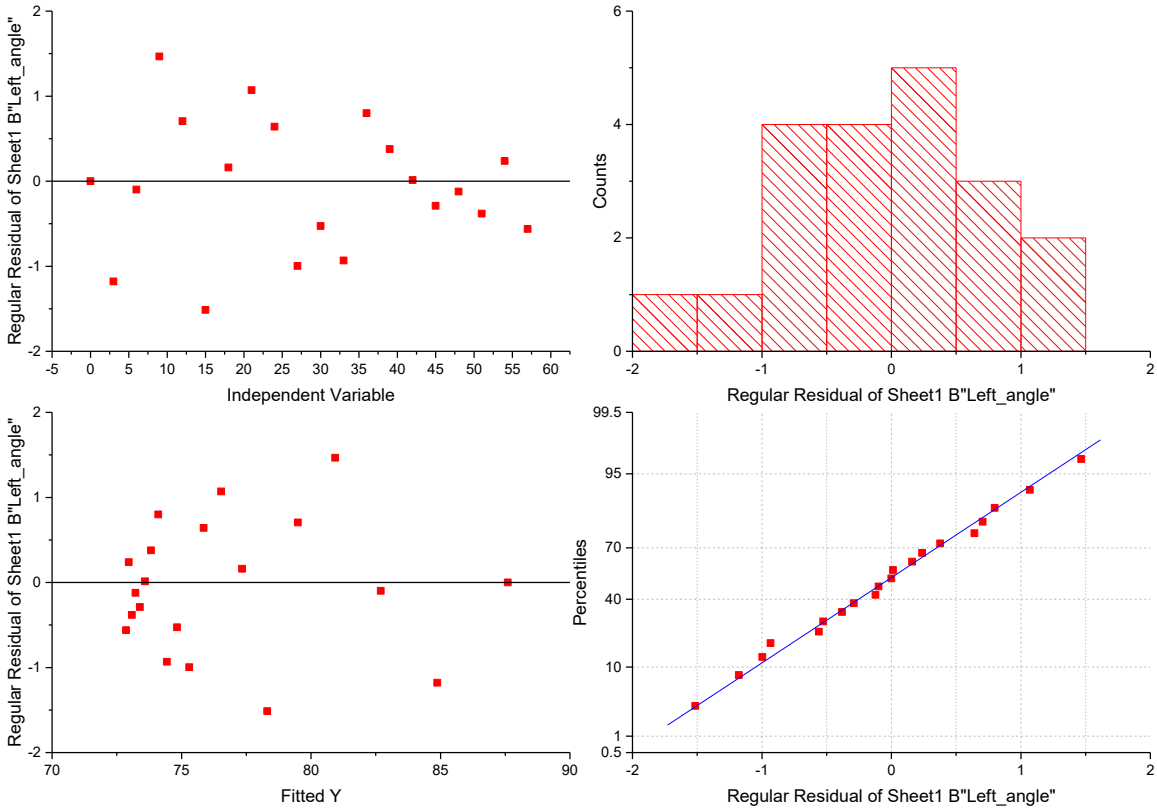

Figure 8.14 Model fitting evaluation for left contact angle (sample #6)

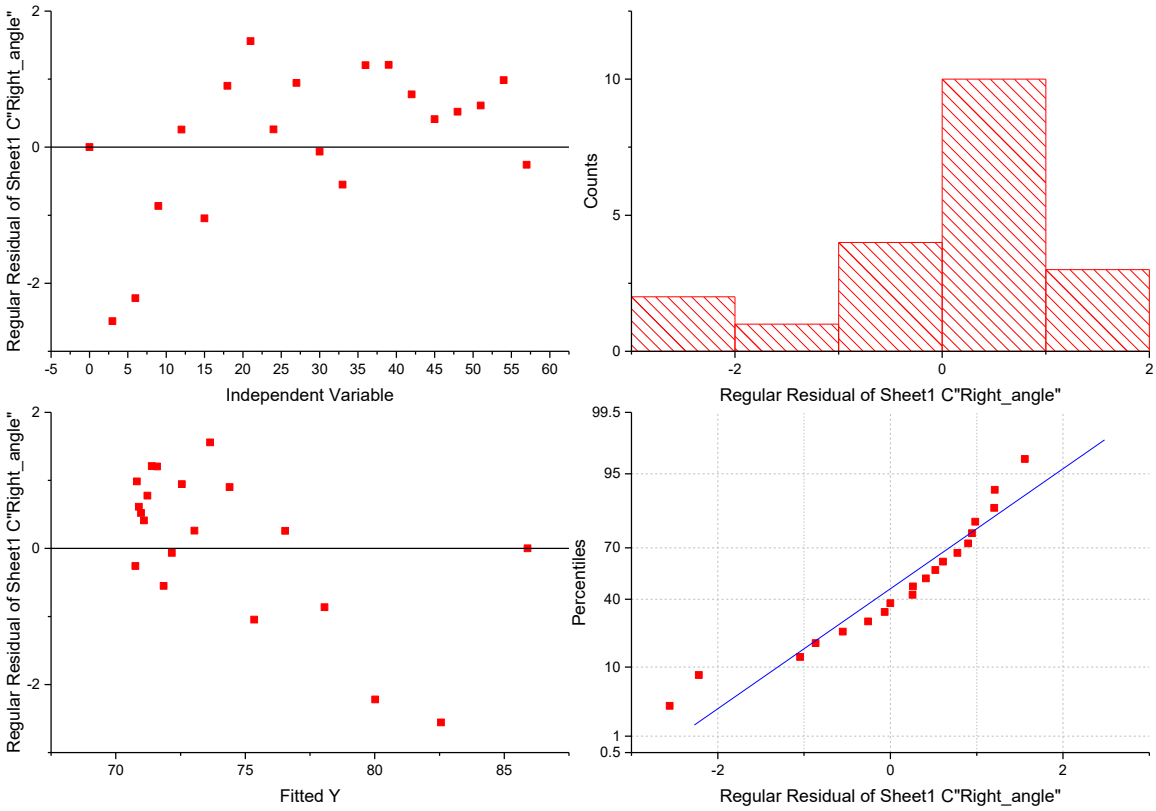

Figure 8.15 Model fitting evaluation for right contact angle (sample #6)

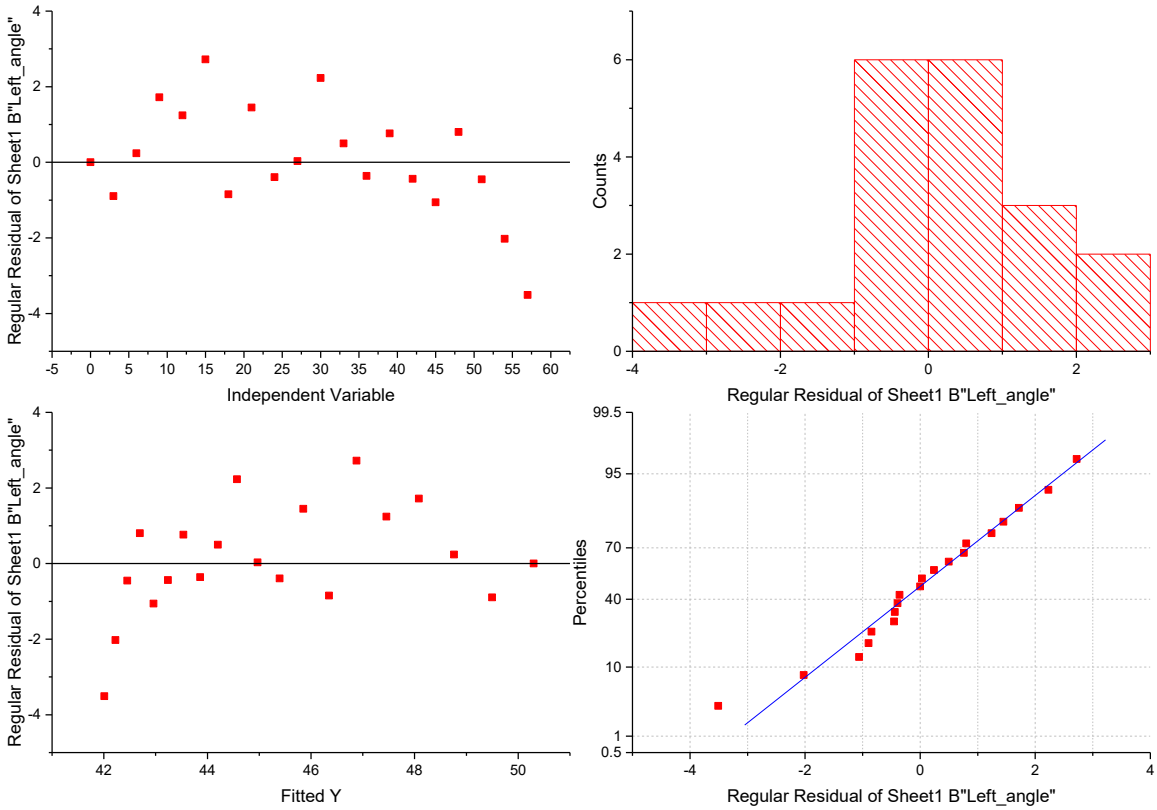

Figure 8.16 Model fitting evaluation for left contact angle (sample #1)

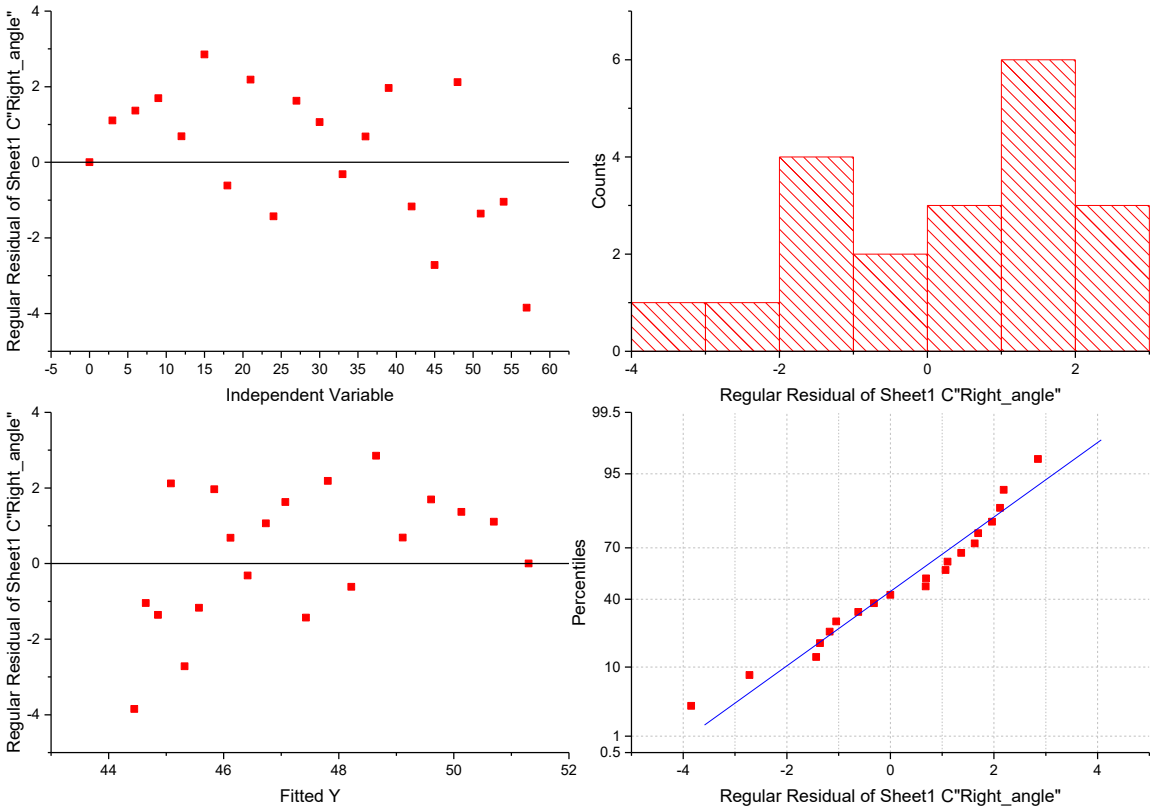

Figure 8.17 Model fitting evaluation for right contact angle (sample #1)

Appendix C

SEM Images of Wheat Straw at 500 Magnification

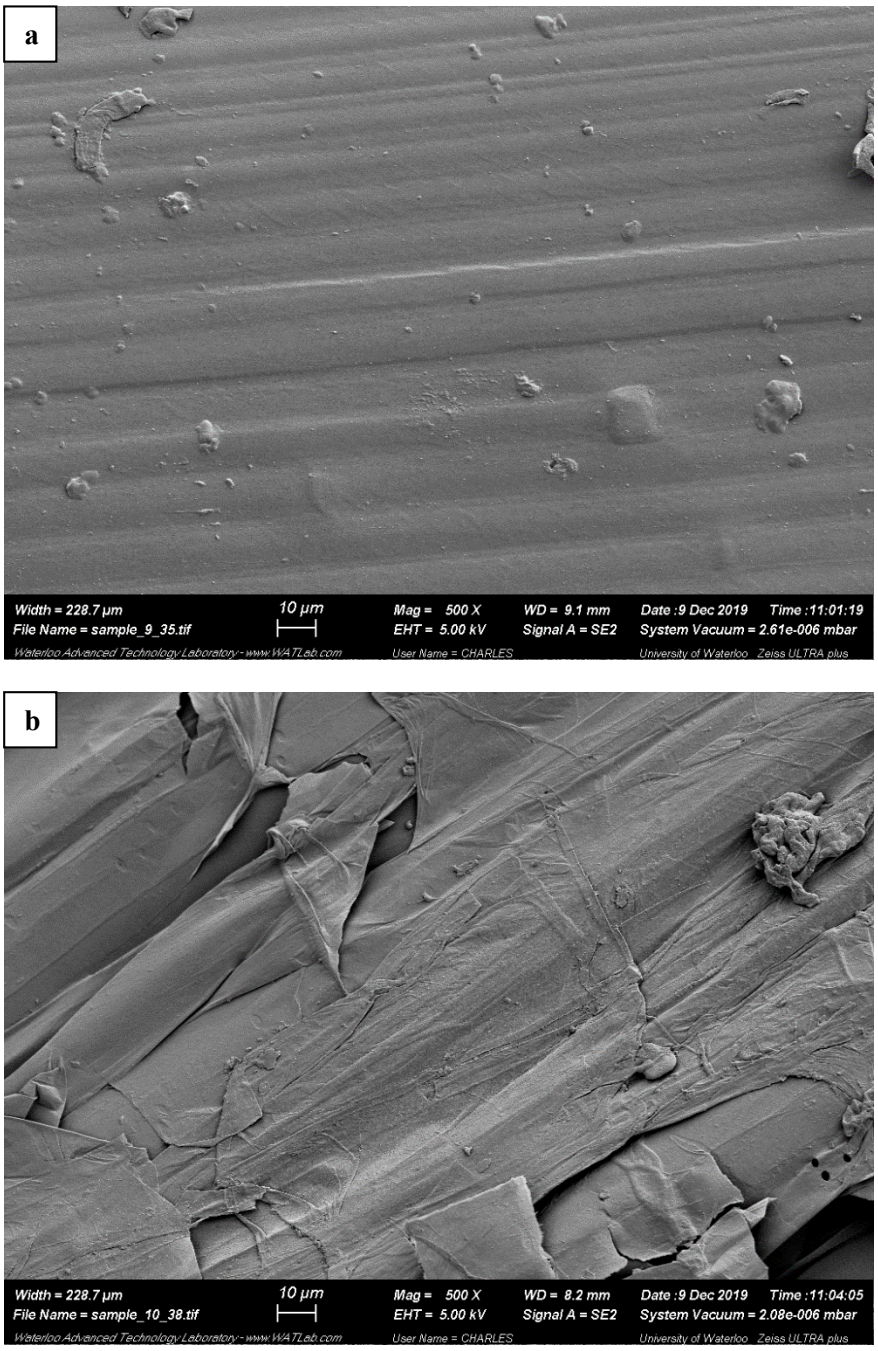

Figure 8.18 Exterior (a) and interior (b) of untreated wheat stem

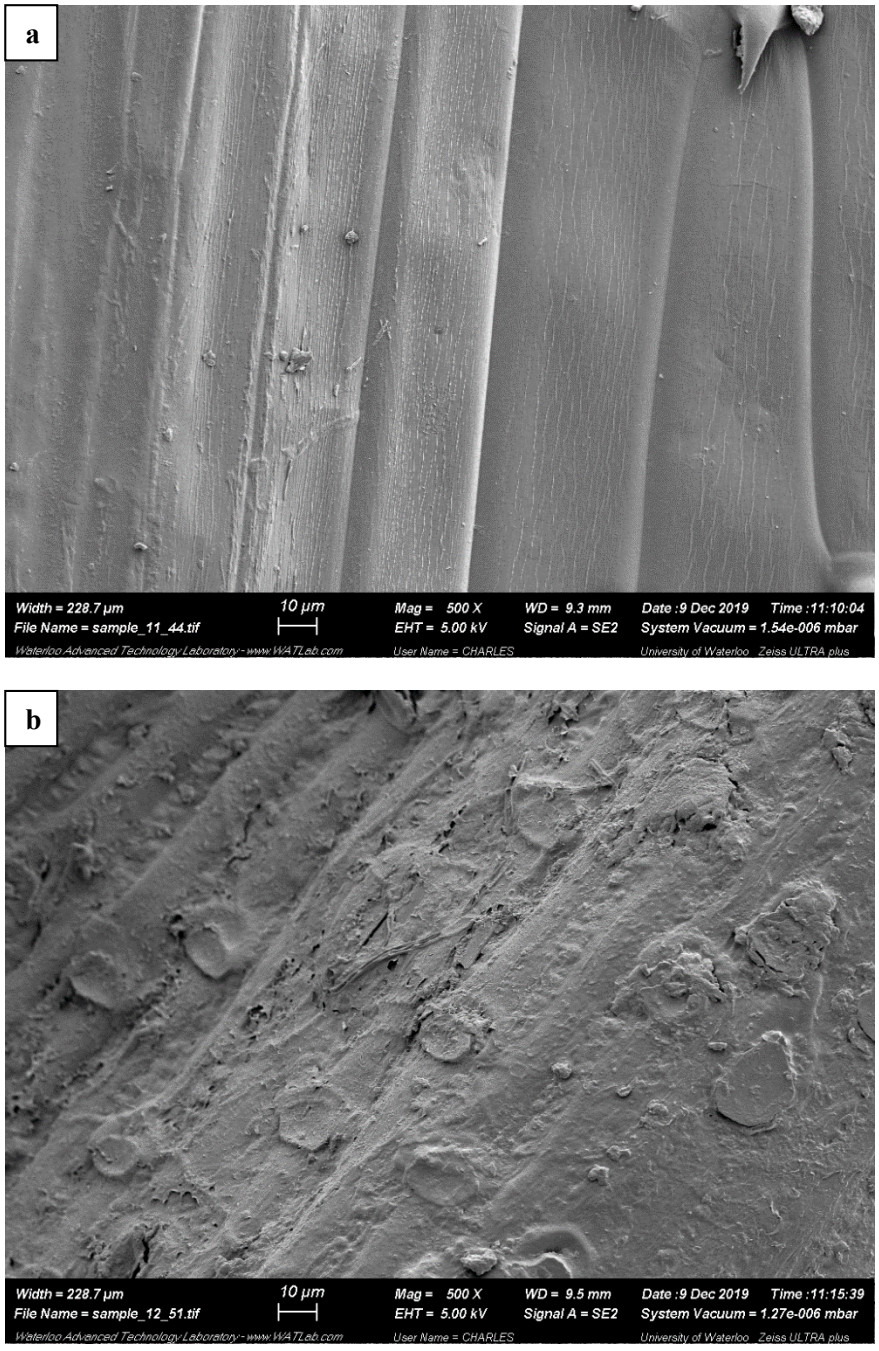

Figure 8.19 Exterior (a) and interior (b) of untreated wheat sheath

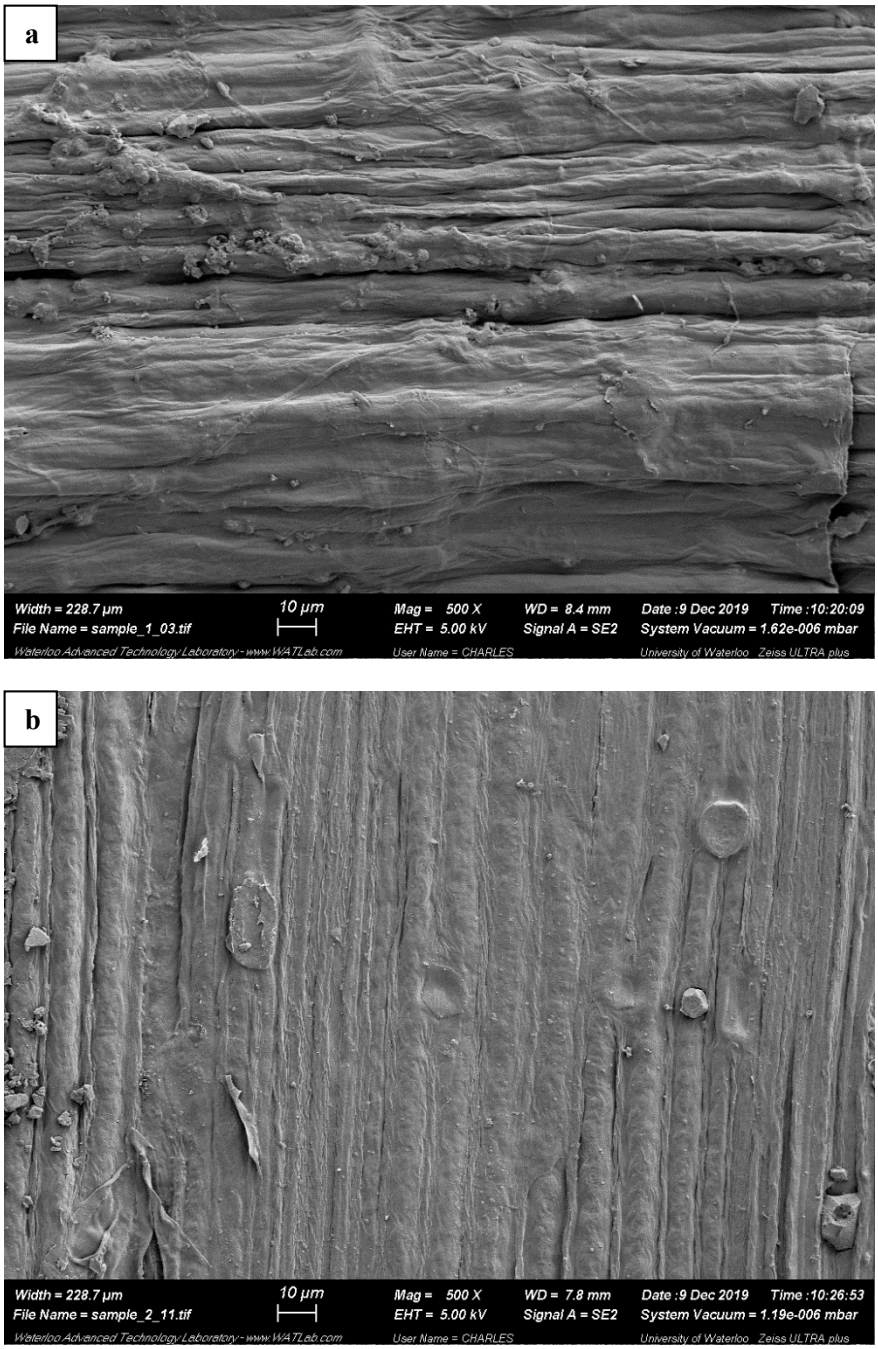

Figure 8.20 Exterior (a) and interior (b) of NaOH treated wheat stem

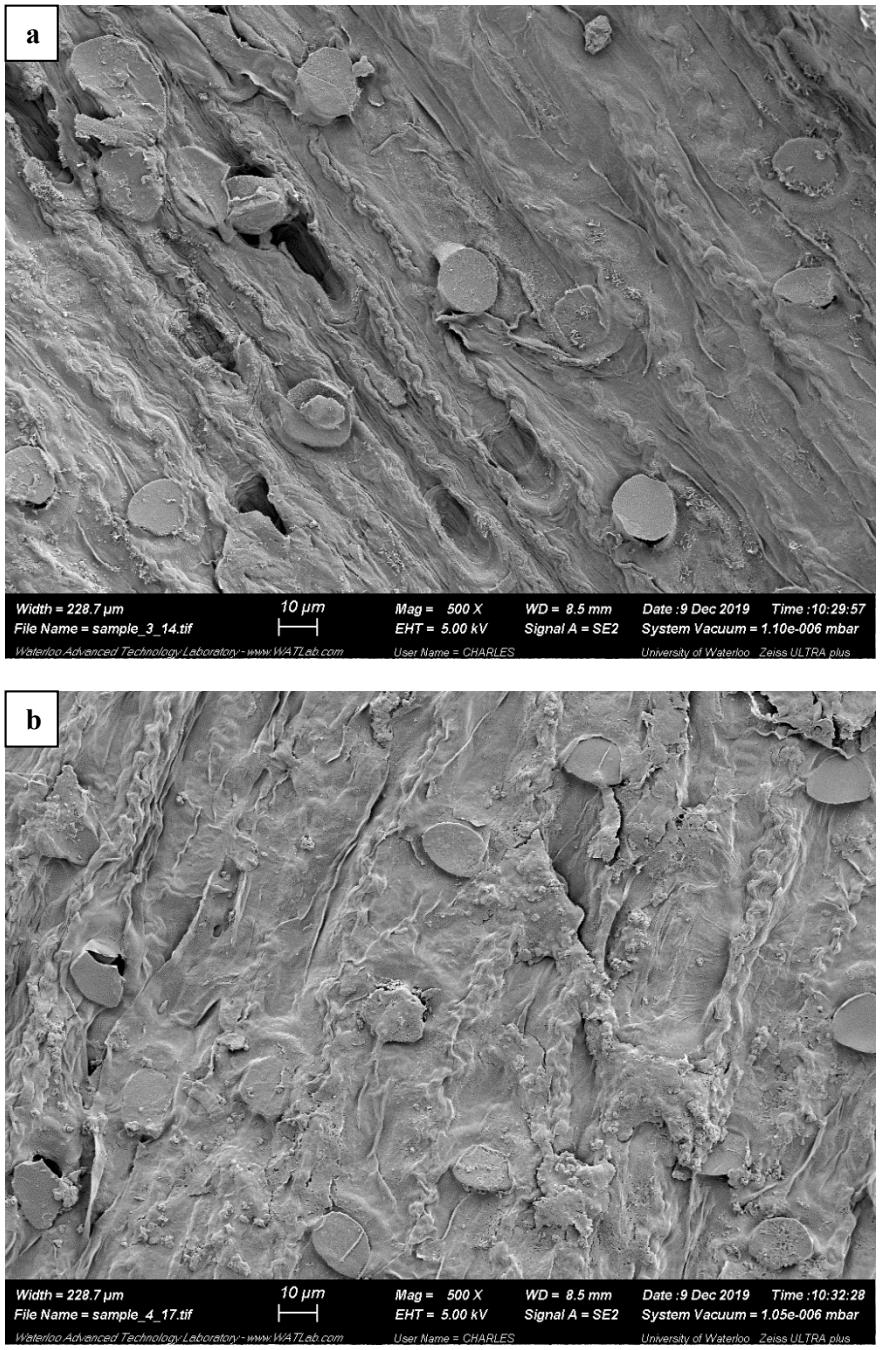

Figure 8.21 Exterior (a) and interior (b) of NaOH treated wheat sheath

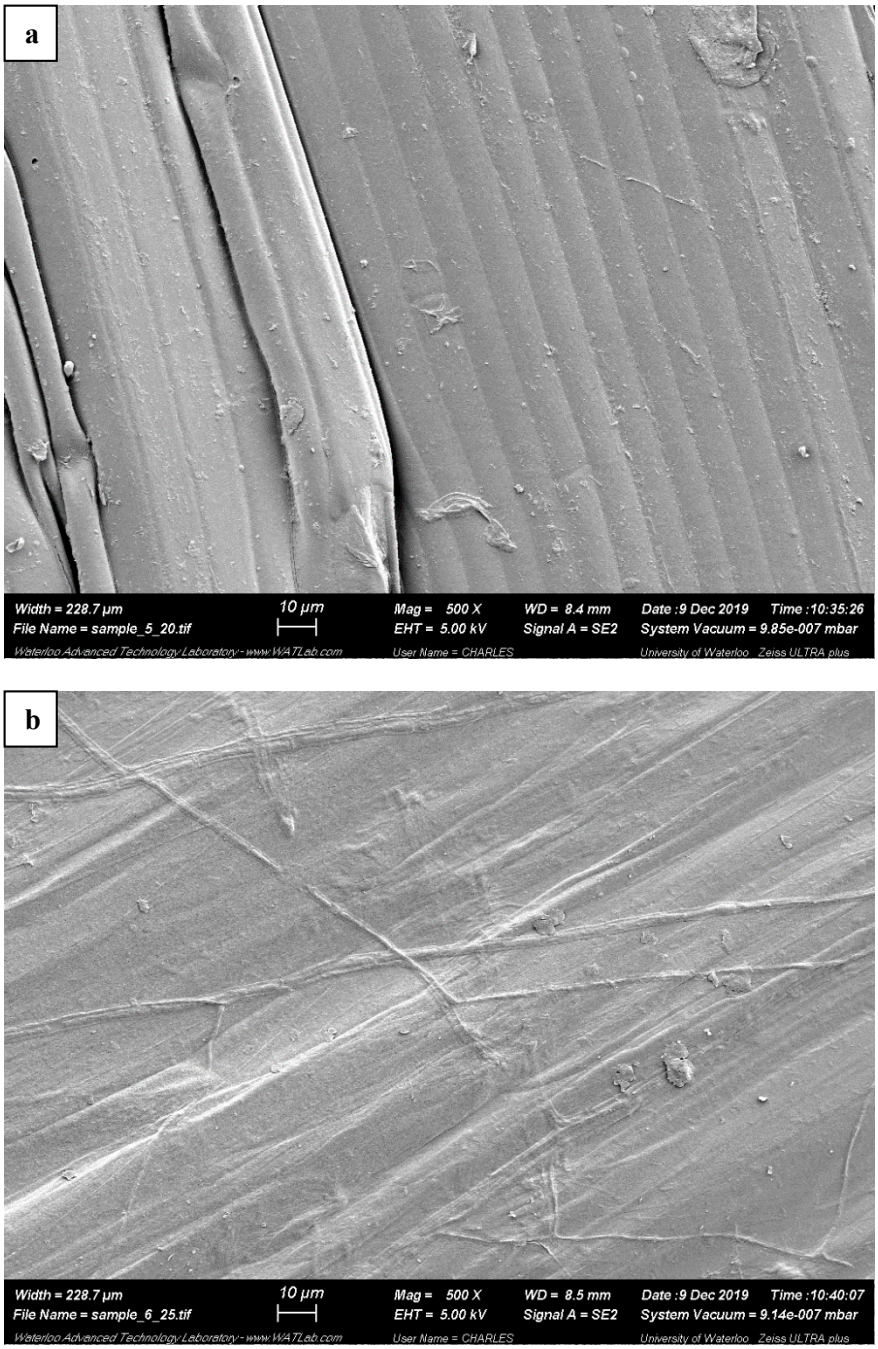

Figure 8.22 Exterior (a) and interior (b) of hot-water treated wheat stem

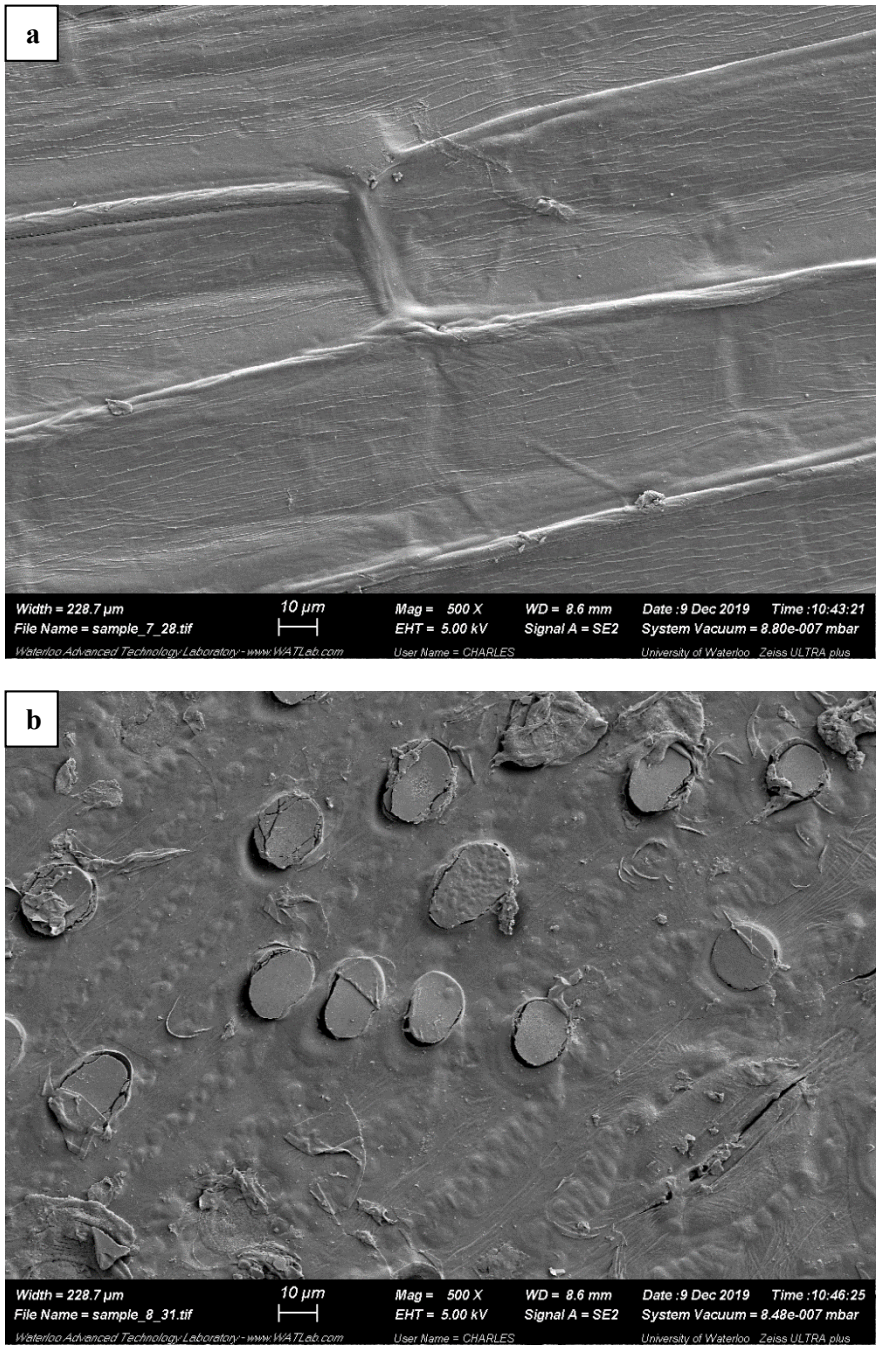

Figure 8.23 Exterior (a) and interior (b) of hot-water treated wheat sheath

Appendix D

Thermal Degradaction of Wheat Straw

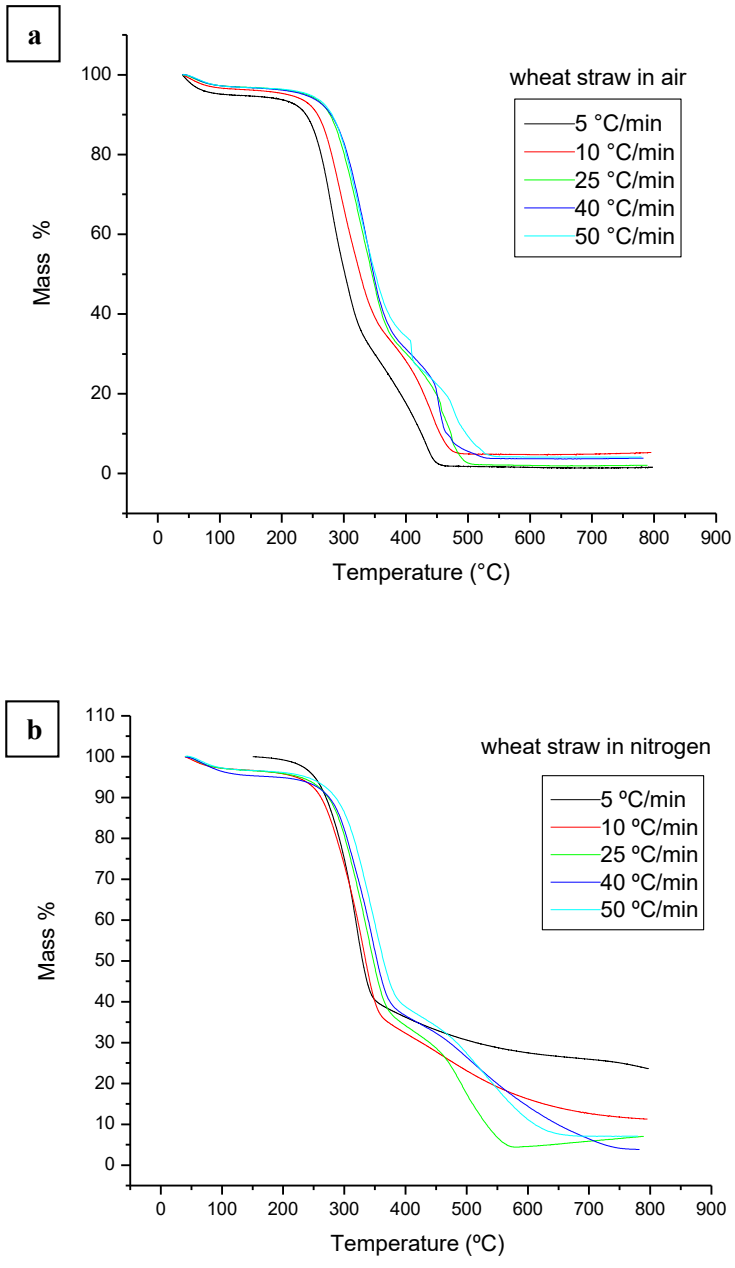

Figure 8.24 TGA thermographs of untreated wheat straw at a series of heating rates in air (a) and in nitrogen (b)

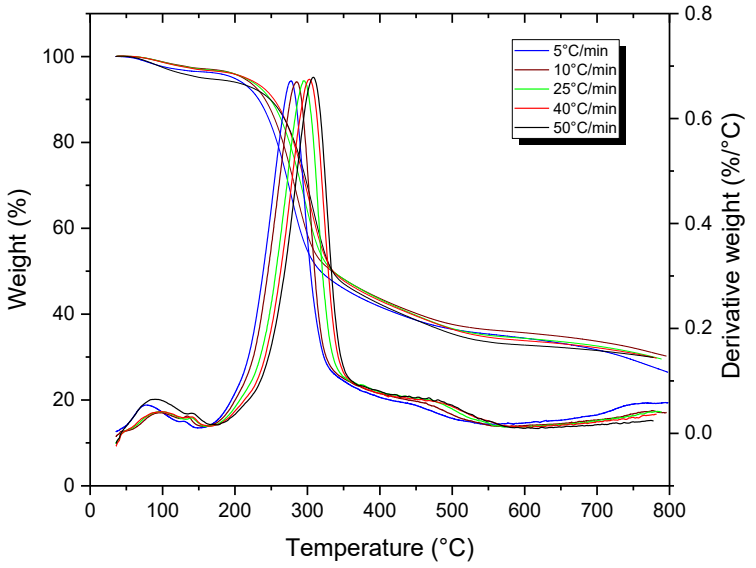

Figure 8.25 TGA thermographs of NaOH treated wheat straw in nitrogen at a series of heating rates

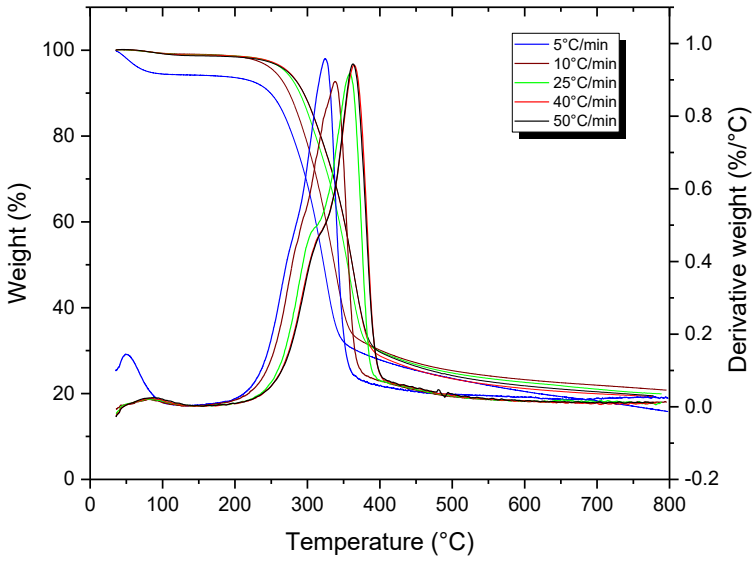

Figure 8.26 TGA thermographs of hot-water treated wheat straw in nitrogen at a series of heating rates

Table 8.6 Activation energies and degradation temperatures of wheat straw in air and nitrogen

Atmosphere	In air	In nitrogen		
Treatment	untreated	untreated	Hot-water treated	NaOH treated
T_{onest} @ 5% conversion (°C)	239–273	251–276	244–272	212–232
Ea @ 5% conversion (kJ/mol)	145.81	200.08	160.81	224.81
Ea @ 10% conversion (kJ/mol)	138.03	188.41	168.32	211.38
Ea @ 20% conversion (kJ/mol)	132.10	194.21	174.32	203.02
Ea @ 30% conversion (kJ/mol)	129.12	207.75	174.56	205.07
Ea @ 40% conversion (kJ/mol)	128.49	203.20	168.00	204.29
Average Ea (kJ/mol)	134.71	198.73	169.20	209.72

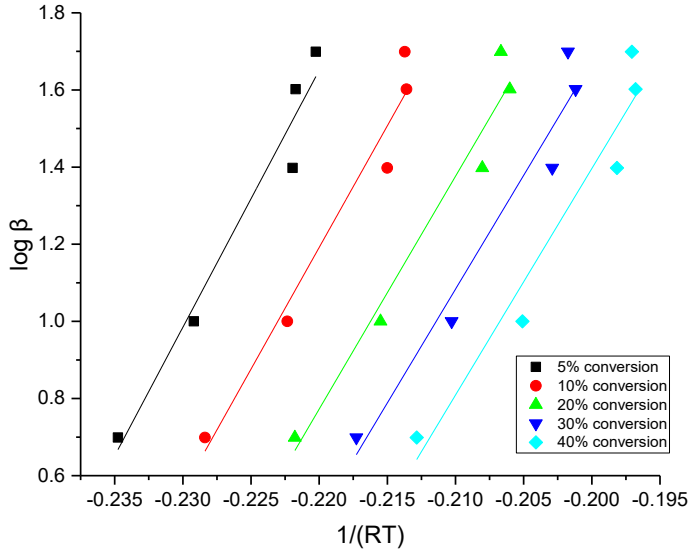

Figure 8.27 Untreated wheat straw in air

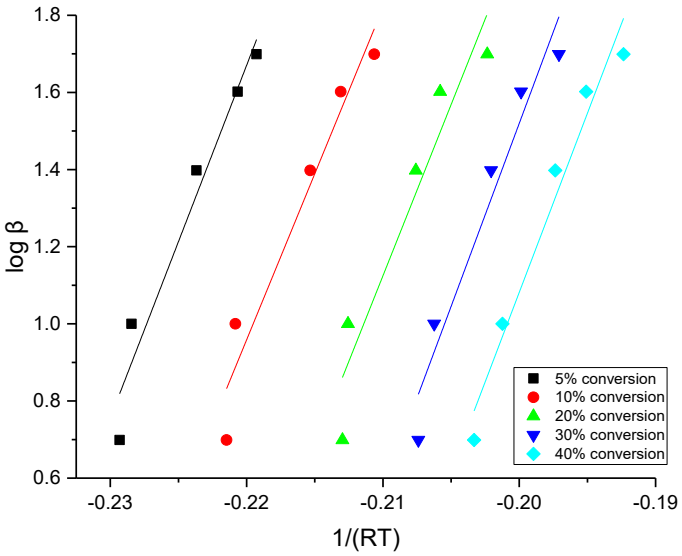

Figure 8.28 Untreated wheat straw in nitrogen

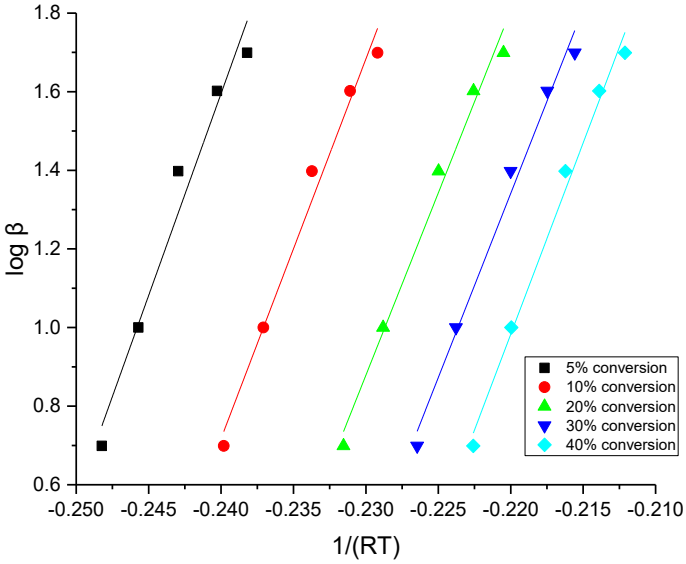

Figure 8.29 NaOH treated wheat straw in nitrogen

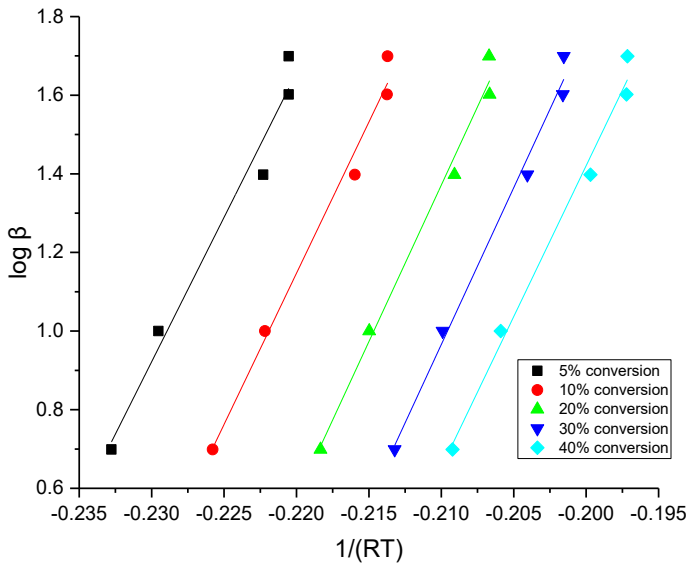

Figure 8.30 Hot-water treated wheat straw in nitrogen

Appendix E

Kinetics of Acrodur Curing

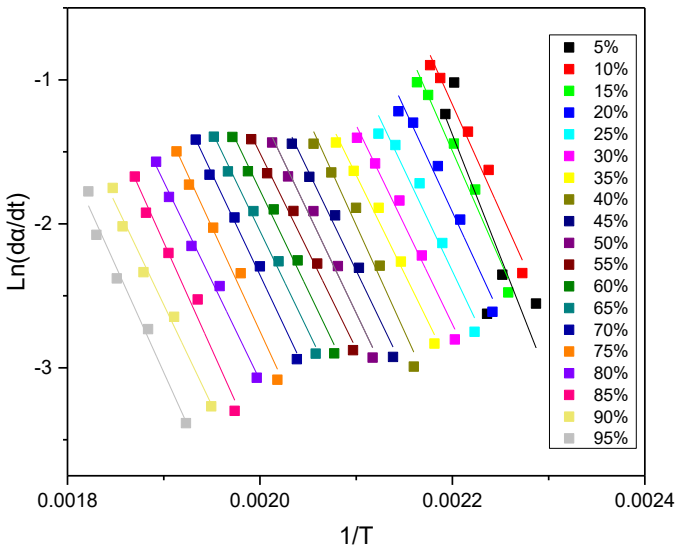

Figure 8.31 ln (dα/dt) vs 1/T plot for isothermal TGA cure of **Thermoset #1**

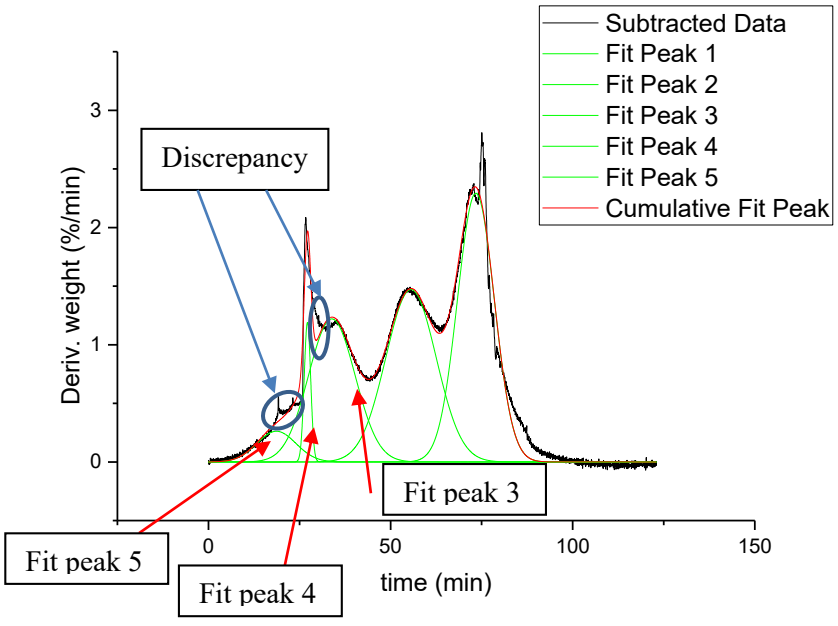

Figure 8.32 Representative illustration of deconvolution of **Thermoset #1** DTG at 5°C/min

Table 8.7 Method and statistics of curve deconvolution

Iteration Algorithm	Levenberg Marquardt
Model (peak type)	Gaussian
Reduced Chi-Sqr	0.01045
Residual Sum of Squares	76.9995
R-Square(COD)	0.9774
Adj. R-Square	0.9774
Fit Status	Succeeded(100)

Table 8.8 Anova of curve deconvolution

	DF	Sum of Squares	Mean Square	F Value	Prob>F
Regression	15	6557.4	437.2	41814.4	0
Residual	7365	77.0	0.01045		
Uncorrected Total	7380	6634.4			
Corrected Total	7379	3413.4			

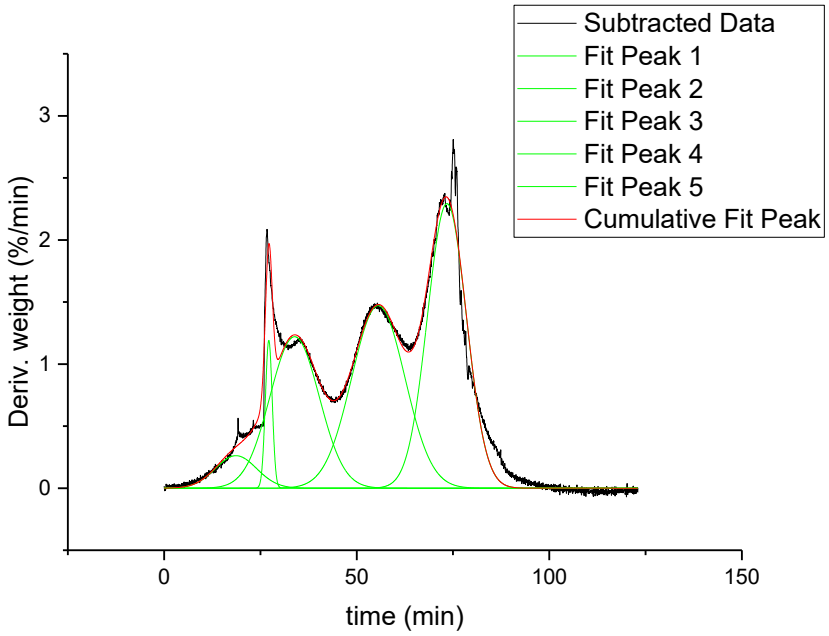

Figure 8.33 Deconvolution of **Thermoset #1** DTG at 5°C/min

Table 8.9 Details of deconvoluted peaks of **Thermoset #1** DTA at 5°C/min

Peak Index	Peak Type	Area Fit	Area FitT	Area FitTP	Center Max	Center Grvty	Max Height	FWHM
1	Gaussian	28.96611	28.96611	36.15761	73.41495	73.41495	2.29266	11.86914
2	Gaussian	25.46497	25.46497	31.78723	55.60836	55.60836	1.47137	16.2588
3	Gaussian	19.54205	19.54205	24.39381	33.86322	33.86322	1.22052	15.04157
4	Gaussian	2.633	2.633	3.2867	27.17139	27.17139	1.19019	2.07827
5	Gaussian	3.5054	3.50456	4.37465	18.65446	18.65446	0.26193	12.57235

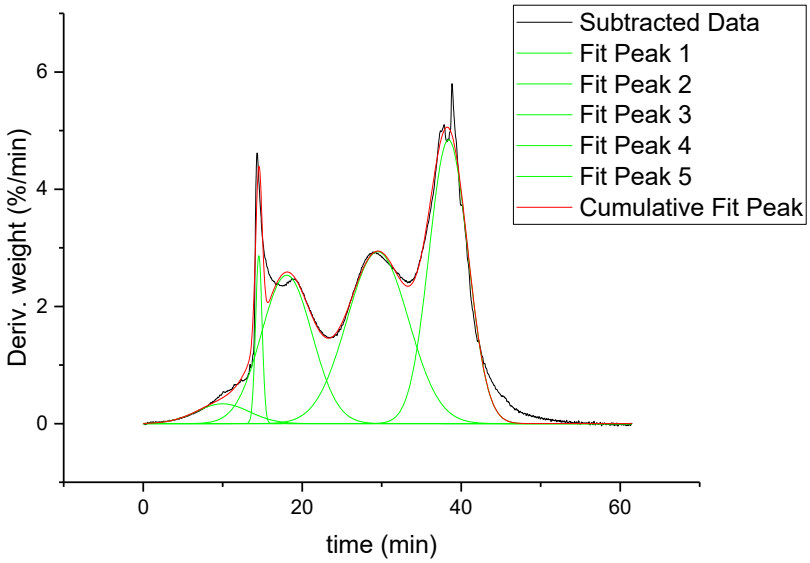

Figure 8.34 Deconvolution of **Thermoset #1** DTG at 10°C/min

Table 8.10 Details of deconvoluted peaks of **Thermoset #1** DTA at 10°C/min

Peak Index	Peak Type	Area Fit	Area FitT	Area FitTP	Center Max	Center Grvty	Max Height	FWHM
1	Gaussian	2.93879	2.93879	3.50234	14.54768	14.54768	2.86556	0.96344
2	Gaussian	2.82898	2.82513	3.36689	9.99641	9.99641	0.33859	7.84922
3	Gaussian	28.39608	28.39608	33.84143	29.50751	29.50751	2.93407	9.09191
4	Gaussian	20.23232	20.23232	24.11215	18.05097	18.05097	2.53245	7.50536
5	Gaussian	29.5169	29.5169	35.17718	38.40736	38.40736	4.84306	5.72557

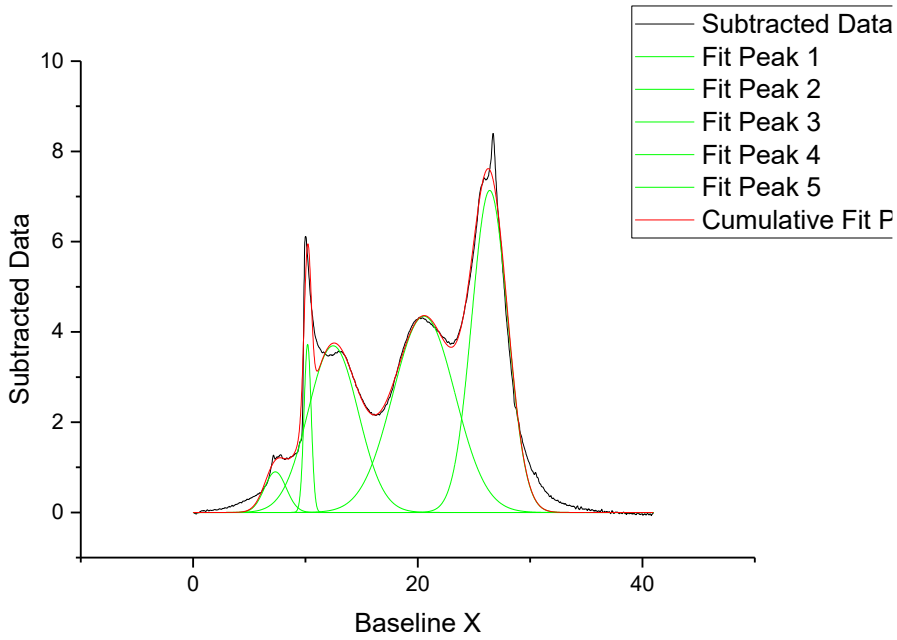

Figure 8.35 Deconvolution of **Thermoset #1** DTG at 15°C/min

Table 8.11 Details of deconvoluted peaks of **Thermoset #1** DTA at 15°C/min

Peak Index	Peak Type	Area Fit	Area FitT	Area FitTP	Center Max	Center Grvty	Max Height	FWHM
1	Gaussian	2.96588	2.96588	3.51627	10.19196	10.19196	3.72456	0.74808
2	Gaussian	20.64961	20.64961	24.4816	12.46226	12.46226	3.69243	5.25373
3	Gaussian	2.17999	2.17999	2.58453	7.31967	7.31967	0.90011	2.27523
4	Gaussian	30.07547	30.07547	35.65665	20.55112	20.55112	4.34889	6.49683
5	Gaussian	28.4765	28.4765	33.76095	26.40214	26.40214	7.13528	3.74924

Table 8.12 Details of deconvoluted peaks of **Thermoset #1** DTA at 20°C/min

Peak Index	Peak Type	Area Fit	Area FitT	Area FitTP	Center Max	Center Grvty	Max Height	FWHM
1	Gaussian	3.71213	3.71213	4.27439	7.98956	7.98956	6.15961	0.56616
2	Gaussian	28.49315	28.49315	32.80889	15.81725	15.81725	5.84969	4.57589
3	Gaussian	20.76516	20.76516	23.91037	9.97451	9.97451	4.87986	3.99756
4	Gaussian	3.31039	3.30116	3.80117	6.07233	6.07233	0.60322	5.15549
5	Gaussian	30.57424	30.57424	35.20519	20.33189	20.33189	9.49588	3.02474

Table 8.13 Details of deconvoluted peaks of **Thermoset #1** DTA at 25°C/min

Peak Index	Peak Type	Area Fit	Area FitT	Area FitTP	Center Max	Center Grvty	Max Height	FWHM
1	Gaussian	2.88382	2.88382	3.34698	6.57714	6.57714	5.79553	0.46746
2	Gaussian	30.0339	30.0339	34.85758	13.01005	13.01005	7.37797	3.82422
3	Gaussian	3.77712	3.75955	4.36336	5.15194	5.15194	0.76076	4.66422
4	Gaussian	20.35102	20.35102	23.61955	8.22003	8.22003	5.80476	3.29359
5	Gaussian	29.13346	29.13346	33.81252	16.48445	16.48445	11.63679	2.35194

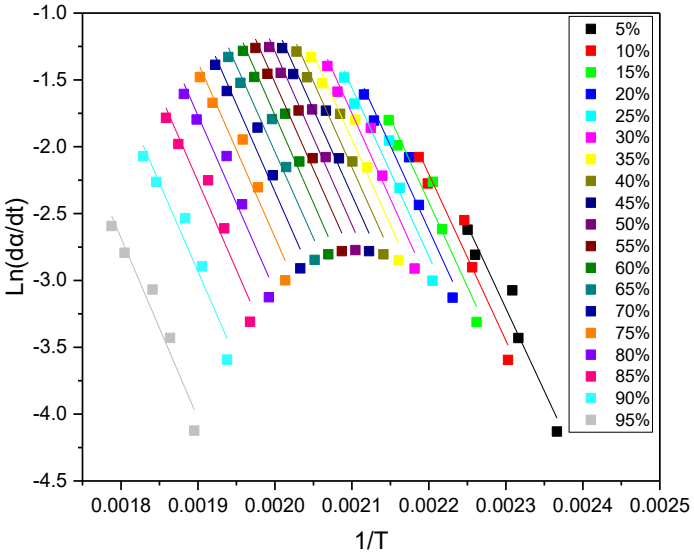

Figure 8.36 ln (dα/dt) vs 1/T plot for isothermal TGA cure of **Thermoset #1**, for single-peak-cure

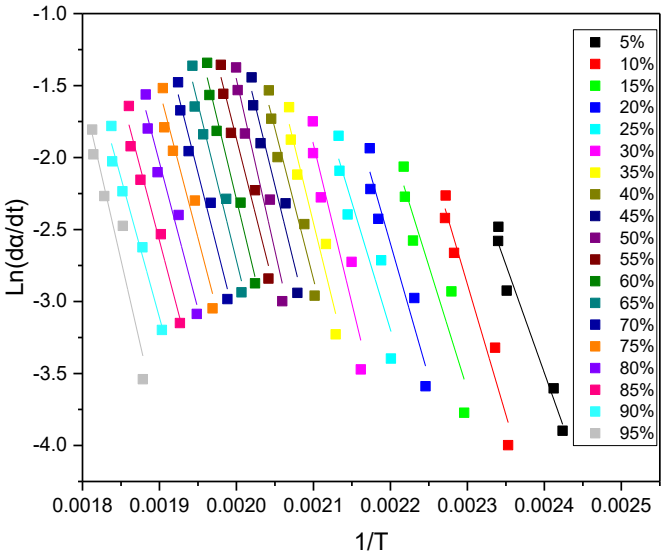

Figure 8.37 ln (dα/dt) vs 1/T plot for isothermal TGA cure of **Thermoset #1** powder

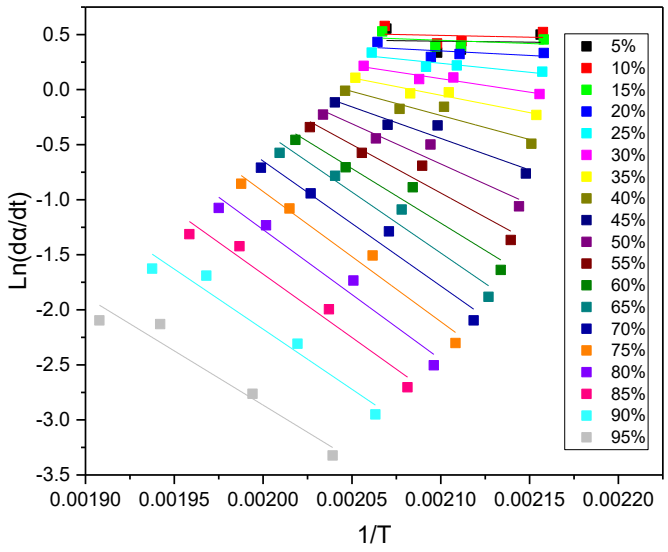

Figure 8.38 ln (dα/dt) vs 1/T plot for isothermal DSC cure of **Thermoset #1**, in hermetic mode

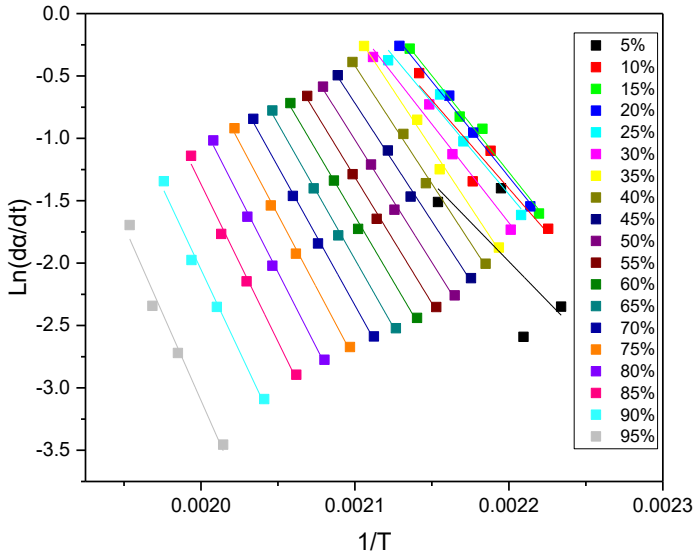

Figure 8.39 ln (dα/dt) vs 1/T plot for dynamic DSC cure of **Thermoset #1**, in non-hermetic mode

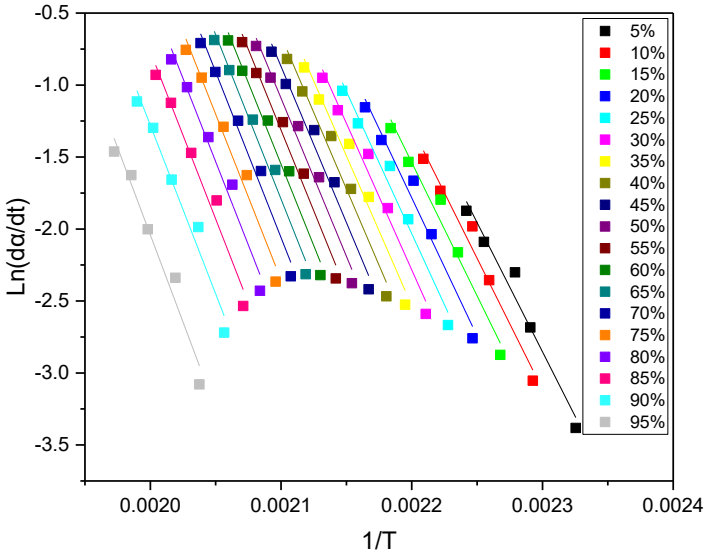

Figure 8.40 ln (dα/dt) vs 1/T plot for dynamic DSC cure of **Thermoset #1** powder, in non-hermetic mode

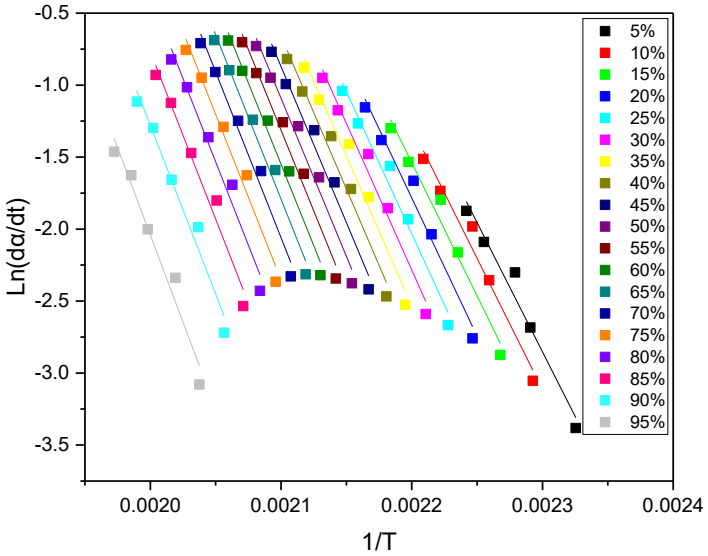

Figure 8.41 ln (dα/dt) vs 1/T plot for dynamic DSC cure of **Thermoset #1** powder, in non-hermetic mode

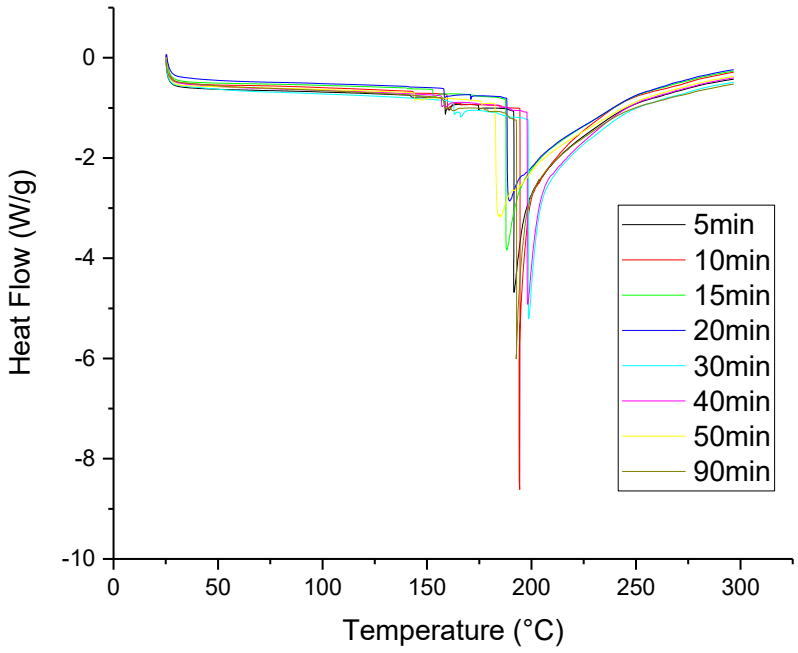

Figure 8.42 Postcure (second heating) of a series of **Thermoset #1** cured isothermally at 130°C for various heating durations, in hermetic mode

Table 8.14 Residual heat and conversion for **Thermoset #1** isothermally cured at 130°C

T_{iso} (°C)	Duration (min)	T_{Peak} (°C)	$\Delta H_{Residual}$ (J/g)
130	5	191	326
130	10	194	309
130	15	188	322
130	20	189	295
130	30	198	271
130	40	198	293
130	50	192	294
130	90	193	280

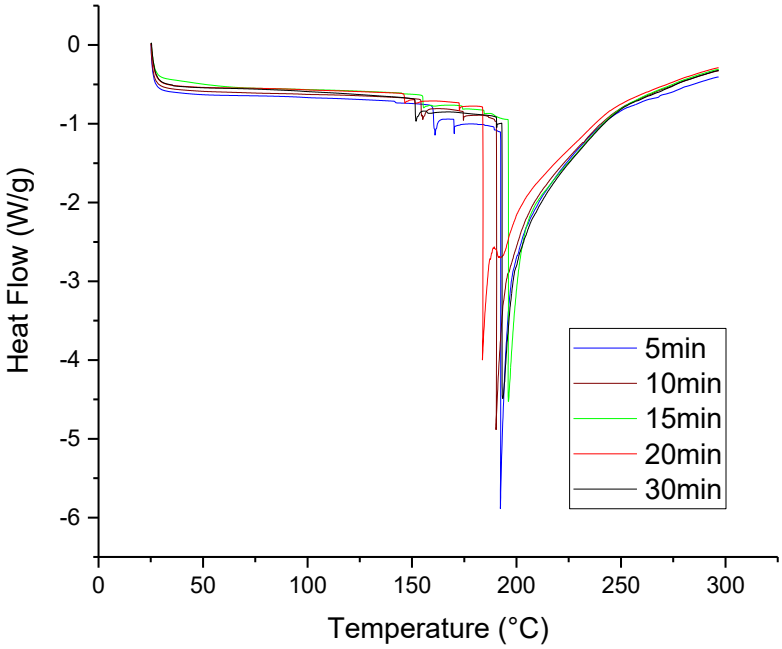

Figure 8.43 Postcure (second heating) of a series of **Thermoset #1** cured isothermally at 140°C for various heating durations, in hermetic mode

Table 8.15 Residual heat and conversion for **Thermoset #1** isothermally cured at 140°C

T_{iso} (°C)	Duration	T_{Peak} (°C)	$\Delta H_{Residual}$ (J/g)
140	5	192	307
140	10	190	316
140	15	196	277
140	20	183	347
140	30	193	315

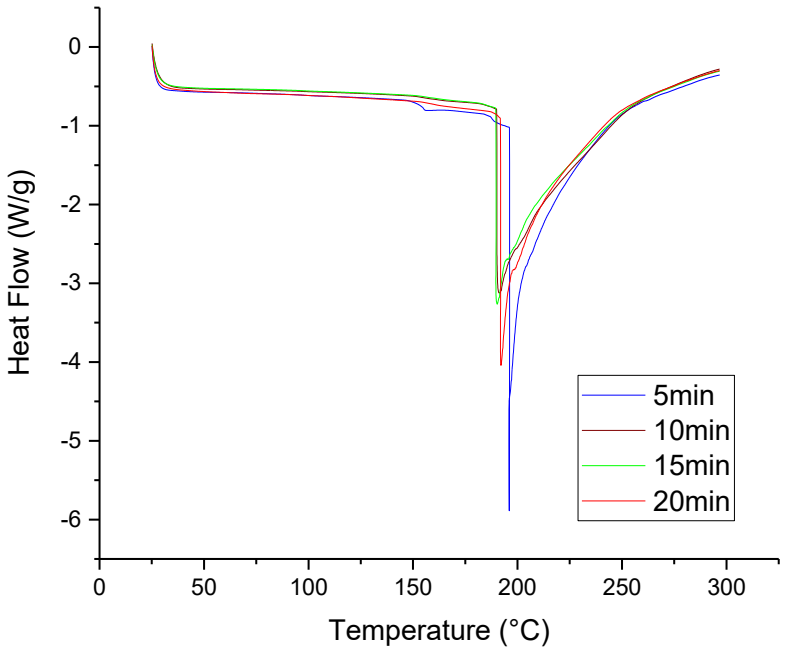

Figure 8.44 Postcure (second heating) of a series of **Thermoset #1** cured isothermally at 150°C for various heating durations, in hermetic mode

Table 8.16 Residual heat and conversion for **Thermoset #1** isothermally cured at 150°C

T_{iso} (°C)	Duration (min)	T_{Peak} (°C)	$\Delta H_{Residual}$ (J/g)
150	5	196	336
150	10	191	370
150	15	190	338
150	20	192	339

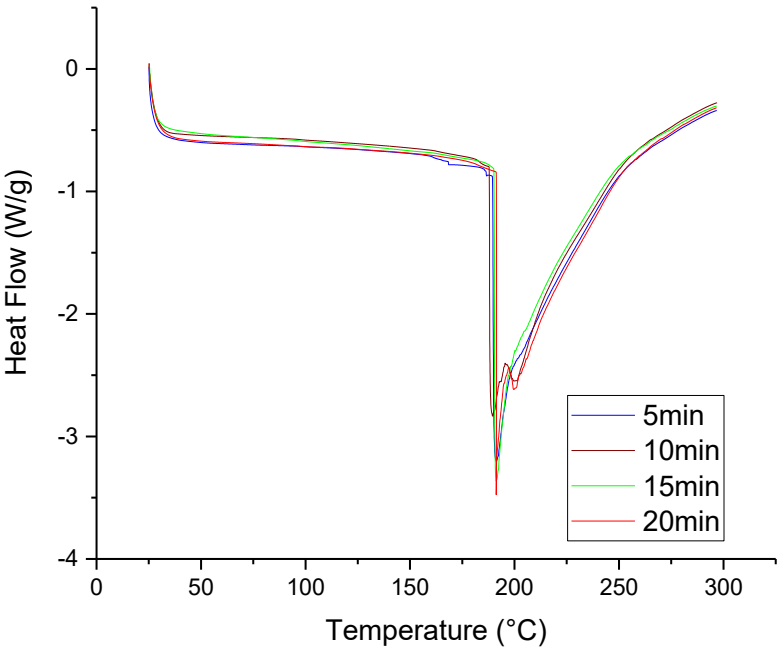

Figure 8.45 Postcure (second heating) of a series of **Thermoset #1** cured isothermally at 160°C for various heating durations, in hermetic mode

Table 8.17 Residual heat and conversion for **Thermoset #1** isothermally cured at 160°C

T_{iso} (°C)	Duration (min)	T_{Peak} (°C)	$\Delta H_{Residual}$ (J/g)
160	5	191	342
160	10	189	362
160	15	191	321
160	20	191	348

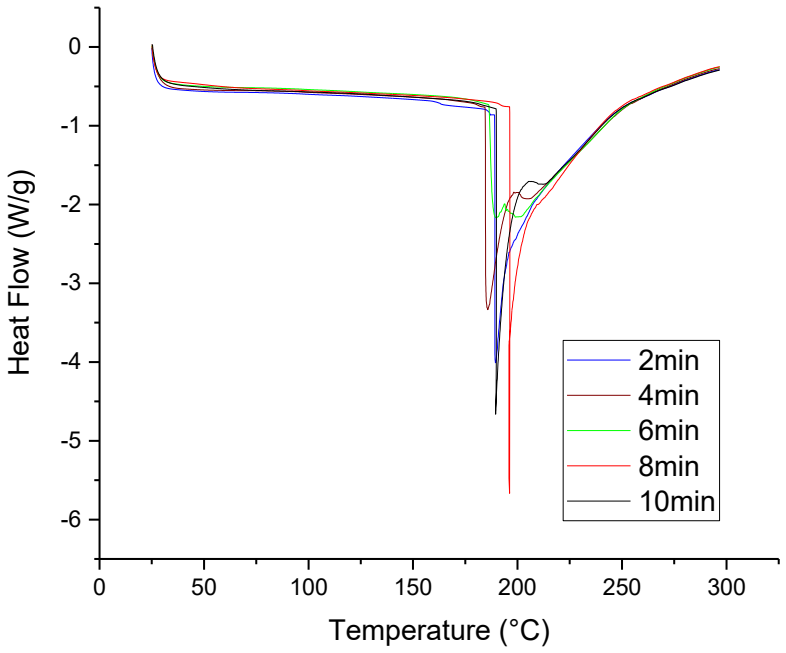

Figure 8.46 Postcure (second heating) of a series of **Thermoset #1** cured isothermally at 170°C for various heating durations, in hermetic mode

Table 8.18 Residual heat and conversion for **Thermoset #1** isothermally cured at 170°C

T_{iso} (°C)	Duration (min)	T_{Peak} (°C)	$\Delta H_{Residual}$ (J/g)
170	2	189	327
170	4	185	362
170	6	190	321
170	8	196	296
170	10	190	321

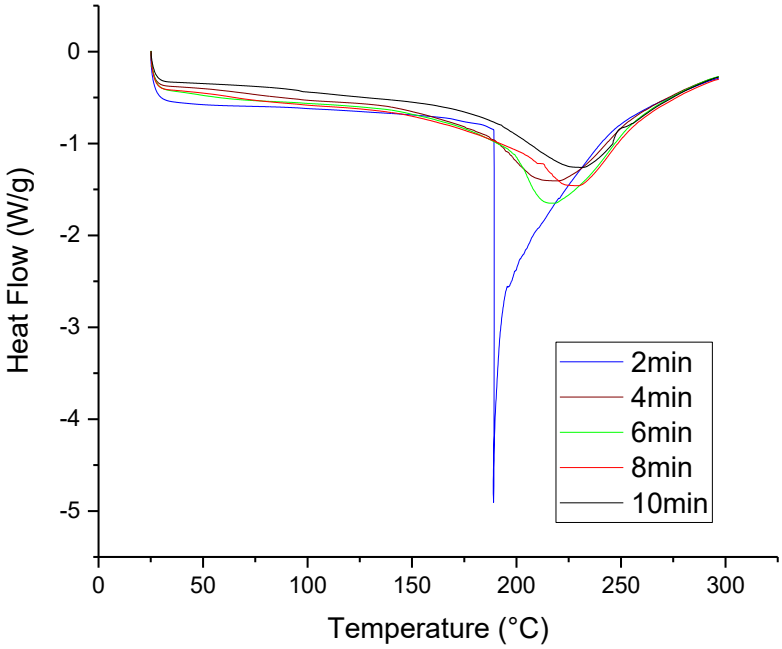

Figure 8.47 Postcure (second heating) of a series of **Thermoset #1** cured isothermally at 180°C for various heating durations, in hermetic mode

Table 8.19 Residual heat and conversion for **Thermoset #1** isothermally cured at 180°C

T_{iso} (°C)	Duration (min)	T_{Onset} (°C)	T_{Peak} (°C)	$\Delta H_{Residual}$ (J/g)	α (%)
180	2	189	189	342	0
180	4	190	212	117	66
180	6	200	213	131	62
180	8	213	232	69	80
180	10	192	233	63	81

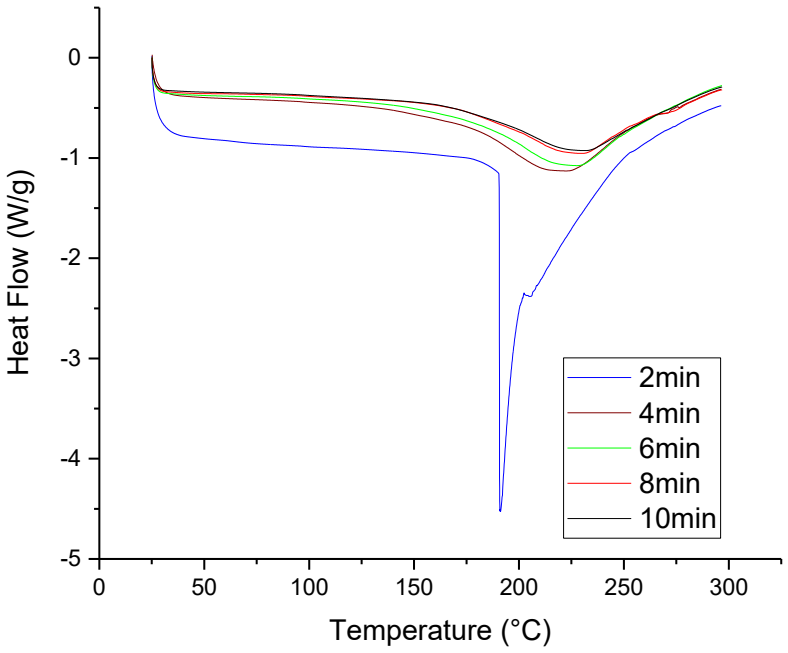

Figure 8.48 Postcure (second heating) of a series of **Thermoset #1** cured isothermally at 190°C for various heating durations, in hermetic mode

Table 8.20 Residual heat and conversion for **Thermoset #1** isothermally cured at 190°C

T_{iso} (°C)	Duration (min)	T_{Onset} (°C)	T_{Peak} (°C)	$\Delta H_{Residual}$ (J/g)	α (%)
190	2	191	191	332	0
190	4	187	225	77	77
190	6	194	230	59	82
190	8	200	232	49	85
190	10	201	233	45	86

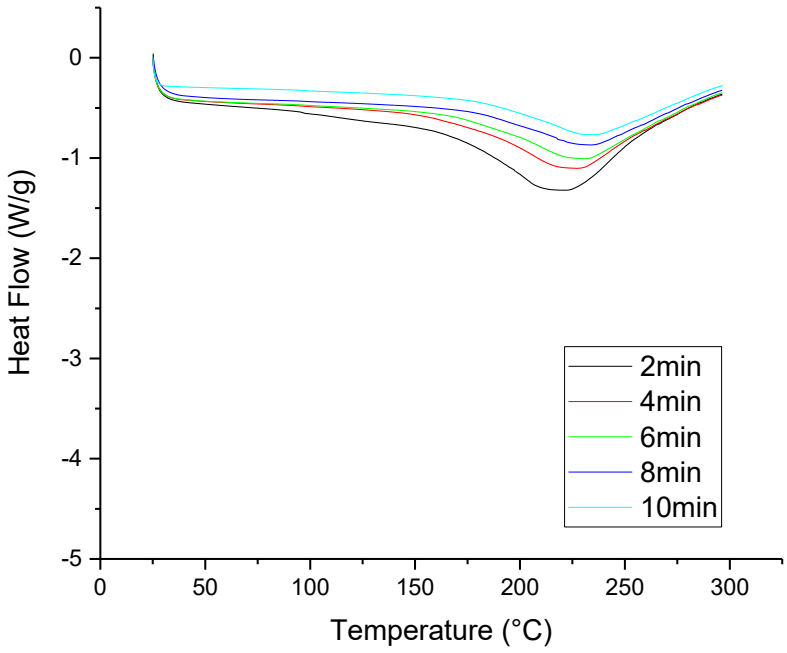

Figure 8.49 Postcure (second heating) of a series of **Thermoset #1** cured isothermally at 200°C for various heating durations, in hermetic mode

Table 8.21 Residual heat and conversion for **Thermoset #1** isothermally cured at 200°C

T_{iso} (°C)	Duration (min)	T_{Onset} (°C)	T_{Peak} (°C)	$\Delta H_{Residual}$ (J/g)	α (%)
200	2	184	224	80	76
200	4	184	228	58	83
200	6	190	232	43	87
200	8	195	232	40	88
200	10	198	230	40	88

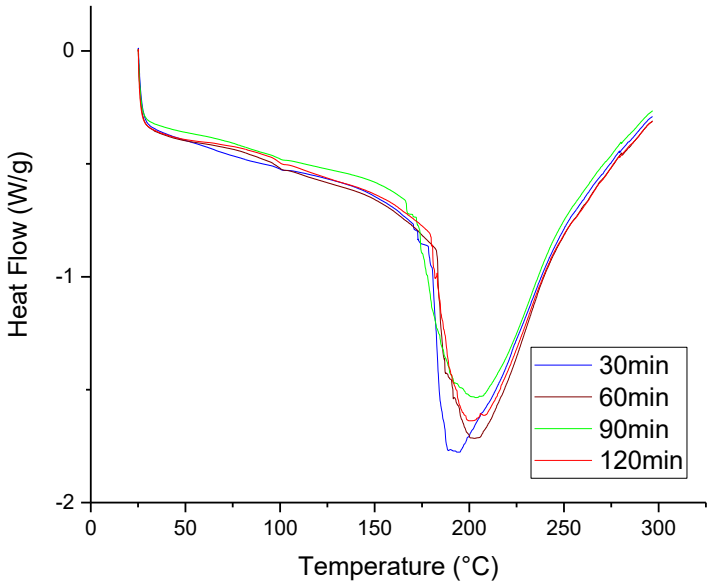

Figure 8.50 Postcure (second heating) of a series of **Thermoset #1** cured isothermally at 130°C for various heating durations

Table 8.22 Characteristic temperature and residual heat of **Thermoset #1** cured isothermally at 130°C

T_{iso} (°C)	Duration (min)	T_{Peak} (°C)	$\Delta H_{Residual}$ (J/g)	α (%)
130	30	195	258	0
130	60	206	210	0
130	90	203	227	0
130	120	200	194	0

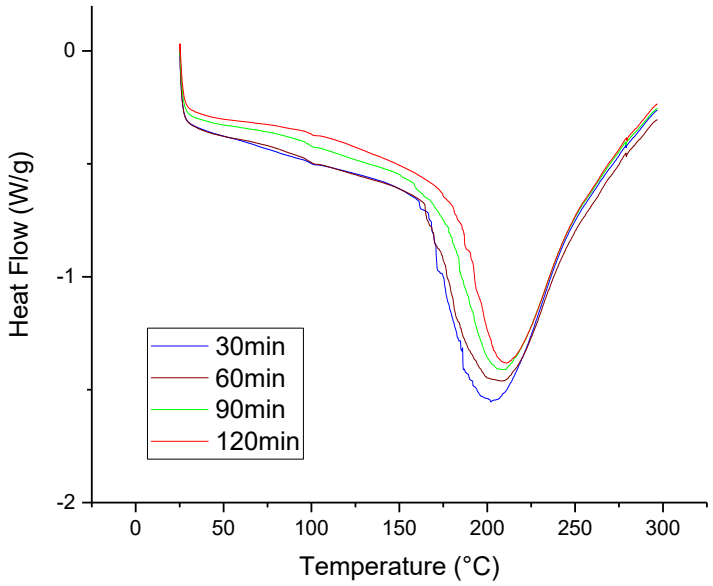

Figure 8.51 Postcure (second heating) of a series of **Thermoset #1** cured isothermally at 140°C for various heating durations

Table 8.23 Characteristic temperature and residual heat of **Thermoset #1** cured isothermally at 140°C

T_{iso} (°C)	Duration (min)	T_{Peak} (°C)	$\Delta H_{Residual}$ (J/g)	α (%)
140	30	202	238	0
140	60	200	189	0
140	90	206	175	3
140	120	210	151	16

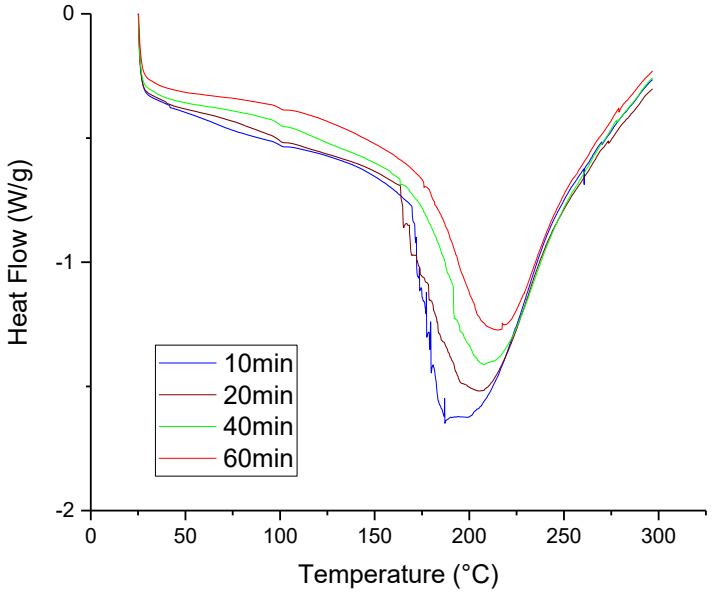

Figure 8.52 Postcure (second heating) of a series of **Thermoset #1** cured isothermally at 150°C for various heating durations

Table 8.24 Characteristic temperature and residual heat of **Thermoset #1** cured isothermally at 150°C

T_{iso} (°C)	Duration (min)	T_{Peak} (°C)	$\Delta H_{Residual}$ (J/g)	α (%)
150	10	187	230	0
150	20	204	214	0
150	40	208	168	7
150	60	214	135	25

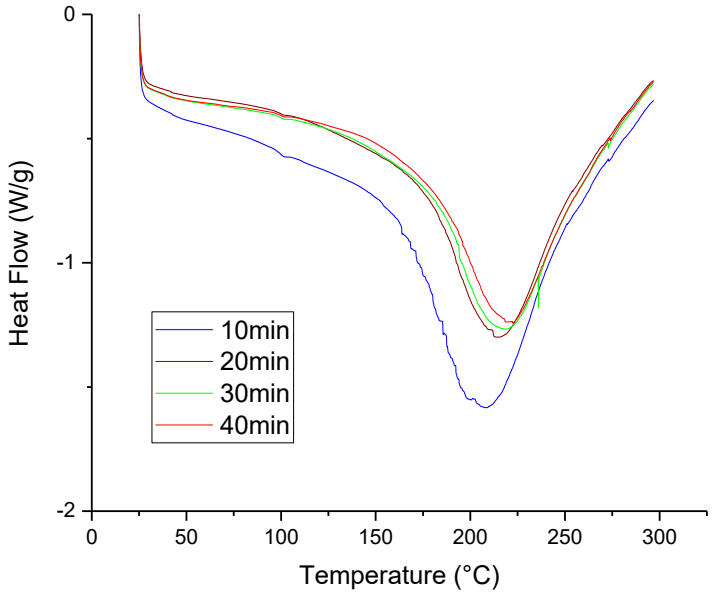

Figure 8.53 Postcure (second heating) of a series of **Thermoset #1** cured isothermally at 160°C for various heating durations

Table 8.25 Characteristic temperature and residual heat of **Thermoset #1** cured isothermally at 160°C

T_{iso} (°C)	Duration (min)	T_{Peak} (°C)	$\Delta H_{Residual}$ (J/g)	α (%)
160	10	206	167	7
160	20	213	108	40
160	30	218	98	46
160	40	219	81	55

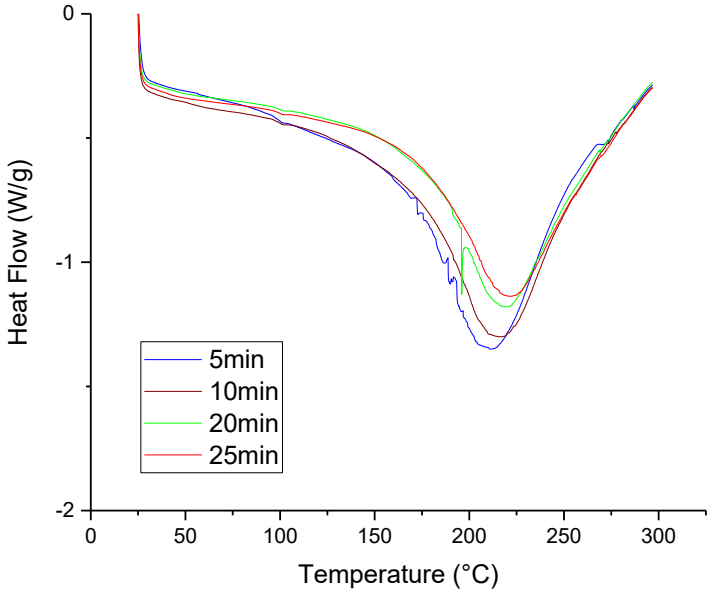

Figure 8.54 Postcure (second heating) of a series of **Thermoset #1** cured isothermally at 170°C for various heating durations

Table 8.26 Characteristic temperature and residual heat of **Thermoset #1** cured isothermally at 170°C

T_{iso} (°C)	Duration (min)	T_{Peak} (°C)	$\Delta H_{Residual}$ (J/g)	α (%)
170	5	211	120	33
170	10	216	97	46
170	20	218	82	54
170	25	219	69	62

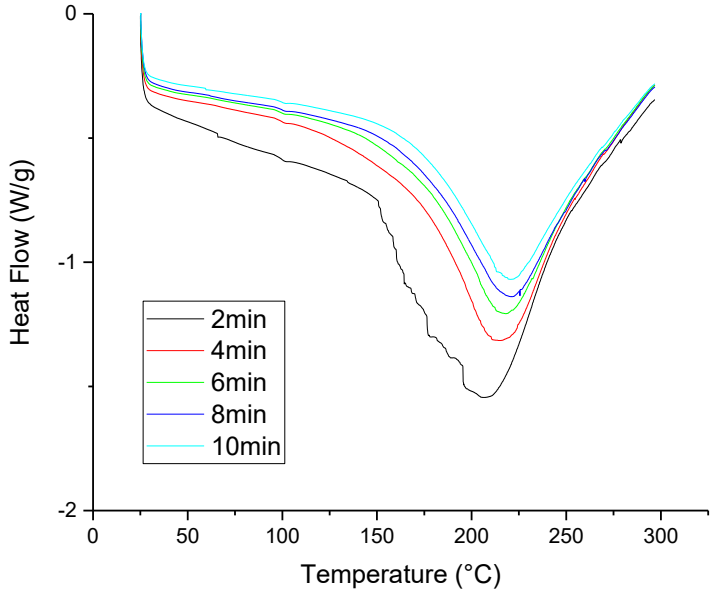

Figure 8.55 Postcure (second heating) of a series of **Thermoset #1** cured isothermally at 180°C for various heating durations

Table 8.27 Characteristic temperature and residual heat of **Thermoset #1** cured isothermally at 180°C

T_{iso} (°C)	Duration (min)	T_{Peak} (°C)	$\Delta H_{Residual}$ (J/g)	α (%)
180	2	205	217	0
180	4	211	74	59
180	6	217	65	64
180	8	220	60	67
180	10	220	45	75

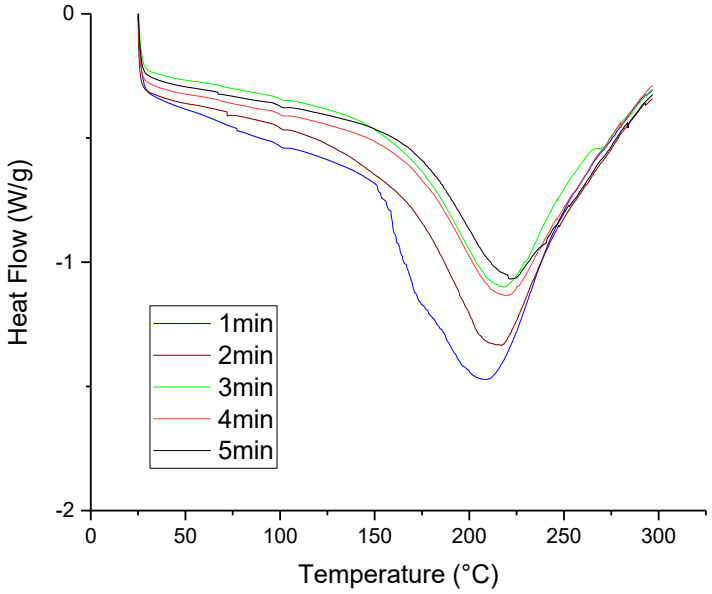

Figure 8.56 Postcure (second heating) of a series of **Thermoset #1** cured isothermally at 190°C for various heating durations

Table 8.28 Characteristic temperature and residual heat of **Thermoset #1** cured isothermally at 190°C

T_{iso} (°C)	Duration (min)	T_{Peak} (°C)	$\Delta H_{Residual}$ (J/g)	α (%)
190	1	207	227	0
190	2	217	78	57
190	3	217	60	67
190	4	220	49	73
190	5	221	43	76

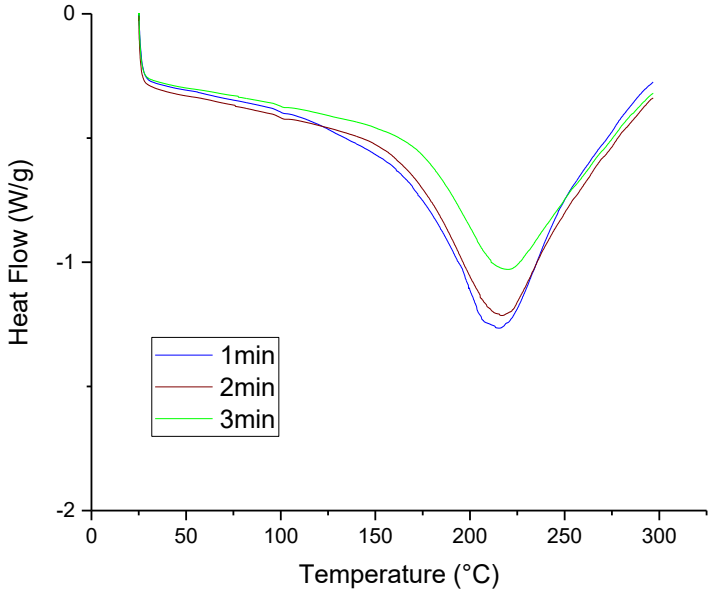

Figure 8.57 Postcure (second heating) of a series of **Thermoset #1** cured isothermally at 200°C for various heating durations

Table 8.29 Characteristic temperature and residual heat of **Thermoset #1** cured isothermally at 200°C

T_{iso} (°C)	Duration (min)	T_{Peak} (°C)	$\Delta H_{Residual}$ (J/g)	α (%)
200	1	214	66	63
200	2	216	44	76
200	3	214	21	88

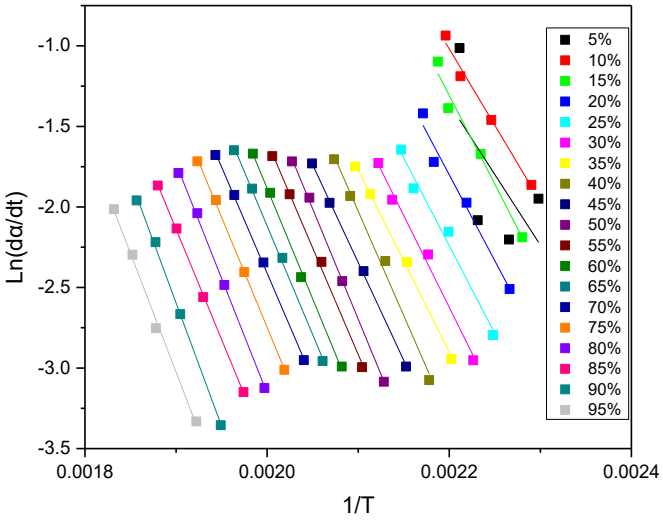

Figure 8.58 Determination of activation energy for isothermal TGA cure of **Thermoset #2** solid

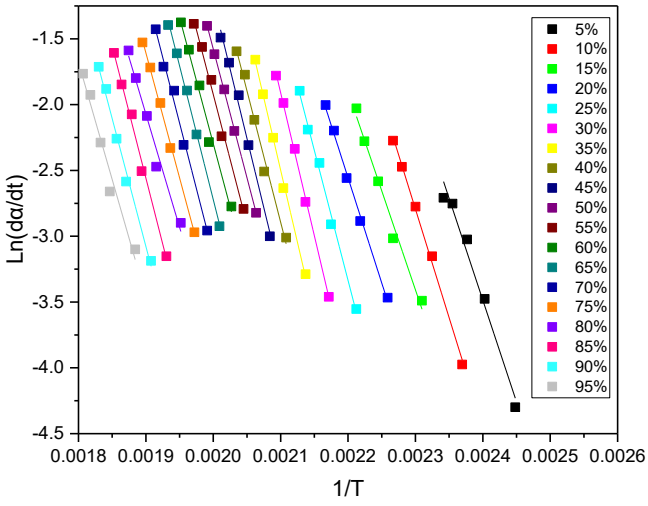

Figure 8.59 Determination of activation energy for isothermal TGA cure of **Thermoset #2** powder

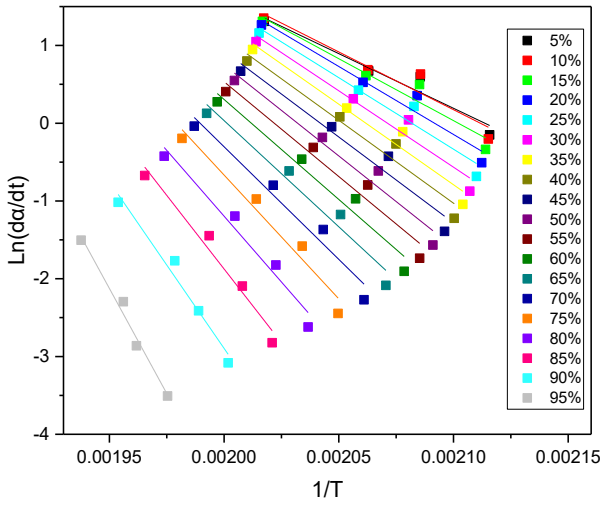

Figure 8.60 Dependence of Ea with the extent of non-isothermal DSC cure of **Thermoset #2** powder in hermetic mode

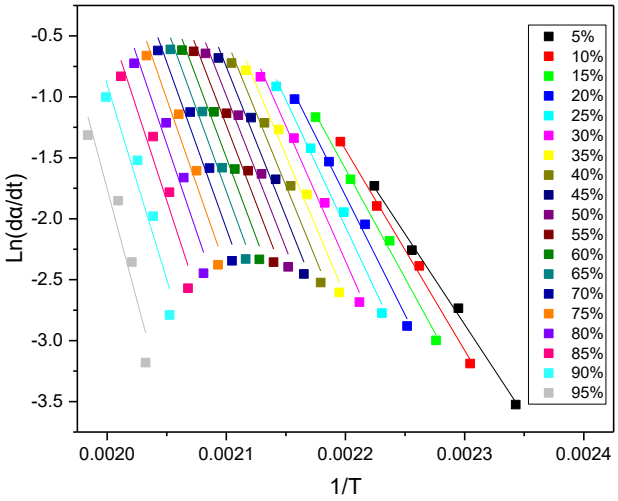

Figure 8.61 Dependence of Ea with the extent of non-isothermal DSC cure of **Thermoset #2** powder in non-hermetic mode

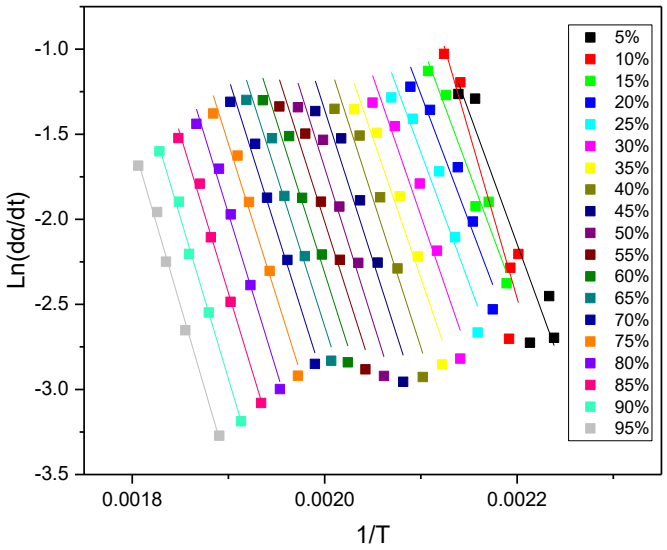

Figure 8.62 Determination of activation energy for isothermal TGA cure of **Thermoset #3** solid

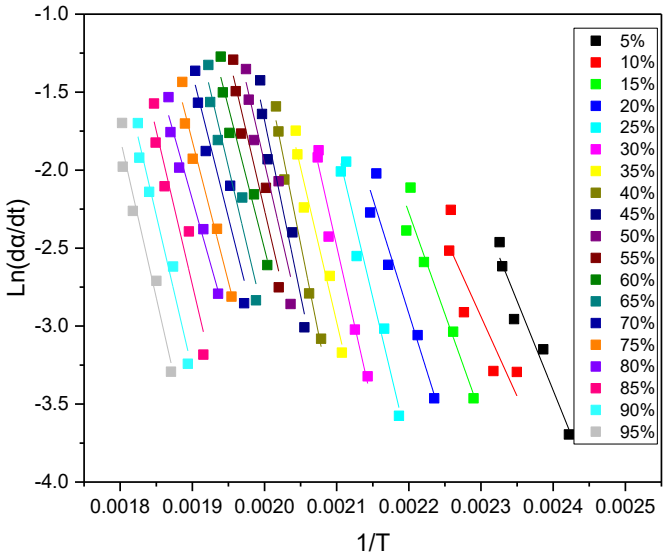

Figure 8.63 Determination of activation energy for isothermal TGA cure of **Thermoset #3** powder

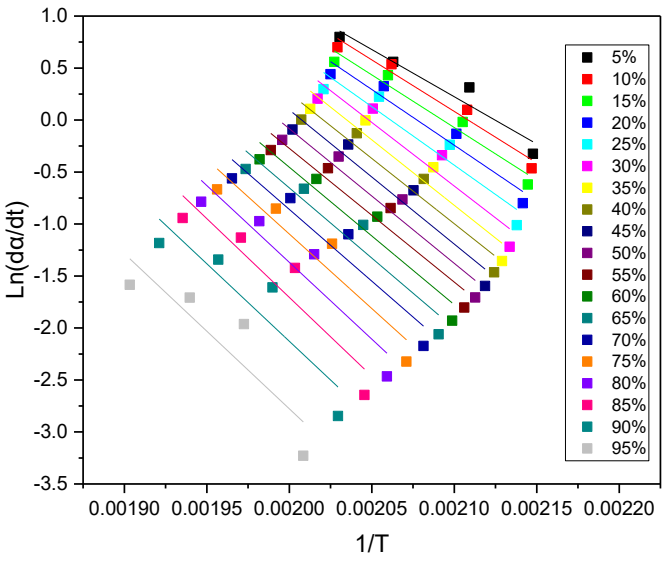

Figure 8.64 Dependence of Ea with the extent of non-isothermal DSC cure of **Thermoset #3** powder in hermetic mode

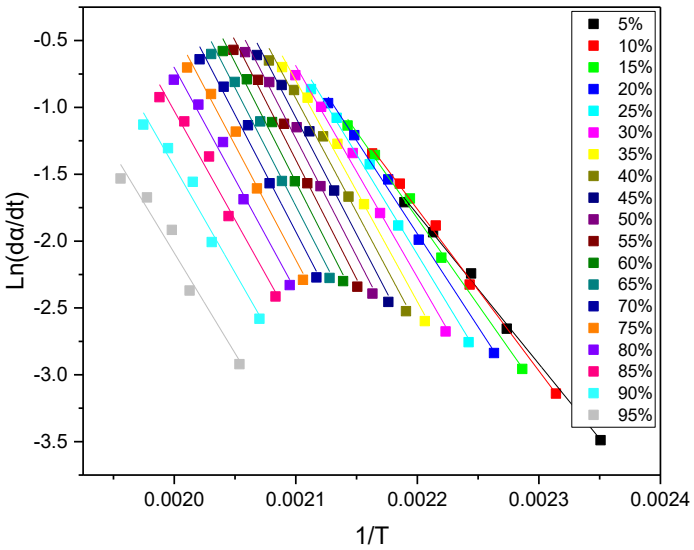

Figure 8.65 Dependence of Ea with the extent of non-isothermal DSC cure of **Thermoset #3** powder in non-hermetic mode

Table 8.30 Replicated 2×2×3 factorial design

Straw size	Fiber (#1)				Particle (#2)			
Concentration	20%		40%		20%		40%	
	$T_{onset/peak}$	ΔH	$T_{onset/peak}$	ΔH	$T_{onset/peak}$	ΔH	$T_{onset/peak}$	ΔH
untreated	219	114	225	127	231	128	218	154
hot-water treated	219	136	210	140	228	124	214	161
NaOH treated	215	107	208	173	213	128	214	166

Table 8.31 ANOVA (analysis of variance)

	$T_{onset/peak}$ (°C)					ΔH (J/g)				
	SS	df	MS	F	$F_{critical}$	SS	df	MS	F	$F_{critical}$
Straw size	216	1	216	8.61	4.17	1250	1	1250	4.49	4.17
Concentration	497	1	497	19.81	4.17	11432	1	11432	41.04	4.17
Treatment	902	2	451	17.98	2.16	1825	2	913	3.28	2.16
Interaction	469	7	67	2.67		4185	7	598	2.15	
Error	828	33	25			9193	33	279		
Total	2911	44	66			27885	44	634		

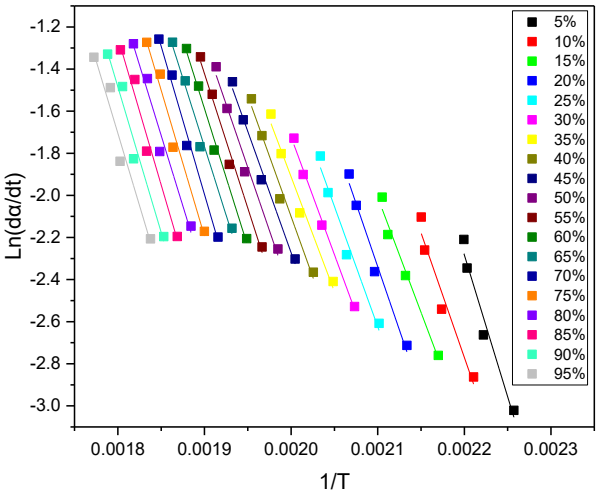

Figure 8.66 Determination of activation energy for isothermal TGA cure of prepregs of untreated wheat straw

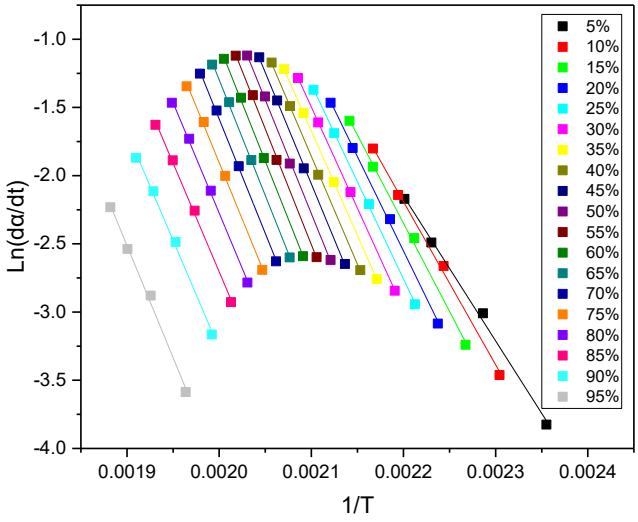

Figure 8.67 Dependence of Ea with the extent of non-isothermal DSC cure of the prepregs of untreated wheat straw and 40% **Thermoset #1** in non-hermetic mode

Appendix F

Raw Data of Replicated 2×2×3 Factorial Design

Table 8.32 Replicated 2×2×3 factorial design

size	Fiber (#1)				Particle (#2)			
Concentration	20%		40%		20%		40%	
	T_{Peak} (°C)	ΔH (J/g)	T_{Peak} (°C)	ΔH (J/g)	T_{Peak} (°C)	ΔH (J/g)	T_{Peak} (°C)	ΔH (J/g)
untreated	220	121	232	129	235	115	224	147
	218	124	219	132	233	141	216	144
	220	109	224	119	228	128	215	170
	217	101			226	126		
hot-water	222	116	215	137	219	116	210	170
	215	138	201	114	234	134	222	109
	220	155	210	174	231	115	211	164
	218	134	214	135	226	130	211	199
NaOH	213	113	211	168	210	129	223	173
	215	114	207	172	216	142	215	174
	218	104	206	175	212	114	203	161
	212	98	207	175			215	155

Appendix G

Wheat Straw-Polyamide 6 Pressboard

Table 8.33 Factors and levels for the Experiment #02

Factors	Low (-)	High (+)
Force (A), lbf	20,000	30,000
Percentage of PA6 (B), %	10	20
WS stem (C), %	0	10

Table 8.34 Design matrix in the Experiment #02

Run	Run order	A	B	C
1)	3	-1	-1	-1
a	7	1	-1	-1
b	4	-1	1	-1
ab	5	1	1	-1
c	6	-1	-1	1
ac	2	1	-1	1
bc	8	-1	1	1
abc	1	1	1	1

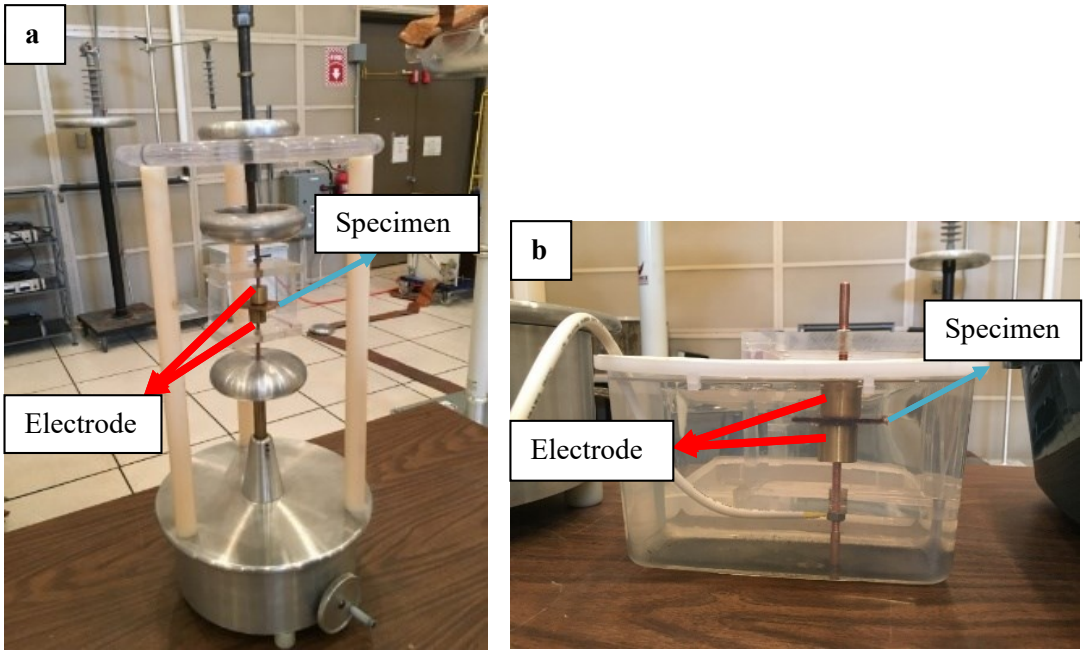

Figure 8.68 Test cell (electrode) for dielectric spectroscopy measurement in air (a) and in insulation oil (b)

Table 8.35 Flexural strength (MPa)

Run	**#01**	**#02**	**#03**	**#04**	**#05**
1)	8.9	11.2	14.3	4.6	5.9
a	7.4	11.3	13.7	8.4	10.0
b	11.8	20.0	8.5	4.4	4.3
ab	8.4	12.0	7.7	9.0	17.0
c	5.9	13.4	11.0	6.6	4.3
ac	12.0	9.2	17.3	6.9	4.7
bc	15.7	24.9	11.9	3.0	6.0
abc	18.7	26.2	14.0	7.9	12.0

Table 8.36 Flexural modulus (MPa)

Run	**#01**	**#02**	**#03**	**#04**	**#05**
1)	770.9	675	841	362.4	424.1
a	559.3	837.3	1258.4	623.5	768.4
b	780.4	760	707	263.6	333.7
ab	685.2	441	460.6	602.7	757
c	348.5	831.5	841	517.5	396.1
ac	637.4	553.3	1375	585.4	401.3
bc	809.9	1097	752.3	203.7	441.3
abc	1176.8	1075.5	1344	491.3	973.8

Table 8.37 Flexural strength and modulus obtained for each pressboard sample manufactured under the combination of 3 factors described in the table (Experiment #02)

Run	Flexural Strength (MPa)	Flexural Modulus (MPa)
a	11.3	836.3
b	20.0	760
ab	16.0	411
c	13.4	831.5
ac	12.4	553.3
bc	24.9	1097
abc	26.2	1,075.5

Table 8.38 Analysis of Variance (ANOVA) for Experiment #02

Source	Effect	SS	df	β	Effective
				16.925	
A=force	-0.9	1.62	1	-0.45	
B=PA6	9.7	188.18	1	4.85	**
C=LWS*	4.6	42.32	1	2.3	
AB	-0.45	0.405	1	-0.225	
AC	1.05	2.205	1	0.525	
BC	2.95	17.405	1	1.475	
ABC	1.6	5.12	1	0.8	

*LWS short for long wheat straw stem; SS stands for sum of squares, DF degree of freedom

Table 8.39 DOE analysis of wheat straw-polyamide 6 pressboard

	Eff	SS	df	β
A	-2.4	11.52	1	-1.2
B	11.2	250.88	1	5.6
C	3.1	19.22	1	1.55
AB	-1.95	7.605	1	-0.975
AC	2.55	13.005	1	1.275
BC	1.45	4.205	1	0.725
ABC	3.1	19.22	1	1.55
				17.675

Table 8.40 NPP of effects

Rank	X	P	Z
1	-2.4	0.071429	-1.46523
2	-1.95	0.214286	-0.79164
3	1.45	0.357143	-0.36611
4	2.55	0.5	0
5	3.1	0.642857	0.366106
6	3.1	0.785714	0.791639
7	11.2	0.928571	1.465234

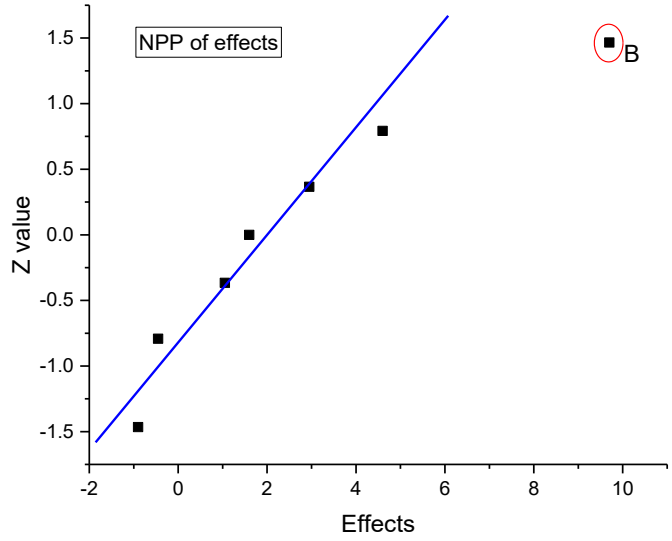

Figure 8.69 Normal probability plot of the effects of the individual factors and factor interactions

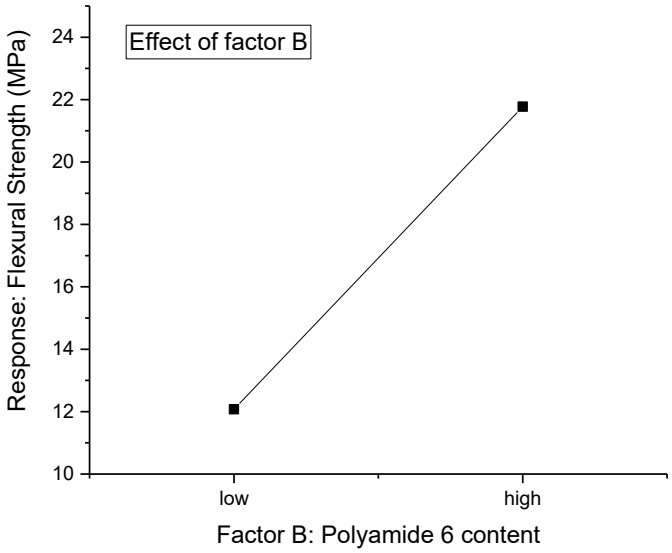

Figure 8.70 Effect of the polyamide 6 content on flexural strength

Table 8.41 BC interaction

B	C	Response
1	1	25.55
1	-1	21
-1	1	12.9
-1	-1	11.25

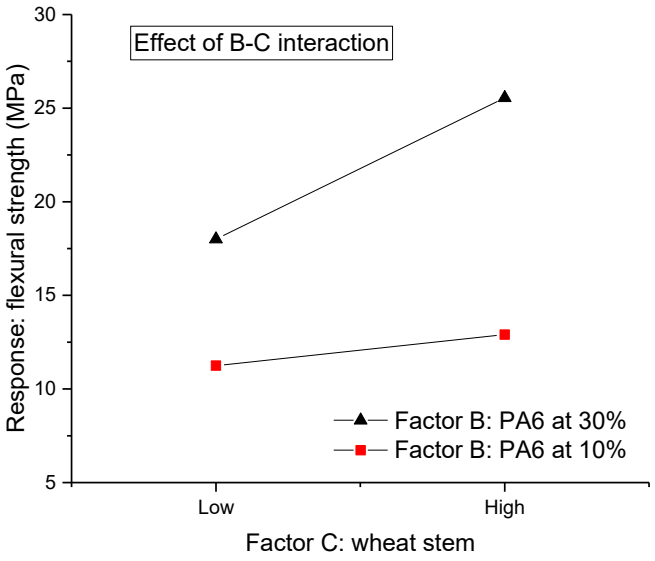

Figure 8.71 Effect of polyamide 6 content–wheat stem interaction on flexural strength

Table 8.42 NNP of residue of BC interaction

Rank	X	P	Z
1	-13.93	0.0625	-1.53412
2	-12.83	0.1875	-0.88715
3	-2.93	0.3125	-0.48878
4	-1.33	0.4375	-0.15731
5	0.88	0.5625	0.157311
6	7.28	0.6875	0.488776
7	10.88	0.8125	0.887147
8	11.98	0.9375	1.534121

Table 8.43 Predicted responses and residuals

y	$\hat{y}$	residual
11.2	12.075	0.88
11.3	21.775	10.48
20	12.075	-7.93
16	21.775	5.78
13.4	12.075	-1.33
12.4	21.775	9.38
24.9	12.075	-12.83
26.2	21.775	-4.43

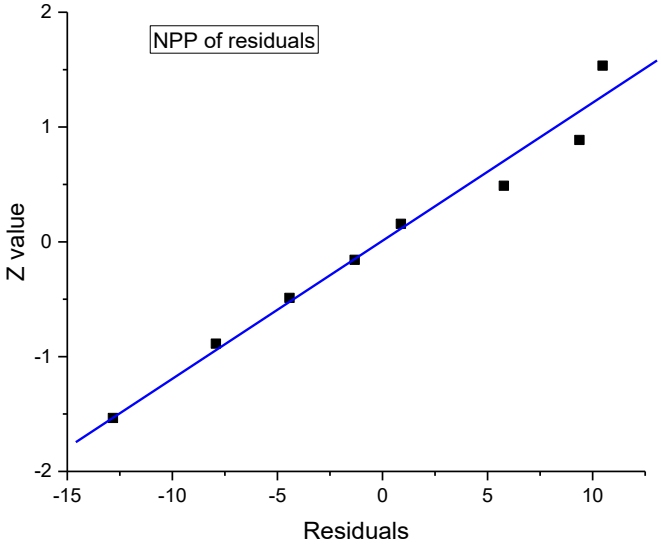

Figure 8.72 Normal probability plot of residual

Appendix H

Wheat Straw-Acrodur Pressboard

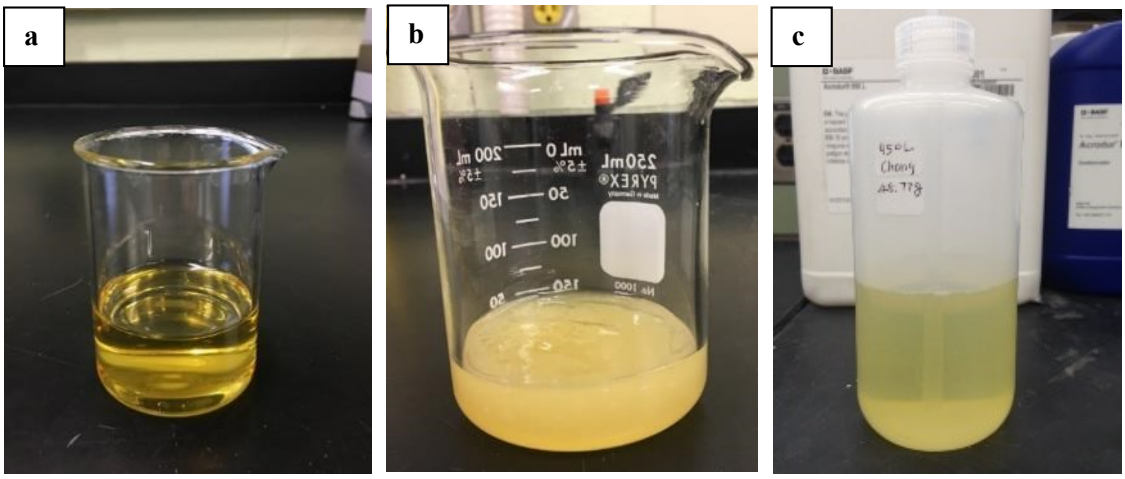

Figure 8.73 **Thermoset #1** (a) and **#2** (b), and **#3** (c)

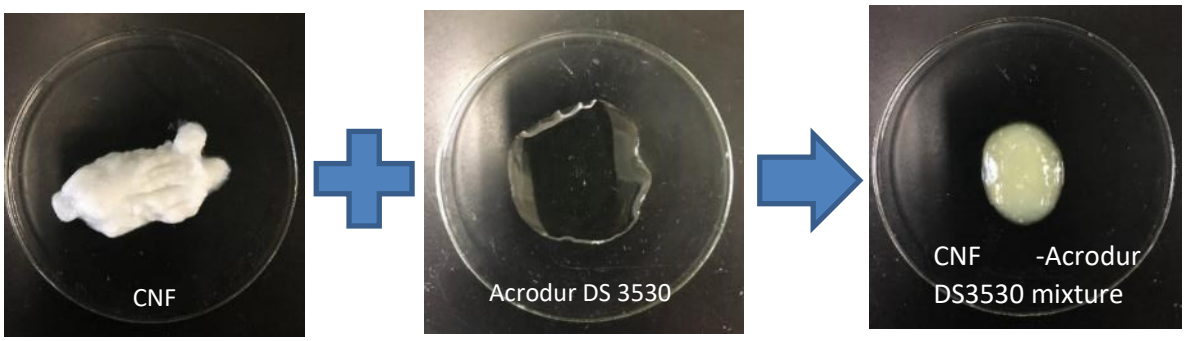

Figure 8.74 **Thermoset #2** made by dispersing CNF in **Thermoset #1** solution

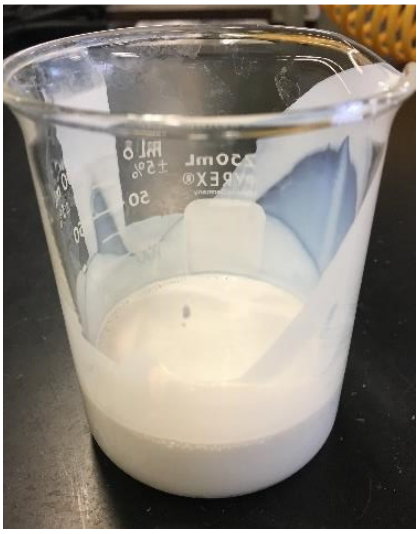

Figure 8.75 **Thermoplastic #5** dispersion